Synthesis and Characterization of Well-Defined Multifunctional Hyperbranched Polyether Polyols

Dissertation

zur Erlangung des Grades

„Doktor der Naturwissenschaften“

im Promotionsfach Chemie

am Fachbereich Chemie, Pharmazie,

Geographie und Geowissenschaften

der Johannes Gutenberg-Universität Mainz

Tobias Kaiser

geboren in Mayen

Mainz, 2020

1. Berichterstatter:

2. Berichterstatter:

Tag der mündlichen Prüfung: 22.06.2020

Erklärung

Die vorliegende Arbeit wurde im Zeitraum von Dezember 2016 bis Mai 2020 am Department of Chemistry der Johannes Gutenberg-Universität angefertigt.

Hiermit versichere ich gemäß § 10 Abs. 3d der Promotionsordnung vom 24.07.2007

a) Ich habe die jetzt als Dissertation vorgelegte Arbeit selbst angefertigt und alle benutzten Hilfsmittel (Literatur, Apparaturen, Material) in der Arbeit angegeben.
b) Ich habe oder hatte die jetzt als Dissertation vorgelegte Arbeit nicht als Prüfungsarbeit für eine staatliche oder andere wissenschaftliche Prüfung eingereicht.
c) Ich hatte weder die jetzt als Dissertation vorgelegte Arbeit noch Teile davon bei einer anderen Fakultät oder einem anderen Fachbereich als Dissertation eingereicht.

Mainz, 18. Mai 2020

Tobias Kaiser

Danksagung

Table of Contents

Motivation and Objectives

During the three decades following their inception in the 1980ies, dendritic polymers have attracted considerable attention establishing them as one of the main classes of polymer architectures. Under this general term, both hyperbranched polymers (HBPs) as well as the perfectly branched dendrimers are summarized, since they show several common traits. For instance, low viscosities both in bulk and solution resulting from an exceptionally compact globular structure and the absence of entanglements are typical for these materials. In addition, dendritic polymers possess multiple functional end-groups clearly distinguishing them from linear polymers. Hyperbranched polymers are typically accessible in a single step, in contrast to the tedious generation-wise synthesis of dendrimers in iterative organic synthesis steps. The facile preparation in one step comes at the cost of a structure determined by polymerization statistics, manifest by linear units interrupting the perfect branching pattern. As a consequence, the degree of branching (DB), which describes the branching perfection of a given polymer, is reduced to values close to 0.5, placing HBPs between linear polymers (DB = 0) and dendrimers (DB = 1). However, since the polymerization typically follows a step-growth mechanism, hyperbranched polymers oftentimes show broad molecular weight distributions (M_w / M_n > 5).

One of the few hyperbranched polymers that can be prepared in a controlled manner is hyperbranched polyglycerol (*hb*PG). Based on the anionic ring-opening polymerization of glycidol, full control of the molar mass and low polydispersities were achieved by slow monomer addition (SMA) to a partially deprotonated polyol core molecule. Hyperbranched polyglycerol combines several extraordinary

features, including a flexible and hydrophilic aliphatic polyether backbone, multiple hydroxyl end-groups, and outstanding biocompatibility, with those typically attributed to dendritic polymers (*vide supra*).

In general, the properties of *hb*PG or any other hyperbranched polymer are dictated by the overall topology as well as the distribution of functional groups. This thesis aims at the manipulation of these fundamental characteristics to prepare well-defined multi-functional polyglycerol or structurally related hyperbranched copolymers beyond previous limitations regarding chemical or physical properties. To this end, two separate approaches are pursued: 1) variation of the polymer architecture (DB and molecular weight), and 2) variation of the polymer functionality (backbone functionality and end-group functionality) (cf. Figure 1).

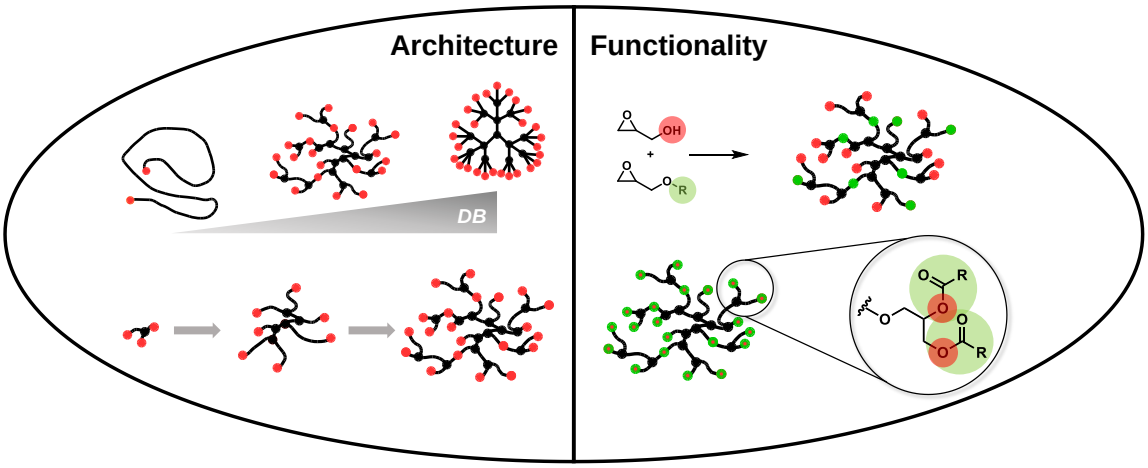

Figure 1. Fundamental characteristics of hyperbranched polymers: polymer architecture (1)) and polymer functionality (2)).

1) The architecture of dendritic polymers is characterized by two parameters: the molecular weight in combination with polydispersity (1a)), and the degree of branching (1b)). To establish detailed structure-property relationships, a

thorough understanding and consequently full control of these characteristics is of highest importance.

a) The slow addition of the latent AB_2 monomer glycidol is a prerequisite to obtain well-defined hyperbranched polyether polyols with control of the molecular weight and polydispersity. This synthetic technique is usually transferable to the copolymerization of glycidol with suitable AB comonomers, i.e. glycidyl ethers, without any obstacles. However, if gaseous comonomers are to be employed, the slow monomer addition using conventional laboratory equipment fails, hence one usually resorts to a batch procedure. To remove this limitation, a universal addition protocol will be developed to prepare well-defined hyperbranched polyether polyols, particularly hyperbranched poly(alkylene oxides), with full control of the molecular weight and polydispersity regardless of the comonomers preferred physical state.

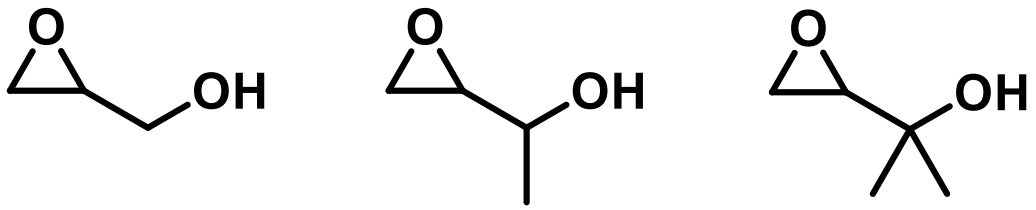

Scheme 1. Structurally related monomers Glycidol, MeGly and DiMeGly.

b) The degree of branching (DB) directly influences the properties unique to dendritic polyethers. By copolymerization of glycidol with monomers prone to anionic ring-opening, the DB is tunable between 0 and 0.5 yielding highly flexible materials with adjustable degree of crystallization, e.g. *hb*PEO. To achieve higher values, the polymerization must be manipulated to yield more branching units. To this end, the reaction mechanism of the anionic

ROMBP of glycidol will be modeled by computer simulations and the steps leading to branching will be identified. To influence these steps, two novel AB_2 monomers will be introduced that structurally resemble glycidol but lead to a variation of the degree of branching.

2) The properties of dendritic polymers are not exclusively governed by the individual architecture, but also to a high degree by the distribution of various functional groups. A distinction can be made between backbone (2a)) and end-group functionality (2b)).

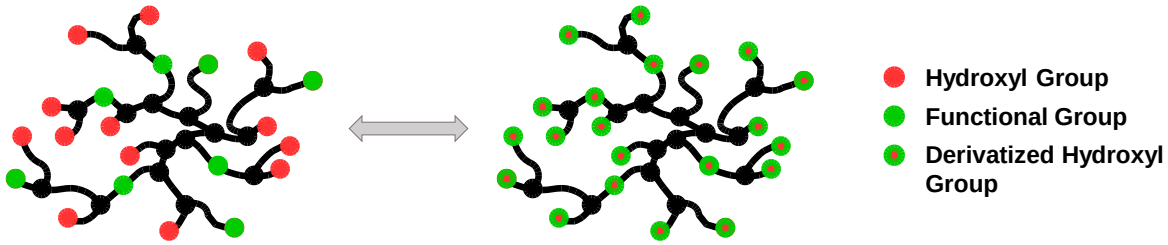

Scheme 2. Schematic differences between backbone and end-group functionalization.

a) Backbone functionalization is typically achieved by the random copolymerization of glycidol with functionalized glycidyl ethers *via* SMA. By variation of the comonomer feed, different ratios of the hydroxy to any functional group are readily available. This thesis aims at the incorporation of tertiary amino moieties to simultaneously introduce pH and thermo-responsive behavior representing novel properties for hyperbranched polyglycerol. In addition to the well-established glycidyl ethers, bulky glycidyl esters will be investigated as a new class of comonomer.

b) The conventional route to end-group functionalization is the derivatization of the termini of *hb*PG. The hydroxyl groups in hyperbranched polyether

polyols undergo typical reactions described for other alcohols, e.g. esterification. By reaction with either fatty acid halides or initiator moieties and subsequent controlled radical polymerization, amphiphilic nanostructures based on *hb*PEO can be prepared in a facile manner in two to three steps. These amphiphilic nanocapsules have potential as nanoreactors with adjustable core and shell domains for the solubilization of a hydrophilic cargo.

Abstract

Aiming at well-defined hyperbranched polyether polyols based on the anionic ring-opening polymerization of glycidol, this thesis presents novel synthetic pathways as well as improved existing strategies to enable full control of the polymer architecture and the overall functionality. Additionally, comprehensive characterization data and theoretical models are provided, enabling a fundamental understanding of the polymer structure.

Chapter 1 summarizes the history of dendritic polymers, in particular hyperbranched polymers (HBPs) as the less branched representatives of this class. In **Chapter 1.1**, a special emphasis is placed on the first decade following the initial reports on hyperbranched polymers. During this time, the synthesis strategies to obtain well-defined HBPs have been continuously improved culminating in the slow monomer addition approach (SMA) representing pseudo chain-growth in contrast to the initial step-growth polymerization. Furthermore, theoretical models for various synthesis strategies are presented, that provide deep insights into different molecular characteristics of hyperbranched polymers, i.e. the degree of branching (DB) and the molar mass. The chapter is concluded by an evaluation of current trends and obstacles regarding HBPs.

Being one of the first well-defined hyperbranched polymers synthesized *via* the SMA approach, hyperbranched polyglycerols (*hb*PG), including structurally related copolymers, have experienced a rapid development regarding synthesis strategies, characterization, and application potential. **Chapter 1.2** summarizes the recent advances concerning hyperbranched polyether polyols obtained by the

anionic ring-opening (co-)polymerization of glycidol and states common limitations encountered during the synthesis and application of this type of hyperbranched polymer.

Different strategies to vary the architecture of hyperbranched polyglycerol and the respective copolymers, i.e. the degrees of branching and molar masses, are presented in **chapter 2**. In particular, **chapter 2.1** introduces the controlled copolymerization of glycidol and ethylene oxide *via* SMA. This synthetic technique is a prerequisite for controlled molar masses and polydispersities and was previously limited to comonomers with a boiling point similar to glycidol. By employing a fully automated reactor setup, a universal synthesis methodology is presented. Following this approach, hyperbranched poly(ethylene oxide) (*hb*PEO) is obtained by the copolymerization of ethylene oxide and glycidol with full control of the molar mass. Furthermore, the synthesis of the first well-defined multi-functional *hb*PEO copolymer, a terpolymer comprising ethylene oxide, glycidol and allyl glycidyl ether, is reported.

Chapter 2.2 on the other hand deals with a detailed study of the fundamental reaction steps during the anionic ring-opening multibranching polymerization of glycidol leading to the formation of branching points. Following simple kinetic considerations, the proton transfer equilibria are identified as the crucial steps towards branching and the DB of *hb*PG at full conversion is simulated. To vary the degree of branching, the AB_2 comonomers MeGly and DiMeGly are introduced, carrying either one or two additional methyl groups adjacent to the hydroxyl group. These compounds show different basicities than glycidol after ring-opening. Thus, the proton transfer equilibria are altered yielding different degrees of branching for homopolymers of MeGly and DiMeGly. Therefore, the AB_2/AB_2 copolymerization

of glycidol with either of the monomers enables tuning of the degree of branching in an unprecedented range. The discussion of the polymer architecture is concluded in **Chapter 2.3** by a thorough hydrodynamic characterization of hyperbranched polyglycerols in a wide range of molar masses. In combination with light scattering approaches, the determination of the absolute molecular weights of *hb*PGs is presented. Additionally, hyperbranched polyglycerols are found to adopt a solid sphere conformation in aqueous solution while simultaneously being highly hydrated.

In contrast to the previous chapter, **Chapter 3** focusses on the functionalization of hyperbranched polyether polyols to tailor the polymer properties. In general, two approaches can be pursued: either copolymerization of glycidol with suitable comonomers yielding multi-functional *hb*PGs (**Chapter 3.1 – 3.2**) or the derivatization of the hydroxyl termini of hyperbranched polyether polyols by common reaction types, e.g. esterification using reactive carboxylic acid derivatives (**Chapter 3.3 – 3.4**).

In **chapter 3.1**, the copolymerization of glycidol with DBuAEGE, a glycidyl ether bearing tertiary amino moieties, is discussed. By simultaneous slow addition of both monomers, a random distribution of the functional groups throughout the polymer is achieved, as suggested by *on-line* NMR monitoring and the thermal analysis of the hyperbranched copolymers. The introduction of the apolar dibutyl amino moieties leads to multi-stimuli responsive behavior resulting in cloud points tunable between 13 and 80 °C, while lower comonomer contents result in full water-solubility. In contrast to other tertiary amines, e.g. tributyl amine, the incorporation of DBuAEGE into the highly hydrophilic polyether backbone leads to an enhanced biocompatibility.

With glycidyl pivalate representing bulky glycidyl esters, a novel class of comonomers is introduced in **chapter 3.2**. The steric hindrance of the ester protecting group has two distinct effects on the copolymerization behavior: although the pivalate group is typically cleaved under basic conditions, no transesterification is observed during polymerization. Additionally, the comonomer is incorporated mainly as a terminal unit. Hence, the copolymerization of glycidol with bulky glycidyl esters leads to the *in-situ* end-group functionalization of *hb*PG with little effect on the degree of branching in contrast to the copolymerization with glycidyl ethers or alkylene oxides.

In **chapter 3.3**, the esterification of the hydroxyl groups of *hb*PEO with various fatty acids is reported to obtain amphiphilic core-shell structures. These unimolecular nanocapsules show phase transfer activity by solubilizing a highly hydrophilic dye in an apolar organic solvent. The average maximum loading capacity was found to depend on the molar mass of the core domain, the degree of functionalization and the type of fatty acid. In comparison to similar structures obtained by the functionalization of *hb*PG, greatly enhanced loading capacities are obtained. While the encapsulated cargo molecule is still addressable for further reactions, it is released only after cleavage of the ester bonds.

By functionalization of *hb*PEO with initiator groups for atom transfer radical polymerization, multi-arm star copolymers with extraordinarily high arm numbers are synthesized by the subsequent controlled polymerization of methyl methacrylate as presented in **chapter 3.4**. The polymerization follows first order kinetics resulting in well-controlled molar masses. With increasing arm lengths, the thermal properties of the apolar PMMA shell approaches those of linear homopolymers despite being attached to a flexible hyperbranched polyether core.

Zusammenfassung

Die vorliegende Dissertation präsentiert neuartige sowie verbesserte bestehende Synthesestrategien basierend auf der anionischen Ringöffnungspolymerisation von Glycidol, um eine umfassende Kontrolle der Polymerarchitektur und der Gesamtfunktionalität zu ermöglichen. Zusätzlich werden ausführliche Charakterisierungsdaten und theoretische Modelle erarbeitet, um ein grundlegendes Verständnis der Polymerstruktur zu ermöglichen.

Kapitel 1 fasst die Geschichte der dendritischen Polymere, insbesondere der hyperverzweigten Polymere (HBPs) als weniger verzweigte Vertreter dieser Klasse zusammen. In **Kapitel 1.1** wird ein besonderer Schwerpunkt auf die ersten Jahre nach der Beschreibung hyperverzweigter Polymere durch Kim und Webster gelegt. Während dieser Zeit wurden die Synthesestrategien zur Darstellung wohldefinierter HBPs kontinuierlich verbessert, sodass durch Entwicklung der langsamen Monomerzugabe (*slow monomer addition*, SMA) schließlich der Stufen-Wachstums-Mechanismus durch ein Pseudo-Kettenwachstum abgelöst wurde. Darüber hinaus werden theoretische Modelle für verschiedene Synthesestrategien vorgestellt, die unterschiedliche fundamentale Eigenschaften hyperverzweigter Polymere beschreiben, etwa der Verzweigungsgrad (DB) oder das Molekulargewicht. Das Kapitel wird durch eine kritische Bewertung aktueller Trends bezüglich Synthese und Charakterisierung hyperverzweigter Polymere abgeschlossen.

Als eines der ersten wohldefinierten hyperverzweigten Polymere, die über den Ansatz der langsamen Monomerzugabe synthetisiert wurden, hat

hyperverzweigtes Polyglycerin (*hb*PG), einschließlich strukturell verwandter Copolymere, eine rasche Entwicklung hinsichtlich möglicher Synthesestrategien, Charakterisierung und Anwendungspotential erfahren. **Kapitel 1.2** fasst die jüngsten Fortschritte in Bezug auf hyperverzweigte Polyether-Polyole zusammen, die durch die anionische Ringöffnungs-(Co-)Polymerisation von Glycidol erhalten wurden, und setzt sich mit Einschränkungen auseinander, die bei der Synthese und Anwendung dieser Art hyperverzweigter Polymere auftreten.

In **Kapitel 2** werden verschiedene Strategien zur Variation der Architektur von hyperverzweigtem Polyglycerin und der jeweiligen Copolymere vorgestellt, etwa der Verzweigungsgrad (DB) sowie das Molekulargewicht. Insbesondere wird in **Kapitel 2.1** die kontrollierte Copolymerisation von Glycidol und Ethylenoxid durch langsame Monomerzugabe vorgestellt. Diese Synthesetechnik ist eine Voraussetzung für eine Kontrolle des Molekulargewichtes und der Polydispersität, war bislang jedoch auf solche Comonomere beschränkt, die einen ähnlichen Siedepunkt wie Glycidol aufweisen. Durch den Einsatz eines vollautomatisierten Reaktors wird eine universelle Synthesemethode vorgestellt, welche es ermöglicht, hyperverzweigtes Poly(ethylenoxid) (*hb*PEO) durch Copolymerisation von Ethylenoxid und Glycidol unter vollständiger Kontrolle der Molmasse zu erhalten. Darüber hinaus wird die Synthese des ersten wohldefinierten *hb*PEO-Terpolymers vorgestellt - ein Copolymers bestehend aus Ethylenoxid, Glycidol und Allylglycidylether.

Kapitel 2.2 befasst sich dagegen mit einer detaillierten Untersuchung der grundlegenden Reaktionsschritte während der anionischen Ringöffnungs-Polymerisation von Glycidol, die zur Bildung von Verzweigungspunkten führen. Anhand einfacher kinetischer Überlegungen werden die Protonentransfergleich-

gewichte als diese entscheidenden Schritte identifiziert und der Verzweigungsgrad von *hb*PG bei vollständiger Umwandlung simuliert. Um den Verzweigungsgrad zu variieren, werden die AB_2-Comonomere MeGly und DiMeGly eingeführt, die entweder eine oder zwei zusätzliche Methylgruppen neben der Hydroxylgruppe tragen. Diese Verbindungen zeigen nach Ringöffnung andere Basizitäten als Glycidol, somit werden die Protonentransfergleichgewichte derart verändert, dass unterschiedliche Verzweigungsgrade für Homopolymere von MeGly und DiMeGly erwartet werden. Daher ermöglicht die AB_2/AB_2-Copolymerisation von Glycidol mit MeGly oder DiMeGly die Einstellung des Verzweigungsgrades in einem bislang beispiellosen Bereich.

Die Diskussion der Polymerarchitektur wird in **Kapitel 2.3** durch eine ausführliche hydrodynamische Charakterisierung von hyperverzweigtem Polyglycerin in einem weiten Bereich von Molekulargewichten abgeschlossen. Neben der Bestimmung absoluter Molekulargewichte, wurde in Kombination mit Lichtstreuexperimenten zusätzlich festgestellt, dass *hb*PG in wässriger Lösung eine feste Kugelkonformation annimmt.

Im Gegensatz zu den vorherigen Kapiteln konzentriert sich **Kapitel 3** auf die Funktionalisierung von hyperverzweigtem Polyglycerin, um die Polymereigenschaften zu variieren. Im Allgemeinen können dazu unterschiedliche Ansätze zielführend sein: entweder die Copolymerisation von Glycidol mit geeigneten Comonomeren zu multifunktionellen *hb*PGs (**Kapitel 3.1** - **3.2**) oder die Derivatisierung der Hydroxylgruppen (**Kapitel 3.3** - **3.4**) durch für niedermolekulare Alkohole typische Reaktionstypen.

In **Kapitel 3.1** wird die Copolymerisation von Glycidol mit DBuAEGE, einem Glycidylether, welcher tertiäre Aminogruppen trägt, diskutiert. Durch gleichzeitige langsame Zugabe beider Monomere wird eine zufällige Verteilung der funktionellen Gruppen im gesamten Polymer erreicht, wie durch Online-NMR-Monitoring und thermische Analyse der hyperverzweigten Copolymere nahegelegt wird. Die Einführung der apolaren Dibutylaminogruppen führt zu Stimuli-responsivem Verhalten, mit frei zwischen 13 und 80 °C einstellbaren Trübungspunkten. Im Gegensatz zu anderen, niedermolekularen tertiären Aminen, wie etwa Tributylamin, führt der Einbau von DBuAEGE in das hydrophile Polyethergerüst zu einer verbesserten Biokompatibilität der Base.

Mit Glycidylpivalat als einfachem Vertreter wird in **Kapitel 3.2** die Klasse der sterisch anspruchsvollen Glycidylester als Alternative zu Glycidylethern für die Copolymerisation mit Glycidol vorgestellt. Der sterische Anspruch der Esterschutzgruppe hat unterschiedliche Auswirkungen auf das Copolymerisations-verhalten: Obwohl die Pivalatgruppe typischerweise unter basischen Bedingungen gespalten wird, wird während der Polymerisation keine Umesterung beobachtet. Zusätzlich wird das Comonomer hauptsächlich als terminale Einheit eingebaut. Im Gegensatz zu den Glycidylethern führt die Copolymerisation von Glycidol mit sperrigen Glycidylestern also zur *in-situ* Endgruppenfunktionalisierung von *hb*PG mit lediglich geringem Einfluss auf den Verzweigungsgrad.

In **Kapitel 3.3** wird die Veresterung der Hydroxygruppen von *hb*PEO mit verschiedenen Fettsäuren vorgestellt, um amphiphile Kern-Schale-Strukturen zu erhalten. Diese sogenannten unimolekularen Nanokapseln zeigen Phasentransferaktivität veranschaulicht durch die Solubilisierung eines hydrophilen Farbstoffs in einem unpolaren organischen Lösungsmittel. Die

durchschnittliche maximale Beladungskapazität dieser Strukturen hängt vom Molekulargewicht der Kerndomäne, dem Funktionalisierungsgrad und der Art der Fettsäure ab. Im Vergleich zu ähnlichen Strukturen, die durch die Funktionalisierung von *hb*PG erhalten wurden, werden verbesserte Beladungskapazitäten erhalten. Während das eingekapselte Gastmolekül noch für weitere Reaktionen adressierbar ist, wird es erst durch Spaltung der Esterbindungen freigesetzt.

Kapitel 3.4 verfolgt einen anderen Ansatz für Kern-Schale-Strukturen. Durch Funktionalisierung der Hydroxylgruppen des *hb*PEO mit ATRP-Initiatorgruppen (atom transfer radical polymerization) werden mehrarmige Sterncopolymere mit außerordentlich hohen Armzahlen durch anschließende kontrollierte Polymerisation von Methylmethacrylat synthetisiert. Die Polymerisation folgt einer Kinetik erster Ordnung, was zu gut kontrollierten Molmassen führt, ohne dass Terminierungsreaktionen auftreten. Mit zunehmender Armlänge nähern sich die thermischen Eigenschaften der apolaren PMMA-Schale denen linearer Homopolymere an, obwohl sie an einen flexiblen hyperverzweigten Polyetherkern gebunden sind.

Graphical Abstract

1.1 Hyperbranched Polymer Architectures: From Flory´s $AB_{(f-1)}$ Polycondensates to Tailor-Made Hyperbranched Polyethers

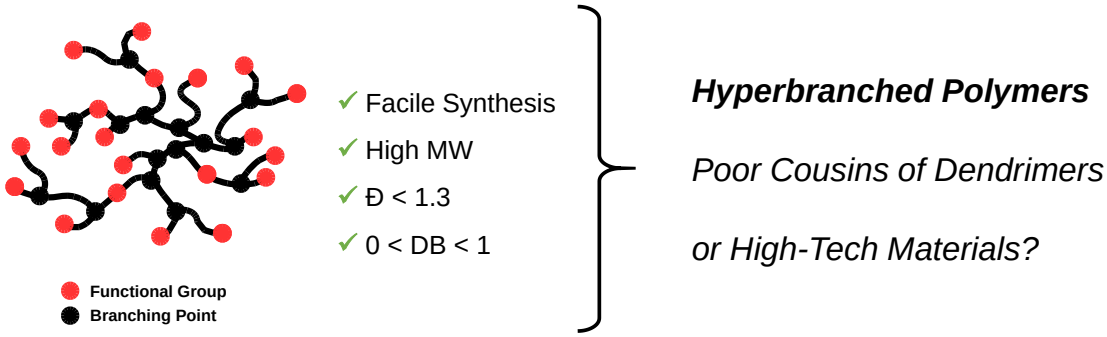

2.1 Control of the Molar Mass of Hyperbranched Poly(ethylene oxide) *via* Slow Monomer Addition

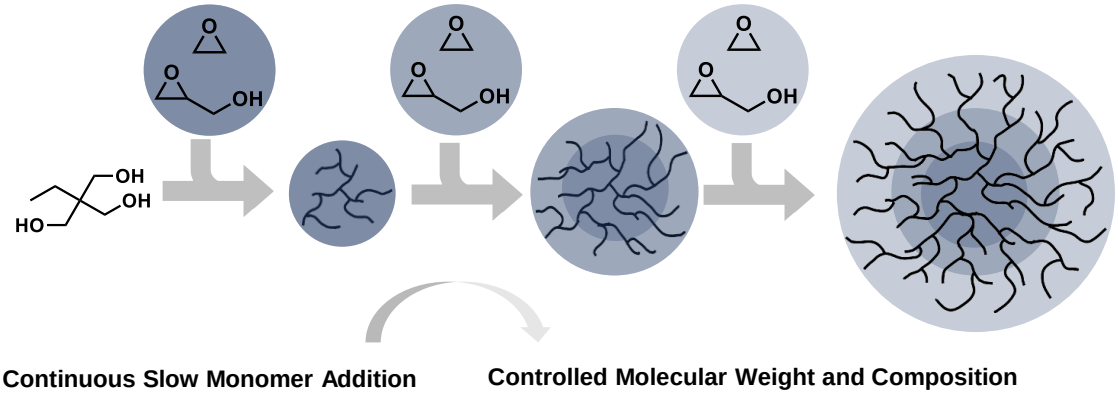

2.2 Variation of the Degree of Branching of Hyperbranched Polyether Polyols by Copolymerization of Glycidol with 1-Substituted Analogs

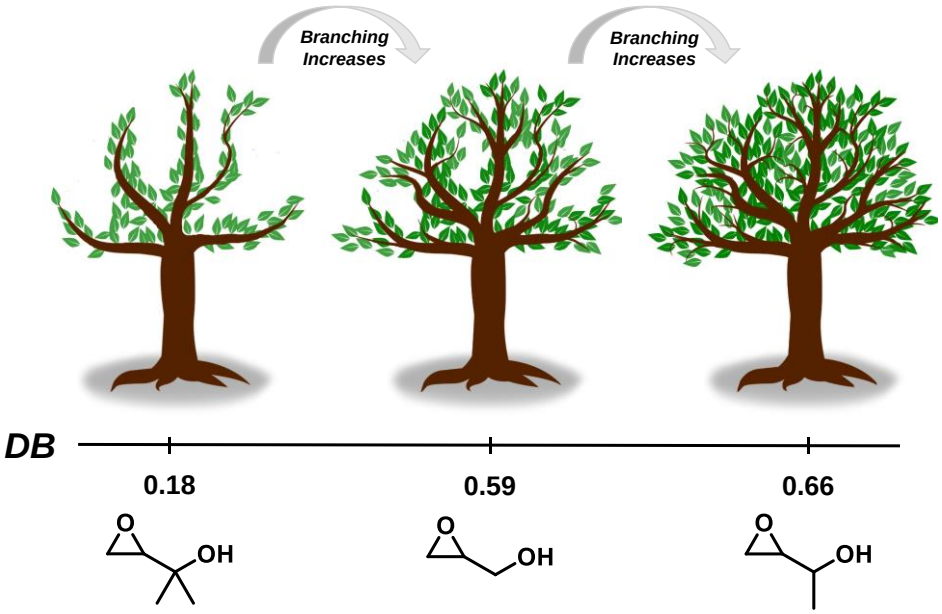

2.3 Hard-Sphere Behavior of Hyperbranched Polyglycerol in Aqueous Solution: Absolute Molecular Weights, Molecular Hydrodynamics and Light Scattering

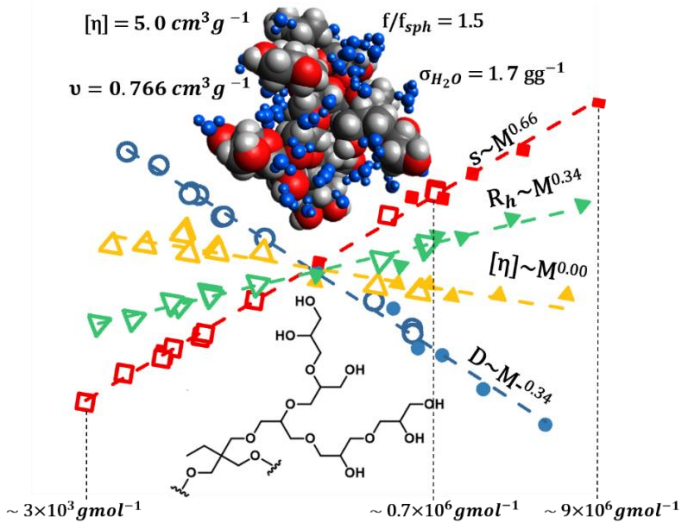

3.1 Synthesis of Biocompatible Organobases by Copolymerization of Glycidol and a *N,N*-Dibutylamino-Functional Glycidyl Ether

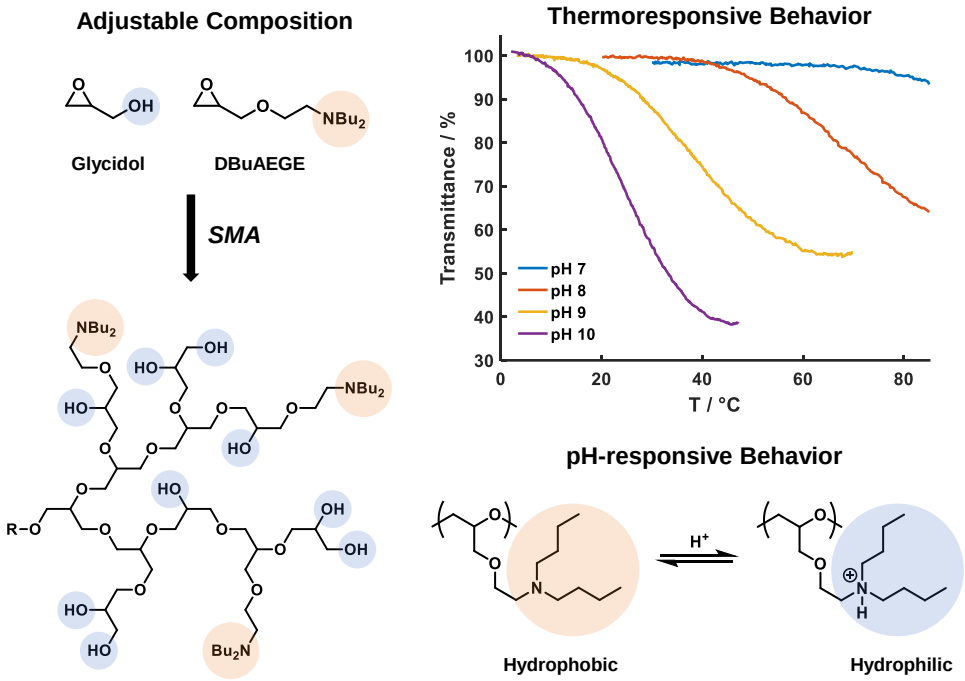

3.2 *In-Situ* End-Group Functionalization of Hyperbranched Polyglycerols by Copolymerization of Glycidol with a Bulky Glycidyl Ester

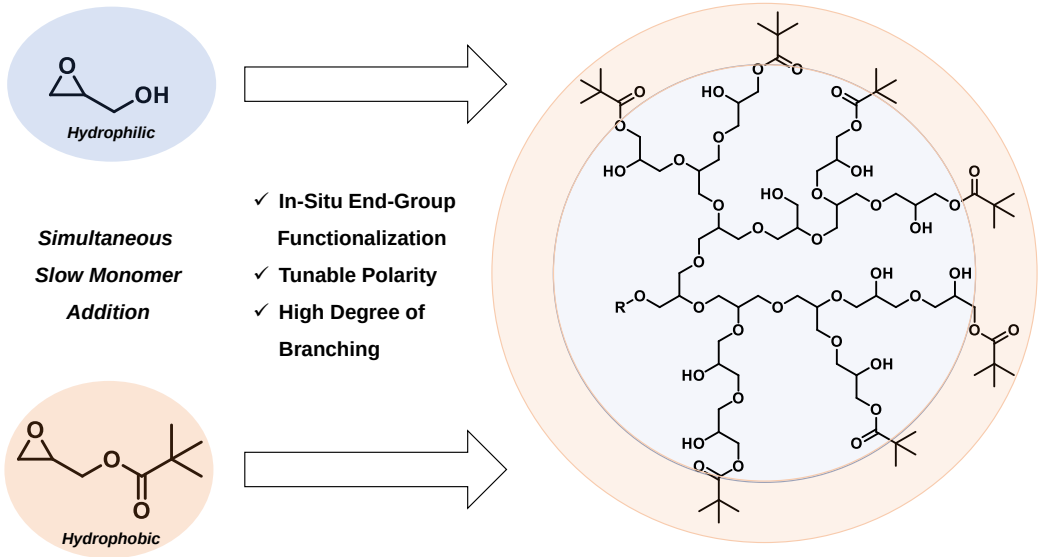

3.3 Synthesis of Unimolecular Nanocapsules by Partial Esterification of Hyperbranched Poly(ethylene oxide)

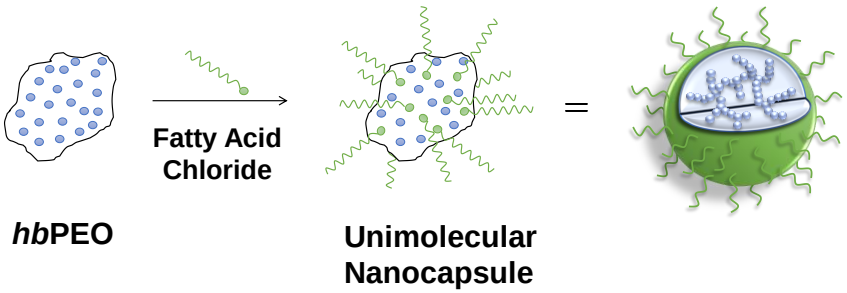

- ✓ ***Facile Two-Step Synthesis***
- ✓ ***Tunable Loading Capacity Y***
- ✓ ***Adressable Core Domain***
- ✓ ***Triggered Cargo Release***

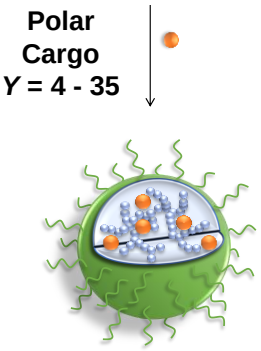

3.4 Synthesis of *hb*PEO-*b*-PMMA Multi-Arm Star Copolymers *via* Atom Transfer Radical Polymerization

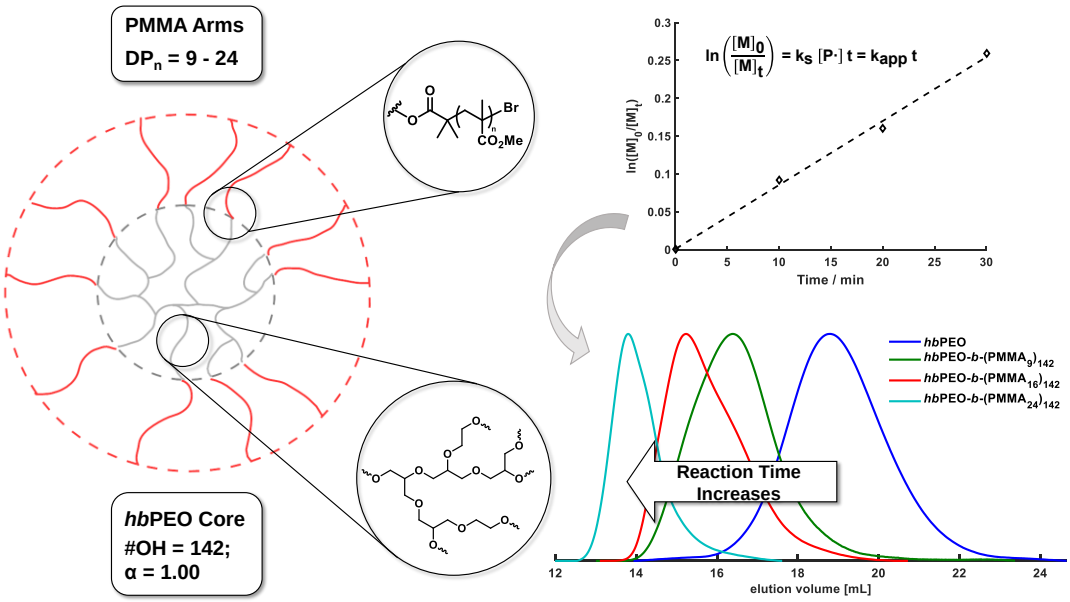

1. Introduction

1.1 Hyperbranched Polymer Architectures: From Flory´s $AB_{(f-1)}$ Polycondensates to Tailormade Hyperbranched Polyether Polyols

*Tobias Kaiser[a], Holger Frey[a,]**

[a]Department of Chemistry, Johannes Gutenberg University, Duesbergweg 10 – 14, 55128 Mainz

To be submitted.

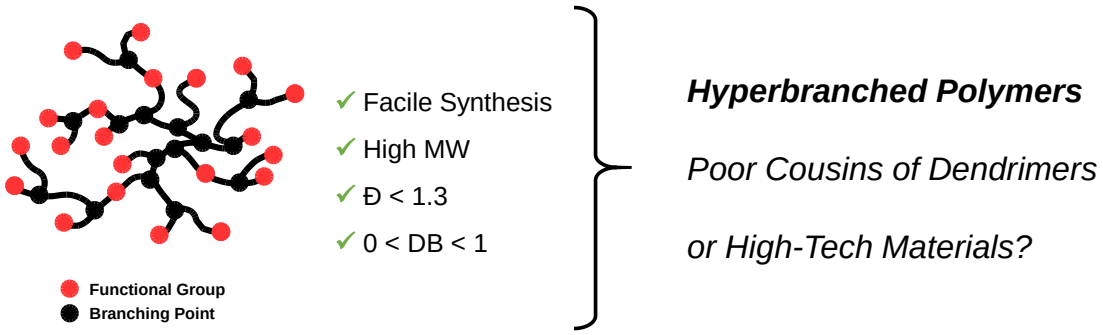

Historical Development of Dendritic Polymers

Celebrating the 100th anniversary of Staudinger's "macromolecular concept",[1] renowned polymer scientists critically evaluate the past developments and future challenges of polymer science, asking: *Quo vadis*, Macromolecular Science?.[2] The main focus in Polymer Science has been on linear polymers until the late 1980ies, with occasional excursions to chain-branched polymers. However, dendritic polymers, i.e. dendrimers and hyperbranched polymers (HBPs), have attracted wide-spread attention in the polymer community following the seminal work of Don Tomalia in 1985 reporting dendritic polyamidoamines possessing a "starburst topology.[3] Already in 1978, Fritz Vögtle presented multifunctional, dendritic ligands synthesized in a similar manner by repeated aza-Michael addition and reduction steps. However, Tomalia realized that dendrimers represent a new type of polymer topology, initializing the "dendrimer hype" of the following decade.[4,5,6]

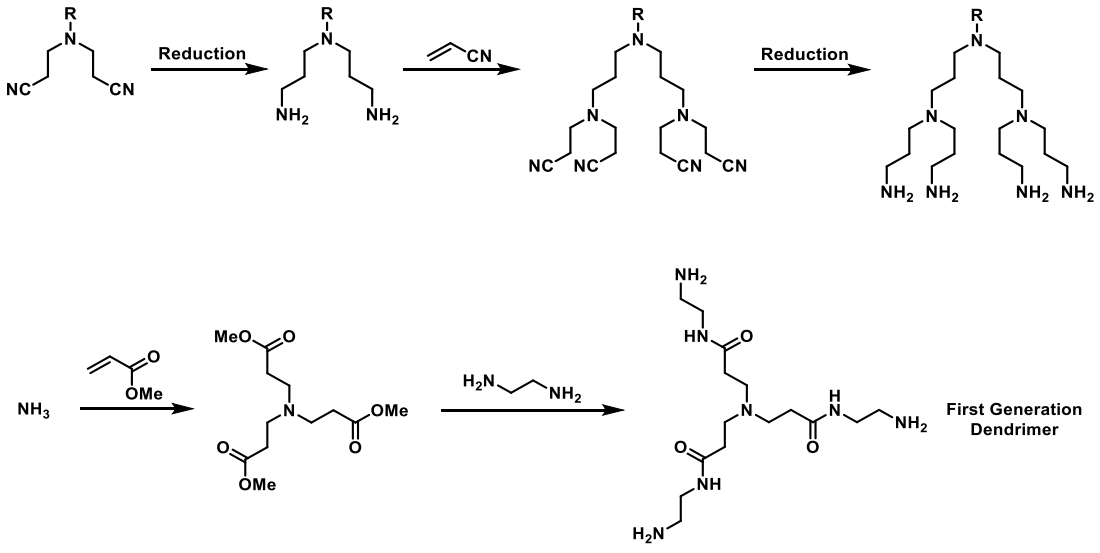

Scheme 1. Top: Vögtle´s synthesis of "cascade-like" polyamines by repeated aza-Michael addition and reduction steps.[4] Bottom: Synthesis of dendritic polyamidoamines by repeated Michael addition and amidation according to Tomalia.[3]

In this topical review article the most important stepping stones during the development of dendritic polymers, focussing on hyperbranched polymers, will be discussed with an emphasis on the rapid innovations in this field during the 1990s – a decade in which the foundation was laid for all future efforts regarding hyperbranched polymers with their tree-like branching pattern. Hence, before we concern ourselves with the state of the art and some thoughts regarding the future of this field, we must take a step back and start by asking: "*Unde Venistis*, Hyperbranched polymers?" Where did you come from?

Branching is a common motive in nature, especially for energy storage macromolecules, for example in polysaccharides.[7] In 1930, Staudinger first described glycogen, dextrane and amylopectin as branched macromolecules,[8] followed by Meyer and Bernfeld proposing a "hyperbranched" structure.[9] The first synthetic approaches towards highly branched polymers, however, can be dated back to the beginning 19th century (cf. Table 1). In an attempt to copolymerize phthalic anhydride (which would later be called a latent A_2-type monomer) or phthalic acid (A_2-type monomer) with glycerol (B_3 type monomer) Watson Smith obtained a insoluble resin.[6] Kienle *et al.* showed that these materials exhibit unexpected properties in comparison to linear polymers, in particular a low viscosity in solution.[10–12] Furthermore, based on an $A_2 + B_3$ reaction, by the condensation of formaldehyde and phenol, Leo H. Baekeland produced the first thermosetting phenol formaldehyde resin, Bakelite.[13] These two polymerizations were prototypes for reactions described much later under the moniker "double monomer" strategy, the step-growth polymerizations using A_2 and B_3 monomers.[14,15] During these reactions, a pronounced risk of gelation exists at a

critical conversion, necessitating careful planning and special reaction parameters, unless cross-linking is expressly desired.

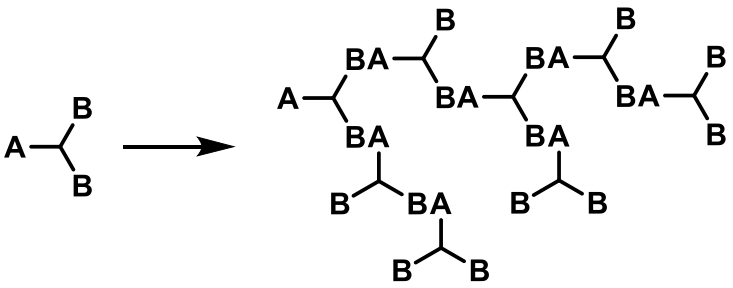

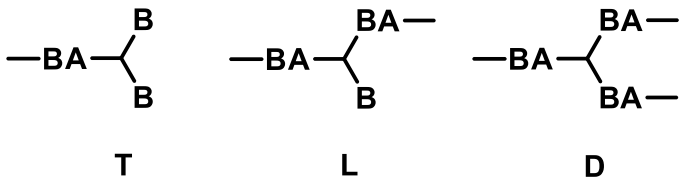

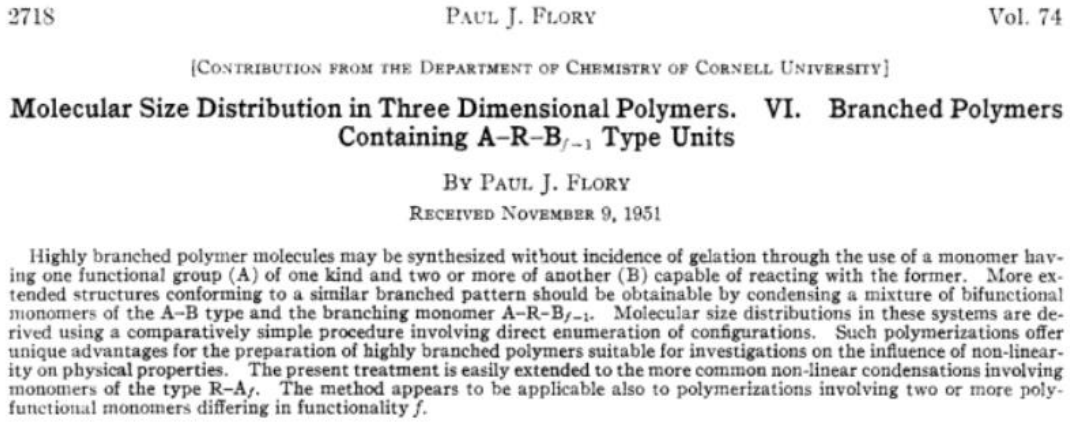

2718 PAUL J. FLORY Vol. 74

[CONTRIBUTION FROM THE DEPARTMENT OF CHEMISTRY OF CORNELL UNIVERSITY]

Molecular Size Distribution in Three Dimensional Polymers. VI. Branched Polymers Containing A–R–B_{f-1} Type Units

BY PAUL J. FLORY

RECEIVED NOVEMBER 9, 1951

Highly branched polymer molecules may be synthesized without incidence of gelation through the use of a monomer having one functional group (A) of one kind and two or more of another (B) capable of reacting with the former. More extended structures conforming to a similar branched pattern should be obtainable by condensing a mixture of bifunctional monomers of the A–B type and the branching monomer A–R–B_{f-1}. Molecular size distributions in these systems are derived using a comparatively simple procedure involving direct enumeration of configurations. Such polymerizations offer unique advantages for the preparation of highly branched polymers suitable for investigations on the influence of non-linearity on physical properties. The present treatment is easily extended to the more common non-linear condensations involving monomers of the type R–A_f. The method appears to be applicable also to polymerizations involving two or more polyfunctional monomers differing in functionality *f*.

Figure 1. Paul J. Flory (left) (Paul J. Flory – Facts. NobelPrize.org. Nobel Media AB 2020. Sat. 28 Mar 2020. https://www.nobelprize.org/prizes/chemistry/1974/flory/facts/); Schematic structure of a hyperbranched polymer based on an AB_2 monomer (right). Bottom: Key publication from 1952 by Flory on branching in A-$B_{(f-1)}$ monomers.[16]

In the 1940s, Paul J. Flory studied the A_2 + B_3 polycondensation of glycerol and phthalic acid in depth. He introduced the important concept of the gelpoint, i.e. the conversion at which gelation/cross-linking starts, and the degree of branching. Additionally, he calculated the molecular weight distributions for a three-

dimensional system approaching gelation.[17–20] Similar efforts concerning polyaddition, representing another type of step-growth reaction, were reported by Walling *et al.*.[21] In 1952, Flory concluded that “highly branched molecules may be synthesized without the incidence of gelation through the use of a monomer having one functional group (A) of one kind and two or more of another (B) capable of reacting with the former”.[16] With this single ingenious work, he defined the common synthetic approach towards highly branched *via* $AB_{(f-1)}$ monomers, where f represents the overall functionality ($f \geq 3$).[7]

However, it took nearly three decades until significant progress concerning the synthesis of highly branched polymers was made.[5,6] Since Vögtle´s first reports on cascade molecules in 1978 (cf. Scheme 1), further contributions to the growing field of perfectly branched dendrimers were made in the following decade by Tomalia *et al*,[3] Newkome *et al.*,[22] as well as Fréchet and coworkers.[23–25] Despite the rapidly growing interest in these structures dendrimer synthesis is demanding and multi-step processes are required to generate these perfectly branched polymers.[5] In fact, sequential organic synthesis strategies are required to obtain perfectly branched dendrimers. The deliberate synthesis of a highly branched polymer by a random one-pot strategy *via* polycondensation was achieved and patented by DuPont researchers Young H. Kim and Owen W. Webster, coining the term “hyperbranched polymer” (HBP). In the vein of Flory´s $AB_{(f-1)}$ polycondensation systems, they prepared highly branched polyphenylene *via* Suzuki polycondensation of bromoaryl boronic acids.[26–29] It is impressive to note that the usually intractable polyphenylene structures become soluble, when incorporating them in a hyperbranched polymer structure. In 1991, Hawker and Fréchet reported their work on highly branched polyesters by polycondensation of

an AB_2 monomer based on a dihydroxy benzoic acid derivative, already adapting to the new terminology of “hyperbranched polymers”.[30] In this work, they furthermore contributed to the structural understanding of branching by introducing an expression for the degree of branching, which describes the relative perfection of the dendritic structure:

$$DB = \frac{D + T}{D + T + L} \qquad 1$$

This equation was suggested on the basis of a comparison of hyperbranched structures with the perfectly branched dendrimers. D, T and L represent the fractions of the repeating units resulting from the polymerization of an AB_2 monomer (cf. Figure 1), usually determined from NMR spectra of the copolymers. Frey and coworkers developed a systematic equation to universally apply to polymers regardless of the molar mass, as in the statistical polymerization of AB_2 monomers the fractions of dendritic and terminal units assume equal values:[31]

$$DB = \frac{2\,D}{2\,D + L} \qquad 2$$

Hence, by definition, linear polymers possess a DB of 0, whereas perfectly branched dendrimers only exhibit dendritic or terminal units resulting in a DB of 1. On the other hand, the maximum DB achieved for hyperbranched polymers prepared in a single batch is 0.5 assuming equal reactivity of all B groups: the relative amounts of repeating (D, L and T) are purely statistical yielding a ratio of 1:2:1.[30–32] However, due to sterical factors and incomplete conversion, DB typically assumes values < 0.5.

In the tailwind of the dendrimer hype, these highly branched structures received broad interest (Figure 2), which ultimately resulted in a detailed understanding of the reaction mechanism and the polymer architecture along with its properties.

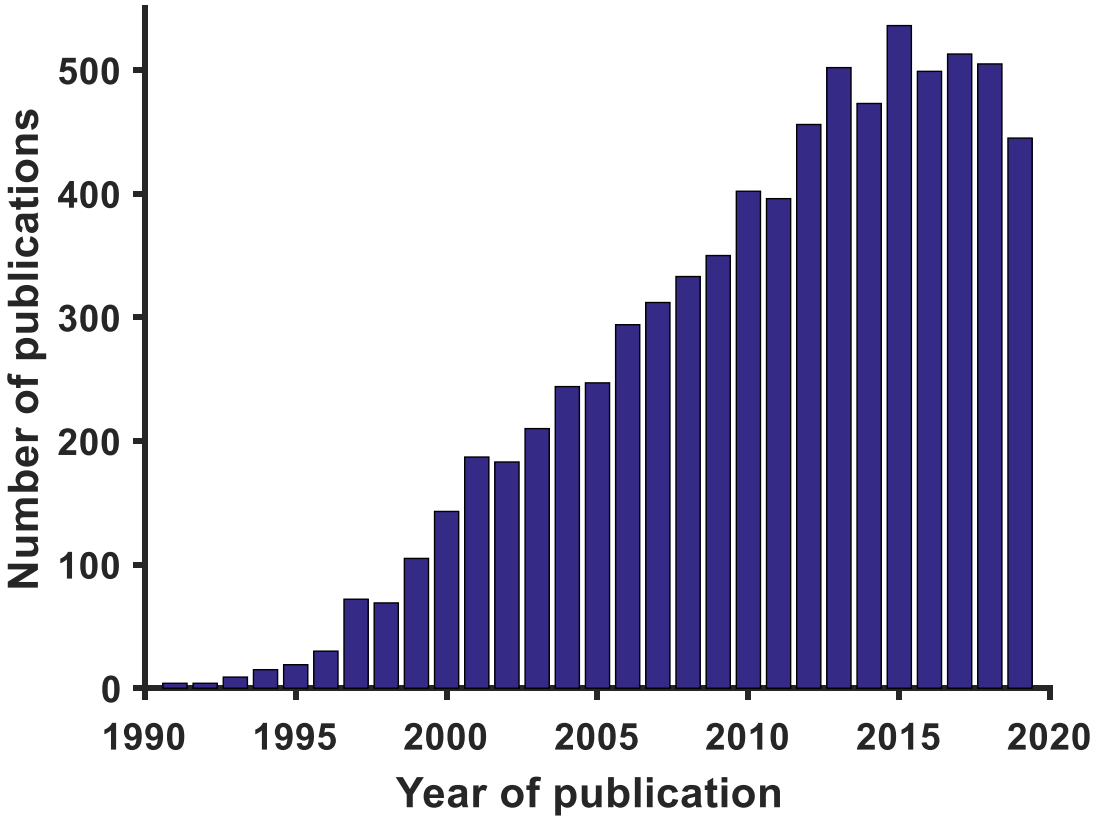

Figure 2. Number of Publications about HBPs between 1990 and today searched by ISI Web of Science.

Since the initial reports on hyperbranched polyphenylenes by Kim and Webster, a vast variety of different AB_2 type monomers has been developed, leading to various types of polymers, including polyphenylenes, poly(phenylacetylenes), polycarbosilanes and polycarboxysilanes, poly(ether ketones) and polyesters.[33–36] Additionally, hyperbranched polyamidoamines prepared by Michael-type polyaddition reactions of $AB_{(f-1)}$ monomers have been developed as well.[37,38]

Table 1. Important cornerstones of the development of hyperbranched polymers.

Type	Year	Monomer	Author	Ref
$A_2 + B_3$	1901	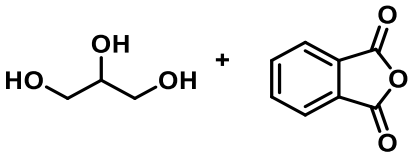	Smith	10
	1909	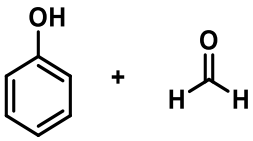	Baekeland	13
AB_2	1988	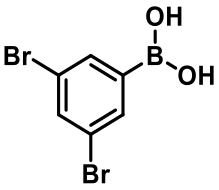	Kim, Webster	26–29
	1991	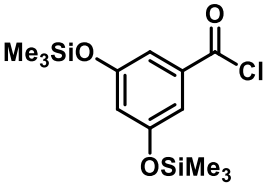	Hawker, Fréchet	30
	1994	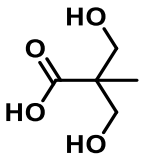	Hult	39
Latent AB_2	1994	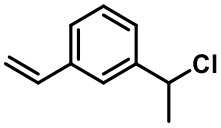	Fréchet	40
	1997	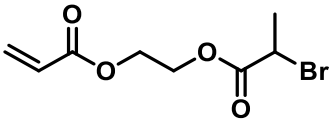	Müller	41
	1999	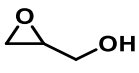	Frey	42

These HBPs were prepared either by polycondensation or polyaddition type reactions, strictly following a step-growth mechanism as already studied by Flory in his seminal work.[6,43] As such, high molar masses, i.e. degrees of polymerization, are only achieved at high conversion according to typical considerations related to polycondensation statistics.[44] The very broad molar mass distributions of these reactions were already described 30 years earlier by Flory, and polydispersities are typically in the range of $M_w / M_n = DP_n / 2$.[16] An additional parameter that could not be treated by Flory´s approach is the occurrence of an intramolecular condensation of the focal A group with any B group of the growing macromolecule (cf. Figure 1, right).[45–49] In fact, this cyclization reduces achievable molecular weights, but also mitigates the polydispersity of an AB_2 (or generally AB_m) polycondensation reaction. Furthermore, in the case of hyperbranched polyesters, transesterification reactions hamper both the molar mass and degree of branching by an uncontrolled scrambling of the resulting structures.

An important iteration away from step-growth with the respective limitations and towards improved control was achieved in 1994, when Fréchet and coworkers reported the of 3-(1-chlorethyl)-ethenylbenzene, relying on a mechanism the authors denominated self-condensing vinyl polymerization (*SCVP*).[40] In this case, a vinyl monomer bearing an initiator moiety that can be activated by an external stimulus (*inimer*), is employed. This inimer can also be described as a “latent” AB_2 monomer, which releases the second B group only after reaction of the A group. Thus, SCVP combines the classical vinyl polymerization (chain-growth) with polycondensation (step-growth) due to coupling of reactive oligomers.

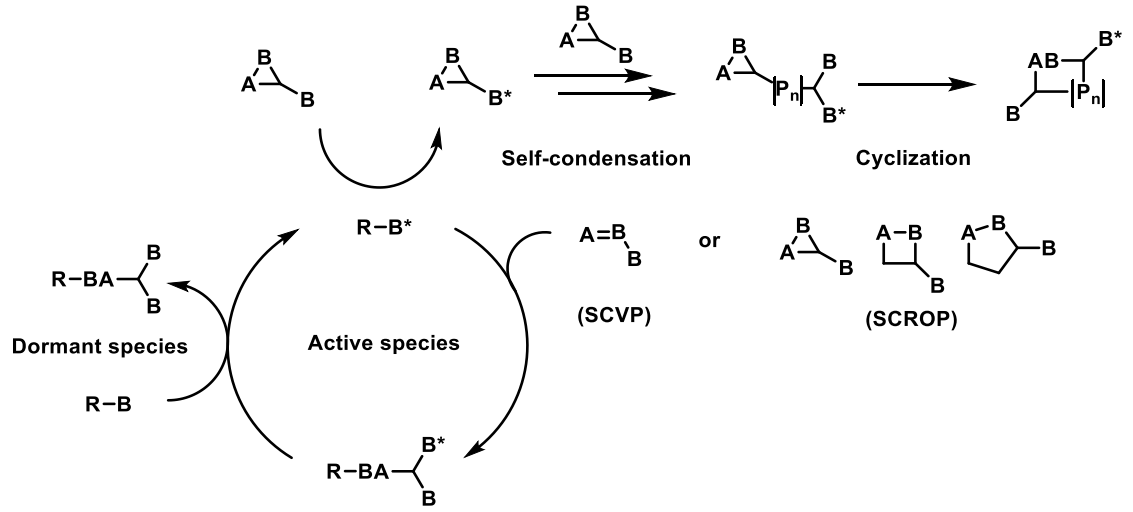

Scheme 2. Schematic mechanism of the self-condensing vinyl polymerization (SCVP) or ring-opening polymerization (SCROP) (reproduced from [7]).

All polymerizations of this kind rely on the reversible (de-)activation of the pendant initiator group B, hence by intra- and intermolecular transfer of the active site, all B groups can initiate chain-growth, but are not active at the same time. Propagation takes place by the attack of an active species at the vinyl bond of the inimer. If the activation of the dormant sites is sufficiently fast, theoretically, all chain-ends propagate simultaneously resulting in a well-defined highly branched polymer. Fréchets initial system relied on the cationic polymerization of the vinyl group, but in the following years many other hyperbranching polymerizations following a reversible-deactivation process were established, including group transfer polymerization[41] and controlled radical polymerization techniques.[50–55]

Besides SCVP, other self-condensing systems, especially heterocycles carrying a pendant initiator group for the self-condensing ring-opening polymerization (*SCROP*), have found broad interest leading to a rapid development, especially in the field of hyperbranched aliphatic polyethers,[56] polyesters[57,58] and polyether carbonates.[59,60] Several methodologies can be applied to prepare hyperbranched

polyether polyols *via* reversible-deactivation polymerization: oxyanionic polymerization (glycidol),[61–63] cationic (glycidol,[64,65] oxetanes[66–68] and anhydrosugars as well as tetrahydrofuran derivatives[69–71]) and transition metal catalysis (glycidol).[72] In comparison to polyesters, the formation of the ether bond is irreversible, adding another dimension of control to the preparation of polyethers.

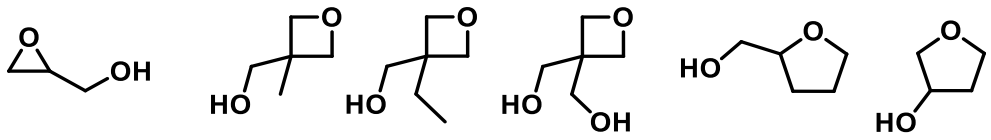

Figure 3. Cyclic inimers for the synthesis of hyperbranched polyether polyols.

Although the reversible-deactivation polymerization as the prevalent process follows a chain-growth mechanism, self-condensation and self-initiation is still feasible: by transfer of the active site to a monomer, a new hyperbranched polymer with a polymerizable core moiety is formed, enabling cyclization and uncontrolled incorporation of these macroinitiators. In this case, molar mass distributions similar to typical polycondensation reactions are expected in a batch polymerization.[16,73]

Since self-condensation leading to macrocycles can only take place, as long as unreacted A groups are present in the reaction system, the simplest way to suppress cyclization is to keep the concentration of A groups as low as possible. To this end, Moore and coworkers immobilized AB_2 monomers onto a solid polystyrene support *via* reaction of the A group.[33] By slowly adding further monomer to a dispersion of the B-functional polystyrene beads, the authors achieved unprecedented control of the molar mass and dispersity by variation both of the addition rate and the ratio of monomer to initiator. Generally speaking, the concentration of A groups can be reduced quite elegantly by slow monomer addition (*SMA*) to a core-forming molecule B_f which only exhibits B groups.[74–76] In

the ideal case, the feed rate should be slower than the propagation rate, thus, all A groups have already reacted before a new batch of monomers is added to the mixture, and the linking reaction must obviously be irreversible. Therefore, the monomer, specifically the A group, can only react with the core B_f or with B groups of the growing hyperbranched polymer, resulting in a pseudo chain-growth polymerization without self-initiation.[7] This concept was first applied successfully by Möck *et al.* to the polymerization of the TMS-protected dihydroxybenzoic acyl chloride (AB_2) introduced by Fréchet in 1991 (Table 1).[77] Shortly after that, Sunder *et al.* were able to synthesize well-defined hyperbranched polyglycerols with low polydispersity *via* SMA of the latent AB_2 monomer glycidol to a partially deprotonated initiator salt. On a theoretical note, Frey as well as Müller and coworkers studied the effect SMA has on the overall topology of the hyperbranched polymer, i.e. molecular weight distribution and degree of branching. By applying SMA, the ratio of the repeating units discussed above (D,T and L) varies, as the formation of linear units is less probable in comparison to batch processes (1:1:1).[75,76,78] According to equation 2, the DB of hyperbranched polymers prepared by SMA is elevated and assumes a maximum value of 0.67. The predictions made by Frey and coworkers regarding the effect of SMA on the polydispersity and molecular weight distribution were eventually verified by a comprehensive set of theoretical considerations by Rabbel *et al.*.[79]

The rapid development in this area led to a fairly complete theoretical understanding of the fundamentals regarding hyperbranched polymers over the course of a single decade. Thus, by the year 2000, a universal methodology was developed for the synthesis of well-defined tailor-made HBPs. Continuously growing research interest in the following years, expressed by an increasing

number of publications per year until 2015, commenced (Figure 2). During that time, a multitude of potential applications for HBPs were explored, where the highly-branched structure is advantageous over linear analogues, e.g. as rheology modifiers, additives, coatings, polymeric electrolytes, nanoreactors and nanocapsules and various biomedical applications. The full scope and application potential has been discussed extensively in a number of excellent review articles.[6,56,80–87]

Today, more than 30 years after Kim and Webster first reported the synthesis of hyperbranched polyphenylenes, dendritic polymers, specifically HBPs, are still as popular as in the first decade after their inception. In 2018 and 2019 alone, there were almost 1000 publications on hyperbranched polymers (cf. Figure 2), dealing either with new synthesis strategies, functionalization, or application prospects. There are various other methods to synthesize hyperbranched polymers, e.g. the polycondensation of symmetric A_2 + B_3 monomer pairs, albeit this strategy has to be adopted to avoid gelation.[14,15]

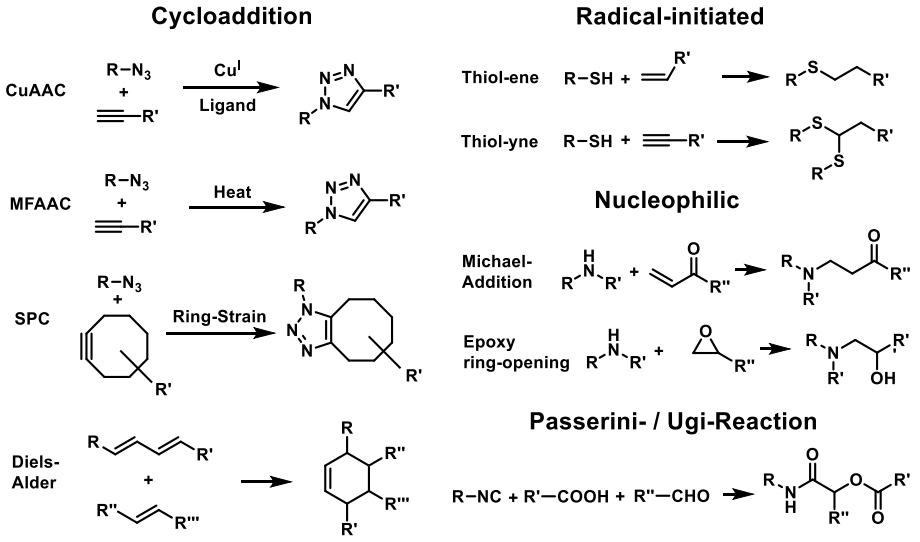

Scheme 3. Different ‘click-chemistries’ employed for the synthesis of hyperbranched polymers (reproduced from [85]).

Due to facile polymerization, reaction robustness and good atom economy, one of the most exciting current developments has been involving click chemistry, (cycloaddition, nucleophilic/electrophilic and radical-initiated click-chemistries) or multicomponent reactions as polymerization techniques (cf. Scheme 3). However, these polymerizations follow a step-growth mechanism. Thus, the aforementioned benefits of the 'click-chemistry' methodology come at the cost of a reduced control of the molecular weight and degree of branching as well as a less defined molecular weight distributions, as discussed earlier. The recent advances utilizing these reactions for the synthesis of HBPs were summarized in an comprehensive review article by Gao and coworkers.[85]

Aside from ongoing efforts regarding new synthesis methodologies, tuning of the HBPs architecture remains a key aspect concerning new developments. Closely related to the polymer architectures is the degree of branching (DB), which directly influences the physical and chemical properties of hyperbranched polymers,[6] e.g. absence of chain entanglements, low mean-square radius of gyration resulting in a compact structure, low viscosity in bulk and solution, amorphous structure, capability of encapsulation, mechanical strength, biocompatibility, and self-assembly-behavior.[56,88–101] Therefore, it is of utmost interest to find ways to reliably vary the degree of branching. The common thread for the variation of DB is the enhancement or reduction of the fraction of linear units. As discussed earlier, using core-forming molecules B_f[102] in combination with SMA[75,77–79] not only grants control of the molar mass yielding narrow molecular weight distributions but also results in enhanced DBs. Furthermore, by post-polymerization reactions, linear units can be transformed into dendritic ones, retroactively increasing the formal DB.[103] If structures with enhanced crystallinity are desired, lower DBs can be obtained by

two major strategies. Generally, the reaction conditions, especially the reaction temperature, were found to be relevant for the degree of branching of the resulting polymer:[104–108] The most feasible strategy, however, involves the copolymerization of AB_2 with AB units introducing strictly linear units (L), which enables lowering of the DB in a controlled manner.[109–111]

As discussed briefly, hyperbranched polyglycerol (*hb*PG) is one of the few hyperbranched polymers that can be prepared in a controlled manner (*vide supra*). The next chapter explores the synthesis, characterization, functionalization, and application potential of this highly branched polyether polyol. Although *hb*PGs can be prepared following a variety of synthesis methodologies, the main emphasis will be placed on the anionic ring-opening polymerization of the latent AB_2 monomer glycidol *via* slow monomer addition as a continuation of the developments summarized in the previous chapter.

Hyperbranched Polyether Polyols by Anionic Ring-Opening Polymerization of Glycidol

Synthesis and Characterization of Hyperbranched Polyglycerol

One of the currently most well-understood classes of HBPs are hyperbranched aliphatic polyether polyols.[56,112] The synthesis of these polymers typically relies on the anionic or cationic ring-opening multibranching polymerization (ROMBP) of cyclic ethers representing latent AB_2 monomers, e.g. glycidol, hydroxyl-substituted oxetanes or hydroxyl-substituted tetrahydrofurans.[56] Particularly hyperbranched polyglycerols received broad interest both in academia and industry, as glycidol can be polymerized by either of the aforementioned methods. Additionally, the synthesis of hyperbranched polyglycerol *via* DMC catalysis has been reported by Tran *et al.* in 2020.[72] A comprehensive overview of the various polyglycerol architectures, i.e. linear and dendritic PG, but also polycarbonates and polyesters, and their respective applications in biomedicine was given by Grinstaff in 2014.[113]

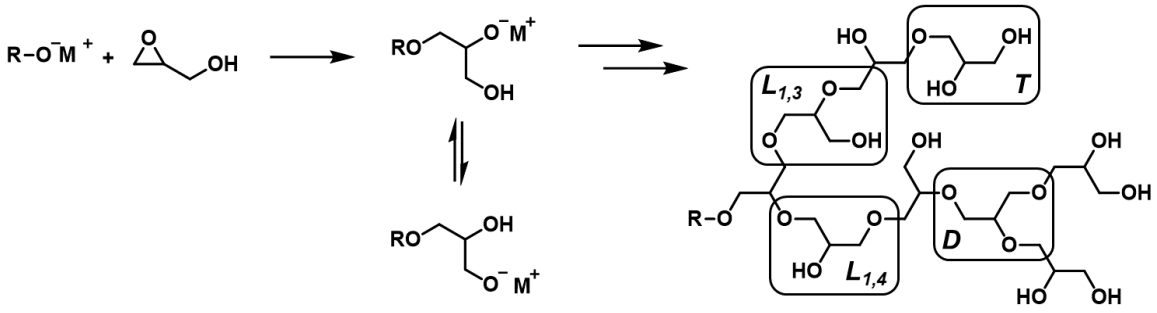

Scheme 4. Schematic synthesis of hyperbranched polyglycerol by anionic ring-opening multibranching polymerization (ROMBP) of glycidol. The different repeating units (terminal, linear and dendritic) are identified.

However, polyglycerol distinguishes itself from the other polyether polyols, e.g. polyoxetanes, by the synthesis *via* anionic ROMBP. The anionic ring-opening of

epoxides leads to the rapid formation of an ether bond. In contrast to the cationic mechanism, this bond formation is irreversible. Thus, no scrambling of the polyether backbone is observed, granting a vastly superior control of the polymerization mechanism.[56]

The anionic polymerization of glycidol was first reported in 1930 by Rider and Hill as a side-reaction resulting from the treatment with pyridine, when they studied the synthesis and stability of the monomer.[61] In the 1960s, Sandler and Berg systematically investigated the polymerization of glycidol. However, instead of a linear polymer, the hydroxyl groups led to transfer reactions, resulting in a branched product.[62] Vandenberg studied the anionic polymerization of glycidol using different bases.[63] Based on a thorough structural investigation of the product by ^{13}C NMR spectroscopy, he proposed a reaction mechanism including self-initiation as well as self-condensing after the deprotonation of glycidol (cf. Scheme 5). As a latent AB_2 monomer (cyclic inimer), the ring-opening polymerization glycidol follows the general mechanism of the SCROP described in the previous chapter. Assuming a fast intra- or intermolecular proton transfer reaction, the reactivities of the primary and secondary alkoxides are similar, leading to uniform growth of the hyperbranched polyether polyol. The occurrence of self-initiation leads to cyclization, this side-reaction always has a pronounced negative impact on the control of the molar mass and the molecular weight distribution of the resulting polymer.[45–48] By slowly adding the latent AB_2 monomer glycidol to a partially deprotonated core-forming molecule B_f, Frey et al. were able overcome this limitation, resulting in a pseudo chain-growth mechanism for the anionic ROMBP of glycidol. In this case, the degrees of polymerization solely depended on the monomer/initiator ratio. The obtained hyperbranched polyglycerols showed

molar masses ranging from 1100 to 6500 g mol^{-1} with moderate to narrow molecular weight distributions (M_w / M_n < 1.5). By employing SMA, elevated degrees of branching (DB) between 0.53 and 0.59 were achieved.[42]

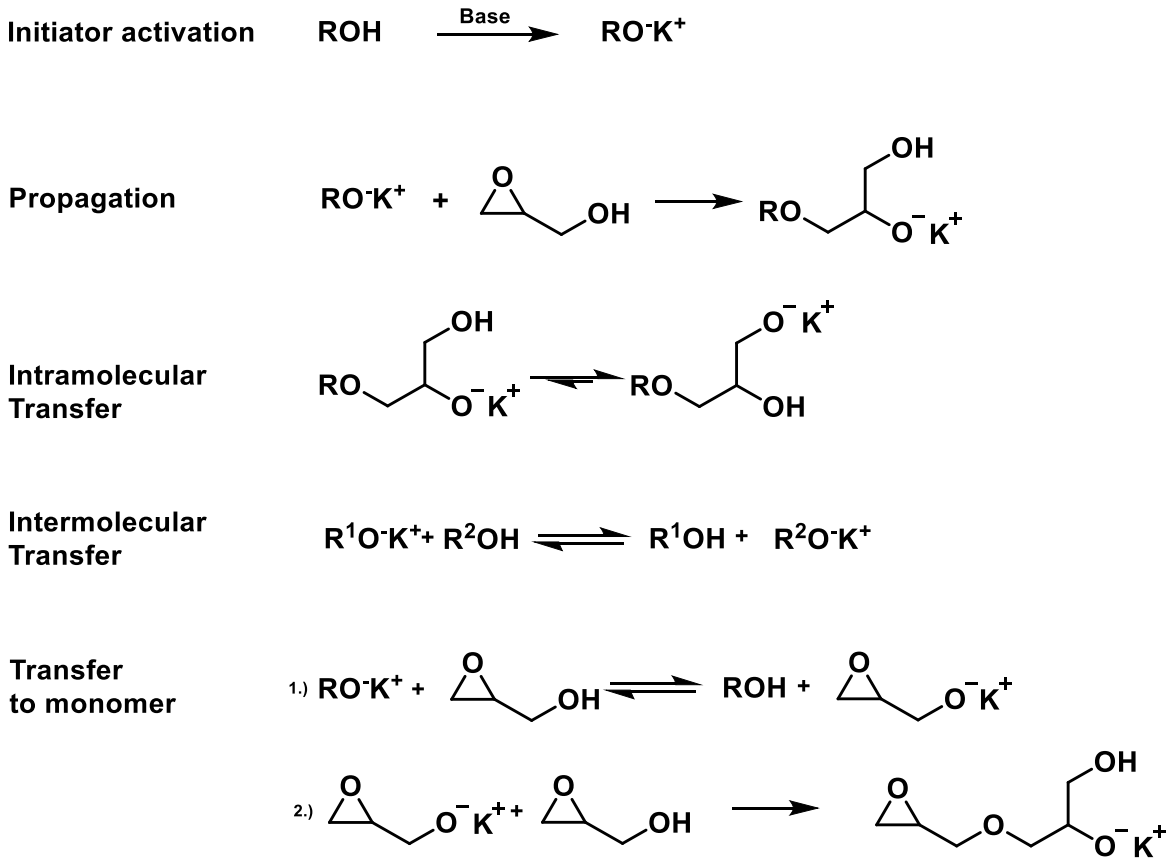

Scheme 5. Mechanism of the anionic ring-opening multibranching polymerization of glycidol using a core-forming molecule ROH.

To reduce the reaction times and experimental efforts during the SMA of glycidol, microreactor technology was also successfully employed to prepare hyperbranched polyglycerols with molar masses up to 1500 g mol^{-1}.[114]

The first polymerizations *via* SMA were conducted without a solvent. As the viscosity increases significantly upon increasing degree of polymerization, however, the range of molar masses was limited. Kautz *et al.* were able to broaden the range of possible molar masses with moderate molecular weight distributions

($M_w / M_n < 1.7$) by increasing the stirring efficiency and conducting the polymerization in solution.[115] By employing a low molar mass *hb*PG as macroinitiator for the polymerization of glycidol, Wilms *et al.* achieved molar masses up to 24000 g mol^{-1}.[116] Brooks and coworkers obtained particularly high molar masses (700 000 g mol^{-1}) by using 1,4-dioxane as an emulsifying agent rather than a solvent.[117] However, in this case the molar masses are independent of the monomer-to-initiator ratio. By employing *hb*PGs obtained by this approach as macroinitiator for the polymerization of glycidol *via* SMA, Grinstaff and Kizhakkedathu obtained particularly high molar masses up to 10^7 g mol^{-1}.[118] Due to a several concurrent reactions with different rate constants, i.e. proton transfer, propagation by ring-opening and self-initiation, the reaction temperature has a distinct impact on the overall reaction control. Haag and coworkers were able to show that elevated temperatures facilitate base-catalyzed as well as thermal self-initiation resulting in a loss of control of the molar mass and molecular weight distribution [119,120] However, high temperatures are required to increase the degree of branching.[121] Hence, a delicate balance between the feed rate and temperature is required to achieve high DBs while suppressing self-initiation to maintain control of the molar mass.

Hyperbranched polymers, in particular hyperbranched polyglycerol, show unique properties as discussed in the previous chapter resulting from a rather compact structure in comparison to linear polymers,.[6,56] Frey and coworkers observed a direct correlation between the overall amount and the chemical nature of the end groups on the glass transition temperature T_g.[122] By facile esterification of the hydroxyl groups with long alkyl chains, the influence on T_g became more pronounced the higher the substituents´ tendency to form highly ordered structures

was. Garamus *et al.* investigated the structure of hyperbranched polyglycerol in dilute aqueous and non-aqueous solutions by small-angle neutron scattering (SANS), observing a compact structure due to branching.[123] Unexpectedly, the highly branched structure was found to prevent aggregation despite the high number of functional groups. Furthermore, by a combination of different hydrodynamic and light scattering approaches, Perevyazko *et al.* found that hyperbranched polyglycerols in a wide range of molar masses (3000 – 700000 g mol^{-1}) and moderate degrees of branching (0.55 – 0.59) adopt a very compact, almost hard-sphere structure in aqueous solution with corresponding exponents of the scaling relationships of $s = 2.16\times10^{-3}M^{0.667}$, $D = 251\times10^{-3}M^{-0.33}$ and $[\eta] = 5.9M^{0}$. Regarding bulk mechanical and rheological properties, Schubert *et al.* detected entanglement behavior for hyperbranched polyglycerols in a broad range of molar masses (400 – 66 000 g mol^{-1}).[124] Peculiarly, the apparent entanglement molar mass was found to be significantly larger than the molar mass between two branching points. They concluded entanglement occurs due to a combination of topological entanglement and associating interactions, i.e. hydrogen bonds.

Brooks and coworkers conducted several toxicity studies comparing both linear and hyperbranched polyglycerols.[98] Although the topology of the polymers was found to have no effect, the biocompatibility for polymers with a molar mass of 6400 g mol^{-1} seems to be similar or better than for commonly applied materials PEG or hetastarch. For high molecular weights of up to 700 000 g mol^{-1} no drastic changes in biocompatibility were found *in vitro* due to the inherently compact structure.[99] However, due to limited urinary excretion, tissue accumulation was observed *in vivo*.[100]

The multitude of functional end groups, low crystallinity, compact structure, and unique properties both in bulk and solution has led to rapidly growing interest in hyperbranched polyether polyols based on glycidol. The fields of applications range from biomedicine, polymer electrolytes, nanoreactors, phase transfer agents among others, as already discussed in a number of excellent review articles.[56,84,112] However, due to hyperbranched polyglycerol possessing a mere polyether scaffold with only hydroxyl end groups, several applications require post-polymerization modification.[122,125–127] On the other hand, by the facile copolymerization of glycidol with suitable , i.e. base-stable, comonomers *via* the SMA approach discussed in the previous chapter, well-defined hyperbranched polyether polyols with tunable properties as well as number and nature of functional end groups can be synthesized (see following chapter).

Multifunctional *hb*PGs by Copolymerization of Glycidol and Functional ABR Monomers

Shortly after their initial reports on the controlled synthesis of hyperbranched polyglycerol *via* the SMA strategy, Sunder *et al.* presented the first copolymerization of glycidol with different ABR monomers, i.e. glycidyl ethers carrying a functional group R.[128] By employing allyl (AGE) or phenyl glycidyl ether (PGE) as the comonomer, control of the molar mass and moderate polydispersities (M_w / M_n < 1.7) were achieved. Furthermore, the copolymerization with AGE granted the possibility of orthogonal functionalization of the different functional groups (hydroxy and allyl). The authors eventually expanded this concept to develop a "modular approach to complex polymer architectures".[112] Typically, the copolymerization of the latent AB_2 monomer with any AB epoxide monomer has a significant impact on the degree of branching of the resulting polymer, since strictly linear units are introduced into the otherwise hyperbranched polymer (see previous chapters).[109–111,128] The influence of the copolymer composition on the degree of branching is expressed by equation 3:

$$DB_{SMA} = \frac{2\,(1 - X_{AB})}{3 - 2\,X_{AB}} \qquad 3$$

$$DB_{Batch} = 2\,\frac{r + 1}{(r+2)^2}\;;\; r = \frac{[AB]}{[AB_2]} \qquad 4$$

Thus, in addition to functionalizing *hb*PGs by copolymerization of glycidol and functional AB comonomers, the intrinsic properties of hyperbranched polyglycerol directly influenced by the degree of branching, e.g. viscosity, hydrodynamic radii and overall number of functional groups (see previous chapter), are tunable as well.

Table 2. Overview of different classes of comonomers suitable for the synthesis of hyperbranched polyether polyols by copolymerization with glycidol either by slow monomer addition (SMA) or batch polymerization.

Class	Comonomer	Structure	Type	Ref
Alkylene Oxide	EO		Batch	129
	PO		Batch	130
	BO	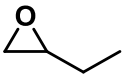	SMA	131
Glycidyl Ethers	AGE	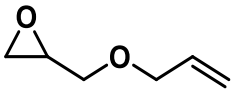	SMA	128
	BGE	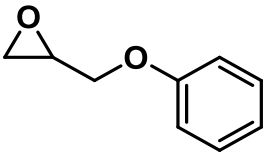	SMA	128
	FGE	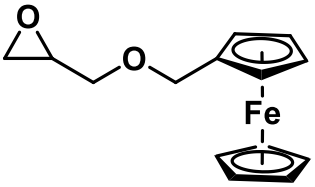	SMA	132
	GPE	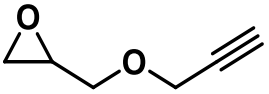	SMA	133
	CAGE	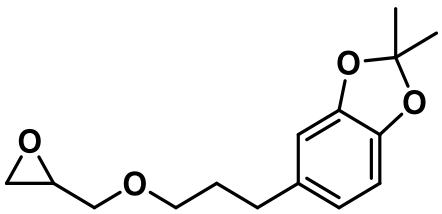	SMA	134
	MTEGE	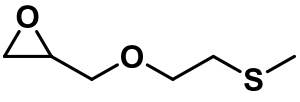	SMA	135

Class	Comonomer	Structure	Type	Ref
Glycidyl Ethers	EEGE	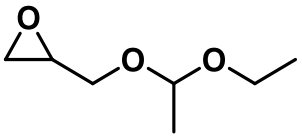	SMA	136
	BBAG	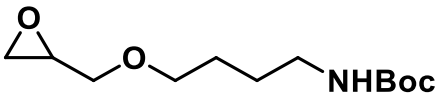	SMA	137
	SSG	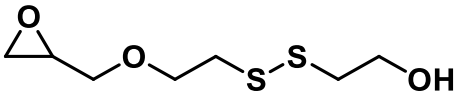	SMA	138
	GEGE	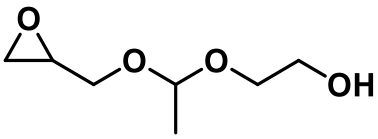	SMA	139
	CHKM	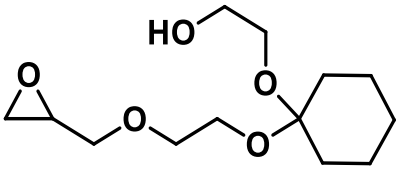	Batch	140
Glycidyl Imides		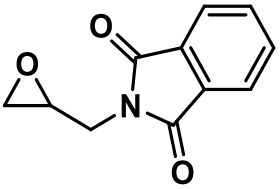	SMA	141
Cyclic Esters	rac-Lactide	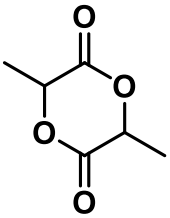	Batch	142
	ε-Caprolactone	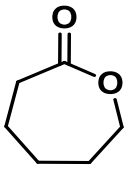	Batch	143
	γ-Butyrolactone	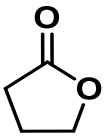	Batch	144

Table 2 gives an overview a cross-section of different comonomer classes for the anionic ring-opening multibranching copolymerization with glycidol, e.g. alkylene oxides, glycidyl ethers and glycidyl amines as well as different lactones and carbon dioxide.

By copolymerization with glycidol, hyperbranched analogs of the commonly used linear alkylene oxides PEO, PPO and PBO could be synthesized resulting in different effects on the individual properties. By copolymerization with EO, water-soluble hyperbranched poly(ethylene oxide)s with adjustable DB and thermal behavior are obtained.[129] On the other hand, the incorporation of propylene oxide or butylene oxide introduces thermo-responsive behavior.[130,131] In this case, the lower critical solution temperature (LCST) is adjustable by variation of the copolymer composition. Due to the low boiling points of EO (T_b = 10.5 °C) and PO (T_b = 35 °C),[145] however, the copolymerization with glycidol usually has to be conducted in a single batch, resulting in interesting copolymer architectures as shown by *in-situ* ^{1}H NMR kinetics experiments.[146]

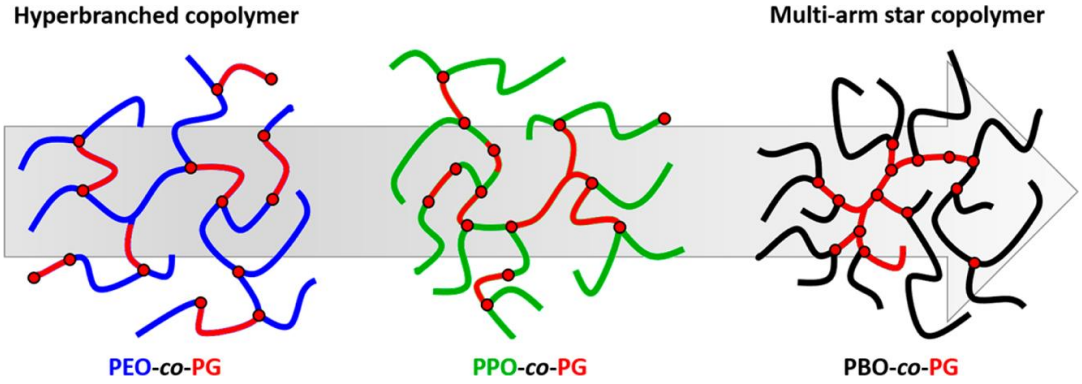

Figure 4. Different polymer topologies found following batch polymerizations to prepare *hb*PEO, *hb*PPO and *hb*PBO.[146]

Random copolymers with numerous functionalities distributed along the backbone are typically formed by the copolymerization of glycidol with different glycidyl

ethers. By variation of the copolymer composition, not only the degree of branching can be adjusted according to equation 3, but also the ratio of functional groups.[128] For example, after acidic deprotection, the incorporation of EEGE leads to hyperbranched polyglycerols with tunable DB.[136] By variation of the substituents, hyperbranched copolymers can be orthogonally functionalized,[128,133,135], show thermo-responsive,[135] pH-responsive,[137] and redox-responsive behavior,[132,135,138] are able to complexate metal-ions,[134] conjugate small molecules,[137] and to adsorb CO_2,[141] or are biodegradable by redox- or acidic means.[138–140] Furthermore, backbone biodegradability *via* acid-catalyzed pathways was also introduced by the batch copolymerization of glycidol cyclic esters, e.g. lactide, caprolactone or butyrolactone.[142–144]

Conclusion

The history of dendritic polymers, i.e. dendritic and hyperbranched polymers (HBPs), initiated in 1952 by the seminal work of Flory and the first dendrimer syntheses in the 1980s, has culminated in a rapid development of both the synthetic strategies and the theoretical understanding of HBPs during the 1990s. By the slow monomer addition (SMA) of a latent AB_2 monomer to a core-forming molecule B_f, the step-growth mechanism of the early AB_2 polycondensation reactions was transformed into pseudo-chain growth, with good control of the molar masses as well as dispersities and increasing understanding of the degree of branching. The knowledge of the structure-property relationship resulted in precise tailoring of the branching-dependent properties, that set dendritic polymers apart from linear structures, i.e. the rather compact structure, high number of functional groups, low crystallinity and low viscosity both in solution and melt.

One of the most prominent examples of a well-defined hyperbranched polymer is the highly branched polyether polyol *hb*PG (hyperbranched polyglycerol). Since the first report on the anionic ring-opening multibranching polymerization of glycidol following the SMA approach in 1999, a deep understanding of the reaction mechanism and the influence of different reaction parameters has enabled the controlled synthesis of well-defined multifunctional *hb*PGs in a wide range of molar masses and functionalities.

Almost 35 years after Don Tomalia´s first reports on a new polymer class, one could argue, that everything might be said and done in the fields of dendritic, specifically hyperbranched polymers. However, each year, new progress is reported either on new synthesis routes, control of the molar mass and dispersity

or different means of functionalization. According to Flory´s work, multibranching polymerizations might not lead to as well-defined materials as obtained by modern controlled/living polymerization techniques, e.g. controlled radical polymerizations or living anionic polymerization. However, the unique properties of dendritic polymers and recent advances in synthesis prove to be invaluable for applications in material science or biomedicine, which are insufficiently covered by linear polymers. One prominent example with increasing relevance is the utilization of hyperbranched polyglycerol in biomedicine for the (non-)covalent conjugation of small molecule drugs, antibody-based drugs, and peptides to improve their stability and bioavailability as well as reduce immunogenicity.[86] Frey and coworkers as well as Klok and coworkers utilized several copolymers based on *hb*PG for protein conjugation, clearly showing advantages over conventional bioconjugation using linear polyethers ('PEGylation').[147,148] Hence, hyperbranched polyglycerols and structurally related copolymers show the potential to contribute to the development of next-generation therapeutics - exemplifying just one promising field, in which hyperbranched polymers might outperform their linear analogs in the near future.

References

(1) Frey, H.; Johann, T. Celebrating 100 years of “polymer science”: Hermann Staudinger's 1920 manifesto. *Polym. Chem.* 2020, *11*, 8–14.

(2) Abetz, V.; Chan, C. H.; Luscombe, C. K.; Matson, J. B.; Merna, J.; Nakano, T.; Raos, G.; Russell, G. T. Quo Vadis, Macromolecular Science? Reflections by the IUPAC Polymer Division on the Occasion of the Staudinger Centenary. *Isr. J. Chem.* 2020, *39*, 12.

(3) Tomalia, D. A.; Baker, H.; Dewald, J.; Hall, M.; Kallos, G.; Martin, S.; Roeck, J.; Ryder, J.; Smith, P. A New Class of Polymers: Starburst-Dendritic Macromolecules. *Polym. J.* 1985, *17*, 117–132.

(4) Buhleier, E.; Wehner, W.; Vögtle, F. "Cascade"- and "Nonskid-Chain-like" Syntheses of Molecular Cavity Topologies. *Synthesis* 1978, *1978*, 155–158.

(5) Fréchet, J. M. J.; Tomalia, D. A. *Dendrimers and other dendritic polymers*; Wiley: Chichester, New York, 2010.

(6) Yan, D.; Gao, C.; Frey, H. *Hyperbranched polymers: Synthesis, properties, and applications*; Wiley series on polymer engineering and technology; Wiley: Hoboken, N.J, 2011.

(7) Sunder, A.; Heinemann, J.; Frey, H. Controlling the Growth of Polymer Trees: Concepts and Perspectives For Hyperbranched Polymers. *Chem. Eur. J.* 2000, *6*, 2499–2506.

(8) Staudinger, H.; Husemann, E. Über hochpolymere Verbindungen. 150. Mitteilung. Über die Konstitution der Stärke. *Justus Liebigs Ann. Chem.* 1937, *527*, 195–236.

(9) Meyer, K. H.; Bernfeld, P. Recherches sur l'amidon V. L'amylopectine. *Helv. Chim. Acta* 1940, *23*, 875–885.

(10) Kienle, R. H.; Hovey, A. G. The Polyhydric Alcohol-Polybasic Acid Reaction. I. Glycerol-Phthalic Anhydride. *J. Am. Chem. Soc.* 1929, *51*, 509–519.

(11) Kienle, R. H.; van Meulen, P. A. d.; Petke, F. E. The Polyhydric Alcohol-Polybasic Acid Reaction. III. Further Studies of the Glycerol-Phthalic Anhydride Reaction. *J. Am. Chem. Soc.* 1939, *61*, 2258–2268.

(12) Kienle, R. H.; van Meulen, P. A. d.; Petke, F. E. The Polyhydric Alcohol-Polybasic Acid Reaction. IV. Glyceryl Phthalate from Phthalic Acid. *J. Am. Chem. Soc.* 1939, *61*, 2268–2271.

(13) Leo H Baekeland. Method of making insoluble products of phenol and formaldehyde. *US 942699A* 1909.

(14) Jikei, M.; Chon, S.-H.; Kakimoto, M.-a.; Kawauchi, S.; Imase, T.; Watanebe, J. Synthesis of Hyperbranched Aromatic Polyamide from Aromatic Diamines and Trimesic Acid. *Macromolecules* 1999, *32*, 2061–2064.

(15) Emrick, T.; Chang, H.-T.; Fréchet, J. M. J. An A 2 + B 3 Approach to Hyperbranched Aliphatic Polyethers Containing Chain End Epoxy Substituents. *Macromolecules* 1999, *32*, 6380–6382.

(16) Flory, P. J. Molecular Size Distribution in Three Dimensional Polymers. VI. Branched Polymers Containing A—R—B f-1 Type Units. *J. Am. Chem. Soc.* 1952, *74*, 2718–2723.

(17) Flory, P. J. Molecular Size Distribution in Three Dimensional Polymers. I. Gelation 1. *J. Am. Chem. Soc.* 1941, *63*, 3083–3090.

(18) Flory, P. J. Molecular Size Distribution in Three Dimensional Polymers. II. Trifunctional Branching Units. *J. Am. Chem. Soc.* 1941, *63*, 3091–3096.

(19) Flory, P. J. Molecular Size Distribution in Three Dimensional Polymers. III. Tetrafunctional Branching Units. *J. Am. Chem. Soc.* 1941, *63*, 3096–3100.

(20) Flory, P. J. Molecular Size Distribution in Three Dimensional Polymers. V. Post-gelation Relationships. *J. Am. Chem. Soc.* 1947, *69*, 30–35.

(21) Walling, C. Gel Formation in Addition Polymerization 1. *J. Am. Chem. Soc.* 1945, *67*, 441–447.

(22) Newkome, G. R.; Yao, Z.; Baker, G. R.; Gupta, V. K. Micelles. Part 1. Cascade molecules: a new approach to micelles. A [27]-arborol. *J. Org. Chem.* 1985, *50*, 2003–2004.

(23) Hawker, C.; Fréchet, J. M. J. A new convergent approach to monodisperse dendritic macromolecules. *J. Chem. Soc., Chem. Commun.* 1990, *17*, 1010–1013.

(24) Hawker, C. J.; Frechet, J. M. J. Control of surface functionality in the synthesis of dendritic macromolecules using the convergent-growth approach. *Macromolecules* 1990, *23*, 4726–4729.

(25) Hawker, C. J.; Frechet, J. M. J. Preparation of polymers with controlled molecular architecture. A new convergent approach to dendritic macromolecules. *J. Am. Chem. Soc.* 1990, *112*, 7638–7647.

(26) Kim, Y. H.; Webster, O. W. *Polym. Prep. (Am. Chem. Soc., Div. Polym. Chem.)* 1988, *29*, 310.

(27) Kim, Y. H. Hyperbranched Polyarylene. *US 4857630* 1989.

(28) Kim, Y. H.; Webster, O. W. Water soluble hyperbranched polyphenylene: "a unimolecular micelle?". *J. Am. Chem. Soc.* 1990, *112*, 4592–4593.

(29) Kim, Y. H.; Webster, O. W. Hyperbranched polyphenylenes. *Macromolecules* 1992, *25*, 5561–5572.

(30) Hawker, C. J.; Lee, R.; Frechet, J. M. J. One-step synthesis of hyperbranched dendritic polyesters. *J. Am. Chem. Soc.* 1991, *113*, 4583–4588.

(31) Hölter, D.; Burgath, A.; Frey, H. Degree of branching in hyperbranched polymers. *Acta Polym.* 1997, *48*, 30–35.

(32) Yan, D.; Müller, A. H. E.; Matyjaszewski, K. Molecular Parameters of Hyperbranched Polymers Made by Self-Condensing Vinyl Polymerization. 2. Degree of Branching. *Macromolecules* 1997, *30*, 7024–7033.

(33) Bharathi, P.; Moore, J. S. Solid-Supported Hyperbranched Polymerization: Evidence for Self-Limited Growth. *J. Am. Chem. Soc.* 1997, *119*, 3391–3392.

(34) Chu, F.; Hawker, C. J. A versatile synthesis of isomeric hyperbranched polyetherketones. *Polymer Bulletin* 1993, *30*, 265–272.

(35) Hawker, C. J.; Chu, F. Hyperbranched Poly(ether ketones): Manipulation of Structure and Physical Properties. *Macromolecules* 1996, *29*, 4370–4380.

(36) Muzafarov, A. M.; Rebrov, E. A.; Gorbacevich, O. B.; Golly, M.; Gankema, H.; Möller, M. Degradable dendritic polymers - A template for functional pores and nanocavities-. *Macromol. Symp.* 1996, *102*, 35–46.

(37) J. Hobson, L.; M. Kenwright, A. A simple ‘one pot’ route to the hyperbranched analogues of Tomalia’s poly(amidoamine) dendrimers. *Chem. Commun.* 1997, *29*, 1877.

(38) Hobson, L. J.; Feast, W.J. Poly(amidoamine) hyperbranched systems: synthesis, structure and characterization. *Polymer* 1999, *40*, 1279–1297.

(39) Malmstroem, E.; Johansson, M.; Hult, A. Hyperbranched Aliphatic Polyesters. *Macromolecules* 1995, *28*, 1698–1703.

(40) Fréchet, J. M.; Henmi, M.; Gitsov, I.; Aoshima, S.; Leduc, M. R.; Grubbs, R. B. Self-condensing vinyl polymerization: an approach to dendritic materials. *Science* 1995, *269*, 1080–1083.

(41) Simon, P. F. W.; Radke, W.; Müller, A. H. E. Hyperbranched methacrylates by self-condensing group transfer polymerization. *Macromol. Rapid Commun.* 1997, *18*, 865–873.

(42) Sunder, A.; Hanselmann, R.; Frey, H.; Mülhaupt, R. Controlled Synthesis of Hyperbranched Polyglycerols by Ring-Opening Multibranching Polymerization. *Macromolecules* 1999, *32*, 4240–4246.

(43) Voit, B. I.; Lederer, A. Hyperbranched and highly branched polymer architectures--synthetic strategies and major characterization aspects. *Chem. Rev.* 2009, *109*, 5924–5973.

(44) Koltzenburg, S.; Maskos, M.; Nuyken, O.; Mülhaupt, R. *Polymere: Synthese, Eigenschaften und Anwendungen*; Springer Spektrum: Berlin, 2014.

(45) Cameron, C.; Fawcett, A. H.; Hetherington, C. R.; Mee, R. A. W.; McBride, F. V. Step growth of an AB2 monomer, with cycle formation. *J. Chem. Phys.* 1998, *108*, 8235–8251.

(46) Dusek, K.; Somvarsky, J.; Smrokova, M.; Simonsick, W. J., JR. Role of cyclization in the degree-of-polymerization distribution of hyperbranched polymers. *Polymer Bulletin* 1999, *42*, 489–496.

(47) Gong, C.; Miravet, J.; Frchet, J. M. J. Intramolecular cyclization in the polymerization of ABx monomers: Approaches to the control of molecular weight and polydispersity in hyperbranched poly(siloxysilane). *J. Polym. Sci. A Polym. Chem.* 1999, *37*, 3193–3201.

(48) Burgath, A.; Sunder, A.; Frey, H. Role of cyclization in the synthesis of hyperbranched aliphatic polyesters. *Macromol. Chem. Phys.* 2000, *201*, 782–791.

(49) Wang, L.; He, X. Investigation of AB n (n = 2, 4) type hyperbranched polymerization with cyclization and steric factors: Influences of monomer

concentration, reactivity, and substitution effect. *J. Polym. Sci. A Polym. Chem.* 2009, *47*, 523–533.

(50) Gaynor, S. G.; Edelman, S.; Matyjaszewski, K. Synthesis of Branched and Hyperbranched Polystyrenes. *Macromolecules* 1996, *29*, 1079–1081.

(51) Matyjaszewski, K.; Gaynor, S. G.; Kulfan, A.; Podwika, M. Preparation of Hyperbranched Polyacrylates by Atom Transfer Radical Polymerization. 1. Acrylic AB* Monomers in “Living” Radical Polymerizations. *Macromolecules* 1997, *30*, 5192–5194.

(52) Matyjaszewski, K.; Gaynor, S. G.; Müller, A. H. E. Preparation of Hyperbranched Polyacrylates by Atom Transfer Radical Polymerization. 2. Kinetics and Mechanism of Chain Growth for the Self-Condensing Vinyl Polymerization of 2-((2-Bromopropionyl)oxy)ethyl Acrylate. *Macromolecules* 1997, *30*, 7034–7041.

(53) Matyjaszewski, K.; Pyun, J.; Gaynor, S. G. Preparation of hyperbranched polyacrylates by atom transfer radical polymerization, 4. The use of zero-valent copper. *Macromol. Rapid Commun.* 1998, *19*, 665–670.

(54) Matyjaszewski, K.; Gaynor, S. G. Preparation of Hyperbranched Polyacrylates by Atom Transfer Radical Polymerization. 3. Effect of Reaction Conditions on the Self-Condensing Vinyl Polymerization of 2-((2-Bromopropionyl)oxy)ethyl Acrylate. *Macromolecules* 1997, *30*, 7042–7049.

(55) Hawker, C. J.; Frechet, J. M. J.; Grubbs, R. B.; Dao, J. Preparation of Hyperbranched and Star Polymers by a "Living", Self-Condensing Free Radical Polymerization. *J. Am. Chem. Soc.* 1995, *117*, 10763–10764.

(56) Schömer, M.; Schüll, C.; Frey, H. Hyperbranched aliphatic polyether polyols. *J. Polym. Sci. A Polym. Chem.* 2013, *51*, 995–1019.

(57) Liu, M.; Vladimirov, N.; Fréchet, J. M. J. A New Approach to Hyperbranched Polymers by Ring-Opening Polymerization of an AB Monomer: 4-(2-Hydroxyethyl)-ε-caprolactone. *Macromolecules* 1999, *32*, 6881–6884.

(58) Trollsås, M.; Löwenhielm, P.; Lee, V. Y.; Möller, M.; Miller, R. D.; Hedrick, J. L. New Approach to Hyperbranched Polyesters: Self-Condensing Cyclic Ester Polymerization of Bis(hydroxymethyl)-Substituted ε-Caprolactone. *Macromolecules* 1999, *32*, 9062–9066.

(59) Motokucho, S.; Sudo, A.; Sanda, F.; Endo, T. Reaction of carbon dioxide with glycidol: The synthesis of a novel hyperbranched oligomer with a carbonate main chain with a hydroxyl terminal. *J. Polym. Sci. A Polym. Chem.* 2004, *42*, 2506–2511.

(60) Scharfenberg, M.; Hofmann, S.; Preis, J.; Hilf, J.; Frey, H. Rigid Hyperbranched Polycarbonate Polyols from CO 2 and Cyclohexene-Based Epoxides. *Macromolecules* 2017, *50*, 6088–6097.

(61) Rider, T. H.; Hill, A. J. Studies of Glycidol. I. Preparation From Glycerol Monochlorohydrin. *J. Am. Chem. Soc.* 1930, *52*, 1521–1527.

(62) Sandler, S. R.; Berg, F. R. Room temperature polymerization of glycidol. *J. Polym. Sci. A Polym. Chem.* 1966, *4*, 1253–1259.

(63) Vandenberg, E. J. Polymerization of glycidol and its derivatives: A new rearrangement polymerization. *J. Polym. Sci. A Polym. Chem.* 1985, *23*, 915–949.

(64) Tokar, R.; Kubisa, P.; Penczek, S.; Dworak, A. Cationic polymerization of glycidol: coexistence of the activated monomer and active chain end mechanism. *Macromolecules* 1994, *27*, 320–322.

(65) Dworak, A.; Walach, W.; Trzebicka, B. Cationic polymerization of glycidol. Polymer structure and polymerization mechanism. *Macromol. Chem. Phys.* 1995, *196*, 1963–1970.

(66) Bednarek, M.; Biedron, T.; Helinski, J.; Kaluzynski, K.; Kubisa, P.; Penczek, S. Branched polyether with multiple primary hydroxyl groups: polymerization of 3-ethyl-3-hydroxymethyloxetane. *Macromol. Rapid Commun.* 1999, *20*, 369–372.

(67) Magnusson, H.; Malmström, E.; Hult, A. Synthesis of hyperbranched aliphatic polyethers via cationic ring-opening polymerization of 3-ethyl-3-(hydroxymethyl)oxetane. *Macromol. Rapid Commun.* 1999, *20*, 453–457.

(68) Yan, D.; Hou, J.; Zhu, X.; Kosman, J. J.; Wu, H.-S. A new approach to control crystallinity of resulting polymers: Self-condensing ring opening polymerization. *Macromol. Rapid Commun.* 2000, *21*, 557–561.

(69) Satoh, T.; Imai, T.; Ishihara, H.; Maeda, T.; Kitajyo, Y.; Narumi, A.; Kaga, H.; Kaneko, N.; Kakuchi, T. Synthesis of Hyperbranched Polysaccharide by Thermally Induced Cationic Polymerization of 1,6-Anhydro-β- d -mannopyranose. *Macromolecules* 2003, *36*, 6364–6370.

(70) Imai, T.; Satoh, T.; Kaga, H.; Kaneko, N.; Kakuchi, T. Synthesis of Hyperbranched Carbohydrate Polymer by Ring-Opening Multibranching Polymerization of 1,4-Anhydroerythritol and 1,4-Anhydro- l -threitol. *Macromolecules* 2004, *37*, 3113–3119.

(71) Bednarek, M.; Kubisa, P. Cationic polymerization of 2-hydroxymethyltetrahydrofuran. *J. Polym. Sci. A Polym. Chem.* 2006, *44*, 6484–6493.

(72) Tran, C. H.; Lee, M. W.; Kim, S. A.; Jang, H. B.; Kim, I. Kinetic and Mechanistic Study of Heterogeneous Double Metal Cyanide-Catalyzed Ring-Opening Multibranching Polymerization of Glycidol. *Macromolecules* 2020, *53*, 2051–2060.

(73) Müller, A. H. E.; Yan, D.; Wulkow, M. Molecular Parameters of Hyperbranched Polymers Made by Self-Condensing Vinyl Polymerization. 1. Molecular Weight Distribution. *Macromolecules* 1997, *30*, 7015–7023.

(74) Hanselmann, R.; Hölter, D.; Frey, H. Hyperbranched Polymers Prepared via the Core-Dilution/Slow Addition Technique: Computer Simulation of Molecular Weight Distribution and Degree of Branching. *Macromolecules* 1998, *31*, 3790–3801.

(75) Radke, W.; Litvinenko, G.; Müller, A. H. E. Effect of Core-Forming Molecules on Molecular Weight Distribution and Degree of Branching in the Synthesis of Hyperbranched Polymers. *Macromolecules* 1998, *31*, 239–248.

(76) Cheng, K.-C.; Chuang, T.-H.; Chang, J.-S.; Guo, W.; Su, W.-F. Effect of Feed Rate on Structure of Hyperbranched Polymers Formed by Self-Condensing Vinyl Polymerization in Semibatch Reactor. *Macromolecules* 2005, *38*, 8252–8257.

(77) Möck, A.; Burgath, A.; Hanselmann, R.; Frey, H. Synthesis of Hyperbranched Aromatic Homo- and Copolyesters via the Slow Monomer Addition Method. *Macromolecules* 2001, *34*, 7692–7698.

(78) Hölter, D.; Frey, H. Degree of branching in hyperbranched polymers. 2. Enhancement of the db: Scope and limitations. *Acta Polym.* 1997, *48*, 298–309.

(79) Schüll, C.; Rabbel, H.; Schmid, F.; Frey, H. Polydispersity and Molecular Weight Distribution of Hyperbranched Graft Copolymers via “Hypergrafting” of AB m Monomers from Polydisperse Macroinitiator Cores: Theory Meets Synthesis. *Macromolecules* 2013, *46*, 5823–5830.

(80) Inoue, K. Functional dendrimers, hyperbranched and star polymers. *Prog. Polym. Sci.* 2000, *25*, 453–571.

(81) Jikei, M.; Kakimoto, M.-a. Hyperbranched polymers: a promising new class of materials. *Prog. Polym. Sci.* 2001, *26*, 1233–1285.

(82) Voit, B. Hyperbranched polymers—All problems solved after 15 years of research? *J. Polym. Sci. A Polym. Chem.* 2005, *43*, 2679–2699.

(83) Wilms, D.; Stiriba, S.-E.; Frey, H. Hyperbranched polyglycerols: from the controlled synthesis of biocompatible polyether polyols to multipurpose applications. *Acc. Chem. Res.* 2010, *43*, 129–141.

(84) Calderón, M.; Quadir, M. A.; Sharma, S. K.; Haag, R. Dendritic polyglycerols for biomedical applications. *Adv. Mater.* 2010, *22*, 190–218.

(85) Zheng, Y.; Li, S.; Weng, Z.; Gao, C. Hyperbranched polymers: advances from synthesis to applications. *Chem. Soc. Rev.* 2015, *44*, 4091–4130.

(86) Abbina, S.; Vappala, S.; Kumar, P.; Siren, E. M. J.; La, C. C.; Abbasi, U.; Brooks, D. E.; Kizhakkedathu, J. N. Hyperbranched polyglycerols: recent advances in synthesis, biocompatibility and biomedical applications. *J. Mater. Chem. B* 2017, *5*, 9249–9277.

(87) Sunder, A.; Krämer, M.; Hanselmann, R.; Mülhaupt, R.; Frey, H. Molecular Nanocapsules Based on Amphiphilic Hyperbranched Polyglycerols. *Angew. Chem. Int. Ed.* 1999, *38*, 3552–3555.

(88) Gao, C.; Yan, D. Y.; Chen, W. Self-Association and Degree of Branching: Fluorescence-Probe Study of Hyperbranched Poly(sulfone-amine)s in Aqueous Solution. *Macromol. Rapid Commun.* 2002, *23*, 465.

(89) Stiriba, S.-E.; Kautz, H.; Frey, H. Hyperbranched molecular nanocapsules: comparison of the hyperbranched architecture with the perfect linear analogue. *J. Am. Chem. Soc.* 2002, *124*, 9698–9699.

(90) Yu, M. Q.; Zhou, Z.; Yan, D. Y. *Chem. J. Chin. Univ.-Chin.* 2003, *24*, 1332.

(91) Mai, Y.; Zhou, Y.; Yan, D. Y. *Chem. J. Chin. Univ.-Chin.* 2004, *25*, 1373.

(92) Krämer, M.; Stumbé, J.-F.; Grimm, G.; Kaufmann, B.; Krüger, U.; Weber, M.; Haag, R. Dendritic polyamines: simple access to new materials with defined treelike structures for application in nonviral gene delivery. *ChemBioChem.* 2004, *5*, 1081–1087.

(93) Mai, Y.; Zhou, Y.; Yan, D.; Hou, J. Quantitative dependence of crystallinity on degree of branching for hyperbranched poly[3-ethyl-3-(hydroxymethyl)oxetane]. *New J. Phys.* 2005, *7*, 42.

(94) Gong, W.; Mai, Y.; Zhou, Y.; Qi, N.; Wang, B.; Yan, D. Effect of the Degree of Branching on Atomic-Scale Free Volume in Hyperbranched Poly[3-ethyl-3-(hydroxymethyl)oxetane]. A Positron Study. *Macromolecules* 2005, *38*, 9644–9649.

(95) Zhu, Q.; Wu, J.; Tu, C.; Shi, Y.; He, L.; Wang, R.; Zhu, X.; Yan, D. Role of branching architecture on the glass transition of hyperbranched polyethers. *J. Phys. Chem. B.* 2009, *113*, 5777–5780.

(96) Cheng, H.; Yuan, X.; Sun, X.; Li, K.; Zhou, Y.; Yan, D. Effect of Degree of Branching on the Self-Assembly of Amphiphilic Hyperbranched Multiarm Copolymers. *Macromolecules* 2010, *43*, 1143–1147.

(97) Perevyazko, I.; Kaiser, T.; Frey, H. Hard Sphere-Behavior of Hyperbranched Polyglycerol in Aqueous Solution: Absolute Molecular Weights, Molecular Hydrodynamics and Light Scattering. *to be submitted* 2020.

(98) Kainthan, R. K.; Janzen, J.; Levin, E.; Devine, D. V.; Brooks, D. E. Biocompatibility testing of branched and linear polyglycidol. *Biomacromolecules* 2006, *7*, 703–709.

(99) Kainthan, R. K.; Hester, S. R.; Levin, E.; Devine, D. V.; Brooks, D. E. In vitro biological evaluation of high molecular weight hyperbranched polyglycerols. *Biomaterials* 2007, *28*, 4581–4590.

(100) Kainthan, R. K.; Brooks, D. E. In vivo biological evaluation of high molecular weight hyperbranched polyglycerols. *Biomaterials* 2007, *28*, 4779–4787.

(101) Petkov, V.; Parvanov, V.; Tomalia, D.; Swanson, D.; Bergstrom, D.; Vogt, T. 3D structure of dendritic and hyper-branched macromolecules by X-ray diffraction. *Solid State Communications* 2005, *134*, 671–675.

(102) Bernal, D. P.; Bedrossian, L.; Collins, K.; Fossum, E. Effect of Core Reactivity on the Molecular Weight, Polydispersity, and Degree of Branching of Hyperbranched Poly(arylene ether phosphine oxide)s. *Macromolecules* 2003, *36*, 333–338.

(103) Lach, C.; Frey, H. Enhancing the Degree of Branching of Hyperbranched Polymers by Postsynthetic Modification. *Macromolecules* 1998, *31*, 2381–2383.

(104) Weimer, M. W.; Frechet, J. M. J.; Gitsov, I. Importance of active-site reactivity and reaction conditions in the preparation of hyperbranched polymers by self-condensing vinyl polymerization: Highly branched vs. linear poly[4-(chloromethyl)styrene] by metal-catalyzed "living" radical polymerization. *J. Polym. Sci. A Polym. Chem.* 1998, *36*, 955–970.

(105) Yan, D.; Hou, J.; Zhu, X.; Kosman, J. J.; Wu, H.-S. A new approach to control crystallinity of resulting polymers: Self-condensing ring opening polymerization. *Macromol. Rapid Commun.* 2000, *21*, 557–561.

(106) Mai, Y.; Zhou, Y.; Yan, D.; Lu, H. Effect of Reaction Temperature on Degree of Branching in Cationic Polymerization of 3-Ethyl-3-(hydroxymethyl)oxetane. *Macromolecules* 2003, *36*, 9667–9669.

(107) Spears, B. R.; Waksal, J.; McQuade, C.; Lanier, L.; Harth, E. Controlled branching of polyglycidol and formation of protein-glycidol bioconjugates via a graft-from approach with "PEG-like" arms. *Chem. Commun.* 2013, *49*, 2394–2396.

(108) Spears, B. R.; Marin, M. A.; Montenegro-Burke, J. R.; Evans, B. C.; McLean, J.; Harth, E. Aqueous Epoxide Ring-Opening Polymerization (AEROP): Green Synthesis of Polyglycidol with Ultralow Branching. *Macromolecules* 2016, *49*, 2022–2027.

(109) Frey, H.; Hölter, D. Degree of branching in hyperbranched polymers. 3 Copolymerization of ABm-monomers with AB and ABn-monomers. *Acta Polym.* 1999, *50*, 67–76.

(110) Litvinenko, G. I.; Simon, P. F. W.; Müller, A. H. E. Molecular Parameters of Hyperbranched Copolymers Obtained by Self-Condensing Vinyl Copolymerization. 1. Equal Rate Constants. *Macromolecules* 1999, *32*, 2410–2419.

(111) Litvinenko, G. I.; Simon, P. F. W.; Müller, A. H. E. Molecular Parameters of Hyperbranched Copolymers Obtained by Self-Condensing Vinyl Copolymerization, 2. † Non-Equal Rate Constants. *Macromolecules* 2001, *34*, 2418–2426.

(112) Sunder, A.; Mülhaupt, R.; Haag, R.; Frey, H. Hyperbranched Polyether Polyols: A Modular Approach to Complex Polymer Architectures. *Adv. Mater.* 2000, *12*, 235–239.

(113) Zhang, H.; Grinstaff, M. W. Recent advances in glycerol polymers: chemistry and biomedical applications. *Macromol. Rapid Commun.* 2014, *35*, 1906–1924.

(114) Wilms, D.; Nieberle, J.; Klos, J.; Löwe, H.; Frey, H. Synthesis of Hyperbranched Polyglycerol in a Continuous Flow Microreactor. *Chem. Eng. Technol.* 2007, *30*, 1519–1524.

(115) Kautz, H.; Sunder, A.; Frey, H. Control of the molecular weight of hyperbranched polyglycerols. *Macromol. Symp.* 2001, *163*, 67–74.

(116) Wilms, D.; Wurm, F.; Nieberle, J.; Böhm, P.; Kemmer-Jonas, U.; Frey, H. Hyperbranched Polyglycerols with Elevated Molecular Weights: A Facile Two-Step Synthesis Protocol Based on Polyglycerol Macroinitiators. *Macromolecules* 2009, *42*, 3230–3236.

(117) Kainthan, R. K.; Muliawan, E. B.; Hatzikiriakos, S. G.; Brooks, D. E. Synthesis, Characterization, and Viscoelastic Properties of High Molecular Weight Hyperbranched Polyglycerols. *Macromolecules* 2006, *39*, 7708–7717.

(118) Anilkumar, P.; Lawson, T. B.; Abbina, S.; Mäkelä, J. T. A.; Sabatelle, R. C.; Takeuchi, L. E.; Snyder, B. D.; Grinstaff, M. W.; Kizhakkedathu, J. N. Mega macromolecules as single molecule lubricants for hard and soft surfaces. *Nat Commun* 2020, *11*, 1517.

(119) Weiss, M. E. R.; Paulus, F.; Steinhilber, D.; Nikitin, A. N.; Haag, R.; Schütte, C. Estimating Kinetic Parameters for the Spontaneous Polymerization of Glycidol at Elevated Temperatures. *Macromol. Theory Simul.* 2012, *21*, 470–481.

(120) Paulus, F.; Weiss, M. E. R.; Steinhilber, D.; Nikitin, A. N.; Schütte, C.; Haag, R. Anionic Ring-Opening Polymerization Simulations for Hyperbranched Polyglycerols with Defined Molecular Weights. *Macromolecules* 2013, *46*, 8458–8466.

(121) Spears, B. R.; Waksal, J.; McQuade, C.; Lanier, L.; Harth, E. Controlled branching of polyglycidol and formation of protein-glycidol bioconjugates via a graft-from approach with "PEG-like" arms. *Chem. Commun.* 2013, *49*, 2394–2396.

(122) Sunder, A.; Bauer, T.; Mülhaupt, R.; Frey, H. Synthesis and Thermal Behavior of Esterified Aliphatic Hyperbranched Polyether Polyols. *Macromolecules* 2000, *33*, 1330–1337.

(123) Garamus, V. M.; Maksimova, T. V.; Kautz, H.; Barriau, E.; Frey, H.; Schlotterbeck, U.; Mecking, S.; Richtering, W. Hyperbranched Polymers: Structure of Hyperbranched Polyglycerol and Amphiphilic Poly(glycerol ester)s in Dilute Aqueous and Nonaqueous Solution. *Macromolecules* 2004, *37*, 8394–8399.

(124) Schubert, C.; Osterwinter, C.; Tonhauser, C.; Schömer, M.; Wilms, D.; Frey, H.; Friedrich, C. Can Hyperbranched Polymers Entangle? Effect of Hydrogen Bonding on Entanglement Transition and Thermorheological Properties of Hyperbranched Polyglycerol Melts. *Macromolecules* 2016, *49*, 8722–8737.

(125) Sunder, A.; Krämer, M.; Hanselmann, R.; Mülhaupt, R.; Frey, H. Molecular Nanocapsules Based on Amphiphilic Hyperbranched Polyglycerols. *Angew. Chem. Int. Ed.* 1999, *38*, 3552–3555.

(126) Haag, R.; Stumbé, J.-F.; Sunder, A.; Frey, H.; Hebel, A. An Approach to Core−Shell-Type Architectures in Hyperbranched Polyglycerols by Selective Chemical Differentiation. *Macromolecules* 2000, *33*, 8158–8166.

(127) Türk, H.; Haag, R.; Alban, S. Dendritic polyglycerol sulfates as new heparin analogues and potent inhibitors of the complement system. *Bioconjug. Chem.* 2004, *15*, 162–167.

(128) Sunder, A.; Türk, H.; Haag, R.; Frey, H. Copolymers of Glycidol and Glycidyl Ethers: Design of Branched Polyether Polyols by Combination of Latent Cyclic AB 2 and ABR Monomers. *Macromolecules* 2000, *33*, 7682–7692.

(129) Wilms, D.; Schömer, M.; Wurm, F.; Hermanns, M. I.; Kirkpatrick, C. J.; Frey, H. Hyperbranched PEG by random copolymerization of ethylene oxide and glycidol. *Macromol. Rapid Commun.* 2010, *31*, 1811–1815.

(130) Schömer, M.; Seiwert, J.; Frey, H. Hyperbranched Poly(propylene oxide): A Multifunctional Backbone-Thermoresponsive Polyether Polyol Copolymer. *ACS Macro Lett.* 2012, *1*, 888–891.

(131) Seiwert, J.; Leibig, D.; Kemmer-Jonas, U.; Bauer, M.; Perevyazko, I.; Preis, J.; Frey, H. Hyperbranched Polyols via Copolymerization of 1,2-Butylene Oxide and Glycidol: Comparison of Batch Synthesis and Slow Monomer Addition. *Macromolecules* 2016, *49*, 38–47.

(132) Alkan, A.; Klein, R.; Shylin, S. I.; Kemmer-Jonas, U.; Frey, H.; Wurm, F. R. Water-soluble and redox-responsive hyperbranched polyether copolymers based on ferrocenyl glycidyl ether. *Polym. Chem.* 2015, *6*, 7112–7118.

(133) Schüll, C.; Gieshoff, T.; Frey, H. One-step synthesis of multi-alkyne functional hyperbranched polyglycerols by copolymerization of glycidyl propargyl ether and glycidol. *Polym. Chem.* 2013, *4*, 4730.

(134) Niederer, K.; Schüll, C.; Leibig, D.; Johann, T.; Frey, H. Catechol Acetonide Glycidyl Ether (CAGE): A Functional Epoxide Monomer for Linear and Hyperbranched Multi-Catechol Functional Polyether Architectures. *Macromolecules* 2016, *49*, 1655–1665.

(135) Seiwert, J.; Herzberger, J.; Leibig, D.; Frey, H. Thioether-Bearing Hyperbranched Polyether Polyols with Methionine-Like Side-Chains: A Versatile Platform for Orthogonal Functionalization. *Macromol. Rapid Commun.* 2017, *38*.

(136) Schubert, C.; Schömer, M.; Steube, M.; Decker, S.; Friedrich, C.; Frey, H. Systematic Variation of the Degree of Branching (DB) of Polyglycerol via Oxyanionic Copolymerization of Glycidol with a Protected Glycidyl Ether and Its Impact on Rheological Properties. *Macromol. Chem. Phys.* 2018, *219*, 1700376.

(137) Song, S.; Lee, J.; Kweon, S.; Song, J.; Kim, K.; Kim, B.-S. Hyperbranched Copolymers Based on Glycidol and Amino Glycidyl Ether: Highly Biocompatible Polyamines Sheathed in Polyglycerols. *Biomacromolecules* 2016, *17*, 3632–3639.

(138) Son, S.; Shin, E.; Kim, B.-S. Redox-Degradable Biocompatible Hyperbranched Polyglycerols: Synthesis, Copolymerization Kinetics, Degradation, and Biocompatibility. *Macromolecules* 2015, *48*, 600–609.

(139) Tonhauser, C.; Schüll, C.; Dingels, C.; Frey, H. Branched Acid-Degradable, Biocompatible Polyether Copolymers via Anionic Ring-Opening Polymerization Using an Epoxide Inimer. *ACS Macro Lett.* 2012, *1*, 1094–1097.

(140) Shenoi, R. A.; Narayanannair, J. K.; Hamilton, J. L.; Lai, B. F. L.; Horte, S.; Kainthan, R. K.; Varghese, J. P.; Rajeev, K. G.; Manoharan, M.; Kizhakkedathu, J. N. Branched multifunctional polyether polyketals: variation of ketal group structure enables unprecedented control over polymer degradation in solution and within cells. *J. Am. Chem. Soc.* 2012, *134*, 14945–14957.

(141) Parzuchowski, P. G.; Stefańska, M.; Świderska, A.; Roguszewska, M.; Zybert, M. Hyperbranched polyglycerols containing amine groups — Synthesis, characterization and carbon dioxide capture. *Journal of CO2 Utilization* 2018, *27*, 145–160.

(142) Pitet, L. M.; Hait, S. B.; Lanyk, T. J.; Knauss, D. M. Linear and Branched Architectures from the Polymerization of Lactide with Glycidol. *Macromolecules* 2007, *40*, 2327–2334.

(143) Mohammadifar, E.; Zabihi, F.; Tu, Z.; Hedtrich, S.; Nemati Kharat, A.; Adeli, M.; Haag, R. One-pot and gram-scale synthesis of biodegradable polyglycerols under ambient conditions: nanocarriers for intradermal drug delivery. *Polym. Chem.* 2017, *8*, 7375–7383.

(144) Hatamvand, R.; Shams, A.; Mohammadifar, E.; Yari, A.; Adeli, M. Synthesis of boronic acid-functionalized poly(glycerol-oligoγ-butyrolactone): Nano-networks for efficient electrochemical sensing of biosystems. *J. Polym. Sci. A Polym. Chem.* 2019, *57*, 1430–1439.

(145) Haynes, W. M. *CRC Handbook of Chemistry and Physics, 92nd Edition*, 92th ed.; CRC Press: Hoboken, 2011.

(146) Leibig, D.; Seiwert, J.; Liermann, J. C.; Frey, H. Copolymerization Kinetics of Glycidol and Ethylene Oxide, Propylene Oxide, and 1,2-Butylene Oxide: From Hyperbranched to Multiarm Star Topology. *Macromolecules* 2016, *49*, 7767–7776.

(147) Wurm, F.; Dingels, C.; Frey, H.; Klok, H.-A. Squaric acid mediated synthesis and biological activity of a library of linear and hyperbranched poly(glycerol)-protein conjugates. *Biomacromolecules* 2012, *13*, 1161–1171.

(148) Wurm, F.; Klos, J.; Räder, H. J.; Frey, H. Synthesis and noncovalent protein conjugation of linear-hyperbranched PEG-poly(glycerol) alpha,omega(n)-telechelics. *J. Am. Chem. Soc.* 2009, *131*, 7954–7955.

2. Synthesis and Characterization of Hyperbranched Polyether Polyols: Variation of the Polymer Architecture

2.1 Control of the Molar Mass of Hyperbranched Poly(ethylene oxide) *via* Slow Monomer Addition

Tobias Kaiser[a], Jan Seiwert[a], Jürgen Vitz[b,c], Jasmin Preis[d], Ivo Nischang[b,c], Ulrich S. Schubert[b,c,e], Holger Frey[a,]*

[a]Institute of Organic Chemistry, Duesbergweg 10-14, Johannes Gutenberg University, 55128 Mainz, Germany

[b]Laboratory of Organic and Macromolecular Chemistry (IOMC), Humboldtstr. 10, Friedrich-Schiller-University Jena, 07743 Jena, Germany

[c]Jena Center for Soft Matter (JCSM), Philosophenweg 7 Friedrich-Schiller-University Jena, 07743 Jena, Germany

[d]PSS Polymer Standards Service GmbH, In der Dalheimer Wiese 5, 55120 Mainz, Germany

[e]Dutch Polymer Institute (DPI), P.O. Box 902, 5600 AX Eindhoven, the Netherlands

To be submitted.

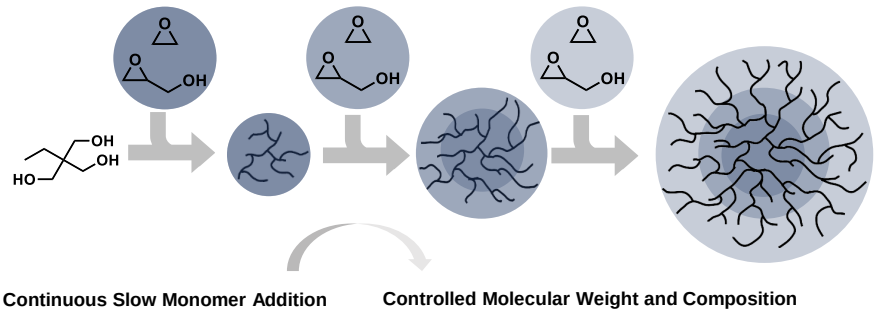

Abstract

We describe the first controlled synthesis of hyperbranched poly(ethylene oxide) copolymers giving access to molar masses up to 40 000 g mol^{-1} and low dispersity. Various hyperbranched poly(ethylene oxide) copolymers with full control of the molar mass and copolymer composition have been prepared by slow monomer addition (SMA) of ethylene oxide and glycidol as a cyclic, branching inimer. Due to vastly different boiling points and resulting safety issues, the slow addition of glycidol and ethylene oxide to a solution of the initiator salt heated to 100 °C requires a fully automated pressure-resistant reactor setup. By variation of the monomer addition rate and the monomer/initiator ratio, a series of *hb*PEO copolymers with glycidol contents between 0.20 and 0.30 and M_n ranging from 1400 to 16 000 g mol^{-1} and narrow molar mass distributions (M_w / M_n = 1.2 - 1.5), determined by SEC. Molar mass averages between 970 and 36700 g mol^{-1} as well as 1500 and 43900 g mol^{-1} were determined by SEC using universal calibration relying on online viscosity measurements and analytical ultracentrifugation (AUC), respectively. Additionally, by terpolymerization of glycidol, ethylene oxide (EO) and allyl glycidyl ether (AGE) hyperbranched poly(ethylene oxide) copolymers functionalized with allyl groups were prepared. An AGE content of 0.10 was targeted while altering the molar mass in the range of 3200 to 6400 g mol^{-1}. The copolymer compositions and molar masses determined using ^{1}H NMR spectroscopy were in good agreement with the targeted values over the whole molecular weight distribution, demonstrating the scope of the slow monomer addition for the preparation of well-defined hyperbranched poly(ethylene oxide) copolymers. The introduction of this synthetic procedure for the controlled

preparation of hyperbranched poly(ethylene oxide) copolymers enables the systematic investigation of structure-property relationships.

Introduction

Poly(ethylene oxide) is considered to be the gold standard polyether for pharmaceutical applications and is a widely used additive in cosmetic formulations and food products due to its extraordinary solubility in aqueous media and its extremely low toxicity.[1,2] The prevalent production process relies on the anionic ring-opening polymerization (AROP) of ethylene oxide (EO). Using common lab glassware, the employment of gaseous monomers, such as ethylene oxide, and the controlled polymerization thereof poses a significant challenge.[3] Vitz *et al.* recently introduced a pressure-resistant and fully automated reactor-setup for the slow addition of ethylene oxide under elevated pressure at high reaction temperatures on the multigram scale.[4]

The utilization of PEO for certain applications can be limited due to crystallinity and the lack of multiple functional groups.[1,2] On the other hand, hyperbranched poly(alkylene oxides) combine the properties of their linear analogues with a dendritic structure, introducing peculiar thermal and rheological properties as well as a multitude of functional groups without the demanding generation-wise synthesis of comparable dendrimers.[5–7]

Recently, our group introduced hyperbranched analogues of the widely used linear poly(alkylene oxides) prepared from EO, propylene oxide (PO) and butylene oxide (BO).[8–10] These materials are typically synthesized by direct anionic copolymerization of glycidol and the respective alkylene oxide in batch procedures.

However, due to a different polymerization mechanism of glycidol in comparison to EO or PO there is little control of the degree of polymerization.[11–15]

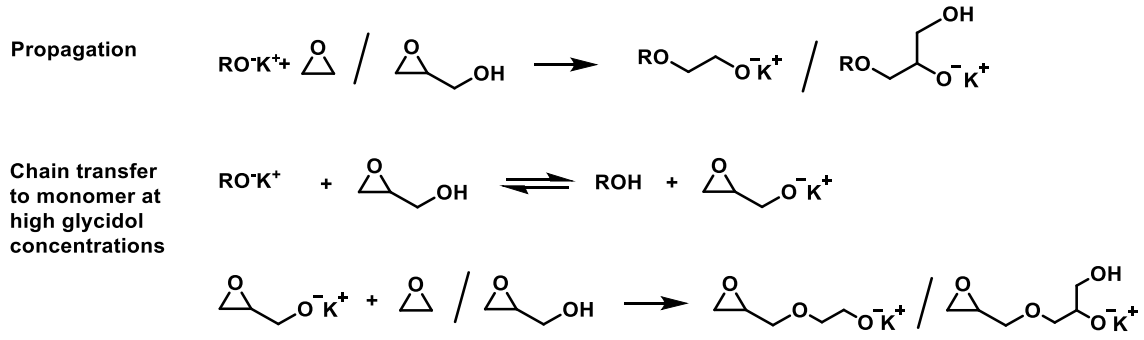

Scheme 1. Desired propagation step in the anionic ring-opening copolymerization of EO and glycidol and self-initiation step at high glycidol concentrations.

Scheme 1 depicts the desired propagation step in the anionic copolymerization of glycidol and EO as well as the prevalent side reaction taking place at high glycidol concentrations. Glycidol acts as an inimer, carrying a hydroxy group capable of initiating chain growth in addition to the polymerizable epoxide ring. Thus, as glycidol can also act as an initiator the control over the degree of polymerization is no longer defined by the monomer-to-initiator ratio when conducting the polymerization in a single batch. Furthermore, low molar mass and cyclic byproducts resulting from backbiting reactions of glycidol initiated chains are to be expected as well.

A variation of the degree of polymerization can be achieved by preparation of *hb*PEO in different solvents. However, the molar masses are either limited to very high values in cyclic ethers or oligomeric products, as observed for the polymerization in DMSO.[16] By having access to *hb*PEO copolymers over a broad range of molar masses Perevyazko *et al.* were able to elucidate the hydrodynamic properties of these materials based on a combination of analytical

ultracentrifugation (AUC), viscometry, translational diffusion and SEC. The resulting scaling factors suggest a compact, sphere-like conformation in solution comparable to perfectly branched dendrimers. Surprisingly, the absolute molar masses determined by AUC were up to 25 times higher than those determined by SEC using linear PEO standards, proving the compact architecture.

In situ ^{1}H NMR kinetic studies of glycidol and ethylene oxide as well as other well established alkylene oxides revealed a slightly higher reactivity of glycidol, resulting in a nearly random hyperbranched gradient copolymer in the case of EO and glycidol. As PO and BO each exhibited a lower reactivity than EO during the copolymerization with glycidol, different microstructures were formed rather resembling multiarm star copolymers with PPO or PBO arms and a hyperbranched polyglycerol core with little to no PO or BO content, respectively. However, as during the entire course of the polymerization new polymer chains are formed due to the self-initiation by glycidol a compositional drift is observed, as chains that are formed during a later stage of the polymerization exhibit a glycidol content that is lower than the initial comonomer feed due to the slightly higher reactivity of glycidol in comparison to ethylene oxide. This ultimately leads to non-uniform hyperbranched structures.

To avoid the chain transfer leading to self-initiation the monomers need to be added slowly to a solution of the initiator to keep the glycidol concentration as low as possible during the entire course of the polymerization. In the case of slow monomer addition of glycidol combined with functional epoxide monomers various well-defined hyperbranched polyether polyols with a variety of functionalities were prepared.[17–25] However, the molar masses achievable by utilizing small molecule initiators, i.e. trimethylolpropane (TMP), is limited. The preparation of

hyperbranched polyglycerol with elevated molar masses and narrow molecular weight distributions by using *hb*PG macroinitiators was reported by our group.[26] This approach cut the overall monomer addition time and maintained the concentration of active reaction sites at a level necessary for sufficient overall reactivity and controlled polymerization.

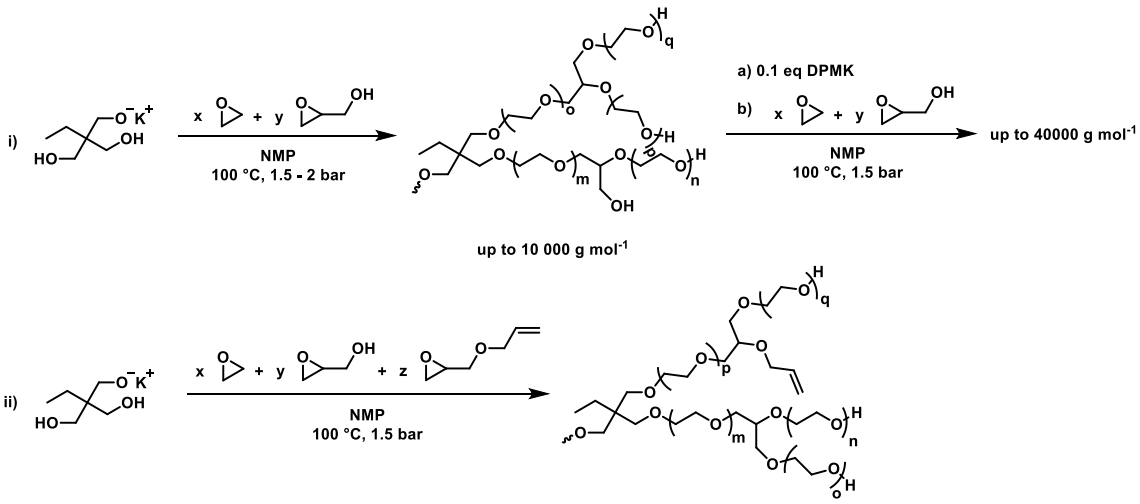

Scheme 2. Synthesis of i) hyperbranched poly(ethylene oxide) copolymers using small molecule and macroinitiators and ii) hyperbranched terpolymers comprised of glycidol, EO and AGE.

As the slow addition of ethylene oxide and propylene oxide to a solution heated well above these monomers´ boiling point (10.5 °C and 34 °C, respectively) poses a significant safety risk, to date only hyperbranched poly(butylene oxide) was prepared employing slow monomer addition.

In this work we present the controlled anionic ring-opening copolymerization of ethylene oxide and glycidol *via* slow monomer addition to prepare well-defined hyperbranched poly(ethylene oxide) copolymers with adjustable molar mass and controlled composition using small molecule initiators as well as macroinitiators (Scheme 2, i)). To ensure controlled addition of the gaseous monomer ethylene

oxide, a fully automated and pressure resistant reactor devised by Schubert, Vitz *et al.* was employed. The scope of this synthetic procedure is highlighted by the preparation of two well-defined hyperbranched terpolymers comprised of glycidol, EO and AGE exhibiting orthogonally addressable functional groups (Scheme 2, ii)).

Experimental Section

Materials

All materials and solvents were purchased from Sigma Aldrich or Linde. Purification of ethylene oxide (EO) was performed in the closed autoclave system under inert conditions: EO (99.9 %) was condensed from the lecture bottle into the dry glass autoclave, dried over sodium and subsequently transferred to the pressure burette *via* distillation. Glycidol (96 %) and 1-Methyl-2-pyrrolidone (NMP, 99.0 %) were purified by distillation over calcium hydride before use. Diphenyl methyl potassium (DPMK) solution in THF was prepared following an established procedure.[27] The exact concentration was determined by titration prior to use. Before use, the (macro-) initiators trimethylol propane (TMP) and *hb*PEO$_{165}$ were dried in high vacuum at 60 °C for 4 and 24 hours, respectively.

Instrumentation

Reactor Setup. The reactor was comprised of two pressure burettes, two mass flow controllers, a cryostat and an automation and control unit. Polymerizations were carried out in two BüchiGlasUster (Uster, Switzerland) small scale PicoClave glass autoclaves (200 and 300 mL, pressure resistant up to 6 bar and 10 bar, respectively). The autoclaves were equipped with a stainless-steel cover, fast action closure, pressure gauge, different valves, a rupture disc and a polycarbonate safety shield. They were dried under vacuum for 24 hours and flushed with argon prior to use.

The pressure burettes consisted of a cylindrical glass tube, equipped with a heating/cooling jacket, inside a stainless-steel frame. They were pressure resistant

up to 12 bar. Both autoclaves and burettes were equipped with PT100 temperature sensors as well as signal to mA converters (GE UNIK 5000, PRelectronics 9113B2 and 9116B), displays (PRelectronics 4501) as well as power supply and control (PRelectronics 9410, 9420). Two Bronkhorst mini CORI-FLOW (M12V14I-PGD-22-K-S, Bronkhorst High-Tech B.V., Ruurlo, Netherlands) mass flow controllers were used (flow ranging from 0.1 to 200g h-1, flow rate accuracy: ± 0.2 %). The temperature was adjusted using a Huber Unistat 390w chiller, enabling a temperature range of -90 °C to 200 °C (Huber Kältemaschinenbau GmbH, Offenburg, Germany), equipped with the following modules: CPU 1212C, 2x SM 1231 AI, CM 1241, RS232, CM 1243-5 Profibus-DP, CSM 1277 Network switch, SM 1207 power supply.

Measurements

NMR spectroscopy. ^{1}H NMR spectra were recorded on a Bruker Avance III HD 300 (5 mm BBFO-SmartProbe with z-gradient and ATM) at 300 MHz, 100 MHz, inverse gated ^{13}C NMR spectra were recorded on a Bruker Avance II HD 400 (5 mm BBFO-SmartProbe with z-gradient and ATM) at 100 MHz. The residual signals of the deuterated solvent were utilized as an internal reference.

Size-exclusion chromatography. SEC measurements in DMF (containing 0.25 g L^{-1} of lithium bromide) were performed using an integrated Agilent 1100 series instrument, equipped with a PSS HEMA column combination ($10^6/10^4/10^2$ Å porosity), UV and RI detector. Calibration is based on linear poly(ethylene oxide) standards (Polymer Standards Service).

SEC with integrated viscosity measurements were performed in DMF (containing 5 g L^{-1} lithium bromide) employing a PSS GRAM column combination (10/300/300 Å porosity), an Agilent MDS refractive index detector and an Agilent MDS viscometer. The calibration is based on linear poly (methyl methacrylate) standards (Polymer Standards Service), molar mass averages were calculated *via* universal calibration.

Hydrodynamic Characterization. Molecular density measurements, basic hydrodynamic characterization in terms of viscosity and sedimentation velocity experiments in analytical ultracentrifugation (AUC) in the solvent water, were performed similar as those described recently.[28,29]

Sedimentation velocity experiment. Sedimentation velocity experiments were performed using a ProteomeLab XL-I analytical ultracentrifuge (Beckman Coulter Instruments, Brea, CA) with an An-50 Ti eight-hole rotor. The cells were equipped with double-sector epon centerpieces with a 12 mm optical path length and filled with 420 µL of the sample in water and with 440 µL of water as the reference. Interference optics detection was used for observation of the sedimentation boundary in respect to time. For all samples, sedimentation velocity experiments were performed with solution concentrations in a range of $0.05 \leq c \leq 0.5\ wt\%$. A rotor speed of 42 000 rpm for up to 24 h and at a temperature of $T = 20\ °C$ was used for experiments. Scans were acquired at five min intervals. A suitable selection of scans was used for data evaluation with Sedfit by numerical solution of the Lamm equation.[30] Differential distributions of sedimentation coefficients and the dependence of inverse sedimentation coefficients against concentration according to the Gralen relation are shown in Figure S 16 and Figure S 17.

Densimetry. The partial specific volume, υ, of each individual hyperbranched macromolecule sample in aqueous solution was determined with a DMA4100 density meter (Anton Paar, Graz, Austria) at $T = 20\,°C$.[29] This allowed for the determination of the partial specific volume, υ, of the samples. The density measurements were performed in a concentration range of $0.1 \leq c \leq 1.4\,wt\%$. Partial specific volumes are displayed in Table S 3.

Viscometry. The relative viscosities of macromolecule solutions, η_r, were determined with an Automated Micro Viscometer (AMVn, Anton Paar, Graz, Austria) at $T = 20\,°C$ *via* a capillary / ball combination and the subsequent determination of the ball times in solvent, t_0, and macromolecule solutions of specific concentrations, t_c.[29] A tilting angle of the capillary of 50° was used for the measurements. The macromolecule solution concentrations, c, were adjusted such that relative viscosities of $\eta_r = t_c/t_0 = 1.2 - 2.5$ were obtained. Extrapolation of linear fits *via* both the Huggins- and Kraemer relations to zero concentration, enabled estimation of the intrinsic viscosity, $[\eta]$ (Figure S 18).

Polymer Synthesis

A detailed overview of the total amount of reagents for each synthesis is presented in the Supporting Information (Table S 1 and Table S 2).

Initiator preparation. The procedure was carried out inside a glove box under dry argon atmosphere. In a glass flask with a screw cap and tube connection, 1 eq. TMP was dissolved in 120 mL NMP. The initiator was partially deprotonated by addition of 0.3 eq. DPMK. Subsequently, the flask was sealed and removed from

the glove box. The solution was homogenized by ultrasonification and transferred to the autoclave *via* a tube under reduced pressure.

Copolymerization of EO/AGE and Glycidol. A solution of glycidol in NMP was transferred to a pressure-resistant glass flask with a screw cap and tube connection. For the synthesis of the hyperbranched terpolymer a mixture of glycidol and AGE was diluted with NMP. The flask was connected to one of the mass flow controllers. The other mass flow controller was connected to a pressure burette containing EO. After heating the initiator solution to 100 °C and applying excess argon pressure of 0.5 bar (1 bar for *hb*PEO_{105} and *hb*PEO_{165}), the slow addition of the glycidol/NMP or glycidol/AGE/NMP mixture and EO at a respective rate of 0.5 g h^{-1} was started. The total addition time, hence total amount of monomers added was adjusted *via* the automated control unit according to the desired molar mass resulting from the monomer-to-initiator ratio. After addition was completed, the autoclave was kept at 100 °C for one hour and then cooled to room temperature. Excess pressure was released through a washing bottle containing a concentrated potassium hydroxide solution in isopropyl alcohol to eliminate residual EO. The polymerization was terminated using a mixture of acetic acid/ethanol. The reaction mixture was transferred to a flask, and solvents were removed by distillation in vacuum. The crude polymers were purified by twofold precipitation in cold diethyl ether and subsequent dialysis against MeOH (MWCO = 1000 g mol^{-1}) to yield *hb*PEO as a brown, viscous oil.

^{1}H NMR (DMSO-d_6, 300 MHz): δ (ppm) = [5.93 – 5.80 (m, CH_2-C<u>H</u>=CH_2), 5.27 – 5.21 (d, -CH=C<u>H</u>$_a$H$_b$), 5.15 – 5.11 (d, -CH=CH$_a$<u>H</u>$_b$)] 4.76 – 4.35 (m, br, -O<u>H</u>), [3.95 – 3.93 (d, -O-C<u>H</u>$_2$-CH=)], 3.90 – 3.15 (m, O-C<u>H</u>-, O-C<u>H</u>$_2$-, polyether backbone), 1.36 – 1.18 (m, 2H, -C<u>H</u>$_2$-CH_3 (TMP)), 0.87 – 0.75 (m, 3H, -C<u>H</u>$_3$ (TMP)).

^{13}C NMR (DMSO-d_6, 100 MHz): δ (ppm) = [135.79 – 135.66 (d, -CH_2-$\underline{C}$H=CH_2), 116.66 (s, =$\underline{C}H_2$)] 80.25 – 79.45 ($L_{1,3G}$), 78.52 – 77.42 (D_G), 73.22 – 72.10 ($L_{1,4G}$), [71.69 – 70.91 (m, -O-$\underline{C}H_2$-CH=CH_2 L_{AGE}, T_{AGE})], 72.04 – 69.62 (D_G, L_{EO}, T_{EO}, 2 T_G), 69.61 – 68.37 ($L_{1,3G}$, $L_{1,4G}$), 63.39 – 62.96 (T_G), 60.87 – 60.07 (T_{EO}, $L_{1,3G}$).

Results and Discussion

To prevent side reactions yielding well-defined copolymers derived from hyperbranched polyglycerol, it is necessary to keep the concentration of glycidol low during the entire polymerization by slowly the adding monomers. However, copolymerization of EO with glycidol *via* SMA is synthetically challenging due to vastly different boiling points of the monomers and the inertia of glycidol at low temperatures on the other hand. Therefore, a safe and controlled addition of the monomers poses the main challenge. While the slow monomer addition of glycidol is easily accomplished and already established using common lab glassware, a pressure resistant and fully automated setup is required to continuously add EO in the liquid state and a mixture of glycidol and NMP to a solution of the partially deprotonated initiator in NMP heated to 100 °C. Using a mass flow controller, an addition rate of as slow as 0.5 g h^{-1} could be realized to ensure a low monomer concentration in the reaction mixture.

By systematically altering the total addition time, also varying the monomer to initiator ratio, a series of polymers with target molar masses ranging from 1400 to 6800 g mol^{-1} and targeted glycidol contents of roughly 0.25 were prepared in quantitative yields. Table 1 summarizes the SEC data for these copolymers.

Table 1. Molar masses determined by different SEC experiments.

Sample[a)]	$M_{n,theo}$ [g mol^{-1}]	M_n[c)] [g mol^{-1}]	M_w / M_n[c)]	M_n[d)] [g mol^{-1}]	M_w / M_n[d)]
*hb*PEO$_{25}$	1400	900	1.23	970	2.40
*hb*PEO$_{83}$	2700	3000	1.23	5200	1.52
*hb*PEO$_{105}$	5200	3600	1.37	7800	1.61
*hb*PEO$_{165}$	6800	4100	1.54	9600	1.96
*hb*PEO$_{Macro}$[b)]	40 000	16 000	1.46	36700	1.91

[a)]Terminology: indices denote the overall degree of polymerization, determined using ^{1}H NMR spectroscopy, [b)]prepared using *hb*PEO$_{165}$ as macroinitiator, [c)]determined using SEC (DMF, 70 °C, linear PEO standard), [d)]values determined by universally calibrated SEC (DMF, 70 °C, linear PMMA standards).

Figure 1 shows the SEC traces for several hyperbranched poly(ethylene oxide) copolymers prepared by slow monomer addition. The SEC traces are shifted to lower elution volume with increasing monomer addition time, corresponding to a higher degree of polymerization. The molar mass averages are in good agreement with the target values calculated from the total addition time. However, with increasing degree of polymerization, the observed molar masses deviate significantly from the target values. These discrepancies are easily explained, since linear PEO standards were employed to estimate molar masses. Hyperbranched polymers typically are expected more compact than linear polymers with comparable molar mass.

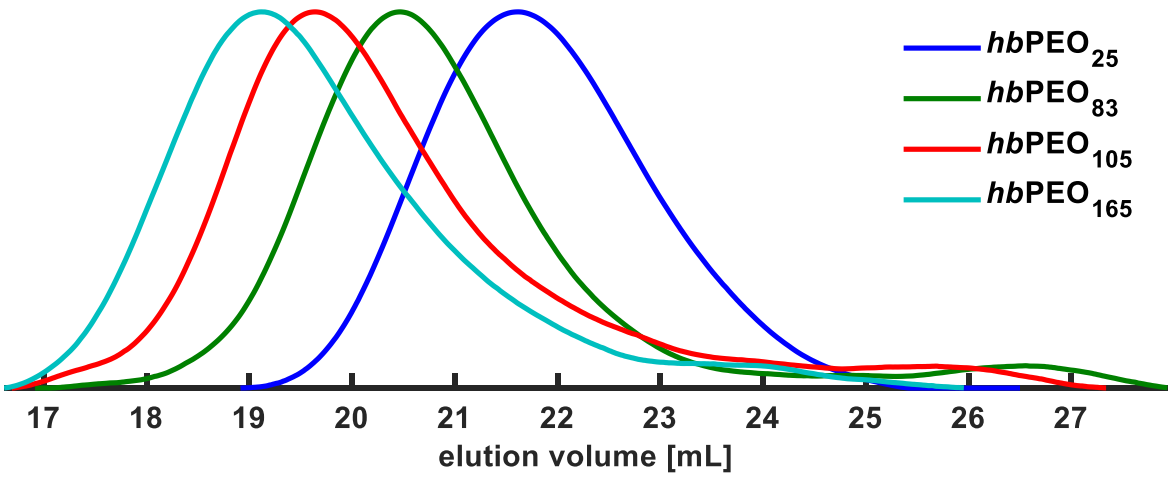

Figure 1. SEC traces of various hyperbranched poly(ethylene oxide) copolymers prepared by slow monomer addition (DMF, after workup by precipitation in diethyl ether and subsequent dialysis (MeOH, MWCO = 1000 g mol^{-1})).

To overcome these shortcomings of standard SEC measurements and to assess the true molar mass values, absolute molar mass values were determined by universal calibration utilizing SEC and subsequent online-viscometry measurements. Due to different means of workup prior to analysis, absolute values are either slightly above or slightly below the target values: in the case of *hb*PEO$_{83}$ – *hb*PEO$_{165}$, low molar mass byproducts were removed by dialysis, whereas in the case of *hb*PEO$_{25}$ workup by dialysis was not feasible due to the compact structure of the polymer, thus this polymer was purified solely by precipitation in diethyl ether. Hence, low molar mass byproducts result in a significantly lower number average molar mass. Considering these findings, the differences between absolute molar masses for *hb*PEO$_{83}$, *hb*PEO$_{105}$ and *hb*PEO$_{165}$ still exactly mirror the intervals provided by the target values. It should be noted, that despite adding the monomers slowly over an extended period of time, there is still a slight low molar mass tailing most likely due to an addition rate of the monomers faster than their consumption resulting in an accumulation of the monomers in the reaction mixture.

This argumentation was suggested by *in situ* IR monitoring of the reaction mixture evaluating the occurrence of an epoxide stretching vibration. However, due to technical limitations, an addition rate slower than 0.5 g h^{-1} could not be realized.

In addition to the analysis by universal calibration, molar masses were determined by analytical ultracentrifugation (AUC), aiming to confirm the controlled character of the synthetic method. Molar masses were calculated from sedimentation-diffusion analysis on sedimentation velocity data and the modified Svedberg equation, i.e. were calculated based on intrinsic sedimentation coefficients and translational frictional ratios (see supporting information, equation S 4).[28,29] Such estimated molar masses appear close to expectations (Table S 3). Notably, however, most of the polymers show a unimodal differential distribution of sedimentation coefficients, in instances fronting toward smaller values of *s* (Figure S 16). The largest molar mass polymer shows a relatively wide distribution of sedimentation coefficients, representative of significant dispersity (Figure S 16). Interestingly, and despite the variation of molar masses as calculated from ultracentrifugation data, the intrinsic viscosity, [*η*], remained largely invariant, hydrodynamically being indicative of the globular and compact shape of the macromolecules.[16]

In analogy to reports by Wilms *et al.*, the products were isolated and used again in SMA as macroinitiator for the synthesis of higher molar mass polymers, as this approach was promising to keep the reaction time sufficiently short and the overall concentration of reactive sites in the growing polymers high.[26] The corresponding SEC trace in DMF (Figure 2) is clearly shifted towards smaller elution volume in comparison to the precursor *hb*PEO_{165} while maintaining a narrow molecular weight distribution. The high molar mass of *hb*PEO_{Macro} results in an even higher

discrepancy of the molar mass determined by SEC from the target values as discussed above. The molar mass of this polymer was determined to be either 36700 g mol^{-1} (universal calibration) or 43900 g mol^{-1} (AUC), thus matching the target value with a slight deviation.

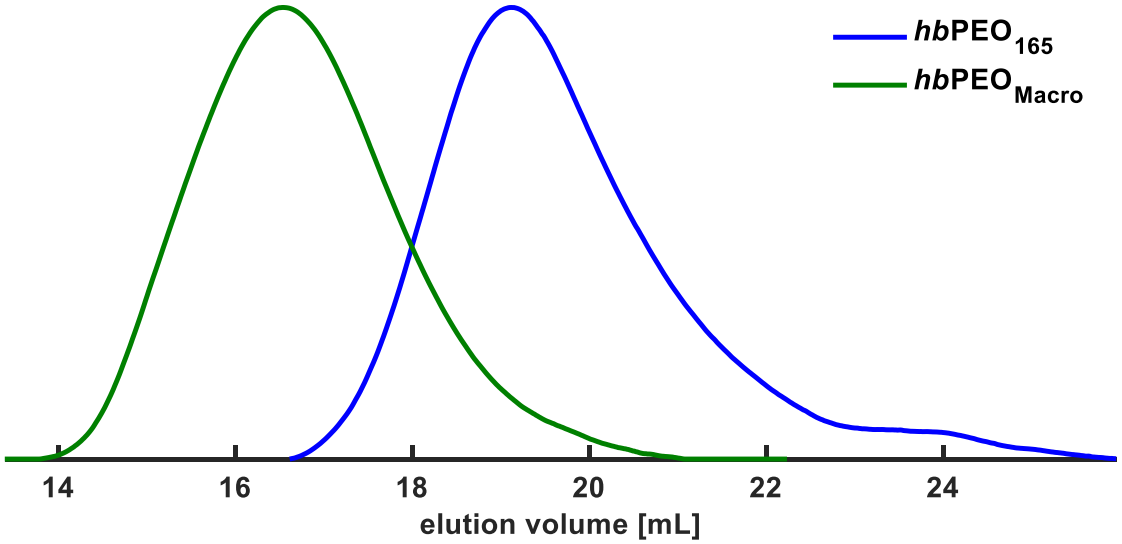

Figure 2. SEC trace of *hb*PEO$_{Macro}$ in comparison to *hb*PEO$_{165}$ (DMF, after workup by dialysis (MeOH, MWCO = 1000 g mol^{-1}).

As SMA ensures initiation exclusively by the initiator TMP ^{1}H NMR spectra measurements can be utilized to determine molar mass averages as well as copolymer compositions of *hb*PEO$_{26}$ – *hb*PEO$_{165}$ and *hb*PEO$_{Macro}$, in contrast to the previously described batch procedure. The respective ^{1}H NMR spectra are found in the supporting information. Owing to an unsatisfactory signal-to-noise ratio in the case of the high molar mass copolymer *hb*PEO$_{Macro}$, no quantitative evaluation of the corresponding ^{1}H NMR spectrum was performed.

Table 2. Molar mass, copolymer composition and degree of branching determined using ^{1}H and ^{13}C NMR spectra.

Sample[a)]	$M_{n,theo}$ [g mol^{-1}]	M_n[b)] [g mol^{-1}]	n_{EO}[b)]	n_G[b)]	$X_{G,theo}$	X_G[b)]	X_G[c)]	DB[c)]	DB_{theo}[d)]
*hb*PEO$_{25}$	1400	1500	19	6	0.23	0.24	0.27	0.28	0.35
*hb*PEO$_{83}$	2700	4400	62	21	0.23	0.25	0.28	0.33	0.36
*hb*PEO$_{105}$	5200	5800	72	33	0.23	0.31	0.37	0.46	0.43
*hb*PEO$_{165}$	6800	8900	114	51	0.27	0.31	0.36	0.47	0.47
*hb*PEO$_{Ma}$	40000	-[e)]	-[e)]	-[e)]	0.24	-[e)]	0.28	0.34	0.36

[a)]Terminology: indices denote the overall degree of polymerization, determined using ^{1}H NMR spectroscopy, [b)]determined using ^{1}H NMR spectroscopy, [c)]determined using inverse gated ^{13}C NMR spectroscopy, [d)]theoretical degree of branching calculated according to literature using the actual glycidol content determined using ^{13}C NMR spectroscopy,[31] [e)]no ^{1}H NMR data available due to an unfavorable signal-to-noise ratio, hence alternative terminology reflecting the utilization of a macroinitiator.

By utilizing the signals of the initiator TMP as a reference the average number of glycidol and ethylene oxide repeating units n_x can be calculated based on the intensity of the signal belonging to the hydroxy group and the polyether backbone. The corresponding equations are presented in detail in the supporting information. The average molar masses can be derived from the total number of repeating units according to equation 1:

$$M_{n,\,hbPEO} = M_{TMP} + 74.1\ g\ mol^{-1} \cdot n_G + 44.1\ g\ mol^{-1} \cdot n_{EO} \qquad 1$$

Such calculated molar masses range from 1500 to 8900 g mol^{-1} for the samples *hb*PEO$_{25}$ - *hb*PEO$_{165}$. Owing to the workup by dialysis, thus removing small molar

mass byproducts, these values are slightly higher than the target molar masses, reiterating the findings of the determination of the molar masses by universal calibration. However, considering the previously mentioned removal of high molar mass compounds, the molar mass of *hb*PEO_{25} should be significantly smaller than the target value. The average amount of glycidol units incorporated into the polymer X_G can be calculated employing equation 2 using the previously determined total number of repeating units n_x:

$$X_G = \frac{n_G}{n_G + n_{EO}} \qquad 2$$

Table 2 summarizes the copolymer compositions as well as molar masses derived from ^{1}H NMR spectroscopy.

In addition to ^{1}H NMR spectroscopy, copolymer compositions were also determined from inverse gated ^{13}C NMR spectroscopy according to equation (3) using the relative amounts of the individual dendritic, linear, and terminal repeating units D, L and G. The ^{13}C NMR spectra are included in the supporting information. The respective repeating units were assigned according to literature.[8]

$$X_G = \frac{D_G + L_{1,3G} + L_{1,4G} + T_G}{D_G + L_{1,3G} + L_{1,4G} + T_G + T_{EO} + L_{EO}} \qquad 3$$

The resulting values as presented in Table 2 are 3 - 6% higher than the corresponding ratio determined according to equation 2. This deviation can be attributed to a worse signal-to-noise-ratio of ^{13}C NMR spectra in comparison to ^{1}H NMR spectra as well as overlapping signals resulting in higher uncertainties of the determined integrals. Except for *hb*PEO_{25}, the glycidol contents are slightly higher than the target ratios. To ensure higher reaction rates by increasing the solubility of the gaseous ethylene oxide during the preparation of *hb*PEO_{105} and *hb*PEO_{165}

the polymerization was performed applying an argon pressure of 1 bar. However, due to the increased pressure in the reaction vessel, ethylene oxide condensed inside the addition tubes, therefore leading to incomplete addition of ethylene oxide, ultimately leading to an increased amount of glycidol incorporated into the polymer. To circumvent condensation of the gaseous comonomer, the following polymerizations were carried out applying a pressure of 0.5 bar, resulting in a smaller deviation from the target comonomer ratio.

The degree of branching is a key parameter to describe polymers with a branched structure. It can assume values ranging from 0 describing linear polymers and 1 for perfectly branched dendrimers. The degree of branching can be determined from IG ^{13}C NMR spectroscopy according to literature.[8,31]

$$DB = \frac{2\,D}{2\,D + L} \qquad 4.1$$

$$DB = \frac{2\,D_G}{2\,D_G + L_{1,3G} + L_{1,4G} + L_{EO}} \qquad 4.2$$

Overall, the degrees of branching determined from ^{13}C NMR spectroscopy are in good agreement with the theoretical values calculated according to literature using the actual glycidol content presented in Table 2**.**[17]

As presented by Leibig *et al.* extensive *in situ* NMR copolymerization kinetical studies of glycidol with ethylene oxide suggest a higher reactivity of glycidol due to intramolecular activation of the strained epoxide ring. When conducted in batch, this leads to a slightly faster incorporation of glycidol into the polymer backbone resulting in a slight gradient. Due to autoinitiation processes prevalent for glycidol, new chains are started at various reaction times. This ultimately leads to a compositional drift of polymers with different molar masses. Therefore, the glycidol

content of the product is non-uniform, polymers with higher molar masses also feature a higher amount of glycidol, whereas polymers, which were initiated during later stages of the polymerization, contain less glycidol due the diverging reactivity of the monomers. Under the assumption that the monomers react faster than they are added to the reaction vessel, all polymers should feature the same composition, regardless of molar mass.

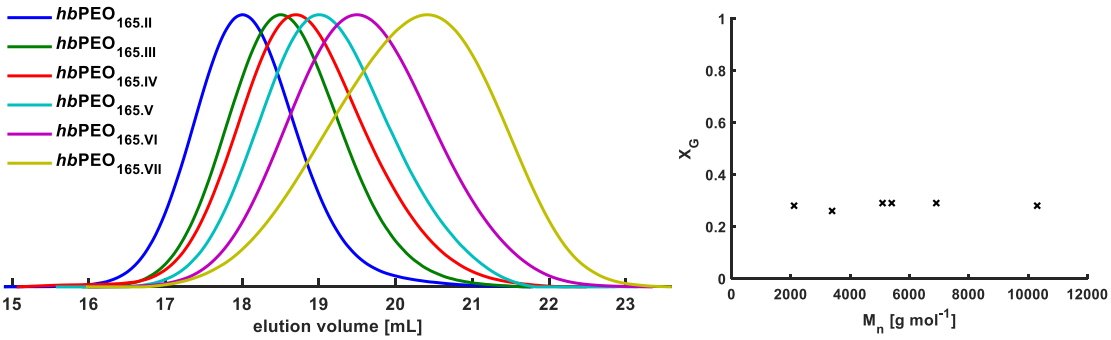

Figure 4. SEC traces of *hb*PEO$_{165}$ after separation by preparative size exclusion chromatography (DMF, linear PEO standards) (left), glycidol content of each fraction *hb*PEO$_{165.II}$ – *hb*PEO$_{165,VII}$ versus the respective molar mass as calculated using ^{1}H NMR spectroscopy (right).

To investigate this assumption, *hb*PEO$_{165}$, a hyperbranched poly(ethylene oxide) copolymer with an overall glycidol fraction of around 0.31, was separated into six fractions using preparative size exclusion chromatography. Figure 4 shows the corresponding SEC traces after fractionation. Table 3 summarizes the data of the fractions obtained by SEC and ^{1}H NMR analysis: the copolymer compositions as determined by ^{1}H NMR spectroscopy range from 0.26 to 0.29 as opposed to 0.31 prior to fractionation. However, no clear trend with varying molar mass, i.e. lower glycidol content the lower the molar mass is, can be observed. Therefore, no compositional drift occurs during the preparation of *hb*PEO copolymers by SMA as

opposed to the previously reported batch procedure, which leads to gradient copolymers of glycidol and ethylene oxide as well as other alkylene oxides.[32] This finding unambiguously proves the well-defined character of the *hb*PEO copolymers synthesized by this method.

Table 3. SEC and ^{1}H NMR data of the samples obtained after fractionation of *hb*PEO_{165} by preparative SEC.

Fraction	M_n[a)] [g mol^{-1}]	M_w / M_n[a)]	M_n[b)] [g mol^{-1}]	X_G[b)]
II	5900	1.13	10300	0.28
III	4600	1.13	6900	0.29
IV	4100	1.17	5400	0.29
V	3600	1.16	5100	0.29
VI	2900	1.18	3400	0.26
VII	2200	1.23	2100	0.28

[a)]Determined from SEC (DMF, linear PEO standard), [b)]determined from ^{1}H NMR spectroscopy.

Creating the basis for the synthesis of well-defined hyperbranched copolymers of ethylene oxide and glycidol the synthetic protocol discussed above may be transferred to the synthesis of hyperbranched terpolymers to introduce new functionalities by the addition of functional epoxide comonomers, which are stable under the applied reaction conditions. Allyl glycidyl ether (AGE) carries an orthogonally addressable double bond, which is stable under basic conditions, rendering this functional glycidyl ether an exceptionally adequate comonomer for

the copolymerization with glycidol and ethylene oxide. The preparation of such a terpolymer comprised of glycidol, ethylene oxide and allyl glycidyl ether was conducted in analogy to synthesis of *hb*PEO copolymers *via* slow monomer addition with the exception of using a glycidol/AGE/NMP mixture instead of a solution of glycidol in NMP. Table 4 shows the NMR and SEC data of two hyperbranched terpolymers composed of ethylene oxide, glycidol and allyl glycidyl ether with target molar masses of 3200 and 6400 g mol^{-1}, respectively, as well as a copolymer composition of EO/glycidol/AGE of 67/23/10.

Table 4. NMR data for two hyperbranched terpolymers comprised of glycidol, ethylene oxide and allyl glycidyl ether.

Sample[a)]	**M_n**[b)] **[g mol^{-1}]**	**M_w/M_n**[b)]	**M_n**[c)] **[g mol^{-1}]**	**X_{AGE}**[c]	**X_G**[c)]	**X_{AGE}**[d)]	**X_G**[d)]	**DB**[d)]	**DB**[e)]
*hb*PEO$_{AGE,72}$	3000	1.28	4400	0.11	0.25	0.18	0.30	0.35	0.36
*hb*PEO$_{AGE,114}$	4100	1.32	6800	0.11	0.24	0.19	0.31	0.35	0.36

[a)]Terminology: indices denote the overall degree of polymerization determined using ^{1}H NMR spectroscopy, [b)]determined using SEC (DMF, linear PEO standard), [c)]determined using ^{1}H NMR spectroscopy, [d)]determined using inverse gated ^{13}C NMR spectroscopy, [e)]theoretical degree of branching calculated according to literature using the actual glycidol content determined from ^{13}C NMR spectroscopy.[31]

The SEC traces as presented in Figure S 15 exhibit monomodal and narrow molecular weight distributions and are shifted towards lower elution volume appropriate to the target molar mass. However, due to the inherent inaccuracy of SEC measurements using linear standards for hyperbranched polymers, the molar mass averages as determined by SEC of 3000 and 4100 g mol^{-1} deviate significantly from the target values. To gain insight into absolute values of the molar

masses as well as the copolymer composition and the degree of branching, ^{1}H and inverse gated ^{13}C NMR spectra were measured. Figure 4 shows an exemplary ^{1}H NMR spectrum of such a hyperbranched terpolymer, the other spectra including the respective ^{13}C date are found in the supporting information (Figure S 12 to Figure S 14).

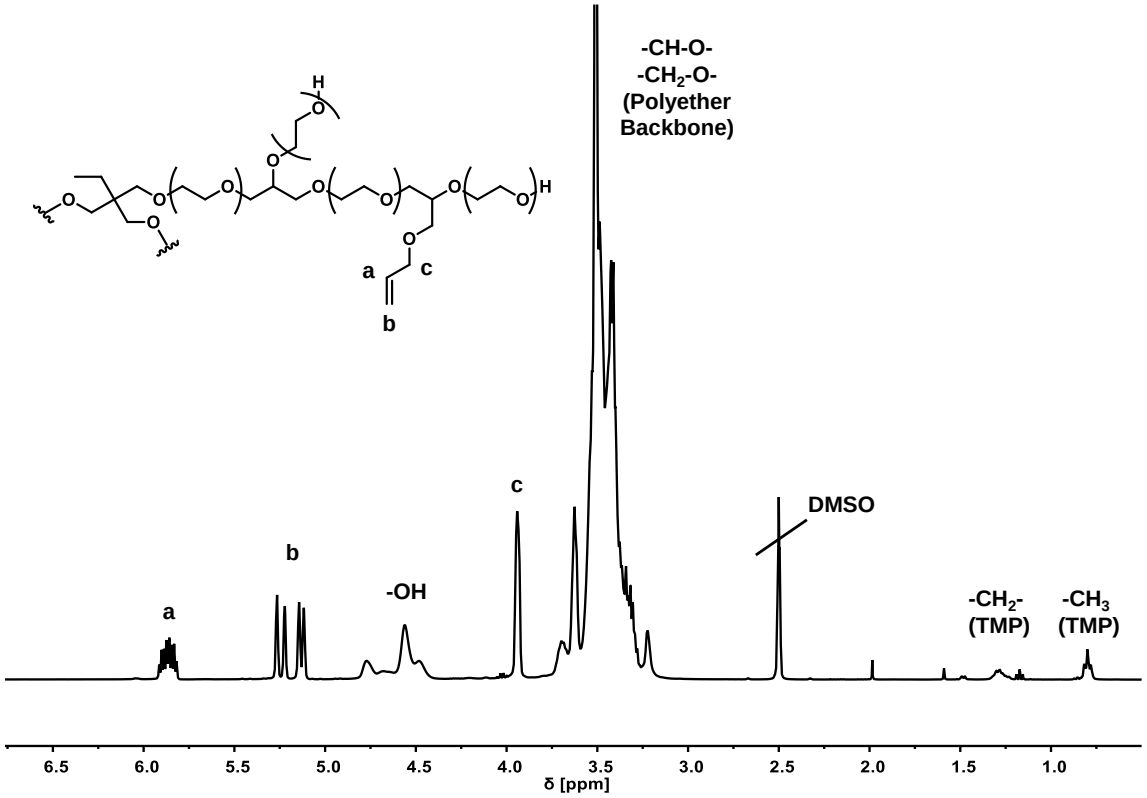

Figure 4. ^{1}H NMR spectrum of *hb*PEO$_{AGE,72}$ (300 MHz, DMSO-d_6).

The olefinic signals of the allyl-bearing comonomer are clearly discernible alongside the broad signals of the polyether backbone and the hydroxy groups. The copolymer composition and molar mass of each polymer can be calculated in analogy to the hyperbranched poly(ethylene oxide) copolymers discussed above by addition of an equation for the total number of AGE repeating units as presented in the supporting information. The results as presented in Table 4 show a slightly higher AGE contents of 0.11 for both terpolymers in comparison to the target

content of 0.10. However, as the glycidol content is also slightly higher than the target these findings are consistent with the previous discussion of the higher glycidol content in hyperbranched poly (ethylene oxide) copolymers: as an argon pressure of 0.5 bar was applied, the addition of EO was incomplete due to the condensation of EO gas in the reactor tubes. The comonomer contents calculated using ^{13}C NMR spectroscopy were found to be 0.18 – 0.19 for AGE and 0.30 – 0.31 glycidol, thus significantly higher than the target values as was the case for the other hyperbranched copolymers presented above. Furthermore, the corresponding degrees of branching of 0.35 are in good agreement with the theoretical ones determined using the actual copolymer composition. However, these results have to be reviewed under reservation, as many signals needed for the calculation overlapped, hence the signal intensities may vary.

Due to the workup by dialysis (MeOH, MWCO = 1000 g mol^{-1}), the molar masses of 4400 and 6800 g mol^{-1} calculated using ^{1}H NMR spectroscopy are slightly higher but overall in good agreement with the target values (3200 and 6400 g mol^{-1}). As discussed thoroughly above, this deviation is higher for the terpolymer with the smaller target molar mass as dialysis has a significant impact on the polymers molecular weight distribution. Nevertheless, the results presented above unambiguously prove the successful preparation of hyperbranched terpolymers *via* SMA and further expand the scope of this synthetic pathway for well-defined hyperbranched polyether polyols.

Conclusion

Five hyperbranched poly(ethylene oxide) copolymers with different molar masses but constant copolymer composition were prepared by anionic ring opening copolymerization of ethylene oxide and glycidol using small molecule initiator (TMP) or a macroinitiator (*hb*PEO_{165}). The control of the degree of polymerization was achieved by slowly adding the monomers to the reaction mixture instead of the batch procedures described in literature. To meet the safety precautions concerning the slow addition of a toxic and explosive monomer to a reaction mixture heated well above its boiling point a fully automated and pressure resistant reactor setup was employed. Molar mass values ranged from 1000 to 37000 g mol^{-1} (determined by universal calibration) or 1500 to 43900 g mol^{-1} (determined by AUC) while maintaining a low dispersity. Furthermore, the intrinsic viscosity, [η], was found to be largely independent from molar mass, indicating a globular and compact shape of the hyperbranched macromolecules. The glycidol content determined *via* ^{1}H and ^{13}C NMR spectra was found to be slightly higher than the comonomer feed suggested due to the incomplete addition of ethylene oxide due to the applied argon pressure. Considering the actual copolymer composition and the retarded ethylene oxide addition, the degrees of branching are in good agreement with the theoretical values confirming the controlled manner of this polymerization technique. By applying slow monomer addition, a compositional drift, as observed for the batch polymerization of glycidol and various alkylene oxides, was eliminated.

The synthetic procedure presented gives access to well-defined hyperbranched poly(ethylene oxide) copolymers with an adjustable degree of polymerization, copolymer composition and amount of end groups. To expand the scope of this

procedure, hyperbranched terpolymers of ethylene oxide, glycidol and allyl glycidyl ether, a base stable functional epoxide monomer, were prepared. Taking control over this new class of hyperbranched poly (ethylene oxide) copolymers can be useful for future biomedical or pharmaceutical applications as the exact knowledge of the polymers size and composition is a prerequisite for the approval.

Acknowledgment

T. K. is grateful for financial support by a fellowship from the “Fonds der Chemischen Industrie (FCI)”. Furthermore, the authors thank Alexander Meier for technical assistance.

References

(1) Herzberger, J.; Niederer, K.; Pohlit, H.; Seiwert, J.; Worm, M.; Wurm, F. R.; Frey, H. Polymerization of Ethylene Oxide, Propylene Oxide, and Other Alkylene Oxides: Synthesis, Novel Polymer Architectures, and Bioconjugation. *Chem. Rev.* **2016**, *116*, 2170–2243.

(2) Dingels, C.; Schömer, M.; Frey, H. Die vielen Gesichter des Poly(ethylenglykol)s. *Chem. Unserer Zeit* **2011**, *45*, 338–349.

(3) Gustin, J.-L. Safety of ethoxylation reactions. *Loss Prevention Bulletin* **2001**, *157*, 11–18.

(4) Vitz, J.; Majdanski, T. C.; Meier, A.; Lutz, P. J.; Schubert, U. S. Polymerization of ethylene oxide under controlled monomer addition via a mass flow controller for tailor made polyethylene oxides. *Polym. Chem.* **2016**, *7*, 4063–4071.

(5) Voit, B. I.; Lederer, A. Hyperbranched and highly branched polymer architectures--synthetic strategies and major characterization aspects. *Chem. Rev.* **2009**, *109*, 5924–5973.

(6) Yan, D.; Gao, C.; Frey, H., Eds. *Hyperbranched polymers: Synthesis, properties, and applications*; Wiley series on polymer engineering and technology; Wiley: Hoboken, N.J, 2011.

(7) Feng, X.-S.; Taton, D.; Chaikof, E. L.; Gnanou, Y. Toward an easy access to dendrimer-like poly(ethylene oxide)s. *J. Am. Chem. Soc.* **2005**, *127*, 10956–10966.

(8) Wilms, D.; Schömer, M.; Wurm, F.; Hermanns, M. I.; Kirkpatrick, C. J.; Frey, H. Hyperbranched PEG by random copolymerization of ethylene oxide and glycidol. *Macromol. Rapid Commun.* **2010**, *31*, 1811–1815.

(9) Schömer, M.; Seiwert, J.; Frey, H. Hyperbranched Poly(propylene oxide): A Multifunctional Backbone-Thermoresponsive Polyether Polyol Copolymer. *ACS Macro Lett.* **2012**, *1*, 888–891.

(10) Seiwert, J.; Leibig, D.; Kemmer-Jonas, U.; Bauer, M.; Perevyazko, I.; Preis, J.; Frey, H. Hyperbranched Polyols via Copolymerization of 1,2-Butylene Oxide and Glycidol: Comparison of Batch Synthesis and Slow Monomer Addition. *Macromolecules* **2016**, *49*, 38–47.

(11) Sandler, S. R.; Berg, F. R. Room temperature polymerization of glycidol. *J. Polym. Sci. Pol. Chem.* **1966**, *4*, 1253–1259.

(12) Tsuruta, T.; Inoue, S.; Koenuma, H. Polymerization of epoxyorganosilanes. *Makromol. Chem.* **1968**, *112*, 58–65.

(13) Vandenberg, E. J. Polymerization of glycidol and its derivatives: A new rearrangement polymerization. *J. Polym. Sci. Polym. Chem. Ed.* **1985**, *23*, 915–949.

(14) Tokar, R.; Kubisa, P.; Penczek, S.; Dworak, A. Cationic polymerization of glycidol: Coexistence of the activated monomer and active chain end mechanism. *Macromolecules* **1994**, *27*, 320–322.

(15) Dworak, A.; Walach, W.; Trzebicka, B. Cationic polymerization of glycidol. Polymer structure and polymerization mechanism. *Macromol. Chem. Phys.* **1995**, *196*, 1963–1970.

(16) Perevyazko, I.; Seiwert, J.; Schömer, M.; Frey, H.; Schubert, U. S.; Pavlov, G. M. Hyperbranched Poly(ethylene glycol) Copolymers: Absolute Values of the Molar Mass, Properties in Dilute Solution, and Hydrodynamic Homology. *Macromolecules* **2015**, *48*, 5887–5898.

(17) Sunder, A.; Türk, H.; Haag, R.; Frey, H. Copolymers of Glycidol and Glycidyl Ethers: Design of Branched Polyether Polyols by Combination of Latent Cyclic AB 2 and ABR Monomers. *Macromolecules* **2000**, *33*, 7682–7692.

(18) Tonhauser, C.; Schüll, C.; Dingels, C.; Frey, H. Branched Acid-Degradable, Biocompatible Polyether Copolymers via Anionic Ring-Opening Polymerization Using an Epoxide Inimer. *ACS Macro Lett.* **2012**, *1*, 1094–1097.

(19) Shenoi, R. A.; Chafeeva, I.; Lai, B. F. L.; Horte, S.; Kizhakkedathu, J. N. Bioreducible hyperbranched polyglycerols with disulfide linkages: Synthesis and biocompatibility evaluation. *J. Polym. Sci. Pol. Chem.* **2015**, *53*, 2104–2115.

(20) Shenoi, R. A.; Narayanannair, J. K.; Hamilton, J. L.; Lai, B. F. L.; Horte, S.; Kainthan, R. K.; Varghese, J. P.; Rajeev, K. G.; Manoharan, M.; Kizhakkedathu, J. N. Branched multifunctional polyether polyketals: variation of ketal group structure enables unprecedented control over polymer degradation in solution and within cells. *J. Am. Chem. Soc.* **2012**, *134*, 14945–14957.

(21) Schüll, C.; Gieshoff, T.; Frey, H. One-step synthesis of multi-alkyne functional hyperbranched polyglycerols by copolymerization of glycidyl propargyl ether and glycidol. *Polym. Chem.* **2013**, *4*, 4730.

(22) Seiwert, J.; Herzberger, J.; Leibig, D.; Frey, H. Thioether-Bearing Hyperbranched Polyether Polyols with Methionine-Like Side-Chains: A Versatile Platform for Orthogonal Functionalization. *Macromol. Rapid Commun.*, *38*.

(23) Son, S.; Shin, E.; Kim, B.-S. Redox-Degradable Biocompatible Hyperbranched Polyglycerols: Synthesis, Copolymerization Kinetics, Degradation, and Biocompatibility. *Macromolecules* **2015**, *48*, 600–609.

(24) Alkan, A.; Klein, R.; Shylin, S. I.; Kemmer-Jonas, U.; Frey, H.; Wurm, F. R. Water-soluble and redox-responsive hyperbranched polyether copolymers based on ferrocenyl glycidyl ether. *Polym. Chem.* **2015**, *6*, 7112–7118.

(25) Niederer, K.; Schüll, C.; Leibig, D.; Johann, T.; Frey, H. Catechol Acetonide Glycidyl Ether (CAGE): A Functional Epoxide Monomer for Linear and Hyperbranched Multi-Catechol Functional Polyether Architectures. *Macromolecules* **2016**, *49*, 1655–1665.

(26) Wilms, D.; Wurm, F.; Nieberle, J.; Böhm, P.; Kemmer-Jonas, U.; Frey, H. Hyperbranched Polyglycerols with Elevated Molecular Weights: A Facile Two-Step Synthesis Protocol Based on Polyglycerol Macroinitiators. *Macromolecules* **2009**, *42*, 3230–3236.

(27) Normant, H.; Angelo, B. Sodation en milieu tétrahydrofuranne par le sodium en présence de naphtalène. *Bull. Soc. Chim. Fr.* **1960**, *2*, 354–359.

(28) Nischang, I.; Perevyazko, I.; Majdanski, T.; Vitz, J.; Festag, G.; Schubert, U. S. Hydrodynamic Analysis Resolves the Pharmaceutically-Relevant Absolute Molar Mass and Solution Properties of Synthetic Poly(ethylene glycol)s Created by Varying Initiation Sites. *Anal. Chem.* **2017**, *89*, 1185–1193.

(29) Grube, M.; Leiske, M. N.; Schubert, U. S.; Nischang, I. POx as an Alternative to PEG? A Hydrodynamic and Light Scattering Study. *Macromolecules* **2018**, *51*, 1905–1916.

(30) Schuck, P. Size-Distribution Analysis of Macromolecules by Sedimentation Velocity Ultracentrifugation and Lamm Equation Modeling. *Biophys. J.* **2000**, *78*, 1606–1619.

(31) Frey, H.; Hölter, D. Degree of branching in hyperbranched polymers. 3 Copolymerization of ABm-monomers with AB and ABn-monomers. *Acta Polym.* **1999**, *50*, 67–76.

(32) Leibig, D.; Seiwert, J.; Liermann, J. C.; Frey, H. Copolymerization Kinetics of Glycidol and Ethylene Oxide, Propylene Oxide, and 1,2-Butylene Oxide: From Hyperbranched to Multiarm Star Topology. *Macromolecules* **2016**, *49*, 7767–7776.

Supporting Information

Reactor Setup

Figure S 1. Photograph of the reactor setup used for the safe addition of ethylene oxide to a preheated reaction mixture.

Polymer Synthesis

Table S 1. Total amounts of reagents used for the synthesis of the hyperbranched poly(ethylene oxide) copolymers *hb*PEO_{25} – *hb*PEO_{Macro}.

Reagent		***hb*PEO$_{25}$**	***hb*PEO$_{83}$**	***hb*PEO$_{105}$**	***hb*PEO$_{165}$**	***hb*PEO$_{Macro}$**
TMP	m [mg]	537	537	268	268	-
	n [mmol]	4	4	2	2	-
hbPEO_{165}	m [mg]	-	-	-	-	1000
	n [mmol]	-	-	-	-	0.1
DPMK	m [mg]	272	272	136	136	120
	n [mmol]	1.32	1.32	0.66	0.66	0.58
Glycidol	m [g]	1.70	3.40	3.40	5.11	1.06
	n [mmol]	23	46	46	69	14
EO	m [g]	3.40	6.79	6.79	10.18 (8.02)	2.11
	n [mmol]	77	154	154	231 (182)	48
NMP	m [g]	1.70	3.40	3.40	5.11	1.06

Table S 2. Total amounts of reagents used for the synthesis of the hyperbranched terpolymers *hb*PEO$_{AGE,72}$ – *hb*PEO$_{AGE,114}$.

Reagent		***hb*PEO$_{AGE,72}$**	***hb*PEO$_{AGE,114}$**
TMP	m [mg]	537	268
	n [mmol]	4	2
DPMK	m [mg]	272	137
	n [mmol]	1.32	0.66
Glycidol	m [g]	3.41	3.41
	n [mmol]	46	46
EO	m [g]	5.90	5.90
	n [mmol]	134	134
AGE	m [g]	2.28	2.28
	n [mmol]	20	20
NMP	m [g]	0.21	0.21

Supplemental NMR Spectra and Data

Calculation of the Average Amount of Each Repeating Unit based on ^{1}H NMR Spectroscopy

$$n_G = I(OH) - 3 \quad \text{S 1}$$

$$n_{EO} = \frac{I(\text{Polyether backbone}) - 5\, n_G - 6}{4} \quad \text{S 2}$$

$$n_{AGE} = I(-CH{=}CH_2) \quad \text{S 3}$$

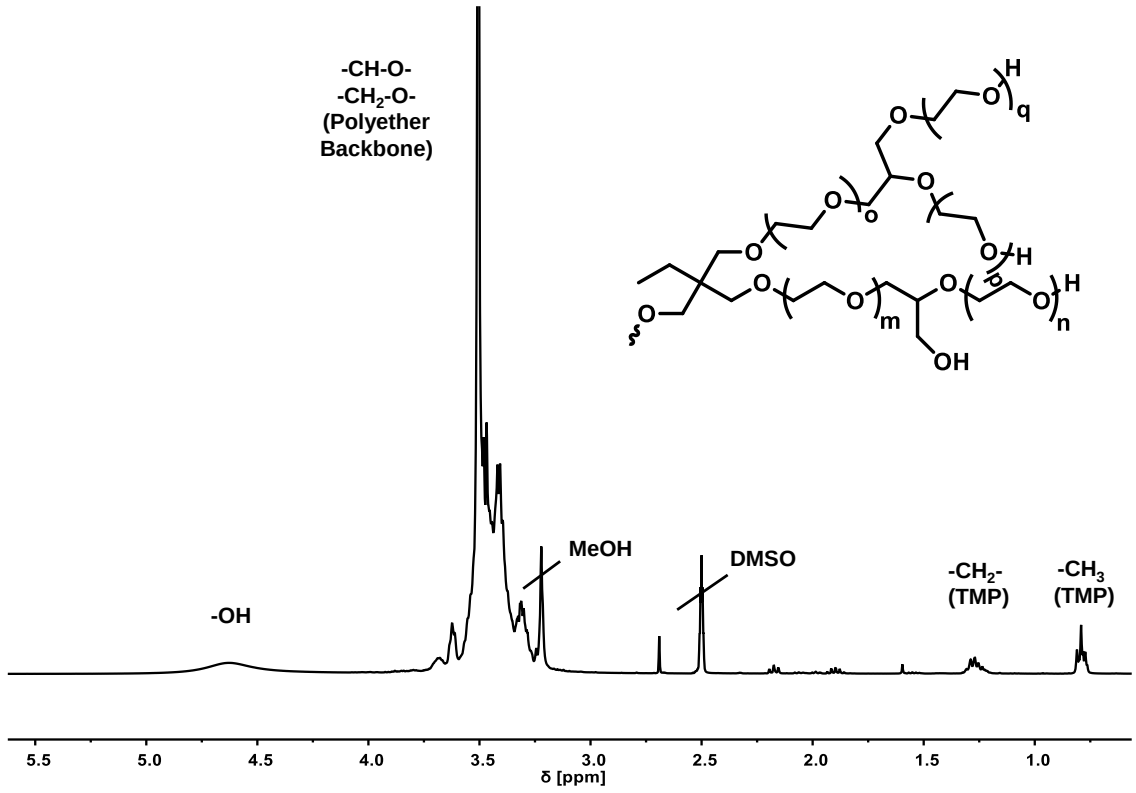

Figure S 2. ^{1}H NMR spectrum of *hb*PEO$_{25}$ (300 MHz, DMSO-d_6).

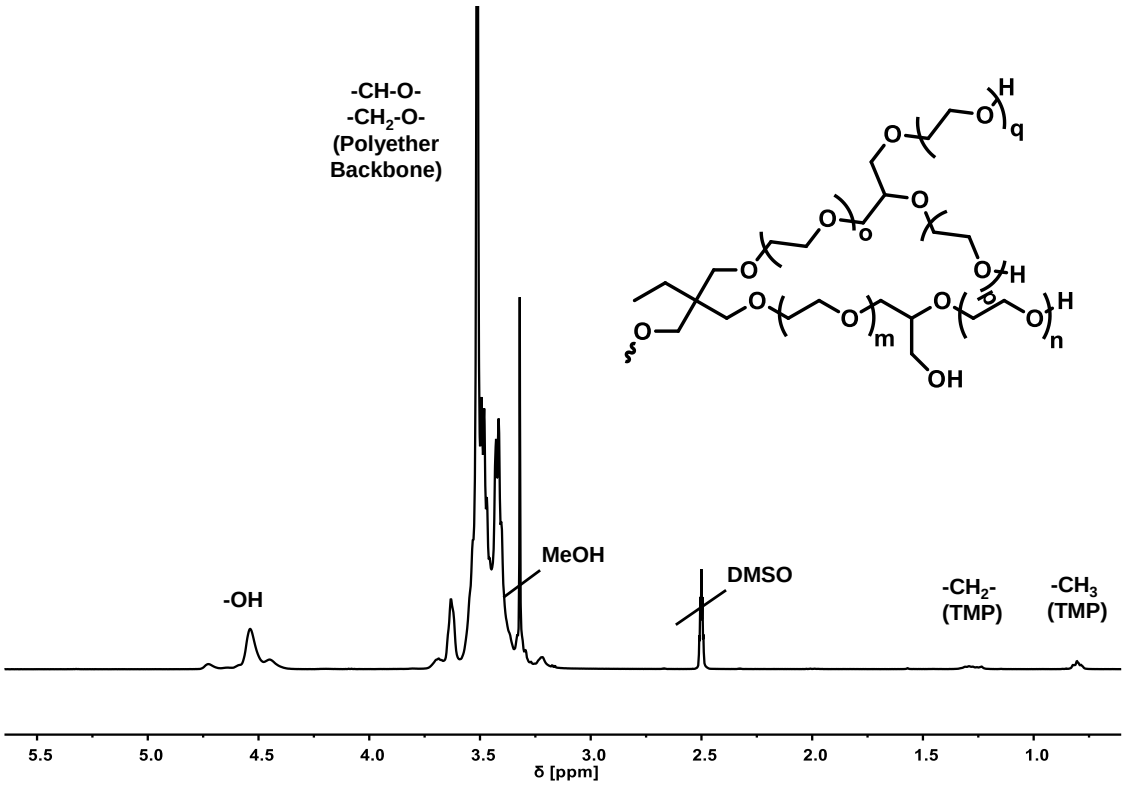

Figure S 3. ^{1}H NMR spectrum of *hb*PEO$_{83}$ (300 MHz, DMSO-d_6).

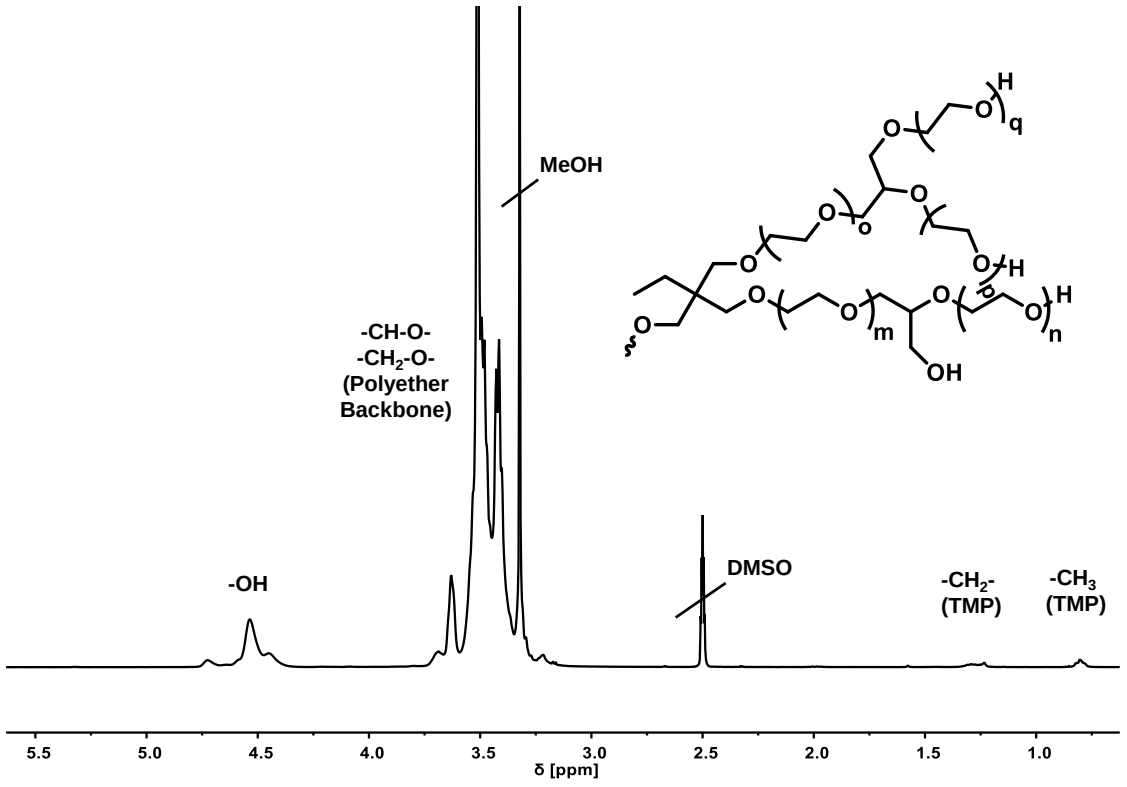

Figure S 4. ^{1}H NMR spectrum of *hb*PEO$_{105}$ (300 MHz, DMSO-d_6).

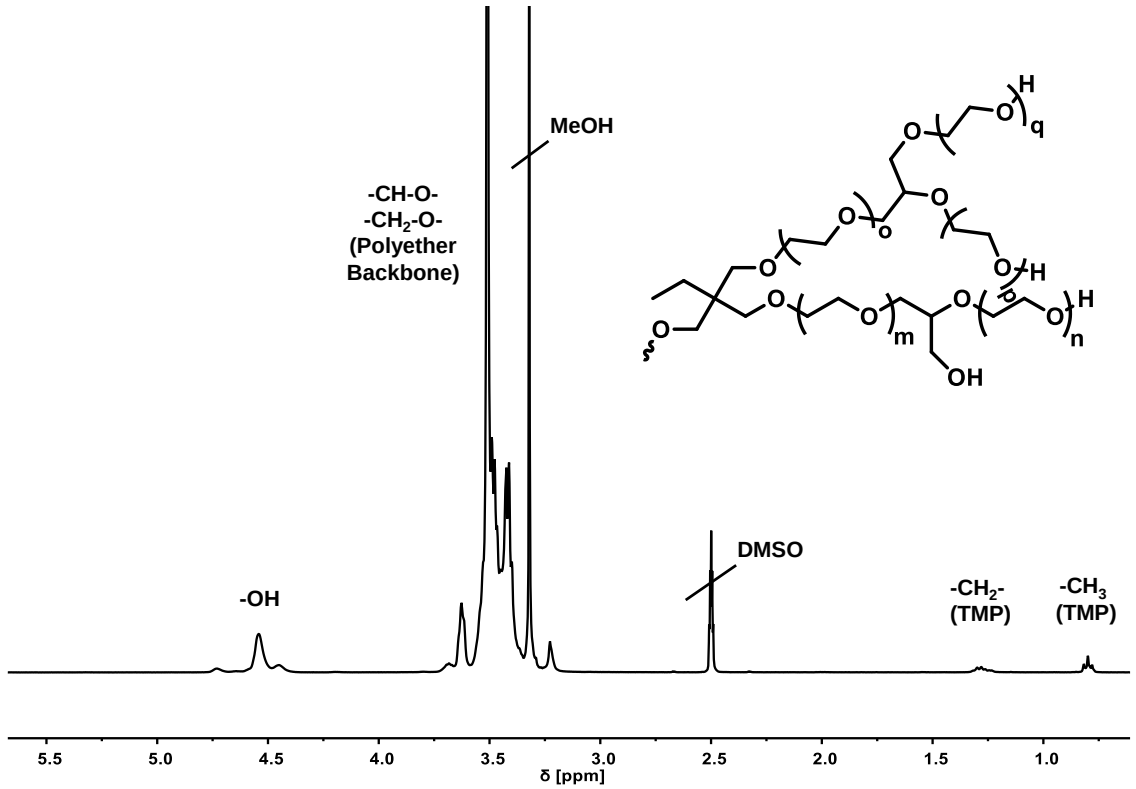

Figure S 5. ^{1}H NMR spectrum of *hb*PEO$_{165}$ (300 MHz, DMSO-d_6).

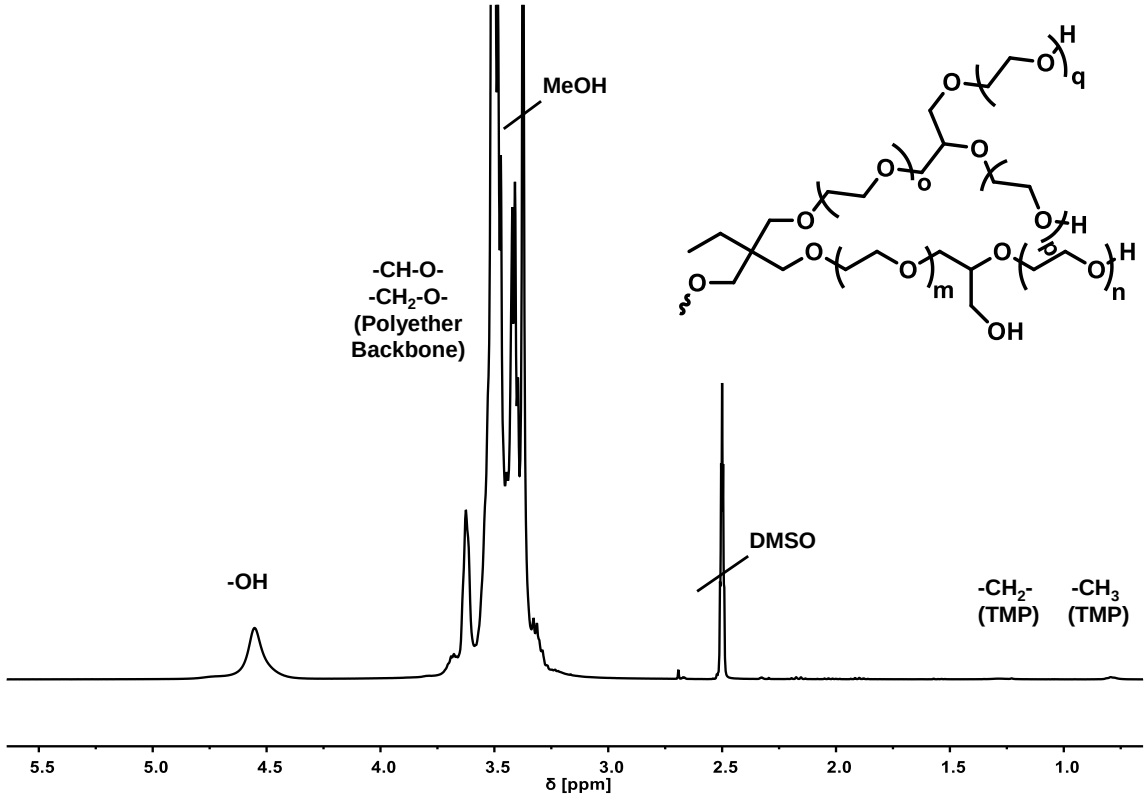

Figure S 6. ^{1}H NMR spectrum of *hb*PEO$_{Macro}$ (300 MHz, DMSO-d_6).

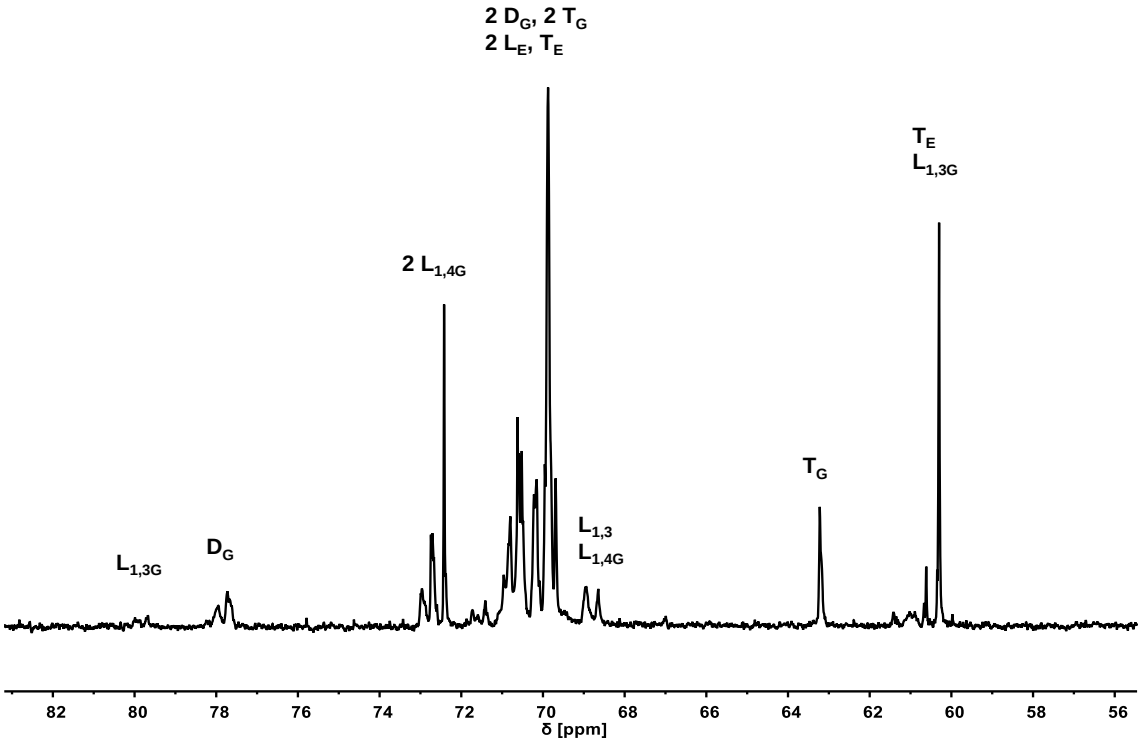

Figure S 7. ^{13}C NMR spectrum of *hb*PEO$_{25}$ (100 MHz, DMSO-d_6).

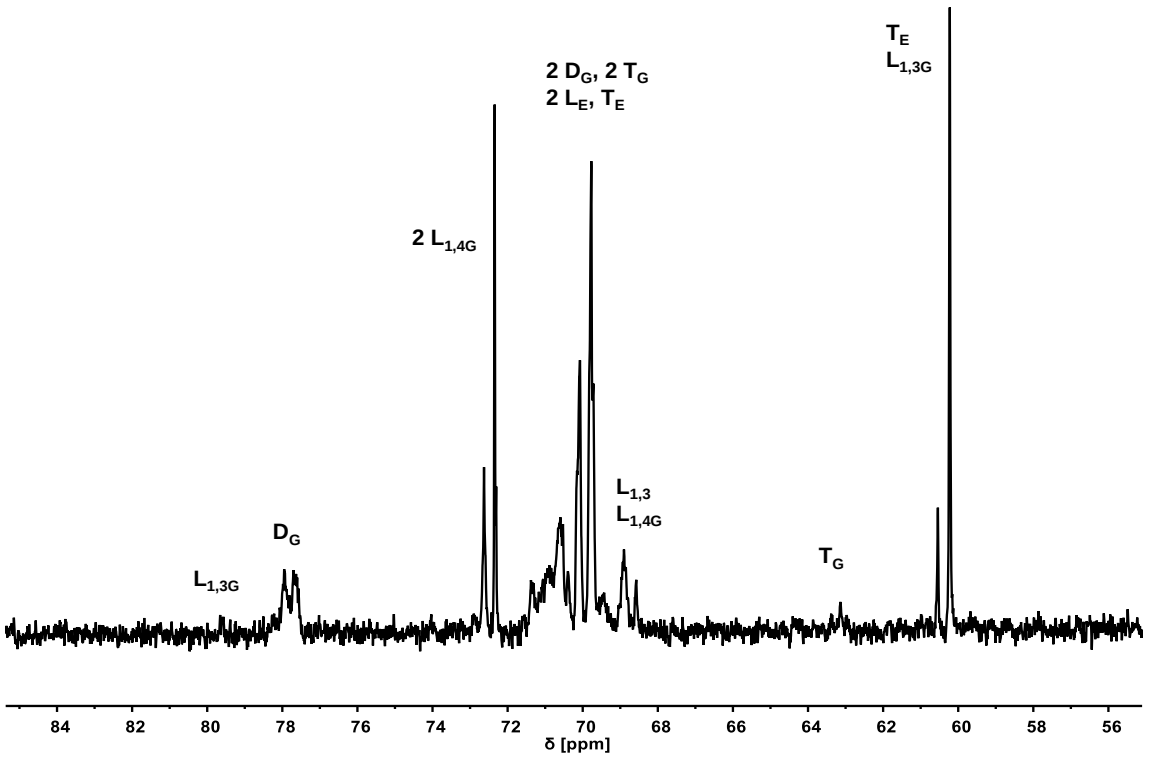

Figure S 8. ^{13}C NMR spectrum of *hb*PEO$_{83}$ (100 MHz, DMSO-d_6).

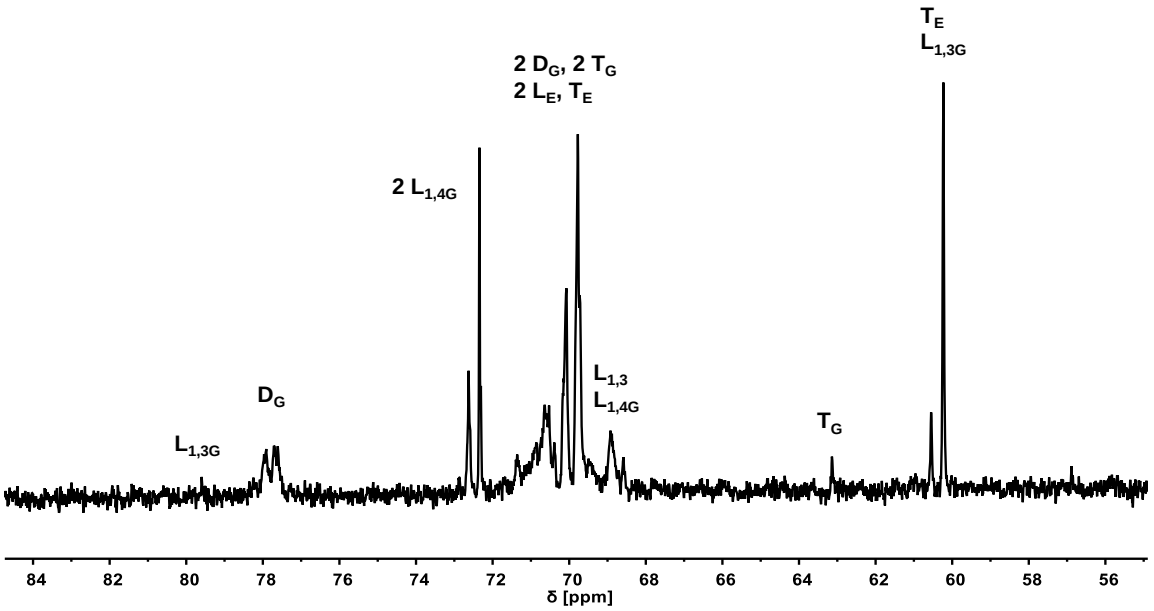

Figure S 9. ^{13}C NMR spectrum of *hb*PEO$_{105}$ (100 MHz, DMSO-d_6).

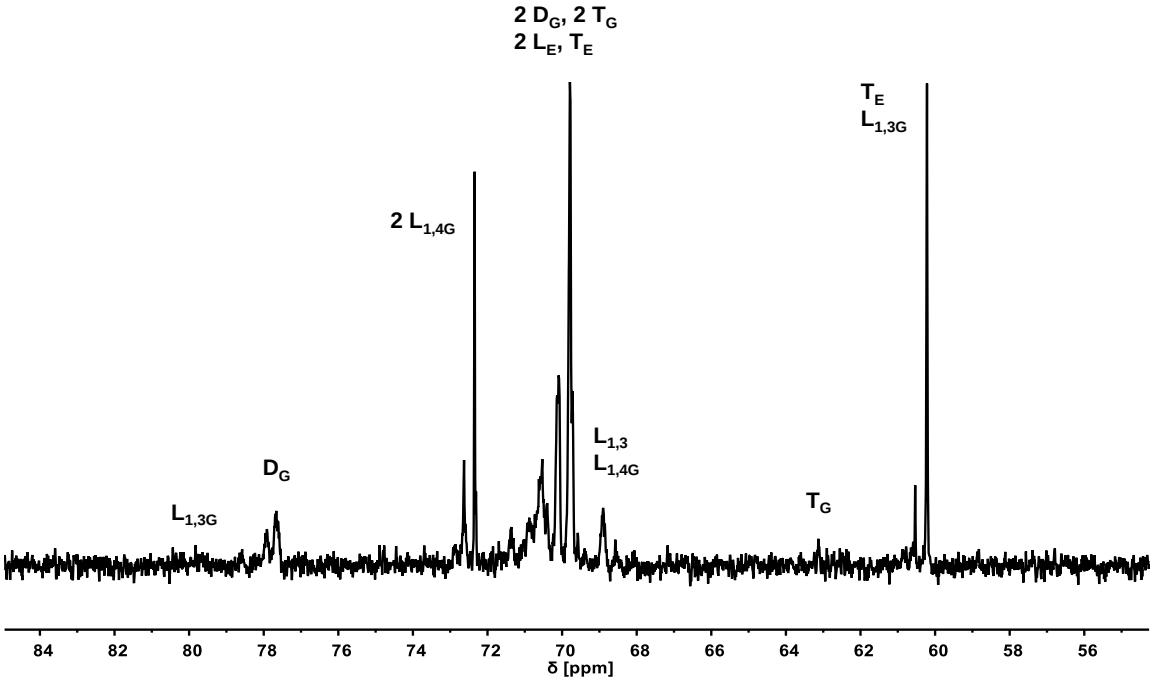

Figure S 10. ^{13}C NMR spectrum of *hb*PEO$_{165}$ (100 MHz, DMSO-d_6).

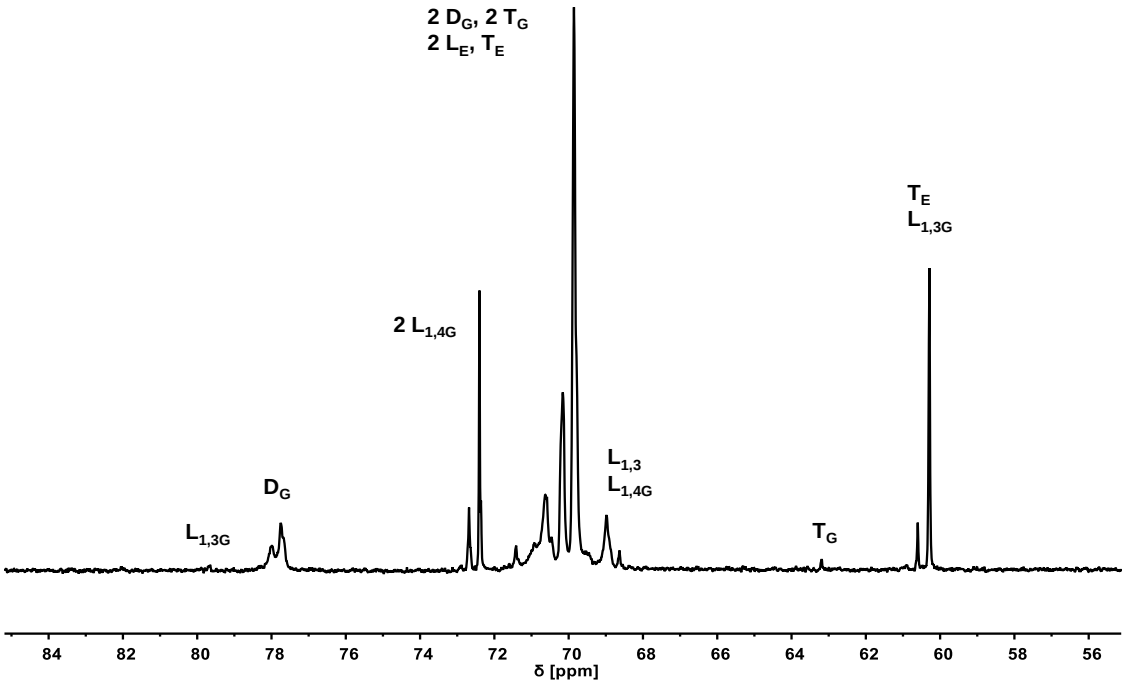

Figure S 11. ^{13}C NMR spectrum of *hb*PEO$_{Macro}$ (100 MHz, DMSO-d_6).

***hb*PEO$_{AGE}$**

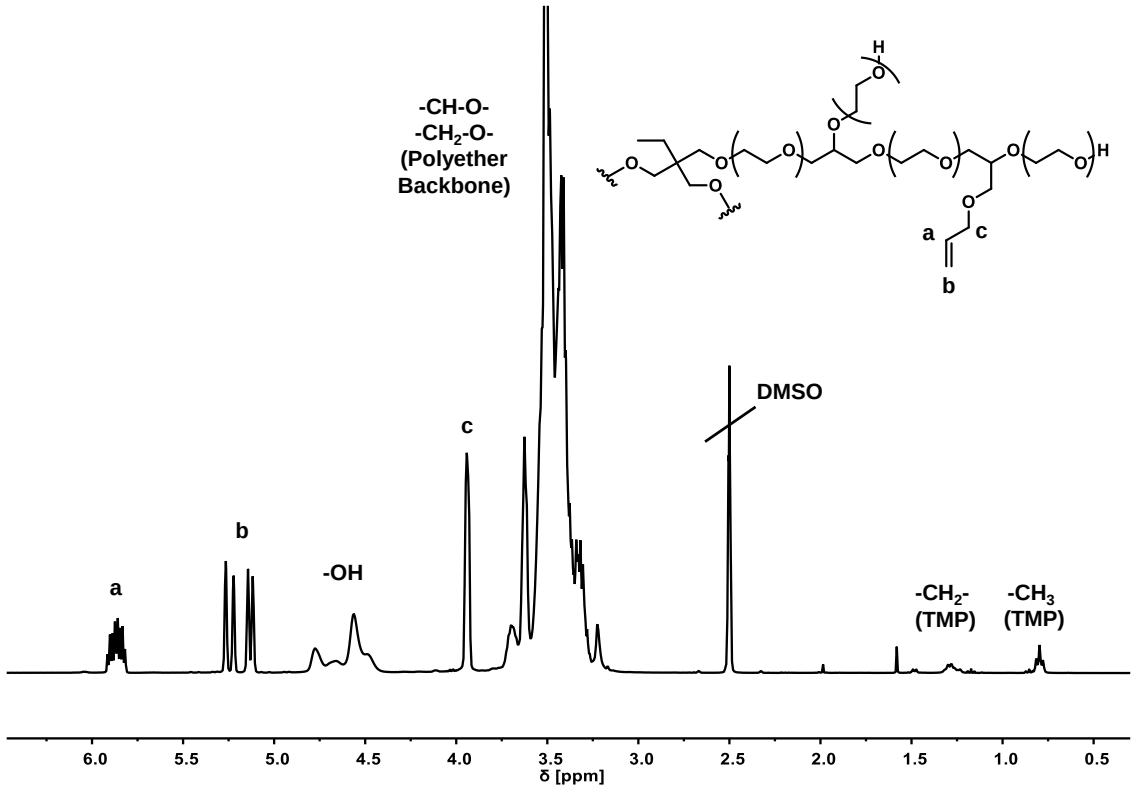

Figure S 12. ^{1}H NMR spectrum of *hb*PEO$_{AGE,114}$ (300 MHz, DMSO-d_6).

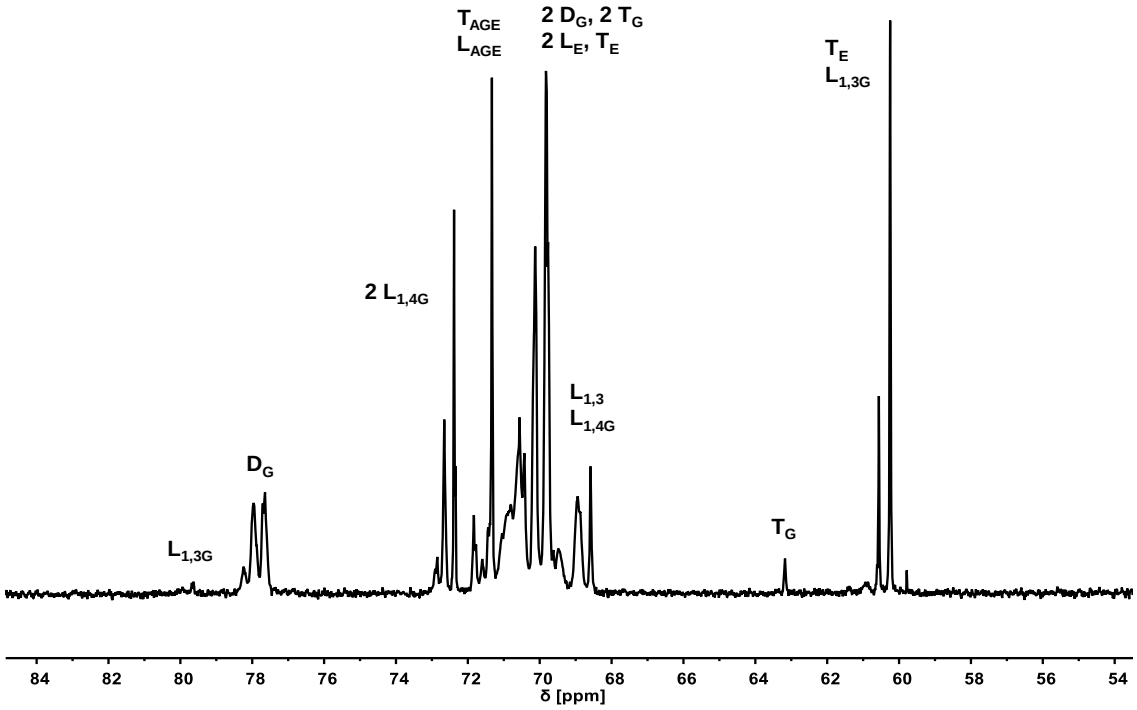

Figure S 13. ^{13}C NMR spectrum of *hb*PEO$_{AGE,72}$ (100 MHz, DMSO-d_6).

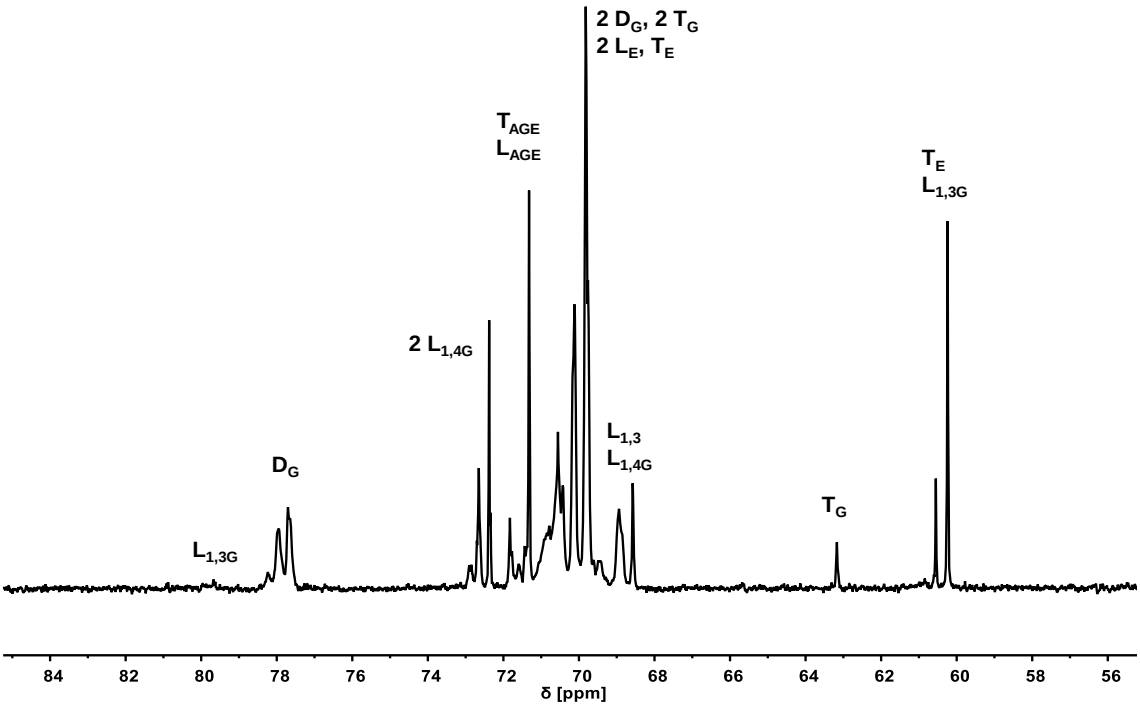

Figure S 14. ^{13}C NMR spectrum of *hb*PEO$_{AGE,114}$ (100 MHz, DMSO-d_6).

Supplemental SEC Data

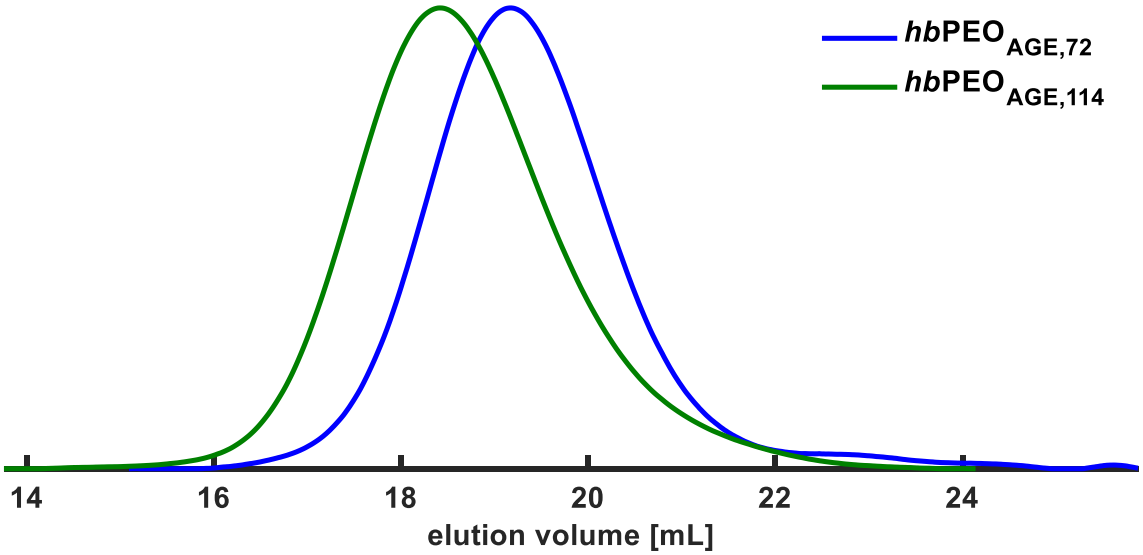

Figure S 15. SEC traces (DMF, RI detector) of the *hb*PEO$_{AGE}$ copolymers after workup by dialysis (MeOH, MWCO = 1000 g mol^{-1}).

Supplemental AUC Data

Modified Svedberg equation:[28,29]

$$M_{s,f} = 9\,\pi\,\sqrt{2}\,N_A\left([s]\,(f/f_{sph})_0\right)^{3/2}\sqrt{v} \qquad \text{S 4}$$

Table S 3. Analytical data obtained by analytical ultracentrifugation, densimetry and viscometry (water, 20 °C).

Sample	$M_{n,theo}$ [g mol^{-1}]	$M_{s,f}$ [g mol^{-1}]	v [cm^3 g^{-1}]	s_0 [S]	f/f_{sph}	[η] [cm^3 g^{-1}]	k_H
*hb*PEO$_{83}$	2700	5200	0.82	0.52	1.35	5.4	2.2
*hb*PEO$_{105}$	5200	7400	0.82	0.77	1.15	4.9	2.6
*hb*PEO$_{165}$	6700	8100	0.80	1.03	1.02	4.9	2.7

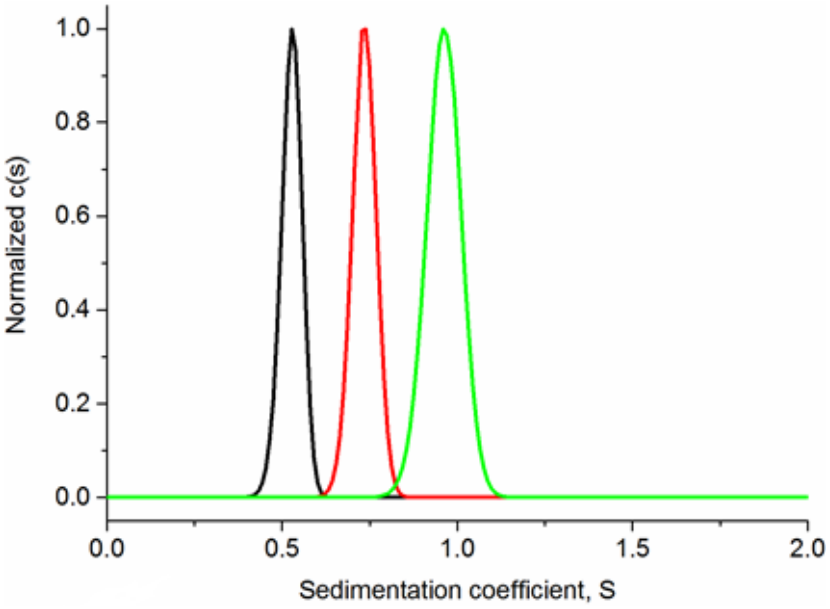

Figure S 16. Normalized distributions of sedimentation coefficients c(s) for the copolymers *hb*PEO$_{83}$, *hb*PEO$_{105}$ and *hb*PEO$_{165}$.

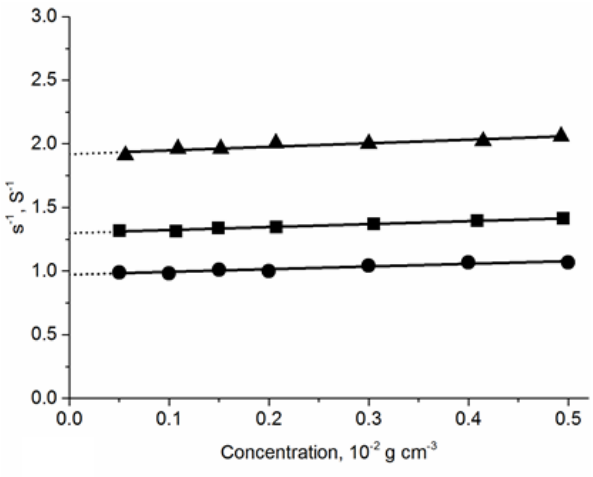

Figure S 17. Inverse sedimentation coefficients s^{-1} plotted against solution concentration for the copolymers *hb*PEO$_{83}$, *hb*PEO$_{105}$ and *hb*PEO$_{165}$. Extrapolations to zero concentration were performed to obtain s_0.

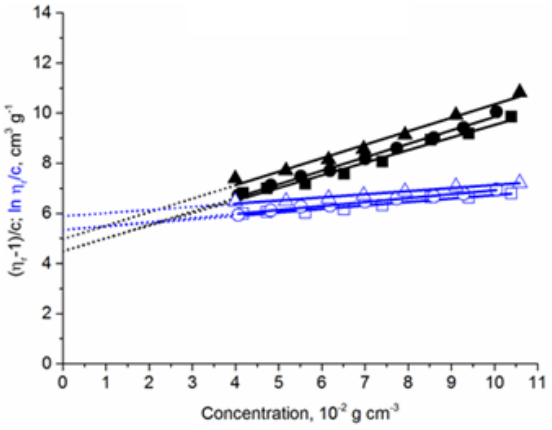

Figure S 18. Huggins (filled black symbols and black lines) and Kraemer (empty blue symbols and lines) plots of *hb*PEO$_{83}$, *hb*PEO$_{105}$ and *hb*PEO$_{165}$. Linear Fits are indicated by solid lines, while extrapolations to zero concentration are represented by dotted lines.

Huggins / Kraemer equation:[28,29]

$$\frac{\eta_r - 1}{c} = [\eta] + k_H [\eta]^2 c + \ldots \qquad \text{S 5}$$

$$\frac{\ln \eta_r}{c} = [\eta] + k_H [\eta]^2 c + \ldots \qquad \text{S 6}$$

2.2 Variation of the Degree of Branching of Hyperbranched Polyether Polyols by Copolymerization of Glycidol with 1-Substituted Analogs

Tobias Kaiser[a], Tobias Johann[a], Holger Frey[a,]*

[a]Department of Chemistry, Johannes Gutenberg University, 55128 Mainz, Germany

To be submitted.

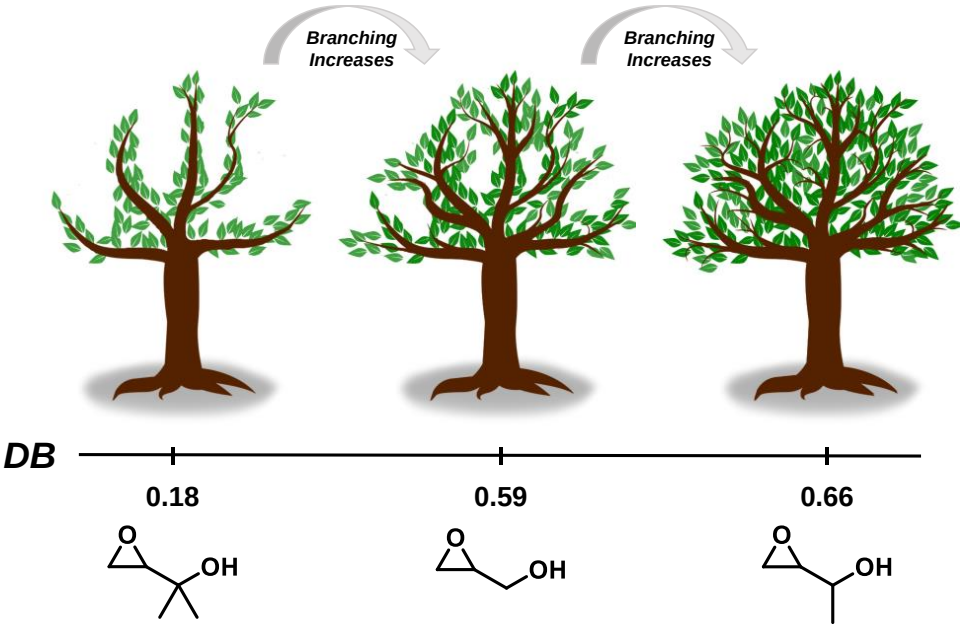

Abstract

Hyperbranched copolymers of glycidol (G) and either 1,2-epoxy-3-butanol (MeGly) or 3,4-epoxy-2-methyl-2-butanol (DiMeGly) have been prepared *via* simultaneous slow monomer addition. By variation of the feed ratio, copolymers with compositions ranging from 0.10 to 0.50 and molar masses between 2200 and 2800 g mol^{-1} were synthesized in the case of G/MeGly while keeping the degrees of polymerization (DP_n) similar, as confirmed by ^{1}H NMR spectroscopy. Regarding G/DiMeGly, compositions were between 0.07 and 0.29 with slightly lower molar masses ranging from 1400 to 2100 g mol^{-1}. The structures of these copolymers were elucidated using 2D NMR experiments and the corresponding degrees of branching (DB) were calculated utilizing inverse gated ^{13}C NMR spectroscopy. The experimental data confirmed a strong dependence of the DB on the copolymer composition. The results were consistent to predictions made by computer simulations using simple kinetical considerations regarding the general mechanism of the ring-opening multibranching polymerization of glycidol and derivatives.

Introduction

Hyperbranched polymers (HBPs) have been the topic of extensive research during the last decades. They are commonly described as dendritic polymers in analogy to the perfectly branched dendrimers.[1–3] However, the synthesis of HBPs is typically a one-pot process, which is inherently more facile than the tedious generation-wise synthesis of dendrimers. Despite exhibiting linear defects resulting in a non-perfectly branched structure, hyperbranched polymers still possess properties similar to dendrimers.[1,2]

Hyperbranched polyether polyols based on the latent AB_2 monomer glycidol are mainly prepared by anionic ring-opening multibranching polymerization (ROMBP) using a partially deprotonated initiator ensuring controlled chain growth (Scheme 10).[4–6] During the polymerization of glycidol a fast proton transfer between repeating units leads to the formation of four different repeating units: dendritic units (D), in which both hydroxy groups have reacted, linear units ($L_{1,3}$ and $L_{1,4}$), in which either one of two hydroxy groups has reacted, and lastly fully unreacted terminal groups (T).[1]

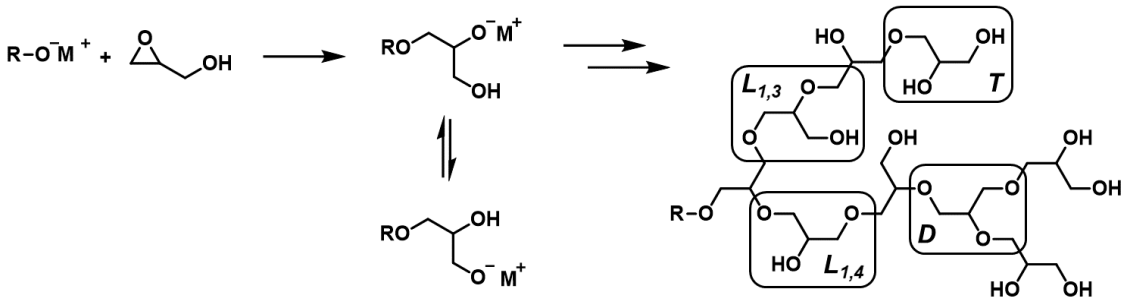

Scheme 1. Different repeating units formed during the anionic ROMBP of glycidol.

The key parameter to describe the structure of hyperbranched polymers is the degree of branching (*DB*), which can assume values between 0 (linear polymers) and 1 (dendrimers). First introduced by Hawker and Fréchet, it is defined by the relative amounts of dendritic and terminal units according to equation 1:[7]

$$DB = \frac{D + T}{D + T + L} \qquad 1$$

Frey and coworkers modified this expression to be universally applicable for hyperbranched polymers regardless of the molar mass:[8]

$$DB = \frac{2\,D}{2\,D + L} \qquad 2$$

For equal reactivity of all B groups, DB can be expressed as a function of the conversion:[9,10]

$$DB = \frac{1}{2} p_A \qquad 3$$

For full conversion ($p_A = 1$), DB is 0.5, which is also commonly found for the one-pot polymerization of AB_2 monomers.[1,8]

The degree of branching is closely related to the polymer architecture and directly influences the physical and chemical properties of the polymers, e.g. free volume, chain entanglement, mean-square radius of gyration, glass-transition temperature (T_g), degree of crystallization, capability of encapsulation, mechanical strength, melting/solution viscosity, biocompatibility, and self-assembly-behavior.[11–21] Therefore, it is of great interest to develop strategies to precisely vary the degree of branching for different applications. Several possibilities to increase the degree of branching have been described before: (i) employing the slow monomer addition technique;[9,22,23] (ii) the use of multifunctional core-forming molecules B_f;[9,22,23] (iii) increased reactivity of the functional B group in linear vs. terminal units;[24] (iv) polymerization of prefabricated dendrons;[25,26] (v) post-polymerization modification the generate dendritic units from linear ones;[27] or (vi) using special catalysts.[28] By employing these techniques, DB is increased to values higher than obtained by a simple one-pot reaction.[28–33] For further control, four different strategies are applicable to tune the degree of branching: (i) copolymerization of AB_n and AB monomers;[34–37] (ii) variation of the reaction conditions;[38–43] as well as (iii) host-guest-inclusion of AB_2 or multifunctional monomers.[44] By copolymerization with AB monomers, strictly linear units are introduced into the otherwise hyperbranched

backbone. Thus, the DB can only be tuned to values lower than 0.5 or 0.66 in the case of slow monomer addition.

In this work, we present the novel AB_2/AB_2 copolymerization of glycidol with analogous monomers 1,2-epoxy-3-butanol (MeGly) and 3,4-epoxy-2-methyl-2-butanol (DiMeGly), carrying either one or two methyl groups adjacent to the hydroxy group. By substituting the protons, the monomers carry either a secondary or a tertiary alcohol resulting in altered reactivities towards proton transfer after initial ring-opening. Consequently, as the proton transfer is one of the crucial steps towards branching, DB is tuneable by variation of the copolymer composition to either assume higher or lower values than the respective homopolymers of glycidol. The individual reactivities of each B group, i.e. primary, secondary or tertiary hydroxy groups, after ring-opening and their influence on DB is modelled by computer simulations following simple kinetical considerations. The results are verified by comparison to the experimental data obtained by copolymerization *via* simultaneous SMA of G/MeGly or G/DiMeGly.

Experimental Section

Materials

All materials were purchased from Sigma Aldrich, TCI or Fisher Scientific. For monomer synthesis all compounds were employed without further purification. Prior to polymerization, glycidol (96 %), MeGly, DiMeGly and 1-methyl-2-pyrrolidone (NMP, 99.0 %) were purified by distillation over calcium hydride. The initiator *N,N*-dibenzyl tris(hydroxymethyl)aminomethane (Bn_2TRIS) was synthesized according to literature.[45]

Instrumentation

NMR spectroscopy. ^{1}H NMR spectra were recorded on a Bruker Avance III HD 300 (5 mm BBFO-SmartProbe with z-gradient and ATM) at 300 MHz. Inverse gated ^{13}C NMR spectra were recorded on a Bruker Avance II HD 400 (5 mm BBFO-SmartProbe with z-gradient and ATM) at 100 MHz. COSY, HSQC, HMBC and the respective one-dimensional spectra were recorded on a Bruker Avance II HD 400 (5 mm BBFO-SmartProbe with z-gradient and ATM) at 400/100 MHz, as well. The residual signals of the deuterated solvent were utilized as an internal reference.

Size-exclusion chromatography. SEC measurements in DMF (containing 0.25 g L^{-1} of lithium bromide) were performed using an integrated Agilent 1100 series instrument, equipped with a PSS HEMA column combination ($10^6/10^4/10^2$ Å porosity), UV and RI detector. Calibration is based on linear poly(ethylene glycol) standards (Polymer Standards Service).

Calculations

Density-functional theory. DFT calculations were performed using the ORCA[46] software suite on the PBEh-3c level.[47] This functional employs DFT-based calculation of the molecule but utilizes several semi-empirical approximations to reduce the computational costs. Thermodynamic properties were calculated at 300 K. All molecules in vacuum exhibited no imaginary frequency and thus represent a local minimum and the probable equilibrium geometry. To account for possible solvent effects the CPCM model was used with DMSO as solvent. In this case occasionally low imaginary frequencies below 50 cm^{-1} were detected due to the peculiarities of the cavity formation of the CPCM algorithm. The 3D illustrations of the molecules were rendered in IBO view.[48]

Branching Simulation. The abundance of the individual repeating units was calculated by numerical solving the polymerization differential equations using the Runge-Kutta 45 approach. The differential equation system was based on the following prerequisites:

- **(i)** There are 4 different OH-Groups (1;1';2;2')
- **(ii)** There are 4 different repeating units ($L_{1,3}$;$L_{1,4}$;D;T)
- **(iii)** All repeating units of one type show the same reactivity (e.g. no penultimate effect)
- **(iv)** All proton reactions are magnitudes faster than the propagation (e.g. proton equilibria are assumed)
- **(v)** OH-Group in glycidol is assumed to be non-reactive

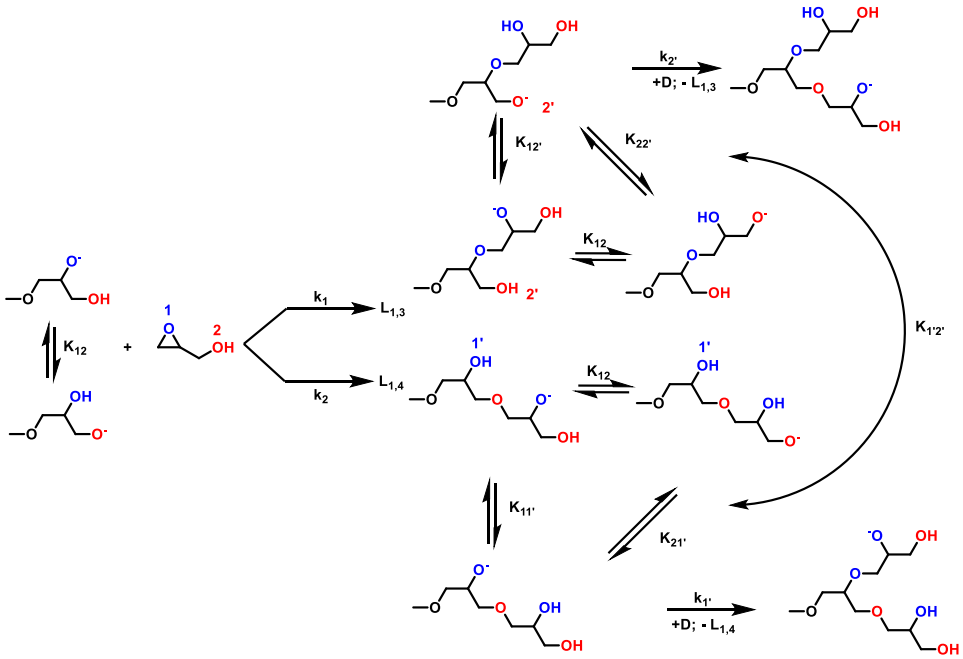

Scheme 2. Polymerization pathway and proton equilibria for glycidol.

The following reactions were included in the differential equation system with "N_X" as the number of the respective repeating unit of type X:

$L_{1,3}$: Produced by reaction of 1 (T) with rate k_1 to yield $L_{1,3}$: N_T = const.; $N_{L1,3}$ = +1

$$\frac{d[L_{1,3}]}{dt} = k_1 * [T] * [G] - k_{2'} * [L_{1,3}] * [G]$$

$L_{1,4}$: Produced by reaction of 2 (T) with rate k_2 to yield $L_{1,4}$: N_T = const.; $N_{L1,4}$ = +1

$$\frac{d[L_{1,4}]}{dt} = k_2 * [T] * [G] - k_{1'} * [L_{1,4}] * [G]$$

D: Produced by reaction of 1' ($L_{1,4}$) with rate $k_{1'}$ or 2' ($L_{1,3}$) with rate $k_{2'}$ to yield D and T: $N_{L1,3}$ = -1 or $N_{L1,4}$ = -1; N_T = +1; N_D = +1

$$\frac{d[D]}{dt} = k_{1'} * [L_{1,4}] * [G] + k_{2'} * [L_{1,3}] * [G]$$

T: Produced simultaneous to each D unit. $N_T = N_D + 1$ (Initiator)

$$\frac{d[T]}{dt} = \frac{d[D]}{dt}$$

Before every calculation step the proton equilibria corresponding to the equilibria constants as shown in Scheme 2 were solved. To estimate the equilibria constants the pKa value of ethanol (15.9) was used as reference for primary alcohols, isopropanol (17.1) as reference for secondary alcohols and tert-butanol (19.0) as reference for tertiary alcohols.

The degree of branching was then calculated by equation 2.

For Glycidol the following assumptions were made:

G_0 = 1 mol/L; Initiator = 0.01 mol/L; Deprotonation = 30%;

- ➔ 1 = sec. alcohol; 2 = prim. alcohol; assumed equilibria constant: for 1->2: 15.8
- ➔ $k_1 = k_{1'} = 0.05$ mol/(L * s) $k_2 = k_{2'} = 0.01$ mol/(L * s)

For MeGly the following assumptions were made:

G_0 = 1 mol/L; Initiator = 0.01 mol/L; Deprotonation = 30%;

- ➔ 1 = sec. alcohol; 2 = sec. alcohol; assumed equilibria constant: for 1->2: 1
- ➔ $k_1 = k_2 = k_{1'} = k_{2'} = 0.01$ mol/(L * s) -> no reactivity differences

For DiMeGly the following assumptions were made:

G_0 = 1 mol/L; Initiator = 0.01 mol/L; Deprotonation = 30%;

- ➔ 1 = sec. alcohol; 2 = tert. alcohol; assumed equilibria constant: for 1->2: 1/80
- ➔ $k_1 = k_{1'} = 0.01$ mol/(L * s) $k_2 = k_{2'} = 0.001$ mol/(L * s)

Monomer Synthesis

The respective allyl alcohol (MeGly: 2-Hydroxy-3-butene, DiMeGly: 2-Methyl-3-buten-2-ol; 58 mmol, 1 eq) was placed in a 500 mL round-bottom flask equipped with a magnetic stirrer and was diluted with 150 mL of dichloromethane. After cooling to 0 °C, 17.9 g meta-chloroperoxybenzoic acid (73 mmol, 1.25 eq) was added in small portions to the solution of the allyl alcohol. Following the complete addition, the reaction mixture was allowed to reach room temperature and was stirred overnight. After filtration to remove precipitated salts the reaction mixture was washed once with saturated aqueous solutions of Na_2SO_3, $NaHCO_3$ and NaCl. The organic phase was isolated and dried with $MgSO_4$. After filtration, the solvent was removed, and the crude product distilled *in vacuo* (p = 26 mbar). MeGly (T_b = 60 – 70 °C) and DiMeGly (T_b = 50 - 60 °C) were isolated as colorless liquids in moderate yields (30 – 40 %).

MeGly: ^{1}H NMR (400 MHz, DMSO-d_6, δ): 4.84 (dd, 1H, -O<u>H</u>); 3.47 – 3.31 (m, 1H, -C<u>H</u>-OH); 2.83 – 2.77 (m, 1H, H_2C-(O)-C<u>H</u>-); 2.67 – 2.64 (m, 1H, <u>H</u>HC-(O)-C*H*-); 2.56 – 2.52 (m, 1H, H<u>H</u>C-(O)-CH-); 1.09 (d, 3H, -C<u>H</u>$_3$).

^{13}C NMR (100 MHz, DMSO-d_6, δ): 66.89 – 65.65 (-<u>C</u>H-OH); 55.90 – 55.08 (H_2C-(O)-<u>C</u>H-); 44.23 – 43.35 (H_2<u>C</u>-(O)-CH-); 19.54 – 19.42 (-<u>C</u>H$_3$).

DiMeGly: ^{1}H NMR (400 MHz, DMSO-d_6, δ): 4.35 (s, 1H, -OH); 2.75 (t, 1H, H_2C-(O)-CH-); 2.52 (d, 1H, H_2C-(O)-CH-); 1.00 (d, 6H, -(CH_3)$_2$).

^{13}C NMR (100 MHz, DMSO-d_6, δ): 57.96 (H_2C-(O)-CH-); 43.00 (H_2C-(O)-CH-); 25.88 – 25.25 (-(CH_3)$_2$).

Copolymerization Protocol

General procedure. In a Schlenk flask equipped with a magnetic stirrer, 67 mg Bn_2TRIS (0.22 mmol, 1 eq) was dissolved in 1 mL methanol. Afterwards, a solution of 11 mg cesium hydroxide monohydrate (0.07 mmol, 0.3 eq) in 1 mL methanol was added and the mixture was stirred for 30 min. Benzene was added and the partially deprotonated initiator salt was dried *in vacuo* overnight at room temperature. The initiator salt was dissolved in 1 mL NMP and heated to 100 °C under argon atmosphere. In another Schlenk flask, the monomers (6 mmol, 27 eq) were mixed in regard to the target composition and diluted with NMP to yield a total volume of 2 mL. Using a syringe pump, the monomer mixture was slowly added to the heated solution of the initiator salt with a rate of 0.1 mL h^{-1}. After complete addition, the mixture was stirred for further 60 min and the polymerization was terminated by adding 1 mL methanol. Afterwards, the reaction mixture was dialyzed (methanol, MWCO = 1000 g mol^{-1}) and the solvent removed. The products were isolated as highly viscous brown oils with yields depending on the initial comonomer ratios.

*hb*P(G-*co*-MeGly): ^{1}H NMR (300 MHz, DMSO-d_6, δ): 7.28 – 7.03 (m, 10H, -N-(CH_2-C_6H_5)$_2$); 4.94 – 4.04 (br, m, -OH); 3.95 (s, 4H, -N-(CH_2-C_6H_5)$_2$); 3.85 - 2.98 (m, -O-CH-, -O-CH_2-); 1.05 (m, -CH-CH_3).

^{13}C NMR (100 MHz, DMSO-d_6, δ): 128.51 – 126.41 (-N-(CH$_2$-C$_6$H$_5$)$_2$); 80.78 – 80.13 ($L_{1,3G}$, $L_{1,3MeGly}$); 78.93 – 77.86 (D_G, D_{MeGly}); 75.00-74.05 (D_{MeGly}, $L_{1,4MeGly}$); 73.81 – 72.82 (2 $L_{1,4G}$, $L_{1,4MeGly}$); 72.49 – 70.51 (2 D_G, 2 T_G, D_{MeGly}, T_{MeGly}); 70.27 – 69.62 ($L_{1,3G}$); 69.60 – 68.72 ($L_{1,4G}$, $L_{1,4MeGly}$); 68.10 – 65.79 (T_{MeGly}, $L_{1,3MeGly}$); 64.13 – 63.12 (T_G, T_{MeGly}); 62.27 – 60.77 ($L_{1,3G}$, $L_{1,3MeGly}$); 54.45 (-N-(CH$_2$-C$_6$H$_5$)$_2$); 19.49 (-CH$_3$).

*hb*P(G-*co*-DiMeGly): ^{1}H NMR (300 MHz, DMSO-d_6, δ): 7.26 – 7.04 (m, 10H, -N-(CH$_2$-C$_6$H$_5$)$_2$); 4.94 – 4.04 (br, m, -OH); 3.95 (s, 4H, -N-(CH$_2$-C$_6$H$_5$)$_2$); 3.85 – 3.03 (m, -O-CH-, -O-CH$_2$-); 1.17 – 0.97 (m, -CH-(CH$_3$)$_2$).

^{13}C NMR (100 MHz, DMSO-d_6, δ): 128.08 – 126.00 (-N-(CH$_2$-C$_6$H$_5$)$_2$); 80.71 – 80.13 ($L_{1,3G}$, $L_{1,3DiMeGly}$); 79.11 – 78.02 (D_G, $D_{GDiMeGly}$); 76.97 – 75.95 ($L_{1,4DiMeGly}$, $D_{DiMeGly}$); 73.75 – 72.81 (2 $L_{1,4G}$, $L_{1,4DiMeGly}$); 72.60 – 70.64 (2 D_G, 2 T_G, $D_{DiMeGly}$, $L_{1,3DiMeGly}$, 2 $T_{DiMeGly}$); 70.46 – 69.69 ($L_{1,3G}$); 69.53 – 68.81 ($L_{1,4G}$, $L_{1,4DiMeGly}$); 63.98 – 63.23 (T_G, $T_{DiMeGly}$); 62.22 – 60.94 (L1,3G, $L_{1,3DiMeGly}$); 54.06 (-N-(CH$_2$-C$_6$H$_5$)$_2$); 27.08 – 24.66 (C-(CH$_3$)$_2$).

Results and Discussion

Computer Simulations

Prior to any polymerization experiments, several computational studies were performed to simulate the polymerization behavior of the novel monomers MeGly and DiMeGly in comparison to glycidol, i.e. reactivity towards anionic ring-opening and the tendency to form branching points.

By DFT calculation, the structures of the monomers in vacuum were simulated (cf. Figure S 1). In the absence of intermolecular interactions, a hydrogen bond between the pendant hydroxy group and oxygen atom of the epoxide is formed for each monomer (Figure 1), as proposed by Leibig *et al.*.[49] Furthermore, the hydrogen bond is significantly shortened by substitution of the protons adjacent to the hydroxy groups (Δd_2 = 7.5 – 9.0 pm). The length of the sterically less hindered C-O bond, which is assumed to be opened during the anionic ROMBP, increases from glycidol to MeGly and to DiMeGly (141.87 pm, 141.90 pm and 141.92 pm). However, the bond lengths are not sufficiently different to derive varying reactivities towards ring-opening.

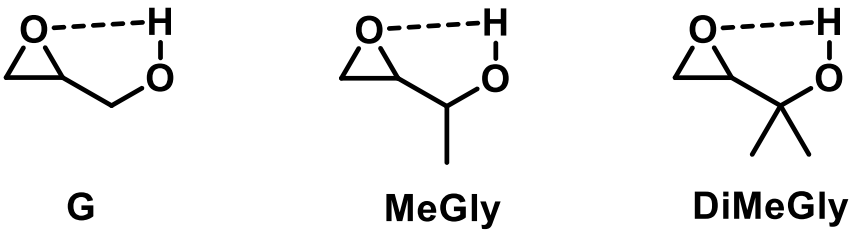

Figure 1. Proposed structures of glycidol and the 1-substituted analogues MeGly and DiMeGly.

Therefore, a single polymerization step was modeled by the attack of potassium methoxide on the unsubstituted carbon atom followed by ring-opening (cf. Scheme

S 1 and Scheme 3). The proposed structures of the active glycidol, MeGly or DiMeGly chain-ends as well as the free enthalpy of the ring-opening reaction were then predicted by DFT calculation (cf. Scheme S 1, Figure S 2 and Table S 2). While the ring-opening of glycidol and MeGly results in similar values for ΔG (-116.21 and -115.69 kJ mol^{-1}), DiMeGly appears less reactive towards ring-opening (ΔG = -110.64 kJ mol^{-1}). Translating these findings to the (co-)polymerization behavior, one might expect random copolymers by the simultaneous ring-opening polymerization of glycidol and MeGly, whereas G/DiMeGly will result in a pronounced gradient structure.

The inter- and intramolecular proton transfer equilibria as well as nucleophilicity of the respective alkoxide are crucial to generate branching during the ring-opening multibranching polymerization of glycidol. Therefore, the DBs of the resulting polymers are dictated by the question, whether one side of the equilibrium is favored over the other, which would ultimately lead to mainly linear units, or whether there is a true equilibrium state (cf. Scheme 1, middle). In the case of glycidol, after ring-opening the equilibrium depends on the reactivities of the secondary and primary alcohol towards deprotonation, i.e. the pK_a values. Considering the different fundamental reaction steps after initial ring-opening of one glycidol unit (Scheme 2), the relative amounts of the different repeating units as well as the degrees of branching obtained by the homopolymerization of glycidol can be modeled using pK_a values of similar model compounds (ethanol for primary alcohols ($pK_{a,primary}$) and isopropanol for secondary ones ($pK_{a,secondary}$)) and estimations for the rate constants k_1 and k_2 (see supporting information for further detail). These considerations differ from efforts discussed in literature, as equal reactivity of each B group is no longer assumed.[9,10,22,23] However, since

estimations are made both for pK_a values and rate constants, the following results show no absolute values for DB and the relative amounts of repeating units.

The apparent upper limit for DB of *hb*PG following these considerations is 0.59 the assumptions discussed above (Figure 2). This finding in conjunction with the relative amounts of the repeating units is in excellent agreement with experimental data commonly found in hyperbranched polyglycerols prepared *via* SMA.[4,50]

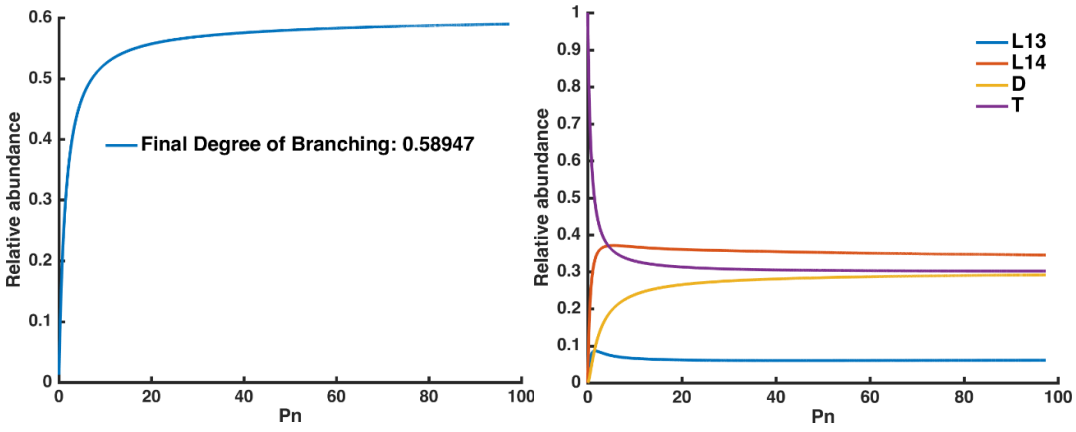

Figure 2. Estimated DB (left) and relative amounts of repeating units (right) of *hb*PG.

By substituting the protons of the methylene group adjacent to the hydroxy group of glycidol, e.g. with one or two methyl groups, the equilibria should be shifted due to the different pKa-values and nucleophilicities of the newly formed secondary or tertiary alcohols (cf. Scheme 3): for MeGly, both groups should show similar reactivity, whereas for DiMeGly, the equilibrium should be reversed (tertiary and primary alcohol).

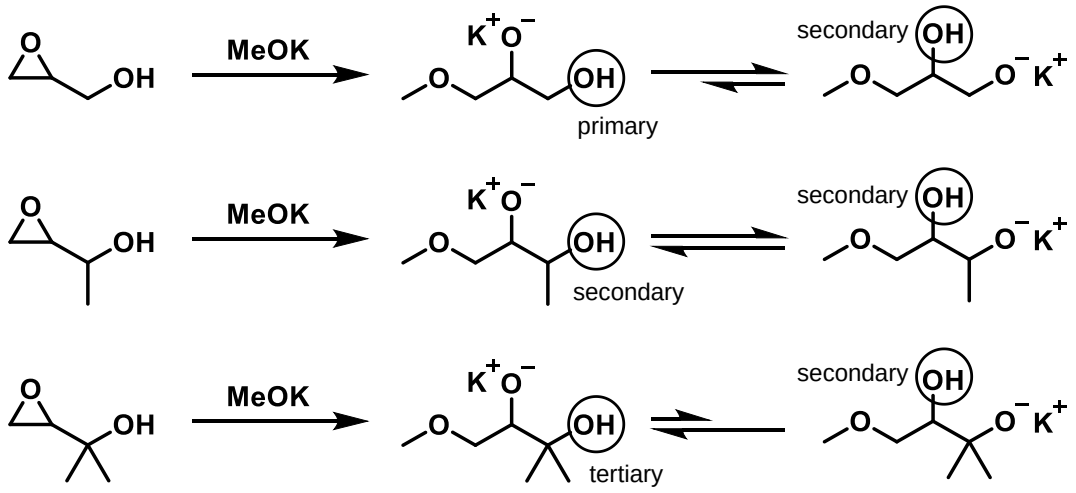

Scheme 3. Proton transfer equilibria after ring-opening of glycidol, MeGly and DiMeGly using potassium methoxide.

Following similar considerations as for glycidol, one can model the *DB*s and relative amounts of repeating units as a function of the degree of polymerization depending on the pKa-values and rate constants:

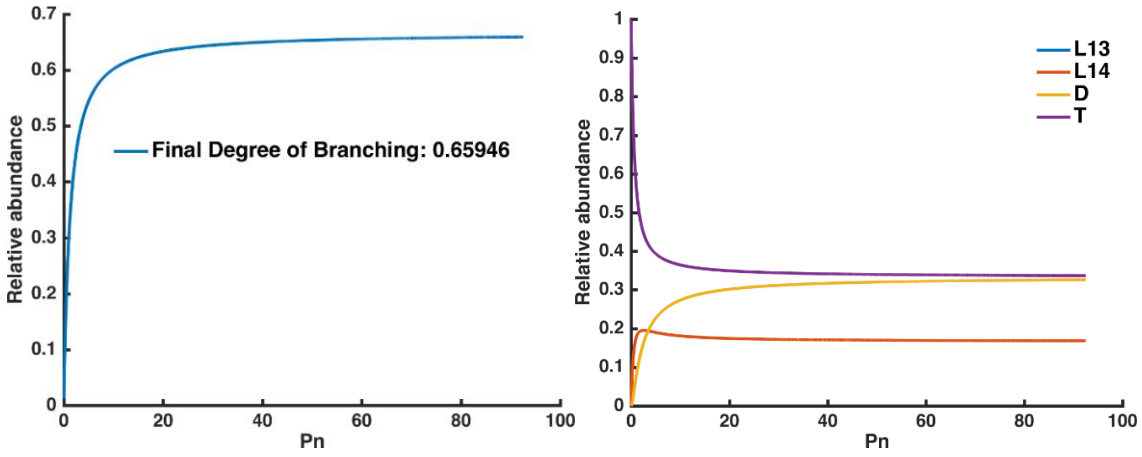

Figure 3. Estimated DB (left) and relative amounts of repeating units (right) of *hb*P(MeGly).

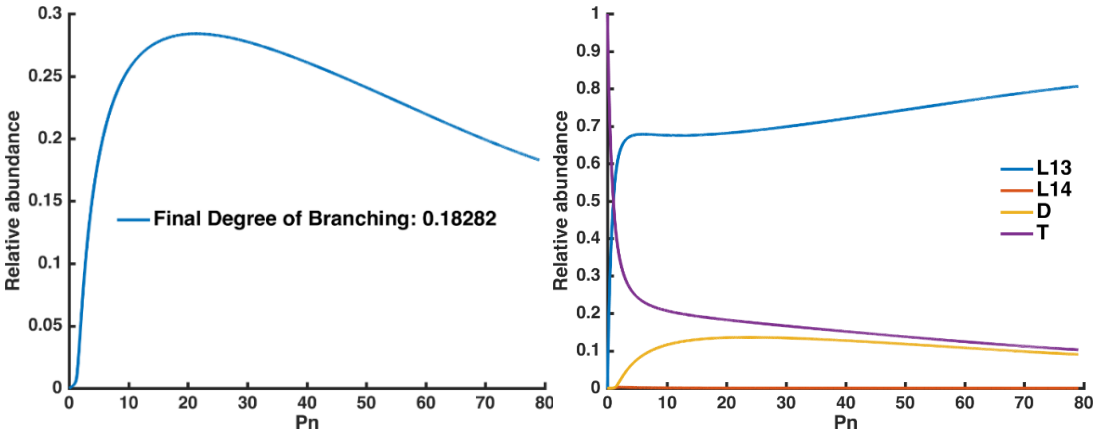

Figure 4. Estimated DB (left) and relative amounts of repeating units (right) of *hb*P(DiMeGly).

Due to equal reactivity of both hydroxy groups, the amounts of $L_{1,3}$ and $L_{1,4}$ units found in *hb*P(MeGly) coincide, while dendritic and terminal units show a higher abundance. As the differences in reactivity are more significant for *hb*P(DiMeGly), little to no $L_{1,4}$ units are formed. In fact, a mainly linear polymer is expected with mostly $L_{1,3}$ units and only little amounts dendritic and terminal units.

In summary, due to differences in basicity going from primary to secondary and tertiary alcohols or alkoxides, the proton transfer equilibrium should be shifted in such a way, that the overall degrees of branching should increase starting from *hb*P(DiMeGly) to *hb*PG and lastly *hb*P(MeGly) with the highest DB (Table 1)

Table 1. Estimated upper limits of the degree of branching of *hb*PG, *hb*P(MeGly) and *hb*P(DiMeGly).

Compound	DB
*hb*PG	0.59
*hb*P(MeGly)	0.66
*hb*P(DiMeGly)	0.18

Polymer Synthesis and Characterization

To investigate the influence of the comonomer on the reaction mechanism, i.e. the DB, in comparison to the computer simulations, several hyperbranched polyether polyols based on glycidol and MeGly as well as DiMeGly were synthesized following a previously published protocol.[51] Scheme 4 summarizes the ring-opening multibranching copolymerization of glycidol and either of the comonomers MeGly or DiMeGly *via* SMA including the synthesis of the respective monomer. The DFT calculations discussed in the previous chapter resulted in random copolymers for G/MeGly and a gradient structure for the batch copolymerization of G and DiMeGly. However due to the rather small differences in reactivity, following the SMA methodology random copolymers are expected as long as the feed rate is sufficiently slow.[51]

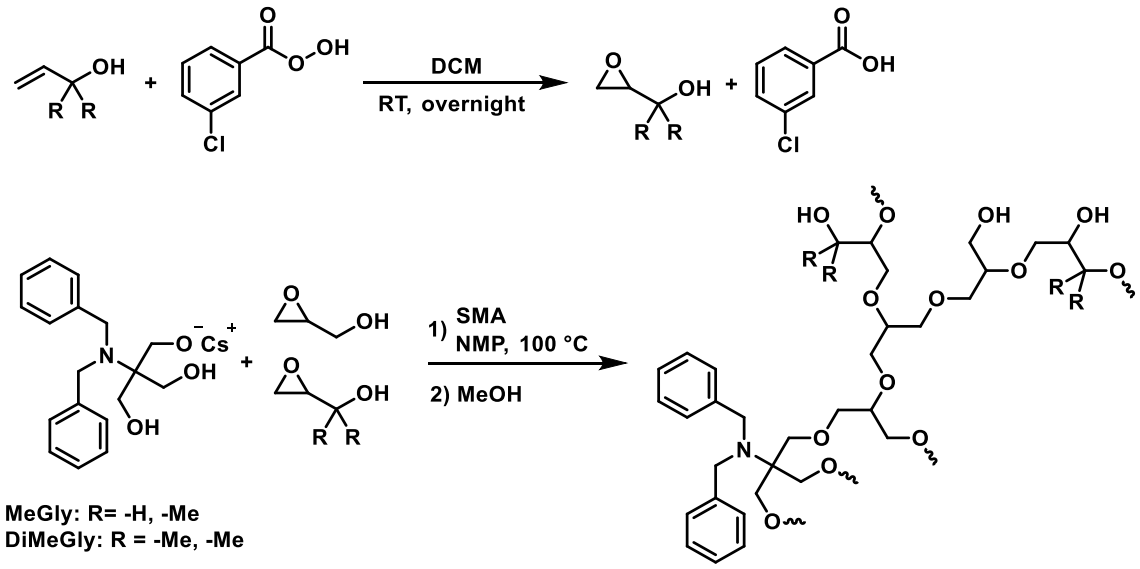

Scheme 4. Synthesis of hyperbranched polyether polyols by copolymerization of glycidol and MeGly or DiMeGly *via* SMA.

The monomers MeGly and DiMeGly were prepared by epoxidation of the commercially available allyl alcohols 2-hydroxy-3-butene and 2-methyl-3-buten-2-ol followed by subsequent aqueous work-up resulting in moderate to low yields. The structures were confirmed by ^{1}H and ^{13}C NMR spectroscopy (see Figure S 3 to Figure S 6). As a single fractionated distillation yielded the compounds in sufficient purity, the monomers were used without further work-up for the following polymerization steps.

As homopolymerization of each monomer was found to yield only oligomeric products with multimodal molecular weight distributions, only copolymers with high glycidol content were prepared. A mixture of either of the monomers and glycidol diluted with NMP was slowly added to a preheated solution of the partially deprotonated initiator Bn_2TRIS in NMP. After full addition, the reaction mixtures were dialyzed in methanol (MWCO = 1000 g mol^{-1}) removing oligomeric side-products as well as most of the solvent NMP. The SEC and NMR data of the resulting copolymers is summarized in Table 2. Preliminary tests resulted in molar masses and copolymer compositions lower than the targeted values the more comonomer was aimed to be introduced (samples I and II). Therefore, the comonomer feed ratio was adjusted for MeGly to obtain copolymers with similar degrees of polymerization (DP_n) while systematically varying the comonomer content between 0.10 and 0.50 (entries 1 to 5).

Table 2. SEC and NMR data of the *hb*P(G-*co*-MeGly) copolymers.

Entry	Sample[a)]	M_n[b)] [g mol^{-1}]	Đ[b)]	DP_n[c)]	M_n[c)] [g mol^{-1}]	X_{MeGly}[c)]
I	*hb*P($G_{0.95}$-*co*-$MeGly_{0.05}$)	550	1.39	11	1100	0.05
II	*hb*P($G_{0.92}$-*co*-$MeGly_{0.08}$)	460	1.24	8	900	0.08
1	*hb*P($G_{0.90}$-*co*-$MeGly_{0.10}$)	730	1.52	21	1900	0.10
2	*hb*P($G_{0.79}$-*co*-$MeGly_{0.21}$)	720	1.57	21	1900	0.21
3	*hb*P($G_{0.68}$-*co*-$MeGly_{0.32}$)	880	1.43	21	1900	0.32
4	*hb*P($G_{0.60}$-*co*-$MeGly_{0.40}$)	930	1.58	32	2800	0.40
5	*hb*P($G_{0.50}$-*co*-$MeGly_{0.50}$)	830	1.44	23	2200	0.50

a)Terminology: indices denote the copolymer composition determined by 1H NMR spectroscopy, b)determined by SEC (DMF, linear PEO standards), c)determined by 1H NMR spectroscopy.

The SEC traces of all copolymers after work-up show monomodal distributions coeluting with traces of the solvent NMP, which is also apparent in the ^{1}H NMR spectra (*vide infra*) and could only be removed risking high losses in yield. The apparent molar masses calculated using linear PEO standards range from 700 to 900 g mol^{-1}, while the distributions are narrow to moderate and generally in good agreement with values expected for trifunctional initiators like TMP (1.43 – 1.63).[23]

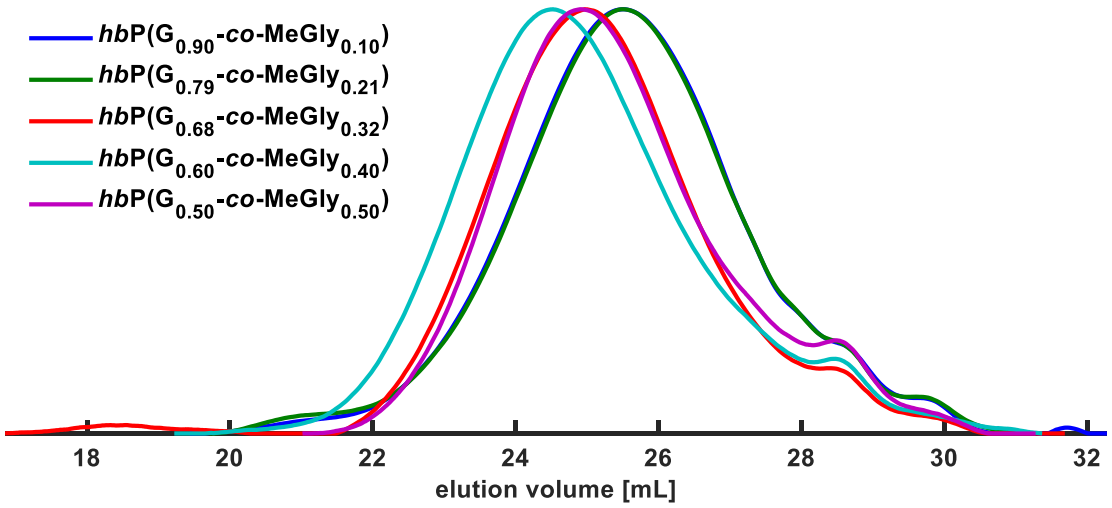

Figure 5. SEC traces of the *hb*P(G-*co*-MeGly) copolymers (DMF, RI detector).

As described elsewhere, hyperbranched polymers are characterized by a more compact structure than similar linear polymers with comparable molar masses or degrees of polymerization.[52] Therefore, molar masses of hyperbranched polymers determined using linear polymer standards tend to be underestimated.

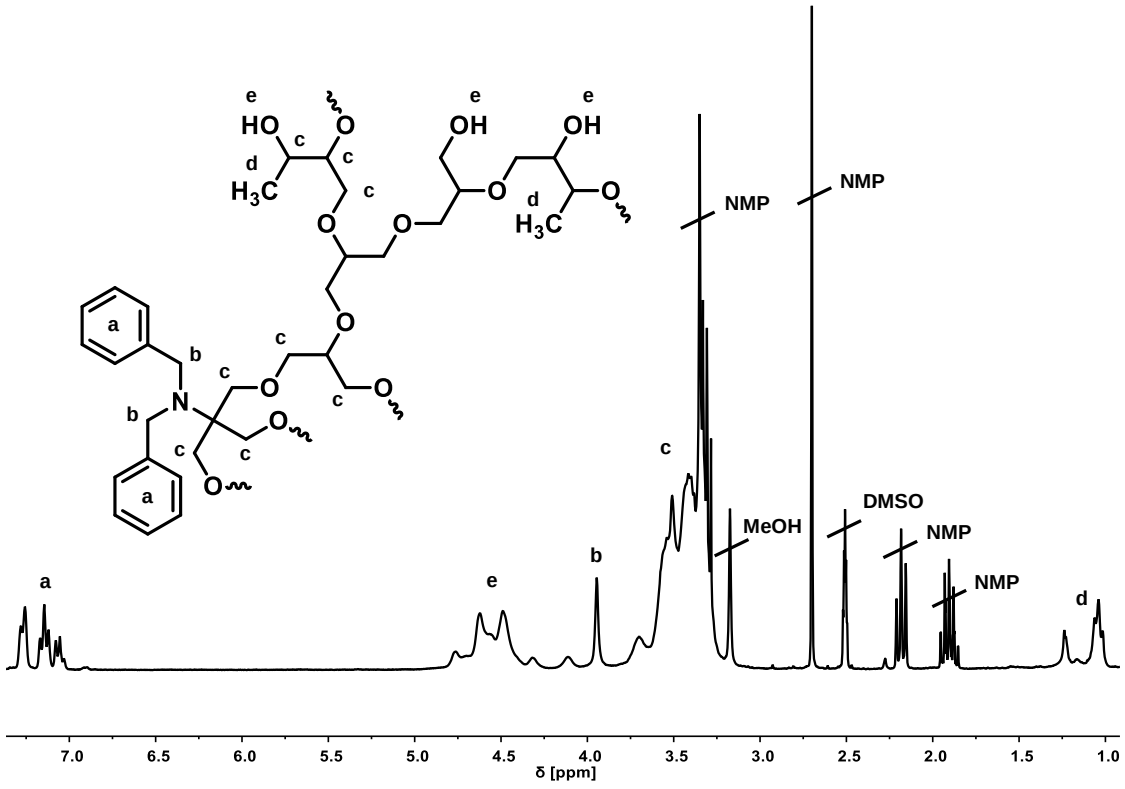

Figure 6. ^{1}H NMR spectrum of *hb*P($G_{0.90}$-*co*-MeGly$0_{.10}$) (300 MHz ,DMSO-d_6).

Figure 6 shows an exemplary ^{1}H NMR spectrum of a *hb*P(G-*co*-MeGly). All signals can be assigned to either solvent residues (NMP, MeOH) or the various structural elements of the hyperbranched polymer. Using the aromatic signals of the initiator (a) as normation, molar masses and copolymer compositions can be calculated: By comparison of the methyl signal (d) and the signal of the hydroxyl groups (e), the copolymer composition can be determined according to equation 4:

$$X_{MeGly} = \frac{I_d}{3\,(I_e - 3)} \qquad 4$$

Furthermore, as each monomer unit introduces exactly one additional hydroxy group into the polymer, the degree of polymerization (DP_n) can be calculated (equation 5).

$$DP_n = I_e - 3 \qquad 5$$

DP_n will be used for comparison to similar hyperbranched polyglycerols rather than the molecular weight when discussing the degrees of branching, as molar masses may deviate due to different molecular weights of the repeating units. The resulting degrees of polymerization typically vary between 21 and 23. As the comonomer feed was adjusted empirically, sample 4 shows a higher deviation concerning DP_n and will be discussed accordingly (*vide infra*).

DiMeGly

Additionally, a set of hyperbranched copolymers based on glycidol and DiMeGly was prepared in analogy to MeGly (*vide supra*). However, the higher the content of DiMeGly in the comonomer feed, the less incorporation was observed. Thus, five copolymers with only limited amounts of DiMeGly were prepared. The SEC and NMR data is summarized in Table 3:

Table 3. SEC and NMR data of the *hb*P(G-*co*-DiMeGly) copolymers.

Entry	Sample[a)]	M_n[b)] [g mol^{-1}]	Đ[b)]	DP_n[c)]	M_n[c)] [g mol^{-1}]	$X_{DiMeGly}$[c)]
6	*hb*P($G_{0.93}$-*co*-DiMeGly$_{0.07}$)	910	1.53	24	2140	0.07
7	*hb*P($G_{0.88}$-*co*-DiMeGly$_{0.12}$)	980	1.41	21	1950	0.12
8	*hb*P($G_{0.84}$-*co*-DiMeGly$_{0.16}$)	640	1.46	18	1730	0.16
9	*hb*P($G_{0.80}$-*co*-DiMeGly$_{0.20}$)	570	1.35	15	1510	0.20
10	*hb*P($G_{0.71}$-*co*-DiMeGly$_{0.29}$)	590	1.34	13	1380	0.29

[a)]Terminology: indices denote the copolymer composition determined by ^{1}H NMR spectroscopy, [b)]determined by SEC (DMF, linear PEO standards), [c)]determined by ^{1}H NMR spectroscopy.

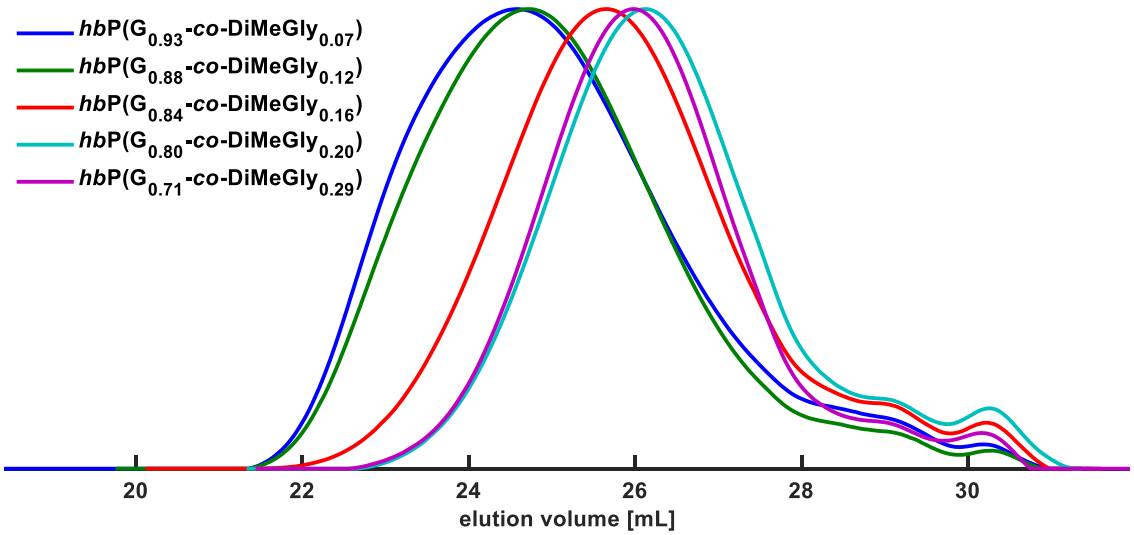

Figure 7. SEC traces of the *hb*P(G-*co*-DiMeGly) copolymers (DMF, RI detector).

Figure 7 depicts the SEC traces of the copolymers based on glycidol and DiMeGly. The SEC traces show monomodal distributions with moderate dispersities between 1.34 and 1.53. The apparent molar masses determined by utilizing linear PEO standards range from 570 to 980 g mol^{-1} and decrease steadily the more comonomer content was targeted.

The copolymer composition, as well as DP_n and molar mass can be calculated in analogy to MeGly. Figure 8 shows an exemplary ^1H NMR spectrum of *hb*P(G-*co*-DiMeGly). As the comonomer only carries an additional methyl group, the signal assignment is congruent with the previous section. After modification of equation 1 in respect to the increased proton count for signal d, the amount of DiMeGly incorporated into the polymer can be calculated according to equation 6, whereas the calculation of DP_n (equation 5) is unaffected by the incorporation of a different monomer:

$$X_{DiMeGly} = \frac{I_d}{6\,(I_e - 3)} \qquad 6$$

The resulting contents of DiMeGly range from 0.07 to 0.29 with increasing deviation from the target values. On the other hand, the overall degrees of polymerization, consequently the resepctive molar masses, decrease from 24 to 13 going from lowest to highest target content.

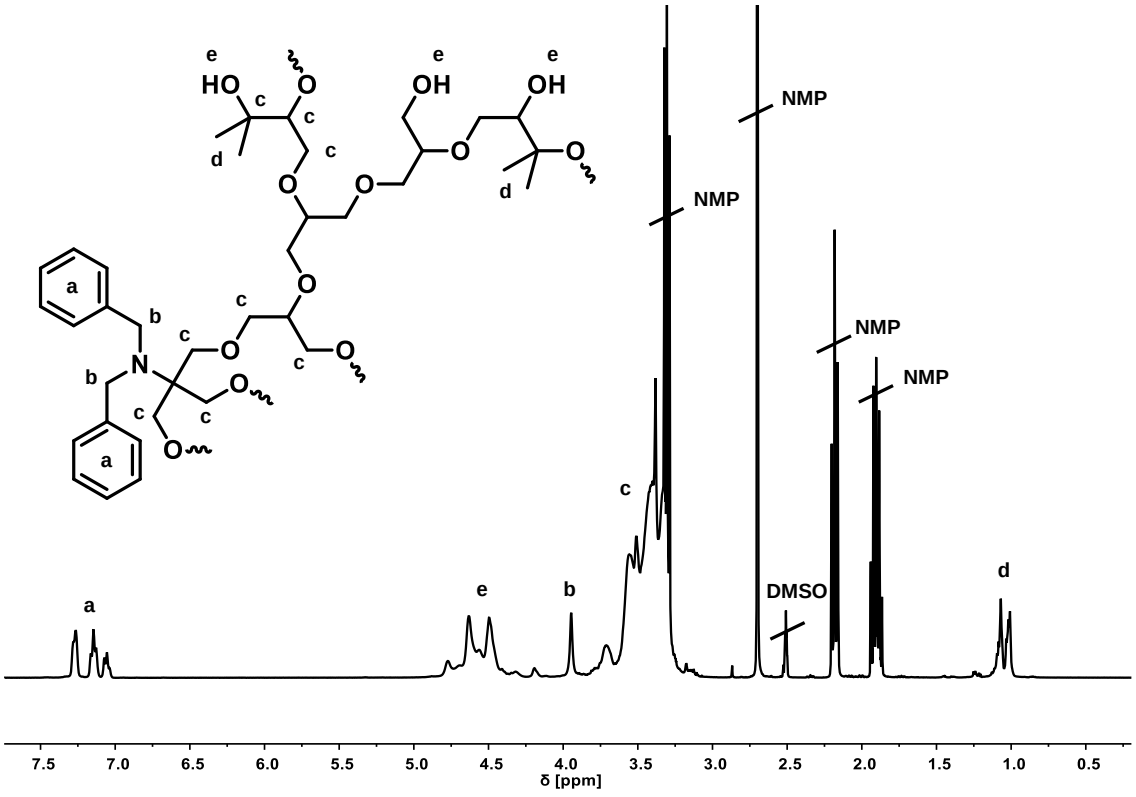

Figure 8. ^{1}H NMR spectrum of *hb*P($G_{0.93}$-*co*-DiMeGly$_{0.07}$) (300 MHz ,DMSO-d_6).

In summary, a number of polymers with similar degrees of polymerization and systematic variation of the content of either MeGly or DiMeGly was obtained. These polymers remain fully soluble in water and exhibit high overall numbers of functional groups. Therefore, the DB is expected to be the only fundamental property of *hb*PG affected by the incorporation of either MeGly or DiMeGly. By systematical investigation of the degrees of branching using inverse gated ^{13}C NMR spectroscopy, the experimental data can be compared to the computationa simulations discussed in the previous section.

Degrees of Branching

Figure 9 shows two typical ^{13}C NMR spectra of the polyether region of *hb*P(G-*co*-MeGly) and *hb*P(G-*co*-DiMeGly). Owing to the unique reaction mechanism, each monomer can form four different repeating units, namely dendritic (D), terminal (T) and two different linear units ($L_{1,3}$ and $L_{1,4}$). Additional analytical data, which was used to assign the various signals of the polyether region to these repeating units, can be found in the supporting information (Figure S 7 to Figure S 20). Due to insufficient signal resolution resulting in signals of both monomers overlapping, no copolymer compositions were calculated from the ^{13}C NMR spectra. However, as according to equation 2 the dendritic and linear units of both comonomers as a whole are used, DBs can be calculated in spite of considerable signal overlap.

By determining the signal intensity ratios of the dendritic and linear units the degree of branching can be calculated according to Frey and coworkers:[8]

$$DB = \frac{2\left(D_{Gly} + D_{(Di-)MeGly}\right)}{2\left(D_{Gly} + D_{(Di-)MeGly}\right) + L_{1,3Gly} + L_{1,4Gly} + L_{1,3(Di-)MeGly} + L_{1,4(Di-)MeGly}} \quad 7$$

The calculated DBs together with the composition of the corresponding copolymers determined by ^{1}H NMR spectroscopy are summarized in Table 4. Compared to the degrees of branching of *hb*PGs with similar degrees of polymerization, various trends can be observed.

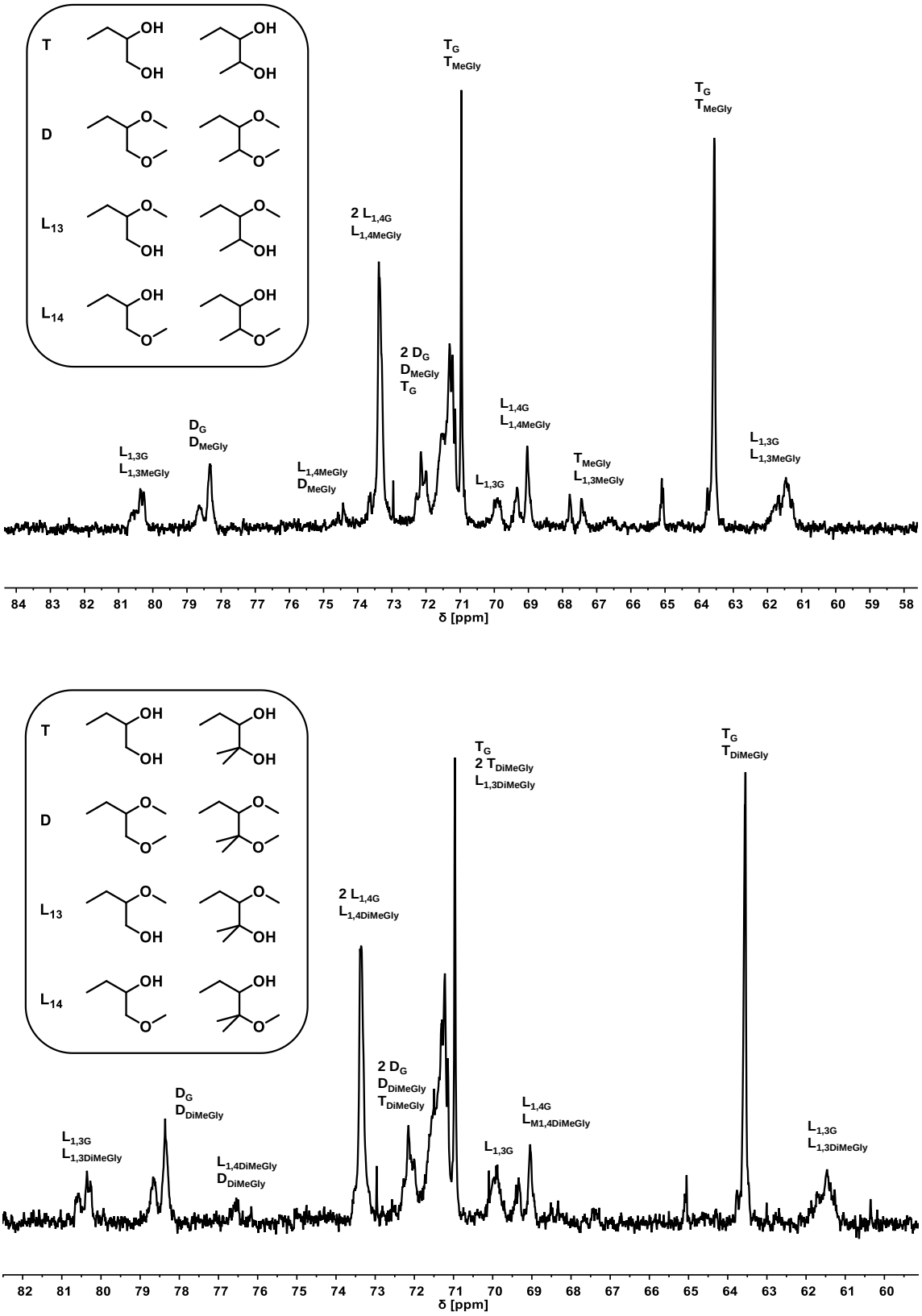

Figure 9. Polyether region in the ^{13}C NMR spectra of *hb*P($G_{0.90}$-*co*-$MeGly_{0.10}$) (top) and *hb*P($G_{0.93}$-*co*-$DiMeGly_{0.07}$) (bottom) (100 MHz ,DMSO-d_6).

Table 4. ^{1}H and ^{13}C NMR data of the copolymers based on glycidol and either MeGly or DiMeGly.

Entry	Sample[a)]	DP_n[b)]	$X_{(Di-)MeGly}$[c)]	DB[c)]	DB_{hbPG}[4]
1	*hb*P($G_{0.90}$-*co*-$MeGly_{0.10}$)	21	0.10	0.52	0.55
2	*hb*P($G_{0.79}$-*co*-$MeGly_{0.21}$)	21	0.22	0.57	0.55
3	*hb*P($G_{0.68}$-*co*-$MeGly_{0.32}$)	20	0.32	0.59	0.55
4	*hb*P($G_{0.60}$-*co*-$MeGly_{0.40}$)	31	0.41	0.60	0.55 – 0.56
5	*hb*P($G_{0.50}$-*co*-$MeGly_{0.50}$)	24	0.50	0.61	0.55
6	*hb*P($G_{0.93}$-*co*-$DiMeGly_{0.07}$)	24	0.07	0.62	0.55
7	*hb*P($G_{0.88}$-*co*-$DiMeGly_{0.12}$)	21	0.12	0.66	0.55
8	*hb*P($G_{0.85}$-*co*-$DiMeGly_{0.15}$)	18	0.15	0.62	0.54?
9	*hb*P($G_{0.80}$-*co*-$DiMeGly_{0.20}$)	15	0.20	0.57	0.53
10	*hb*P($G_{0.71}$-*co*-$DiMeGly_{0.29}$)	13	0.29	0.56	0.53

[a)]Terminology: indices denote the copolymer composition determined by ^{1}H NMR spectroscopy, [b)]determined by ^{1}H NMR spectroscopy, [c)]determined by ^{13}C NMR spectroscopy, [d)]degrees of branching of *hb*PG with similar DP_n.[4]

For a more feasible visualization, Figure 10 shows the degrees of branching plotted against the comonomer content for the different copolymers based on glycidol and MeGly as well as glycidol and DiMeGly.

For copolymers containing MeGly, the degrees of branching increase to values well above what is expected for hyperbranched polyglycerols with similar degrees of polymerization (dashed lines) the more comonomer is incorporated.[4]

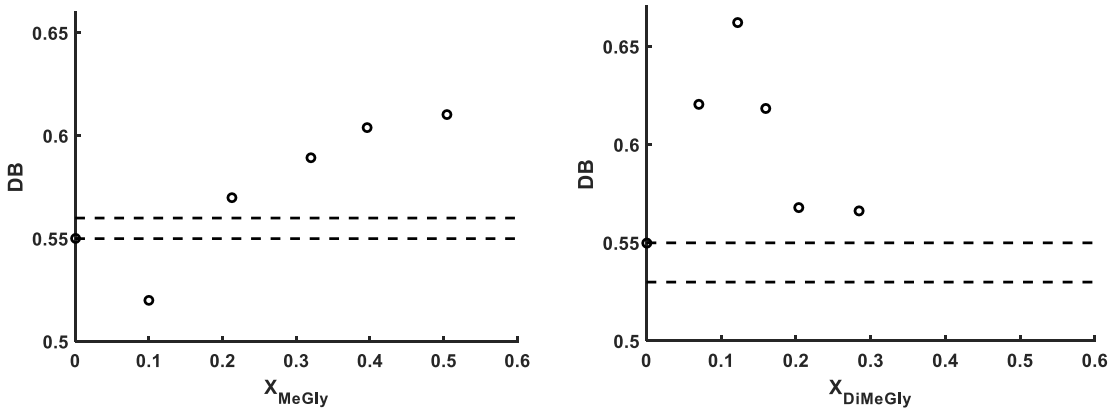

Figure 10. Degrees of branching plotted against the respective copolymer composition $X_{(Di-)MeGly}$ for *hb*P(G-*co*-MeGly) (left) and *hb*P(G-*co*-DiMeGly) (right).

However, for MeGly contents below 0.20 lower degrees of branching than for hyperbranched polyglycerols are observed. For DiMeGly, the trend is reversed: at low contents, the degrees of branching increase to values at the upper theoretical limit for hyperbranched polymers prepared by slow monomer addition (DB ≈ 0.66).[9] Furthermore, in both cases the degree of branching is mainly dictated by the copolymer composition rather than the molar mass or degree of polymerization: comparing sample 4 to 5 or sample 6 to 7, the degree of branching still increases, although the degree of polymerization decreases, which is in stark contrast to the computer simulation regarding homopolymerization presented above as well as experimental data discussed in literature.[4] Furthermore, for samples 7 to 10, DB decreases at a much steeper rate than what is described in literature, since halving DP_n should decrease DB only by 0.02.[4]

The aforementioned observations are explained considering the reaction mechanism and the computer modeling regarding the homopolymerization of MeGly and DiMeGly in the previous chapter. Especially for low comonomer contents, the proton transfer equilibrium between the primary and secondary

alcohol of glycidol is the determining factor for the overall DB. Therefore, MeGly and DiMeGly can be considered as auxiliary bases during the ring-opening multibranching polymerization of glycidol. By addition of MeGly, the overall concentration of secondary alcohols is increased resulting in a shift towards primary alkoxides of the already existing equilibrium, thus increasing the amount of $L_{1,4}$ units decreasing the probability of branching even further. Tertiary hydroxy groups, characterized by a higher pK_a value compared to secondary ones, are introduced by the copolymerization with DiMeGly. As the deprotonation and thus propagation from the secondary alcohol of glycidol is more favorable in the presence of DiMeGly, more $L_{1,3}$ and D units are formed and the overall degree of branching of the *hb*PG copolymer increases. On the other hand, at higher comonomer ratios, the proton transfer equilibrium of the comonomer dictates the formation of branching points. Hence, at comonomer contents of 0.10 and above, the influence of the copolymer composition on the DB follows the trends predicted by computer simulations.

Conclusion

Hyperbranched copolymers based on glycidol and either MeGly or DiMeGly have been introduced in order to influence certain steps of the reaction mechanism to alter the degree of branching. The polymers were prepared *via* simultaneous slow monomer addition of both monomers to a solution of a partially deprotonated initiator salt in NMP as solvent. While preparing copolymers of glycidol and MeGly, the copolymer compositions were varied systematically between 0.10 and 0.50, maintaining constant degrees of polymerization (determined by ^{1}H NMR spectroscopy) to allow comparison to similar hyperbranched polyglycerols. Molar masses determined by SEC were in the range of 720 to 930 g mol^{-1} with moderate dispersities between 1.43 and 1.58. The control over the copolymer composition and degree of polymerization of *hb*P(G-*co*-DiMeGly) copolymers proved to be less viable: The DiMeGly content was varied between 0.07 and 0.29. However, the degrees of polymerization decreased with higher comonomer fraction from 24 to 13. The DBs calculated using inverse gated ^{13}C NMR spectroscopy showed a strong dependence on the content of either MeGly or DiMeGly. To understand the experimental data regarding DB, the relative abundances of the different repeating units (D, T, $L_{1,3}$ and $L_{1,4}$) and consequently DB as a function of DP_n were predicted by DFT calculations and computer simulations of the reaction mechanism of the homopolymerization of either G, MeGly or DiMeGly. It was concluded, that at comonomer fractions below 0.10, the comonomers act as auxiliary bases strongly influencing the proton transfer reaction of glycidol and shifting this equilibrium to either side. As a result, significantly lower DBs than homopolymer of glycidol and vice versa are observed. Only at higher contents, the trends predicted by computer simulations were found, as the ring-opening and subsequent proton transfer of a

MeGly or DiMeGly chain end becomes the determining factor in the formation of branching. Furthermore, the influence of DP_n on DB was found to be negligible in comparison to content of the comonomers MeGly or DiMeGly.

By introducing the novel comonomers MeGly and DiMeGly, the degree of branching of *hb*PG can be altered while maintaining fundamental properties like water-solubility or a larger number of functional groups. Thus, the variation of the comonomer content allows for the fine-tuning of properties that are only dependent on the DB.

Acknowledgment

T. K. is grateful for financial support by a fellowship from the “Fonds der Chemischen Industrie (FCI)”. Furthermore, the authors thank Monika Schmelzer and Ulrike Kemmer-Jonas for technical assistance.

References

(1) Yan, D.; Gao, C.; Frey, H. *Hyperbranched polymers: Synthesis, properties, and applications*; Wiley series on polymer engineering and technology; Wiley: Hoboken, N.J, 2011.

(2) Voit, B. I.; Lederer, A. Hyperbranched and highly branched polymer architectures--synthetic strategies and major characterization aspects. *Chem. Rev.* **2009**, *109*, 5924–5973.

(3) Kim, Y. H. Hyperbranched polymers 10 years after. *J. Polym. Sci. A Polym. Chem.* **1998**, *36*, 1685–1698.

(4) Sunder, A.; Hanselmann, R.; Frey, H.; Mülhaupt, R. Controlled Synthesis of Hyperbranched Polyglycerols by Ring-Opening Multibranching Polymerization. *Macromolecules* **1999**, *32*, 4240–4246.

(5) Herzberger, J.; Niederer, K.; Pohlit, H.; Seiwert, J.; Worm, M.; Wurm, F. R.; Frey, H. Polymerization of Ethylene Oxide, Propylene Oxide, and Other Alkylene Oxides: Synthesis, Novel Polymer Architectures, and Bioconjugation. *Chem. Rev.* **2016**, *116*, 2170–2243.

(6) Schömer, M.; Schüll, C.; Frey, H. Hyperbranched aliphatic polyether polyols. *J. Polym. Sci. A Polym. Chem.* **2013**, *51*, 995–1019.

(7) Hawker, C. J.; Lee, R.; Frechet, J. M. J. One-step synthesis of hyperbranched dendritic polyesters. *J. Am. Chem. Soc.* **1991**, *113*, 4583–4588.

(8) Hölter, D.; Burgath, A.; Frey, H. Degree of branching in hyperbranched polymers. *Acta Polym.* **1997**, *48*, 30–35.

(9) Hölter, D.; Frey, H. Degree of branching in hyperbranched polymers. 2. Enhancement of the db: Scope and limitations. *Acta Polym.* **1997**, *48*, 298–309.

(10) Yan, D.; Müller, A. H. E.; Matyjaszewski, K. Molecular Parameters of Hyperbranched Polymers Made by Self-Condensing Vinyl Polymerization. 2. Degree of Branching. *Macromolecules* **1997**, *30*, 7024–7033.

(11) Yu, M. Q.; Zhou, Z.; Yan, D. Y. *Chem. J. Chin. Univ.-Chin.* **2003**, *24*, 1332.

(12) Self-Association and Degree of Branching: Fluorescence-Probe Study of Hyperbranched Poly(sulfone-amine)s in Aqueous Solution.

(13) Cheng, H.; Yuan, X.; Sun, X.; Li, K.; Zhou, Y.; Yan, D. Effect of Degree of Branching on the Self-Assembly of Amphiphilic Hyperbranched Multiarm Copolymers. *Macromolecules* **2010**, *43*, 1143–1147.

(14) Gong, W.; Mai, Y.; Zhou, Y.; Qi, N.; Wang, B.; Yan, D. Effect of the Degree of Branching on Atomic-Scale Free Volume in Hyperbranched Poly[3-ethyl-3-(hydroxymethyl)oxetane]. A Positron Study. *Macromolecules* **2005**, *38*, 9644–9649.

(15) Krämer, M.; Stumbé, J.-F.; Grimm, G.; Kaufmann, B.; Krüger, U.; Weber, M.; Haag, R. Dendritic polyamines: simple access to new materials with defined treelike structures for application in nonviral gene delivery. *ChemBioChem* **2004**, *5*, 1081–1087.

(16) Mai, Y.; Zhou, Y.; Yan, D. Y. *Chem. J. Chin. Univ.-Chin.* **2004**, *25*, 1373.

(17) Mai, Y.; Zhou, Y.; Yan, D.; Hou, J. Quantitative dependence of crystallinity on degree of branching for hyperbranched poly[3-ethyl-3-(hydroxymethyl)oxetane]. *New J. Phys.* **2005**, *7*, 42.

(18) Schubert, C.; Osterwinter, C.; Tonhauser, C.; Schömer, M.; Wilms, D.; Frey, H.; Friedrich, C. Can Hyperbranched Polymers Entangle? Effect of Hydrogen Bonding on Entanglement Transition and Thermorheological Properties of Hyperbranched Polyglycerol Melts. *Macromolecules* **2016**, *49*, 8722–8737.

(19) Stiriba, S.-E.; Kautz, H.; Frey, H. Hyperbranched molecular nanocapsules: comparison of the hyperbranched architecture with the perfect linear analogue. *J. Am. Chem. Soc.* **2002**, *124*, 9698–9699.

(20) Zhu, Q.; Wu, J.; Tu, C.; Shi, Y.; He, L.; Wang, R.; Zhu, X.; Yan, D. Role of branching architecture on the glass transition of hyperbranched polyethers. *J. Phys. Chem. B* **2009**, *113*, 5777–5780.

(21) Zhang, C.; Fan, Y.; Zhang, Y.; Yu, C.; Li, H.; Chen, Y.; Hamley, I. W.; Jiang, S. Self-Assembly Kinetics of Amphiphilic Dendritic Copolymers. *Macromolecules* **2017**, *50*, 1657–1665.

(22) Hanselmann, R.; Hölter, D.; Frey, H. Hyperbranched Polymers Prepared via the Core-Dilution/Slow Addition Technique: Computer Simulation of Molecular Weight Distribution and Degree of Branching. *Macromolecules* **1998**, *31*, 3790–3801.

(23) Radke, W.; Litvinenko, G.; Müller, A. H. E. Effect of Core-Forming Molecules on Molecular Weight Distribution and Degree of Branching in the Synthesis of Hyperbranched Polymers. *Macromolecules* **1998**, *31*, 239–248.

(24) Wang, J.; Johnson, D. M. Design, synthesis and polymerization of highly branched pseudodendrimers through tandem reactions. *Polym. Int.* **2009**, *58*, 1234–1245.

(25) Ishida, Y.; Sun, A. C. F.; Jikei, M.; Kakimoto, M.-a. Synthesis of Hyperbranched Aromatic Polyamides Starting from Dendrons as AB x Monomers: Effect of Monomer Multiplicity on the Degree of Branching. *Macromolecules* **2000**, *33*, 2832–2838.

(26) Jikei, M.; Kakimoto, M.-a. Hyperbranched Polymers: a promising new class of materials. *Prog. Polym. Sci.* **2001**, *26*, 1233–1285.

(27) Lach, C.; Frey, H. Enhancing the Degree of Branching of Hyperbranched Polymers by Postsynthetic Modification. *Macromolecules* **1998**, *31*, 2381–2383.

(28) Huang, W.; Su, L.; Bo, Z. Hyperbranched polymers with a degree of branching of 100% prepared by catalyst transfer Suzuki-Miyaura polycondensation. *J. Am. Chem. Soc.* **2009**, *131*, 10348–10349.

(29) Smet, M.; Schacht, E.; Dehaen, W. Synthesis, Characterization, and Modification of Hyperbranched Poly(arylene oxindoles) with a Degree of Branching of 100 %. *Angew. Chem. Int. Ed.* **2002**, *41*, 4547–4550.

(30) Fu, Y.; van Oosterwijck, C.; Vandendriessche, A.; Kowalczuk-Bleja, A.; Zhang, X.; Dworak, A.; Dehaen, W.; Smet, M. Hyperbranched Poly(arylene oxindole)s with a Degree of Branching of 100% for the Construction of Nanocontainers by Orthogonal Modification. *Macromolecules* **2008**, *41*, 2388–2393.

(31) Sinananwanich, W.; Higashihara, T.; Ueda, M. Synthesis of a Hyperbranched Polymer with Perfect Branching Based on Piperidine-4-one. *Macromolecules* **2009**, *42*, 994–1001.

(32) Kono, S.; Sinananwanich, W.; Shibasaki, Y.; Ando, S.; Ueda, M. Synthesis of Hyperbranched Polymer with Degree of Branching of Approximately 100% by Polycondensation of 2-(4-Phenoxyphenoxy)fluorenone. *Polymer Journal* **2007**, *39*, 1150–1156.

(33) Jim, C. K. W.; Qin, A.; Lam, J. W. Y.; Liu, J.; Haeussler, M.; Tang, B. Z. *Sci. China, Ser. B Chem.* **2008**, *51*.

(34) Frey, H.; Hölter, D. Degree of branching in hyperbranched polymers. 3 Copolymerization of ABm-monomers with AB and ABn-monomers. *Acta Polym.* **1999**, *50*, 67–76.

(35) Schubert, C.; Schömer, M.; Steube, M.; Decker, S.; Friedrich, C.; Frey, H. Systematic Variation of the Degree of Branching (DB) of Polyglycerol via Oxyanionic Copolymerization of Glycidol with a Protected Glycidyl Ether and Its Impact on Rheological Properties. *Macromol. Chem. Phys.* **2018**, *219*, 1700376.

(36) Wilms, D.; Schömer, M.; Wurm, F.; Hermanns, M. I.; Kirkpatrick, C. J.; Frey, H. Hyperbranched PEG by random copolymerization of ethylene oxide and glycidol. *Macromol. Rapid Commun.* **2010**, *31*, 1811–1815.

(37) Möck, A.; Burgath, A.; Hanselmann, R.; Frey, H. Synthesis of Hyperbranched Aromatic Homo- and Copolyesters via the Slow Monomer Addition Method. *Macromolecules* **2001**, *34*, 7692–7698.

(38) Mai, Y.; Zhou, Y.; Yan, D.; Lu, H. Effect of Reaction Temperature on Degree of Branching in Cationic Polymerization of 3-Ethyl-3-(hydroxymethyl)oxetane. *Macromolecules* **2003**, *36*, 9667–9669.

(39) Weimer, M. W.; Frechet, J. M. J.; Gitsov, I. Importance of active-site reactivity and reaction conditions in the preparation of hyperbranched polymers by self-condensing vinyl polymerization: Highly branched vs. linear poly[4-(chloromethyl)styrene] by metal-catalyzed "living" radical polymerization. *J. Polym. Sci. A Polym. Chem.* **1998**, *36*, 955–970.

(40) Yan, D.; Hou, J.; Zhu, X.; Kosman, J. J.; Wu, H.-S. A new approach to control crystallinity of resulting polymers: Self-condensing ring opening polymerization. *Macromol. Rapid Commun.* **2000**, *21*, 557–561.

(41) Mohammadifar, E.; Bodaghi, A.; Dadkhahtehrani, A.; Nemati Kharat, A.; Adeli, M.; Haag, R. Green Synthesis of Hyperbranched Polyglycerol at Room Temperature. *ACS Macro Lett.* **2017**, *6*, 35–40.

(42) Spears, B. R.; Marin, M. A.; Montenegro-Burke, J. R.; Evans, B. C.; McLean, J.; Harth, E. Aqueous Epoxide Ring-Opening Polymerization (AEROP): Green Synthesis of Polyglycidol with Ultralow Branching. *Macromolecules* **2016**, *49*, 2022–2027.

(43) Spears, B. R.; Waksal, J.; McQuade, C.; Lanier, L.; Harth, E. Controlled branching of polyglycidol and formation of protein-glycidol bioconjugates via a graft-from approach with "PEG-like" arms. *Chem. Commun.* **2013**, *49*, 2394–2396.

(44) Chen, L.; Zhu, X.; Yan, D.; Chen, Y.; Chen, Q.; Yao, Y. Controlling polymer architecture through host-guest interactions. *Angew. Chem. Int. Ed.* **2005**, *45*, 87–90.

(45) Schüll, C.; Nuhn, L.; Mangold, C.; Christ, E.; Zentel, R.; Frey, H. Linear-Hyperbranched Graft-Copolymers via Grafting-to Strategy Based on Hyperbranched Dendron Analogues and Reactive Ester Polymers. *Macromolecules* **2012**, *45*, 5901–5910.

(46) Neese, F. The ORCA program system. *WIREs Comput. Mol. Sci.* **2012**, *2*, 73–78.

(47) Grimme, S.; Brandenburg, J. G.; Bannwarth, C.; Hansen, A. Consistent structures and interactions by density functional theory with small atomic orbital basis sets. *J. Chem. Phys.* **2015**, *143*, 54107.

(48) Knizia, G. Intrinsic Atomic Orbitals: An Unbiased Bridge between Quantum Theory and Chemical Concepts. *J. Chem. Theory Comput.* **2013**, *9*, 4834–4843.

(49) Leibig, D.; Seiwert, J.; Liermann, J. C.; Frey, H. Copolymerization Kinetics of Glycidol and Ethylene Oxide, Propylene Oxide, and 1,2-Butylene Oxide: From Hyperbranched to Multiarm Star Topology. *Macromolecules* **2016**, *49*, 7767–7776.

(50) Paulus, F.; Weiss, M. E. R.; Steinhilber, D.; Nikitin, A. N.; Schütte, C.; Haag, R. Anionic Ring-Opening Polymerization Simulations for Hyperbranched Polyglycerols with Defined Molecular Weights. *Macromolecules* **2013**, *46*, 8458–8466.

(51) Seiwert, J.; Herzberger, J.; Leibig, D.; Frey, H. Thioether-Bearing Hyperbranched Polyether Polyols with Methionine-Like Side-Chains: A Versatile Platform for Orthogonal Functionalization. *Macromol. Rapid Commun.* **2017**, *38*.

(52) Perevyazko, I.; Seiwert, J.; Schömer, M.; Frey, H.; Schubert, U. S.; Pavlov, G. M. Hyperbranched Poly(ethylene glycol) Copolymers: Absolute Values of the Molar Mass, Properties in Dilute Solution, and Hydrodynamic Homology. *Macromolecules* **2015**, *48*, 5887–5898.

Supporting Information

Supplemental Data obtained from DFT calculations

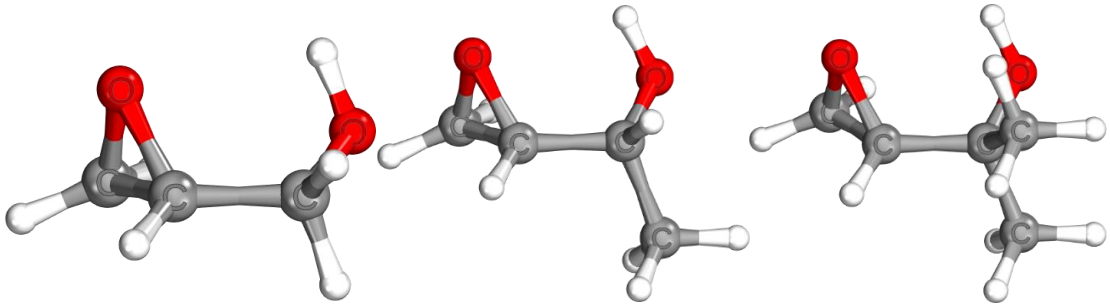

Figure S 1. Proposed structures of the monomers G (left), MeGly (middle) and DiMeGly (right) in vacuum.

Table S 1. Relevant bond lengths d found in G, MeGly, DiMeGly.

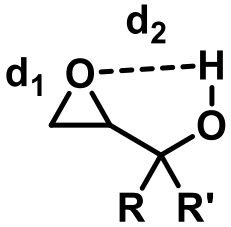	**d_1 [pm]**	**d_2 [pm]**
G: R = R’ = -H	141.87	246.54
MeGly: R = -H, R’ = -CH_3	141.90	237.49
DiMeGly: R = R’ = -CH_3	141.92	239.04

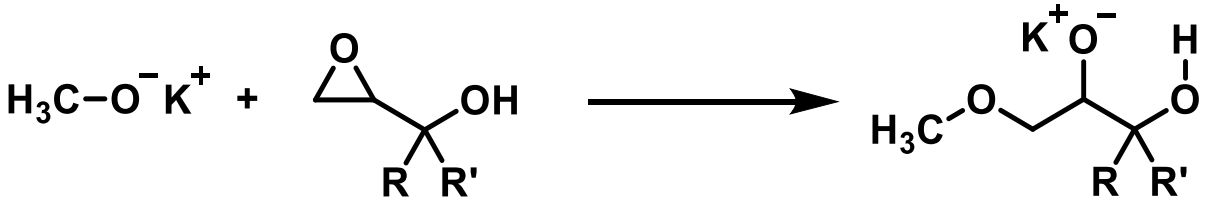

Scheme S 1. Model compounds as active chain ends after ring-opening using potassium methoxide.

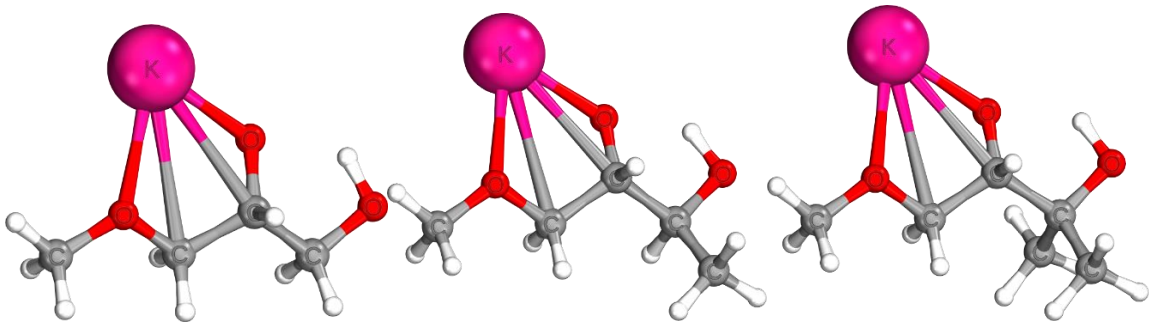

Figure S 2. Proposed of structures of G, MeGly or DiMeGly terminated active chain-ends in vacuum.

Table S 2. Gibbs free enthalpy of the ring-opening of G, MeGly or DiMeGly using potassium methoxide in vacuum at 300 K.

Chain-End	**ΔG** **[kJ mol^{-1}]**
G	-116.21
MeGly	-115.69
DiMeGly	-110.64

Supplemental ^{1}H and ^{13}C NMR Spectra

MeGly

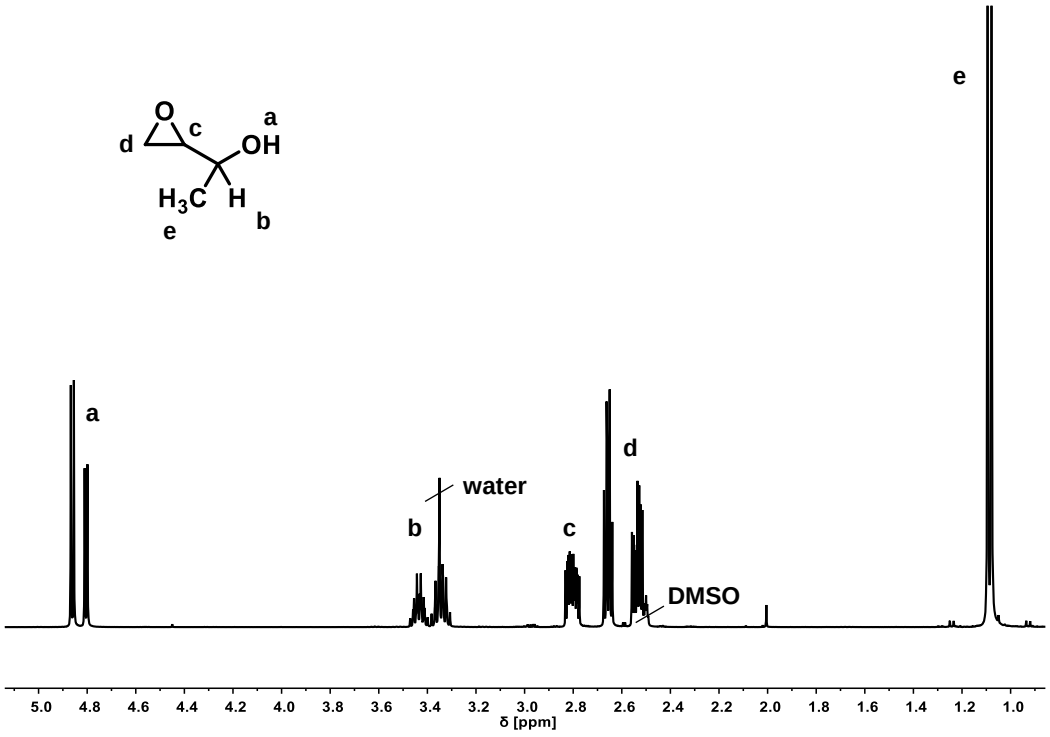

Figure S 3. ^{1}H NMR spectrum of MeGly (400 MHz, DMSO-d_6).

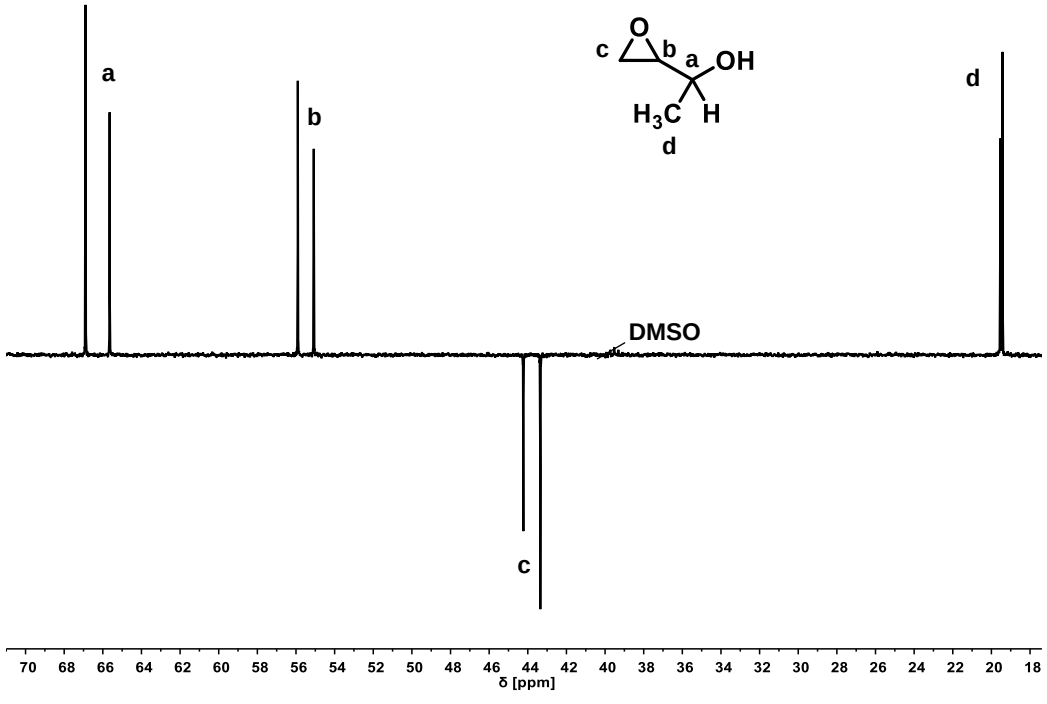

Figure S 4. ^{13}C NMR spectrum (DEPT) of MeGly (100 MHz, DMSO-d_6).

DiMeGly

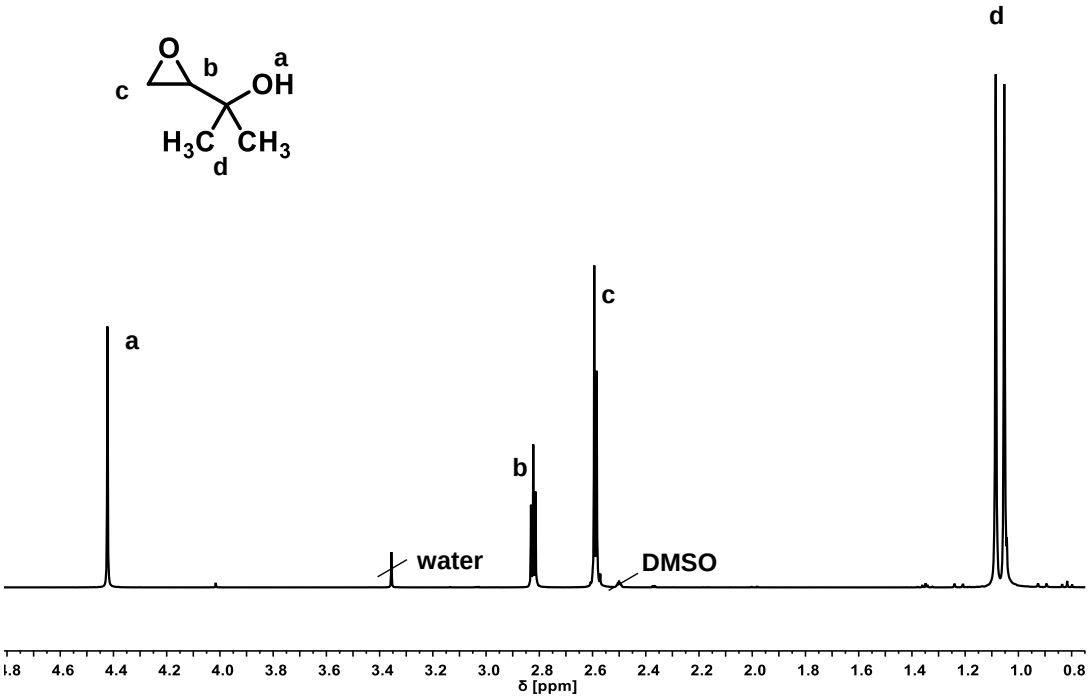

Figure S 5. ^{1}H NMR spectrum of DiMeGly (400 MHz, DMSO-d_6).

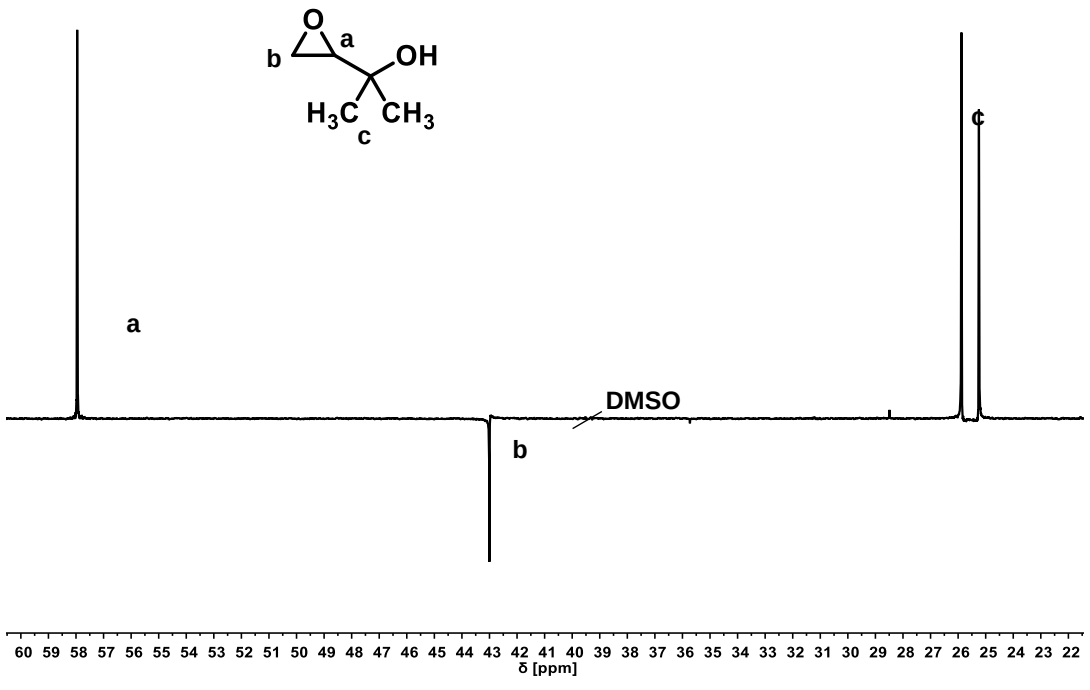

Figure S 6. ^{13}C NMR spectrum (DEPT) of DiMeGly (100 MHz, DMSO-d_6).

***hb*P(G-*co*-MeGly)**

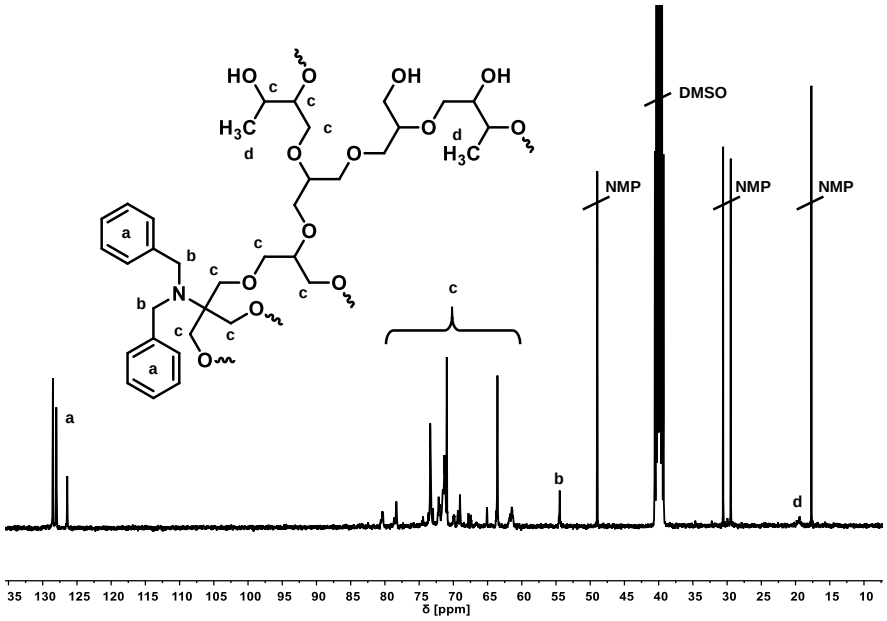

Figure S 7. Inverse gated ^{13}C NMR spectrum of *hb*P($G_{0.90}$-*co*-$MeGly_{0.10}$) (300 MHz, DMSO-d_6).

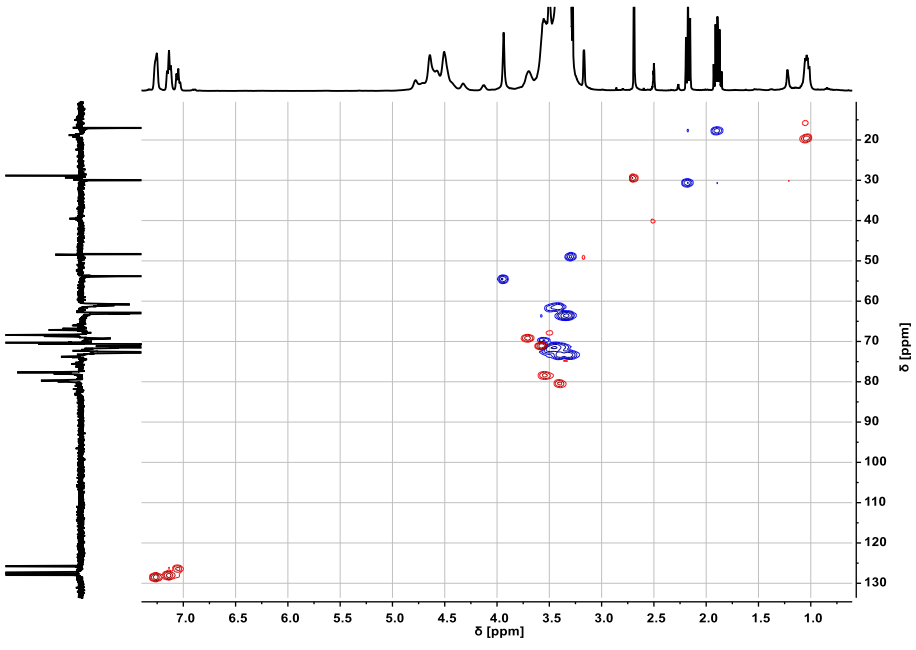

Figure S 8. ^{1}H-^{13}C HSQC NMR spectrum of *hb*P($G_{0.90}$-*co*-$MeGly_{0.10}$) (400/100MHz, DMSO-d_6). ^{1}H and ^{13}C NMR spectra can be found on the horizontal and vertical axis, respectively. Phase correlation is given by correlation of cross peaks (red: methyl, methine, Blue: methylene).

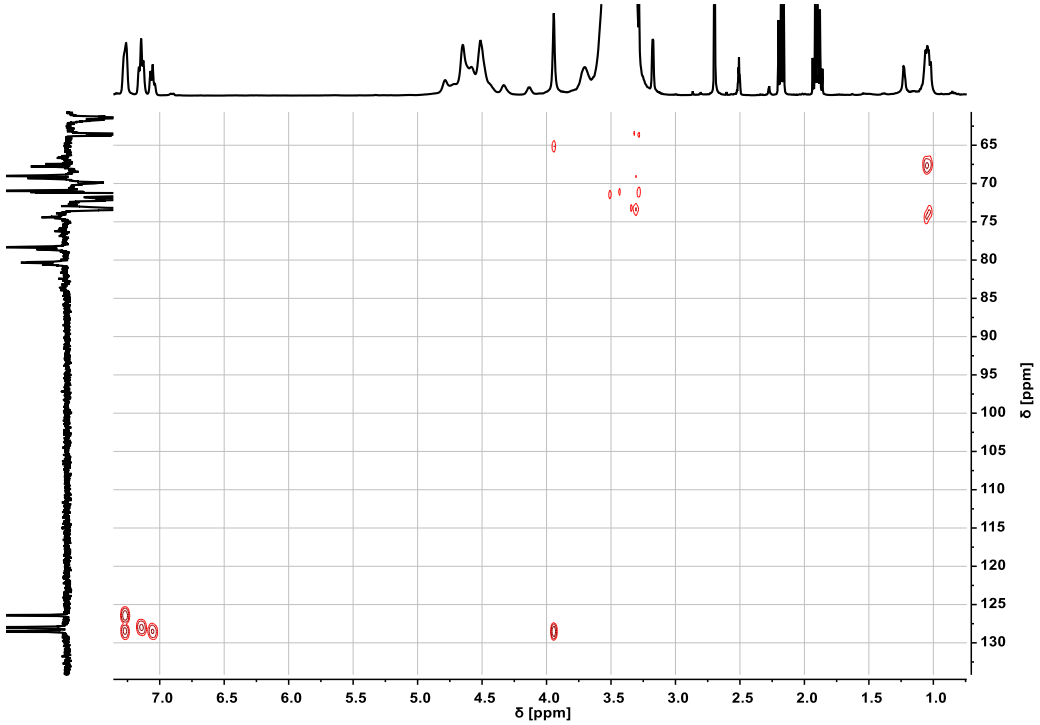

Figure S 9. ^{1}H-^{13}C HMBC NMR spectrum of *hb*P(G$_{0.90}$-*co*-MeGly$_{0.10}$) (400/100 MHz, DMSO-d_6). ^{1}H and ^{13}C NMR spectra can be found on the horizontal and vertical axis, respectively.

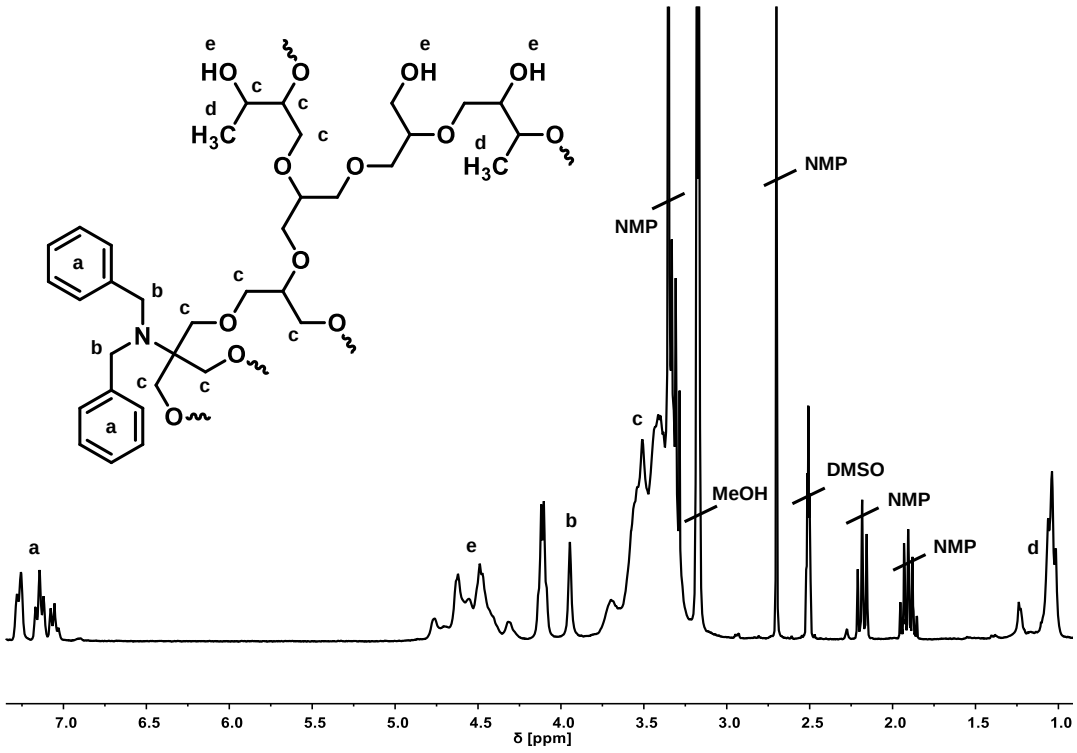

Figure S 10. ^{1}H NMR spectrum of *hb*P(G$_{0.79}$-*co*-MeGly$_{0.21}$) (400 MHz, DMSO-d_6).

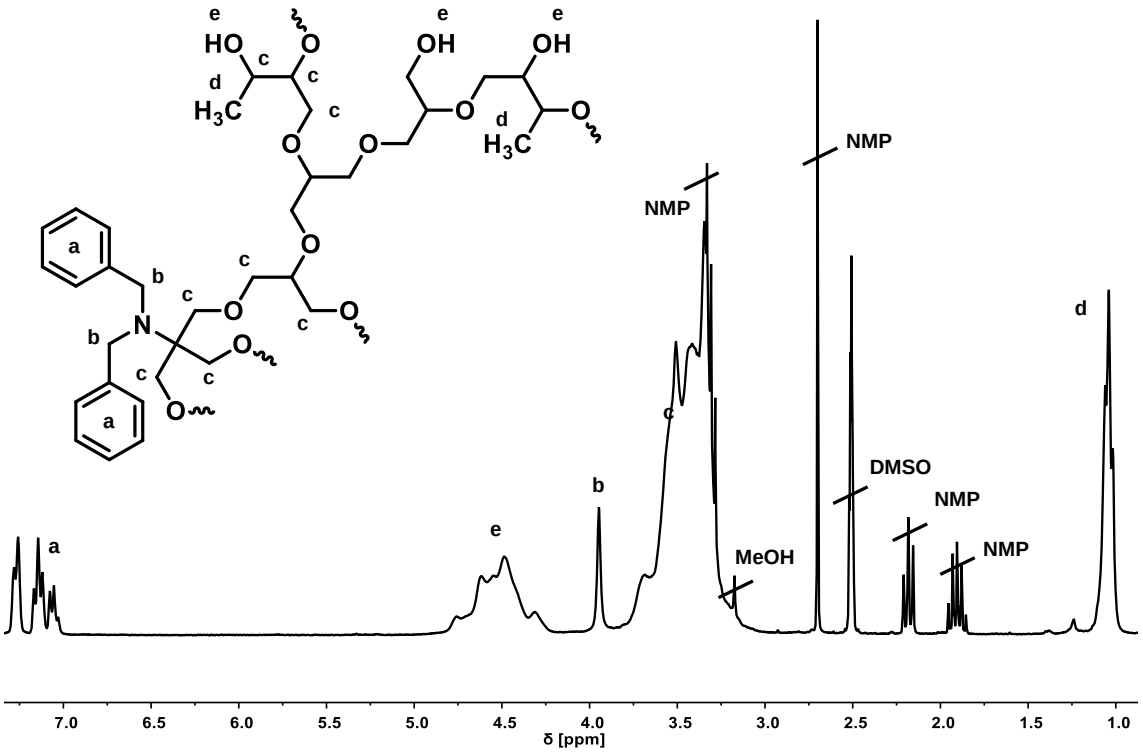

Figure S 11. ^{1}H NMR spectrum of *hb*P($G_{0.68}$-*co*-MeGly$_{0.32}$) (400 MHz, DMSO-d_6).

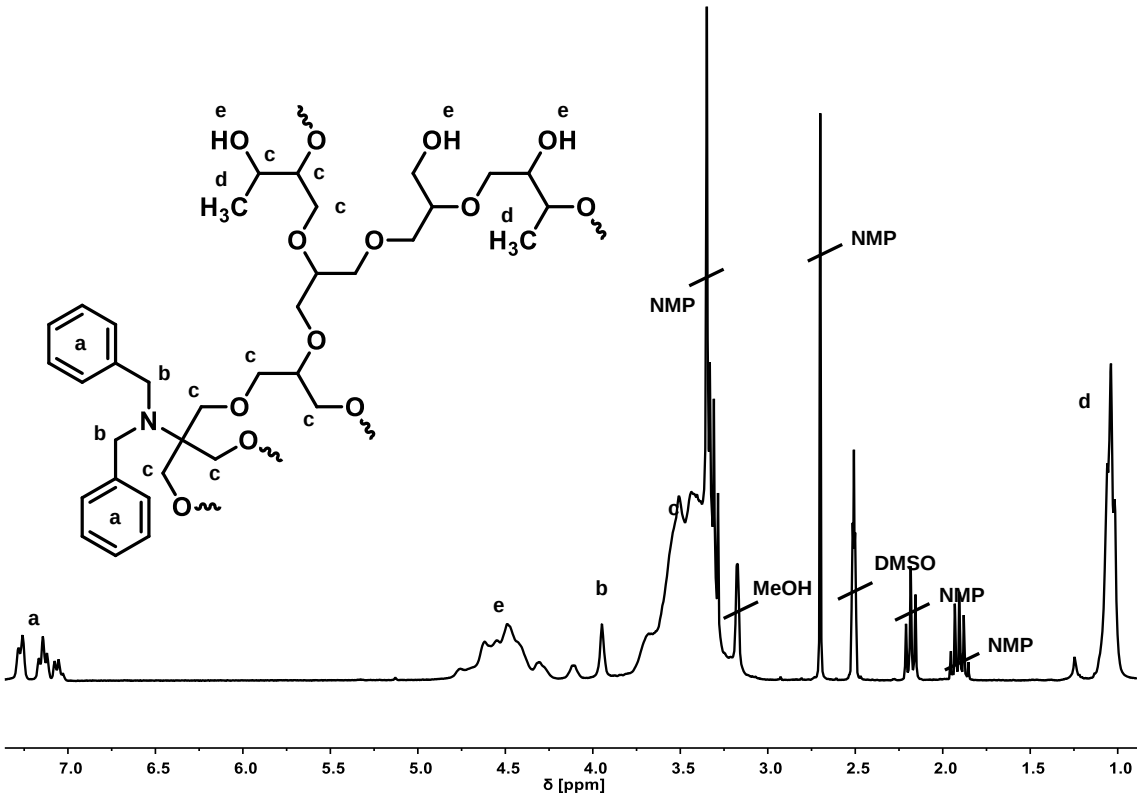

Figure S 12. ^{1}H NMR spectrum of *hb*P($G_{0.60}$-*co*-MeGly$_{0.40}$) (400 MHz, DMSO-d_6).

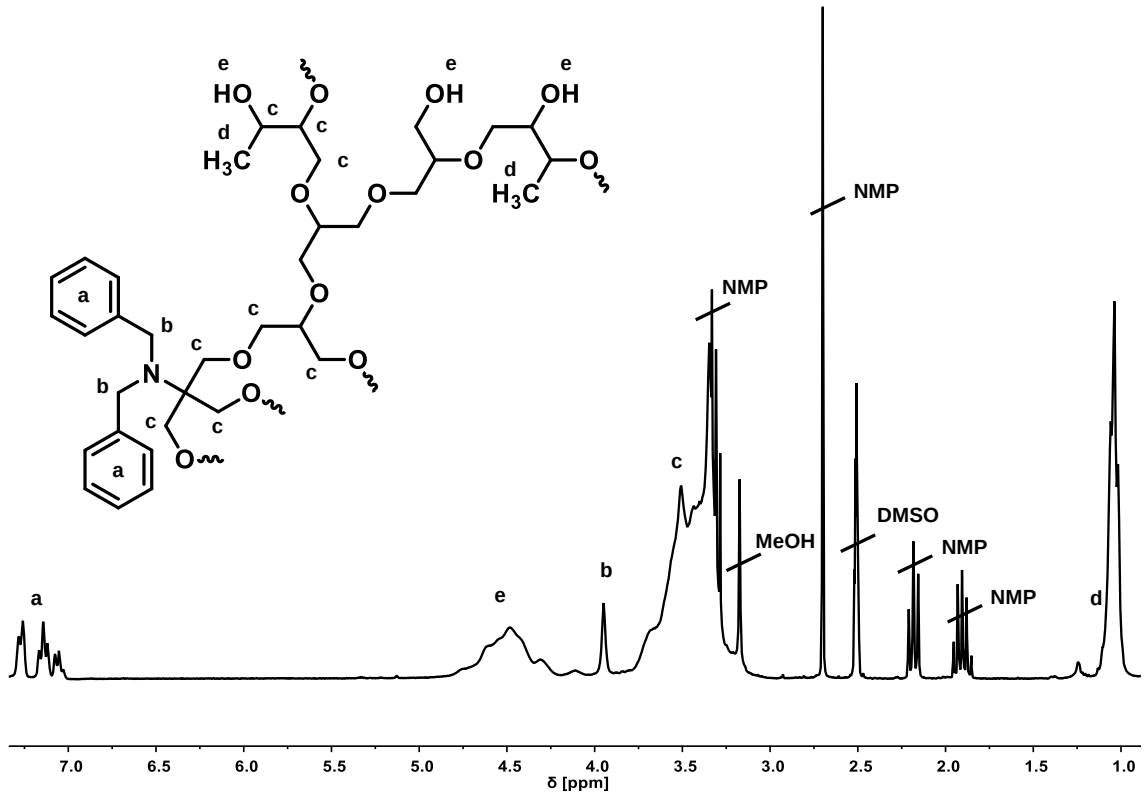

Figure S 13. ^{1}H NMR spectrum of *hb*P($G_{0.50}$-*co*-MeGly$_{0.50}$) (400 MHz, DMSO-d_6).

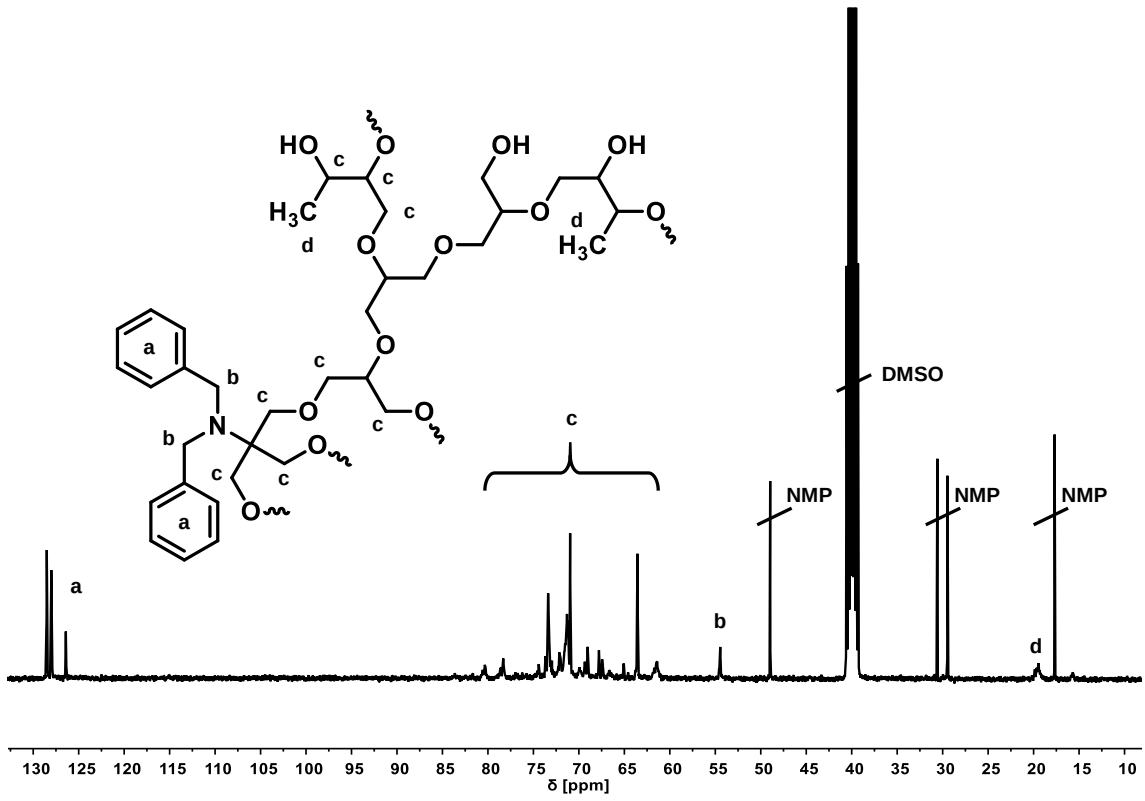

Figure S 14. ^{13}C NMR spectrum of *hb*P($G_{0.79}$-*co*-MeGly$_{0.21}$) (100 MHz, DMSO-d_6).

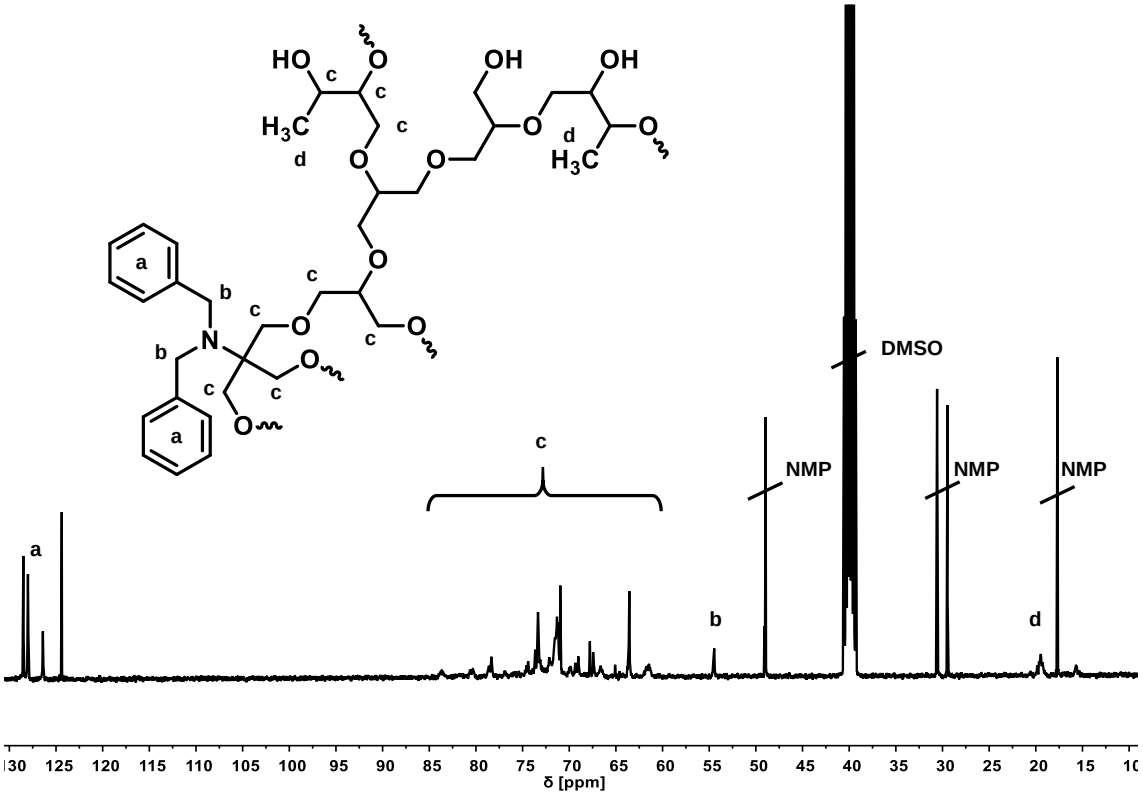

Figure S 15. ^{13}C NMR spectrum of *hb*P($G_{0.69}$-*co*-MeGly$_{0.32}$) (100 MHz, DMSO-d_6).

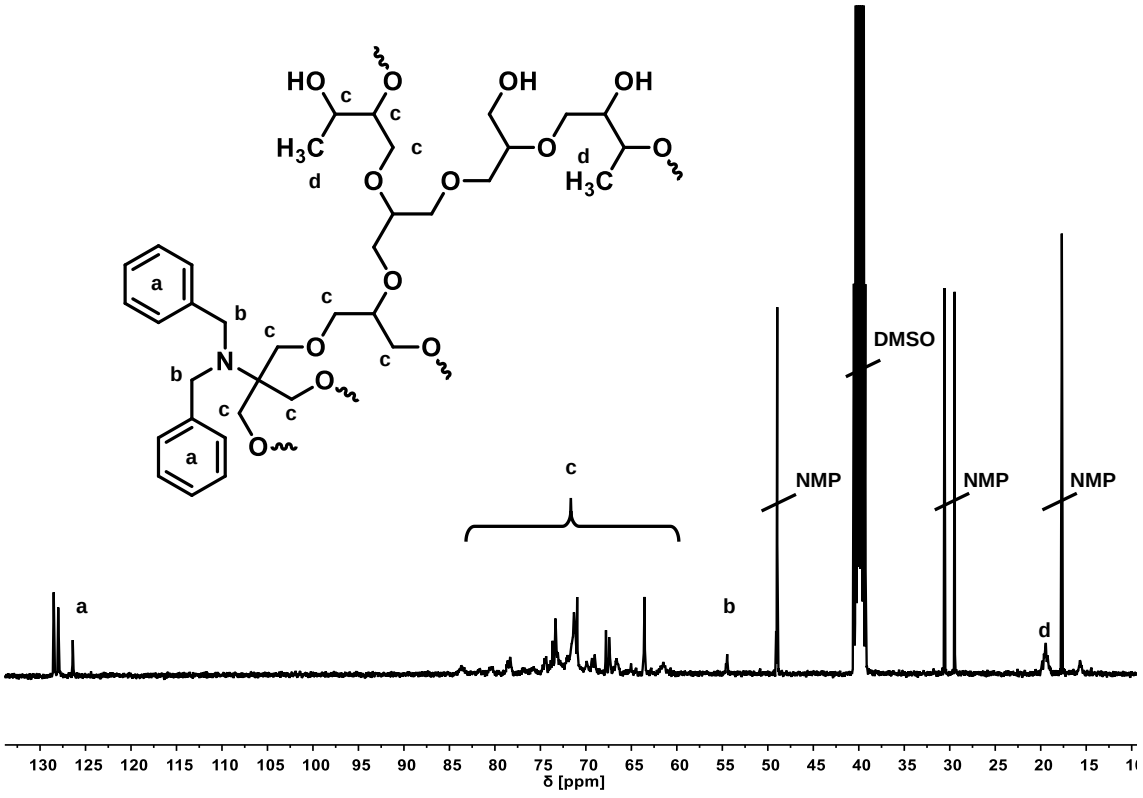

Figure S 16. ^{13}C NMR spectrum of *hb*P($G_{0.60}$-*co*-MeGly$_{0.40}$) (100 MHz, DMSO-d_6).

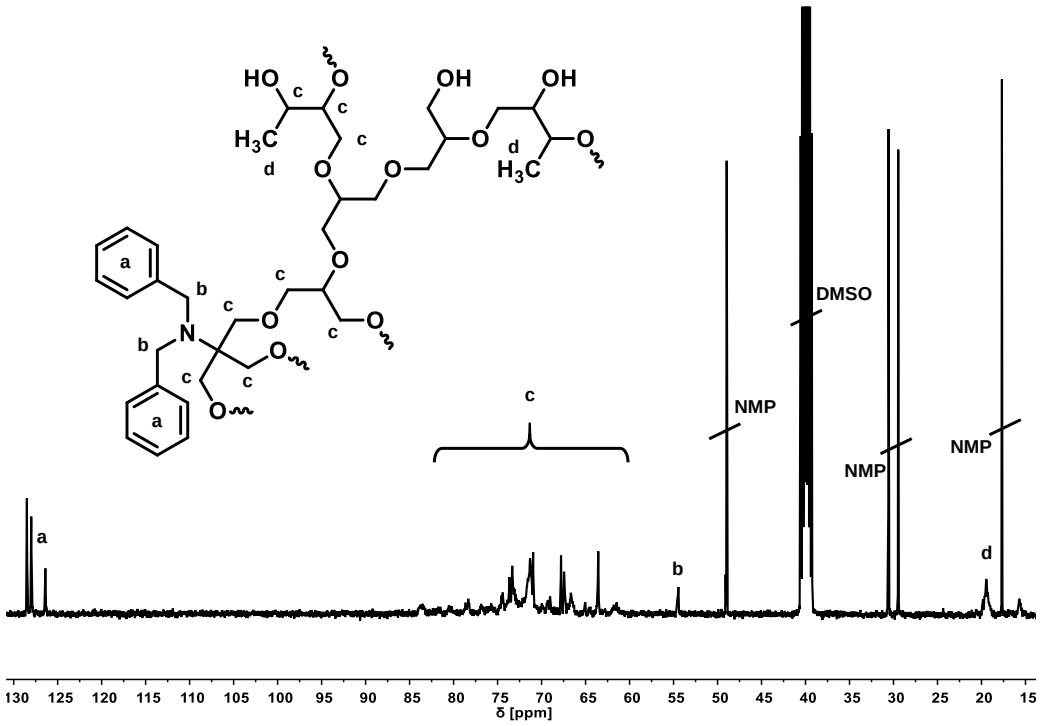

Figure S 17. ^{13}C NMR spectrum of *hb*P($G_{0.50}$-*co*-MeGly$_{0.50}$) (100 MHz, DMSO-d_6).

*hb*P(G-*co*-DiMeGly)

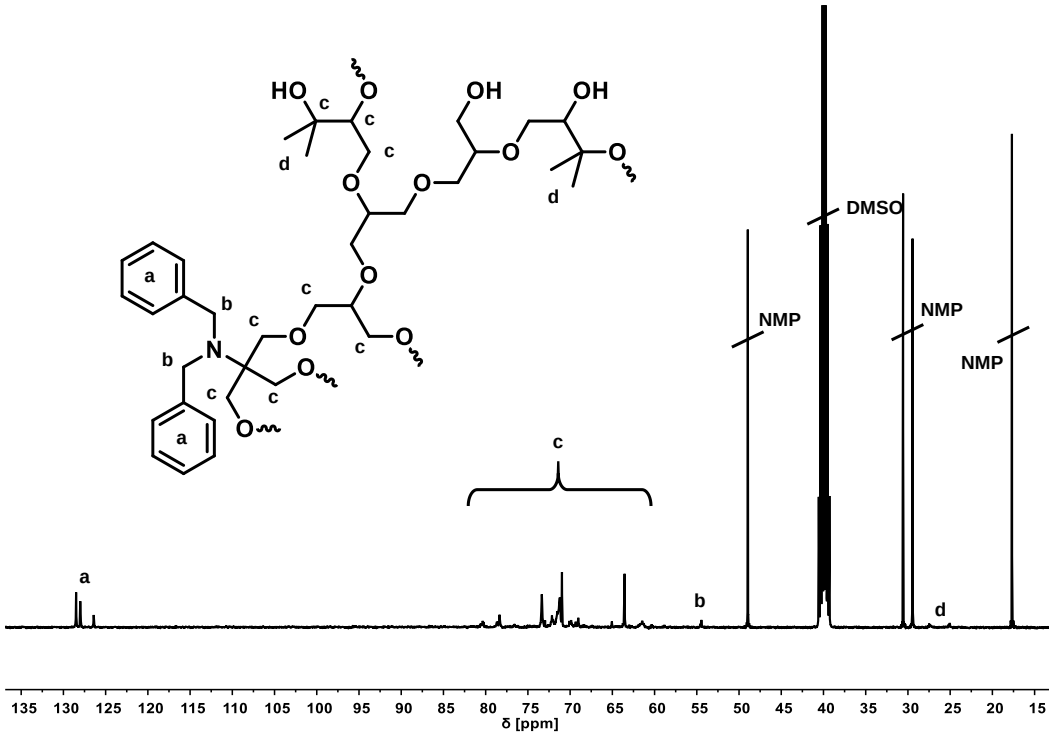

Figure S 18. Inverse gated ^{13}C NMR spectrum of *hb*P($G_{0.93}$-co-DiMeGly$_{0.07}$) (300 MHz, DMSO-d_6).

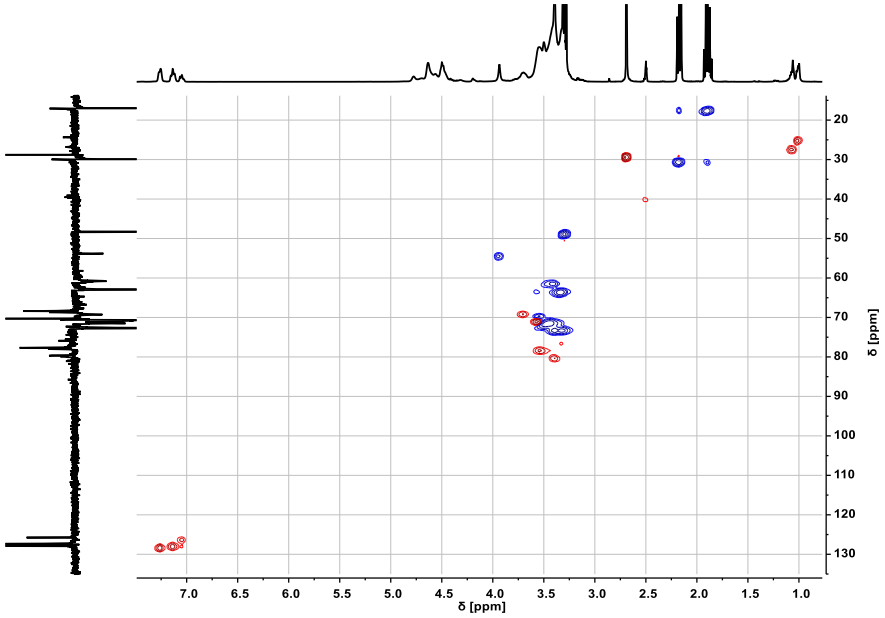

Figure S 19. ^{1}H-^{13}C HSQC NMR spectrum of *hb*P(G$_{0.93}$-*co*-DiMeGly$_{0.07}$) (400/100MHz, DMSO-d_6). ^{1}H and ^{13}C NMR spectra can be found on the horizontal and vertical axis, respectively. Phase correlation is given by correlation of cross peaks (red: methyl, methine, Blue: methylene).

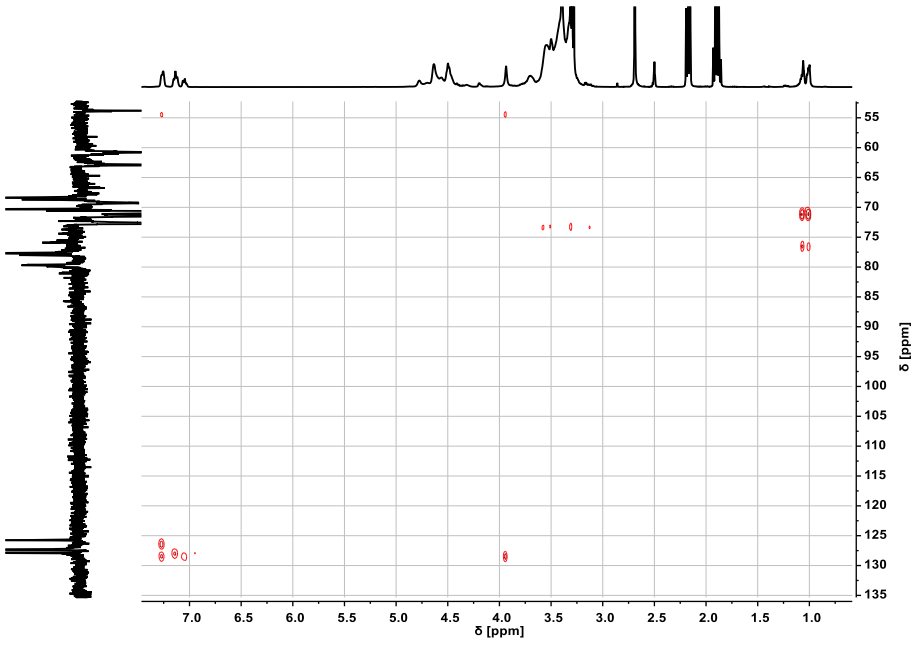

Figure S 20 ^{1}H-^{13}C HMBC NMR spectrum of *hb*P(G$_{0.93}$-*co*-DiMeGly$_{0.07}$) (400/100 MHz, DMSO-d_6). ^{1}H and ^{13}C NMR spectra can be found on the horizontal and vertical axis, respectively.

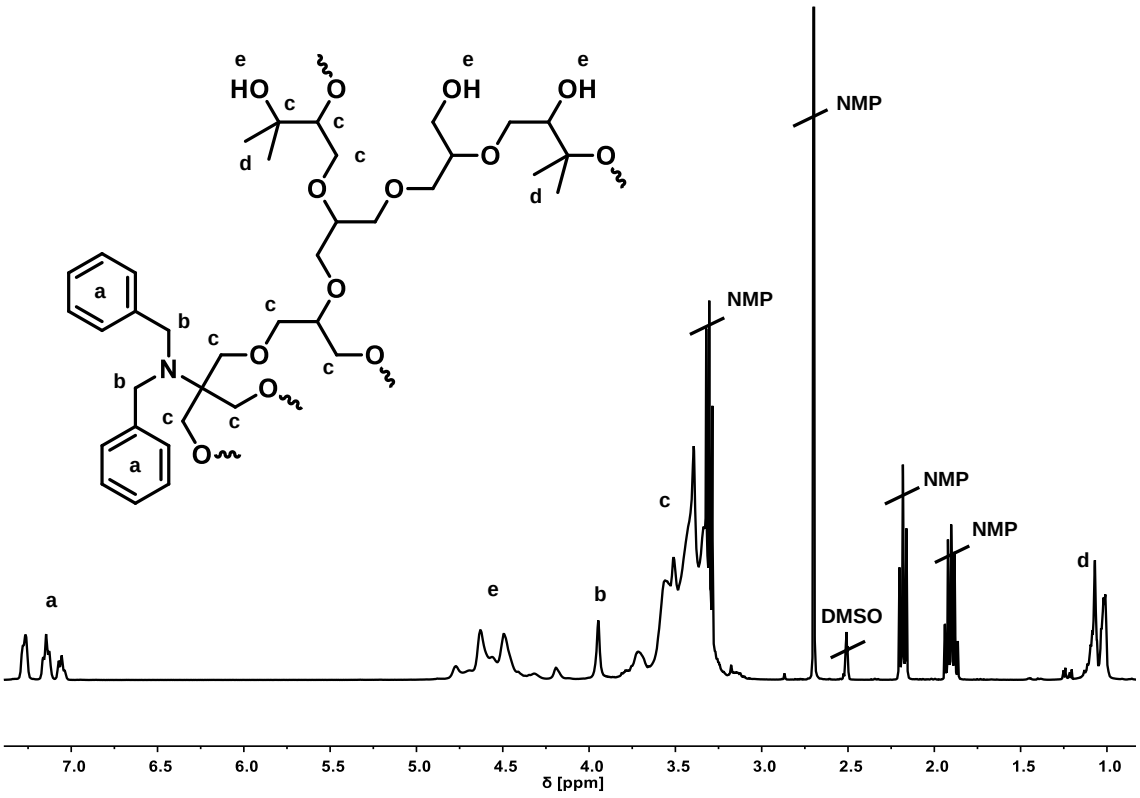

Figure S 21. ^{1}H NMR spectrum of *hb*P($G_{0.88}$-*co*-DiMeGly$_{0.12}$) (400 MHz, DMSO-d_6).

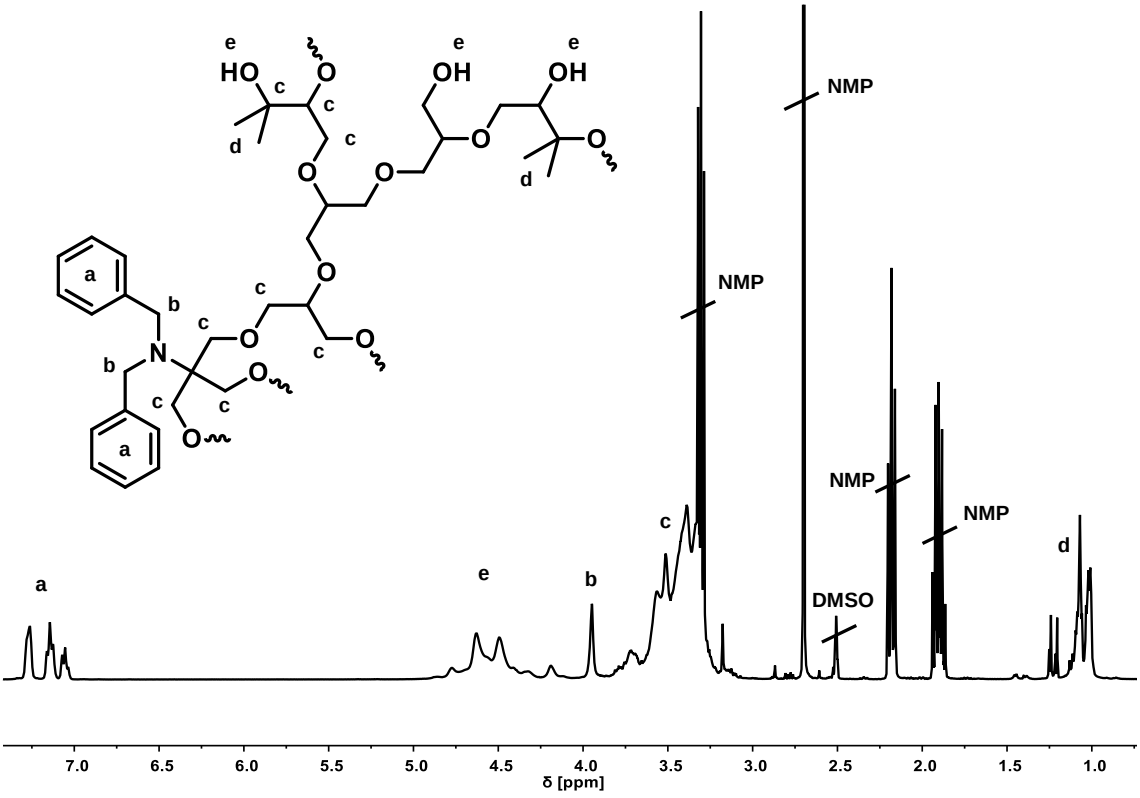

Figure S 22. ^{1}H NMR spectrum of *hb*P($G_{0.85}$-*co*-DiMeGly$_{0.15}$) (400 MHz, DMSO-d_6).

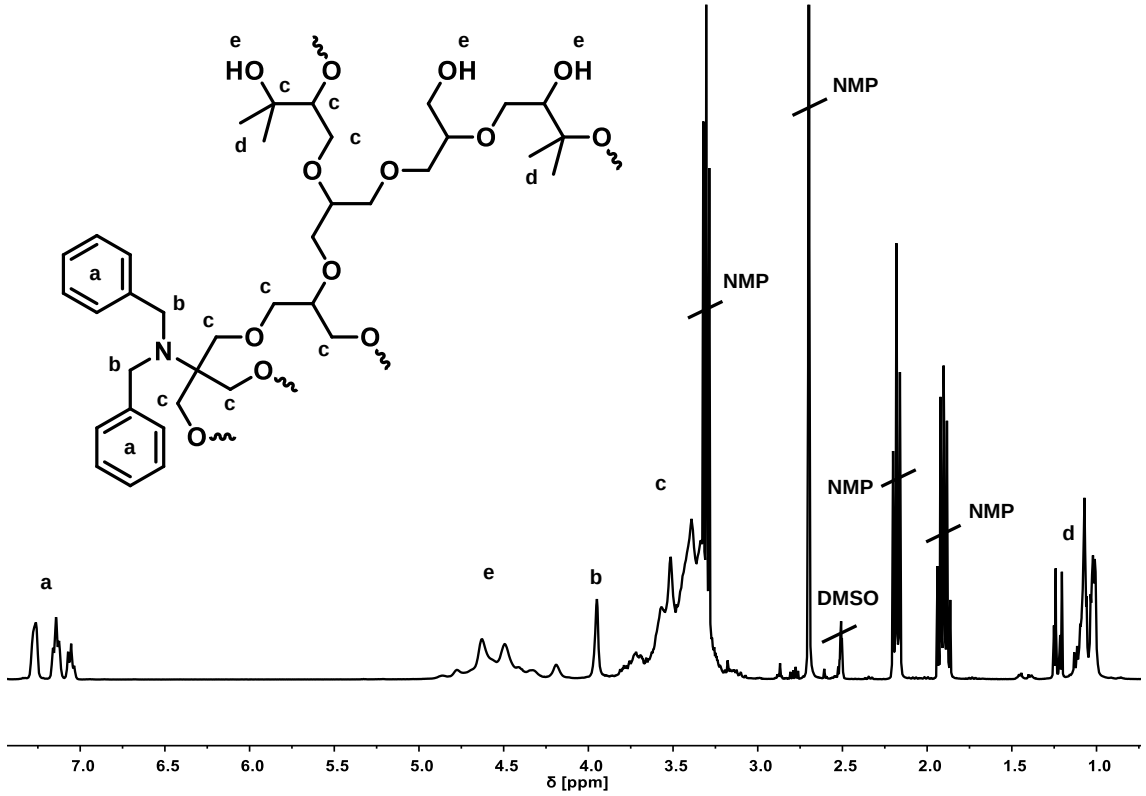

Figure S 23. ^{1}H NMR spectrum of *hb*P($G_{0.80}$-*co*-DiMeGly$_{0.20}$) (400 MHz, DMSO-d_6).

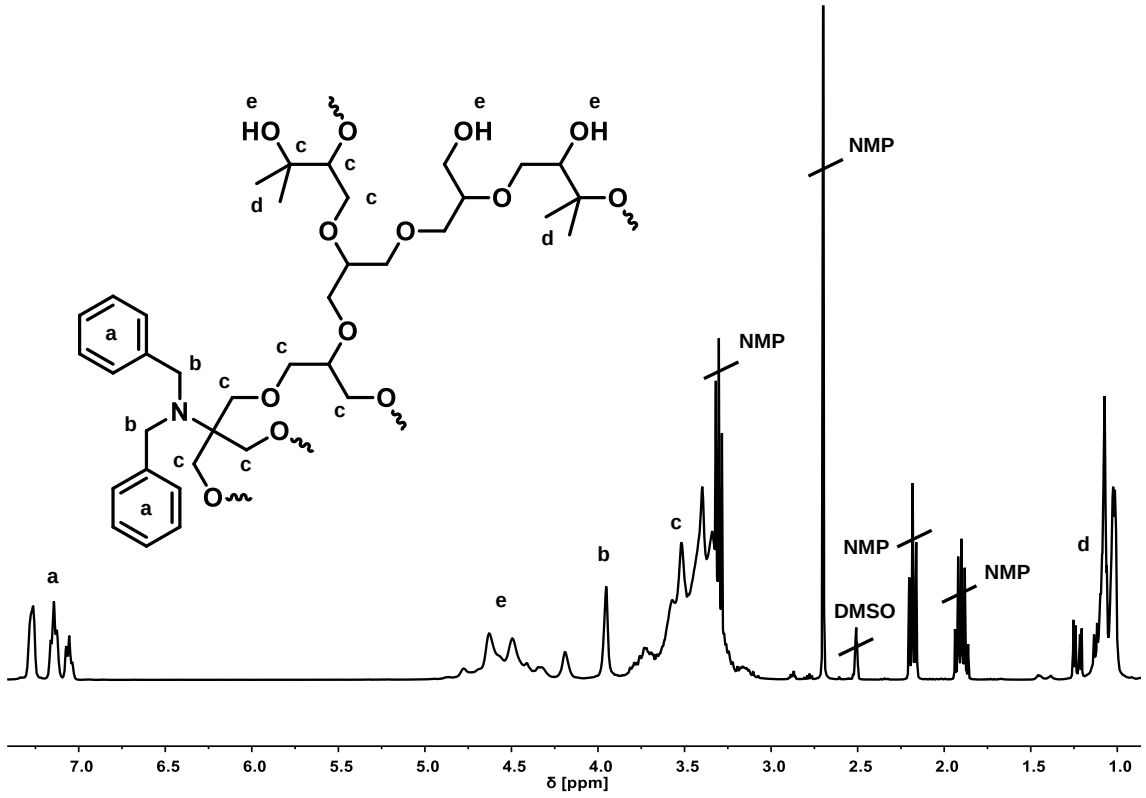

Figure S 24. ^{1}H NMR spectrum of *hb*P($G_{0.71}$-*co*-DiMeGly$_{0.29}$) (400 MHz, DMSO-d_6).

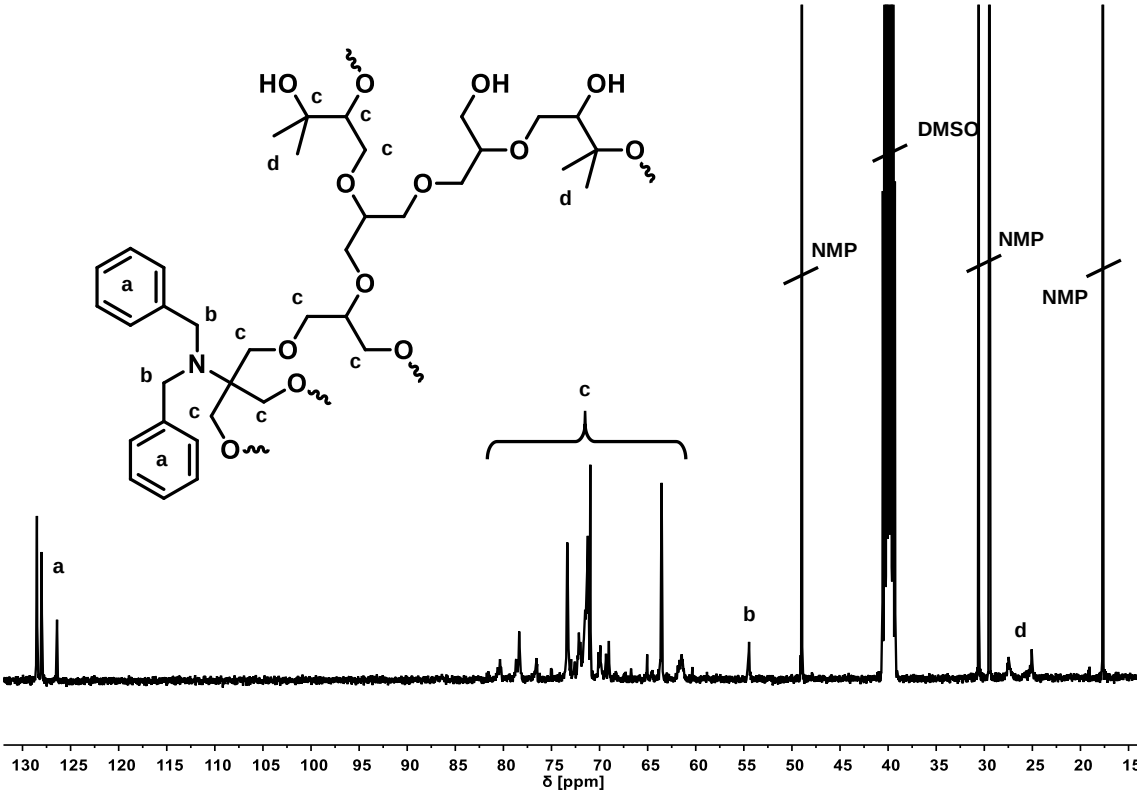

Figure S 25. ^{13}C NMR spectrum of *hb*P($G_{0.88}$-*co*-DiMeGly$_{0.12}$) (100 MHz, DMSO-d_6).

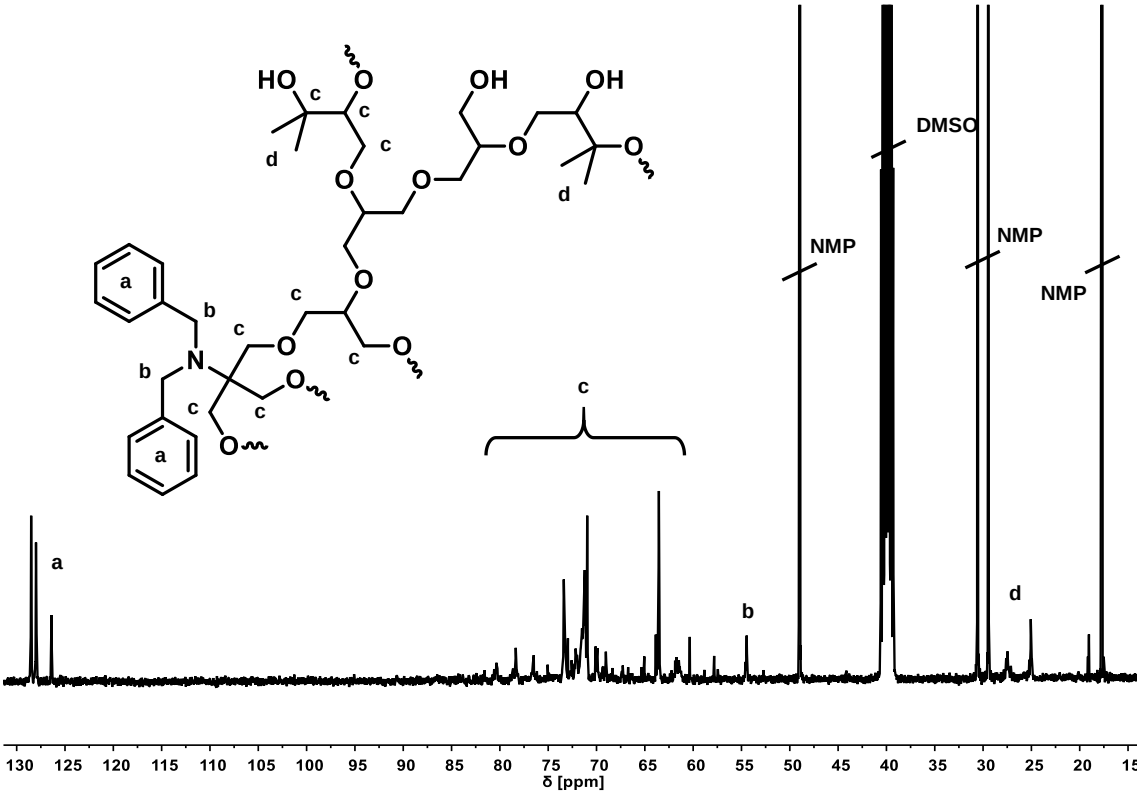

Figure S 26. ^{13}C NMR spectrum of *hb*P($G_{0.85}$-*co*-DiMeGly$_{0.15}$) (100 MHz, DMSO-d_6).

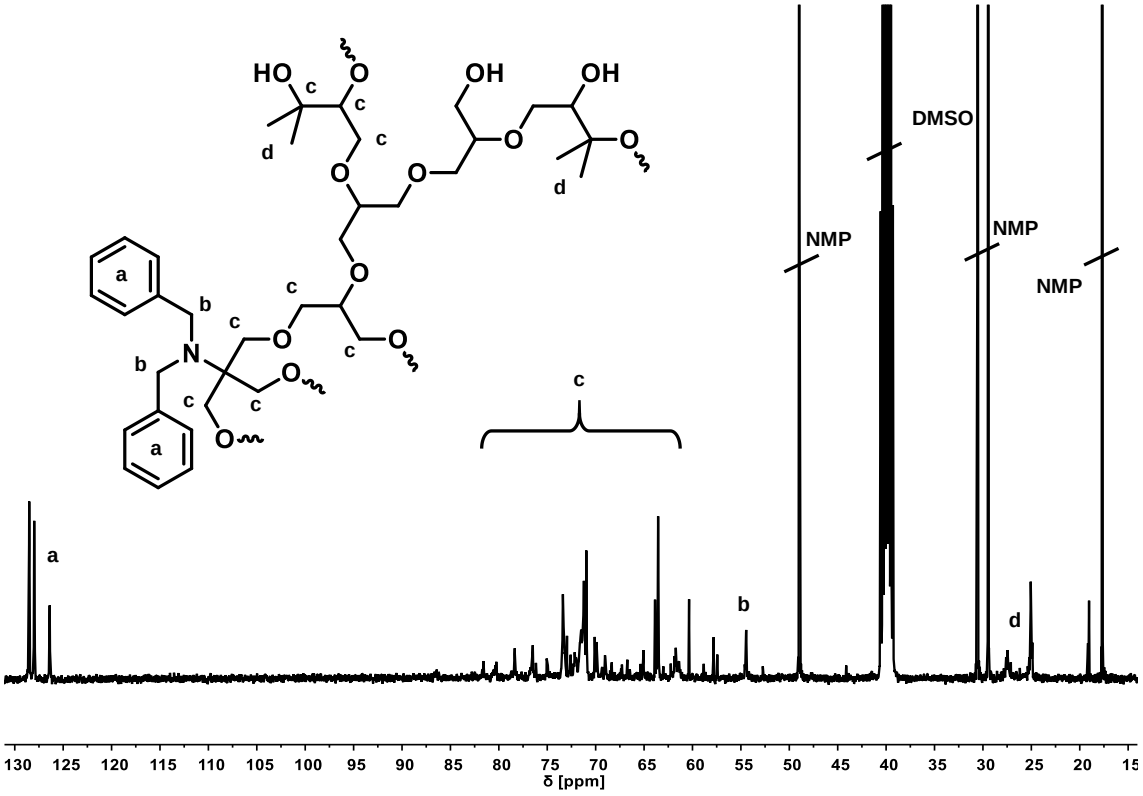

Figure S 27. ^{13}C NMR spectrum of *hb*P($G_{0.80}$-*co*-DiMeGly$_{0.20}$) (100 MHz, DMSO-d_6).

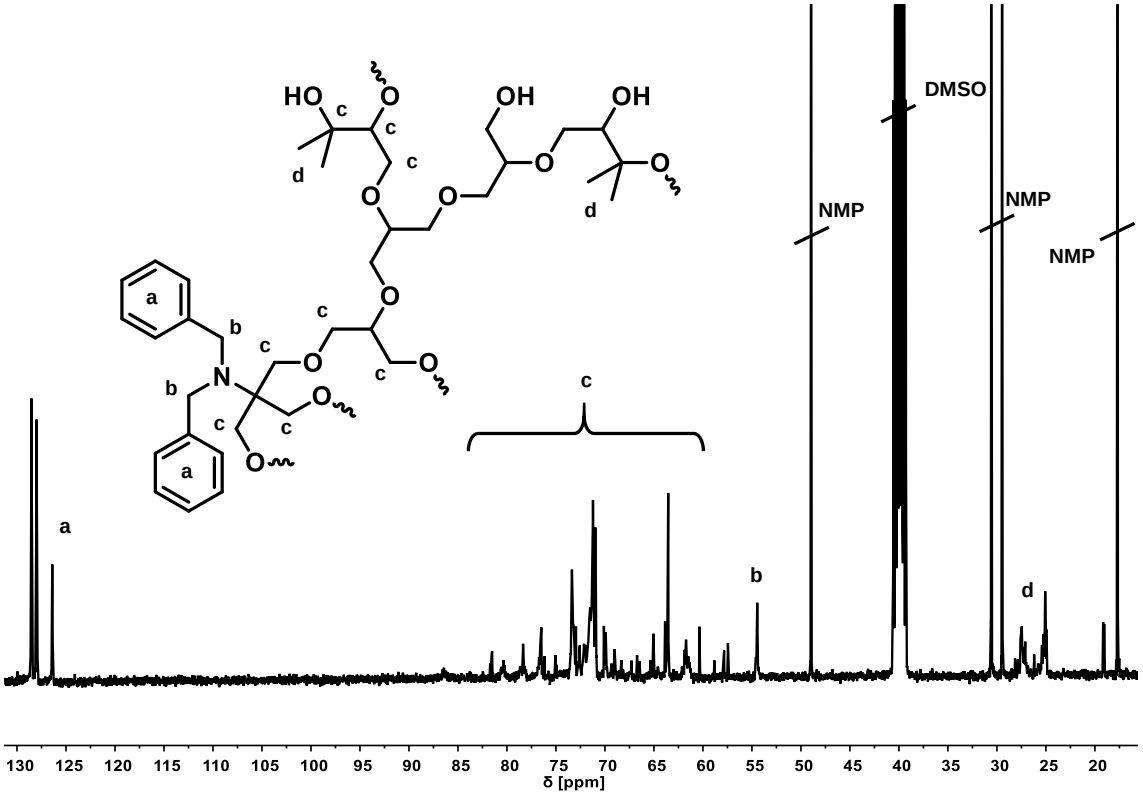

Figure S 28. ^{13}C NMR spectrum of *hb*P($G_{0.71}$-*co*-DiMeGly$_{0.29}$) (100 MHz, DMSO-d_6).

2.3 “Hard” Sphere-Behavior of “Soft”, Globular Hyperbranched Polyglycerols – Extensive Molecular Hydrodynamic and Light Scattering Studies

Alexey Lezov[a], Alexander Gubarev[a], Tobias Kaiser[b], Nikolay Tsvetkov[a], Ivo Nischang[c,d,], Ulrich S. Schubert[c,d], Holger Frey[b], Igor Perevyazko[a,*]*

[a]Department of Physics St. Petersburg University St. Petersburg, Russia

[b]Institute of Organic Chemistry, Johannes Gutenberg University, Duesbergweg 10-14, 55128 Mainz, Germany

[c]Laboratory of Organic and Macromolecular Chemistry (IOMC), Friedrich Schiller University Jena, Humboldtstr. 10, 07743 Jena, Germany

[d]Jena Center for Soft Matter (JCSM), Friedrich Schiller University Jena, Philosophenweg 7, 07743 Jena, Germany

To be submitted.

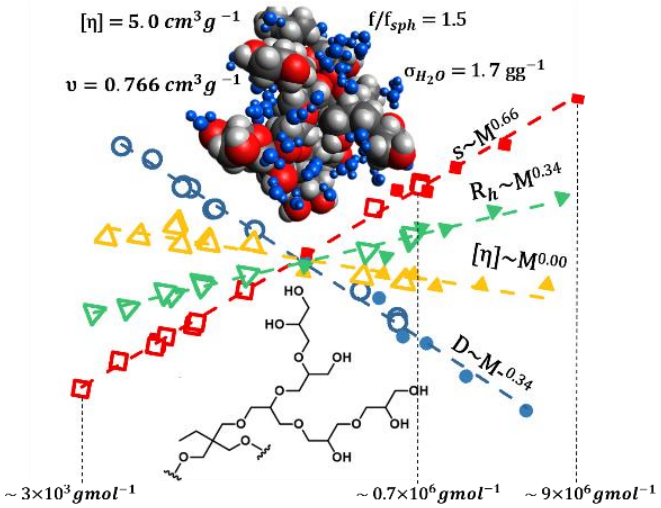

Abstract

Whether or not hyperbranched polymers behave like quasi “hard spheres” in solution is the subject of numerous fundamental discussions, also motivated by research on the perfectly branched dendritic structures. Experimentally targeting this question, a homologous series of hyperbranched polyglycerols (*hb*PGs) was prepared in a wide range of molar masses from ca. $3\,000$ to $700\,000\ gmol^{-1}$ and an overall moderate degree of branching (DB) between 0.55 and 0.59. *hb*PG samples have been investigated by a comprehensive set of experimental hydrodynamic and light scattering approaches, *i.e*. sedimentation velocity studies in analytical ultracentrifugation, dynamic and static light scattering experiments, isothermal diffusion experiments, intrinsic viscosities, and size exclusion chromatography (SEC), coupled with multi-angle laser light scattering (MALLS). The physical soundness of the received average molar masses, evaluated by the different, arguably, absolute approaches to molar mass estimations was verified *via* the concept of the hydrodynamic invariants, which, was found to assume average values of $A_0 = (2.6 \pm 0.4) \times 10^{-10}\ g\ cm^2\ s^{-2}\ K^{-1}\ mol^{-1/3}$ for the here studied and other branched macromolecular topologies. The hyperbranched polyglycerols were found to adopt a very compact, globular like conformation in solution. The compact structure, similar to dendrimers is nevertheless accompanied by a very high level of hydration giving in average 1.7 g of water per 1 g *hb*PG macromolecule. The corresponding, experimentally determined scaling relationships, show values that are characteristic for the hard sphere conformation: $s = 2.16 \times 10^{-3} M^{0.67}, D = 251 \times 10^{-3} M^{-0.33}, [\eta] = 5.9 M^{0}$. The high level of molecular compactness is also reflected in the contraction factors, which show

significantly reduced molecular volumes of *hb*PGs at high molar mass compared to their linear analogs.

Introduction

Hyperbranched polymers are densely branched macromolecules that contain a combination of dendritic, linear, and terminal units determined by the statistics of the formation process. In contrast to perfectly branched dendrimers, that are characterized by a very high, arguably perfect, level of branching symmetry, hyperbranched polymers are randomly branched polymers with a more irregular architecture.[1] These materials were first synthesized based on a multifunctional AB_n – type polycondensation reaction from suitable monomeric precursors *via* a typically employed and desired “one pot” strategy. The drawback of the conventional AB_n polycondensation approach is the high dispersity of the resulting polymers in respect to both the molar mass and the obtained degree of branching (DB).[2] However, the resulting dispersity regarding molar masses and their distributions can be diminished to a certain extent by using the controlled polymerization techniques or, alternatively, the slow monomer addition approach in the semi-batch polymerizations.[3-6]

Hyperbranched polyglycerols (*hb*PGs) can be considered as one of the most intensely studied and promising examples of the ”class” of hyperbranched polymers; such polyethers are molecularly water-soluble and show excellent biocompatibility and low toxicity.[4, 7] The large number of hydroxyl groups of the *hb*PGs enables to tune the chemical and solution, respectively functional properties. Finally, yet importantly, this also permits the creation of polymer

conjugates to biological macromolecules, ultimately aiming at gene and drug delivery systems, tissue engineering applications, and other implementations of such macromolecular systems.[7-10]

The unique structure-property relationship of hyperbranched macromolecules has its origin in their corresponding physical and chemically-defined structure, typically determined by the chosen monomeric precursors, their structural organization in the macromolecules, as well as their resulting molecular, conformational, and yet to be studied hydrodynamic characteristics. In this context, the basic objective of the physicochemical characterization of such macromolecular structures is to establish the fundamental structure-property relationships, urgently required at present. Those are reconciled from the systematic experiments under well-defined conditions. The fundamental information, concerning the molecular structure and conformational properties can thus be obtained, for example, by using high resolution techniques such as X-ray or neutron small-angle scattering. An alternative route to such structure-property relationships are the experimental approaches of macromolecular hydrodynamics and light scattering. Those comprise macromolecular solution viscometry and densimetry, analytical ultracentrifugation, dynamic-, and static-light scattering experiments. The application of these classical experimental approaches has already led to a commonly-accepted understanding of macromolecular behavior in solutions of choice and serve as basement of today’s polymer solution physics.[11] Compared to the arguably nearly-perfect dendrimers, hyperbranched macromolecular structures exhibit distinctly different behavior, for example, as a rule of thumb they do not show any maximum in the double logarithmic scaling dependence of the intrinsic viscosity on the molar mass.[12] However, despite the significant interest in such

nanoscale structures in solution, the knowledge concerning their molecular and conformational solution characteristics, in particular of *hb*PGs, is still very limited currently. The first dilute solution characteristics of *hb*PGs were reported by Richtering *et al*., relying on experimental results obtained from small-angle neutron scattering (SANS).[13] Later, Kainthan *et al*. studied a series of *hb*PG samples by means of SEC coupled to viscometric- and multi-angle laser light scattering-detectors.[14] Kizhakkedathu *et al.* published an analysis of ultra-high molar mass *hb*PGs by means of viscosity, SEC-multi-angle light scattering, and some other related techniques.[15] Apart from the *hb*PGs, currently, there is a very limited amount of systematic studies of hyperbranched macromolecular systems, particularly those shedding light on the very much desired structure-property relationships in solution. The majority of such studies is related to a variety of hyperbranched poly(esters/ether)s in suitable organic solvents, as those published by Turner *et al.*[16, 17], Gelade *et al.*[18], de Luca *et al.*[19], Lederer *et al.*[20], and Boye *et al.*[21]. The study of related macromolecular systems comprises hyperbranched polystyrenes[22-24], poly(pyridyl-phenylene)s[25] or glycogens[26] of natural origin in typically utilized organic solvents. The predominant analytical techniques employed to study branched or hyperbranched macromolecular structures in solution are the light-scattering and molecular viscometric studies.[1, 12] The classical hydrodynamic methods, combining (intrinsic) viscosity measurements, sedimentation velocity analysis by analytical ultracentrifugation, and the fundamental translational diffusion studies, all in solution, have rarely been applied for hyperbranched macromolecular structures in a systematic manner.[25, 27, 28]

In the current study, we have investigated a homologous series of *hb*PGs over a wide range of molar masses by diverse hydrodynamic- and light-scattering

techniques: (i) Sedimentation velocity analytical ultracentrifugation, (ii) intrinsic viscosity measurements, (iii) isothermal diffusion measurements, (iv) dynamic light and (v) static light scattering experiments, and finally (vi) size exclusion chromatography coupled to multi-angle laser light scattering (SEC-MALLS). Particular attention is paid to the sedimentation-diffusion analysis by the numerical solution of the Lamm equation as well as the isothermal diffusion measurements. These experimental attempts aim at a detailed investigation of the hydrodynamic, the macromolecular, and the conformational characteristics of the hyperbranched macromolecules in solution, and finally their respective scientific correlation.

Experimental Section

Materials

All materials were purchased from Sigma Aldrich, TCI or Fisher Scientific. For monomer synthesis all compounds were employed without further purification. Prior to polymerization, glycidol (96 %), 1,4-dioxane and bis(2-methyoxyethyl) ether were purified by distillation over calcium hydride.

Instrumentation

Analytical Ultracentrifugation (AUC). Sedimentation velocity experiments were performed with a ProteomeLab XLI analytical ultracentrifuge (Beckman Coulter, Brea, CA), using double-sector Epon centerpieces with a $12\ mm$ optical path length and a four-hole rotor (An-60Ti). The rotor speed was varied between $40\,000$ to $60\,000\ rpm$, depending on the sample. The sector-shaped cell compartments were filled with $420\ \mu L$ of sample solution and $440\ \mu L$ of the solvent water in the reference sector. Before the run, the rotor was equilibrated for approximately $1\ h$ at $T = 25.0\ °C$ in the centrifuge. Sedimentation velocity profiles were recorded by the interference / refractive index (RI) optics at $T = 25.0\ °C$.

Viscometry. Viscosity measurements were conducted using an AMVn microviscometer (Anton Paar, Graz, Austria), with a capillary / ball combination as the physical core of the measuring system. The respective ball times for the solvent, t_0, and the polymer solutions, t, of polymer solutions of a certain concentration, were measured at $T = 25.0$ ℃, while the relative viscosities of $\eta_r = t/t_0$ in the range of ~ 1.2 to ~ 2.5 were monitored for data evaluation.

Dynamic and static light scattering. Batch dynamic light scattering (DLS) and static light scattering (SLS) experiments were carried out using a “PhotoCor-Complex” apparatus (Photocor Instruments Inc., Moscow, Russia), equipped with a real-time correlator (288 channels, minimal correlation time of $\tau = 10\,ns$). The laser`s wavelength was $\lambda = 405\ \mathrm{nm}$; the intensity fluctuations were recorded at scattering angles (ϑ) ranging from a $30°$ to a $140°$ scattering angle. The experiments were performed at a temperature of $T = 25.0\ ℃$. The obtained autocorrelation functions of the scattered light intensities were processed using the DynaLS software, which provides the respective distributions $\rho(\tau)$ of the scattered light intensities by the respective known relaxation times, τ. The dependence between $1/\tau$ (where τ is the maximum intensity of the $\rho(\tau)$ distribution) and the squared scattering vector $q^2 = (4\pi n/\lambda \sin(\vartheta/2))^2$ for all the studied macromolecule populations was observed being a straight line passing through the plot origin, representing the diffusional processes recorded. The translational diffusion coefficients at the particularly measured macromolecule concentrations in solutions, D, was calculated from the slope of this recorded line according to the following relationship: $1/\tau = Dq^2$.[29] The translational diffusion coefficients at infinite dilutions, D_0, were determined by extrapolation of the $D(c)$ dependences to infinite dilution *via* the following relationship: $D_0 = D(1 + c2A_2M)$, where c is the polymer concentration, and A_2 is the second viral coefficient of the macromolecules in solution. The weight-average molar masses, M_W, of the studied macromolecular samples were determined from such batch static light scattering data according to the following equation: $Hc/R_\vartheta|_{\vartheta\to 0} = 1/M_W + 2A_2$, where $H = 4\pi^2 n_0^2(\partial n/\partial c)^2/(\lambda^4 N_A)$, R_ϑ is the Rayleigh ratio, A_2 is the second virial coefficient, $\frac{\partial n}{\partial c}$ is the refractive index increment, and N_A is the Avogadro number.

SEC-Multi-angle Laser Light Scattering. SEC-MALLS was performed as described recently.[30, 31] The dn/dc values of the here described macromolecules were determined in the isothermal diffusion experiments and appeared largely nvariant $dn/dc = 0.110\ cm^3\ g^{-1}$, the determined value is in a good correlation with the literature data.[15] For this study, we used a Zimm plot of $Hc/R(\theta)$ against $\sin^2(\theta/2)$ constructed at each recorded elution slice in SEC-MALLS. This allowed for determination of the resultant intercept from each elution slice by extrapolation to $\sin^2(\theta/2) = 0$ and, by its inverse, the molar mass of such elution slice, M_i, of the respective elution fraction of disperse populations.[30] *Via* the well-known relation in treating such elution populations, the weight-average molar mass, M_w, of the macromolecule populations was calculated. This is possible by making use of the concentration-sensitive refractive index (RI) detector and the mass-sensitive MALLS detector.

Isothermal diffusion measurements. A solution to solvent diffusion boundary was created in a glass cell with a thickness of $h = 30\ mm$ along the utilized beam path, by using an average solution concentration of $c = 1\ mg\ ml^{-1}$ for all of the macromolecular samples. Lebedev’s polarizing interferometer was utilized as the optical detection system for recording the solvent to solution boundary concentration over time.[32, 33]

Partial specific volume determination. The density measurements were carried out in a density meter (DMA 5000M, Anton Paar, Graz, Austria) according to the procedure of Kratky *et al*[34] and used in diverse recent experimental studies.[27, 30, 31, 35, 36]

NMR Spectroscopy. ^{1}H NMR spectra were recorded on a Bruker Avance III HD 300 (5 mm BBFO-SmartProbe with z-gradient and ATM) at 300 MHz, inverse gated ^{13}C NMR spectra were recorded on a Bruker Avance II HD 400 (5 mm BBFO-SmartProbe with z-gradient and ATM) at 100 MHz. The residual signals of the deuterated solvent were utilized as the internal reference. The degrees of branching (DB) were calculated utilizing the ^{13}C-NMR signals according to literature.[3]

Synthesis of Hyperbranched Polyglycerol Samples (*hb*PGs)

General procedure: In a Schlenk flask equipped with a magnetic stirrer, $67\ mg$ ($0.5\ mmol$, $1.0\ eq$) trimethylolpropane (TMP) was dissolved in methanol, partially deprotonated with $28\ mg$ ($0.17\ mmol$, $0.3\ eq$) cesium hydroxide monohydrate and dried *in vacuo* overnight at room temperature. To vary the molar masses, different solvents were employed for the polymerizations:[37] For molar masses up to $10\,000\ g\ mol^{-1}$, the initiator salt was dissolved in 1 mL of dried bis(2-methyoxyethyl) ether (diglyme) and heated to a temperature of $100\ °C$ under an argon atmosphere. A solution of glycidol monomer in diglyme in a volumetric ratio of $1{:}1$ was added to the initiator at a rate of $0.2\ ml\ h^{-1}$ using a syringe pump. For creation of higher molar masses, the respective initiator was dissolved in dioxane and the glycidol monomer was added without dilution according to the procedure introduced by Brooks et al..[7] The polymerization reaction was terminated by the addition of an excess of methanol solvent after the complete addition of the monomer. Subsequently, the solvent was removed, and the crude product was precipitated from MeOH into cold diethyl ether. After drying *in vacuo,* the resultant

polymers were obtained as dark yellow oils or honey-like materials depending on the molar masses aimed at (in yields of 80 – 90 %).

^{1}H NMR (300 MHz, DMSO-d_6, δ): 4.80 – 4.10 (br, OH); 3.80 – 3.00 (m, O-CH, O-CH_2); 1.40 – 1.10 (m, 2H, C$\underline{H_2}$-CH_3 (TMP)); 0.90 – 0.70 (m, 3H, -CH_2-CH_3 (TMP)).

^{13}C NMR (100 MHz, DMSO-d_6, δ): 81.0 – 80.0 (m, CH $L_{1,3}$); 79.0 – 78.0 (m, CH D); 73.5 – 72.5 (s, 2 CH_2 $L_{1,4}$); 72.5 – 70.5 (m, 2 CH_2 D, CH T, CH_2 T); 70.5 – 68.5 (m, CH_2 $L_{1,3}$, CH-OH $L_{1,4}$); 64.0 – 63.0 (s, CH_2-OH T); 62.5 – 60.5 (m, CH_2-OH $L_{1,3}$).

Results and Discussion

The behavior of macromolecular populations in solution can generally be described by a distinctive set of hydrodynamic characteristics such as the intrinsic viscosity $[\eta]$, $in\,[\,cm^3g^{-1}]$, the partial specific volume υ, $in\,[\,cm^3g^{-1}]$, the sedimentation coefficient s, $in\,[S]$, and the translational diffusion coefficient D, $in\,[cm^2s^{-1}]$. These primary hydrodynamic characteristics depend on the fundamental macromolecular characteristics that define their behavior in solution, *i.e.* the molar masses and the average hydrodynamic sizes / shapes. In the following, we first discuss the evaluation of the basic hydrodynamic data. Then, we move to the evaluation of the actual molar mass averages using the different hydrodynamic and light scattering approaches and, subsequently, verify the obtained values of such estimates *via* the concept of the hydrodynamic invariants.[38] Subsequently, we will discuss the gross conformation of the hyperbranched macromolecular structures in solution, their corresponding hydrodynamic sizes from different measurements, and the influence of the hydration and branching on estimations of such. Special interest will be paid to peculiarities of sedimentation-diffusion analysis *via* the Lamm equation modeling. Finally, we will attempt to complement the research by the global comparison of *hb*PGs with other known branched polymer systems found in the literature.

Solution Characteristics of Hyperbranched Polyglycerol

Intrinsic Viscosity and Partial Specific Volume

The intrinsic viscosity, $[\eta]$, is related to the volume and the molar mass of macromolecules and can be defined as:

$$[\eta] = N_A \frac{V_s}{M} \nu(p);\ V_s = \left(\upsilon + \frac{\delta}{\rho_0}\right) \quad 1$$

where N_A is the Avogadro number, M is the molar mass, V_s is the specific volume of the macromolecules in solutions, $\nu(p)$ is the viscosity increment (the so-called Simha function),[39] υ is the partial specific volume, ρ_0 is the density of the solvent, and δ is the hydration of the macromolecules.

In the case of hard, non-hydrated spherical particles, eq. 1 will take the form of the Einstein’s relation for the intrinsic viscosity, *i.e*. $[\eta] = 2.5\upsilon$. The intrinsic viscosities, $[\eta]$, were determined by utilizing the classical Huggins and Kraemer extrapolation procedures, and the average values from both were considered as the value of the intrinsic viscosity. The experimentally determined values of $[\eta]$, together with the Huggins and Kraemer viscometric constants are summarized in Table 1, while the experimental dependencies can be found in Figure S 1 of the supporting information (SI).

Table 1. Intrinsic viscosities $[\eta]$, Huggins, k_H, and Kraemer, k_K, constants, sedimentation coefficients, s, and Gralen coefficients, k_s, of *hb*PGs in water at $T = 25.0$ °C.

Sample	[η] [cm³ g⁻¹]	k_H	k_K	s [S]	k_s [cm³g⁻¹]
1	4.3	1.5	0.3	0.49	30
2	4.7	1.9	0.4	0.79	30
3	6.2	0.7	0.1	1.11	40
4	4.6	1.9	0.4	1.24	70
5	5.9	0.9	0.03	1.05	10
6	5.2	2.1	0.4	1.53	35
7	5.0	2.6	0.5	1.62	15
8	5.5	2.1	0.3	2.83	40
9	4.5	2.5	0.6	12.0	20
10	4.6	2.6	0.6	18.9	10
11	4.6	2.0	0.4	18.1	15

Regardless of the macromolecular sample population, the measured intrinsic viscosities fluctuate around an average value of $[\eta] = 5.0 \pm 0.6\, cm^3 g^{-1}$. This situation is typical for macromolecular objects with a compact, spherical-like conformation in solution, since the average rotational friction coefficient will have the same proportionality to the volume as the average molar mass of sample populations. The value of the Huggins viscometric constant, k_H, for a particular macromolecular sample can be used to obtain information regarding the macromolecule-solvent interactions – flexible polymer chains show k_H values in between 0.3 to 0.8, with a general tendency to increase for thermodynamically poorer solvents. The here found numerical values do not show a trend depending

on the macromolecular sample and molar mass, reflecting on average $k_H = 1.9 \pm 0.6$, a quite large value compared to linear macromolecular sample populations.[31] This is in line with the known characteristic values for compact macromolecular structures and conformations in solution, particularly the hyperbranched macromolecular structures.[27, 40, 41] The partial specific volume $\upsilon,\ in\ [cm^3 g^{-1}]$ that, according to eq. 1, is a prominent component of the intrinsic viscosity, reflects the change of a volume of a system upon the addition of a unity of mass of macromolecules at constant temperature and pressure. It is, however, in a first approximation often considered as the reciprocal value of the molecular density of macromolecules. Furthermore, it is a mandatory parameter for molar mass value and size determinations *via* the sedimentation-diffusion analysis. For a homologous series of macromolecule sample populations, the value of υ is not expected to change with the average molar mass values.[35, 42, 43] The experimental data for the determination of υ are shown in Figure S2 of the SI. All studied macromolecular sample populations follow the same dependence, resulting in an average value of $\upsilon = 0.766 \pm 0.009\ cm^3 g^{-1}$ from the corresponding buoyancy factor of $(1 - \upsilon\rho_0) = 0.236$, with the solvent density of water being $\rho_0 = 0.99714\ g\ cm^3$ at a temperature of 25 °C.

Sedimentation Velocity Experiments and Analysis by the Lamm Equation Modeling

Further insights regarding the molecular characteristics and solution behavior of *hb*PGs were gained from sedimentation velocity experiments in the AUC, treated with state-of-the-art numerical analytical approaches for data analysis. The temporarily resolved primary experimental data that are recorded during the AUC runs is the radial distribution of the sedimentation concentration profiles. Typical examples of these are shown in Figures 1A, 1B, 1C, and 1D for the macromolecular samples 1, 4, 8, and 11, respectively. The shape of the sedimentation profiles, in macromolecular terms, is determined by the molar mass / hydrodynamic size and as well by the heterogeneity / dispersity of a particular macromolecular sample system. The analysis of the sedimentation velocity data was performed by applying the continuous $c(s)$ distribution analysis,[44] and the $c(s, f/f_0)$ analysis,[45] implemented into the SEDFIT program. The $c(s)$ and $c(s, f/f_0)$ models allow for a numerical solution of the Lamm equation that describes the mass transport by sedimentation and diffusion in the AUC cells during the sedimentation velocity centrifugation experiments:

$$\frac{dc}{dt} = \frac{1}{r}\frac{\partial}{\partial r}\left[\left(D\frac{\partial c}{\partial r} - \omega^2 rsc\right)r\right] \qquad 2$$

where s and D are sedimentation and translational diffusion coefficients, c is the concentration, r is the radial distance, and t is the time at which the profiles are recorded.

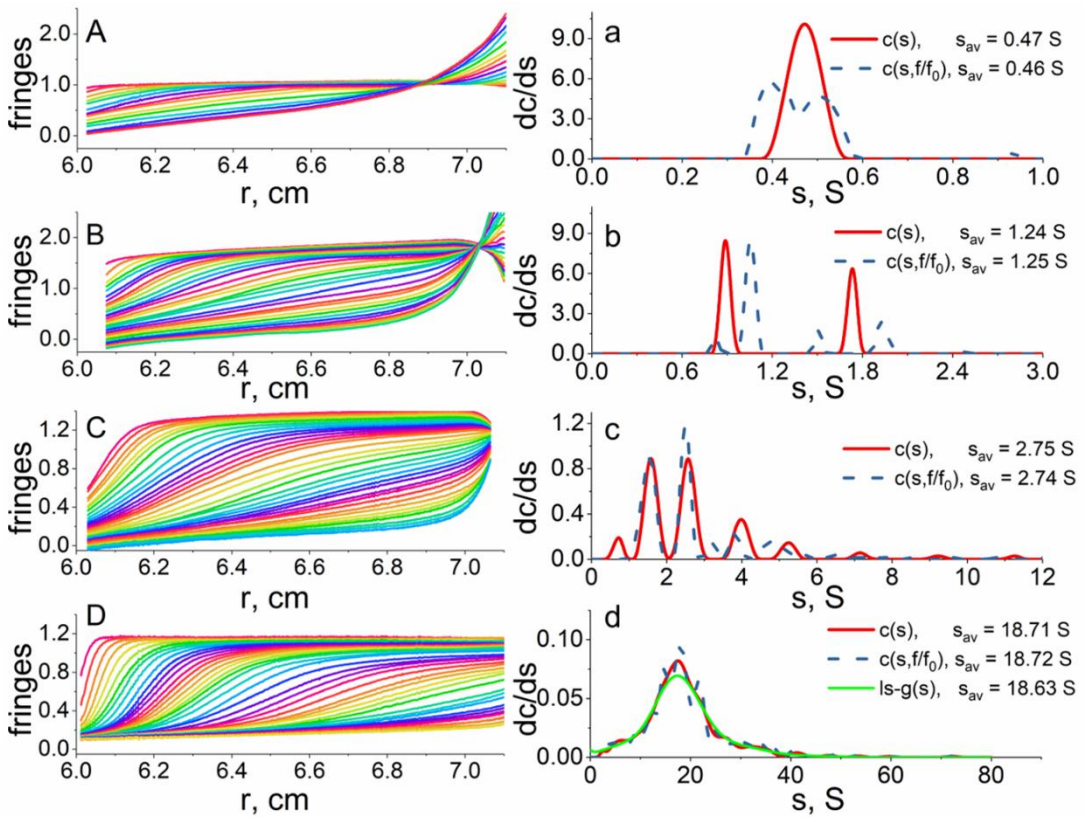

Figure 1. A, **B**, **C**, **D** – initial experimental concentration distribution sedimentation profiles for the *hb*PG samples 1, 4, 8, and 11 at a concentration of $c \approx 0.05\%$. **a**, **b**, **c**, **d** – corresponding differential distributions of sedimentation coefficients evaluated with the $c(s)$ and $c(s, f/f_0)$ analysis models in SEDFIT for the *hb*PG samples 1, 4, 8, and 11.

The $c(s)$ model is intrinsically confined within the hydrodynamic equivalent sphere model with the corresponding scaling between the sedimentation and the molar mass $s \sim M^{2/3}$, while the $c(s, f/f_0)$ presenting herself as a “model free” approach without any of such scaling presumptions. It is apparent that, independent of the applied numerical model solutions, ($c(s)$ or $c(s, f/f_0)$), the differential distributions of sedimentation coefficients are more disperse when increasing the average molar masses of the samples (Figures 1, B, C, D and Figure S3). The increase of the apparent dispersity of macromolecular sample populations at increased average molar masses can be considered typical for hyperbranched polymers. This is due

to the statistical nature of the utilized polymerization processes, *i.e*., higher molar mass macromolecules formed during polymerization will have an overall higher probability to react with the present monomer due to the increased amount of the available reactive groups of the formed macromolecules, inevitably leading to a higher overall macromolecule population dispersity.[6, 46]

However, in spite of the same general tendency reflecting higher dispersity, we do see that in the case of relatively low molar mass samples (distributions a and b in Figure 1) the differential distributions obtained by $c(s)$ and $c(s, f/f_0)$ are markedly different. Both $c(s)$ and $c(s, f/f_0)$ afford the sedimentation coefficient distributions by fitting the sedimentation boundary *via* the numerical solution of the Lamm equation. As we pointed out above, the shape of the concentration profiles will depend on the sedimentation and diffusion (in other words the molar mass / hydrodynamic size) and heterogeneity / dispersity of the macromolecular system. In case of relatively low molar mass samples the shape of the sedimentation profiles will be as well highly affected by the high diffusion rate causing an overall spreading of the profiles. The fundamental problem that such spreading can both be caused by the molecular dispersity / heterogeneity and the diffusion, and the adequate decomposition of the corresponding contributions in the Lamm equation analysis remains difficult.[30] This means that mathematically both of these distributions are equally possible, which is in turn reflected by the same level of the root-mean-square deviation. For high molar mass samples, the diffusion contribution becomes less significant and the corresponding distributions coincide to a large extent. Furthermore, in this case a model considering the sedimentation of non-diffusing species, the $ls - g^*(s)$ model can be applied, giving apparently the same overall distribution of the sedimentation coefficients of the particular high

molar mass sample for which the diffusion contribution may in sedimentation velocity experiments is of a minor importance (Figure 1 d). It is also important to note that the average sedimentation coefficients, independent of the applied model can be considered similar within the experimental error.

The signal (weight) average sedimentation coefficients were evaluated from different solute concentrations by integrating over the entire differential sedimentation coefficient distributions. The determined sedimentation coefficients were then plotted and extrapolated to infinite dilution according to the relation $s^{-1} = s_0^{-1}(1 + k_s c)$, where k_s is the concentration-sedimentation, *i.e*. the Gralen coefficient. The corresponding concentration dependences are shown in Figure S 4 (SI) while the extrapolated sedimentation coefficients at infinite dilution and the corresponding Gralen coefficients $k_s, in\ [cm^3 g^{-1}]$ are summarized in Table 1.

The numerical solution of the Lamm equation assumes evaluation of the both the sedimentation and translational diffusion coefficients. The diffusion coefficients are initially represented in the form of frictional ratios f/f_0; a common analytical construct in the area of bio- and polymer-physics, where f is the weight-average translational friction coefficient of the studied macromolecule / particle and f_0 or f_{sph} is the translational friction coefficient of the corresponding spherical particle having the same anhydrous volume and mass. The translational diffusion coefficient at infinite dilution, D_0, can be calculated using the frictional ratio at infinite dilution, $(f/f_0)_0$, together with the determined sedimentation coefficient at infinite dilution, s_0, and the determined partial specific volume, υ as:

$$D_0 = \frac{k_B T}{\eta_0^{3/2} 9\pi\sqrt{2}} \left(\frac{1-\upsilon\rho}{\upsilon}\right)^{1/2} (f/f_0)_0^{-3/2} s_0^{-1/2} \qquad 3$$

The evaluated frictional ratios (Table 1 of the SI) and the corresponding diffusion coefficients are clearly different (Table 2): the $c(s, f/f_0)$ analysis results in an average of $30\,\%$ higher frictional ratios, and correspondingly lower diffusion coefficients than the ones evaluated by the $c(s)$ analysis. In general, hyperbranched macromolecules are expected to have a compact, spherical like conformation in solution, so the $\frac{f}{f_0} \gg 1$ can either reflect the non-spherical / globular shape of the macromolecules or their hydration. This, and the consistency of the evaluated data, will be discussed later (*vide infra)*.

Dynamic Light Scattering and Isothermal Diffusion Measurements

Independently from the sedimentation velocity analysis, the translational diffusion coefficients were evaluated by dynamic light scattering (D_{DLS}) and isothermal diffusion measurements ($D_{isother}$). The estimated values are displayed in Table 2.

Table 2. Translational diffusion coefficients of *hb*PG samples in water determined by DLS (D_{DLS}), isothermal diffusion measurements ($D_{isotherm}$), from the $c(s)$ ($D_{c(s)}$), and $c(s,f/f)$ ($D_{c(s,f/f)}$) models by SEDFIT from sedimentation-diffusion analysis at a temperature of $T = 25.0$ ℃.

Sample	$D_{c(s)}\times10^7$ [cm² s⁻¹]	$D_{c(s,f/f)}\times10^7$ [cm² s⁻¹]	$D_{DLS}\times10^7$ [cm² s⁻¹]	$D_{isother}\times10^7$ [cm² s⁻¹]
1	24.8	22.7	17.5	21.0
2	17.0	14.5	13.3	14.9
3	14.3	10.5	10.7	13.5
4	16.9	10.1	10.1	11.6
5	15.1	11.4	9.38	12.5
6	12.8	7.4	8.70	8.94
7	10.7	7.4	8.92	8.09
8	8.7	6.0	6.46	6.70
9	5.9	3.5	3.61	3.72
10	4.0	2.1	2.72	3.14
11	5.0	2.3	2.95	2.81

The corresponding concentration dependencies of the estimated diffusion coefficients from DLS are presented in Figure S 5 (SI). The isothermal diffusion measurements represent a classical approach for the determination of the diffusion coefficients, which is based on the simple observation of the solution / solvent boundary dispersion (σ) over time as reflected by the experimental differential diffusion interferograms (e.g. Figure 3 A, sample 10) from which the dispersion over time, *i.e*. the diffusion coefficients can be calculated.[47] The slope of the

corresponding dependence of diffusion dispersion, σ^2, over time, (Figure 3B) ($\sigma^2 = \sigma_0^2 + 2Dt$), allows for calculation of the diffusion coefficients.

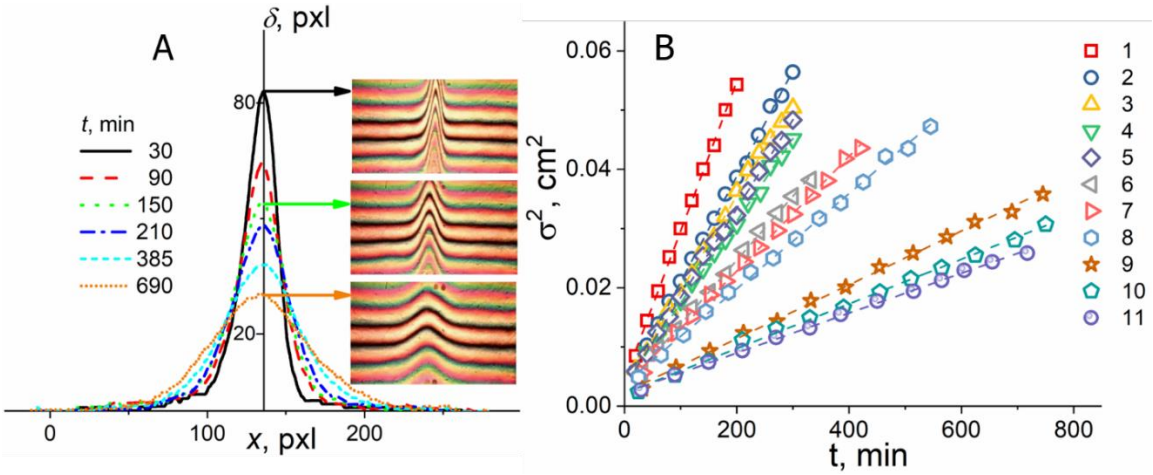

Figure 2. A – Differential diffusion interferograms at different periods of time for the macromolecular sample population 10; **B** – Dispersion of the diffusion boundary (σ^2) against time (t) for *hb*PG samples in water at a temperature of at $T = 25.0$ ℃.

The diffusion coefficients evaluated by DLS – D_{DLS}, isothermal diffusion measurements $D_{isotherm}$ and *via* numerical solution of the Lamm equation on sedimentation velocity data using the $c(s, f/f_0)$ model, $D_{c(s,f/f)}$, are in reasonable agreement, while the ones evaluated *via* the $c(s)$ model $D_{c(s)}$ show the highest diffusion coefficient values in all cases, indicating inconsistency in the data. Further discussion regarding the adequacy of the determined values of the diffusion coefficients will be provided later (*vide infra*).

Molar Mass Estimations

Based on the determined sedimentation coefficients at infinite dilution, the differently determined diffusion coefficients / frictional ratios at infinite dilution and the partial specific volume enables us to calculate the average molar masses of the macromolecular sample populations, using the following forms of the Svedberg equation:

$$M_{s,D} = \frac{RTs_0}{(1-\upsilon\rho_0)D_0} = R\frac{[s]}{[D]} \equiv M_{s,f}9\pi\sqrt{2}N_A([s]\,(f/f_0)_0)^{3/2}\sqrt{\upsilon} \qquad 4$$

where R is the universal gas constant, $[s] = \frac{s_0\eta_0}{(1-\upsilon\rho_0)}$ is the intrinsic sedimentation coefficient, and $[D] = \frac{D_0\eta_0}{T}$ is the intrinsic diffusion coefficient, η_0 and ρ_0 are the dynamic viscosity and density of the solvent.

The correspondingly calculated values, M_{sD}, obtained by using the respective diffusion coefficients listed in Table 2 are displayed in Table 3.

Table 3. Molar masses of *hb*PGs determined by the different approaches utilized in this study.

Sample	$M_{sD(DdIs)}$ [g mol^{-1}]	$M_{sD(Disotherm)}$ [g mol^{-1}]	$M_{w,SLS}$ [g mol^{-1}]	$M_{w,SEC-MALLS}$ [g mol^{-1}]	$M_{c(s,f/f)}$ [g mol^{-1}]	$M_{c(s)}$ [g mol^{-1}]
1	2 900	2 500*	2 000*	3 600	2 300*	2 100*
2	6 200	5 600	4 800*	5 800	5 700	4 900*
3	10 900	8 600*	8 300*	9 000*	11 100	8 100*
4	12 900	11 200	12 400	13 400	12 800	7 700*
5	11 800	8 800*	14 400	15 900*	9 700	7 300*
6	18 500	18 000	18 800	22 000	21 700	12 500*
7	19 100	21 000	19 600	20 800	22 900	15 900*
8	46 000	44 400	43 200	38 000	49 600	34 300*
9	349 700	339 400	351 000	324 000	357 500	214 000*
10	730 200	632 500	1080 000*	794 600	959 500*	498 300*
11	643 400	675 400	799 800	1018 000*	821 800	377 400*

*****Excluded from the averaging according to inadequate values of the hydrodynamic invariant, A_0 (equation 4).

In addition to the sedimentation-diffusion analysis, the molar masses were independently determined by size exclusion chromatography coupled to multi-angle laser light scattering experiments ($M_{w,SEC-MALLS}$) and also by the batch static light scattering experiments ($M_{w,SLS}$). Figure 3A shows normalized refractive index (RI) elution traces for the macromolecular sample populations and Figure 3B also the MALLS@90° elution traces, as well as the resulting molar mass trace, M_i, for sample 4.

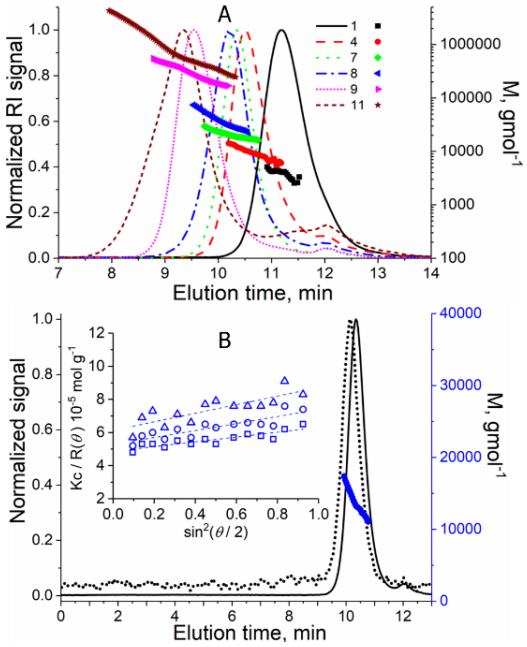

Figure 3. A – Normalized SEC refractive index (RI) elution profiles and the respective molar mass traces, M_i, in regions with sufficient signal-to-noise ratio for both the concentration and mass sensitive detector of the selected *hb*PG samples in water, at a temperature of $T = 25.0$ °C. **B** – Refractive index and MALLS@90° elution trace as well as the resultant molar mass trace, M_i, for macromolecular sample 4 and the example Zimm plots for selected elution slices.

It is clear, that MALLS as well as refractive index traces are characterized by varying detector responses, a situation not surprising in view of the nature of the concentration- and mass-sensitive detectors.[48] Care was taken to perform integration and M_i estimations for elution slices having a sufficient signal-to-noise-ratio from both detectors. The molar mass trace, M_i, derived from Zimm plots (e.g. Figure 3B, inset) shows typical behavior as expected for an SEC elution mode, with decreasing molar masses, M_i, at increased elution times. The corresponding Zimm plots from the static light scattering (SLS) experiments are shown in Figure S6 of the SI. The evaluated molar masses from such macromolecular sample populations are summarized in Table 3.

Consistency of the Experimental Data and Molar Masses

Based on the primary experimental results summarized above, *i.e*. the intrinsic viscosities, sedimentation coefficients at infinite dilution, determined translational diffusion coefficients by the different techniques, and the average molar mass estimates, we now attempt further interrelation of the data. The diffusion coefficients and corresponding molar masses were determined by DLS, the boundary spreading experiments ($D_{isother}$) and by the sedimentation-diffusion analysis using the $c(s, f/f_{sph})$ and $c(s)$ models using sedimentation velocity data, respectively. Furthermore, absolute molar masses (in addition to the sedimentation-diffusion analysis) were evaluated by the SLS and the $SEC-MALLS$ experiments. SLS, $SEC-MALLS$ and the sedimentation-diffusion analysis afford independent measurements of the molar masses and are considered as primarily absolute techniques for molar mass estimations of the synthetic macromolecule populations. However, as can be seen in Table 3, each of these approaches lead to similar, yet different values of the average molar masses. In many cases, the discrepancy between the different techniques is relatively low and can likely be explained by unavoidable experimental errors found in each of these techniques, while, for several low and high molar mass samples, the deviation appears to be substantial as seen in Table 3. In terms of average macromolecular characteristics, particularly considering the molar mass, the term “absolute” may be misleading, because no exact value can be established, since the macromolecular samples are disperse by virtue of the “nature” of their creation. In this case, one can only refer to the statistically most relevant / suitable, and yet physically sound values of the molar masses, that describe this population of the macromolecules at hand.[30] A clarification regarding the “most relevant” values of such molar masses appears

possible through the hydrodynamic invariant concept.[38, 49] This concept assumes invariance or low variations of the product of $[s]$, $[D]$, and $[\eta]$ for a distinct type of polymer system independent of the molar mass:

$$A_0 = (R[s][D]^2[\eta])^{\frac{1}{3}} \quad 5$$

Due to the highest exponential power, the largest influence on A_0 will stem from the diffusion coefficients, which are the most cumbersome hydrodynamic characteristic to determine for disperse sample populations. Substitution of $[s]$ or $[D]$ by the average molar masses using the classical Svedberg relationship (equation 3) gives the following alternative opportunities of equation 5:

$$A_0 = R[s][\eta]^{1/3}M^{-2/3} \quad 5a$$

$$A_0 = [D][\eta]^{1/3}M^{1/3} \quad 5b$$

In the literature, distinct characteristic values of $A_0,\ in\ [\ g\ cm^2\ s^{-2}\ K^{-1}\ mol^{-1/3}]$ for all basic macromolecular systems in solution are available in principle. In general, for linear flexible polymer chains the average value of $A_0 = (3.2 \pm 0.2) \times 10^{-10}$ was found, while for rigid chain macromolecules, the average value of A_0 is $(3.7 \pm 0.4) \times 10^{-10}$ is found to be characteristic for such polymer systems . However, for branched and hyperbranched polymer systems systematic studies of the A_0 values are scarce and practically absent in the literature. Previously studied hyperbranched poly(ethylene glycol) copolymers showed average values of $A_0 = (2.4 \pm 0.3) \times 10^{-10}$;[27] the average value obtained by Pavlov *et al.* for different dendrimer generations with up to 128 end groups is $A_0 = (2.53 \pm 0.05) \times 10^{-10}$.[50-56] Calculated based on the recently studied by Parambath *et al.*[15] “mega” *hb*PGs with up to $\approx 9 \times 10^6 gmol^{-1}$ molar masses average values of A_0 are $(2.5 \pm$

$0.3) \times 10^{-10}$. The experimental values around 2.5 are very peculiar since it notably lower than the theoretical minimum limit predicted for a solid impermeable sphere, *i.e.* $A_0 = 2.914$.[38] A more general overview on the variation of the hydrodynamic invariants for various, differently branched synthetic and natural polymer macromolecules the available data on which is sufficient to calculate the A_0 is shown in Figure 4. [15, 19, 25, 26, 28, 55-58]

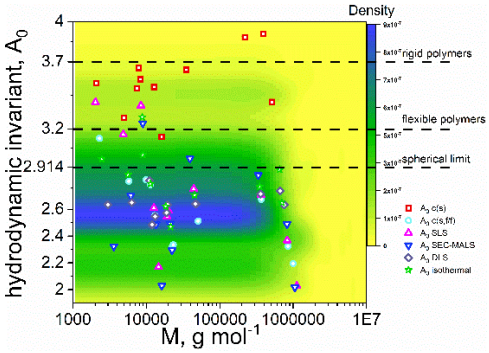

Figure 4. 2D multivariate kernel density estimation of the A_0 values from the literature data on the dendritic, branched and hyperbranched polymer systems. Dash lines represent average experimental values for the rigid and flexible chain polymers and the theoretical limit for rigid impermeable sphere. The data points represent experimental values calculated for the here studied *hb*PGs using SLS (A_{SLS}), SEC-MALLS ($A_{SEC-MALLS}$), sedimentation-diffusion analysis (A_{sD}), and sedimentation-diffusion analysis using Sedfit with the c(s) model ($A_{f/f}$).

Figure 4 is a 2D multivariate kernel density estimation based on 112 data points. The values calculated for the studied samples by various techniques reported here are shown by symbols in Figure 4. The statistical “density” of the A_0 values is reflected by the color intensity in Figure 4 (see the “density” bar) and shows that the majority of the experimental values of A_0 calculated over the entire set of the available literature data are, as a rule of thumb, were found to be the following

$A_0 = (2.6 \pm 0.4) \times 10^{-10}\ [g\ cm^2\ s^{-2}\ K^{-1}\ mol^{-1/3}]$,[14, 19, 25, 27, 28, 52, 55-57, 59]. Up to date this the first reported summarized experimental values for basically complete family of branched polymer systems. An experimental error of ± 0.4 is means an approximately $\approx 20\%$ shift of the sample molar mass. Such rather large experimental variations are of typical for A_0 – not surprising since it contains experimental data of three independently determined hydrodynamic characteristics. Notwithstanding this fact, the use of A_0 provide real opportunity to intercorrelate hydrodynamic data and molar masses from different sources and to arbitrate on their physical consistence.

Consequently, instead of the simple averaging of the molar masses from the used in here absolute techniques, we will use such average value of A_0 to perform a selection of the most relevant and consistent values of the molar masses and corresponding diffusion coefficients. First of all, we see that the use of $D_{c(s)}$ leads to the hydrodynamic invariants that are far off from the calculated average value of A_0 for branched macromolecules known from the literature and is more typical for linear flexible macromolecular chains, while the $D_{c(s,f/f)}$ and $M_{c(s,f/f)}$ position themselves in the expected range of the A_0 values. This is by excluding macromolecular Sample 1 and 10 only. The diffusion coefficients determined by DLS were found to give appropriate estimates of invariants for all samples, while the isothermal diffusion experiments data for the macromolecular Samples 1, 3, and 5 were found to be off an acceptable range only. The SEC-MALLS and batch SLS analysis, in general, give comparable and physically-sound results of estimations, excluding though macromolecular Samples 1, 2, 3, and 10 from SLS and Samples 3, 5, and 11 from the SEC-MALLS data. The argued excluded values, according to A_0, of M and / or D are indicated by an asterisk in the Table 3. The

thus obtained average molar mass values from the techniques, M_{av}, and the corresponding average diffusion coefficients, D_{av}, used for calculation, together with the respective hydrodynamic invariants, A_{av} are shown in Table 4.

In addition, and based on the established final values of the diffusion coefficients, D_{av}, we also recalculated the corresponding average frictional ratios $(f/f_0)_{av}$ (Table 4). These, such obtained consistent hydrodynamic characteristics and the resultant molar masses are then used to establish the following conclusions regarding the conformational properties of the hyperbranched polyglycerols in aqueous solution detailed below.

Table 4. Average molar masses, diffusion coefficients, frictional ratios, and hydrodynamic invariants for *hb*PG samples in water at a temperature of $T = 25.0$ °C.

Sample	$M_{av} \pm \Delta M$ [g mol^{-1}]	$(D_{av} \pm \Delta D) \times 10^{-7}$ [cm^2 s^{-1}]	$(f/f_0)_{av} \pm \Delta(f/f_0)$	$A_{av} \times 10^{10}$ [g cm^{2}s^{-2}K^{-1} mol$^{-1/3}$]
1	3 200 ± 400	15.8 ± 2.0	1.55 ± 0.20	2.5
2	5 800 ± 300	14.2 ± 0.7	1.42 ± 0.07	2.8
3	11 000 ± 100	10.6 ± 0.1	1.54 ± 0.01	2.8
4	12 500 ± 800	10.4 ± 0.7	1.50 ± 0.10	2.6
5	10 700 ± 1 400	10.3 ± 1.4	1.60 ± 0.20	2.6
6	19 800 ± 1 900	8.1 ± 0.8	1.66 ± 0.15	2.5
7	20 700 ± 1 500	8.6 ± 1.1	1.56 ± 0.20	2.6
8	44 300 ± 4 100	6.7 ± 0.6	1.53 ± 0.15	2.7
9	344 000 ± 13 000	3.7 ± 0.1	1.41 ± 0.05	2.7
10	719 000 ± 82 000	2.8 ± 0.3	1.46 ± 0.17	2.7
11	735 000 ± 89 000	2.6 ± 0.3	1.55 ± 0.19	2.5

Power Law Dependencies of Scaling Relationships

Dendritic, branched, or hyperbranched macromolecules are known to exhibit a compact and less asymmetric conformation in solution in comparison to their linear analogues.[12] For a homologous series of polymers, the macromolecular conformation in solution can be established *via* the classical scaling relationships that relate values of s, D, and $[\eta]$ against the molar mass :

$$[\eta] = K_\eta \cdot M^{b_{[\eta]}} \quad (6)$$

$$s = K_s \cdot M^{b_s} \quad (7)$$

$$D = K_D \cdot M^{b_D} \quad (8)$$

In principle similar scalings can be established between each pair of the hydrodynamic characteristics and molar mass, for example:

$$f/f_0 = K_{f/f} \cdot M^{b_{f/f}} \quad (9)$$

$$R_h = K_{R_h} \cdot M^{b_{R_h}} \quad (10)$$

The double-logarithmic scaling behavior of the hydrodynamic characteristics of various branched polymer systems against the molar mass in a double-logarithmic sense is common for the intrinsic viscosity and / or radius of gyration.[60] Dendrimers exhibit a maximum of the intrinsic viscosity as a function of the molar mass.[60] A similar phenomenological behavior was also predicted for hyperbranched macromolecules, however, experimental results reported so far do not clearly evidence such conclusion.[1, 60] Typical values of the scaling indices for the intrinsic viscosities of hyperbranched macromolecular structures are usually in the range of ca. 0.3 to 0.5.[21,25] The scaling dependencies for the studied *hb*PGs, in all cases, show linear behavior over the entire range of the studied molar masses, indicating

the hydrodynamic self-similarity of the studied macromolecule populations. The magnitude of the obtained scaling indices is related to the limiting case of a compact, spherical like conformation, *i.e.*: $s{\sim}M^{\frac{2}{3}}, D{\sim}M^{-\frac{1}{3}}, [\eta]{\sim}M^{0}$ (Table 5). The detailed estimated parameters of the scaling relationships can be found in Table 5.

In order to sketch physically wider picture concerning the gross conformation of the *hb*PGs in addition to the in here studied samples we also would like to use recent data from Kizhakkedathu *et al*[15]; they report the synthesis and corresponding characterization of extra high molar mass *hb*PGs. The literature data are shown as filled symbols in Figure 5 and ideally fits to the in here obtained dependence. The overall molar mass range is from $\sim 3\,000\ gmol^{-1}$ to $\sim 9 \times 10^{6}\ gmol^{-1}$ the widest considered up to date. Furthermore, using the above literature data, authors calculated missing sedimentation coefficients and frictional ratios of such “mega” *hb*PGs (Figure 5). The scaling indices changes very slightly, reflecting in turn the same behavior of literature and in here studied samples (Table 5).

Interestingly, even if we use the highly underestimated values of the molar masses from the $c(s)$ analysis or simply, a complete average of molar mass populations and perform the exponential scaling analysis, we still arrive at basically the same scaling indices: $s{\sim}M^{0.69}, D{\sim}M^{-0.34}, [\eta]{\sim}M^{0.01}$. This underpins that the molar mass estimations, if systematically biased, result of course in similar exponential parameters.

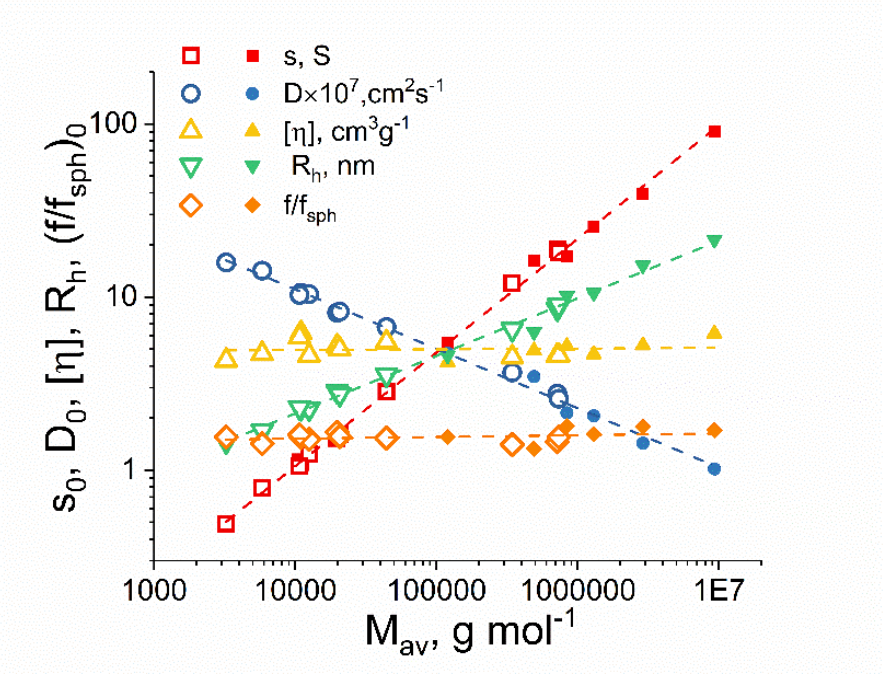

Figure 5. Double logarithmic dependencies of s, D, and $[\eta]$ on the average molar masses of the *hb*PGs samples in water, studied at a temperature of $T = 25.0$ ℃.

Table 5. Parameters of the scaling relationships for *hb*PG in water, studied at a temperature of $T = 25.0$ ℃

Scaling	**$b_i \pm \Delta b_i$**	**$K_i \pm \Delta K_i$**	**$b_i \pm \Delta b_i$***	**$K_i \pm \Delta K_i$***
	3 < M, kDa < 735		3 < M, kDa < 9 300	
s_0-M	0.673 ± 0.008	(2.10±0.04)×10^{-3}	0.657±0.008	(2.49±0.04)×10^{-3}
D_0-M	-0.326 ± 0.008	221 ± 4	-0.343± 0.008	261 ± 4
[η]-M	-0.02 ± 0.02	5.9 ± 0.7	0.00± 0.01	4.7 ± 0.5
R_h-M	0.326 ± 0.008	0.106 ± 0.003	0.333± 0.008	0.099
f/f_0-M	-0.008± 0.008	1.7 ± 0.3	0.010± 0.008	1.4 ± 0.4

* “global” scaling indices obtained over extended molar mass region[15]

Average Hydrodynamic Sizes and Hydration

The scaling indices indicate that the *hb*PGs possess an ideal, spherical conformation / shape in solution on average. However, the estimated translational frictional ratios show an average value of $(f/f_0)_0 = 1.5 \pm 0.2$ (Table 2), *i.e*. independent on the average molar masses, as we see at the corresponding scaling behavior. The presented $(f/f_0)_0$ average value is only based on the inhere obtained data without considering the literature data since it lies closely within the mentioned region. A deviation of f/f_0 from that of an ideal solid sphere, *i.e*. 1 should be in the present case solely interpreted by the hydration of macromolecules. This is because, the f/f_{sph} value depends on both the shape parameter P (the Perrin friction factor) and the hydration δ:

$$(f/f_0)_0 = P\left(\frac{\delta}{\upsilon\rho_0} + 1\right)^{1/3} \qquad 11$$

By virtue of definition, the hydration δ represents the amount of the contained, or better associated, water per macromolecule mass, in terms of $[g/g]$. It can be defined as:

$$\delta = \left(\frac{V_{hyd}}{V_{anh}} - 1\right)\upsilon\rho_0 \qquad 12$$

where $V_{hyd} = \frac{4}{3}\pi R_h^3$ is the hydrated volume of the macromolecular sample, with R_h being the average hydrodynamic radius and $V_{anh} = \frac{M\upsilon}{N_A}$ being the respective anhydrous volume of such.

Furthermore, re-arrangement of equation 1 established for the intrinsic viscosity $[\eta]$ leads one to the following relationship for the value of hydration:

$$\delta = \left(\frac{[\eta]}{\nu(p)} - \upsilon\right)\rho_0 \qquad 13$$

The so-called Simha function, $\nu(p)$, for spherical anhydrous particles will be equal to a value of 2.5. Consequently, one can calculate the hydration using equations 11 and 13, assuming the solid spherical shape approximation. In other words, we set $P = 1$ and $\nu(p) = 2.5$. On the other hand, the hydration can also be calculated by using equation 12 if the hydrodynamic size is available from an experimental estimation. The hydrodynamic radius can be calculated using the sedimentation, diffusion, or intrinsic viscosity data and the average molar masses of the macromolecules:

$$R_s = \frac{3}{\sqrt{2}}\sqrt{[s]\upsilon}\left(f/f_{sph}\right)^{3/2} \qquad 14$$

$$R_D = \frac{kT}{6\pi\eta_0 D} \qquad 15$$

$$R_\eta = \left(\frac{3}{10\pi N_A}\right)^{\frac{1}{3}}(M[\eta])^{\frac{1}{3}} \qquad 16$$

The calculated hydrodynamic radii, together with the corresponding hydration values, are summarized in Table 6.

Table 6. Hydrodynamic radii and the calculated hydration values for *hb*PGs in water at $T = 25.0$ °C.

Sample	R_s [nm]	R_{DLS} [nm]	R_η [nm]	R_g* [nm]	$\delta \pm \Delta\delta$ [g g^{-1}]
1	1.5	1.3	1.3	1.6	1.7 ± 0.7
2	1.7	1.7	1.6	1.9	1.3 ± 0.2
3	2.3	2.0	2.1	2.4	1.9 ± 0.2
4	2.4	2.2	2.1	2.5	1.6 ± 0.4
5	2.5	2.2	2.3	2.4	2.1 ± 0.5
6	3.0	2.8	2.5	2.9	2.2 ± 0.8
7	2.9	2.9	2.5	2.9	1.8 ± 0.5
8	3.6	3.7	3.3	3.9	1.8 ± 0.3
9	6.7	6.6	6.2	7.8	1.3 ± 0.2
10	8.8	8.4	8.1	10.0	1.4 ± 0.3
11	9.5	8.4	8.1	10.1	1.8 ± 0.6

* Calculated according to $R_g = 0.102M^{0.34}$ (Garamus *et al*[13]).

The average hydrodynamic radii do not exceed an upper limit of 10 nm in the present work, even for the highest molar mass sample populations. This reflects a very compact solution structure of the *hb*PGs. The hydration values listed in Table 6 are average values calculated using equations 11, 12, and 13. We note, that the hydration values calculated based on the intrinsic viscosities (equation 13) are, on average, as much as 60% lower than the ones calculated by equations 11 or 12. Despite such different estimations, the average values of the hydration are quite high, showing that on average 1.7 g of water is associated with $1\,g$ of a *hb*PG

macromolecular sample. In comparison to the typical globular proteins, having values of $\delta \approx 0.35\ g g^{-1}$ or to the carboxymethylcellulose[61] with $\delta \approx 0.8\ g g^{-1}$ this appears to be quite substantial.[62]

According to the classical hydration paradigm, a “layer” of bound water, which is assumed to have a constant thickness, covers an anhydrous particle and / or macromolecular structure.[62] This concept can be applied to the globular proteins or nanoparticles, while in the case of (hyperbranched) macromolecules of very compact conformation, the situation will be more complex, since water molecules can also be expected inside the polymeric branched structure, further amplified by potential defects in such structure, when considering the possible irregular branching, unresolvable by the current experiments.

The contribution of hydration to the overall determined hydrodynamic size of the *hb*PGs can simply be estimated as the ratio of the hydrodynamic effective size (equations 14, 15 and 16) to the straightforwardly calculated anhydrous size: $R_{anh} = \left(\frac{3}{4}\frac{M\upsilon}{\pi N_A}\right)^{\frac{1}{3}}$, which results in an expansion factor of approximately 1.5 compared to the solid sphere approximation.

Contraction Factors

Quantitatively, the effect of a branched / hyperbranched architecture on the macromolecular hydrodynamic characteristics can be described by the contraction factors that are represented by the ratio of the corresponding hydrodynamic characteristics of the branched macromolecules to their linear analogs of the same molar mass:

$$g = \frac{R_{g,b}^2}{R_{g,lin}^2}; g' = \frac{[\eta]_b}{[\eta]_{lin}}; h = \frac{f_b^t}{f_{lin}^t} = \left(\frac{s_b}{s_l}\right)^{-1} \quad 17$$

Initially, such ratios were introduced for the radius of gyration, (g) by Zimm and Stockmayer and later by Stockmayer and Fixman for the intrinsic viscosity (g'); similar relationships can also be written for the translational friction coefficients, h, or the ratio of the sedimentation coefficients (equation 17).[12] The radius of gyration, R_g, for the here studied *hb*PGs was estimated based on the scaling relationships obtained by Richtering *et al.* for *hb*PGs in D_2O, i.e. $R_g = 0.102M^{0.34}$.[13] The data on the radius of gyration and translational friction coefficients of linear polyglycerols were taken from the literature with $D = 1.72 \times 10^{-4} M_w^{-0.542}, (in\ cm^2 s^{-1}); R_g = 0.00297M^{0.71}$.[63] For the intrinsic viscosity, the scaling of $[\eta] = 0.02M_{sD}^{0.7}, (in\ cm^3 g^{-1})$ was used (unpublished results). The corresponding individual values for g, g', and h are listed in Table 7. The corresponding dependence on the molar masses is shown in Figure S 7 of the SI and the respective parameters for the scaling relationships are summarized in Table S 2 of the SI.

Table 7. Contraction factors g, g' and h for the *hb*PG series in aqueous solution.

Sample	g	g’	h
1	3.08	0.77	1.38
2	1.91	0.54	1.12
3	1.31	0.50	1.07
4	1.09	0.31	1.01
5	1.10	0.40	1.11
6	0.78	0.26	1.01
7	0.77	0.24	0.96
8	0.44	0.16	0.79
9	0.10	0.03	0.48
10	0.05	0.02	0.43
11	0.05	0.02	0.45

The basic relationship between the contraction factor, g' (based on the intrinsic viscosities), and g (for the radii of gyration) remains, yet, unclear. This situation likely has its origin in the different Flory hydrodynamic parameters (Φ) of the branched polymers in comparison to their linear analogues.[60] The experimental values vary from ca. 0.3 to 2.5, depending on the type of the branched macromolecular system.[1, 64] For the *hb*PG samples studied here, we obtain values of $g' \cong g^{0.97\pm0.03}$. The corresponding scaling relation between g and h is found to be in reasonable agreement with the theoretically predicted scaling of $g' \cong h^3$, i.e. $g' \cong h^{3.3\pm0.1}$. The corresponding double logarithmic scaling dependencies between the contraction factors are shown in Figure 8 of the SI, and the corresponding parameters of the established scaling relationships are summarized in Table 7.

Sedfit Data Analysis Review

We have seen that in terms of the average sedimentation coefficients, different analytical models implemented into the Sedfit software result in similar average values within experimental error. The distributions of the sedimentation coefficients though may have certain variations whether the $c(s)$ or the $c(s, f/f)$ model is used, especially for the low molar masses, where diffusive contributions to the sedimentation profiles become significant.

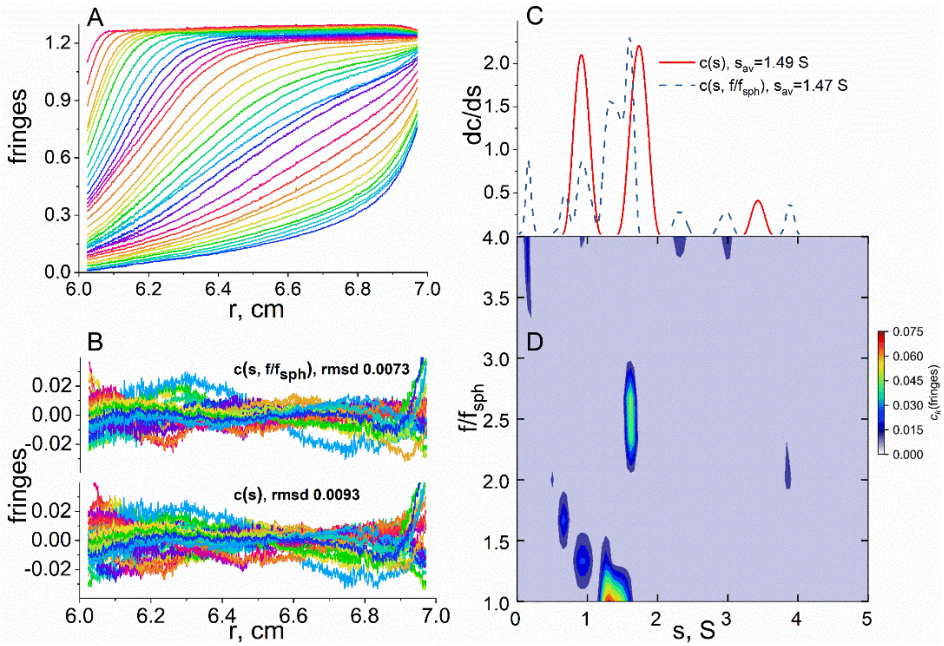

Figure 6. A – differential distributions of the sedimentation coefficients evaluated by c(s) – solid line and $c(s, f/f)$ models (dash line). Bottom – distribution of frictional ratios with a corresponding intensity color bar, obtained by $c(s, f/f)$ modeling. In both cases, resolution of modelled sedimentation coefficients was 100, and resolution of frictional ratios was 10. A Tikhonov-Phillips regularization procedure with a confidence level of 0.9 was used.

Some examples were already presented above in Figure 1, now we would like to show and discuss another very interesting example in Figure 6, *i.e*. results from the $c(s)$ and the $c(s, f/f)$ analysis of the *hb*PG sample 6, that has an average

molar mass of ca $20\,000\ gmol^{-1}$ (see Tables 3 and 4). The numerical solutions were performed with the same modelling parameters (see Figure 6 capture for details). Figure 6 D shows 2D map distribution of sedimentation coefficients s versus the frictional ratio , f/f_{sph}. Standard limits for the f/f boundaries (1 to 4) were chosen for the fits. The value of $f/f_{sph} = 4$ as upper boundary means that in the case of using ellipsoid of revolution model the corresponding aspect ratios a/b will be around 100 – highly asymmetric, rod like structures probably.[65] Yet we do see some minor species characterized by unreasonably high f/f_{sph} values (≈ 4). This is especially curios for species in the region of very small sedimentation coefficients as one can see for example in Figure 6 C and D, where the first peak stands at $\approx 0.15\,S$ – some “oligomerically” small species, which in general physically can be present in solution but cannot have such high asymmetry in solution. At the same time in spite of high f/f_{sph} value the corresponding concentration signal is very small and does not contribute much to the frictional ratio over entire population. The c(s) model appears to result in less heterogeneous and more “natural” distributions. Also the highly compact spherical like conformation of the hyperbranched macromolecules should positively contribute to the successful analysis by the $c(s)$ model[27] which assumes the spherical model in its very core, however as it is turned out it was unable to correctly resolve the diffusion coefficients / frictional ratios. Such behavior can probably be explained by the substantial hydration and the presence of water molecules inside and outside on the surface which will contribute to the hydrodynamic non-ideality effects.

Conformation and Solution Behavior

We have performed a series of hydrodynamic and light scattering experiments that formed an initial matrix of primary hydrodynamic characteristics and established molar masses. The verification of such matrix was made based on the hydrodynamic invariant concept – revealing the statistically most relevant molecular characteristics of hyperbranched polyglycerols in aqueous solution. These characteristics were then used to establish the statistically most likely conformation of the hyperbranched macromolecule sample populations in solution using the very classical power law dependencies. This illuminated the self-similarity and highly compact spherical like conformation of such macromolecules in solution (Table 5). Further insights into the macromolecular conformation could be obtained by introducing the ratio R_g/R_h, which represents the actual segment density of hyperbranched macromolecules as a result of the corresponding hydrodynamic “interactions” in solution. For spherical (solid) particles the ratio is expected being 0.778; dendrimers show an average value of ~ 0.98, while hyperbranched macromolecules are usually characterized by a rather large value of ~ 1.23. The hyperbranched polyglycerols resemble an average value of 1.07 ± 0.06 that could be attributed to the so-called Gaussian “soft sphere” conformation, an average value also typical for dendrimers. In fact, the hyperbranched polyglycerols and their copolymers show the most compact macromolecular conformation in aqueous solution among all other studied hyperbranched polymer systems to date. Figure 7 compares the different branched macromolecular systems in terms of their effective hydrodynamic volume, determined as $[\eta]M$. The data on *hb*PGs are consist of literature, in here studied samples, and show a direct proportionality

between the determined macromolecular volume and the molar masses, which is typical for the spherical particles and dendritic structures.

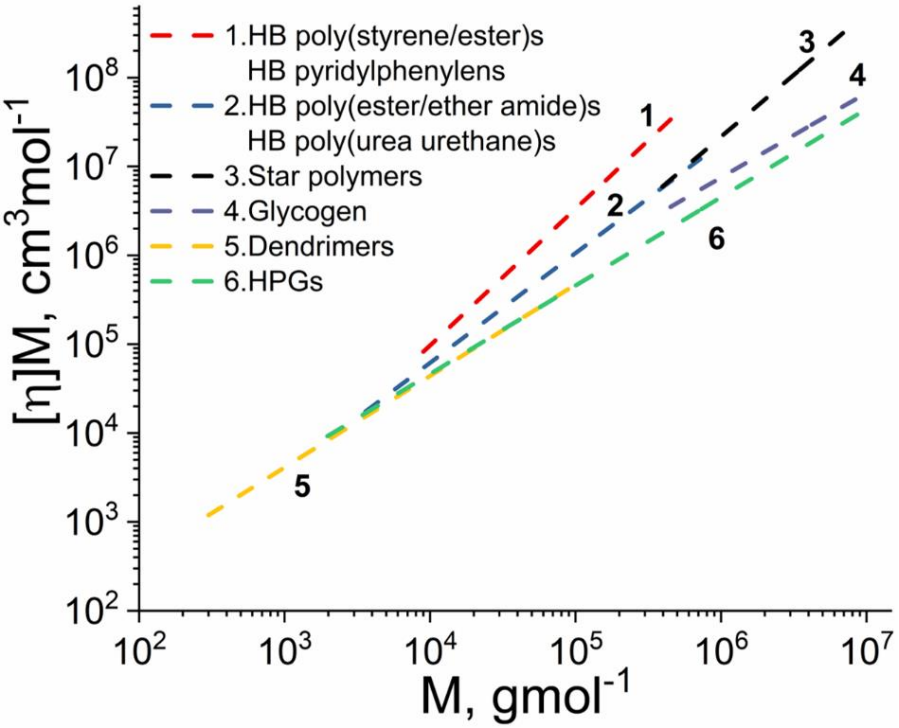

Figure 7. Double logarithmic plot of the hydrodynamic volume, [η]M, against the molar mass, M, for the various branched macromolecular systems: 1 – hyperbranched poly(styrene)s, poly(ester)s and pyridylphenylenes, 2 – hyperbranched poly(ester amide)s, poly (ether amide)s, poly(urea urethane)s, 3 – star polymers with 64 and 128 arms, 4 – Glycogen, 5 – dendrimers 6 – hyperbranched *hb*PGs and *hb*PGs copolymers.

Conclusions

We have presented an in-depth physico-chemical and analytical investigation of hyperbranched polyglycerols, by applying a combination of hydrodynamic and light-scattering approaches, namely sedimentation velocity analytical ultracentrifugation, batch dynamic- and static-light scattering measurements, intrinsic viscosity, and SEC-MALLS measurements. As a result, a complete set of macromolecular hydrodynamic, molecular-, and conformational-characteristics was established for hyperbranched polyglycerols. It was shown, that hyperbranched polyglycerol macromolecule populations are apparently highly hydrated and, yet, adopt the most compact and regular conformation in solution among all other studied hyperbranched systems characterized to date. Despite the admittedly irregular structure and inherent dispersity of the hyperbranched polyglycerols, hydrodynamically they cannot be distinguished from the perfectly structured dendrimers and corresponding experimental scaling relationships show the book values for the hard sphere conformation. In reality, as it is turned out, the *hb*PG macromolecular coils resemble highly hydrated and yet very compact spherical/globular particles in solution with the effective hydrodynamic volume being approximately 50 lower than corresponding linear analogues. Based on the calculations using available literature data on different branched polymer systems, an average value, and the corresponding suitable range for the hydrodynamic invariants, was re-established. The experimental global value of A_0 for *hb*PGs was found to be much lower than the theoretically predicted value for solid spheres. The sedimentation velocity analysis from analytical ultracentrifugation data enabled with the “model free” numerical solutions of the Lamm equation was shown to provide adequate average molar mass values, apparent hydrodynamic

sizes, and dispersities of the studied *hb*PGs. Therefore, we could demonstrate a self-sufficient physico-chemical analytical approach for the analysis of such disperse macromolecular structures in solution.

Acknowledgment

Perevyazko, Gubarev and Lezov are grateful for the support by a grant from the Russian Foundation for Basic Research (project № 18-33-20013). Nischang gratefully acknowledges support of this study through the DFG-funded Collaborative Research Center PolyTarget (SFB 1278—project number 316213987, project Z01). The authors thank U. Kemmer-Jonas for technical assistance.

References

1. Voit, B. I.; Lederer, A. Hyperbranched and Highly Branched Polymer Architectures—Synthetic Strategies and Major Characterization Aspects. *Chem. Rev.* **2009,** 109 (11), 5924-5973 DOI: 10.1021/cr900068q.

2. Flory, P. J. Molecular Size Distribution in Three Dimensional Polymers. VI. Branched Polymers Containing A—R—Bf-1 Type Units. *J. Am. Chem. Soc.* **1952,** 74 (11), 2718-2723 DOI: 10.1021/ja01131a008.

3. Sunder, A.; Hanselmann, R.; Frey, H.; Mülhaupt, R. Controlled Synthesis of Hyperbranched Polyglycerols by Ring-Opening Multibranching Polymerization. *Macromolecules* **1999,** 32 (13), 4240-4246 DOI: 10.1021/ma990090w.

4. Zheng, Y. C.; Li, S. P.; Weng, Z. L.; Gao, C. Hyperbranched polymers: advances from synthesis to applications. *Chem. Soc. Rev.* **2015,** 44 (12), 4091-4130 DOI: 10.1039/c4cs00528g.

5. Schüll, C.; Rabbel, H.; Schmid, F.; Frey, H. Polydispersity and Molecular Weight Distribution of Hyperbranched Graft Copolymers via Hypergrafting, of ABm Monomers from Polydisperse Macroinitiator Cores: Theory Meets Synthesis. *Macromolecules* **2013,** 46 (15), 5823-5830 DOI: 10.1021/ma401119r.

6. Hanselmann, R.; Hölter, D.; Frey, H. Hyperbranched Polymers Prepared via the Core-Dilution/Slow Addition Technique: Computer Simulation of Molecular Weight Distribution and Degree of Branching. *Macromolecules* **1998,** 31 (12), 3790-3801 DOI: 10.1021/ma971197r.

7. Wang, D. L.; Zhao, T. Y.; Zhu, X. Y.; Yan, D. Y.; Wang, W. X. Bioapplications of hyperbranched polymers. *Chem. Soc. Rev.* **2015,** 44 (12), 4023-4071 DOI: 10.1039/c4cs00229f.

8. Abbina, S.; Vappala, S.; Kumar, P.; Siren, E. M. J.; La, C. C.; Abbasi, U.; Brooks, D. E.; Kizhakkedathu, J. N. Hyperbranched polyglycerols: recent advances in synthesis, biocompatibility and biomedical applications. *Journal of Materials Chemistry B* **2017,** 5 (47), 9249-9277 DOI: 10.1039/C7TB02515G.

9. Kainthan, R. K.; Janzen, J.; Levin, E.; Devine, D. V.; Brooks, D. E. Biocompatibility Testing of Branched and Linear Polyglycidol. *Biomacromolecules* **2006,** 7 (3), 703-709 DOI: 10.1021/bm0504882.

10. Kasza, G.; Gyulai, G.; Abraham, A.; Szarka, G.; Ivan, B.; Kiss, E. Amphiphilic hyperbranched polyglycerols in a new role as highly efficient multifunctional surface active stabilizers for poly(lactic/glycolic acid) nanoparticles. *Rsc Advances* **2017,** 7 (8), 4348-4352 DOI: 10.1039/c6ra27843d.

11. Flory, P. J. Spatial configuration of macromolecular chains. *Science* **1975,** 188 (4195), 1268-76 DOI: 188/4195/1268 [pii]

10.1126/science.188.4195.1268.

12. Lederer, A.; Burchard, W., *Hyperbranched Polymers: Macromolecules in between Deterministic Linear Chains and Dendrimer Structures*. The Royal Society of Chemistry: Cambridge, 2015.

13. Garamus, V. M.; Maksimova, T. V.; Kautz, H.; Barriau, E.; Frey, H.; Schlotterbeck, U.; Mecking, S.; Richtering, W. Hyperbranched Polymers: Structure of Hyperbranched Polyglycerol and Amphiphilic Poly(glycerol ester)s in Dilute Aqueous and Nonaqueous Solution. *Macromolecules* **2004,** 37 (22), 8394-8399 DOI: 10.1021/ma0490909.

14. Kainthan, R. K.; Muliawan, E. B.; Hatzikiriakos, S. G.; Brooks, D. E. Synthesis, Characterization, and Viscoelastic Properties of High Molecular Weight

Hyperbranched Polyglycerols. *Macromolecules* **2006,** 39 (22), 7708-7717 DOI: 10.1021/ma0613483.

15. Anilkumar, P.; Lawson, T. B.; Abbina, S.; Mäkelä, J. T. A.; Sabatelle, R. C.; Takeuchi, L. E.; Snyder, B. D.; Grinstaff, M. W.; Kizhakkedathu, J. N. Mega macromolecules as single molecule lubricants for hard and soft surfaces. *Nature Communications* **2020,** 11 (1), 2139 DOI: 10.1038/s41467-020-15975-6.

16. Turner, S. R.; Walter, F.; Voit, B. I.; Mourey, T. H. Hyperbranched Aromatic Polyesters with Carboxylic Acid Terminal Groups. *Macromolecules* **1994,** 27 (6), 1611-1616 DOI: 10.1021/ma00084a051.

17. Turner, S. R.; Voit, B. I.; Mourey, T. H. All-aromatic hyperbranched polyesters with phenol and acetate end groups: synthesis and characterization. *Macromolecules* **1993,** 26 (17), 4617-4623 DOI: 10.1021/ma00069a031.

18. Geladé, E. T. F.; Goderis, B.; de Koster, C. G.; Meijerink, N.; van Benthem, R. A. T. M.; Fokkens, R.; Nibbering, N. M. M.; Mortensen, K. Molecular Structure Characterization of Hyperbranched Polyesteramides. *Macromolecules* **2001,** 34 (11), 3552-3558 DOI: 10.1021/ma001266t.

19. De Luca, E.; Richards, R. W. Molecular characterization of a hyperbranched polyester. I. Dilute solution properties. *J. Polym. Sci., Part B: Polym. Phys.* **2003,** 41 (12), 1339-1351 DOI: 10.1002/polb.10463.

20. Lederer, A.; Voigt, D.; Clausnitzer, C.; Voit, B. Structure characterization of hyperbranched poly(ether amide)s. *J. Chromatogr.* **2002,** 976 (1), 171-179 DOI: http://dx.doi.org/10.1016/S0021-9673(02)00937-8.

21. Boye, S.; Komber, H.; Friedel, P.; Lederer, A. Solution properties of selectively modified hyperbranched polyesters. *Polymer* **2010,** 51 (18), 4110-4120 DOI: 10.1016/j.polymer.2010.06.037.

22. Li, L.; Lu, Y.; An, L.; Wu, C. Experimental and theoretical studies of scaling of sizes and intrinsic viscosity of hyperbranched chains in good solvents. *The Journal of Chemical Physics* **2013,** 138 (11), 114908.

23. Hutchings, L. R.; Dodds, J. M.; Roberts-Bleming, S. J. HyperMacs: Highly Branched Polymers Prepared by the Polycondensation of AB2 Macromonomers, Synthesis and Characterization. *Macromolecules* **2005,** 38 (14), 5970-5980 DOI: 10.1021/ma047419k.

24. Li, L.; He, C.; He, W.; Wu, C. Formation Kinetics and Scaling of “Defect-Free” Hyperbranched Polystyrene Chains with Uniform Subchains Prepared from Seesaw-Type Macromonomers. *Macromolecules* **2011,** 44 (20), 8195-8206 DOI: 10.1021/ma201687s.

25. Gubarev, A. S.; Lezov, A. A.; Senchukova, A. S.; Vlasov, P. S.; Serkova, E. S.; Kuchkina, N. V.; Shifrina, Z. B.; Tsvetkov, N. V. Diels–Alder Hyperbranched Pyridylphenylene Polymer Fractions as Alternatives to Dendrimers. *Macromolecules* **2019,** 52 (4), 1882-1891 DOI: 10.1021/acs.macromol.8b02388.

26. Ioan, C. E.; Aberle, T.; Burchard, W. Solution Properties of Glycogen. 1. Dilute Solutions. *Macromolecules* **1999,** 32 (22), 7444-7453 DOI: 10.1021/ma990600m.

27. Perevyazko, I.; Seiwert, J.; Schömer, M.; Frey, H.; Schubert, U. S.; Pavlov, G. M. Hyperbranched Poly(ethylene glycol) Copolymers: Absolute Values of the Molar Mass, Properties in Dilute Solution, and Hydrodynamic Homology. *Macromolecules* **2015,** 48 (16), 5887-5898 DOI: 10.1021/acs.macromol.5b01020.

28. Filippov, A.; Amirova, A. I.; Kirila, T.; Belyaeva, E. V.; Sheremetyeva, N. A.; Muzafarov, A. M. Influence of branching regularity on the behavior of

hyperbranched polymers in solution. *Polym. Int.* **2015,** 64 (6), 780-786 DOI: 10.1002/pi.4852.

29. Berne, B.; Pecora, R., *Dynamic Light Scattering: with Applications to Chemistry, Biology, and Physics*. Dover Publications: New York 2000; p 384.

30. Grube, M.; Perevyazko, I.; Heinze, T.; Schubert, U. S.; Nischang, I. Revisiting very disperse macromolecule populations in hydrodynamic and light scattering studies of sodium carboxymethyl celluloses. *Carbohydr. Polym.* **2020,** 229, 115452 DOI: 10.1016/j.carbpol.2019.115452.

31. Nischang, I.; Perevyazko, I.; Majdanski, T.; Vitz, J.; Festag, G.; Schubert, U. S. Hydrodynamic Analysis Resolves the Pharmaceutically-Relevant Absolute Molar Mass and Solution Properties of Synthetic Poly(ethylene glycol)s Created by Varying Initiation Sites. *Anal. Chem.* **2017,** 89 (2), 1185-1193 DOI: 10.1021/acs.analchem.6b03615.

32. Tsvetkov, V. N., *Rigid-chain polymers: hydrodynamic and optical properties in solution*. Plenum Press: New York, 1989.

33. Tsvetkov, V. N.; Eskin, V. E.; Frenkel, S. Y., *Structure of macromolecules in solution*. Nat. Lend. Library Sci.&Technol.: Boston, 1971.

34. Kratky, O.; Leopold, H.; Stabinger, H. The determination of the partial specific volume of proteins by the mechanical oscillator technique. *Methods Enzymol.* **1973,** 27, 98-110.

35. Perevyazko, I.; Lezov, A.; Gubarev, A. S.; Lebedeva, E.; Festag, G.; Guerrero-Sanchez, C.; Tsvetkov, N.; Schubert, U. S. Structure-property relationships via complementary hydrodynamic approaches: Poly(2-(dimethylamino)ethyl methacrylate)s. *Polymer* **2019,** 182, 121828 DOI: 10.1016/j.polymer.2019.121828.

36. Perevyazko, I.; Gubarev, A. S.; Tauhardt, L.; Dobrodumov, A.; Pavlov, G. M.; Schubert, U. S. Linear poly(ethylene imine)s: true molar masses, solution properties and conformation. *Polymer Chemistry* **2017,** 8 (46), 7169-7179 DOI: 10.1039/c7py01634d.

37. Wilms, D.; Wurm, F.; Nieberle, J.; Böhm, P.; Kemmer-Jonas, U.; Frey, H. Hyperbranched Polyglycerols with Elevated Molecular Weights: A Facile Two-Step Synthesis Protocol Based on Polyglycerol Macroinitiators. *Macromolecules* **2009,** 42 (9), 3230-3236. DOI: 10.1021/ma802701g

38. Tsvetkov, V. N.; Lavrenko, P. N.; Bushin, S. V. Hydrodynamic Invariant of Polymer-Molecules. *J. Polym. Sci., Part A: Polym. Chem.* **1984,** 22 (11), 3447-3486.

39. Harding, S. E.; Dampier, M.; Rowe, A. J. The viscosity increment for ellipsoids of revolution: Some observations on the simha formula. *Biophys. Chem.* **1982,** 15 (3), 205-208 DOI: https://doi.org/10.1016/0301-4622(82)80003-3.

40. Morawetz, H., *Macromolecules in Solution*. Second ed.; Wiley: New York, 1975.

41. Pamies, R.; Cifre, J. G. H.; Martinez, M. D. L.; de la Torre, J. G. Determination of intrinsic viscosities of macromolecules and nanoparticles. Comparison of single-point and dilution procedures. *Colloid. Polym. Sci.* **2008,** 286 (11), 1223-1231 DOI: 10.1007/s00396-008-1902-2.

42. Pavlov, G. M.; Perevyazko, I. Y.; Okatova, O. V.; Schubert, U. S. Conformation parameters of linear macromolecules from velocity sedimentation and other hydrodynamic methods. *Methods* **2011,** 54 (1), 124-35 DOI: 10.1016/j.ymeth.2011.02.005.

43. Pavlov, G. M.; Perevyazko, I.; Schubert, U. S. Velocity Sedimentation and Intrinsic Viscosity Analysis of Polystyrene Standards with a Wide Range of Molar Masses. *Macromol. Chem. Phys.* **2010,** 211 (12), 1298-1310 DOI: 10.1002/macp.200900602.

44. Schuck, P. Size-distribution analysis of macromolecules by sedimentation velocity ultracentrifugation and lamm equation modeling. *Biophys. J.* **2000,** 78 (3), 1606-19 DOI: 10.1016/S0006-3495(00)76713-0.

45. Brown, P. H.; Schuck, P. Macromolecular size-and-shape distributions by sedimentation velocity analytical ultracentrifugation. *Biophys. J.* **2006,** 90 (12), 4651-61 DOI: 10.1529/biophysj.106.081372.

46. Radke, W.; Litvinenko, G.; Müller, A. H. E. Effect of Core-Forming Molecules on Molecular Weight Distribution and Degree of Branching in the Synthesis of Hyperbranched Polymers. *Macromolecules* **1998,** 31 (2), 239-248 DOI: 10.1021/ma970952y.

47. Lavrenko, V. P.; Gubarev, A. S.; Lavrenko, P. N.; Okatova, O. V.; Pavlov, G. M.; Panarin, E. F. Processing of Digital Interference Images Obtained on Tsvetkov Diffusometer. *Indus. Lab.* **2013,** 79 (7-1), 33-36.

48. Grube, M.; Leiske, M. N.; Schubert, U. S.; Nischang, I. POx as an Alternative to PEG? A Hydrodynamic and Light Scattering Study. *Macromolecules* **2018,** 51 (5), 1905-1916 DOI: 10.1021/acs.macromol.7b02665.

49. Mandelkern, L.; Flory, P. J. The Frictional Coefficient for Flexible Chain Molecules in Dilute Solution. *The Journal of Chemical Physics* **1952,** 20 (2), 212-214.

50. Pavlov, G. M.; Korneeva, E. V.; Nepogod’ev, S. A.; Jumel, K.; Harding, S. E. Translational and Rotational Friction of Lactodendrimer Molecules in Solution. *Polymer Science Series A* **1998,** 40, 1282.

51. Pavlov, G.; Korneeva, E.; Jumel, K.; Harding, S.; Meijer, E. W.; Peerlings, H. W. I.; Stoddart, J. F.; Nepogodiev, S. Hydrodynamic properties of carbohydrate-coated dendrimers. *Carbohydr. Polym.* **1999,** 38 (3), 195-202 DOI: http://dx.doi.org/10.1016/S0144-8617(98)00091-5.

52. Pavlov, G. M.; Korneeva, E. V.; Roy, R.; Michailova, N. A.; Ortega, P. C.; Perez, M. A. Sedimentation, translational diffusion, and viscosity of lactosylated polyamidoamine dendrimers. *Prog. Colloid Polym. Sci.* **1999,** 113, 150-157 DOI: 10.1007/3-540-48703-4_21.

53. Pavlov, G. M.; Korneeva, E. V.; Michailova, N. A.; Roy, R.; Cejas Ortega, P.; Alamino Perez, M.; . Translational and rotational friction of lactopolyamidoamin-dendrimers in solutions. *Vysokomolekul. soedin Ser.A* **1999,** 41, 1810-1815.

54. Pavlov, G. M.; Errington, N.; Harding, S. E.; Korneeva, E. V.; Roy, R. Molecular and Structural Characteristics of Lactodendrimers Based on Poly(amidoamine). *Polymer Sci. Ser. A* **2001,** 43, 118.

55. Pavlov, G. M.; Errington, N.; Harding, S. E.; Korneeva, E. V.; Roy, R. Dilute solution properties of lactosylated polyamidoamine dendrimers and their structural characteristics. *Polymer* **2001,** 42 (8), 3671-3678 DOI: http://dx.doi.org/10.1016/S0032-3861(00)00617-0.

56. Pavlov, G. M.; Korneeva, E. V.; Meijer, E. W. Molecular characteristics of poly(propylene imine) dendrimers as studied with translational diffusion and viscometry. *Colloid. Polym. Sci.* **2002,** 280 (5), 416-423 DOI: 10.1007/s00396-001-0625-4.

57. Tsvetkov, N. V.; Gubarev, A. S.; Lebedeva, E. V.; Lezov, A. A.; Mikhailova, M. E.; Kolomiets, I. P.; Mikusheva, N. G.; Akhmadeeva, L. I.; Kuchkina, N. V.; Serkova, E. S.; Shifrina, Z. B. Conformational and hydrodynamic parameters of hyperbranched pyridylphenylene polymers. *Polym. Int.* **2017,** 66 (4), 583-592 DOI: 10.1002/pi.5298.

58. Pavlov, G. M.; Korneeva, E. V.; Roy, R.; Michailova, N. A.; Ortega, P. C.; Perez, M. A. In *Sedimentation, translational diffusion, and viscosity of lactosylated polyamidoamine dendrimers*, Berlin, Heidelberg, 1999; Springer Berlin Heidelberg: Berlin, Heidelberg, 1999; pp 150-157.

59. Morris, G. A.; Ang, S.; Hill, S. E.; Lewis, S.; Schäfer, B.; Nobbmann, U.; Harding, S. E. Molar mass and solution conformation of branched α(1→4), α(1→6) Glucans. Part I: Glycogens in water. *Carbohydr. Polym.* **2008,** 71 (1), 101-108 DOI: 10.1016/j.carbpol.2007.05.029.

60. Burchard, W., Solution Properties of Branched Macromolecules. In *Branched Polymers II*, Roovers, J., Ed. Springer Berlin Heidelberg: 1999; Vol. 143, pp 113-194.

61. Talik, P.; Hubicka, U. The DSC approach to study non-freezing water contents of hydrated hydroxypropylcellulose (HPC). *J. Therm. Anal. Calorim.* **2018,** 132 (1), 445-451 DOI: 10.1007/s10973-017-6889-9.

62. García de la Torre, J. Hydration from hydrodynamics. General considerations and applications of bead modelling to globular proteins. *Biophys. Chem.* **2001,** 93 (2), 159-170 DOI: https://doi.org/10.1016/S0301-4622(01)00218-6.

63. Rangelov, S.; Trzebicka, B.; Jamroz-Piegza, M.; Dworak, A. Hydrodynamic Behavior of High Molar Mass Linear Polyglycidol in Dilute Aqueous Solution. *The*

Journal of Physical Chemistry B **2007,** 111 (38), 11127-11133 DOI: 10.1021/jp074485q.

64. Mori, H.; Müller, A. H. E.; Simon, P. F. W., Linear Versus (Hyper)branched Polymers. In *Macromolecular Engineering*, Wiley-VCH Verlag GmbH & Co. KGaA: 2007; pp 973-1005.

65. Harding, S. E.; Colfen, H. Inversion Formulas for Ellipsoid of Revolution Macromolecular Shape Functions. *Anal. Biochem.* **1995,** 228 (1), 131-142 DOI: 10.1006/abio.1995.1324.

Supporting Information

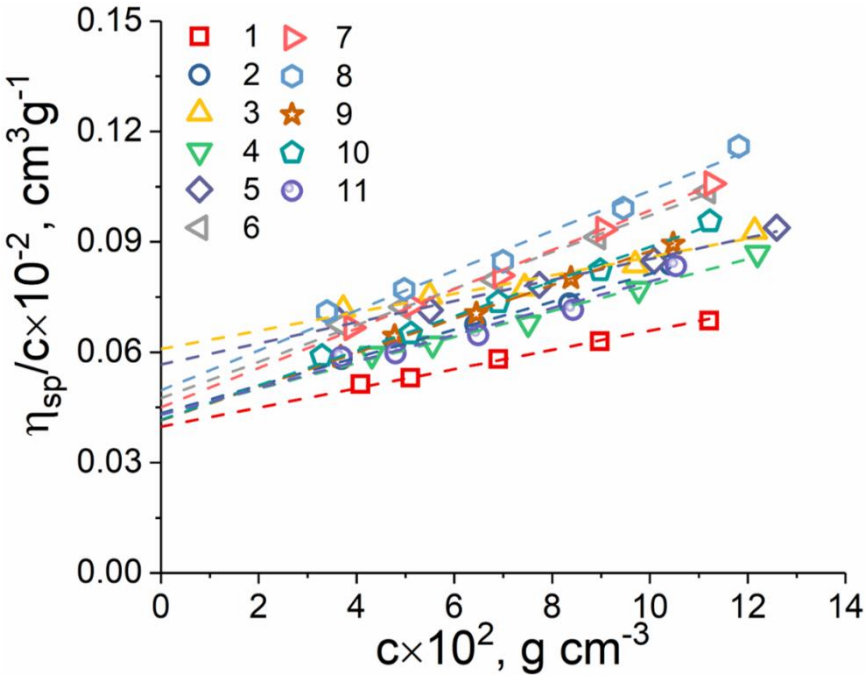

Figure S 1. Intrinsic viscosity Huggins extrapolation procedures for the *hb*PG in water at T = 25 °C.

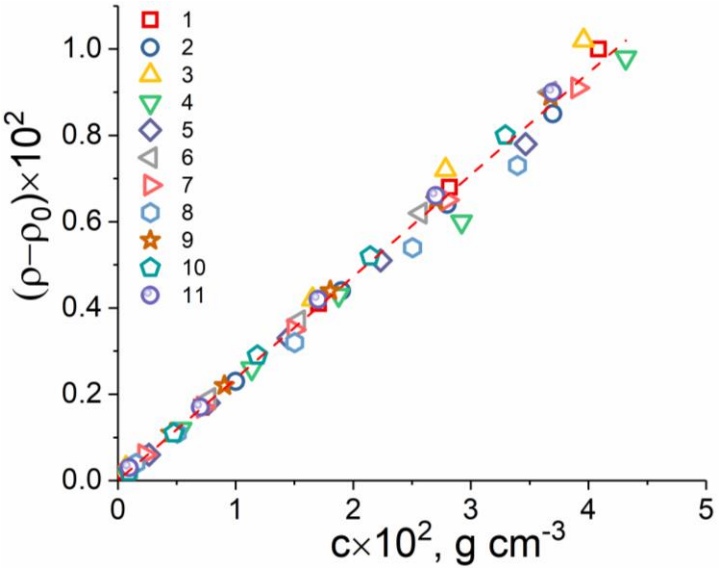

Figure S 2. Partial specific volume determination for the *hb*PG in water at T = 25 °C.

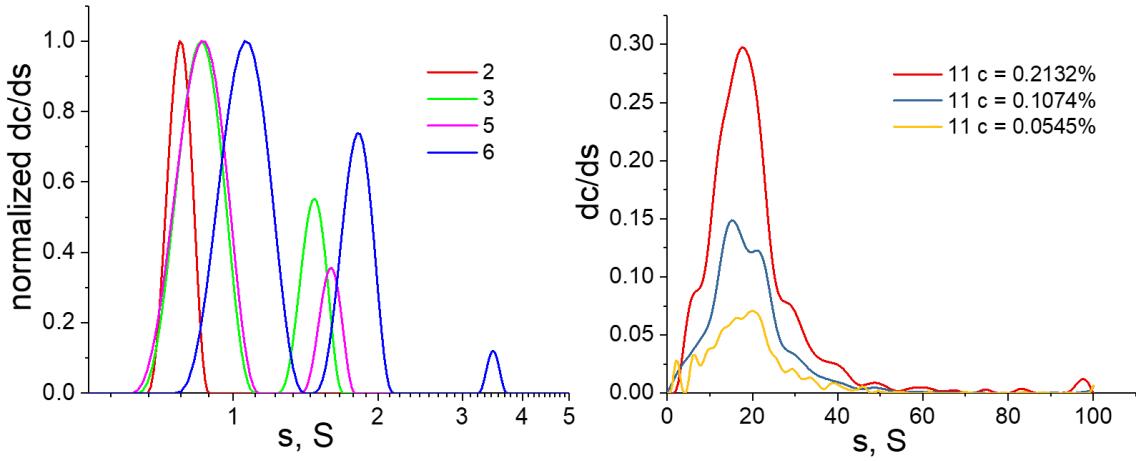

Figure S 3. Differential distributions of the sedimentation coefficients for *hb*PG samples (2, 3, 5, 6) in water at T = 25 ℃.

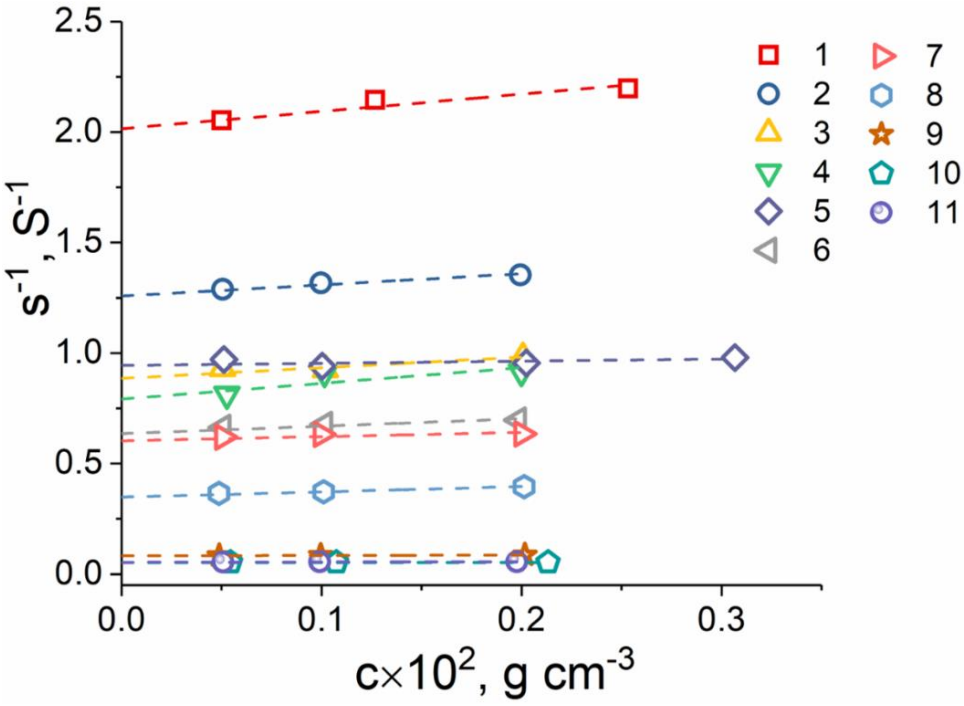

Figure S 4. Concentration dependences of the sedimentation coefficients for the *hb*PG in water at T = 25 ℃.

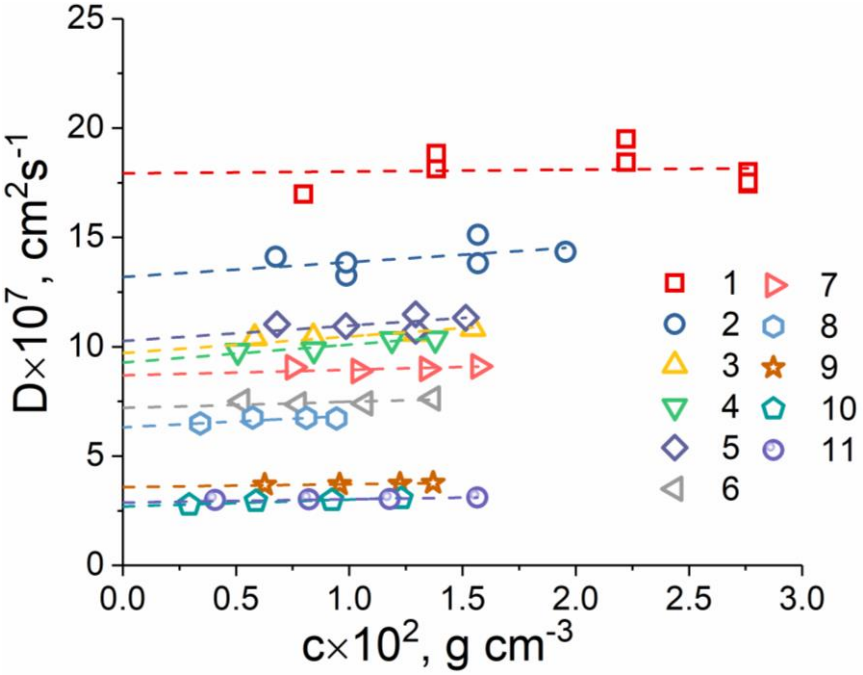

Figure S 5. Concentration dependences of the translation diffusion coefficients determined by the dynamic light scattering experiments in water T = 25 °C.

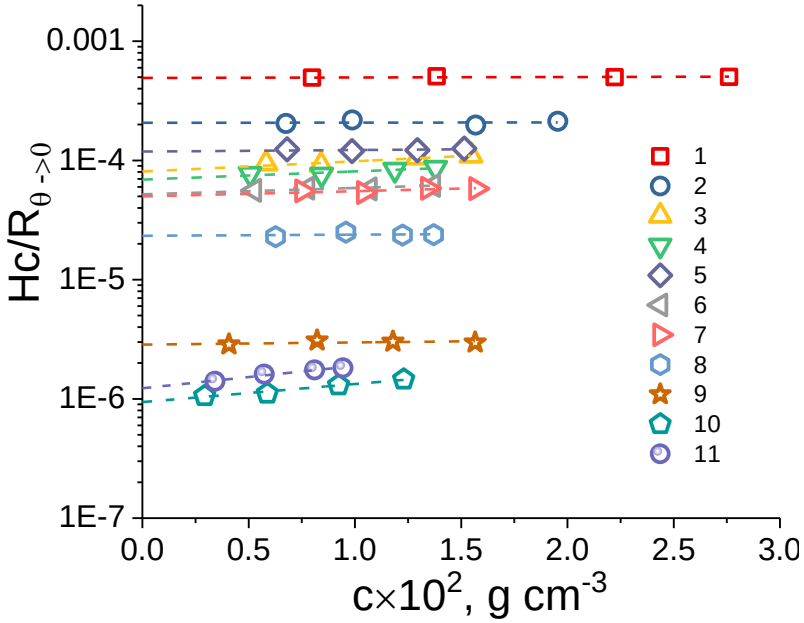

Figure S 6. Static light scattering dependence of Hc/R_θ on the polymer concentration of *hb*PG at T = 25 °C.

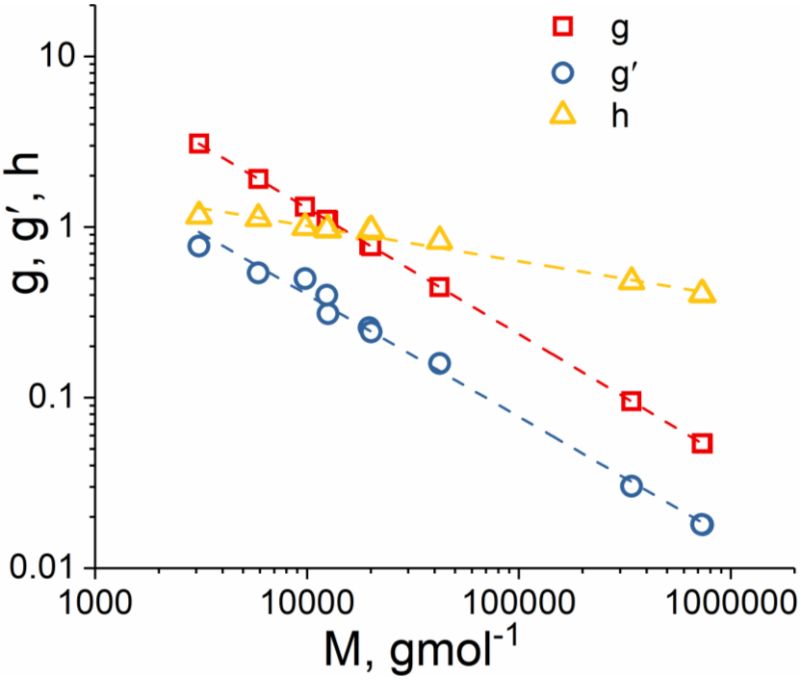

Figure S 7. Double logarithmic scaling dependences of the g, g' and h on the molar mass for the *hb*PG samples in water, $T = 25.0$ ℃, the corresponding scaling indices are listed in Table 6.

Table S 1. Frictional ratios evaluated by c(s) and c(s,f/f) models for *hb*PG macromolecules in water, $T = 25.0$ ℃.

Sample	$(f/f_0)_{c(s)}$	$(f/f_0)_{c(s,f/f)}$
1	1.15	1.22
2	1.26	1.40
3	1.26	1.55
4	1.09	1.53
5	1.24	1.50
6	1.22	1.76
7	1.35	1.72
8	1.29	1.65
9	1.03	1.45
10	1.15	1.78
11	1.00	1.68

Table S 2. Scaling parameters for the corresponding log-log dependences of the contraction factors.

Scaling	$b_i \pm \Delta b_i$	$K_i \pm \Delta K_i$	$\lvert r_i \rvert$
g-M	-0.74	1179	1
g`-M	-0.72±0.02	296	0.9966
h-M	-0.21±0.01	6.85	0.9890
g`-g	0.97±0.03	0.313	0.9966
g`-h	3.3±0.1	0.375	0.9912
g-h	0.28±0.01	0.946	0.9890

Supplemental ^{1}H and ^{13}C NMR Spectroscopy

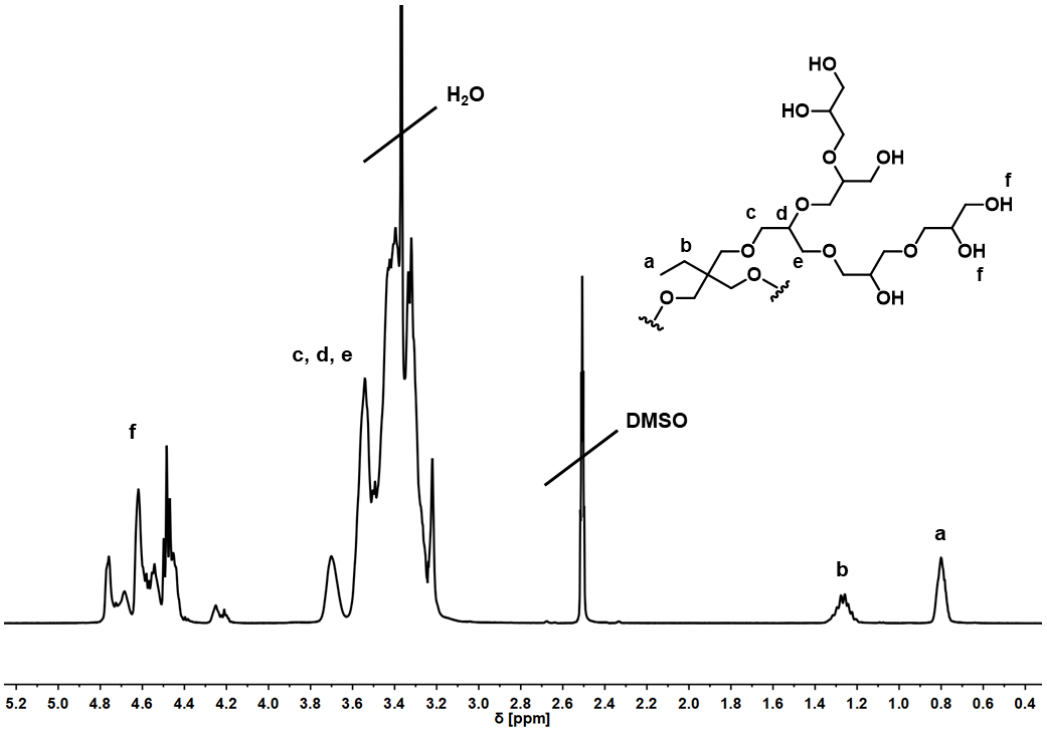

Figure S 8. ^{1}H NMR spectrum of sample 1 (300 MHz, DMSO-d_6).

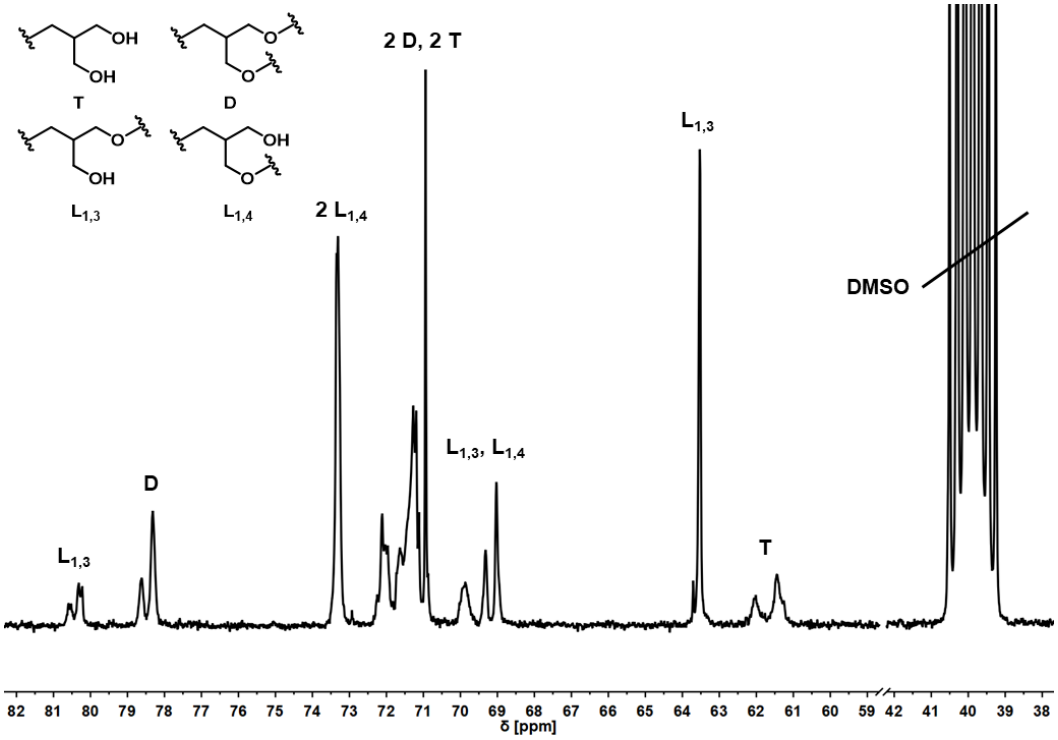

Figure S 9. Inverse gated ^{13}C NMR spectrum of sample 1 (100 MHz, DMSO-d_6).

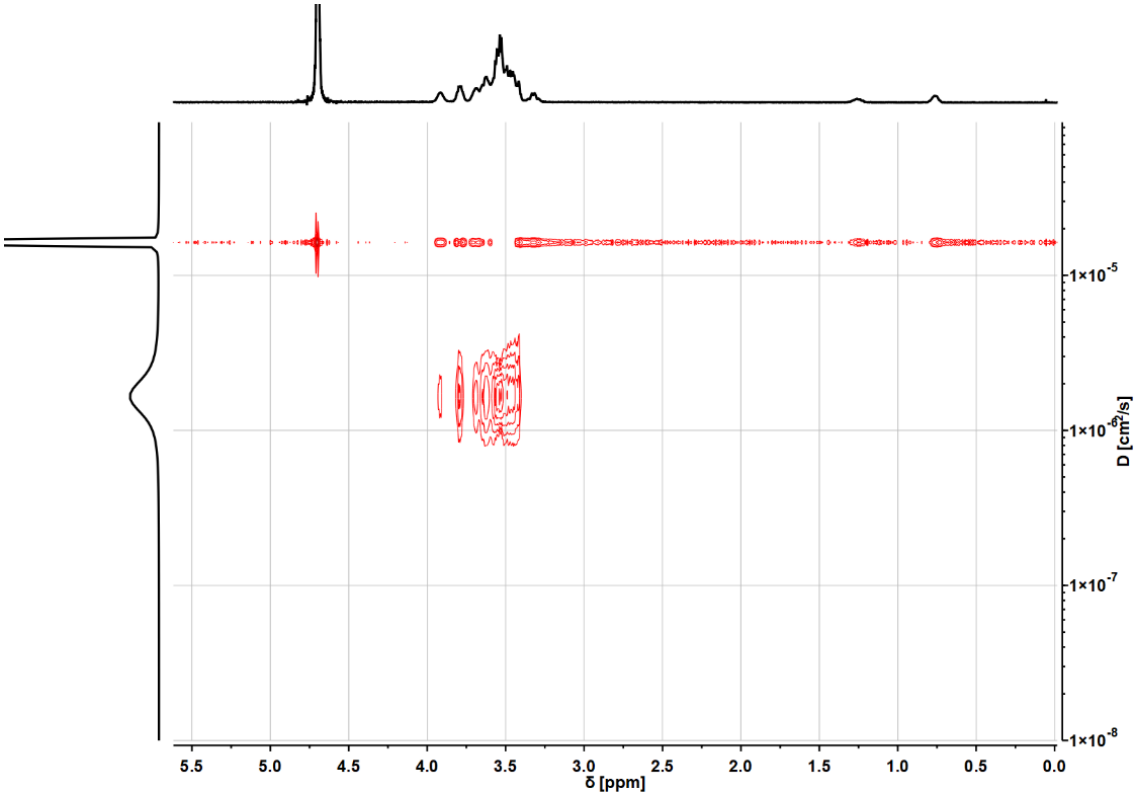

Figure S 10. DOSY NMR spectrum of sample 1 (300 MHz, D_2O).

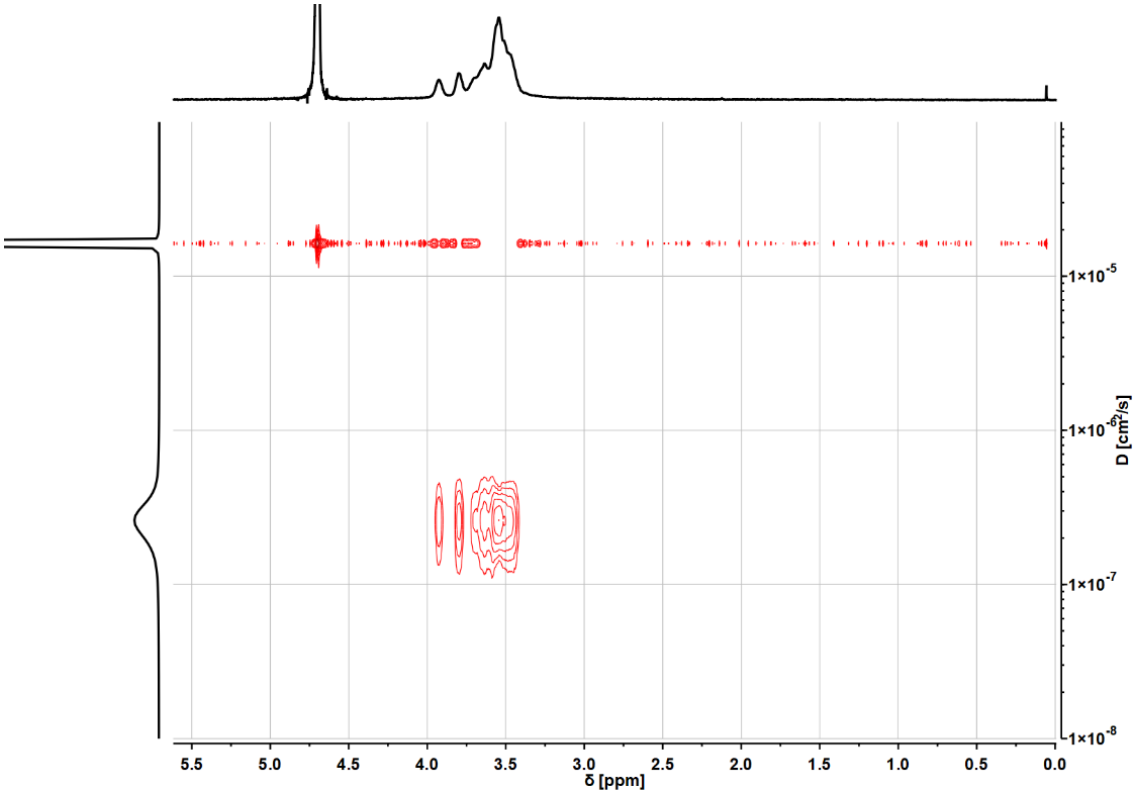

Figure S 11. DOSY NMR spectrum of sample 10 (300 MHz, D_2O).

3. Synthesis and Characterization of Hyperbranched Polyether Polyols: Variation of the Polymer Functionality

3.1 Synthesis of Stimuli-Responsive Organobases by Copolymerization of Glycidol and a *N,N*-Dibutylamino-Functional Glycidyl Ether

Tobias Kaiser[a], Mika Donabauer[a], Matthias Bros[b], Holger Frey[a,]*

[a]Department of Chemistry, Johannes Gutenberg University, 55128 Mainz, Germany

[b]Department of Dermatology, University Medical Center of the Johannes Gutenberg University Mainz, 55131 Mainz

In preparation.

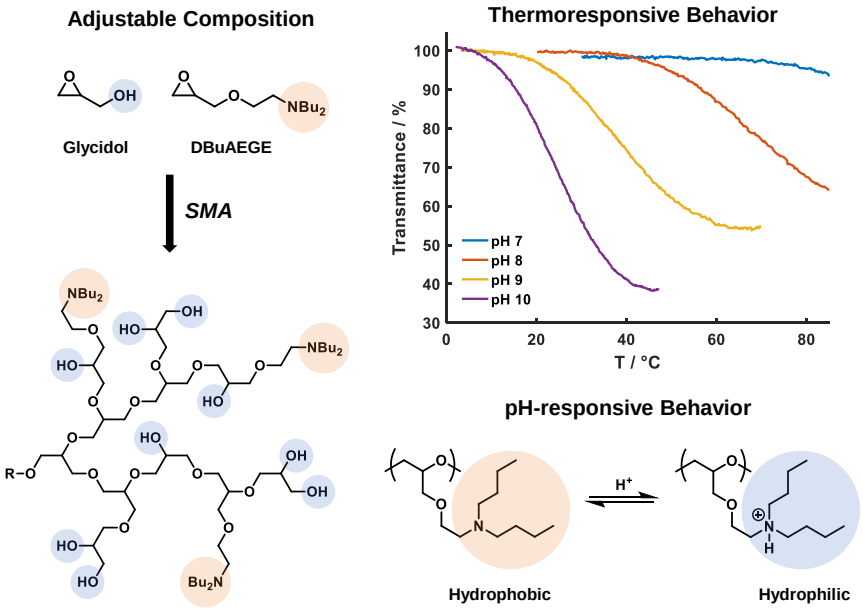

Abstract

Several multi-amino functional hyperbranched polyether polyols have been prepared by the copolymerization of glycidol and *N,N*-dibutylaminoethyl glycidyl ether (DBuAEGE) following a slow monomer addition (SMA) protocol. By variation of the comonomer ratio in the initial mixture, comonomer contents $X_{DBuAEGE}$ between 0.10 and 0.36 and similar molar masses ranging from 2300 to 290 g mol^{-1} were obtained as confirmed by ^{1}H NMR spectroscopy. The SEC traces show monomodal distributions independent of the copolymer composition with moderate dispersities between 1.33 and 1.46. Structure elucidation by ^{13}C NMR and online NMR kinetics reveals a mostly random copolymer with a slight abundance of terminal DBuAEGE moieties, also supported by a linear decrease of the glass transition temperature depending on the composition. By the introduction of the apolar dibutyl amino moieties, multi-stimuli responsive behavior is introduced into the otherwise fully water-soluble *hb*PG backbone. Varying the copolymer composition and the pH value of the aqueous medium, the water-solubility, i.e. the cloud point, can be adjusted continuously. Furthermore, by incorporation into the highly hydrophilic polyether scaffold, the tertiary amine groups show increased biocompatibility, allowing for a wide range of different applications.

Introduction

Poly(ethylene glycol) is considered the gold standard polyether for a plethora of applications, e.g. biomedicine, among others. However, the amount of functional groups is limited to the termini.[1] By copolymerization with suitable comonomers, multi-functional PEG copolymers are accessible. Very promising candidates for a

multitude of applications, i.e. surface modification, catalysis or biomedicine, are multi amino-functional polyethers.[2] Especially the introduction of tertiary amino groups results in intriguing properties, i.e. multi-stimuli responsive behavior.[3] An elegant pathway to tertiary amino-functional PEGs is the direct copolymerization of ethylene oxide with suitable comonomers *via* anionic ring-opening polymerization. Following this strategy, our group has reported on the direct copolymerization of ethylene oxide with several, sterically hindered glycidyl amines, forming gradient copolymers.[4–6] On the other hand, to form random copolymers, Lynd and coworkers introduced the glycidyl ether DEGE, carrying a tertiary *N,N*-diisopropyl amine unit,[7] whereas Ziegler *et al.* employed a *N,N*-dibutyl amino-functional glycidyl ether.[8] However, by copolymerization only the amount of amino groups is adjustable whereas the hydroxy functionality is exclusive to the end group, restricting the field of possible applications.

On the other hand, hyperbranched polyether polyols based on glycidol carry a multitude of functional hydroxy groups without the necessity of copolymerization or post-polymerization modification.[9–11] Hyperbranched polyglycerols (*hb*PG) are typically prepared by the anionic ring-opening polymerization of glycidol using a partially deprotonated initiator salt *via* slow monomer addition.[12] The incorporation of a glycidol unit introduces exactly one hydroxy group in addition to the initiator moiety. Therefore, the total number of functional groups #OH is directly affected by the average degree of polymerization, i.e. molar mass. Several methods to tune the molar mass of *hb*PGs have been reported, e.g. using various solvents with different polarity.[13–16] Furthermore, by the statistical copolymerization of glycidol and suitable, base-stable, glycidyl ethers, a multitude of different functional groups can be introduced in addition to the hydroxy groups.[17–21] In this case, the average

amount of either functional group is facilely adjusted by variation of the copolymer composition.[22] In addition, hyperbranched analogs of commonly used linear poly(alkylene oxide)s have been prepared to modify the water-solubility of *hb*PGs.[23–26] The introduction of primary amino groups was achieved by the copolymerization of glycidol with either glycidyl phthalimide[27] or an amino functional glycidyl ether carrying a BOC protection group[28] and subsequent deprotection. However, as of now, no tertiary amino-functional *hb*PG obtained exclusively by copolymerization has been described.

Tributylamine

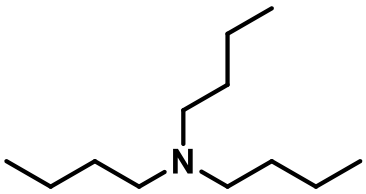

✓ High Basicity
✗ Poor Solubility in Water
✗ Highly Toxic
✗ Low Flash Point

***hb*P(G-*co*-DBuAEGE)**

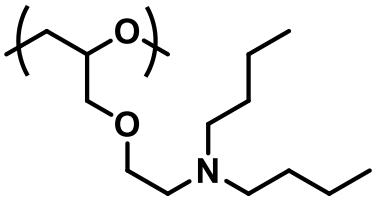

✓ High Basicity
✓ Soluble in Water
✓ Biocompatible
✓ No Vapor Pressure

Scheme 1. Comparison of a DBuAEGE repeating unit and the structurally related tributylamine.[29]

In this work, we report the synthesis of hyperbranched copolymers based on glycidol and the novel glycidyl ether *N,N*-dibutylaminoethyl glycidyl ether (DBuAEGE), introducing dibutylamino moieties into the polyether polyol.[8] The *N,N*-dibutylamino moiety shows a strong resemblance to tributyl amine, an organic compound commonly used for a wide variety of applications, e.g. as a proton accepting catalyst in organic synthesis and polyurethane preparation (Scheme 1).[30] In contrast to the low molecular weight model compound, the hyperbranched copolymers show thermo- and pH responsive behavior resulting in tunable water-solubility. Furthermore, the random distribution throughout the polyether polyol leads to an enhanced biocompatibility of the amine groups.[31–34]

Experimental Section

Materials

All materials were purchased from Sigma Aldrich, TCI or Fisher Scientific. The compounds used for monomer synthesis were employed without further purification. Prior to polymerization, glycidol (96 %), *N,N*-dibutylaminoethyl glycidyl ether (DBuAEGE) and 1-methyl-2-pyrrolidone (NMP, 99 %) were purified by distillation over calcium hydride. The initiator *N,N*-dibenzyl tris(hydroxymethyl)aminomethane (Bn_2TRIS) was synthesized according to literature.[35]

Instrumentation

NMR spectroscopy. ^{1}H and ^{13}C NMR spectra as well as HSQC and HMBC were recorded on a Bruker Avance II HD 400 (5 mm BBFO-SmartProbe with z-gradient and ATM) at 400/100 MHz. Inverse gated ^{13}C NMR spectra were recorded on a Bruker Avance II HD 400 (5 mm BBFO-SmartProbe with z-gradient and ATM) at 100 MHz. The residual signals of the deuterated solvent were utilized as an internal reference.

Size-exclusion chromatography. SEC measurements in DMF (containing 0.25 g L^{-1} of lithium bromide) were performed using an integrated Agilent 1100 series instrument, equipped with a PSS HEMA column combination ($10^6/10^4/10^2$ Å porosity), UV and RI detector. Calibration is based on linear poly(ethylene glycol) standards (Polymer Standards Service).

Turbidimetry. Cloud points were determined using a Jasco V 630 photospectrometer with a Jasco ETC-717 Peltier element and observed by optical transmittance of light beam (λ = 630 nm) through a 1 cm quartz cell. The intensity of the transmitted light was recorded versus the temperature of the sample cell. The heating-cooling rate was 10 K min^{-1} and values were recorded in 1 K intervals.

Fourier-transform infrared spectroscopy (FTIR). FTIR measurements were performed using a Nicolet iS10 FTIR spectrometer (Thermo Fisher Scientific) equipped with diamond ATR sample holder.

Differential Scanning Calorimetry. DSC measurements were performed using a PerkinElmer 8500 thermal analysis system and a Perkin-Elmer CLN2 thermal analysis controller in the temperature range of -90 to +150 °C at a heating rate of 10 K min^{-1}.

Monomer Synthesis

A three-necked flask equipped with a dropping funnel, reflux condenser and thermometer was filled with 24.5 mL epichlorohydrin (28.9 g, 0.31 mol, 5 eq.), 15 mL aqueous NaOH solution (50 wt%) and tetrabutylammonium hydrogensulfate (0.81 g, 2.39 mmol, cat.) and cooled to 0 °C. 12 mL *N,N*-dibutylaminoethanol (10.3 g, 0.06 mol, 1 eq.) was added dropwise under vigorous stirring. After complete addition, the reaction was quenched with ice water and the organic phase was separated. The aqueous phase was extracted with diethyl ether and the combined organic phases washed with aqueous NaCl (sat.) and subsequently dried with anhydrous $MgSO_4$. After filtration to remove solids, the solvents were removed *in vacuo*. The crude product was purified by successive fractional

distillations (T_b = 115 °C, p = 2 10^{-2} mbar) to yield a colorless liquid in moderate yields (53 -60 %).

^{1}H NMR (400 MHz, $CDCl_3$): δ (ppm) = 3.72 (dd, 1H, H_2C-(O)-CH-CH<u>H</u>-O-); 3.55 (m, 2H, -O-C<u>H</u>$_2$-CH_2-NR_2); 3.39 (dd, 1H, H_2C-(O)-CH-C<u>H</u>H-O-); 3.13 (m, 1H, H_2C-(O)-C<u>H</u>-); 2.78 (dd, 1H, <u>H</u>HC-(O)-CH-); 2.64 (t, 2H, -O-CH_2-C<u>H</u>$_2$-NR_2); 2.59 (dd, 1H, H<u>H</u>C-(O)-CH-); 2.43 (m, 4H, -N-(C<u>H</u>$_2$-CH_2-CH_2-CH_3)$_2$); 1.40 (m, 4H, -N-(CH_2-C<u>H</u>$_2$-CH_2-CH_3)$_2$); 1.28 (m, 4H, -N-(CH_2-CH_2-C<u>H</u>$_2$-CH_3)$_2$); 0.89 (m, 6H, -N-(CH_2-CH_2-CH_2-C<u>H</u>$_3$)$_2$).

^{13}C NMR (100 MHz, $CDCl_3$): δ (ppm) = 71.89 (H_2C-(O)-CH-<u>C</u>H$_2$-O-); 70.20 (-O-<u>C</u>H$_2$-CH_2-NR_2); 54.71 (-N-(<u>C</u>H$_2$-CH_2-CH_2-CH_3)$_2$); 53.57 (-O-CH_2-<u>C</u>H$_2$-NR_2); 50.94 (H_2C-(O)-<u>C</u>H-); 44.41 (H_2<u>C</u>-(O)-CH-); 29.35 (-N-(CH_2-<u>C</u>H$_2$-CH_2-CH_3)$_2$); 20.77 (-N-(CH_2-CH_2-<u>C</u>H$_2$-CH_3)$_2$); 14.18 (-N-(CH_2-CH_2-CH_2-<u>C</u>H$_3$)$_2$).

Copolymerization Protocol

General procedure: In a Schlenk flask equipped with a magnetic stirrer, 67 mg Bn_2TRIS (0.22 mmol, 1 eq) was dissolved in 1 mL methanol. Afterwards, a solution of 11 mg cesium hydroxide monohydrate (0.07 mmol, 0.3 eq) in 1 mL methanol was added and the mixture was stirred for 30 min. The partially deprotonated initiator salt was mixed with 2 mL benzene evacuated overnight at room temperature. The initiator salt was then dissolved in 1 mL NMP and heated to 100 °C under argon atmosphere. In another Schlenk flask, the monomers were mixed in regard to the target composition and diluted with NMP. Using a syringe pump, the monomer mixture was slowly added to the heated solution of the initiator salt with a rate of 0.1 mL h^{-1}. Subsequent to complete addition, the mixture was

stirred for another 60 min and the polymerization was terminated by adding 1 mL methanol. Afterwards, the reaction mixture was dialyzed (methanol, MWCO = 1000 g mol^{-1}) and the solvent evaporated. The products were isolated as highly viscous brown oils.

^{1}H NMR (300 MHz, DMSO-d_6, δ): 7.30 – 7.01 (m, 10H, -N-(CH_2-$C_6\underline{H}_5$)$_2$); 5.02 – 4.26 (br, m, -O$\underline{H}$); 3.95 (s, 4H, -N-($C\underline{H}_2$-C_6H_5)$_2$); 3.87 – 3.10 (m, -O-C$\underline{H}$-, -O-C$\underline{H}_2$-); 2.57 – 2.47 (-O-CH_2-C$\underline{H}_2$-NR_2); 2.43 – 2.32 (-N-(CH_2-C$\underline{H}_2$-CH_2-CH_3)$_2$); 1.41 – 1.18 (-N-(CH_2-CH_2-C$\underline{H}_2$-CH_3)$_2$); 0.91 – 0.80 (-N-(CH_2-CH_2-CH_2-C$\underline{H}_3$)$_2$).

^{13}C NMR (100 MHz, DMSO-d_6, δ): 128.18 – 125.83 (-N-(CH_2-$\underline{C}_6H_5$)$_2$); 80.41 – 79.63 ($L_{1,3G}$); 78.39 – 77.63 (D_G, $L_{DBuAEGE}$); 73.32 – 72.65 (2 $L_{1,4G}$); 72.65 – 72.27 (2 $T_{DBuAEGE}$); 72.00 – 70.19 (2 T_G, 2 D_G, 2 $L_{DBuAEGE}$); 69.92 – 69.27 ($L_{1,3G}$, $L_{DBuAEGE}$, $T_{DBuAEGE}$); 69.11 – 68.30 ($L_{1,4G}$, $T_{DBuAEGE}$); 63.41 – 62.90 (T_G); 61.52 – 60.61 ($L_{1,3G}$); 54.30 – 53.95 (-N-($\underline{C}H_2$-C_6H_5)$_2$); 53.95 – 53.66 (-N-($\underline{C}H_2$-CH_2-CH_3)$_2$); 53.23 – 52.95 (-O-CH_2-$\underline{C}H_2$-NR_2); 29.33 – 28.81 (-N-(CH_2-$\underline{C}H_2$-CH_2-CH_3)$_2$); 20.30 – 19.77 (-N-(CH_2-CH_2-$\underline{C}H_2$-CH_3)$_2$); 14.19 – 13.70 (-N-(CH_2-CH_2-CH_2-$\underline{C}H_3$)$_2$).

In-situ NMR Monitoring of the Copolymerization

The online NMR-monitoring was performed following a literature procedure.[26] 6 mg Bn_2TRIS (0.02 mmol, 1.0 eq.) and 1 mg cesium hydroxide monohydrate (0.3 eq.) were placed in a Schlenk tube and dissolved in methanol. Benzene was added and the mixture was stirred for 30 min to prepare the initiator salt. Afterwards, the tube was evacuated, and the initiator dried overnight. Under inert atmosphere, the initiator salt was dissolved in 0.1 mL DMSO-d_6 and the solution transferred to a

pressure-resistant NMR tube equipped with a Teflon seal. 30 µL glycidol (0.44 mmol, 22 eq.) and 65 µL DBuAEGE (0.29 mmol, 15 eq.) were added and the mixture was diluted with DMSO-d_6 to yield a total volume of 0.5 mL. The NMR tube was sealed and placed in the NMR spectrometer at 60 °C. During the first hour, spectra were recorded with 16 scans at 2-minute intervals, then at 5-minute intervals for 2 hours and at 10-minute intervals for the remainder of the experiment. To complete the reaction, the NMR tube was placed in an oil-bath heated to 60 °C overnight. Afterwards, a final ^{1}H NMR spectrum was recorded, which was used as the end-point equaling full conversion of both monomers.

Results and Discussion

By variation of the comonomer feed, several hyperbranched copolymers based on glycidol and *N,N*-dibutylaminoethylglycidyl ether (DBuAEGE) with different compositions were prepared.

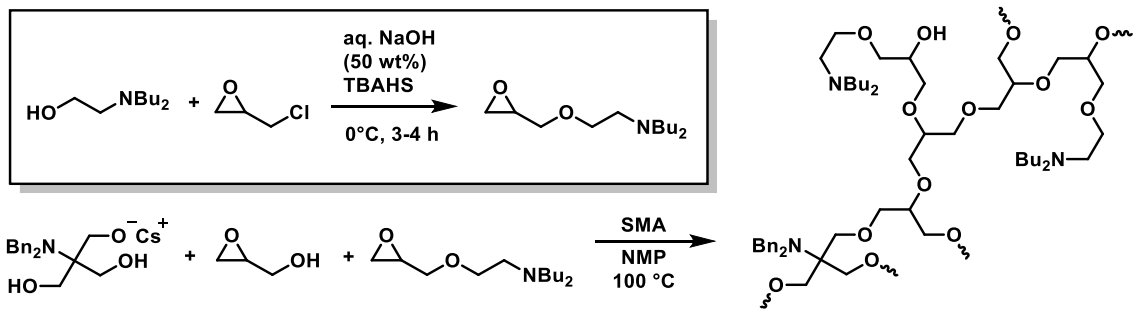

Scheme 2. Schematic synthesis of DBuAEGE and anionic ring-opening copolymerization of glycidol and DBuAEGE *via* SMA.

The monomer DBuAEGE was synthesized from the corresponding alcohol and epichlorohydrin *via* a two-phase reaction in moderate yields. After several distillations, the monomer was received as a colorless liquid, which rapidly turns yellow when in contact with moisture or air. The structure of the compound was confirmed by ^{1}H, ^{13}C and HSQC NMR spectroscopy (see Figure S 1 to Figure S 4) also revealing a sufficient purity for the following polymerization steps.

The polymerization followed a typical protocol for the synthesis of hyperbranched copolymers *via* slow monomer addition.[20] A mixture of both monomers was added to a solution of the partially deprotonated initiator Bn_2TRIS in NMP preheated to 100 °C. After the complete addition, the polymerization was terminated by adding an excess of methanol. Subsequently, the crude reaction mixture was dialyzed in methanol (MWCO = 1000 g mol^{-1}) to yield the polymers as brownish, highly viscous oils. By variation of the comonomer feed, different copolymer compositions were

targeted while maintaining a constant molar mass. Table 1 gives an overview of the analytical data obtained by SEC and ^{1}H NMR spectroscopy for the different *hb*P(G-*co*-DBuAEGE) copolymers.

Table 1. SEC and NMR characterization data of the *hb*P(G-*co*-DBuAEGE) copolymers.

Sample[a)]	**M_n**[b)] **[g mol^{-1}]**	**Đ**	**M_n**[c)] **[g mol^{-1}]**	**X**[c)]	**DB**[d)]	**X**[d)]
*hb*P($G_{0.90}$-*co*-DBuAEGE$_{0.10}$)	800	1.46	2600	0.10	0.42	0.06
*hb*P($G_{0.80}$-*co*-DBuAEGE$_{0.20}$)	900	1.45	2900	0.20	0.41	0.17
*hb*P($G_{0.73}$-*co*-DBuAEGE$_{0.27}$)	900	1.46	2700	0.27	0.47	0.18
*hb*P($G_{0.64}$-*co*-DBuAEGE$_{0.36}$)	1000	1.33	2300	0.36	0.42	0.26

[a)]Terminology: indices denote the copolymer composition determined by ^{1}H NMR spectroscopy, [b)]determined by SEC (DMF, linear PEO standards), [c)]molar masses and DBuAEGE content determined by ^{1}H NMR spectroscopy, [d)]determined by inverse gated ^{13}C NMR spectroscopy.

The SEC traces (Figure 1) of each copolymer show monomodal distributions with residual solvents appearing at higher elution volume. The molar masses determined using linear PEG standards range from 800 to 1000 g mol^{-1} with moderate dispersities between 1.33 and 1.46. As discussed in the literature,[10] molar masses of hyperbranched polymers obtained from SEC using linear standards are typically underestimated due to the compact structure resulting from the highly branched architecture.

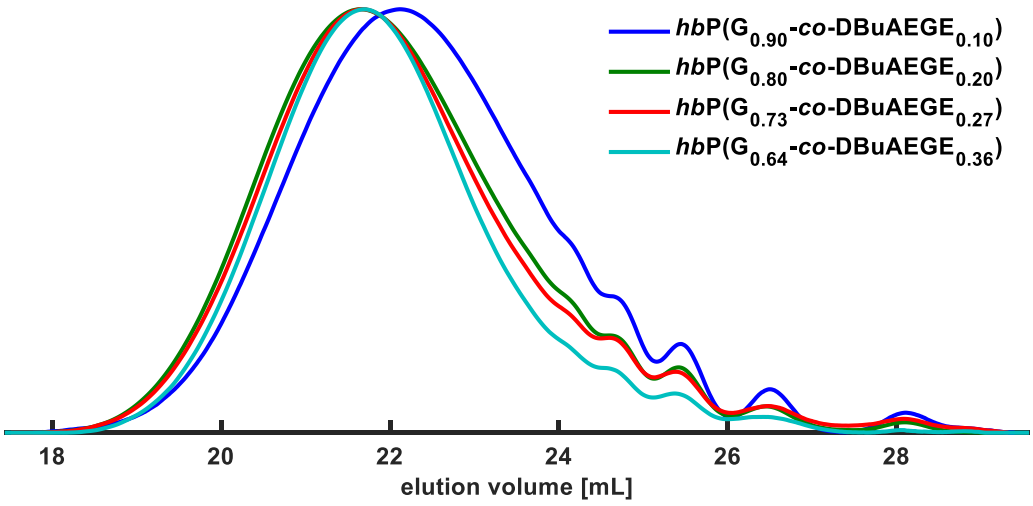

Figure 1. SEC traces of the *hb*P(G-*co*-DBuAEGE) copolymers (DMF, RI detector).

The analysis by ^{1}H NMR spectroscopy, on the other hand offers, valuable insights into the polymer architecture, i.e. copolymer composition as well as absolute values of the molar mass. Figure 2 shows an exemplary ^{1}H NMR spectrum of *hb*P(G$_{0.80}$-*co*-DBuAEGE$_{0.20}$), further spectra are found in the supporting information (Figure S 6 to Figure S 8).

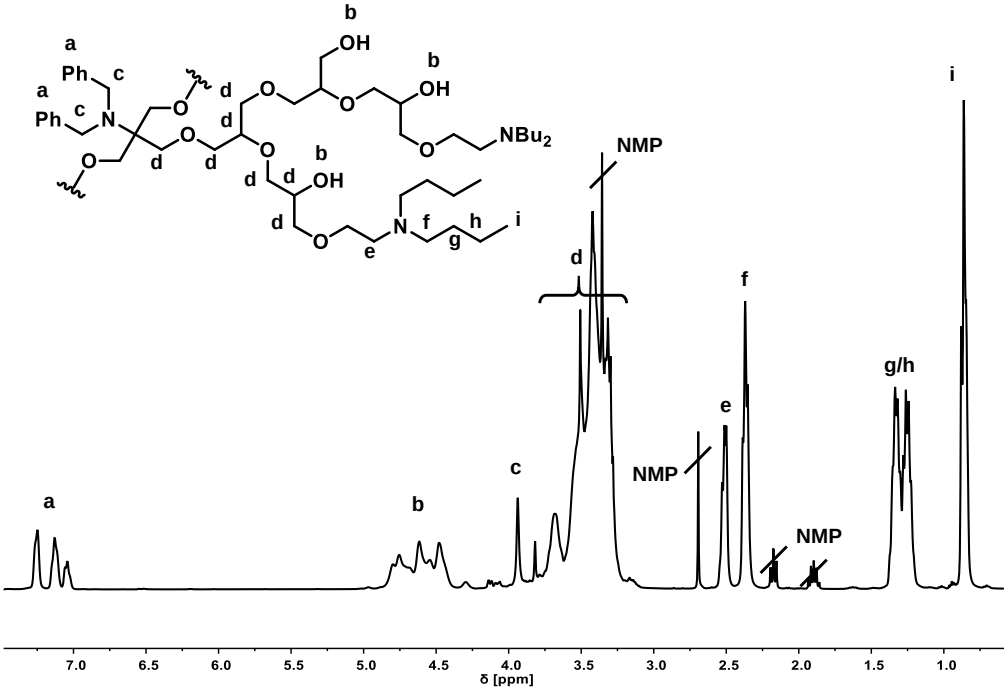

Figure 2. ^{1}H NMR spectrum of *hb*P(G$_{0.80}$-*co*-DBuAEGE$_{0.20}$) (400 MHz, DMSO-d_6).

The signals of the various structural units of the polymer are clearly distinguishable, including the benzyl protecting group a and c of the initiator (7.32 - 6.98 ppm and 3.97 – 3.87 ppm), the hydroxy groups b (4.86 – 4.37 ppm), the polyether backbone d (3.87 – 3.07 ppm) and the signals of the butyl substituents e - i (2.57 – 0.75 ppm), while no signals of side-products aside solvent residue (NMP) are evident. Using the aromatic signals of the initiator as normation, the average molar mass and copolymer composition can be calculated using equation 1 by comparing the average degrees of polymerization of each comonomer. As the incorporation of each glycidol unit increases the overall number of hydroxy groups by one, the intensity of signal b (I_b) can be used to calculate the average degree of polymerization of glycidol ($DP_{n,G}$), whereas any of the signals of the butyl substituents, e.g. signal i (I_i) can be used to calculate $DP_{n,\,DBuAEGE}$ (see equations 1 and 2).

$$DP_{n,\,G}=I_b-3 \qquad (1)$$

$$DP_{n,\,DBuAEGE}=\frac{I_i}{6} \qquad (2)$$

$$X_{DBuAEGE}=\frac{DP_{n,\,DBuAEGE}}{DP_{n,\,DBuAEGE}+DP_{n,\,G}} \qquad (3)$$

$$M_n=M_{Initiator}+\left(DP_{n,\,G}\;M_G\right)+\left(DP_{n,\,DBuAEGE}\;M_{DBuAEGE}\right) \qquad (4)$$

The results of these calculations are presented in Table 1. The copolymer compositions increase from 0.10 to 0.36, whereas the molar masses determined by ^{1}H NMR spectroscopy are similar ranging from 2300 to 2900 g mol^{-1}. With increasing comonomer content a higher deviation from the target values (0.1 to 0.4) is observed. Furthermore, the molar masses determined by ^{1}H NMR spectroscopy assume values lower than targeted. As stated above, the

comonomer DBuAEGE tends to degradate when not stored under inert conditions. Due to the slow monomer addition over an extended period, the monomer mixture might inherently be exposed to air or ambient moisture, leading to side-reactions impeding full conversion of either monomer. By the combination of NMR and SEC, one can conclude, that work-up by dialysis is sufficient to remove said byproducts and to yield well-defined hyperbranched polymers despite not quite mirroring the targeted values.

The highly branched structure of hyperbranched polyglycerol and other HBPs results in peculiar properties in solution or melt separating these architectures from comparable linear polymers. The key parameter to describe the branched structure is the degree of branching (DB). Frey and coworkers modified the definition of DB reported in literature, where D and L represent the amounts of dendritic and linear units typically obtained from ^{13}C NMR spectroscopy:[36,37]

$$DB = \frac{2D}{2D + L} \quad (5)$$

Figure 3 shows a section of the ^{13}C NMR spectrum of *hb*P(G$_{0.80}$-*co*-DBuAEGE$_{0.20}$) representing the polyether region. The full spectra of each copolymer can be found in the supporting information (Figure S 9 to Figure S 12).

By a combination of 2D NMR experiments, the signals of the polyether region in the ^{13}C NMR spectrum can be assigned and utilized to calculate the relative amounts of possible repeating units (T, L and D). Furthermore, the copolymer composition is also obtained from ^{13}C NMR spectroscopy:

$$X_{DBuAEGE} = \frac{T_{DBuAEGE} + L_{DBuAEGE}}{T_G + L_G + D_G + T_{DBuAEGE} + L_{DBuAEGE}} \quad (6)$$

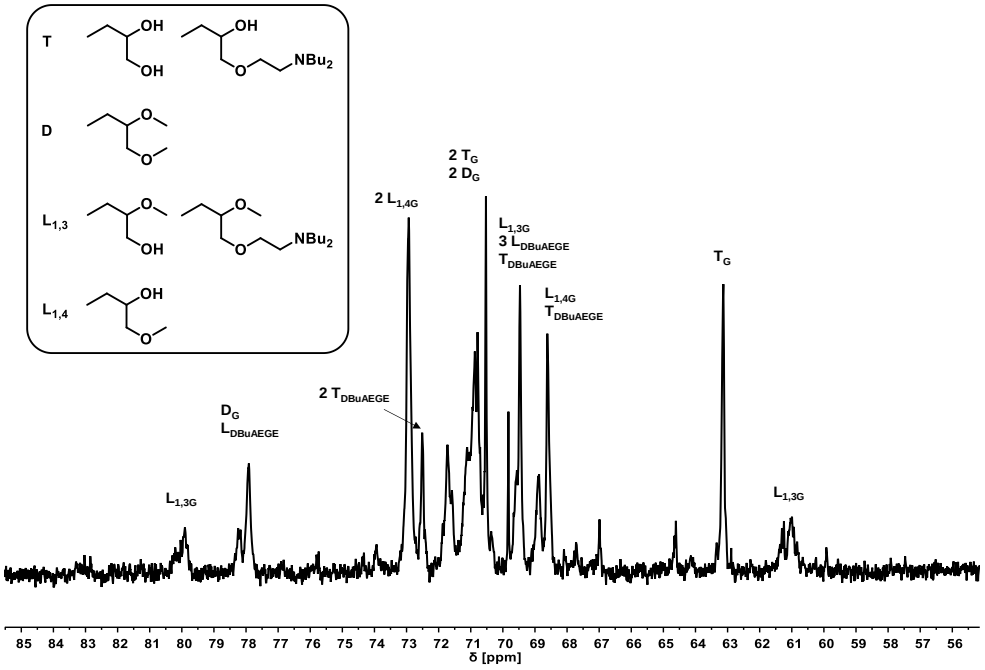

Figure 3. Polyether region in the ^{13}C NMR spectrum of *hb*P($G_{0.80}$-*co*-DBuAEGE$_{0.20}$) (400 MHz, DMSO-d_6).

The results of the calculations are summarized in Table 1. The degrees of branching range from 0.41 to 0.47 regardless of the copolymer composition or the molar mass. However, due to pronounced overlap of the signals essential for the calculation of either DB or $X_{DBuAEGE}$, the results presented above tend to underestimate the values for X obtained from ^1H NMR spectroscopy and the typical range of DBs obtained by the copolymerization of an AB_2 with an AB monomer at full conversion and in the absence of side-reactions (cf. supporting information, Table S 1 and Figure S 16).[38,39] Nevertheless, the branched structure is confirmed by the occurrence of the various repeating units.

The investigation of the copolymerization kinetics by *in-situ* ^1H NMR monitoring provides further structural insights. By performing the batch copolymerization of glycidol and DBuAEGE inside an NMR tube, the single monomer conversion can be observed in real-time as a reduction of the intensity of the signal corresponding

to the respective comonomer. Figure 4 (left) shows the individual monomer conversions plotted against the total conversion. The conversion of glycidol is significantly faster than DBuAEGE, which is mainly incorporated only after most of glycidol has reacted. The corresponding reactivity ratios of each monomer were calculated following the Fineman-Ross formalism (see the supporting information for further detail): r_G = 4.80 and $r_{DBuAEGE}$ = 0.17.[40]

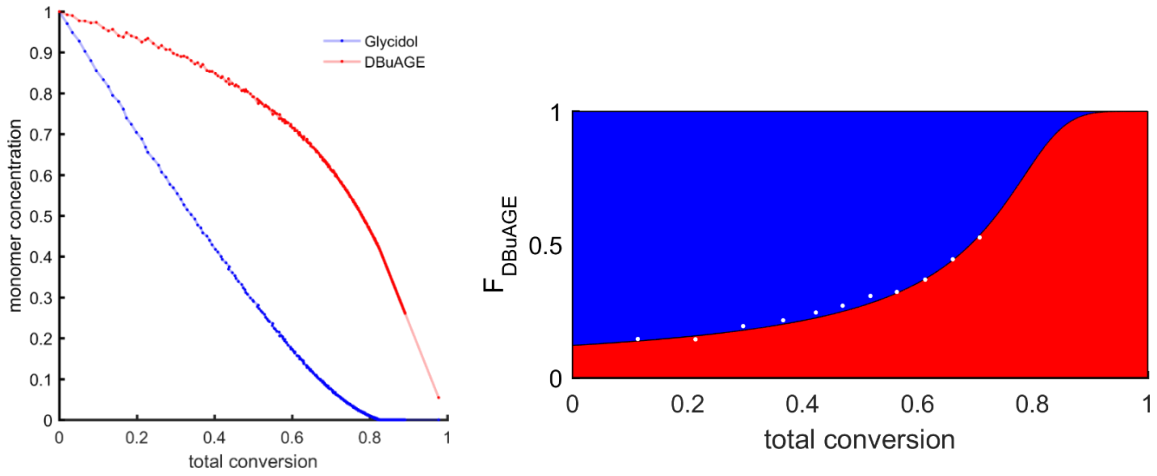

Figure 4. Single Monomer concentration vs total conversion during batch copolymerization of glycidol and DBuAEGE (left); visualization of the proposed gradient structure (right).

Similar reactivity ratios have been found for the batch copolymerization of glycidol and propylene oxide (r_G = 4.70 and r_{PO} = 0.17), forming a pronounced gradient structure with a glycidol-rich center and a comonomer-rich periphery.[26] Despite forming a gradient copolymer during the batch polymerization, in a semi-batch setup following the SMA strategy, assuming the monomer addition is sufficiently slow, little to no accumulation of unreacted comonomer is expected. A similar observation was made for the copolymerization of glycidol and MTEGE (r_G = 3.70 and r_{MTEGE} = 0.27) where an addition rate of 0.2 mL h^{-1} resulted in a random distribution of the comonomer throughout the hyperbranched polymer.[20] The

random copolymer structure is corroborated by the thermal analysis of the polymers *via* differential scanning calorimetry (DSC). For each of the *hb*P(G-*co*-DBuAEGE) copolymers only a single glass transition temperature (T_g) is observed depending on the amount of copolymer: With increasing copolymer content, the T_g decreases linearly from -35 to -48 °C. In fact, the different T_gs coincide with a linear dependence between the glass transition temperatures of the individual homopolymers *hb*PG[12] and linear P(DBuAEGE),[8] strongly supporting a random distribution of the DBuAEGE and glycidol monomers.

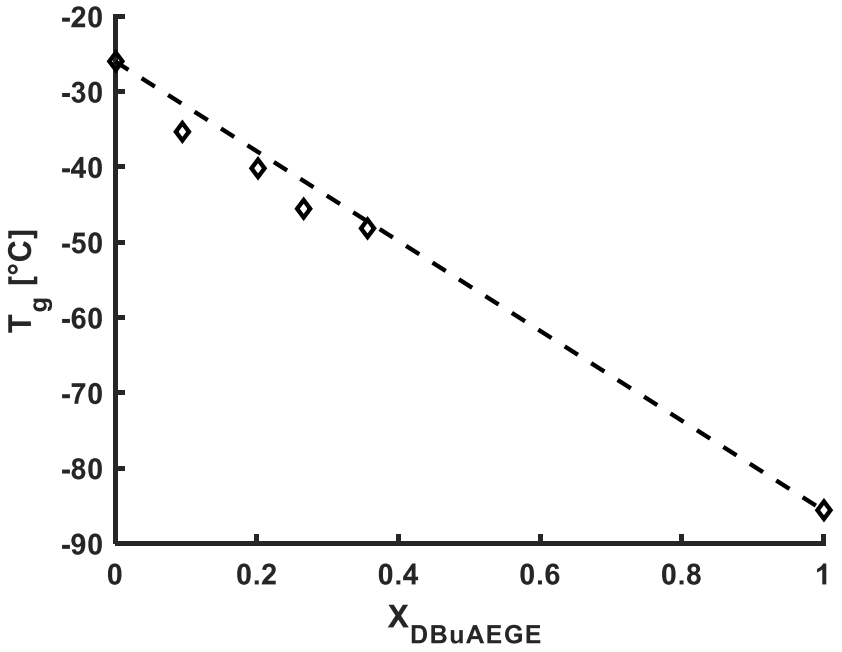

Figure 5. Glass transition temperatures T_g vs. comonomer content $X_{DBuAEGE}$. A linear decrease of T_gs with increasing $X_{DBuAEGE}$ is observed.

By the incorporation of the apolar, basic *N,N*-dibutylamino moieties throughout the hyperbranched polyether polyol properties, which are uncommon for hyperbranched polyglycerols, are introduced. Depending on the composition, the copolymers show varying degrees of thermoresponsive and pH responsive behavior. As an example, Figure 6 shows several turbidity curves of buffered

aqueous solutions (c = 1 mg mL^{-1}) of *hb*P($G_{0.80}$-co-DBuAEG$E_{0.20}$) recorded at pH 7, 8 and 9. With increasing pH value, the water-solubility decreases upon heating as the solution turns turbid at lower temperatures. For pH values below 7, the polymer is fully water-soluble as a result from protonation of the tertiary amine.

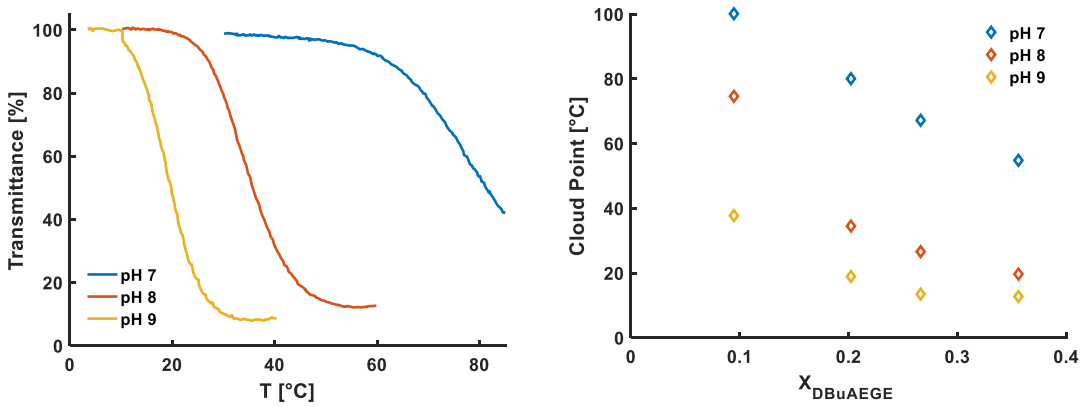

Figure 6. Turbidimetry measurement of buffered aqueous solutions of *hb*P($G_{0.80}$-*co*-DBuAEG$E_{0.20}$) at different pH values (1 mg mL^{-1}) (left) and dependence of the cloud points on the copolymer composition different pH values (right).

The turbidimetric measurements were repeated for each of the *hb*P(G-*co*-DBuAEGE) copolymers and are depicted in the supporting information (cf. Figure S 18 to Figure S 20). For each polymer solution at different pH values the cloud points were determined as the temperature at the inflection point of the turbidity curve (Table 2).

With increasing copolymer content, the fraction of apolar moieties increases leading to poorer water-solubility. Protonation of the amine groups on the other hand facilitates solubility in water by the formation of highly polar ammonium salts. Thus, temperatures, at which the cloud points are observed, decrease with increasing copolymer content and increasing pH value (see Figure 6, right).

Table 2. Results of the turbidity measurements for each polymer at different pH values.

Sample	$X_{DBuAEGE}$	Cloud Point [°C]			
		pH 7	pH 8	pH 9	pH 10
*hb*P($G_{0.90}$-*co*-DBuAEGE$_{0.10}$)	0.10	>100	75[a)]	38	24
*hb*P($G_{0.80}$-*co*-DBuAEGE$_{0.20}$)	0.20	80[a)]	35	19	-
*hb*P($G_{0.73}$-*co*-DBuAEGE$_{0.27}$)	0.27	67	27	14	-
*hb*P($G_{0.64}$-*co*-DBuAEGE$_{0.36}$)	0.36	55	20	13	-

[a)]Estimation based on extrapolated inflection point.

Due to their good biocompatibility and water-solubility, hyperbranched polyglycerols and derivatives thereof find wide-spread use for various applications.[11] On the other hand, common tertiary amines, e.g. tributylamine, are oftentimes harmful or even toxic.[29] By the incorporation of the amine moieties into a hyperbranched polyether polyol structure, an increased biocompatibility is expected due to pronounced hydration and subsequent shielding.[31,41,42] Three *hb*(P-*co*-DBuAEGE) copolymers with comonomer contents between 0.06 and 0.10 were synthesized to investigate the biocompatibility (see supporting information). The polymers exhibit complete solubility in water under physiological conditions, i.e. the onset of turbidity at pH = 7.42 occurs at temperatures higher than 37.5 °C (cf. Figure S 25). To observe potential cytotoxic effects of *hb*P($G_{0.94}$-*co*-DBuAEGE$_{0.06}$), *hb*P($G_{0.92}$-*co*-DBuAEGE$_{0.08}$) and *hb*P($G_{0.90}$-*co*-DBuAEGE$_{0.10}$) on immune cells, their metabolic activity was assessed after incubation with varying doses of the copolymers. To this end, spleen cells obtained from C57BL/6 mice were seeded into wells of 96 well cluster plates (10^6 cells/100 µL/well). The

polymers were applied to triplicates of seeded spleen cells at different concentrations as indicated. Untreated samples and samples incubated with DMSO at a high dose (10%) inducing cytotoxicity served as controls. On the next day, 20 µL of water-soluble MTT (3-[4,5-Dimethylthiazol-2-yl]-2,5-diphenyltetrazoliumbromid) reagent were applied (Promega, Madison, WI). Mitochondrial dehydrogenase activity reduces MTT to a purple water-insoluble formazan product. The reaction was terminated after 3 – 5 h by applying Stop/Lysis buffer (100 µL, Promega). Absorbance (570 nm) was assessed by employing a Spark multimode microplate reader (TECAN, Männedorf, Switzerland).

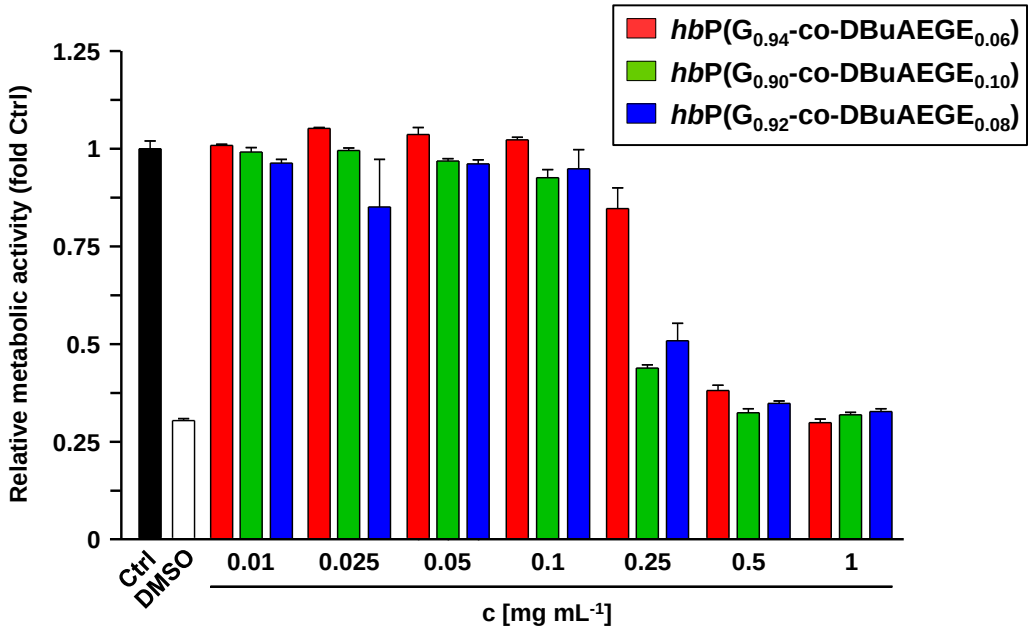

Figure 7. Metabolic activity of murine spleen cells incubated overnight with *hb*P($G_{0.94}$-*co*-DBuAEGE$_{0.06}$), *hb*P($G_{0.92}$-*co*-DBuAEGE$_{0.08}$) and *hb*P($G_{0.90}$-*co*-DBuAEGE$_{0.10}$) at different concentrations. Data denote the results of one experiment (mean±SEM of triplicates) representative for 3 independent experiments.

As indicated in Figure 7, low concentrations of the hyperbranched copolymers do not show any effect on the metabolic activity of splenic immune cells. At higher

concentrations (> 0.1 mg mL^{-1}), a considerable decrease in their metabolic activity was observed, which was less severe for *hb*P($G_{0.94}$-*co*-$DBuAEGE_{0.06}$) exhibiting the lowest DBuAEGE content. Hence, hyperbranched copolymers based on glycidol and DBuAEGE in this range of compositions are biocompatible over a wide range of concentrations, and therefore constitute suitable candidates for various applications.

By the combination of the analytical data presented above, the hyperbranched polyether polyol structure and the responsivity towards different stimuli, namely pH and temperature, have been confirmed. Including the results of the biocompatibility testing, these materials show several advantages over tributylamine (cf. Scheme 1),[29] offering the potential to replace this compound for various applications, e.g. as catalysts for the preparation of polyurethane foams. In this case, the polyether polyol backbone even enables incorporation of the catalyst into the PU material.[30,43–46] By employing such auto-catalytic polyol components, no migratory amine catalyst emission is expected resulting in a reduction of health-hazards, unpleasant odors or degradation of the material, since no volatile tertiary amines are used as catalysts.[30]

Conclusion

We have reported the synthesis of water-soluble, biocompatible organobases by the anionic ring-opening copolymerization of glycidol and the *N,N*-dibutylamino-functional glycidyl ether DBuAEGE (AB_2 + AB) *via* slow monomer addition. By variation of the comonomer feed, several copolymers with comonomer contents ranging from 0.10 to 0.36, as confirmed by ^{1}H NMR spectroscopy, were prepared,

while maintaining similar molar masses (2300 – 2900 g mol^{-1}). Analysis by SEC, however, yielded molar masses between 800 and 1000 g mol^{-1} with narrow dispersities (M_w / M_n = 1.33 – 1.46). By a combination of different NMR experiments, including real time kinetics by online ^{1}H NMR monitoring, an in-depth structure elucidation was performed. The reactivity ratios calculated following the Fineman-Ross methodology would lead to a pronounced gradient structure in batch similar to hyperbranched poly(propylene oxide), whereas following the SMA approach leads to a random distribution of the comonomer throughout the hyperbranched polyether polyol.

The incorporation of the hydrophobic dibutylamino moieties into the highly hydrophilic polyether polyol backbones introduces thermo- and pH-responsive behavior. By variation of the comonomer content and the pH value between 7 and 10 of the aqueous media, the water-solubility can be tailored precisely with cloud points ranging from 13 to 80 °C, while also finding full solubility or insolubility. Furthermore, copolymers in a range of compositions, that enable water-solubility under physiological conditions, exhibit enhanced biocompatibility in comparison to other tertiary amines, e.g. tributylamine.

Acknowledgment

T. K. is grateful for financial support by a fellowship from the “Fonds der Chemischen Industrie (FCI)”. Furthermore, the authors thank Monika Schmelzer and Ulrike Kemmer-Jonas for technical assistance.

References

(1) Dingels, C.; Schömer, M.; Frey, H. Die vielen Gesichter des Poly(ethylenglykol)s. *Chem. Unserer Zeit* **2011**, *45*, 338–349.

(2) Wilms, V. S.; Frey, H. Aminofunctional polyethers: smart materials for applications in solution and on surfaces. *Polym. Int.* **2013**, *62*, 849–859.

(3) Herzberger, J.; Niederer, K.; Pohlit, H.; Seiwert, J.; Worm, M.; Wurm, F. R.; Frey, H. Polymerization of Ethylene Oxide, Propylene Oxide, and Other Alkylene Oxides: Synthesis, Novel Polymer Architectures, and Bioconjugation. *Chem. Rev.* **2016**, *116*, 2170–2243.

(4) Reuss, V. S.; Werre, M.; Frey, H. Thermoresponsive copolymers of ethylene oxide and N,N-diethyl glycidyl amine: polyether polyelectrolytes and PEGylated gold nanoparticle formation. *Macromol. Rapid Commun.* **2012**, *33*, 1556–1561.

(5) Kurzbach, D.; Wilms, V. S.; Frey, H.; Hinderberger, D. Impact of Amino-Functionalization on the Response of Poly(ethylene glycol) (PEG) to External Stimuli. *ACS Macro Lett.* **2013**, *2*, 128–131.

(6) Herzberger, J.; Kurzbach, D.; Werre, M.; Fischer, K.; Hinderberger, D.; Frey, H. Stimuli-Responsive Tertiary Amine Functional PEGs Based on N , N -Dialkylglycidylamines. *Macromolecules* **2014**, *47*, 7679–7690.

(7) Lee, A.; Lundberg, P.; Klinger, D.; Lee, B. F.; Hawker, C. J.; Lynd, N. A. Physiologically relevant, pH-responsive PEG-based block and statistical copolymers with N,N-diisopropylamine units. *Polym. Chem.* **2013**, *4*, 5735–5742.

(8) Ziegler, A.; Weißenfels, M.; Herzberger, J.; Fischer, K.; Frey, H. One-Step Synthesis of Amino-Functional Polyether. *unpublished results* **2018**.

(9) Yan, D.; Gao, C.; Frey, H. *Hyperbranched polymers: Synthesis, properties, and applications*; Wiley series on polymer engineering and technology; Wiley: Hoboken, N.J, 2011.

(10) Voit, B. I.; Lederer, A. Hyperbranched and highly branched polymer architectures--synthetic strategies and major characterization aspects. *Chem. Rev.* **2009**, *109*, 5924–5973.

(11) Schömer, M.; Schüll, C.; Frey, H. Hyperbranched aliphatic polyether polyols. *J. Polym. Sci. A Polym. Chem.* **2013**, *51*, 995–1019.

(12) Sunder, A.; Hanselmann, R.; Frey, H.; Mülhaupt, R. Controlled Synthesis of Hyperbranched Polyglycerols by Ring-Opening Multibranching Polymerization. *Macromolecules* **1999**, *32*, 4240–4246.

(13) Kautz, H.; Sunder, A.; Frey, H. Control of the molecular weight of hyperbranched polyglycerols. *Macromol. Symp.* **2001**, *163*, 67–74.

(14) Kainthan, R. K.; Muliawan, E. B.; Hatzikiriakos, S. G.; Brooks, D. E. Synthesis, Characterization, and Viscoelastic Properties of High Molecular Weight Hyperbranched Polyglycerols. *Macromolecules* **2006**, *39*, 7708–7717.

(15) ul-haq, M. I.; Shenoi, R. A.; Brooks, D. E.; Kizhakkedathu, J. N. Solvent-assisted anionic ring opening polymerization of glycidol: Toward medium and high molecular weight hyperbranched polyglycerols. *J. Polym. Sci. A Polym. Chem.* **2013**, *51*, 2614–2621.

(16) Moore, E.; Zill, A. T.; Anderson, C. A.; Jochem, A. R.; Zimmerman, S. C.; Bonder, C. S.; Kraus, T.; Thissen, H.; Voelcker, N. H. Synthesis and Conjugation of Alkyne-Functional Hyperbranched Polyglycerols. *Macromol. Chem. Phys.* **2016**, *217*, 2252–2261.

(17) Schüll, C.; Gieshoff, T.; Frey, H. One-step synthesis of multi-alkyne functional hyperbranched polyglycerols by copolymerization of glycidyl propargyl ether and glycidol. *Polym. Chem.* **2013**, *4*, 4730.

(18) Alkan, A.; Klein, R.; Shylin, S. I.; Kemmer-Jonas, U.; Frey, H.; Wurm, F. R. Water-soluble and redox-responsive hyperbranched polyether copolymers based on ferrocenyl glycidyl ether. *Polym. Chem.* **2015**, *6*, 7112–7118.

(19) Niederer, K.; Schüll, C.; Leibig, D.; Johann, T.; Frey, H. Catechol Acetonide Glycidyl Ether (CAGE): A Functional Epoxide Monomer for Linear and Hyperbranched Multi-Catechol Functional Polyether Architectures. *Macromolecules* **2016**, *49*, 1655–1665.

(20) Seiwert, J.; Herzberger, J.; Leibig, D.; Frey, H. Thioether-Bearing Hyperbranched Polyether Polyols with Methionine-Like Side-Chains: A Versatile Platform for Orthogonal Functionalization. *Macromol. Rapid Commun.* **2017**, *38*.

(21) Schubert, C.; Schömer, M.; Steube, M.; Decker, S.; Friedrich, C.; Frey, H. Systematic Variation of the Degree of Branching (DB) of Polyglycerol via Oxyanionic Copolymerization of Glycidol with a Protected Glycidyl Ether and Its Impact on Rheological Properties. *Macromol. Chem. Phys.* **2018**, *219*, 1700376.

(22) Sunder, A.; Türk, H.; Haag, R.; Frey, H. Copolymers of Glycidol and Glycidyl Ethers: Design of Branched Polyether Polyols by Combination of Latent Cyclic AB 2 and ABR Monomers. *Macromolecules* **2000**, *33*, 7682–7692.

(23) Wilms, D.; Schömer, M.; Wurm, F.; Hermanns, M. I.; Kirkpatrick, C. J.; Frey, H. Hyperbranched PEG by random copolymerization of ethylene oxide and glycidol. *Macromol. Rapid Commun.* **2010**, *31*, 1811–1815.

(24) Schömer, M.; Seiwert, J.; Frey, H. Hyperbranched Poly(propylene oxide): A Multifunctional Backbone-Thermoresponsive Polyether Polyol Copolymer. *ACS Macro Lett.* **2012**, *1*, 888–891.

(25) Seiwert, J.; Leibig, D.; Kemmer-Jonas, U.; Bauer, M.; Perevyazko, I.; Preis, J.; Frey, H. Hyperbranched Polyols via Copolymerization of 1,2-Butylene Oxide and Glycidol: Comparison of Batch Synthesis and Slow Monomer Addition. *Macromolecules* **2016**, *49*, 38–47.

(26) Leibig, D.; Seiwert, J.; Liermann, J. C.; Frey, H. Copolymerization Kinetics of Glycidol and Ethylene Oxide, Propylene Oxide, and 1,2-Butylene Oxide: From Hyperbranched to Multiarm Star Topology. *Macromolecules* **2016**, *49*, 7767–7776.

(27) Parzuchowski, P. G.; Stefańska, M.; Świderska, A.; Roguszewska, M.; Zybert, M. Hyperbranched polyglycerols containing amine groups — Synthesis, characterization and carbon dioxide capture. *Journal of CO2 Utilization* **2018**, *27*, 145–160.

(28) Song, S.; Lee, J.; Kweon, S.; Song, J.; Kim, K.; Kim, B.-S. Hyperbranched Copolymers Based on Glycidol and Amino Glycidyl Ether: Highly Biocompatible Polyamines Sheathed in Polyglycerols. *Biomacromolecules* **2016**, *17*, 3632–3639.

(29) GESTIS Substance database. Tributylamine. http://gestis.itrust.de/nxt/gateway.dll/gestis_de/029500.xml?f=templates$fn=default.htm$3.0 (accessed March 19, 2020).

(30) Ionescu, M. *Chemistry and technology of polyols for polyurethanes*; Rapra Technology Ltd: Shawbury, U.K, 2005.

(31) Perevyazko, I.; Kaiser, T.; Frey, H. Hard Sphere-Behavior of Hyperbranched Polyglycerol in Aqueous Solution: Absolute Molecular Weights, Molecular Hydrodynamics and Light Scattering. *to be submitted.*

(32) Kainthan, R. K.; Janzen, J.; Levin, E.; Devine, D. V.; Brooks, D. E. Biocompatibility testing of branched and linear polyglycidol. *Biomacromolecules* **2006**, *7*, 703–709.

(33) Kainthan, R. K.; Hester, S. R.; Levin, E.; Devine, D. V.; Brooks, D. E. In vitro biological evaluation of high molecular weight hyperbranched polyglycerols. *Biomaterials* **2007**, *28*, 4581–4590.

(34) Kainthan, R. K.; Brooks, D. E. In vivo biological evaluation of high molecular weight hyperbranched polyglycerols. *Biomaterials* **2007**, *28*, 4779–4787.

(35) Schüll, C.; Nuhn, L.; Mangold, C.; Christ, E.; Zentel, R.; Frey, H. Linear-Hyperbranched Graft-Copolymers via Grafting-to Strategy Based on Hyperbranched Dendron Analogues and Reactive Ester Polymers. *Macromolecules* **2012**, *45*, 5901–5910.

(36) Hölter, D.; Burgath, A.; Frey, H. Degree of branching in hyperbranched polymers. *Acta Polym.* **1997**, *48*, 30–35.

(37) Hölter, D.; Frey, H. Degree of branching in hyperbranched polymers. 2. Enhancement of the db: Scope and limitations. *Acta Polym.* **1997**, *48*, 298–309.

(38) Frey, H.; Hölter, D. Degree of branching in hyperbranched polymers. 3 Copolymerization of ABm-monomers with AB and ABn-monomers. *Acta Polym.* **1999**, *50*, 67–76.

(39) Sunder, A.; Türk, H.; Haag, R.; Frey, H. Copolymers of Glycidol and Glycidyl Ethers: Design of Branched Polyether Polyols by Combination of Latent Cyclic AB 2 and ABR Monomers. *Macromolecules* **2000**, *33*, 7682–7692.

(40) Fineman, M.; Ross, S. D. Linear method for determining monomer reactivity ratios in copolymerization. *J. Polym. Sci. A Polym. Chem.* **1950**, *5*, 259–262.

(41) Abbina, S.; Vappala, S.; Kumar, P.; Siren, E. M. J.; La, C. C.; Abbasi, U.; Brooks, D. E.; Kizhakkedathu, J. N. Hyperbranched polyglycerols: recent advances in synthesis, biocompatibility and biomedical applications. *J. Mater. Chem. B* **2017**, *5*, 9249–9277.

(42) Calderón, M.; Quadir, M. A.; Sharma, S. K.; Haag, R. Dendritic polyglycerols for biomedical applications. *Adv. Mater.* **2010**, *22*, 190–218.

(43) Wegener, G.; Brandt, M.; Duda, L.; Hofmann, J.; Klesczewski, B.; Koch, D.; Kumpf, R.-J.; Orzesek, H.; Pirkl, H.-G.; Six, C.*; et al.* Trends in industrial catalysis in the polyurethane industry. *Applied Catalysis A: General* **2001**, *221*, 303–335.

(44) Silva, A. L.; Bordado, J. C. Recent Developments in Polyurethane Catalysis: Catalytic Mechanisms Review. *Catalysis Reviews* **2004**, *46*, 31–51.

(45) Zia, K. M.; Bhatti, H. N.; Ahmad Bhatti, I. Methods for polyurethane and polyurethane composites, recycling and recovery: A review. *React. Funct. Polym.* **2007**, *67*, 675–692.

(46) Akindoyo, J. O.; Beg, M. D. H.; Ghazali, S.; Islam, M. R.; Jeyaratnam, N.; Yuvaraj, A. R. Polyurethane types, synthesis and applications – a review. *RSC Adv.* **2016**, *6*, 114453–114482.

Supporting Information

Supplemental NMR Analytical Data

DBuAEGE

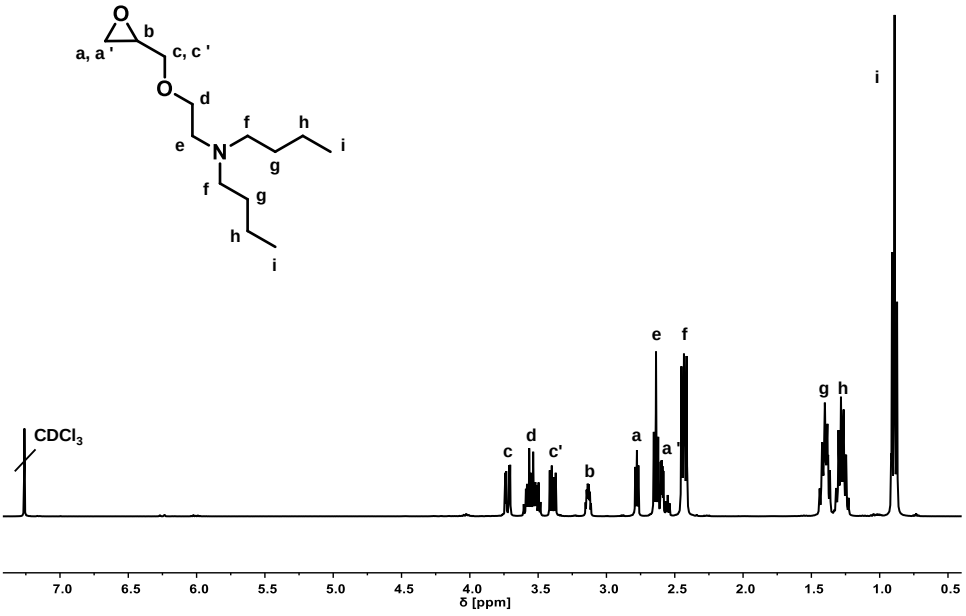

Figure S 1. ^{1}H NMR spectrum of DBuAEGE (400 MHz, $CDCl_3$).

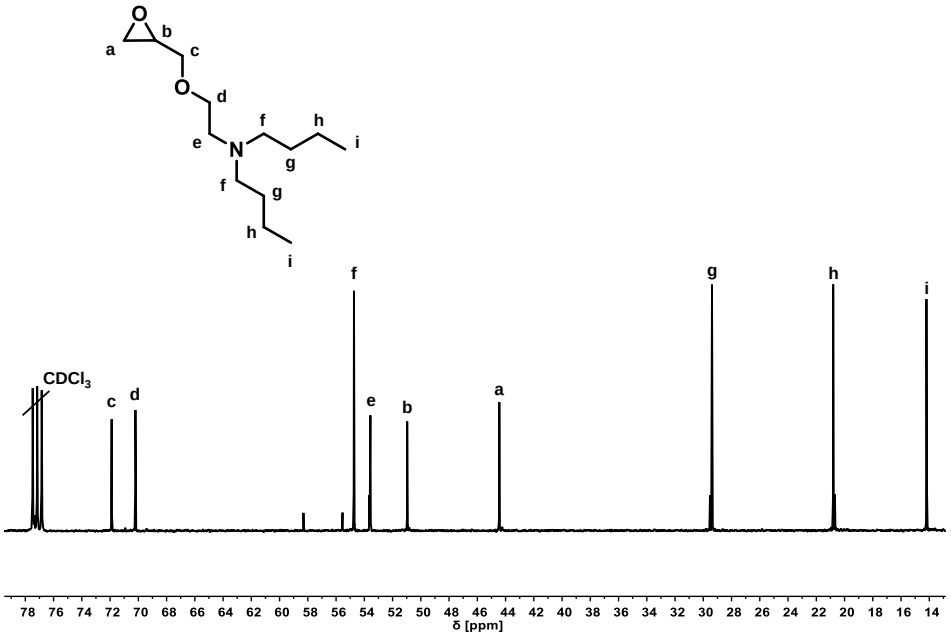

Figure S 2. ^{13}C NMR spectrum of DBuAEGE (100 MHz, $CDCl_3$).

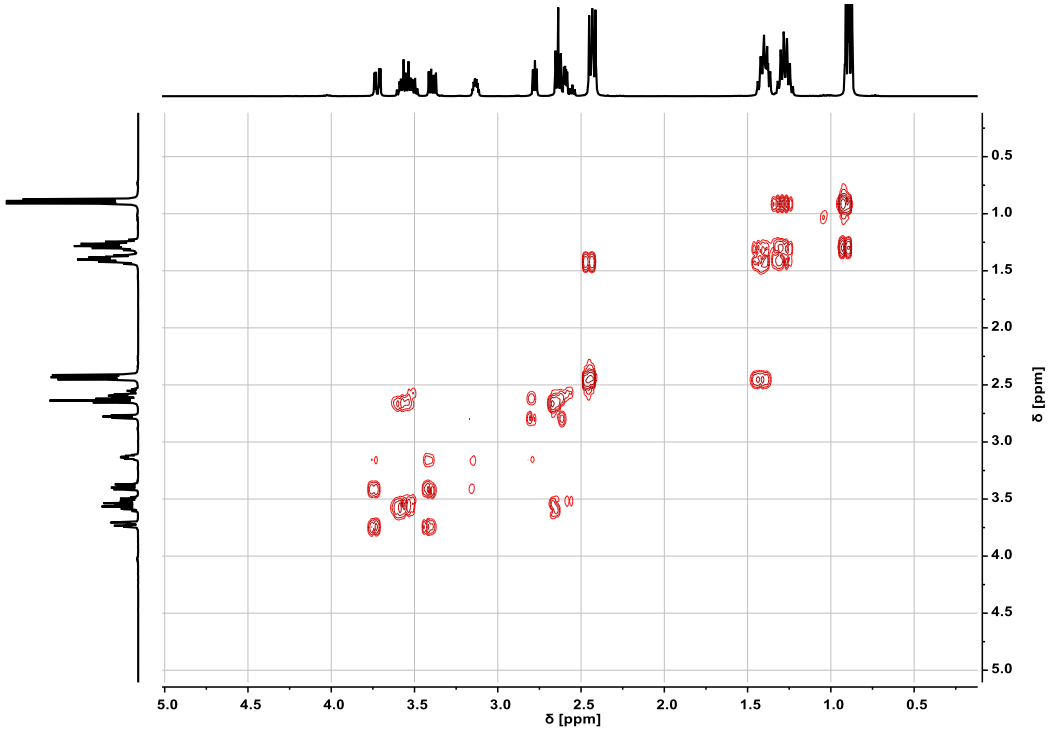

Figure S 3. ^{1}H-^{1}H COSY NMR spectrum of DBuAEGE (400/400MHz, $CDCl_3$).

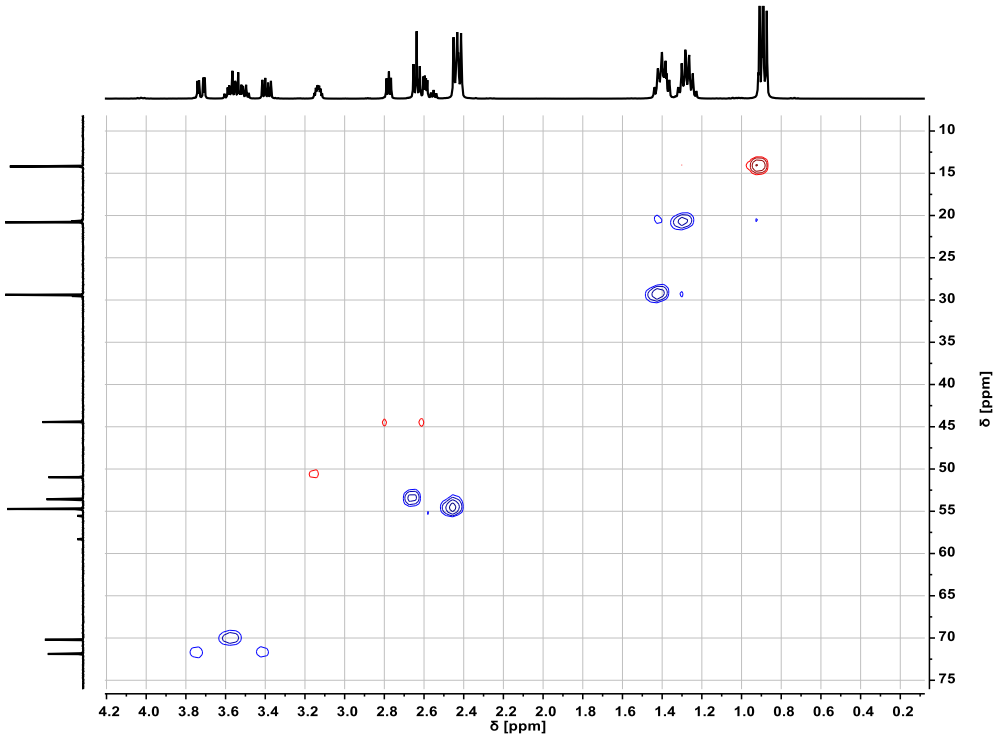

Figure S 4. ^{1}H-^{13}C HSQC NMR spectrum of DBuAEGE (400/100MHz, $CDCl_3$). ^{1}H and ^{13}C NMR spectra can be found on the horizontal and vertical axis, respectively. Phase correlation is given by correlation of cross peaks (red: methyl, methine, Blue: methylene).

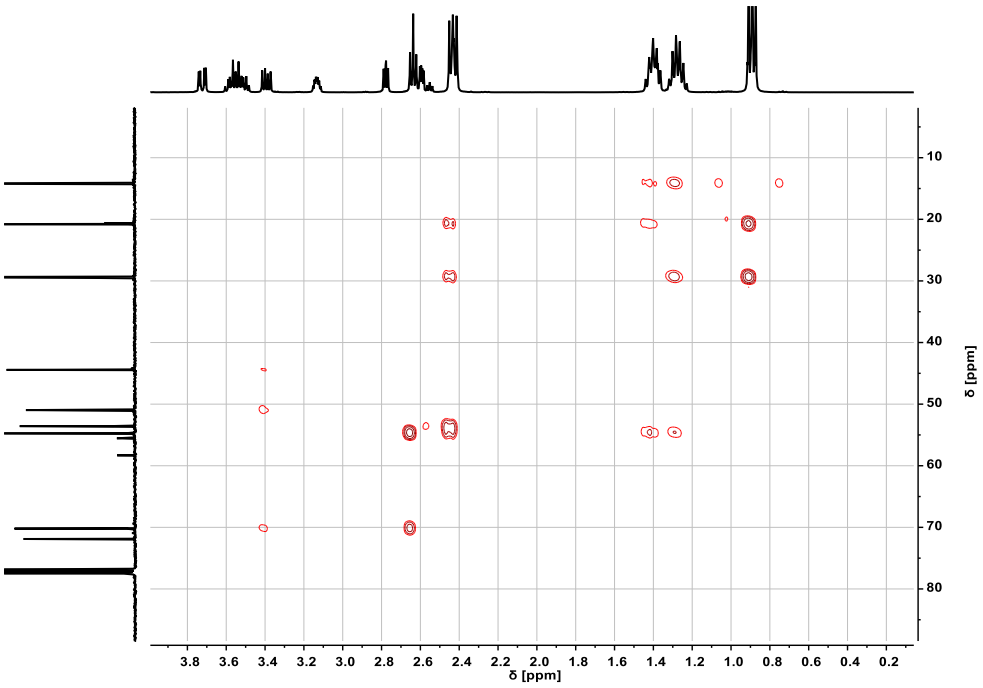

Figure S 5. ^{1}H-^{13}C HMBC NMR spectrum of *hb*P(G$_{0.80}$-*co*-DBuAEGE$_{0.20}$) (400/100MHz, DMSO-d_6). ^{1}H and ^{13}C NMR spectra can be found on the horizontal and vertical axis, respectively.

*hb*P(G-*co*-DBuAEGE)

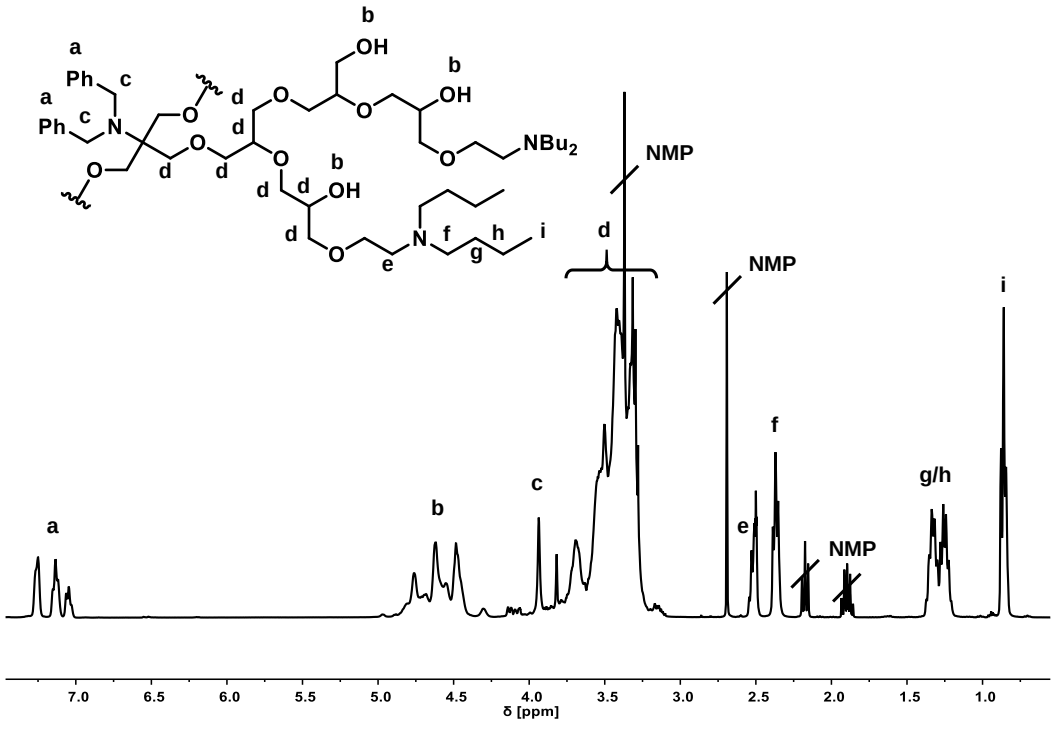

Figure S 6. ^{1}H NMR spectrum of *hb*P(G$_{0.90}$-*co*-DBuAEGE$_{0.10}$) (400 MHz, DMSO-d_6).

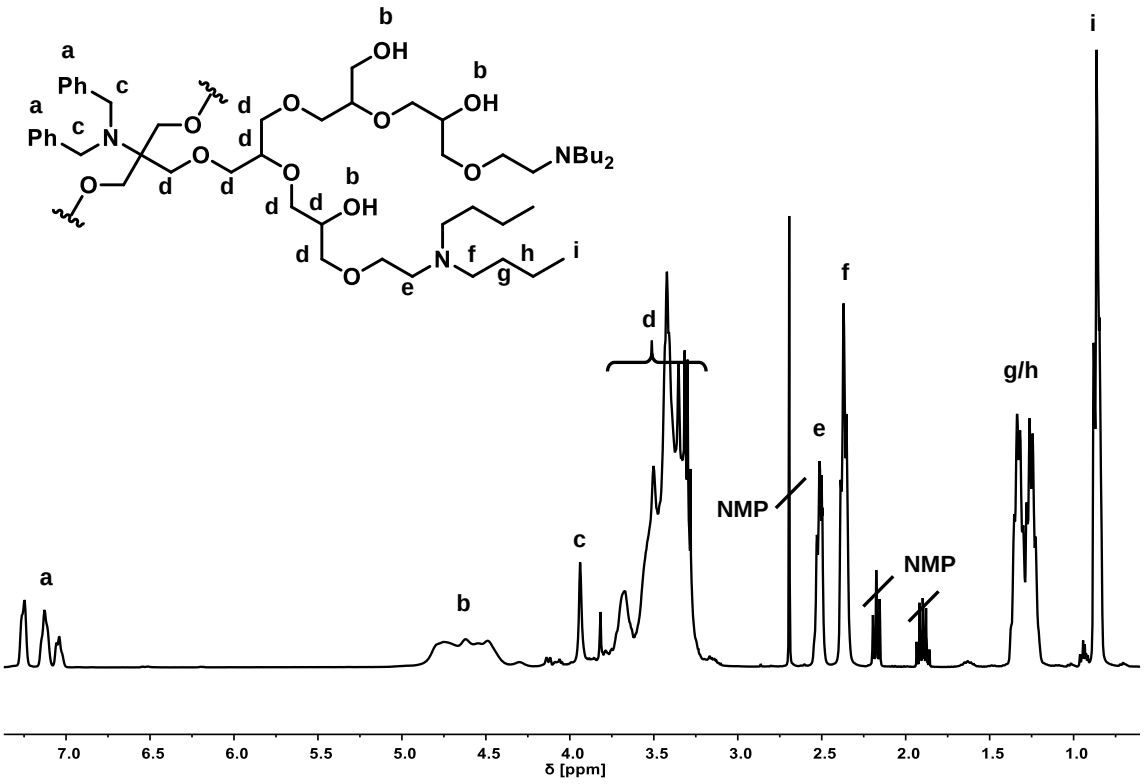

Figure S 7. ^{1}H NMR spectrum of *hb*P($G_{0.73}$-*co*-DBuAEGE$_{0.27}$) (400 MHz, DMSO-d_6).

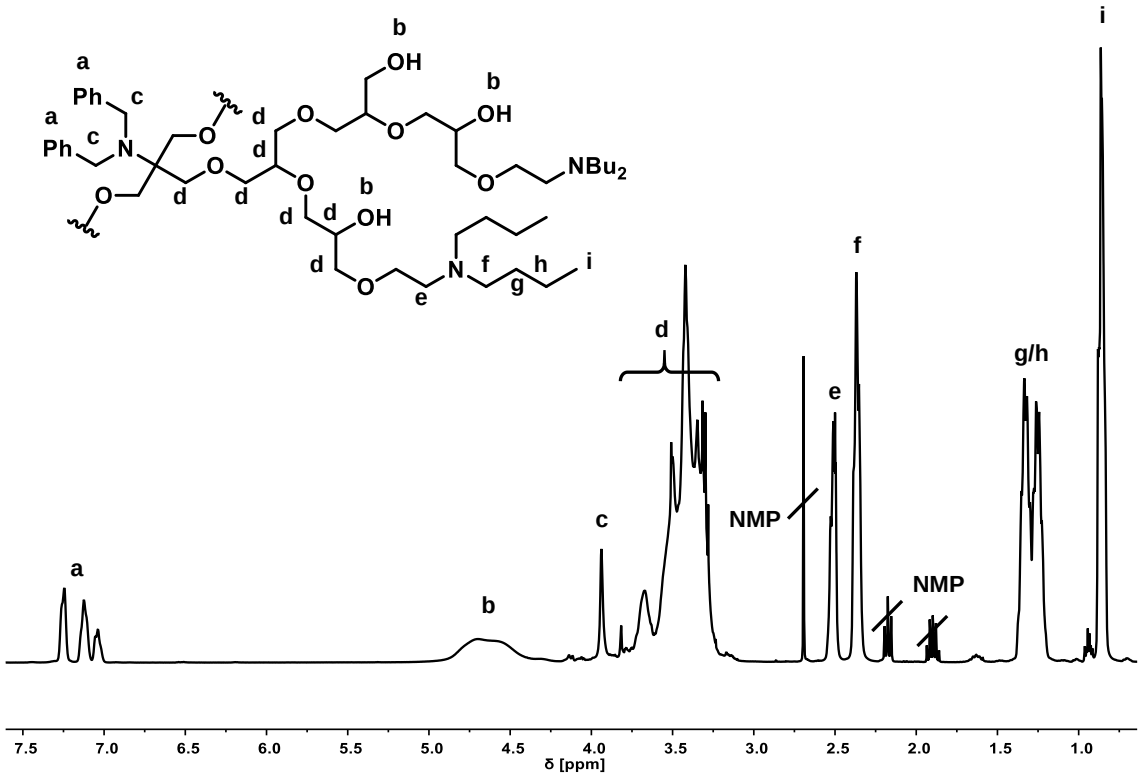

Figure S 8. ^{1}H NMR spectrum of *hb*P($G_{0.64}$-*co*-DBuAEGE$_{0.36}$) (100 MHz, DMSO-d_6).

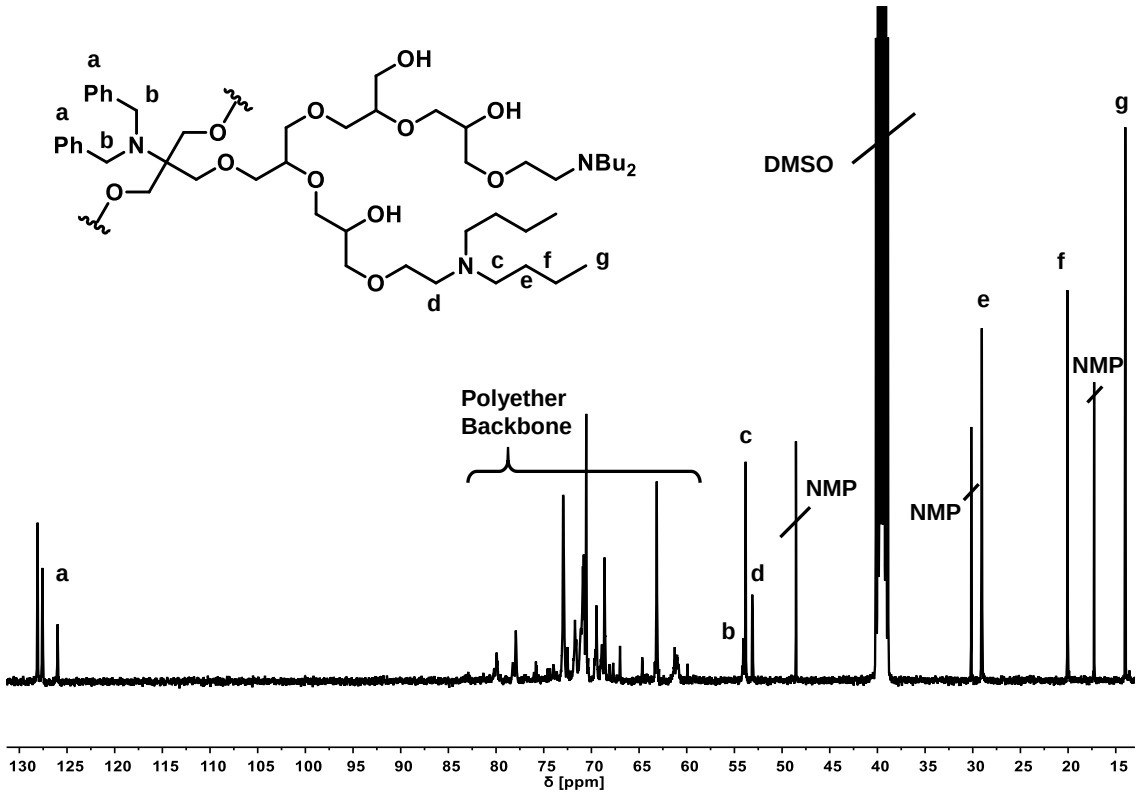

Figure S 9. ^{13}C NMR spectrum of *hb*P($G_{0.90}$-*co*-DBuAEGE$_{0.10}$) (100 MHz, DMSO-d_6).

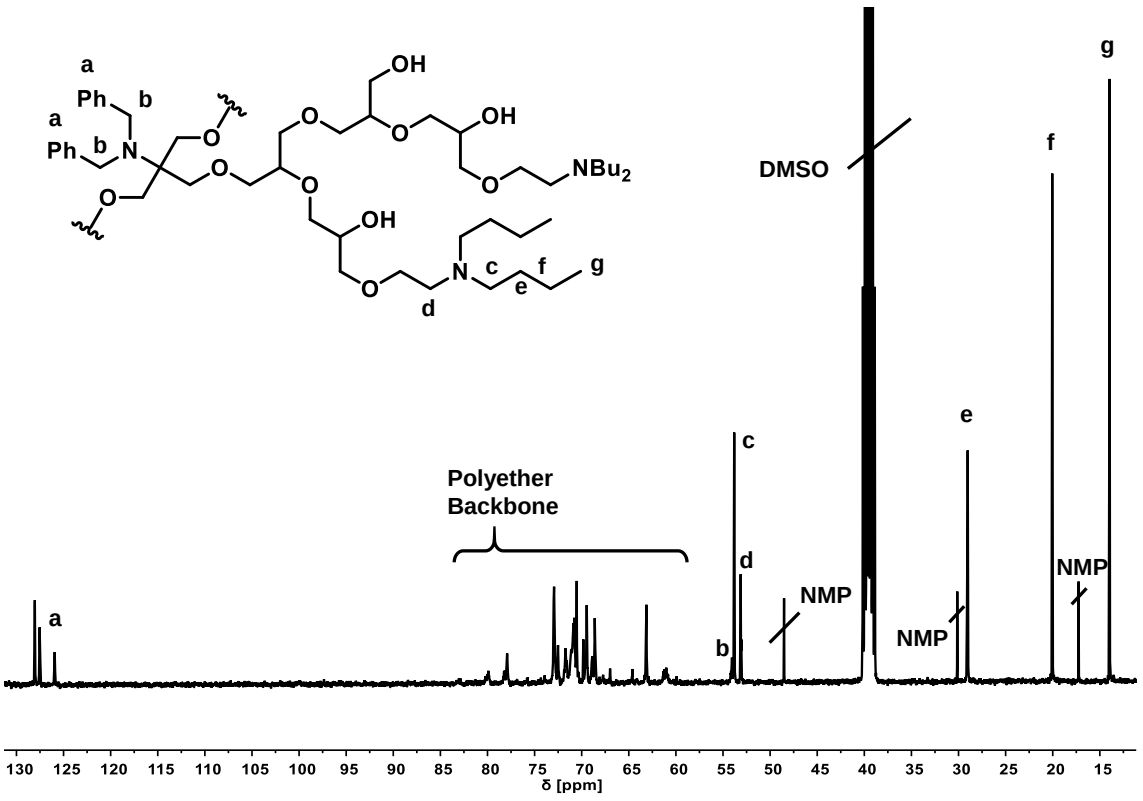

Figure S 10. ^{13}C NMR spectrum of *hb*P($G_{0.80}$-*co*-DBuAEGE$_{0.20}$) (100 MHz, DMSO-d_6).

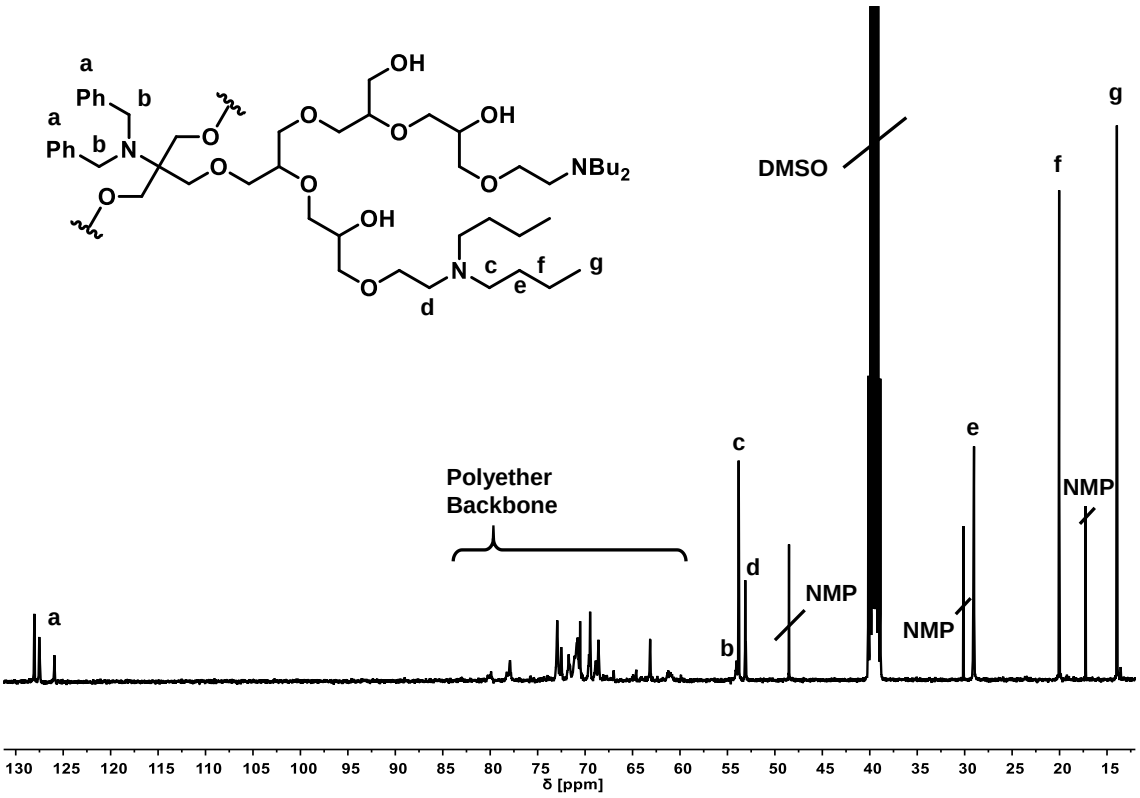

Figure S 11. ^{13}C NMR spectrum of *hb*P($G_{0.73}$-*co*-DBuAEGE$_{0.27}$) (100 MHz, DMSO-d_6).

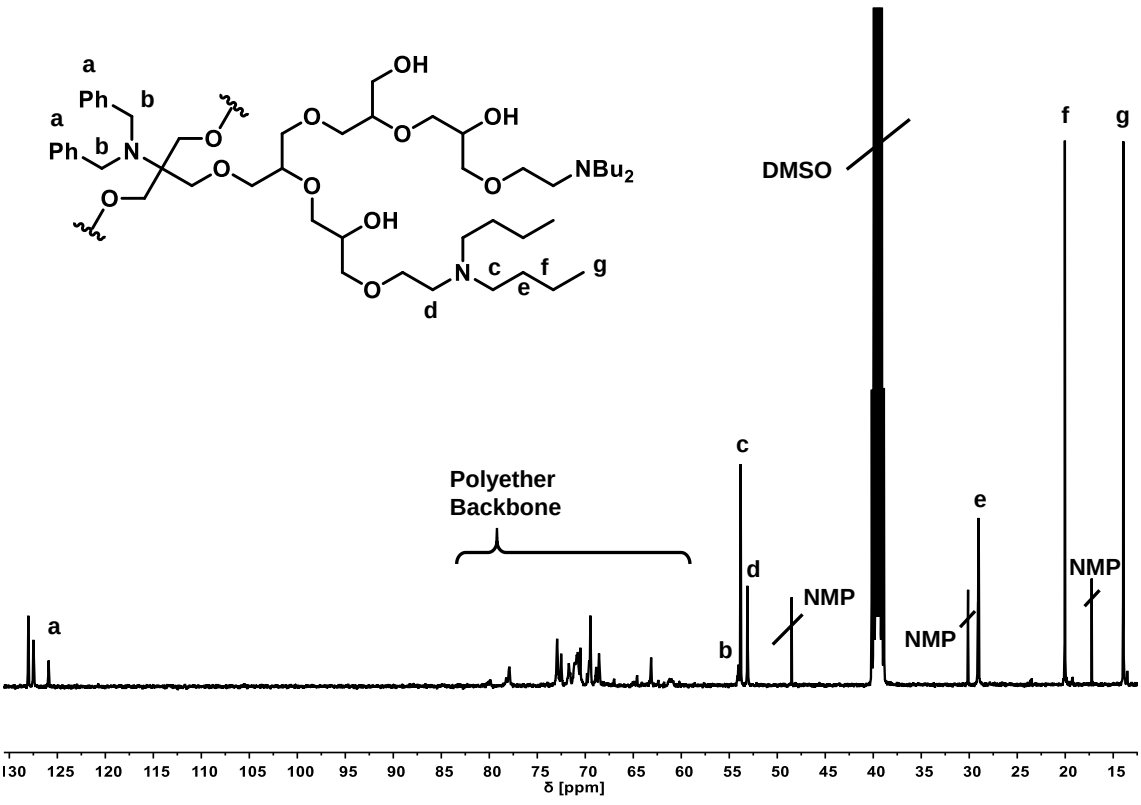

Figure S 12. ^{13}C NMR spectrum of *hb*P($G_{0.64}$-*co*-DBuAEGE$_{0.36}$) (100 MHz, DMSO-d_6).

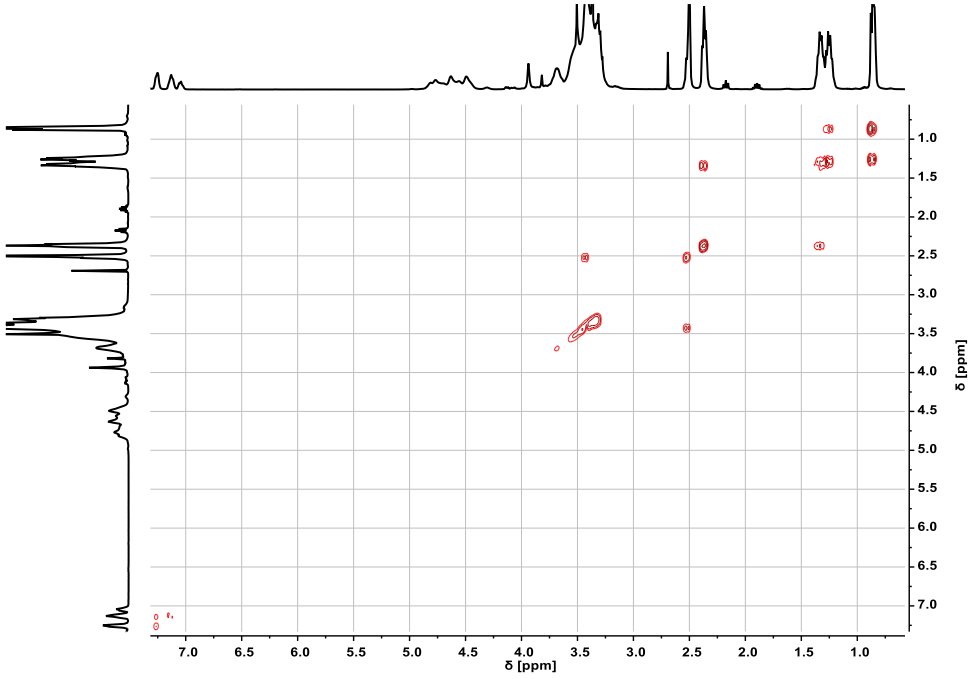

Figure S 13. ^{1}H-^{1}H COSY NMR spectrum of *hb*P(G$_{0.80}$-*co*-DBuAEGE$_{0.20}$) (400/400MHz, DMSO-d_6).

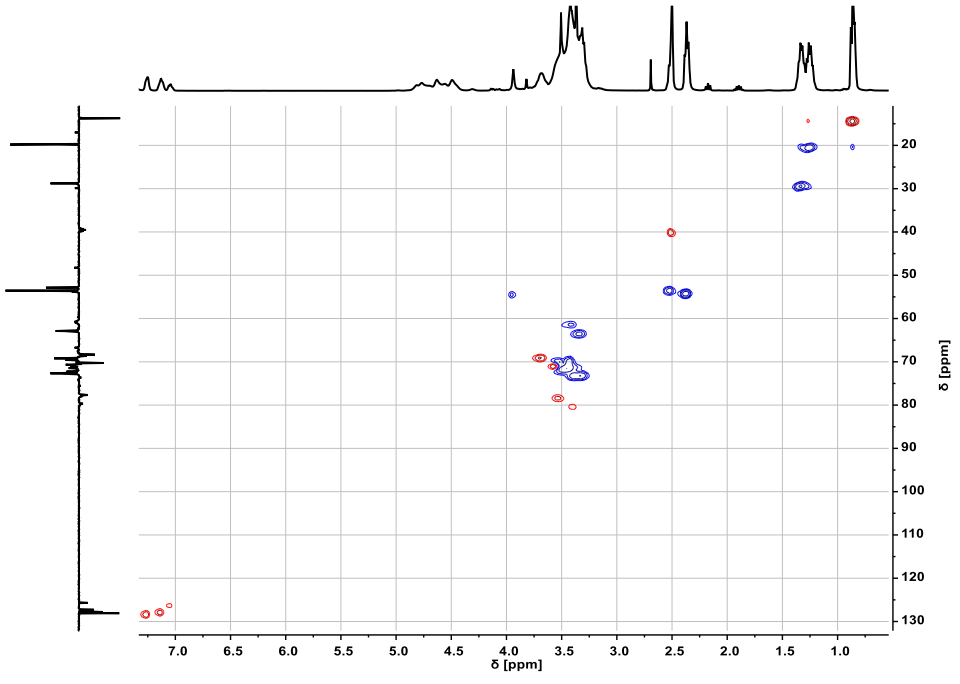

Figure S 14. ^{1}H-^{13}C HSQC NMR spectrum of *hb*P(G$_{0.80}$-*co*-DBuAEGE$_{0.20}$) (400/100MHz, DMSO-d_6). ^{1}H and ^{13}C NMR spectra can be found on the horizontal and vertical axis, respectively. Phase correlation is given by correlation of cross peaks (red: methyl, methine, Blue: methylene).

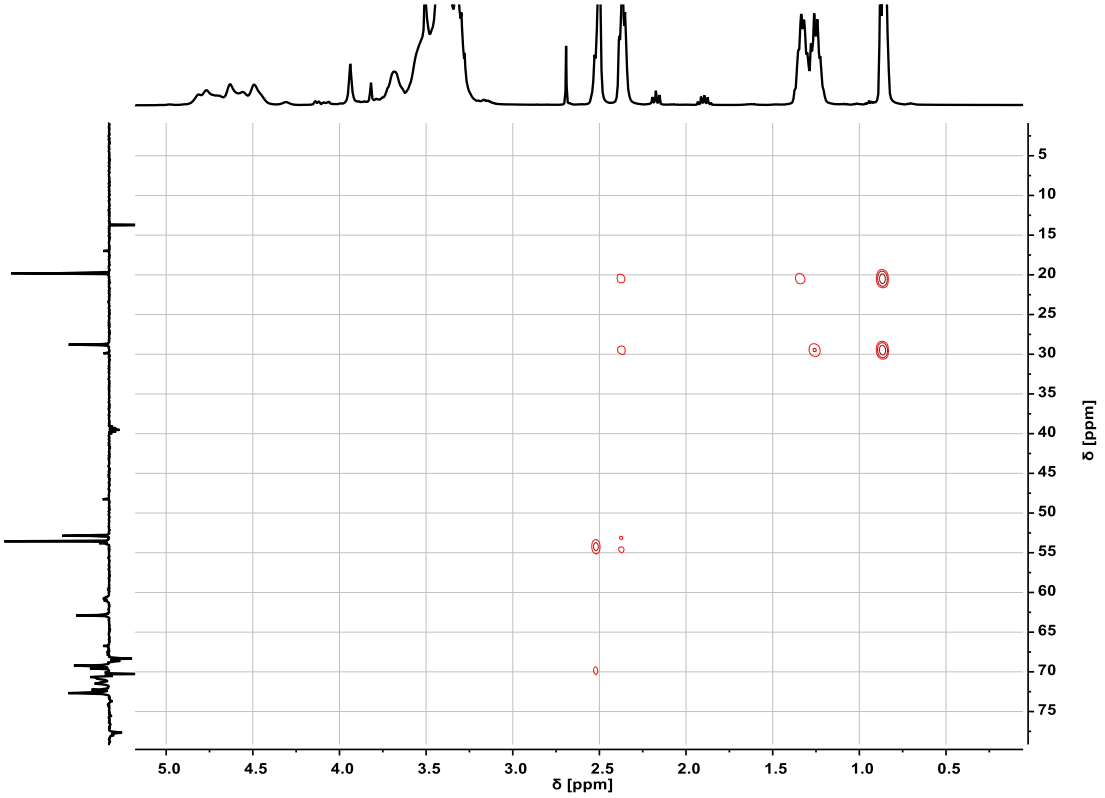

Figure S 15. ^{1}H-^{13}C HMBC NMR spectrum of *hb*P(G$_{0.80}$-*co*-DBuAEGE$_{0.20}$) (400/100MHz, DMSO-d_6). ^{1}H and ^{13}C NMR spectra can be found on the horizontal and vertical axis, respectively.

Degree of Branching for the Copolymerization of AB_2 with AB Monomers

Modified equation for DB for the system AB_2 + AB under ideal SMA conditions (full conversion, no side-reactions, no sterical hindrance) according to Frey and coworkers:[39]

$$DB = \frac{2\,(1- X_{AB})}{3 - 2\,X_{AB}} \qquad \text{S 1}$$

Table S 1. Copolymer compositions and the values for DB determined either experimentally or calculated according to equation S 1.

Sample[a)]	$X_{DBuAEGE}$[b)]	DB[c)]	$DB_{AB/AB2}$[d)]
*hb*P($G_{0.90}$-*co*-DBuAEG$E_{0.10}$)	0.10	0.42	0.64
*hb*P($G_{0.80}$-*co*-DBuAEG$E_{0.20}$)	0.20	0.41	0.62
*hb*P($G_{0.73}$-*co*-DBuAEG$E_{0.27}$)	0.27	0.47	0.59
*hb*P($G_{0.64}$-*co*-DBuAEG$E_{0.36}$)	0.36	0.42	0.56

[a)]Terminology: indices denote the copolymer composition determined by ^{1}H NMR spectroscopy, [b)]determined by ^{1}H NMR spectroscopy, [d)]determined by inverse gated ^{13}C NMR spectroscopy, [d)]calculated according to equation S 1 using $X_{DBuAEGE}$[b)].

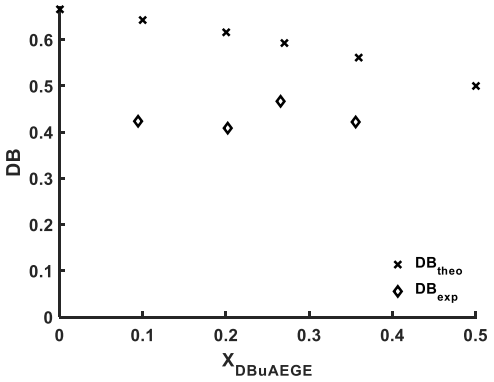

Figure S 16. Comparison of the DBs determined experimentally and calculated by equation S 1 plotted against $X_{DBuAEGE}$.

Copolymerization Kinetics

$$P_1^- + M_1 \xrightarrow{k_{11}} P_1M_1^-$$

$$P_1^- + M_2 \xrightarrow{k_{12}} P_1M_2^-$$

$$P_2^- + M_1 \xrightarrow{k_{21}} P_2M_1^-$$

$$P_2^- + M_2 \xrightarrow{k_{22}} P_2M_2^-$$

P_1^-; P_2^-: active chain end; M_1; M_2: monomer; *k*: reactivity constant

Fineman-Ross equation:[40]

$$x \cdot \frac{1-y}{y} = \frac{x^2}{y} r_1 - r_2;\ r_1 = \frac{k_{11}}{k_{12}} \text{ and } r_2 = \frac{k_{22}}{k_{21}} \qquad \text{S 3}$$

x = mole fraction of the stock; y = mole fraction of the polymer at certain mole fractions of the stock; r_1 = reactivity ratio for monomer M_1; r_2 = reactivity ratio for monomer M_2.

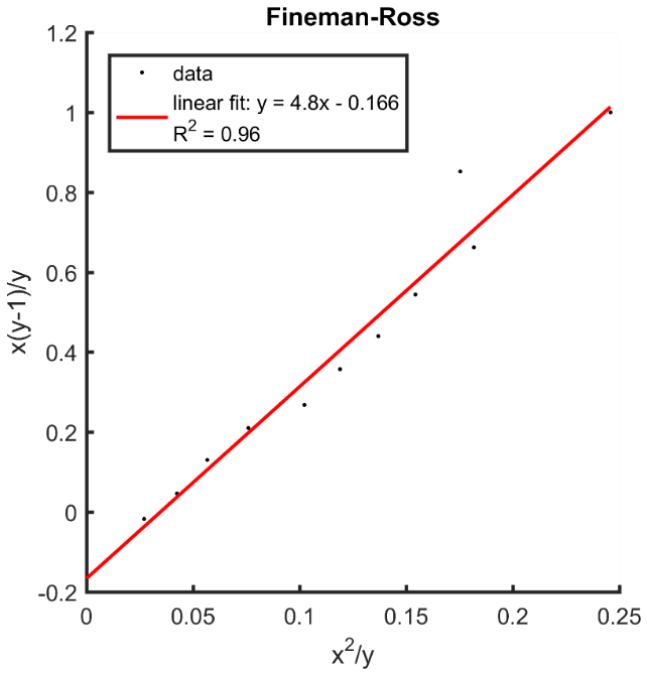

Figure S 17. Fineman-Ross plot to determine the reactivity ratios r_1 and r_2.

Turbidimetric Measurements

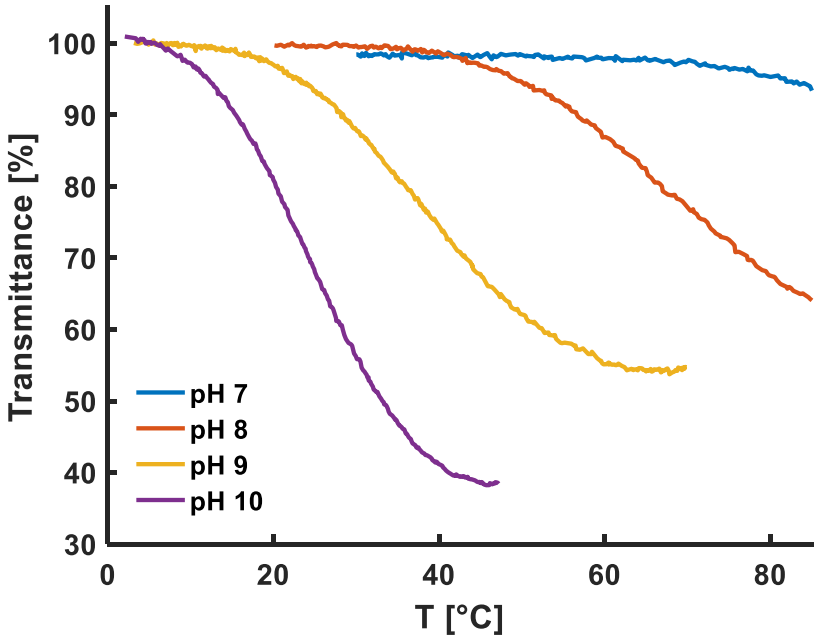

Figure S 18. Turbidimetry measurement of buffered aqueous solutions of *hb*P(G$_{0.90}$-*co*-DBuAEGE$_{0.10}$) at different pH values (1 mg mL^{-1}).

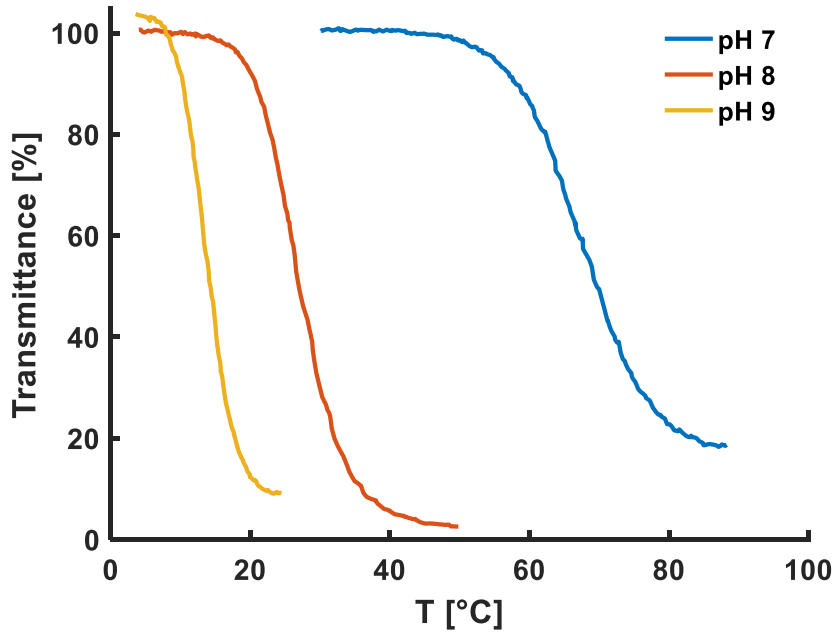

Figure S 19. Turbidimetry measurement of buffered aqueous solutions of *hb*P(G$_{0.73}$-*co*-DBuAEGE$_{0.27}$) at different pH values (1 mg mL^{-1}).

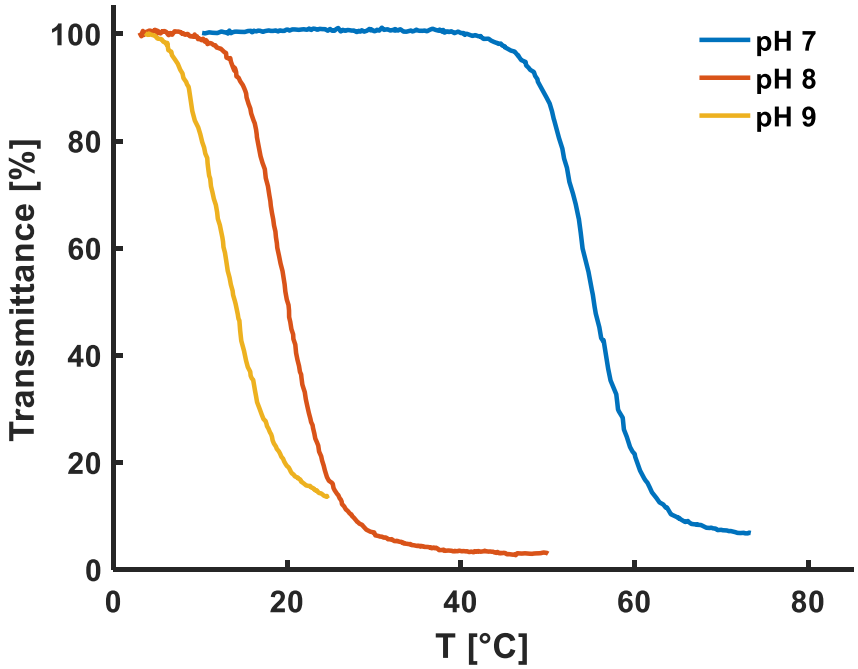

Figure S 20. Turbidimetry measurement of buffered aqueous solutions of *hb*P($G_{0.64}$-*co*-DBuAEG$E_{0.36}$) at different pH values (1 mg mL^{-1}).

Supplemental Analysis for Biocompatibility Testing

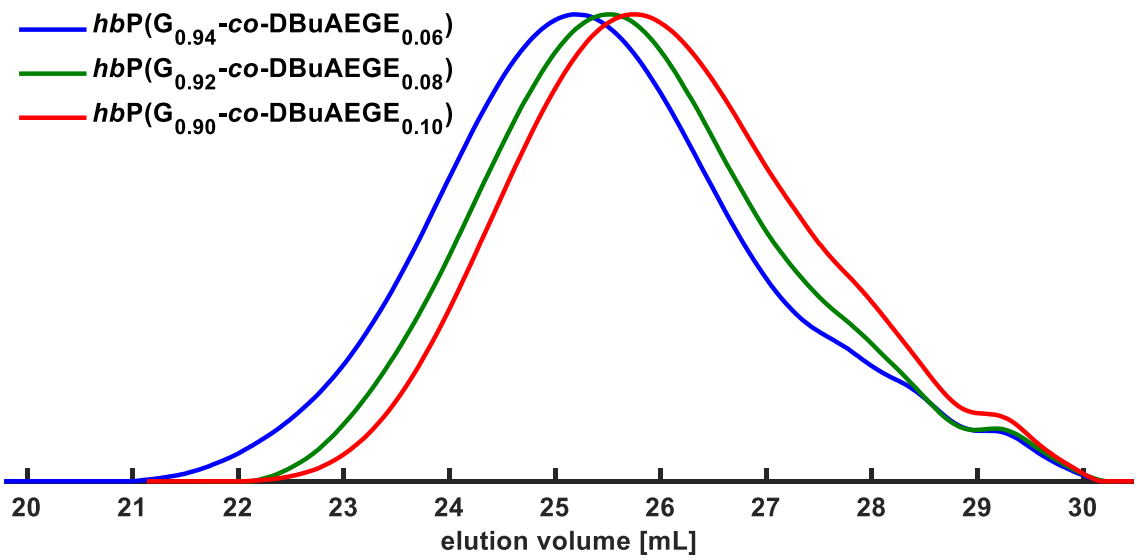

Figure S 21. SEC traces of *hb*P(G$_{0.94}$-*co*-DBuAEGE$_{0.06}$), *hb*P(G$_{0.92}$-*co*-DBuAEGE$_{0.08}$) and *hb*P(G$_{0.90}$-*co*-DBuAEGE$_{0.10}$) (DMF) used for viability testing.

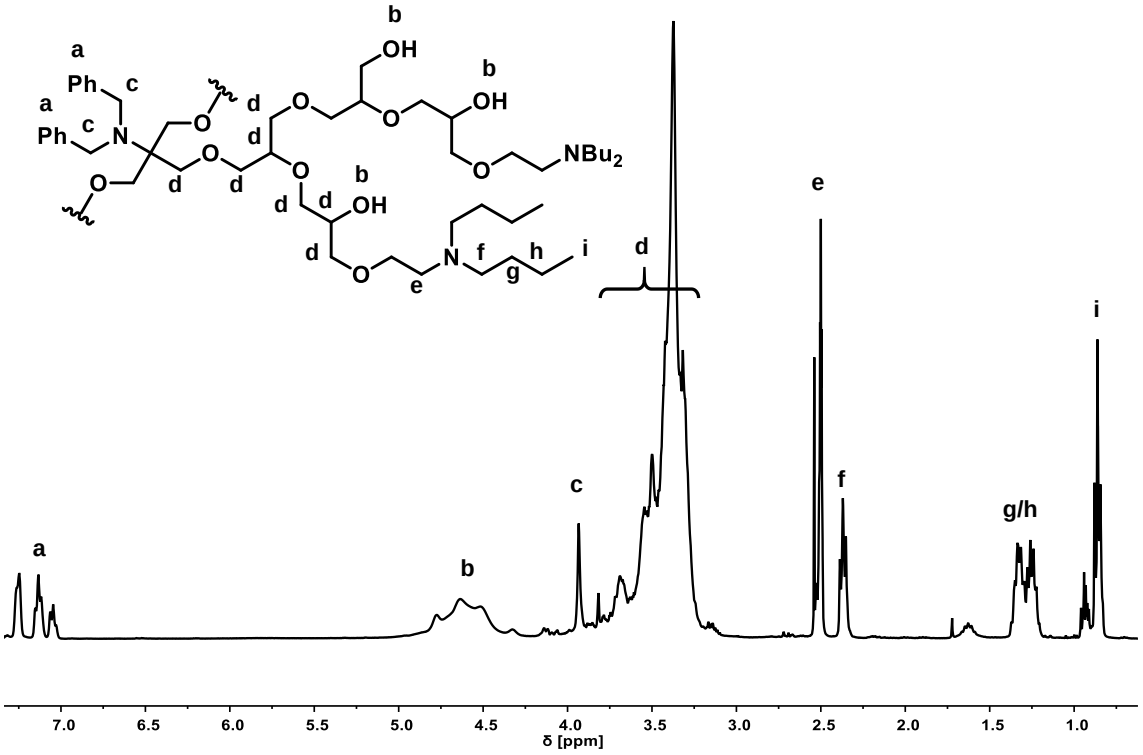

Figure S 22. ^{1}H NMR spectrum of *hb*P(G$_{0.94}$-*co*-DBuAEGE$_{0.06}$) (400 MHz, DMSO-d_6).

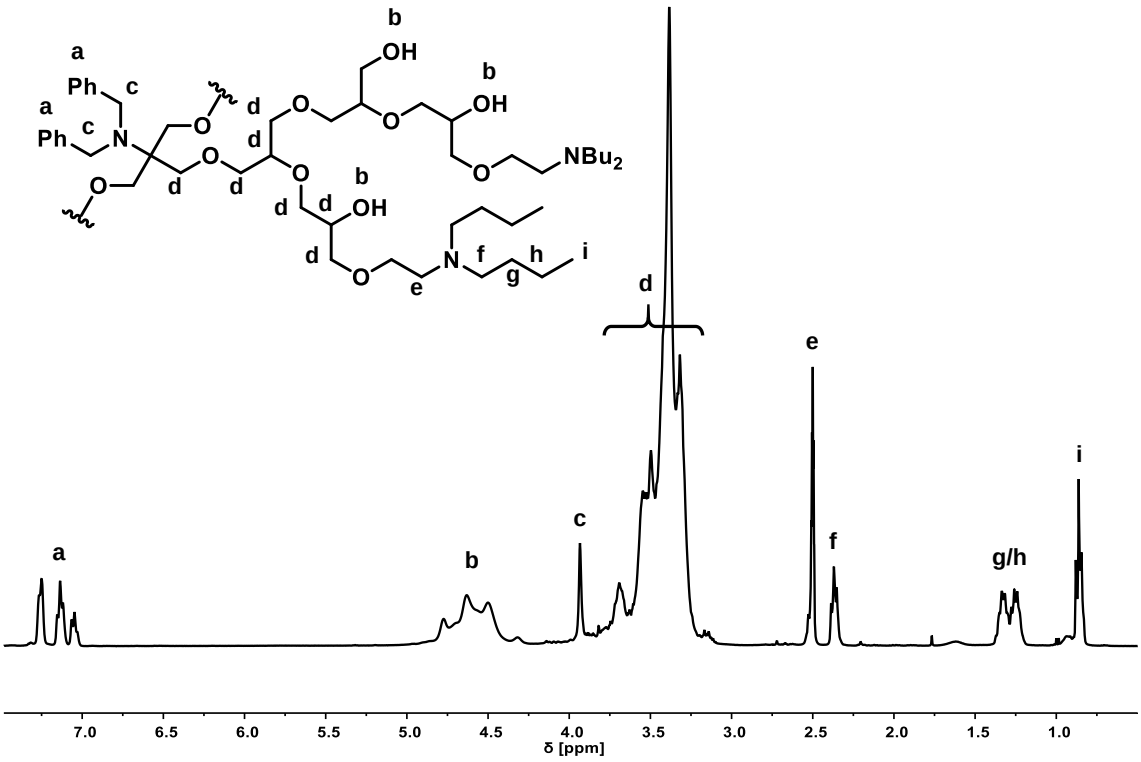

Figure S 23. ^{1}H NMR spectrum of *hb*P($G_{0.92}$-*co*-DBuAEGE$_{0.08}$) (400 MHz, DMSO-d_6).

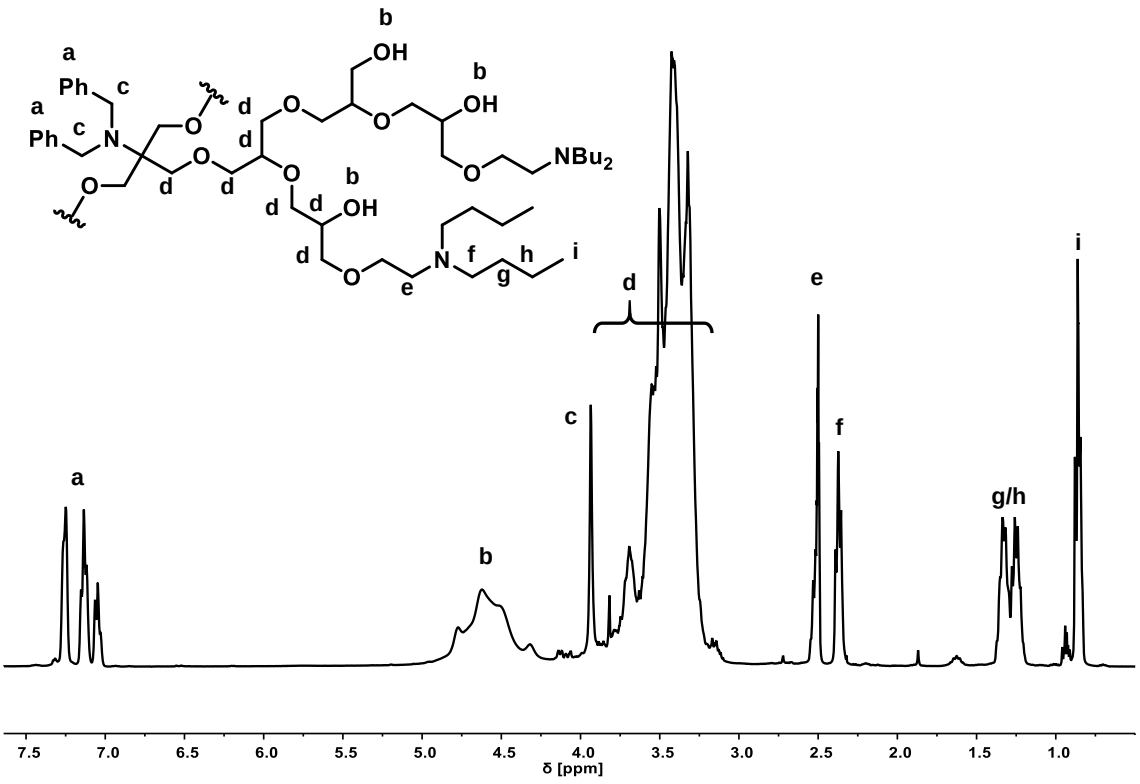

Figure S 24. ^{1}H NMR spectrum of *hb*P($G_{0.90}$-*co*-DBuAEGE$_{0.10}$) (400 MHz, DMSO-d_6).

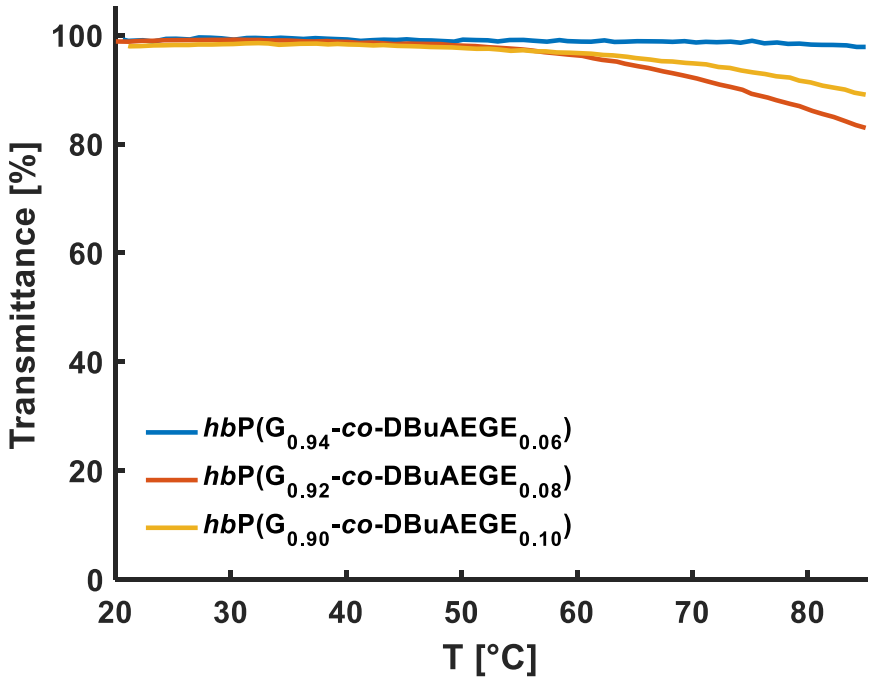

Figure S 25. Turbidimetry measurement of PBS buffered solutions of *hb*P($G_{0.94}$-*co*-$DBuAEGE_{0.06}$), *hbP*($G_{0.92}$-*co*-$DBuAEGE_{0.08}$) and *hb*P($G_{0.90}$-*co*-$DBuAEGE_{0.10}$) (1 mg mL^{-1}) to confirm full solubility under physiological conditions.

3.2 *In-Situ* End-Group Functionalization of Hyperbranched Polyglycerols by Copolymerization of Glycidol with a Bulky Glycidyl Ester

Tobias Kaiser[a], Holger Frey[a,]*

[a]Department of Chemistry, Johannes Gutenberg University, 55128 Mainz, Germany

To be submitted.

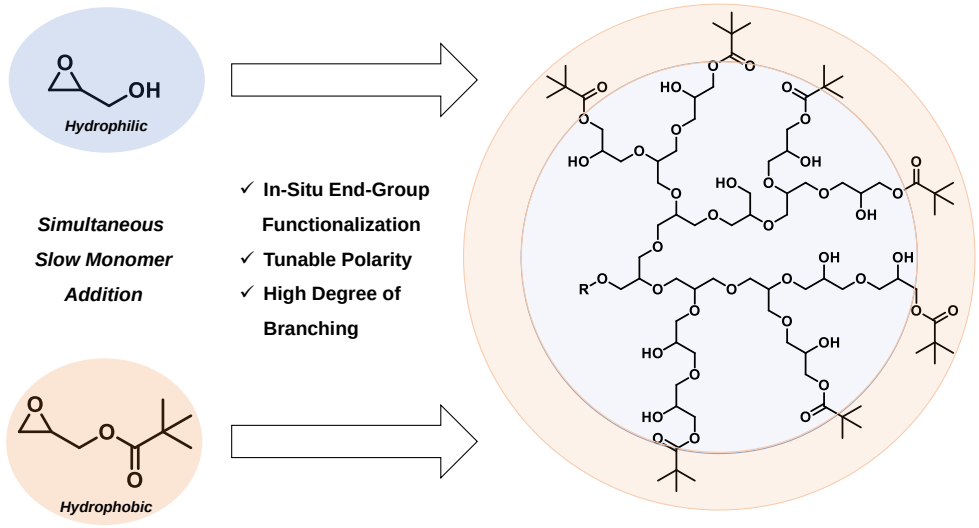

Abstract

Hyperbranched copolymers of glycidol and an ester-protected glycidol derivative, glycidyl pivalate (GlyPiv), have been prepared *via* simultaneous slow monomer addition. Comonomer contents ranging from 0.03 to 0.37 and degrees of polymerization between 19 and 25 were obtained as confirmed by ^{1}H NMR spectroscopy. The molar masses determined using either SEC or ^{1}H NMR were between 740 and 1000 or 2000 and 2300 g mol^{-1}, respectively. Additionally, successful copolymerization was also confirmed by FTIR spectroscopy, representing structural units of both comonomers. Structure elucidation by a combination of different 2D NMR experiments showed no signals linked to transesterification. Hence, the pivalate protecting group is assumed to be stable under the reaction conditions. Additionally, the thorough evaluation of ^{13}C NMR spectra suggested incorporation of the comonomer GlyPiv mainly as terminal units into the otherwise hyperbranched polyether polyol backbone, only to a lesser extent as linear units. Since terminal units have no influence on the degree of branching (DB) according to literature reports, DBs were found to be mostly unaffected by the variation of the comonomer content. Thus, GlyPiv behaves rather as a chain-stopper than a conventional comonomer. This type of copolymerization can function as a gateway to introducing various functional groups without decreasing DB.

Introduction

Hyperbranched polymers are a special class of materials which have gained scientific interest during the last decades, as they combine properties typically

associated with dendrimers with a facile one-pot synthesis.[1,2] Generally, due to their highly branched architecture, these polymers have a more compact structure, i.e. hydrodynamic radius, than linear analogues, resulting in low viscosities in melts and solution. Furthermore, a large number of functional end-groups leads to better solubilities and numerous pathways for modification.[3–14]

As a common subclass, hyperbranched polyether polyols are typically prepared by the anionic ring-opening multibranching polymerization (ROMBP) of the latent AB_2 monomer glycidol following a slow monomer addition (SMA) protocol.[15,16] According to Frey and coworkers, the degree of branching (DB) as a key parameter to describe the hyperbranched architecture can be calculated using the relative amounts of each repeating unit, i.e. dendritic (D), linear (L) and terminal (T):[17]

$$DB = \frac{D + T}{D + T + L} = \frac{2D}{2D + L} \quad (1)$$

A commonly discussed strategy to introduce other functionalities into the polyether backbone is the copolymerization of glycidol with various suitable, i.e. base-stable, comonomers. If the copolymerization is conducted following the SMA approach, random copolymers with numerous functionalities distributed equally along the backbone are formed. For instance, the copolymerization of glycidol with glycidyl ethers enables hyperbranched polyglycerols to show metal interactions, thermoresponsive and pH responsive behavior and orthogonal functionalization.[18–23] The copolymerization of glycidol with alkylene oxides leads to hyperbranched analogues of the common linear polyethers PEO, PPO and PBO with tunable thermoresponsive behavior.[24–27] However, these functionalizations strongly influence the DB of the resulting polymers as by copolymerization of the AB_2 monomer glycidol with AB type monomers strictly linear units are randomly

introduced into the otherwise highly branched backbone.[28] If the aforementioned hyperbranched poly(alkylene oxide)s, however, are synthesized in a one-pot reaction, interesting topologies are formed: due to vastly different reactivities of glycidol and butylene oxide, multiarm star polymers are formed with a more or less unscathed hyperbranched polyglycerol core functioning as the macroinitiator for PBO chains.[27] A suitable alternative without the drawback of adding linear units or resorting to batch polymerizations is the reversible post-polymerization modification of the different secondary and primary hydroxy groups found in hyperbranched polyglycerol. For example, the hydroxy groups of hyperbranched polyglycerols undergo typical reactions described for small molecules[29–33] and can also be used as macroinitiators for the ring-opening polymerization of functional epoxides[34,35] or cyclic esters.[36–38]

Here, we present the anionic copolymerization of glycidol with an ester-protected glycidol moiety, glycidyl pivalate, *via* simultaneous slow monomer addition. Due to the steric demand of the pivalate protecting group, propagation from a GlyPiv is hindered, resulting in a high fraction of terminal GlyPiv units. According to equation 1, the degree of branching of these copolymers is unaffected by a variation of the comonomer content. The discussed copolymerization strategy combines both advantages of the methodologies described in literature: reversible *in situ* functionalization without significantly influencing the degree of branching.

Experimental Section

Materials

All materials were purchased from Sigma Aldrich, TCI or Fisher Scientific. All compounds used for monomer synthesis were employed without further purification. Prior to polymerization, glycidol (96 %), glycidyl pivalate and 1-methyl-2-pyrrolidone (NMP, 99.0 %) were purified by distillation over calcium hydride.

Instrumentation

NMR spectroscopy. ^{1}H and ^{13}C NMR spectra as well as COSY, HSQC and HMBC experiments were recorded on a Bruker Avance II HD 400 (5 mm BBFO-SmartProbe with z-gradient and ATM) at 400/100 MHz. Inverse gated ^{13}C NMR spectra were recorded on a Bruker Avance II HD 400 (5 mm BBFO-SmartProbe with z-gradient and ATM) at 100 MHz. The residual signals of the deuterated solvent were utilized as an internal reference.

Size-exclusion chromatography. SEC measurements in DMF (containing 0.25 g L^{-1} of lithium bromide) were performed using an integrated Agilent 1100 series instrument, equipped with a PSS HEMA column combination ($10^6/10^4/10^2$ Å porosity), UV and RI detector. Calibration is based on linear poly(ethylene glycol) standards (Polymer Standards Service).

Turbidimetry. Cloud points were determined using a Jasco V 630 photo spectrometer with a Jasco ETC-717 Peltier element and observed by optical transmittance of light beam (λ = 630 nm) through a 1 cm quartz cell. The intensity

of the transmitted light was recorded versus the temperature of the sample cell. The heating cooling rate was 10 K min^{-1} and values were recorded in 1 K intervals.

Monomer Synthesis

To generate potassium pivalate, 15.18 g pivalic acid (0.15 mol, 1 eq.) and 8.34 g potassium hydroxide (0.15 mol, 1 eq.) were placed in a 250 mL round-bottom flask equipped with reflux condenser and a magnetic stirrer and dissolved in 150 mL THF. After stirring for 2 without additional heating, the solvent was evaporated, and residual traces were removed azeotropically using toluene *in vacuo*. The dried potassium pivalate was dissolved in 80 mL acetonitrile and 2.42 g tetra-n-butylammonium bromide (7.51 mmol, cat.) as well as 35 mL epichlorohydrin (0.45 mol, 3 eq.) were added. The reaction mixture was stirred vigorously and heated to reflux for 2.5 h. Afterwards, the suspension was allowed to cool to room temperature. After filtration to remove any precipitated salts, the solvent was evaporated, and the residue dissolved in 70 mL dichloromethane. The solution was washed with saturated aqueous solutions of $NaHCO_3$ and NaCl and the organic phase was dried using $MgSO_4$. After filtration the solvent was removed and the crude product was distilled repeatedly *in vacuo* (p = 0.01 mbar, T_b = 80 – 100 °C). GlyPiv was obtained as a colorless liquid in moderate yields.

^{1}H NMR (400 MHz, $CDCl_3$): δ (ppm) = 4.40 (dd, 1H, -C<u>H</u>H-O-); 3.92 (dd, 1H, -CH<u>H</u>-O-); 3.20 (m, 1H, H_2C-(O)-C<u>H</u>-); 2.83 (dd, 1H, <u>H</u>HC-(O)-CH-); 2.64 (dd, 1H, H<u>H</u>C-(O)-CH-); 1.22 (s, 9H, -(C<u>H</u>$_3$)$_3$).

^{13}C NMR (100 MHz, $CDCl_3$): δ (ppm) = 178.40 (-O<u>C</u>OR); 64.78 (-<u>C</u>H_2-OPiv); 49.61 (H_2C-(O)-<u>C</u>H-); 44.63 (H_2<u>C</u>-(O)-CH-); 38.97 (-<u>C</u>-(CH_3)$_3$); 27.29 (-(<u>C</u>H_3)$_3$).

Copolymerization Protocol

General procedure: In a Schlenk flask equipped with a magnetic stirrer, 33 mg TMP (0.25 mmol, 1 eq) was dissolved in 1 mL methanol. Afterwards, a solution of 12 mg cesium hydroxide monohydrate (0.07 mmol, 0.3 eq) in 1 mL methanol was added and the mixture was stirred for 30 min. The partially deprotonated initiator salt was dried *in vacuo* overnight at room temperature. The initiator salt was then dissolved in 1 mL NMP and heated to 100 °C under argon atmosphere. In another Schlenk flask, the monomers (6.64 mmol, 27 eq) were mixed in respect to the target composition and diluted with NMP to yield a total volume of 2 mL. Using a syringe pump, the monomer mixture was slowly added to the heated solution of the initiator salt with a rate of 0.1 mL h^{-1}. After complete addition, the mixture was stirred for further 60 min and the polymerization was terminated by adding 1.48 mL of a solution of acetic acid in ethanol (c = 0.05 mol L^{-1}, 1 eq.). Afterwards, the reaction mixture was dialyzed (methanol, MWCO = 1000 g mol^{-1}) and the solvent removed. The polymers were isolated as highly viscous brown oils with yields depending on the initial comonomer ratios.

*hb*P(G-*co*-GlyPiv): ^{1}H NMR (400 MHz, DMSO-d_6, δ): 5.16 – 4.21 (br, m, -O<u>H</u>); 4.21 – 3.00 (m, -O-C<u>H</u>-, -O-C<u>H</u>$_2$-); 1.42 – 1.20 (m, -C<u>H</u>$_2$-CH$_3$); 1.19 – 1.07 (m, -C-(C<u>H</u>$_3$)$_3$); 0.88 – 0.73 (m, -CH$_2$-C<u>H</u>$_3$).

^{13}C NMR (100 MHz, DMSO-d_6, δ): 177.96 – 177.24 (C=O); 81.11 – 80.14 ($L_{1,3G}$); 79.03 – 77.98 (D_G); 77.75 – 75.95 (L_{GlyPiv}); 73.77 – 73.10 (2 $L_{1,4G}$); 72.95 – 72.49 (T_{GlyPiv}); 72.46 – 70.29 (2 D_G, 2 T_G); 70.28 – 69.59 ($L_{1,3G}$); 69.51 – 68.69 ($L_{1,4G}$); 68.62 – 67.05 (T_{GlyPiv}); 66.20 – 65.52 (T_{GlyPiv}); 64.91 – 63.75 (L_{GlyPiv}); 63.70 – 63.20 (T_G); 61.82 – 61.08 ($L_{1,3G}$); 60.53 – 60.12 (L_{GlyPiv}); 38.92 – 38.57 (C-$(CH_3)_3$); 27.62 – 26.98 (C-(CH_3)$_3$); 23.36 – 22.42 (-CH_2-CH_3); 8.17 – 7.61 (-CH_2-CH_3).

FTIR: $\tilde{\nu}$ (cm^{-1}) = 3600 – 3000 (-OH); 1700 (C=O); 1377 (-CH_3); 1100 (C-O-C).

Results and Discussion

Several hyperbranched polyether polyols based on glycidol and glycidyl pivalate (GlyPiv) were prepared to investigate the copolymerization behavior of a bulky glycidyl ester during the anionic ring-opening copolymerization. The pivalate protecting was specifically chosen due to the lack of CH-acidity in α-position to the carbonyl group. The steric demand of other possible protecting groups, i.e. benzoic acid derivatives, was believed to be insufficient to efficiently shield the ester bond. A particularly intriguing question is whether transesterification takes place or if the otherwise base-labile pivalate protecting group is stable under the reaction conditions of an anionic ROMBP. This would affect the degree of branching in two ways: i) if no transesterification takes place, the comonomer is incorporated as an AB unit, introducing solely linear (L) or terminal (T) units; ii) if transesterification takes place, glycidol repeating units of the growing chains could be transformed into GlyPiv units, ultimately affecting the reactivity of glycidol linear or terminal units and reducing the abundance of dendritic ones.

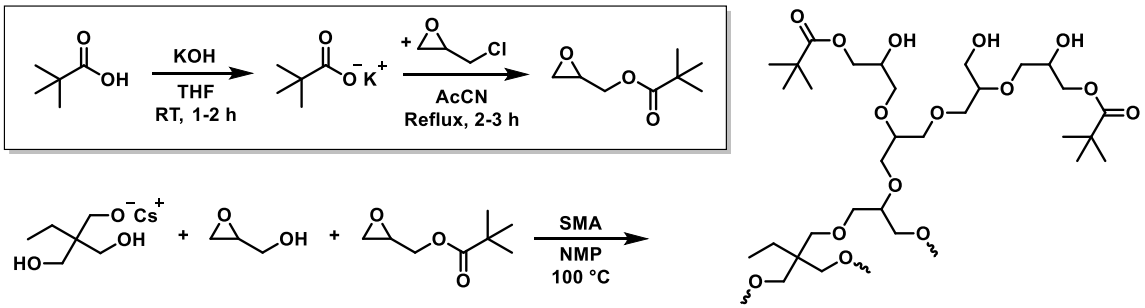

Scheme 1. Schematic monomer synthesis and copolymerization of glycidol and glycidyl pivalate *via* SMA.

The monomer GlyPiv was successfully prepared by the reaction of potassium pivalate with epichlorohydrin *via* a two-phase reaction using the phase transfer

catalyst TBAB (Scheme 1). The structure of the monomer was confirmed by ^{1}H and ^{13}C spectroscopy as well as several 2D NMR experiments (Figure S 1 to Figure S 5). Repeated fractionated distillations yielded the compound in sufficient purity for a subsequent use in anionic ring-opening polymerizations.

Table 1. ^{1}H NMR and SEC data of the copolymers based on glycidol and GlyPiv.

Sample[a)]	**DP_n**[b)]	**X_{GlyPiv}**[b)]	**M_n**[b)] **[g mol^{-1}]**	**M_n**[c)] **[g mol^{-1}]**	**Đ**[c)]
*hb*P($G_{0.97}$-*co*-GlyPiv$_{0.03}$)	24	0.03	2000	860	1.81
*hb*P($G_{0.94}$-*co*-GlyPiv$_{0.06}$)	25	0.06	2100	740	1.53
*hb*P($G_{0.88}$-*co*-GlyPiv$_{0.12}$)	24	0.12	2200	800	1.65
*hb*P($G_{0.80}$-*co*-GlyPiv$_{0.20}$)	23	0.20	2300	1000	1.94
*hb*P($G_{0.63}$-*co*-GlyPiv$_{0.37}$)	19	0.37	2100	870	1.57

[a)]Terminology: indices denote the copolymer composition determined by ^{1}H NMR spectroscopy [b)]determined by ^{1}H NMR spectroscopy, [c)]determined by SEC (DMF, linear PEO standards).

The hyperbranched polyether polyols were prepared by simultaneous SMA of a mixture of glycidol and GlyPiv to a solution of the partially deprotonated initiator TMP in NMP heated to 100 °C. After complete monomer addition and further reaction time the polymerization was terminated by the addition of stoichiometric amounts of acetic acid to avoid premature cleavage of the ester bonds. Subsequent dialysis of the crude reaction mixture in methanol (MWCO = 1000 g mol^{-1}) yielded the hyperbranched copolymers as highly viscous brown oils. The degrees of polymerization P_n (≈ 27) were specifically selected to

yield hyperbranched polyglycerols with molar masses of 2000 g mol^{-1} after eventual cleavage of the ester bond. Scheme 1 depicts the monomer synthesis alongside the copolymerization of glycidol and GlyPiv *via* SMA. Five hyperbranched polyether polyols with systematically varied GlyPiv content (X_{GlyPiv}) were prepared, while maintaining a similar degree of polymerization. Table 1 summarizes the SEC and ^{1}H NMR data of the copolymers. The SEC traces of the copolymers (Figure 1) show monomodal distributions with moderate dispersities and molar masses, determined using linear PEG standards, range from 740 to 1000 g mol^{-1}. Deviations from the theoretical values are due to the inherently compact structure of hyperbranched polymers, i.e. hydrodynamic volume, in comparison to linear analogues, typically resulting in an underestimation of the molar masses by conventional SEC methods.[39]

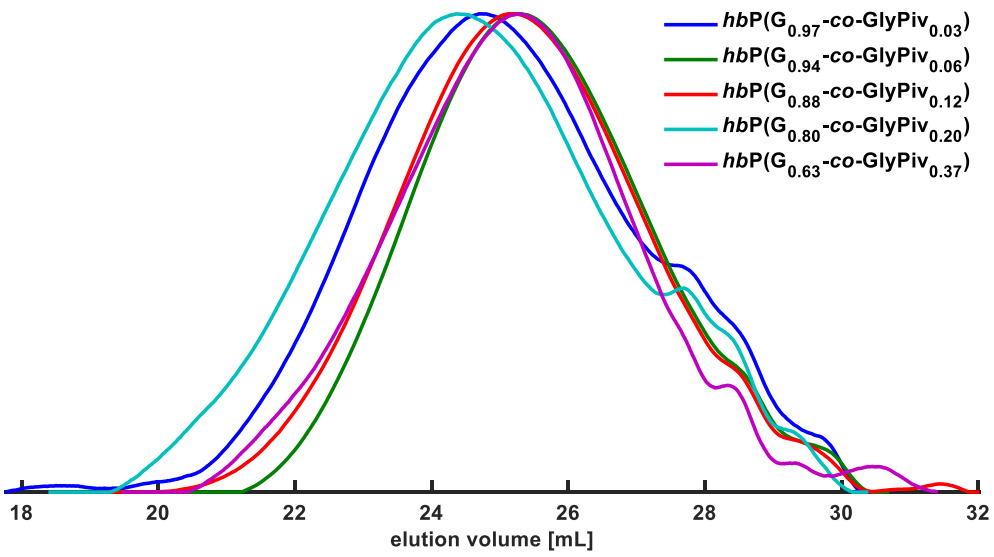

Figure 1. SEC traces of the *hb*P(G-*co*-GlyPiv) copolymers (DMF, RI detector).

Figure 2 shows an exemplary spectrum of *hb*P(G$_{0.80}$-*co*-GlyPiv$_{0.20}$), the NMR spectra of every other copolymer is found in the supporting information (cf. Figure S 11 to Figure S 18). Disregarding several solvent traces, the signals can be

assigned to each of the structural units of either glycidol or glycidyl pivalate: the hydroxy groups (a) from 5.13 to 4.23 ppm, the combined signals of the polyether backbone (b + c) from 4.22 to 3.09 ppm, the methyl groups of the pivalate protecting groups (e) at 1.14 ppm and lastly the methylene and methyl group of the initiator TMP (d + f, 1.31 – 1.21 and 0.86 – 0.73 ppm).

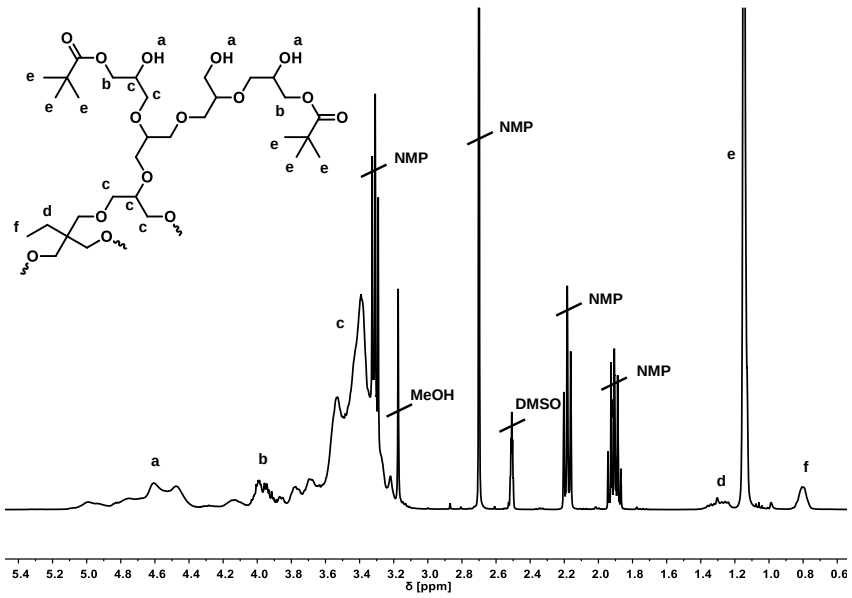

Figure 2. ^{1}H NMR spectrum of *hb*P($G_{0.80}$-*co*-GlyPiv$_{0.20}$) (400 MHz, DMSO-d_6).

Using signal f as normation, the degree of polymerization, comonomer content and the average molar mass can be calculated using equations 1 - 3 by comparison of the signals of the hydroxy groups (a) and the methyl groups of the comonomer GlyPiv (e):

$$DP_n = \left(\frac{I_e}{6}\right) + (I_a\text{-}3) \qquad 1$$

$$X_{GlyPiv} = \frac{I_a}{6\ DP_n} \qquad 2$$

$$M_n = M_{TMP} + M_{Glycidol}\ (I_a\text{-}3) + M_{GlyPiv}\ \left(\frac{I_e}{6}\right) \qquad 3$$

The resulting degrees of polymerization typically vary between 19 and 25 and decrease with increasing target comonomer content. Furthermore, the comonomer content X_{GlyPiv}, ranging from 0.03 to 0.37, decreases the higher the target values. Hence, neither glycidol nor GlyPiv show full conversion, suggesting a strong influence of GlyPiv on the reaction mechanism. Furthermore, DOSY NMR and FTIR spectroscopy also confirm the successful copolymerization of glycidol and glycidyl pivalate, the corresponding spectra are found in the supporting information (cf. Figure S 10 and Figure S 19). However, using only ^{1}H NMR spectroscopy, no definitive statements can be made about the general mechanism regarding the initial questions of transesterification and manner of incorporation. Typically, ^{13}C NMR spectroscopy is used to elucidate structural characteristics of hyperbranched polyether polyols (see Figure S 6). Particularly interesting is the region from 55 to 85 ppm representing the polyether backbone (Figure 3), which is significant for observations regarding the DB, transesterification, and general reaction mechanism.

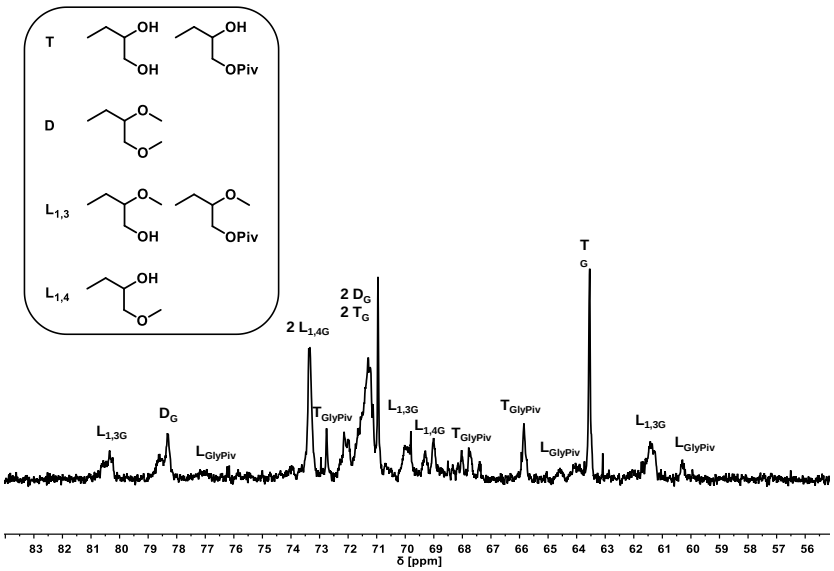

Figure 3. Polyether region in ^{13}C NMR spectrum of *hb*P($G_{0.80}$-*co*-$GlyPiv_{0.20}$) (100 MHz, DMSO-d_6).

By a combination of different 2D NMR experiments all signals can be assigned (see Figure S 7 to Figure S 9). While the signals of each repeating unit of glycidol (D, $L_{1,3}$, $L_{1,4}$ and T) can be found in the spectra, the GlyPiv units demand further discussion. As little to no signal of a methine carbon in vicinity to an ester moiety is found in either of the 2D experiments, two different possibilities regarding transesterification, i.e. transfer of the pivalate moiety to an active chain end, need to be discussed: Transesterification either happens exclusively by the attack of a sterically less hindered primary alkoxide on the carbonyl carbon or the steric hindrance of the protecting group grants sufficient shielding, successfully preventing the attack of the equally bulky alkoxide nucleophile. The former reaction, however, would not be detectable, since the same repeating units are obtained afterwards affecting neither the DB nor the overall reactivity. Therefore, one can assume, that no transesterification takes place and the copolymerization of glycidol with glycidyl esters can in fact be described as an AB_2/AB system, if the stability of the ester bond due the sterically hindrance is sufficient.

Following the structure elucidation and signal assignment, the degree of branching can be calculated according to Frey and coworkers based on the signal intensities of the different repeating units found in hyperbranched polymers (equation 4):

$$DB = \frac{2\,D}{2\,D + L_{Glycidol} + L_{GlyPiv}} \qquad 4$$

For copolymerizations of AB_2 monomers with linear AB comonomers, the degree of branching is reduced by the introduction of strictly linear unit, thus increasing the ratio of L in equation 3 (see supporting information for further detail). Table S 1 summarizes the results of the DB calculations. Peculiarly, the degrees of branching obtained by equation 3 range from 0.50 to 0.53 and appear to be independent of

both the molar masses and copolymer compositions up to $X_{GlyPiv} = 0.20$. The incorporation of GlyPiv as terminal units is more favorable than as linear units (see Figure 3 L_{GlyPiv} vs T_{GlyPiv}). Due to the steric demand of the pendant pivalate moiety propagation from a glycidyl pivalate chain end either by glycidol or glycidyl pivalate is likely hindered, resulting in mainly terminal units and, to a lesser extent, linear ones. Therefore, GlyPiv rather acts as a chain stopper than a linear AB comonomer. Consequently, no pronounced effect of the copolymer composition on the degree of branching up to 0.20 is observed. However, the DBs tend to be smaller than those obtained under ideal SMA conditions, since the introduction of GlyPiv as a chain-stopper prohibits full conversion. Hence the degrees of branching assume values between those typically expected for ideal batch and ideal SMA AB_2/AB copolymerizations.[18,28] Only for a glycidyl pivalate content of 0.37 DB decreases similar to the equations discussed in literature (cf. supporting information), as statistically, by an increase of the comonomer feed more glycidyl pivalate units are incorporated as linear units.

The combination of no occurrence of transesterification and incorporation mainly as terminal units allows for the *in-situ* end-group functionalization of hyperbranched polyether polyols by copolymerization with bulky glycidyl esters in limited ratios up to 0.20 – 0.30. For instance, by copolymerization of glycidol with the apolar comonomer GlyPiv, thermoresponsive behavior can be introduced, whereas hyperbranched polyglycerol is fully water-soluble otherwise.[15] Figure 4 shows the results of two turbidimetric measurements of aqueous solutions of *hb*P($G_{0.80}$-*co*-$GlyPiv_{0.20}$) with different concentrations.

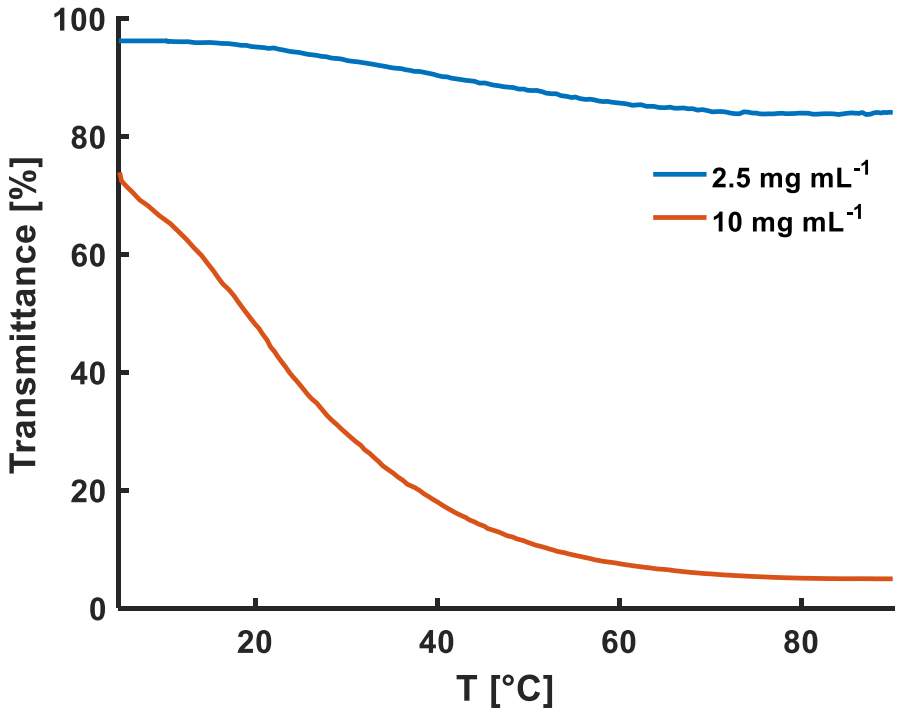

Figure 4. Turbidimetry measurement of aqueous solutions of *hb*P($G_{0.80}$-*co*-Gly$Piv_{0.20}$) with different concentrations.

By the introduction of 20 % of the apolar ester moiety, turbidity already occurs at room temperature. In comparison to other thermoresponsive hyperbranched polyether polyols, e.g. hyperbranched polypropylene, where a propylene oxide contents of approximately 70 % and higher are necessary to show significant turbidity, much less comonomer is necessary to achieve similar effects. However, in contrast to *hb*PPO, the apolar ester moiety is facilely removable by saponification of the ester bond, e.g. with aqueous solutions of potassium or sodium hydroxide.[40]

However, also other esters, bearing different functional groups, should by utilizable, as long as the ester bond is shielded. For example, Sunder *et al.* already studied the post-polymerization of hyperbranched polyglycerols by facile esterification as a promising pathways interesting materials, e.g. unimolecular

nanocapsules by employing fatty acids or liquid-crystalline materials by the attachment of mesogens.[29,30,41] By using glycidyl esters instead, the necessity of the post-polymerization modification is obsolete, reducing the number of reaction steps.

Conclusion

Hyperbranched polyether polyols based on glycidol and the bulky comonomer glycidyl pivalate have been introduced to investigate, whether the otherwise base-labile pivalate moiety undergoes transesterification during the anionic ring-opening multibranching polymerization. By simultaneous slow monomer addition of both monomers to a solution of a partially deprotonated initiator, several copolymers were synthesized. In order to vary the copolymer composition, different comonomer feed ratios were employed targeting overall degrees of polymerization of 27 resulting in hyperbranched polyglycerol with a molar mass of 2000 g mol-1 after removal of the protecting group. The SEC traces of all copolymers exhibited monomodal distributions M_w / M_n = 1.53 – 1.94) with molar masses between 740 and 1000 g mol^{-1}, as determined using linear PEG standards. The degrees of polymerization typically ranged from 23 to 25 for comonomer contents between 0.03 and 0.20, as confirmed by ^{1}H NMR spectroscopy. With increasing comonomer content (X_{GlyPiv} = 037), however, the degree of polymerization decreased to 19. This observation is based on the unique copolymerization characteristics of the monomer pair glycidol and glycidyl pivalate. The structure elucidation of the copolymers resulted in two important observations owing to the bulky pivalate moiety: i) no transesterification takes place, as only methylene groups were found

adjacent to the ester protecting group; and ii) propagation from a glycidyl pivalate is suppressed, thus GlyPiv is mainly incorporated as a terminal units, only to a lesser extent as a linear one, functioning as a chain-stopper rather than a comonomer. Consequently, for comonomer contents between 0.03 and 0.20, the degree of branching is unaffected by the incorporation of the terminal GlyPiv units ranging from 0.50 to 0.53 showing no influence of the degree of polymerization or the copolymer composition. Hence, the simultaneous polymerization of glycidol and GlyPiv results in the *in-situ* end-group functionalization of a hyperbranched polyglycerol core. All copolymers presented here show thermoresponsive behavior in aqueous solution depending on the copolymer concentration. In comparison to other systems discussed in literature, e.g. *hb*PPO, less comonomer content is needed to achieve similar effects. This synthesis strategy might be expanded to a universal methodology to generate ester-functionalized hyperbranched polyglycerols reducing the number of reaction steps reported so far.

Acknowledgment

T. K. is grateful for financial support by a fellowship from the “Fonds der Chemischen Industrie (FCI)”. Furthermore, the authors thank Monika Schmelzer and Ulrike Kemmer-Jonas for technical assistance.

References

(1) Voit, B. I.; Lederer, A. Hyperbranched and highly branched polymer architectures--synthetic strategies and major characterization aspects. *Chem. Rev.* **2009**, *109*, 5924–5973.

(2) Yan, D.; Gao, C.; Frey, H. *Hyperbranched polymers: Synthesis, properties, and applications*; Wiley series on polymer engineering and technology; Wiley: Hoboken, N.J, 2011.

(3) Zhou, Y.; Yan, D. Supramolecular self-assembly of amphiphilic hyperbranched polymers at all scales and dimensions: progress, characteristics and perspectives. *Chem. Commun.* **2009**, 1172–1188.

(4) Voit, B. New developments in hyperbranched polymers. *J. Polym. Sci. A Polym. Chem.* **2000**, *38*, 2505–2525.

(5) Wilms, D.; Stiriba, S.-E.; Frey, H. Hyperbranched polyglycerols: from the controlled synthesis of biocompatible polyether polyols to multipurpose applications. *Acc. Chem. Res.* **2010**, *43*, 129–141.

(6) Schubert, C.; Osterwinter, C.; Tonhauser, C.; Schömer, M.; Wilms, D.; Frey, H.; Friedrich, C. Can Hyperbranched Polymers Entangle? Effect of Hydrogen Bonding on Entanglement Transition and Thermorheological Properties of Hyperbranched Polyglycerol Melts. *Macromolecules* **2016**, *49*, 8722–8737.

(7) Peleshanko, S.; Tsukruk, V. V. The architectures and surface behavior of highly branched molecules. *Prog. Polym. Sci.* **2008**, *33*, 523–580.

(8) Kim, Y. H. Hyperbranched polymers 10 years after. *J. Polym. Sci. A Polym. Chem.* **1998**, *36*, 1685–1698.

(9) Jikei, M.; Kakimoto, M.-a. Hyperbranched polymers: a promising new class of materials. *Prog. Polym. Sci.* **2001**, *26*, 1233–1285.

(10) Inoue, K. Functional dendrimers, hyperbranched and star polymers. *Prog. Polym. Sci.* **2000**, *25*, 453–571.

(11) Hult, A.; Johansson, M.; Malmström, E. Hyperbranched Polymers. In *Branched polymers*; Roovers, J., Ed.; Advances in Polymer Science 143; Springer: Berlin [u.a.], 1999; pp 1–34.

(12) Gao, C.; Yan, D. Hyperbranched polymers: from synthesis to applications. *Prog. Polym. Sci.* **2004**, *29*, 183–275.

(13) Carlmark, A.; Hawker, C.; Hult, A.; Malkoch, M. New methodologies in the construction of dendritic materials. *Chem. Soc. Rev.* **2009**, *38*, 352–362.

(14) Calderón, M.; Quadir, M. A.; Sharma, S. K.; Haag, R. Dendritic polyglycerols for biomedical applications. *Adv. Mater.* **2010**, *22*, 190–218.

(15) Sunder, A.; Hanselmann, R.; Frey, H.; Mülhaupt, R. Controlled Synthesis of Hyperbranched Polyglycerols by Ring-Opening Multibranching Polymerization. *Macromolecules* **1999**, *32*, 4240–4246.

(16) Schömer, M.; Schüll, C.; Frey, H. Hyperbranched aliphatic polyether polyols. *J. Polym. Sci. A Polym. Chem.* **2013**, *51*, 995–1019.

(17) Hölter, D.; Burgath, A.; Frey, H. Degree of branching in hyperbranched polymers. *Acta Polym.* **1997**, *48*, 30–35.

(18) Sunder, A.; Türk, H.; Haag, R.; Frey, H. Copolymers of Glycidol and Glycidyl Ethers: Design of Branched Polyether Polyols by Combination of Latent Cyclic AB 2 and ABR Monomers. *Macromolecules* **2000**, *33*, 7682–7692.

(19) Schüll, C.; Gieshoff, T.; Frey, H. One-step synthesis of multi-alkyne functional hyperbranched polyglycerols by copolymerization of glycidyl propargyl ether and glycidol. *Polym. Chem.* **2013**, *4*, 4730.

(20) Alkan, A.; Klein, R.; Shylin, S. I.; Kemmer-Jonas, U.; Frey, H.; Wurm, F. R. Water-soluble and redox-responsive hyperbranched polyether copolymers based on ferrocenyl glycidyl ether. *Polym. Chem.* **2015**, *6*, 7112–7118.

(21) Niederer, K.; Schüll, C.; Leibig, D.; Johann, T.; Frey, H. Catechol Acetonide Glycidyl Ether (CAGE): A Functional Epoxide Monomer for Linear and Hyperbranched Multi-Catechol Functional Polyether Architectures. *Macromolecules* **2016**, *49*, 1655–1665.

(22) Seiwert, J.; Herzberger, J.; Leibig, D.; Frey, H. Thioether-Bearing Hyperbranched Polyether Polyols with Methionine-Like Side-Chains: A Versatile Platform for Orthogonal Functionalization. *Macromol. Rapid Commun.* **2017**, *38*.

(23) Schubert, C.; Schömer, M.; Steube, M.; Decker, S.; Friedrich, C.; Frey, H. Systematic Variation of the Degree of Branching (DB) of Polyglycerol via Oxyanionic Copolymerization of Glycidol with a Protected Glycidyl Ether and Its Impact on Rheological Properties. *Macromol. Chem. Phys.* **2018**, *219*, 1700376.

(24) Seiwert, J.; Leibig, D.; Kemmer-Jonas, U.; Bauer, M.; Perevyazko, I.; Preis, J.; Frey, H. Hyperbranched Polyols via Copolymerization of 1,2-Butylene Oxide and Glycidol: Comparison of Batch Synthesis and Slow Monomer Addition. *Macromolecules* **2016**, *49*, 38–47.

(25) Wilms, D.; Schömer, M.; Wurm, F.; Hermanns, M. I.; Kirkpatrick, C. J.; Frey, H. Hyperbranched PEG by random copolymerization of ethylene oxide and glycidol. *Macromol. Rapid Commun.* **2010**, *31*, 1811–1815.

(26) Schömer, M.; Seiwert, J.; Frey, H. Hyperbranched Poly(propylene oxide): A Multifunctional Backbone-Thermoresponsive Polyether Polyol Copolymer. *ACS Macro Lett.* **2012**, *1*, 888–891.

(27) Leibig, D.; Seiwert, J.; Liermann, J. C.; Frey, H. Copolymerization Kinetics of Glycidol and Ethylene Oxide, Propylene Oxide, and 1,2-Butylene Oxide: From Hyperbranched to Multiarm Star Topology. *Macromolecules* **2016**, *49*, 7767–7776.

(28) Frey, H.; Hölter, D. Degree of branching in hyperbranched polymers. 3 Copolymerization of ABm-monomers with AB and ABn-monomers. *Acta Polym.* **1999**, *50*, 67–76.

(29) Sunder, A.; Krämer, M.; Hanselmann, R.; Mülhaupt, R.; Frey, H. Molecular Nanocapsules Based on Amphiphilic Hyperbranched Polyglycerols. *Angew. Chem. Int. Ed.* **1999**, *38*, 3552–3555.

(30) Sunder, A.; Quincy, M.-F.; Mülhaupt, R.; Frey, H. Hyperbranched Polyether Polyols with Liquid Crystalline Properties. *Angew. Chem. Int. Ed.* **1999**, *38*, 2928–2930.

(31) Haag, R.; Stumbé, J.-F.; Sunder, A.; Frey, H.; Hebel, A. An Approach to Core−Shell-Type Architectures in Hyperbranched Polyglycerols by Selective Chemical Differentiation. *Macromolecules* **2000**, *33*, 8158–8166.

(32) Türk, H.; Haag, R.; Alban, S. Dendritic polyglycerol sulfates as new heparin analogues and potent inhibitors of the complement system. *Bioconjugate Chem.* **2004**, *15*, 162–167.

(33) Barriau, E.; Frey, H.; Kiry, A.; Stamm, M.; Gröhn, F. Negatively charged hyperbranched polyether-based polyelectrolytes. *Colloid Polym. Sci.* **2006**, *284*, 1293–1301.

(34) Knischka, R.; Lutz, P. J.; Sunder, A.; Mülhaupt, R.; Frey, H. Functional Poly(ethylene oxide) Multiarm Star Polymers: Core-First Synthesis Using Hyperbranched Polyglycerol Initiators. *Macromolecules* **2000**, *33*, 315–320.

(35) Sunder, A.; Mülhaupt, R.; Frey, H. Hyperbranched Polyether−Polyols Based on Polyglycerol: Polarity Design by Block Copolymerization with Propylene Oxide. *Macromolecules* **2000**, *33*, 309–314.

(36) Burgath, A.; Sunder, A.; Neuner, I.; Mülhaupt, R.; Frey, H. Multi-arm star block copolymers based on ε-caprolactone with hyperbranched polyglycerol core. *Macromol. Chem. Phys.* **2000**, *201*, 792–797.

(37) Gottschalk, C.; Wolf, F.; Frey, H. Multi-Arm Star Poly(L-lactide) with Hyperbranched Polyglycerol Core. *Macromol. Chem. Phys.* **2007**, *208*, 1657–1665.

(38) Wolf, F. K.; Fischer, A. M.; Frey, H. Poly(glycolide) multi-arm star polymers: Improved solubility via limited arm length. *Beilstein J. Org. Chem.* **2010**, *6*.

(39) Perevyazko, I.; Seiwert, J.; Schömer, M.; Frey, H.; Schubert, U. S.; Pavlov, G. M. Hyperbranched Poly(ethylene glycol) Copolymers: Absolute Values of the Molar Mass, Properties in Dilute Solution, and Hydrodynamic Homology. *Macromolecules* **2015**, *48*, 5887–5898.

(40) Wuts, P. G. M.; Greene, T. W., Eds. *Greene's Protective Groups in Organic Synthesis*; John Wiley & Sons, Inc: Hoboken, NJ, USA, 2006.

(41) Sunder, A.; Bauer, T.; Mülhaupt, R.; Frey, H. Synthesis and Thermal Behavior of Esterified Aliphatic Hyperbranched Polyether Polyols. *Macromolecules* **2000**, *33*, 1330–1337.

Supporting Information

Supplemental NMR Spectra and Data

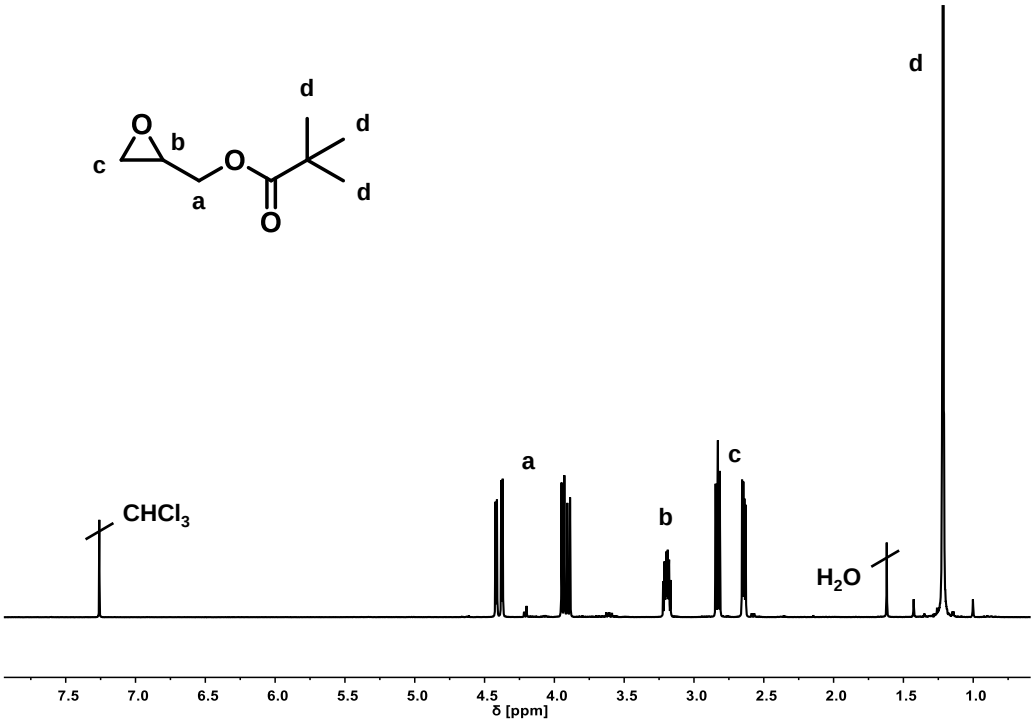

Figure S 1. ^{1}H NMR spectrum of GlyPiv (400 MHz, $CDCl_3$).

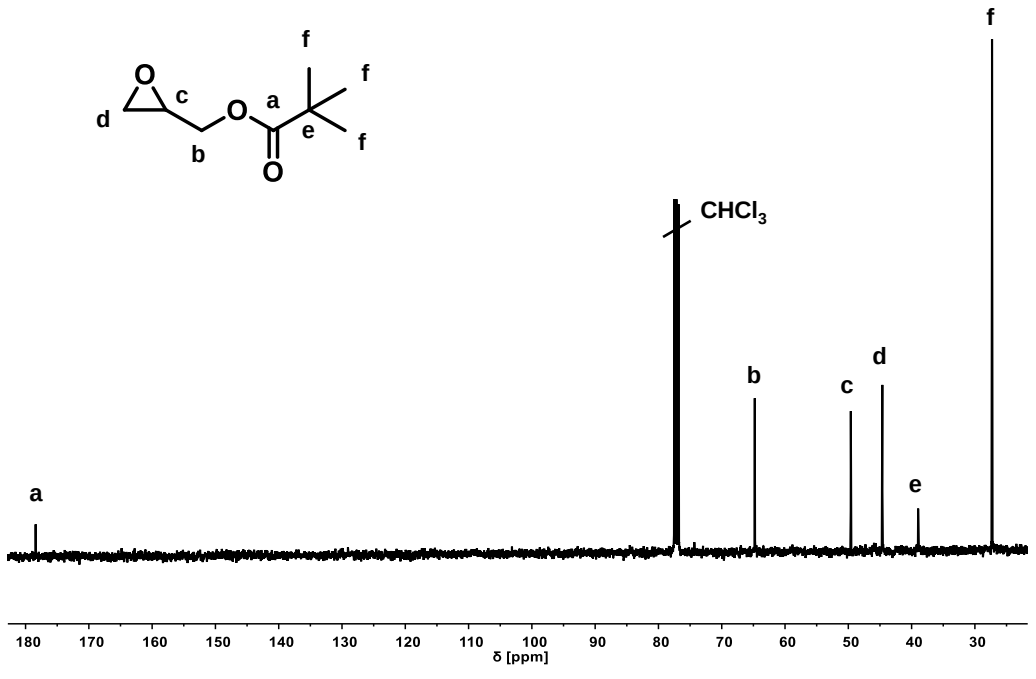

Figure S 2. ^{13}C NMR spectrum of GlyPiv (100 MHz, $CDCl_3$).

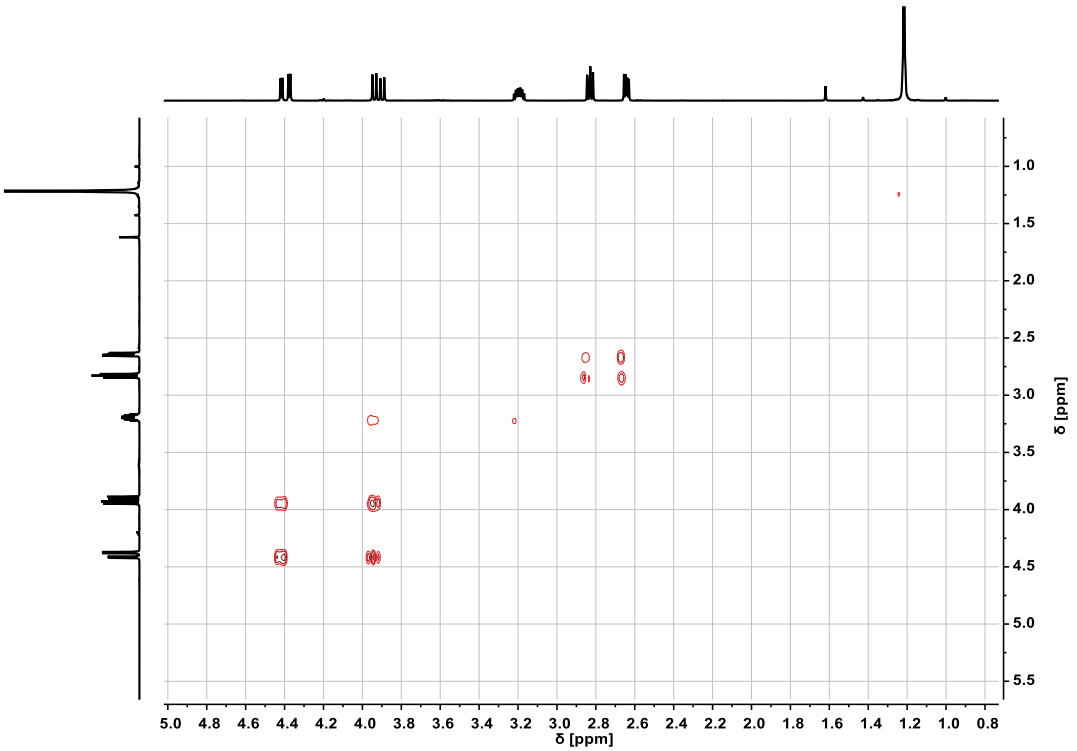

Figure S 3. ^{1}H-^{1}H COSY NMR spectrum of GlyPiv (400 MHz, $CDCl_3$).

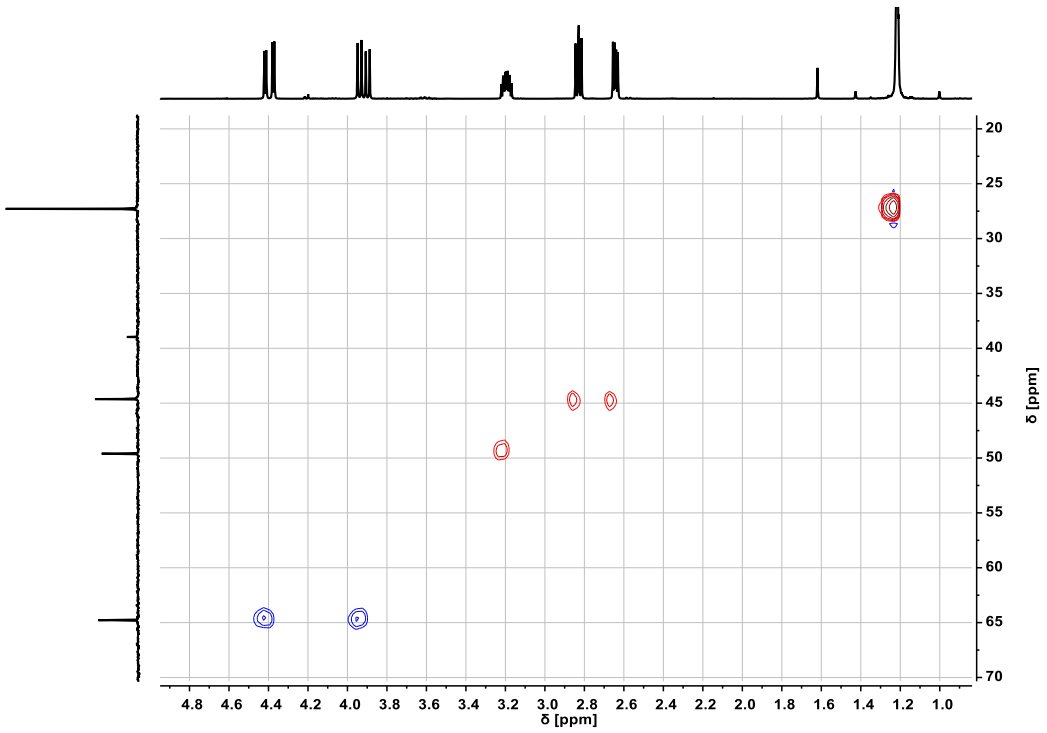

Figure S 4. ^{1}H-^{13}C HSQC NMR spectrum of GlyPiv (400/100MHz, $CDCl_3$). ^{1}H and ^{13}C NMR spectra can be found on the horizontal and vertical axis, respectively. Phase correlation is given by correlation of cross peaks (red: methyl, methine, Blue: methylene).

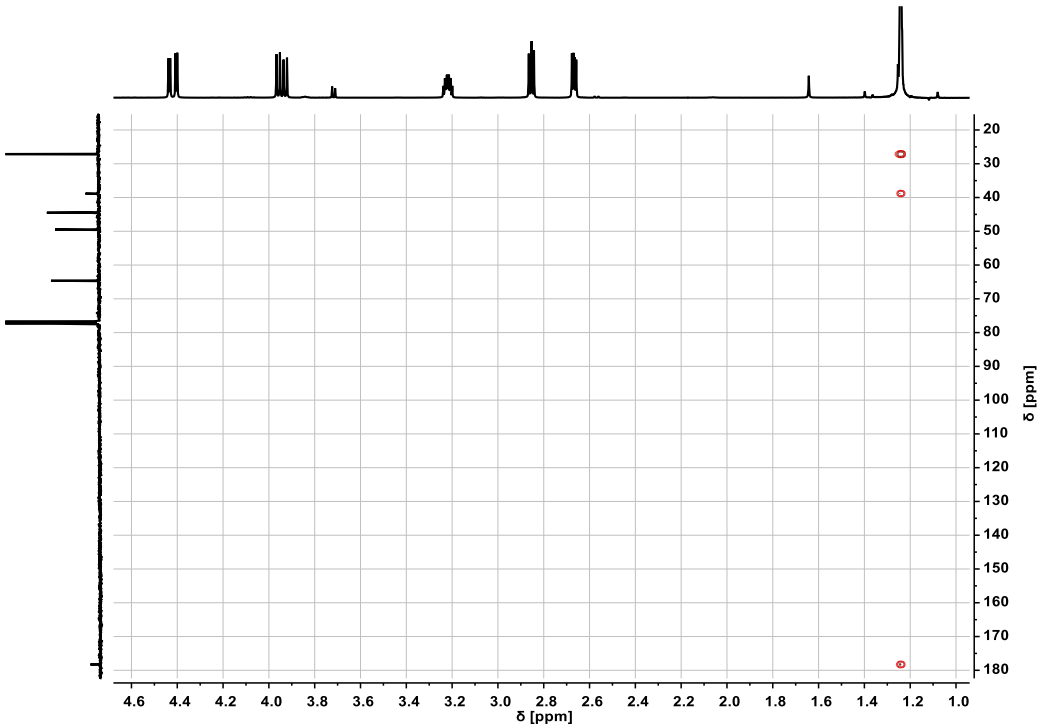

Figure S 5. ^{1}H-^{13}C HMBC NMR spectrum of GlyPiv (400/100 MHz, $CDCl_3$). ^{1}H and ^{13}C NMR spectra can be found on the horizontal and vertical axis, respectively.

*hb*P(G-*co*-GlyPiv)

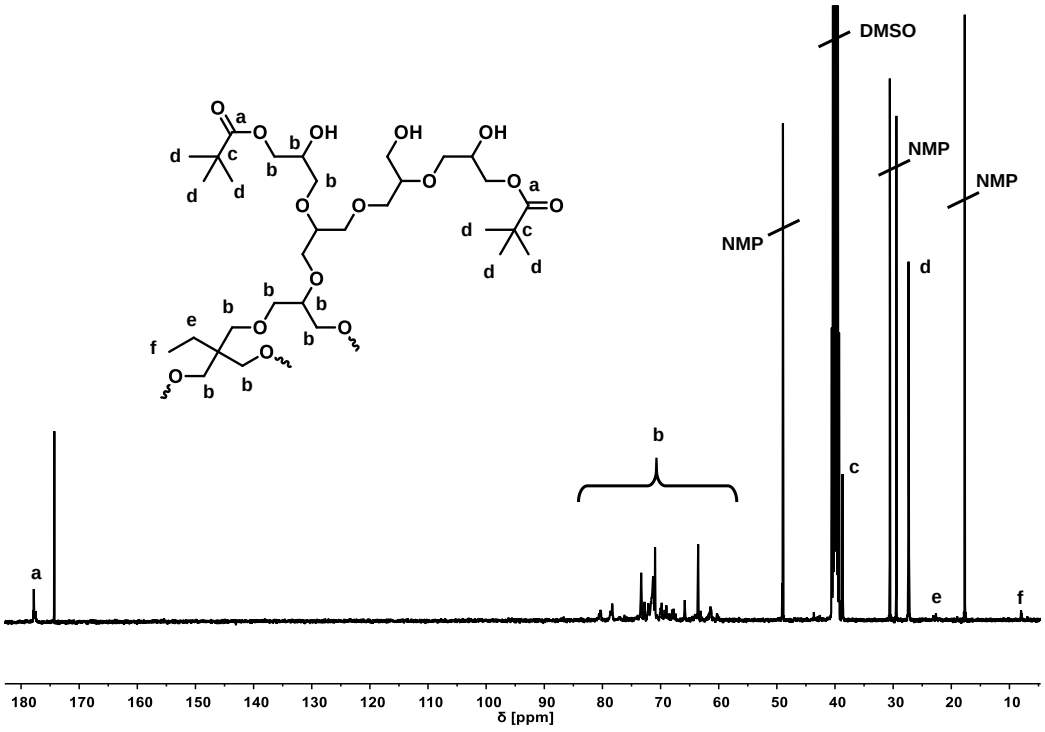

Figure S 6. ^{13}C NMR spectrum of *hb*P($G_{0.80}$-*co*-GlyPiv$_{0.20}$) (100 MHz, DMSO-d_6).

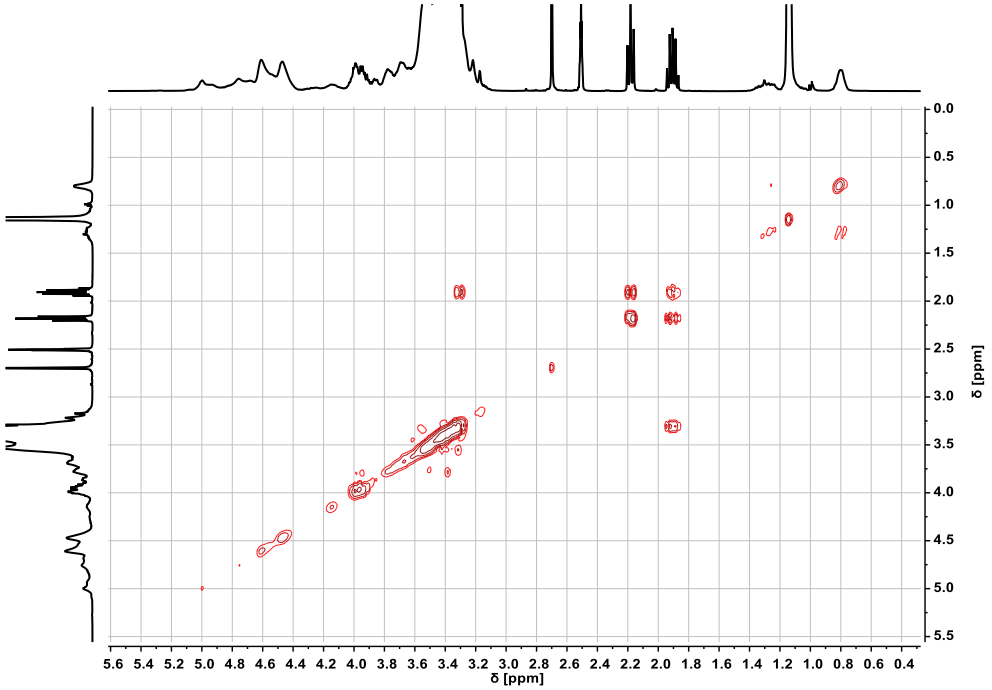

Figure S 7. ^{1}H-^{1}H COSY NMR spectrum of *hb*P(G$_{0.80}$-*co*-GlyPiv$_{0.20}$) (100/100 MHz, DMSO-d_6).

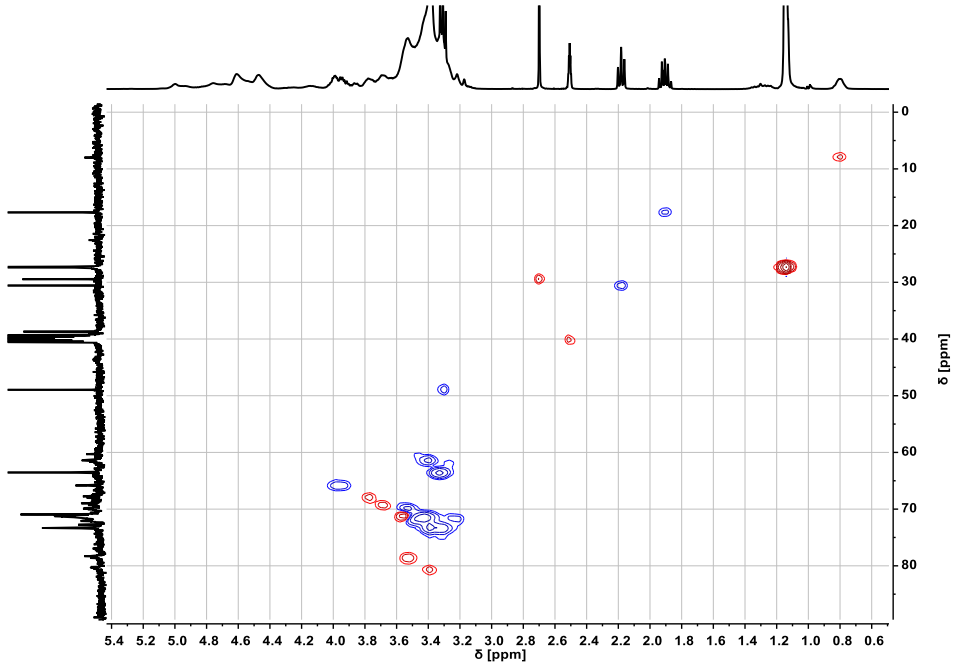

Figure S 8. ^{1}H-^{13}C HSQC NMR spectrum of *hb*P(G$_{0.80}$-*co*-GlyPiv$_{0.20}$) (400/100MHz, DMSO-d_6). ^{1}H and ^{13}C NMR spectra can be found on the horizontal and vertical axis, respectively. Phase correlation is given by correlation of cross peaks (red: methyl, methine, Blue: methylene).

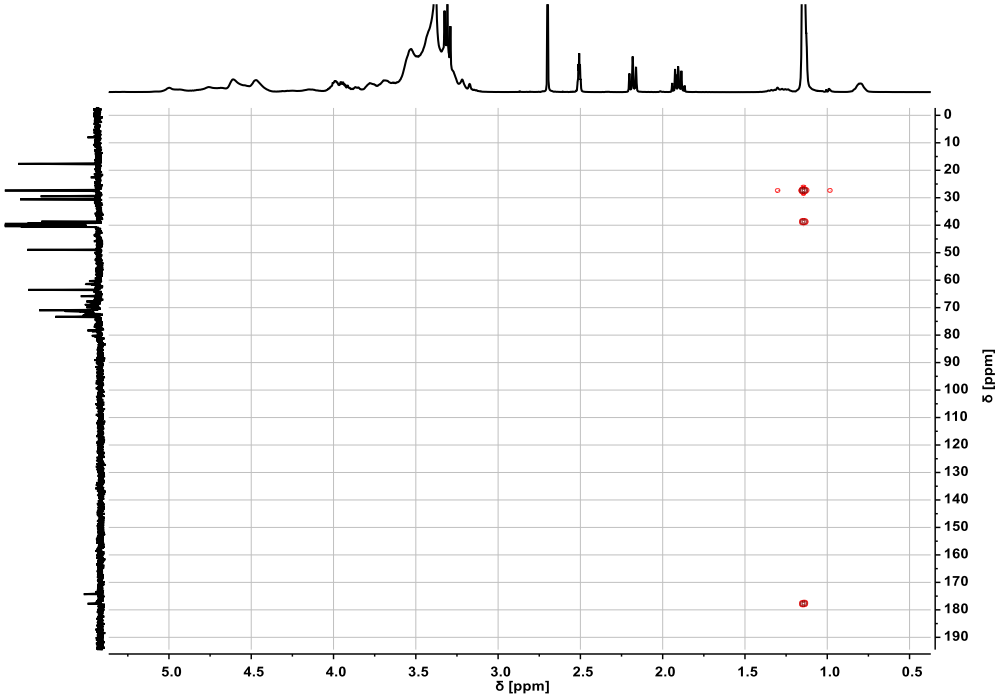

Figure S 9. ^{1}H-^{13}C HSQC NMR spectrum of *hb*P(G$_{0.80}$-*co*-GlyPiv$_{0.20}$) (400/100MHz, DMSO-d_6). ^{1}H and ^{13}C NMR spectra can be found on the horizontal and vertical axis, respectively.

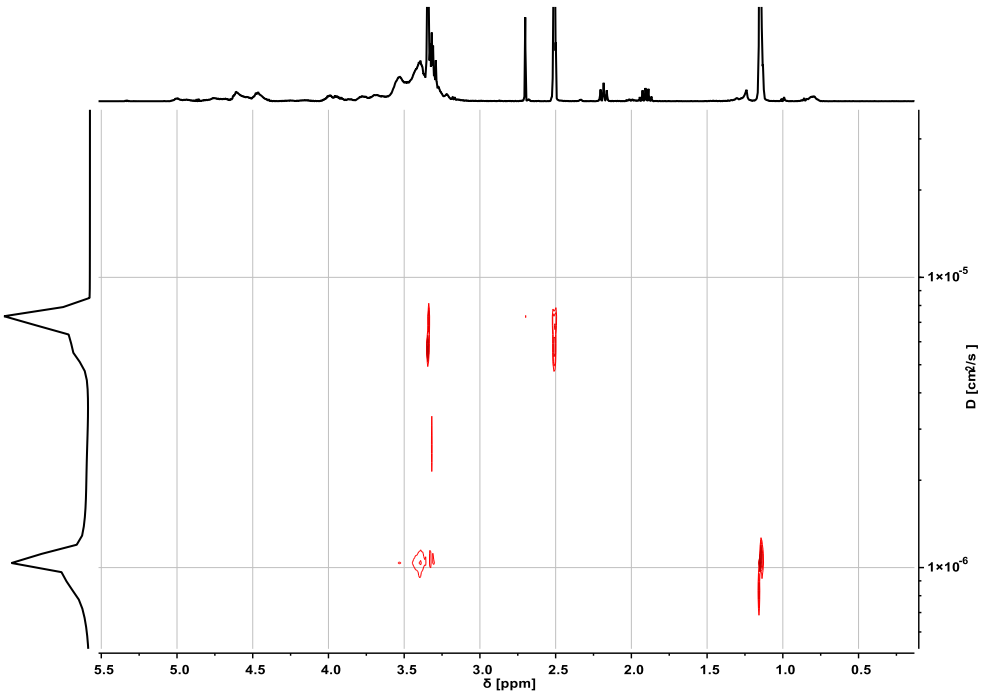

Figure S 10. DOSY NMR spectrum of *hb*P(G$_{0.80}$-*co*-GlyPiv$_{0.20}$) (400 MHz, DMSO-d_6). The ^{1}H NMR spectrum and the diffusion coefficient D [cm^2 s^{-1}] can be found on the horizontal and the vertical axis, respectively.

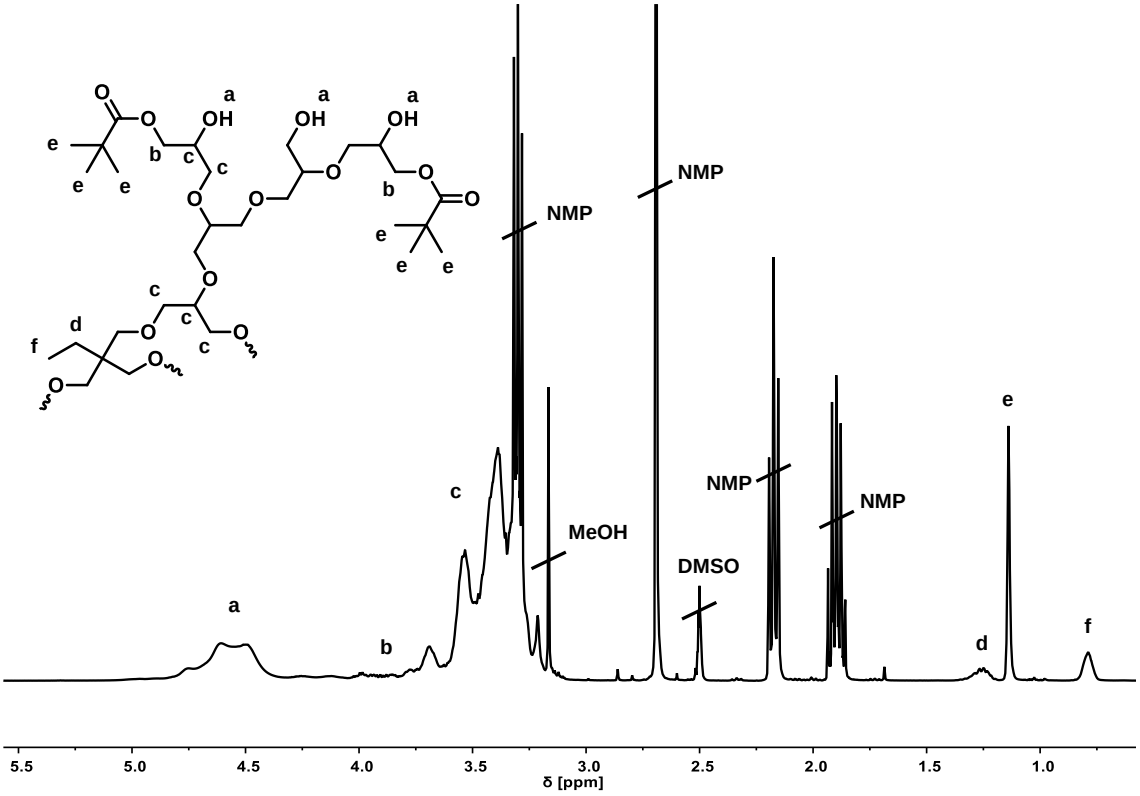

Figure S 11. ^{1}H NMR spectrum of *hb*P($G_{0.97}$-*co*-GlyPiv$_{0.03}$) (400 MHz, DMSO-d_6).

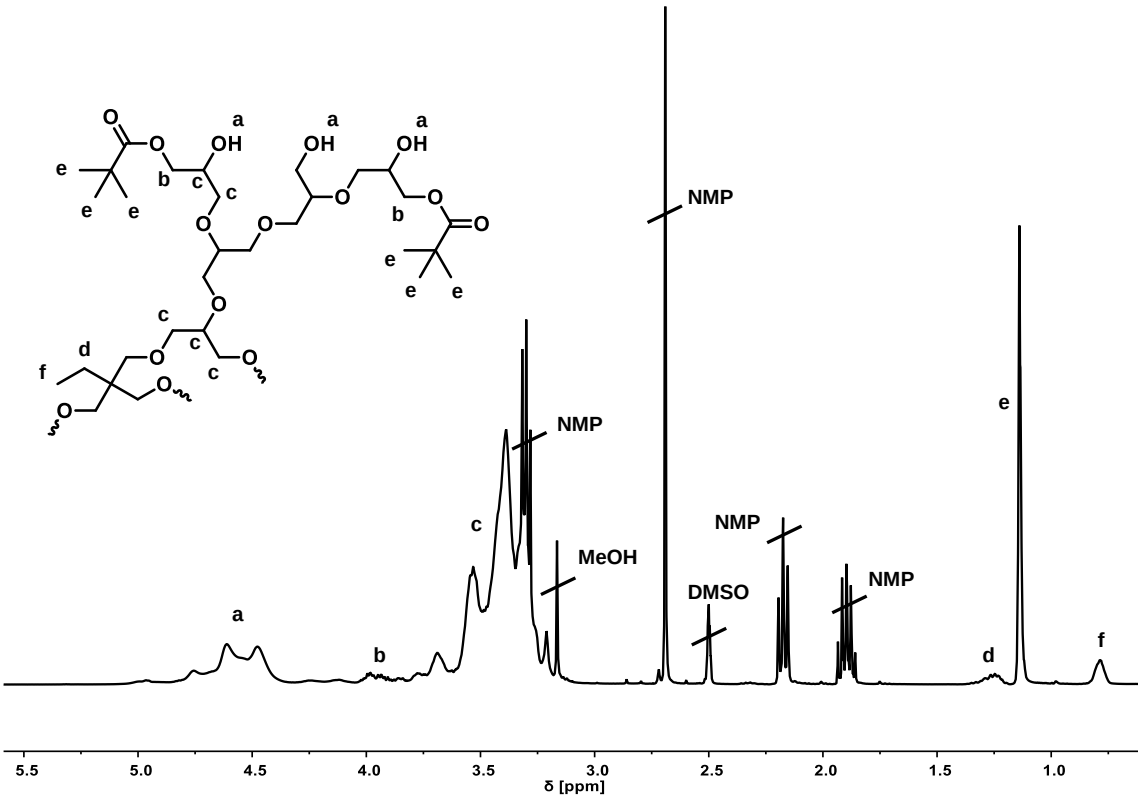

Figure S 12. ^{1}H NMR spectrum of *hb*P($G_{0.94}$-*co*-GlyPiv$_{0.06}$) (400 MHz, DMSO-d_6).

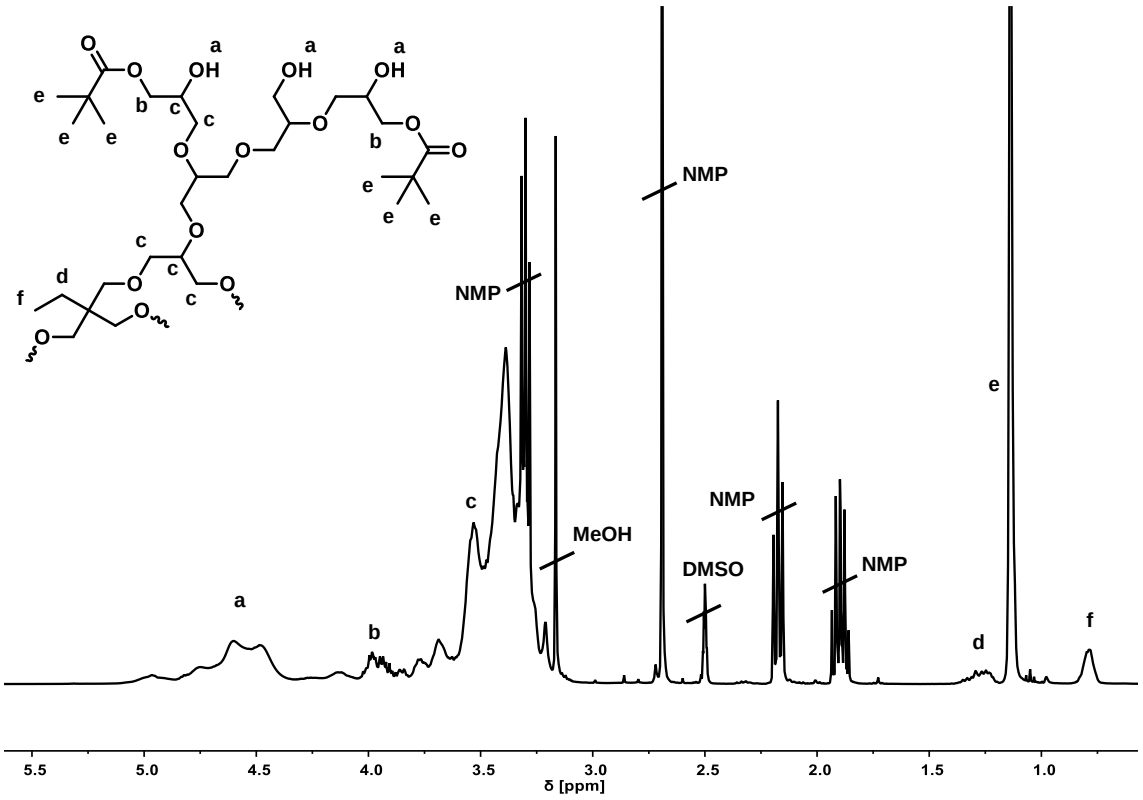

Figure S 13. ^{1}H NMR spectrum of *hb*P($G_{0.88}$-*co*-GlyPiv$_{0.12}$) (400 MHz, DMSO-d_6).

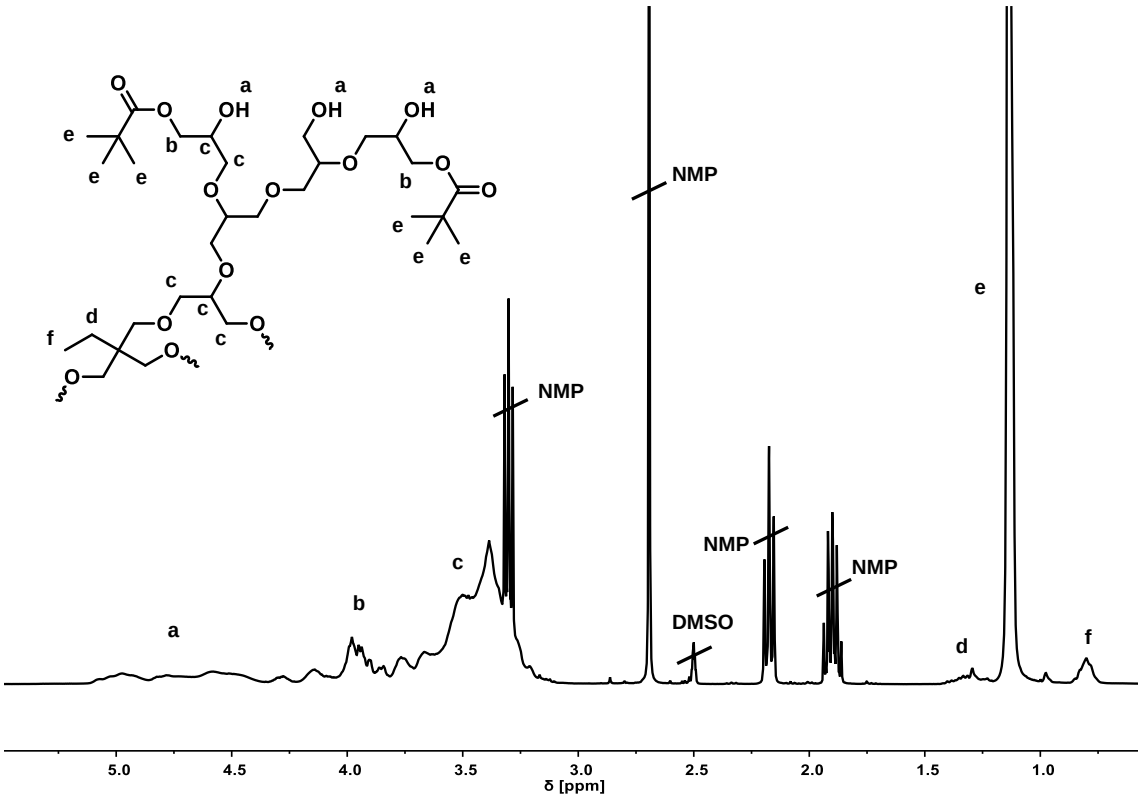

Figure S 14. ^{1}H NMR spectrum of *hb*P($G_{0.63}$-*co*-GlyPiv$_{0.37}$) (400 MHz, DMSO-d_6).

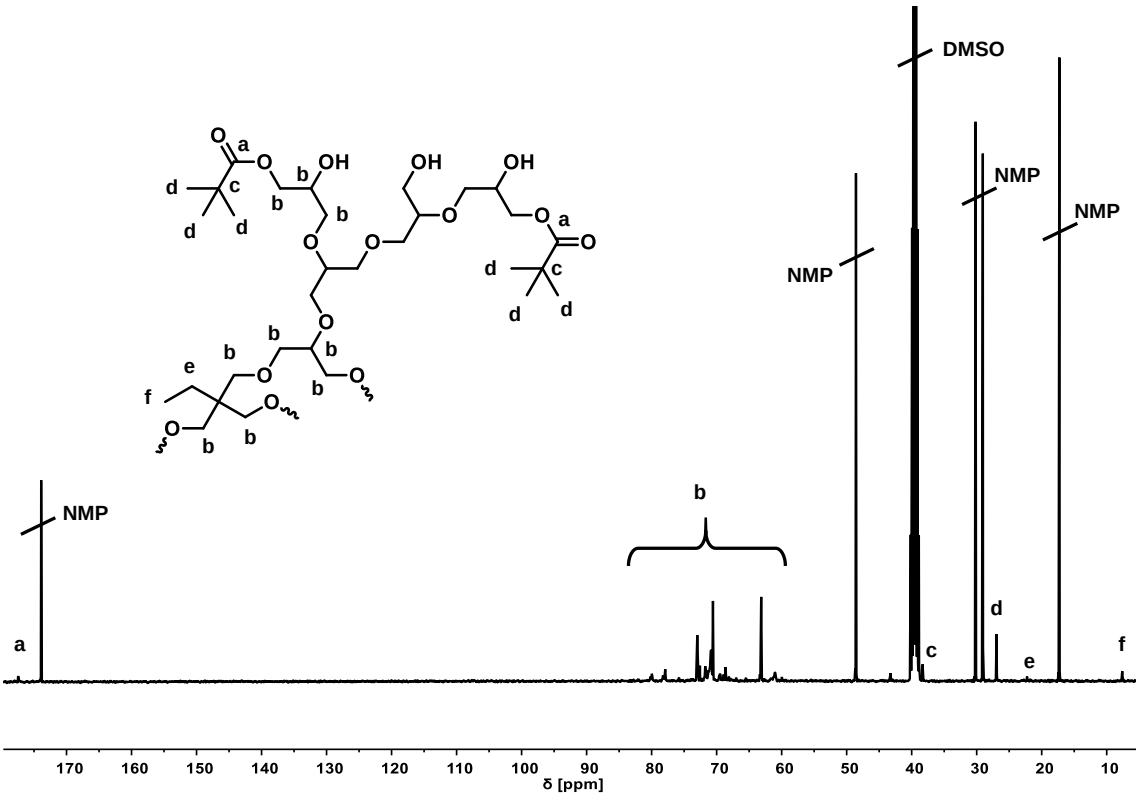

Figure S 15. ^{13}C NMR spectrum of *hb*P($G_{0.97}$-*co*-GlyPiv$_{0.03}$) (100 MHz, DMSO-d_6).

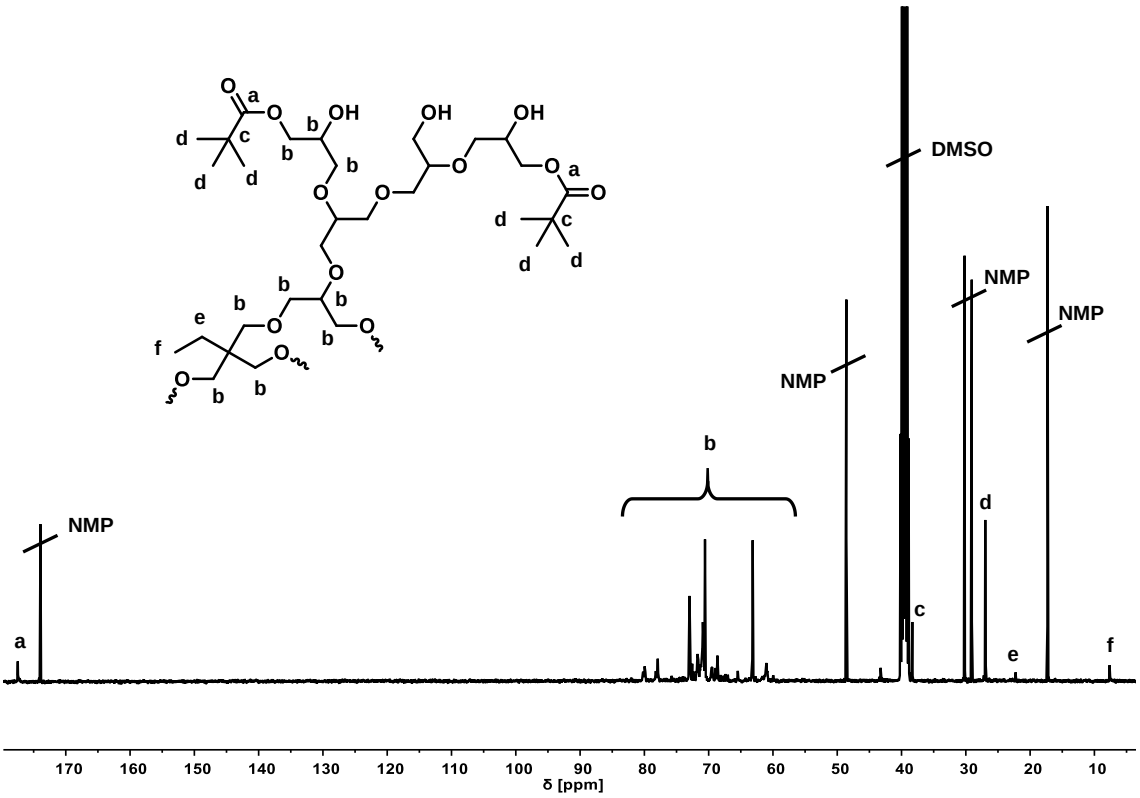

Figure S 16. ^{13}C NMR spectrum of *hb*P($G_{0.94}$-*co*-GlyPiv$_{0.06}$) (100 MHz, DMSO-d_6).

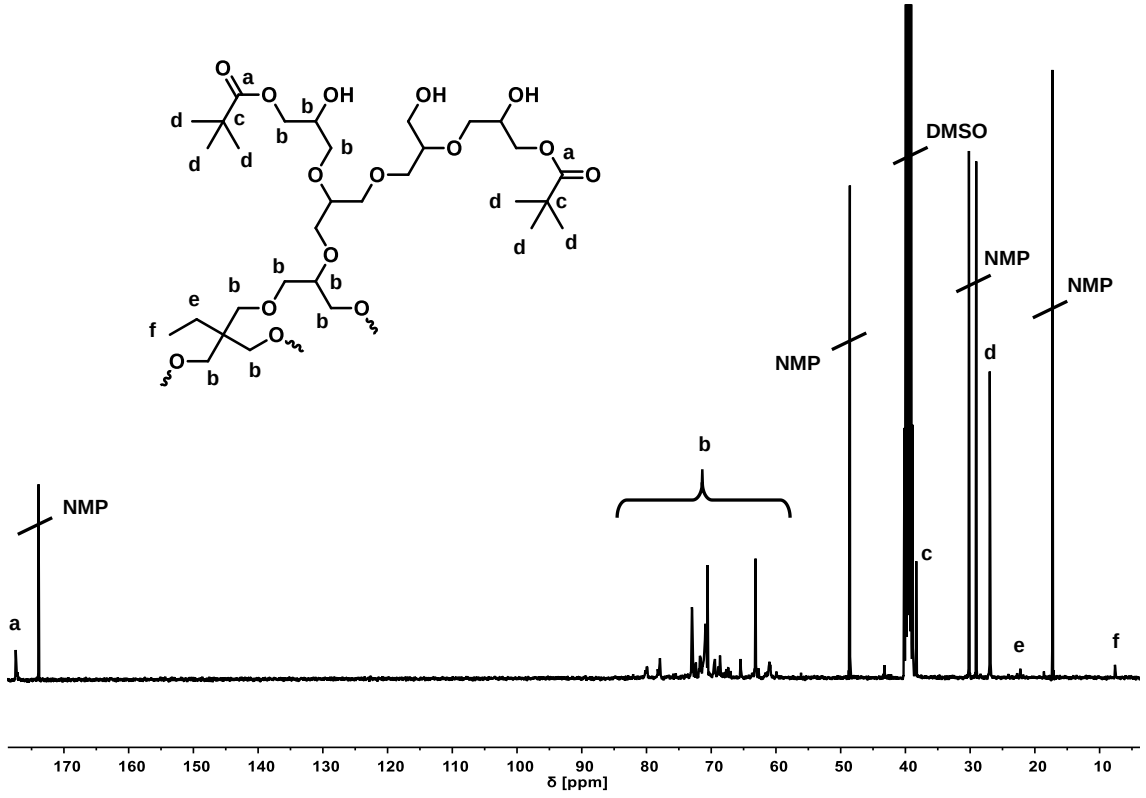

Figure S 17. ^{13}C NMR spectrum of *hb*P($G_{0.88}$-*co*-GlyPiv$_{0.12}$) (100 MHz, DMSO-d_6).

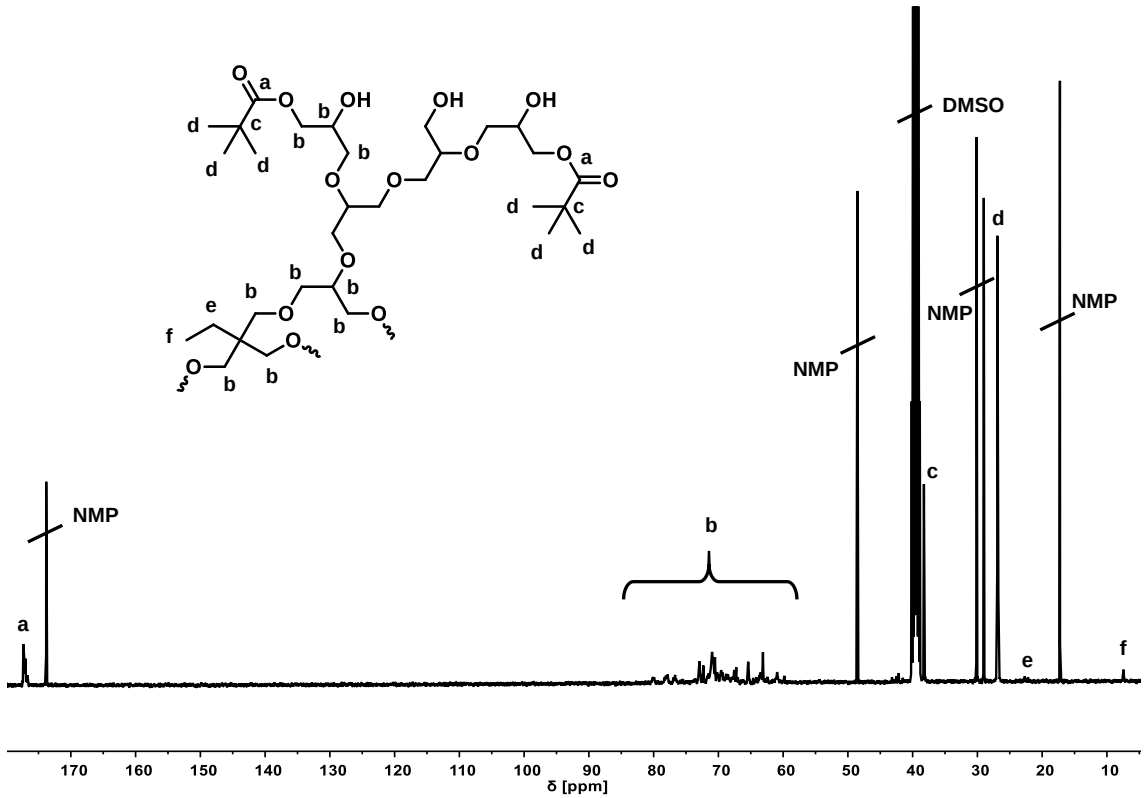

Figure S 18. ^{13}C NMR spectrum of *hb*P($G_{0.63}$-*co*-GlyPiv$_{0.37}$) (100 MHz, DMSO-d_6).

Calculation of the Degrees of Branching

Calculation of the Degree of Branching according to Frey and coworkers under ideal SMA and batch conditions)no side-reactions, full conversion).[18,28]

$$DB^{SMA} = \frac{2\,(1- X_{AB})}{3 - 2\,X_{AB}} \qquad \text{S 1}$$

$$DB^{Batch} = 2\,\frac{r + 1}{(r + 2)^2}\; r = \frac{X_{GlyPiv}}{X_{Glycidol}} \qquad \text{S 2}$$

Table S 1. DP_n, X_{GlyPiv} and DB of the hbP(G-co-GlyPiv) copolymers.

Sample[a)]	**DP_n**[b)]	**X_{GlyPiv}**[b)]	**DB**[c)]	**DB**[d)]	**DB**[e)]
*hb*P($G_{0.97}$-*co*-$GlyPiv_{0.03}$)	24	3	0.53	0.50	0.65
*hb*P($G_{0.94}$-*co*-$GlyPiv_{0.06}$)	25	6	0.50	0.50	0.65
*hb*P($G_{0.88}$-*co*-$GlyPiv_{0.12}$)	24	12	0.50	0.50	0.64
*hb*P($G_{0.80}$-*co*-$GlyPiv_{0.20}$)	23	20	0.52	0.49	0.61
*hb*P($G_{0.63}$-*co*-$GlyPiv_{0.37}$)	19	37	0.47	0.47	0.56

[a)]Terminology: indices denote the copolymer composition determined by ^{1}H NMR spectroscopy, [b)]determined by ^{1}H NMR spectroscopy, [c)]determined ^{13}C NMR spectroscopy, [d)]theoretical values under ideal batch conditions using X_{GlyPiv}, [e)]theoretical values under ideal SMA conditions.

Supplemental FTIR Spectroscopy

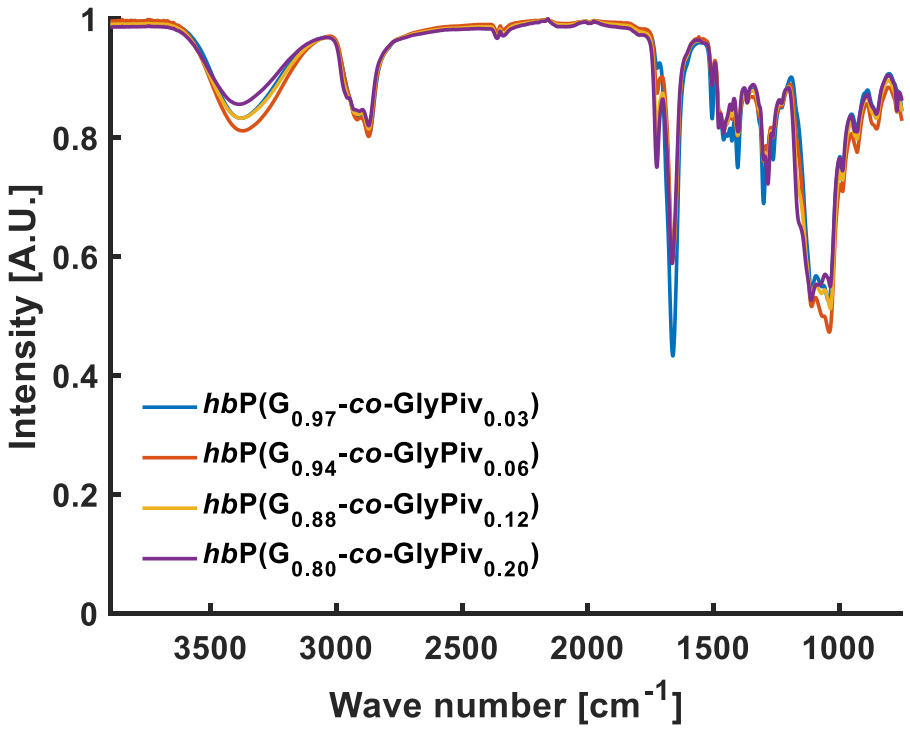

Figure S 19. FTIR spectra of *hb*P($G_{0.97}$-*co*-$GlyPiv_{0.03}$), *hb*P($G_{0.94}$-*co*-$GlyPiv_{0.06}$), *hb*P($G_{0.88}$-*co*-$GlyPiv_{0.12}$) and *hb*P($G_{0.80}$-*co*-$GlyPiv_{0.20}$).

3.3 Synthesis of Unimolecular Nanocapsules by Partial Esterification of Hyperbranched Poly(ethylene oxide)

Tobias Kaiser[a], Jessica Emsermann[a], Jasmin Preis[b], Holger Frey[a,]*

[a]Department of Chemistry, Johannes Gutenberg University, 55128 Mainz, Germany

[b]PSS Polymer Standards Service GmbH, In der Dalheimer Wiese 5, 55120 Mainz, Germany

To be submitted.

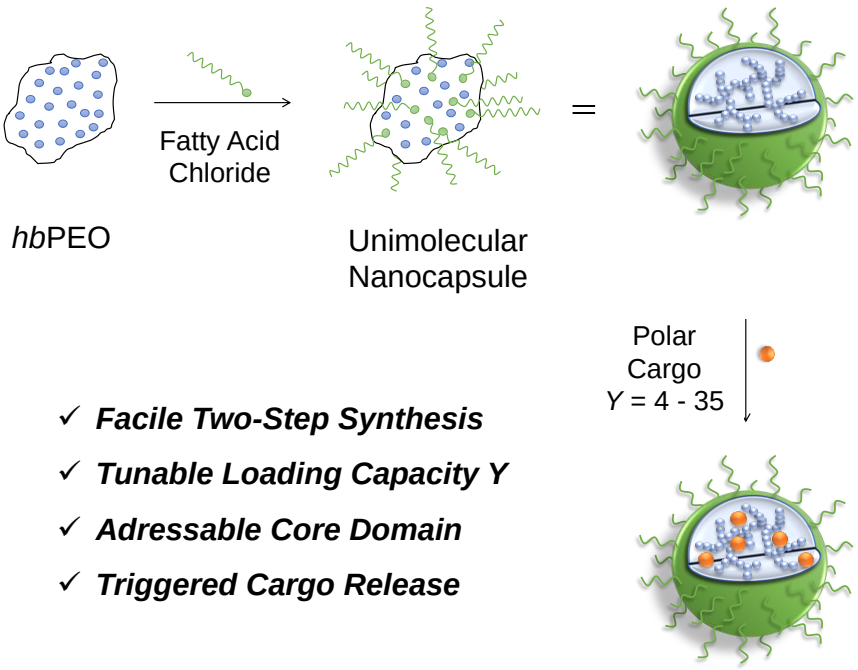

Abstract

The synthesis of unimolecular nanocapsules based on hyperbranched poly(ethylene oxide) (*hb*PEO) is reported. Two *hb*PEO copolymers were prepared by direct anionic copolymerization of glycidol and ethylene oxide in a single batch. Utilizing 1,4-dioxane as solvent, molar masses of 374 000 and 438 000 g mol^{-1} with moderate dispersities as determined by universally calibrated SEC were obtained. The glycidol content varied between 0.34 and 0.45 and was confirmed by ^{13}C NMR spectroscopy. Consequently, degrees of branching (DB) between 0.38 and 0.45 and total numbers of functional groups (#OH) between 1700 and 2600 were calculated. Following an Einhorn methodology, degrees of functionalization α of 0.25 and 1.00 were achieved by esterification of the hydroxy groups with either lauroyl chloride (C12) or oleoyl chloride (C18) as observed by ^{1}H NMR and FTIR spectroscopy. The phase-transfer behavior of the unimolecular nanocapsules was investigated by the solubilization of the hydrophilic dye congo red in chloroform and quantified by UV-Vis spectroscopy. The average loading capacities Y varied from 4 to 35 subject to the degree of functionalization α, alkyl chain length and molar mass of the micellar core domain.

Introduction

Amphiphilic core-shell structures based on dendrimers and dendritic polymers show properties usually associated with micelles, i.e. unimolecular micelles.[1] These nanocapsules are stable upon dilution and applying sheer forces, whereas polymeric micelles dissociate into free polymer chains when diluted below the critical micelle concentration (CMC).[2] However, the synthesis of dendrimers is a

tedious generation-wise process.[3] Hyperbranched polymers (HBP) are a type of polymer architecture formally derived from dendrimers. They combine the properties of dendrimers, i.e. a large number of functional groups, a relatively compact structure and molecular cavities due to branching, with a simple one-pot synthesis.[4] However, linear defects are introduced in contrast to the perfectly branched dendrimers. Due to these defects, the functional groups are distributed randomly throughout their globular structure.[5,6]

As a prominent example of the controlled synthesis of hyperbranched polymers, hyperbranched polyether polyols are typically prepared by the anionic ring-opening polymerization of glycidol. In this case the total number of functional groups directly correlates to the degree of polymerization of glycidol.[7–9] Several approaches to amphiphilic core-shell structures in a simple two-step manner have been reported. The derivatization of the high number of functional hydroxy end groups can be achieved esterification with various fatty acid chlorides, acetalization or the reaction with epoxide-functional long alkyl chains.[10–13] Unimolecular nanocapsules obtained by derivatization of hyperbranched polyglycerol show intriguing properties, e.g. encapsulation and phase-transfer of small molecules, resulting in a wide range of possible applications in the fields of catalysis, drug delivery and other medical applications.[14–21] Since Garamus *et al.* could show that these architectures feature no aggregation in dilute solutions,[22] the phase-transfer properties of these reverse unimolecular nanocapsules are solely attributed to the unique amphiphilic core-shell structure. Furthermore, comparative studies showed no phase-transfer behavior of similar linear polymers.[23,24] Due to the random distribution of the functional groups throughout the polymer, hydroxy groups are still present in the core domain after functionalization. As a consequence, these

hydroxy groups facilitate the encapsulation by hydrogen bonding to the hydrophilic cargo molecule.[25] The loading capacity of such unimolecular nanocapsules largely depends on the size of the core domain.[12] Several methods have been discussed in literature in order to increase the size of hyperbranched core domain, represented by the hydrodynamic radius.[5,6] Utilizing different types of solvents leads to an increase of the molar mass whereas random copolymerization of glycidol with linear AB type monomers decreases DB, both resulting in an enhanced hydrodynamic radius[26–28]

Our group has recently introduced a number of hyperbranched polyether polyol analogues of commonly used linear poly(alkylene oxides).[29–31] Due to the random incorporation, excellent water-solubility and good biocompatibility, hyperbranched copolymers of glycidol and ethylene oxide are of particular interest among these.[29,32] By the introduction of strictly linear AB units into the hyperbranched polymer backbone the degree of branching is significantly reduced leading to less compact structures.[28,33]

Here, we present the synthesis of unimolecular nanocapsules based on hyperbranched poly(ethylene oxide) copolymers *via* a simple two-step process. First, the hyperbranched polyether polyols were synthesized by direct anionic copolymerization of ethylene oxide and glycidol. Subsequently, the copolymers were esterified by using either lauroyl or oleoyl chloride to yield amphiphilic core-shell structures, whose phase-transfer properties allow for the encapsulation of a high number of hydrophilic guest molecules.

Experimental Section

Materials

All materials were purchased from Sigma Aldrich, TCI chemicals, VWR chemicals, Fisher Scientific and Deutero. Glycidol (96 %) and 1,4-dioxane were dried over calcium hydride and distilled under reduced pressure before use. Ethylene oxide was used without further purification. Prior to use, lauroyl chloride and oleoyl chloride were distilled under reduced pressure.

Measurements

NMR spectroscopy: ^{1}H NMR spectra were either recorded on a Bruker Avance III HD 300 (5 mm BBFO-SmartProbe with z-gradient and ATM) at 300 MHz or on a Bruker Avance II HD 400 (5 mm BBFO-SmartProbe with z-gradient and ATM) at 400 MHz. Inverse gated ^{13}C NMR spectra were recorded on a Bruker Avance II HD 400 (5 mm BBFO-SmartProbe with z-gradient and ATM) at 100 MHz. The residual signals of the deuterated solvent were utilized as an internal reference.

Size-exclusion chromatography (SEC). SEC measurements in DMF (containing 0.25 g L^{-1} of lithium bromide) were performed using an integrated Agilent 1100 series instrument, equipped with a PSS HEMA column combination ($10^6/10^4/10^2$ Å porosity), UV and RI detector. Calibration is based on linear poly (ethylene oxide) standards (Polymer Standards Service).

SEC with integrated viscosity measurements were performed in DMF (containing 5 g L^{-1} lithium bromide) employing a PSS GRAM column combination (10/300/300 Å porosity), an Agilent MDS refractive index detector and an Agilent MDS

viscometer. The calibration is based on linear poly (methyl methacrylate) standards (Polymer Standards Service), molar mass averages were calculated *via* universal calibration.

Fourier-transform infrared spectroscopy (FTIR). FTIR measurements were performed using a Nicolet iS10 FTIR spectrometer (Thermo Fisher Scientific) equipped with diamond ATR sample holder.

Ultraviolet-visible spectroscopy (UV-Vis). UV-Vis spectroscopy was conducted using a JASCO V-630 UV-Vis spectrophotometer. Absorption was measured from 400 to 700 nm (400 nm min^{-1}) at 25 °C after dark and baseline correction.

Synthesis of the *hb*PEO polymers

A two-neck flask equipped with a septum, Teflon seal and magnetic stirrer was connected to a vacuum line. 44 mg (0.3 mmol, 1 eq) of trimethylolpropane (TMP) was mixed with a solution of 11 mg (0.1 mmol, 0.3 eq) potassium tert-butoxide in 1 mL methanol to partially deprotonate the initiator. After the addition of 5 mL benzene and stirring of the resulting emulsion, the flask was evacuated over night to remove traces of water and other volatile compounds. To dissolve the initiator salt, 20 mL 1,4-dioxane were added. After the introduction of glycidol through the septum *via* cannula, gaseous ethylene oxide was transferred to the reaction flask under vacuum. Afterwards, the reaction mixture was immediately heated to 80 °C and stirred for 24 h. After completion of the reaction, the solution was diluted by the addition of methanol and neutralized by filtration over an acidic ion exchange resin (DOWEX® 50WX8). The crude copolymers were precipitated in cold diethyl

ether and subsequently dialyzed in methanol (MWCO = 3500 g mol^{-1}) to yield *hb*PEO as highly viscous brownish oils.

^{1}H NMR (DMSO-d_6, 400 MHz): δ (ppm) = 4.76 – 4.35 (m, br, -O<u>H</u>), 3.90 – 3.15 (m, -O-C<u>H</u>-, -O-C<u>H_2</u>-), 1.36 – 1.18 (m, 2H, -C<u>H_2</u>-CH_3 (TMP)), 0.87 – 0.75 (m, 3H, -CH_2-C<u>H_3</u> (TMP)).

^{13}C NMR (DMSO-d_6, 100 MHz): δ (ppm) = 80.25 – 79.45 ($L_{1,3G}$), 78.52 – 77.42 (D_G), 73.22 – 72.10 ($L_{1,4G}$), 72.04 – 69.62 (D_G, L_E, T_E, 2 T_G), 69.61 – 68.37 ($L_{1,3G}$, $L_{1,4G}$), 63.39 – 62.96 (T_G), 60.87 – 60.07 (T_E, $L_{1,3G}$).

FTIR: $\tilde{\nu}$ (cm^{-1}) = 3470 (-OH), 1100 (C-O-C).

Esterification

A solution of 200 mg of the hyperbranched polyether polyol in 2 mL methanol was transferred to a round bottom flask and mixed with 3 mL of benzene. The polymer was dried *in vacuo* overnight at room temperature. Afterwards, 20 mL pyridine were added under inert gas atmosphere and the solution was cooled to 0 °C. The fatty acid chloride (0.25 or 1.1 eq) was added dropwise and the resulting mixture was stirred over night at room temperature. After the addition of potassium carbonate (1.1 eq regarding the fatty acid chloride) and stirring for 30 minutes, precipitated solids were removed by filtration and pyridine was removed azeotropically *in vacuo* using toluene. The crude product was dialyzed in chloroform (benzoylated cellulose, MWCO = 2000 g mol^{-1}) to yield the products as pale yellow to brown waxes.

Lauroyl chloride: ^{1}H NMR (DMSO-d_6, 300 MHz): δ (ppm) = 4.26 – 4.10 (-C$\underline{H}_2$-OCOR); 3.90 – 3.15 (m, -O-C$\underline{H}$-, -O-C$\underline{H}_2$-); 2.40 - 2.15 (-C$\underline{H}_2$-COO-); 1.80 – 1.40 (-C$\underline{H}_2$-CH$_2$-COO-); 1.40 – 0.90 ((-C$\underline{H}_2$-)$_8$); 1.36 – 1.18 (-C$\underline{H}_2$-CH$_3$ (TMP)); 0.90 – 0.65 (-C$\underline{H}_3$); 0.87 – 0.75 (CH$_2$-C$\underline{H}_3$ (TMP)).

Oleoyl chloride: ^{1}H NMR (DMSO-d_6, 300 MHz): δ (ppm) = 5.43 – 5.20 (-C$\underline{H}$=C$\underline{H}$-); 4.26 – 4.10 (-C$\underline{H}_2$-OCOR); 3.90 – 3.15 (m, -O-C$\underline{H}$-, -O-C$\underline{H}_2$-); 2.45 - 2.20 (-C$\underline{H}_2$-COO-); 2.11 – 1.91 (-C$\underline{H}_2$-CH=CH-C$\underline{H}_2$-)); 1.72 – 1.50 (-C$\underline{H}_2$-CH$_2$-COO-); 1.42 – 1.11 ((-C$\underline{H}_2$-)$_4$, (-C$\underline{H}_2$-)$_6$); 0.94 – 0.74 (-C$\underline{H}_3$).

FTIR: $\tilde{\nu}$ (cm^{-1}) = 1100 vs (C-O), 1377 w (-CH$_3$ def), 1736 m (C=O), 3470 w, br (-OH).

Results and Discussion

Various unimolecular nanocapsules were prepared by esterification of two *hb*PEO copolymers with different fatty acid chlorides (Scheme 1).[34] First, two hyperbranched polyether polyols (*hb*PEO$_{0.34}$ and *hb*PEO$_{0.45}$) were synthesized *via* direct copolymerization of ethylene oxide and glycidol in 1,4-dioxane according to literature, resulting in high molar masses of 374.000 and 438.000 g mol^{-1} and glycidol contents of 0.34 and 0.45, respectively.[27,29,33] After full conversion of the gaseous monomer ethylene oxide the polymerization was terminated by the addition of an excess of methanol. Following neutralization, the polymers were isolated by precipitation in cold diethyl ether. Subsequently, either lauroyl chloride (*C12*) or oleoyl chloride (C18) were employed in different ratios to investigate the effect of the alkyl chain-length, the degree of functionalization and the molar mass of the core domain on the encapsulation and solubilization properties of the resulting nanocapsules.

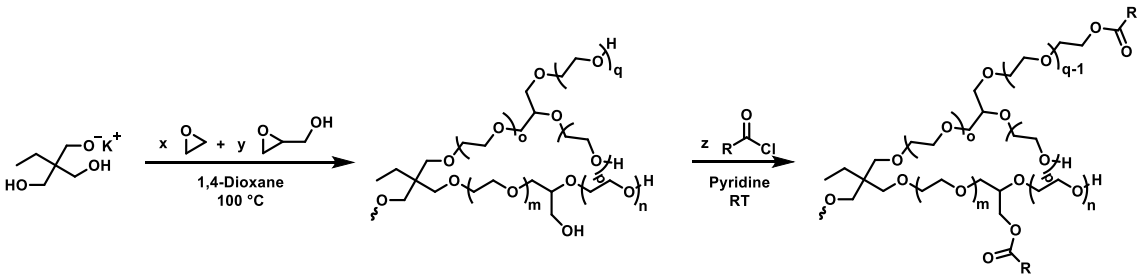

Scheme 1. Schematic synthesis of unimolecular nanocapsules in two steps by partial esterification of hyperbranched poly(ethylene oxide) copolymers.

Table 1 presents the most relevant analytical data of both hyperbranched poly(ethylene oxide) copolymers used in this study. The corresponding SEC traces and NMR spectra are found in the supporting information (cf. Figure S 1 to Figure S 6).

Table 1. SEC and ^{13}C NMR data of *hb*PEO$_{0.45}$ and *hb*PEO$_{0.34}$.

Sample[a)]	M_n[b)] [g mol^{-1}]	Đ[b)]	M_n[c)] [g mol^{-1}]	Đ[c)]	X_G[d)]	DB[d)]	#OH[e)]
*hb*PEO$_{0.45}$	47000	1.25	438 000	2.08	0.45	0.45	2600
*hb*PEO$_{0.34}$	73000	1.26	374 000	2.52	0.34	0.38	1700

[a)]Terminology: indices denote the glycidol content determined by ^{13}C NMR spectroscopy, [b)]determined by SEC (DMF, linear PEO standards), [c)]determined by universally calibrated SEC (DMF, 70 °C, linear PMMA standards), [d)]determined by ^{13}C NMR spectroscopy, [e)]calculated using equation 1.

Typically, the molar masses of hyperbranched poly(ethylene oxide) copolymers determined by conventional SEC analysis are underestimated due to their compact structure resulting in a smaller hydrodynamic volume as compared to their linear analogues.[33] Nevertheless, the polymers exhibit monomodal distribution with low dispersities. Universally calibrated SEC *via* on-line viscosimetry yielded more accurate values, ranging from 374 000 to 438 000 g mol^{-1}. For further insight into the polymer architecture, including copolymer composition and degree of branching, ^{1}H and ^{13}C NMR analysis is generally more suited. Figure S 3 to Figure S 6 show the ^{1}H and ^{13}C NMR spectra of *hb*PEO$_{0.45}$ and *hb*PEO$_{0.34}$ as well as the signal assignment according to literature.[29] This can be used to calculate the glycidol content as well as the degree of branching (see equation S 1, supporting information). Furthermore, as each glycidol repeating unit introduces exactly one additional hydroxy group into the polymer, the total number #OH can be calculated according to equation 1:

$$\#OH = f_{Initiator} + \frac{M_n \cdot [G]}{M_G} = 3 + \frac{M_n \cdot [G]}{M_G} \quad (1)$$

Consequently, both polymers vary in absolute molar mass and comonomer content, leading to different total numbers of addressable hydroxy groups per polymer, i.e. 1700 and 2600.

In a second step, the hydroxy groups were either partially or quantitatively esterified using lauroyl chloride (C12) or oleoyl chloride (C18) in pyridine.[34] Table 2 gives a brief overview of the esters studied in this work. Using different ratios of the fatty acid chlorides to the hydroxy groups, degrees of functionalization α of 0.25 or 1.00 were targeted.

Table 2. Degrees of functionalization and molar masses of the esters based on *hb*$PEO_{0.45}$ and *hb*$PEO_{0.34}$.

Entry	Sample[a)]	α[b)]	M_n[c)] [kg mol^{-1}]
1	*hb*$PEO_{0.45}$-$C12_{0.26}$	0.26	567
2	*hb*$PEO_{0.45}$-$C12_{1.00}$	1.00	928
3	*hb*$PEO_{0.34}$-$C12_{0.23}$	0.23	445
4	*hb*$PEO_{0.34}$-$C12_{0.95}$	0.95	667
5	*hb*$PEO_{0.34}$-$C18_{1.00}$	1.00	822

[a)]Terminology *hb*PEO_x-CY_z: x = glycidol content determined from IG ^{13}C NMR spectroscopy, y = chain-length of corresponding fatty acid, z = degree of functionalization, [b)]Estimation based on the reaction feed, [c)]calculated using absolute molar masses and estimated degrees of functionalization α.

Figure 1 shows the ^{1}H NMR spectrum of *hb*PEO$_{0.34}$ after quantitative functionalization with C18 (Table 2, sample 6). The signals of the polyether backbone and the oleic acid chain are easily distinguishable: the olefinic signals of the fatty acid (5.43 – 5.20 ppm, g), the methylene and methine groups of the polyether backbone (4.26 – 3.15 ppm, signal f and polyether backbone) and the remaining hydrocarbon signals of the fatty acid (2.45 – 0.74 ppm, a - e).

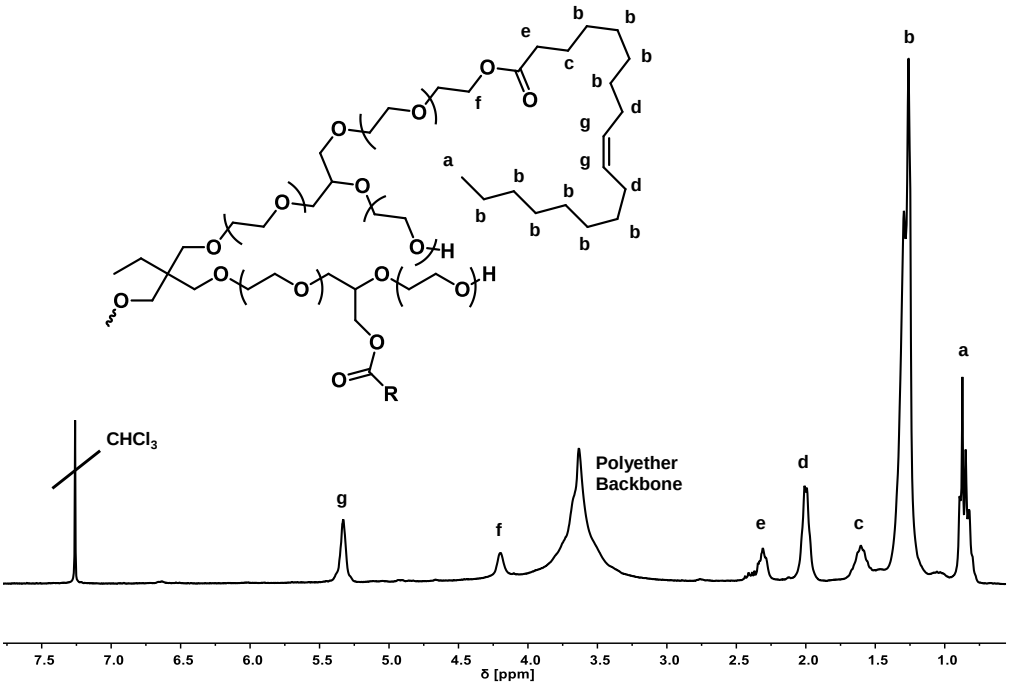

Figure 1. ^{1}H NMR spectrum of *hb*PEO$_{0.34}$-C18$_{1.00}$ (300 MHz, $CDCl_3$).

Interestingly, as the olefinic signals of C18 (g) are still observed, subsequent functionalization reactions of the hydrophobic shell domain are feasible. For instance, to improve the long-term stability of the unimolecular micelles, the oleic acid moieties could be crosslinked by radical or other mechanisms.[35] Furthermore, only the signal of the methylene groups adjacent to primary hydroxy groups (Figure S 6, T_G, T_E and $L_{1,3G}$ units) has shifted downfield upon esterification (Figure 1, signal f).[36] Signals corresponding to esterified secondary hydroxy groups (Figure

S 6, T_G and $L_{1.4G}$ units) are not observed owing to the high abundance of ethylene oxide units (X_{EO} = 0.66). The determination of the degree of functionalization by ^{1}H NMR spectroscopy proved impracticable due to poor signal resolution of the hydroxy groups in $CDCl_3$. Consequently, only the theoretically targeted values of α molar masses are summarized in Table 2.

To investigate quantitative functionalization, a FTIR spectrum of both *hb*PEO (blue) and the corresponding ester (orange) was recorded (Figure 2): after the reaction with an excess of acid halide, the band of the hydroxy group (3400 cm^{-1}) is reduced in intensity to a weak residual signal, whereas the introduction of the carbonyl band (1736 cm^{-1}) proves the formation of the ester moieties. This observation is in accordance with the prior discussion concerning NMR spectroscopy.

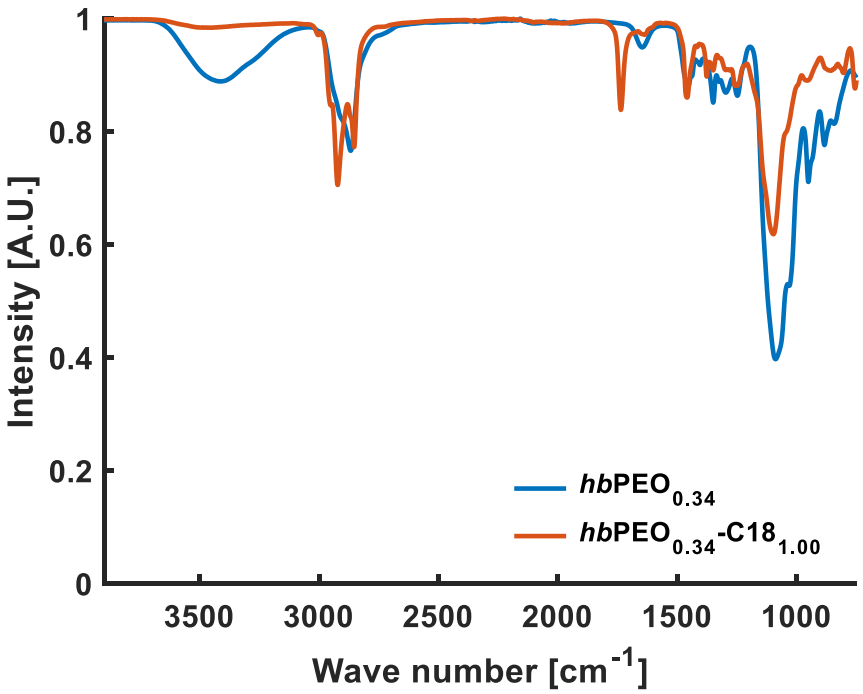

Figure 2. FTIR spectrum of *hb*$PEO_{0.34}$ and *hb*$PEO_{0.34}$-$C18_{1.00}$.

In analogy to similar structures based on *hb*PG, the esterified hyperbranched poly(ethylene oxide) copolymers are expected to act as amphiphilic unimolecular

nanocapsules, possessing the ability to encapsulate and solubilize small hydrophilic guest, e.g. water-soluble dyes. To investigate the phase transfer behavior, a 0.01 wt% solution of the polymer in chloroform was mixed with aqueous solutions of congo red of varying concentrations and agitated briefly. Figure 3 depicts the resulting mixtures after phase-separation.

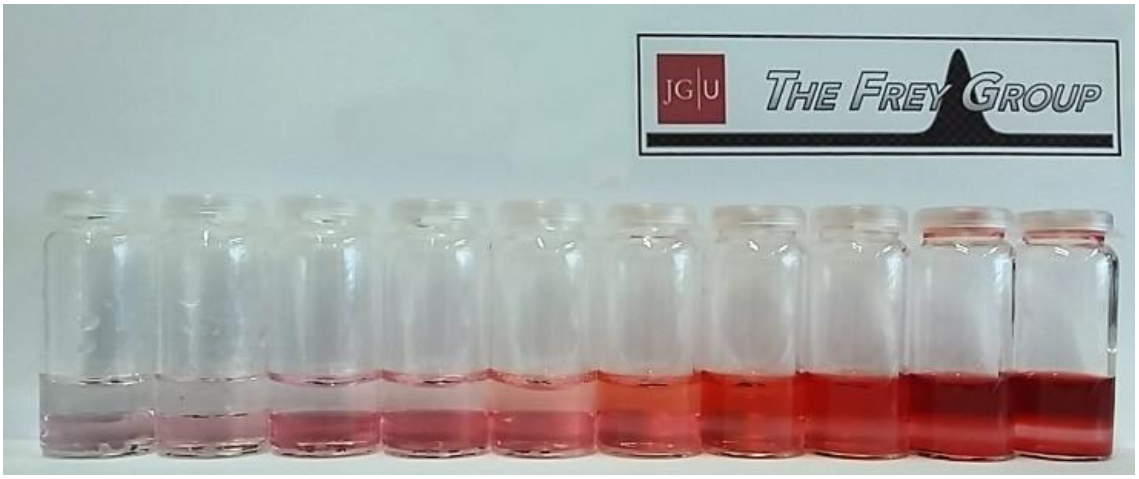

Figure 3. Phase transfer of congo red from aqueous solution (top layer) to chloroform (bottom layer) containing *hb*$PEO_{0.34}$-$C18_{1.00}$ (c = 0.01 wt%). The concentration of congo red in the aqueous layer increases from left to right.

The coloring of the organic layer (bottom) confirms the extraction and hence phase-transfer of the highly hydrophilic dye, which is otherwise insoluble in chloroform and other common organic solvents. After phase separation, the organic phase was investigated by UV-Vis spectroscopy to determine the dye concentration (Figure 4, left). Regardless of the polymer structure (molecular weight, glycidol content or degree of functionalization) the color intensity of the organic phase increased sharply with higher dye concentrations in the aqueous phase. Furthermore, saturation of the organic phase occurred above a certain concentration due to the spatial confinement of the core domain (see the rightmost vials in Figure 3 and Figure 4). Below the saturation point, congo red is almost

quantitatively extracted from the aqueous phase into the chloroform layer (see Figure 3, leftmost vials).

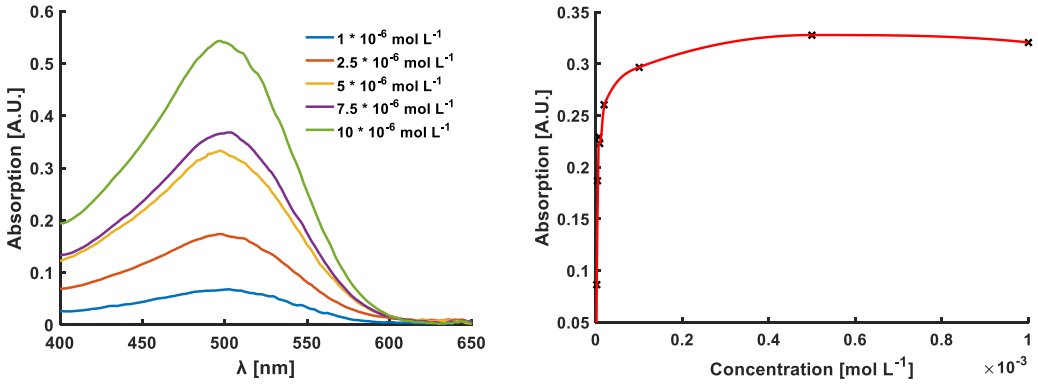

Figure 4. UV-Vis absorption spectra (λ = 400 – 650 nm) of *hb*PEO$_{0.34}$-C18-$_{1.00}$ in chloroform (c = 0.01 wt%) after mixing with aqueous solutions of congo red with increasing concentration (left); Absorption at λ = 495 nm (A_{495nm}) of the organic phases plotted against the concentration of congo red in the aqueous phase.

The average number of dye molecules per nanocapsules (loading capacity Y) can be calculated by comparing the concentration of dye c_{Dye} in the organic phase to the concentration of unimolecular nanocapsules $c_{Nanocapsule}$ (equation 2.1).

$$Y = \frac{c_{Dye}}{c_{Nanocapsule}} \qquad 2.1$$

Therefore, a calibration curve was prepared to correlate the absorption of the dye solution the corresponding concentration (see Figure S 13 and Figure S 14). Under the assumption that the absorption of the dye congo red is unaffected by encapsulation, the slope m of the resulting linear graph can be used to calculate the number of guest molecules using equation 2.2. The absorption A at λ = 495 nm was used for all further calculations to ensure consistency, as the UV-Vis spectra of the aqueous dye solutions of congo red showed the highest absorption at this particular wavelength.

$$Y = \frac{A_{495} \cdot M_n}{m \cdot w \cdot \rho_{CHCl3}} \qquad 2.2$$

Table 3 summarizes the results of the UV-Vis measurements and resulting calculations. The comparison of entries 1 and 3 as well 4 and 5 shows higher loading capacities Y with increasing degrees of functionalization.[12] Additionally, the loading capacity is enhanced by a bigger size of the core domain of the nanocapsule, i.e. higher molar mass of the hyperbranched poly(ethylene oxide) copolymer at a constant degree of functionalization (entries 1 and 4 as well 3 and 5).

Table 3. Absorption A_{495} (λ = 495 nm)) and loading capacity Y of the unimolecular nanocapsules based on *hb*$PEO_{0.45}$ and *hb*$PEO_{0.34}$.

Sample	Name[a)]	α[b)]	M_n[c)] [kg mol^{-1}]	A_{495} [A.U.]	Y[d)]
1	*hb*$PEO_{0.45}$-$C12_{0.26}$	0.26	567	0.0547	4.27
3	*hb*$PEO_{0.45}$-$C12_{1.00}$	1.00	928	0.1149	14.66
4	*hb*$PEO_{0.34}$-$C12_{0.23}$	0.23	445	0.0258	1.58
5	*hb*$PEO_{0.34}$-$C12_{0.95}$	0.95	667	0.0500	4.59
6	*hb*$PEO_{0.34}$-$C18_{1.00}$	1.00	822	0.3125	35.33

[a)]Terminology *hb*PEO_x-CY_z: x = glycidol content determined from IG ^{13}C NMR spectroscopy, y = chain-length of corresponding fatty acid, z = degree of functionali-zation, [b)]Estimation based on reaction feed, [c)]calculation using absolute molar masses and estimated degrees of functionalization, [d)]calculated using equation 2.

The influence of the alkyl chain length is illustrated by entries 5 and 6, showing that more dye molecules are incorporated the longer the chain is. Interestingly, for

*hb*PEO$_{0.34}$-C18$_{1.00}$ the loading capacity is more than seven times higher than *hb*PEO$_{0.34}$-C12$_{0.95}$, although the difference in alkyl chain length is rather marginal. More importantly, oleic acid carries a double bond in cis configuration representing a defect in the hydrophobic shell. This defect leads to a less densely packed hydrophobic shell, hence resulting in an easier uptake of the dye molecules. Notably, the dye was only released upon saponification of the ester bonds by reaction with concentrated aqueous NaOH indicating irreversible encapsulation (cf. Figure S 18).

In this study, the molar masses of polyether polyols and the alkyl chain-length were investigated as possible influences on the loading capacity Y. A vastly higher number of guest molecules was achieved by employing high molar mass hyperbranched poly(ethylene oxide) copolymers compared to nanocapsules based on *hb*PG, exhibiting maximum loading capacities between 0.7 and 2.7.[12]

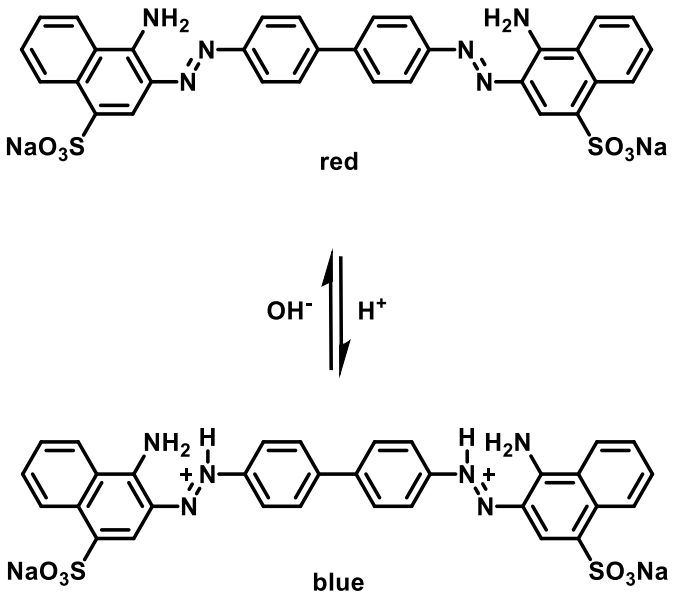

Figure 5. Color Change of congo red resulting from pH changes.

To use these loaded nanocapsules for further applications, the core including the guest molecules needs to be addressable for chemical reactions.[17,18,23,24] As a simple model reaction, the color change of the dye from red to blue at pH 3.0 – 5.2 was investigated (cf. Figure 5). Figure S 19 shows a solution of the dye loaded nanocapsule *hb*PEO$_{0.34}$-C18$_{1.00}$ in chloroform (lower layer) after mixing with aqueous solutions of hydrochloric acid of varying concentrations. With increasing concentration of HCl in the aqueous phase the color of the organic phase changes from red to blue, (left to right vial) clearly indicating the addressability of encapsulated guest molecules for chemical reactions. Therefore, the common applications discussed for unimolecular nanocapsules based on *hb*PG, i.e. as nanoreactors or for spatial confinement of catalysts and preparation of naoparticles,[17–20] can be transferred to the materials reported here. Additionally, unimolecular nanocapsules based on high molar mass *hb*PEO significantly enhance the loading capacity Y. Consequently, the turnover numbers or nanoparticle sizes can be tuned in wider range than before.

Conclusion

Unimolecular nanocapsules prepared by the esterification of the hydroxy groups hyperbranched polyether polyols have been thoroughly investigated in the past. They were used for the encapsulation of hydrophilic cargo, but also as spatially confined nanoreactors for the synthesis of nanoparticles. However, relying on hyperbranched polyglycerol, the size range of these nanocapsules is rather limited. Thus, the resulting average maximum loading ranges from 0.7 to 2.7 congo red molecules per polymer.

Employing high molar mass *hb*PEO polyether polyol cores, these parameters could be enhanced. By direct anionic ring-opening copolymerization of glycidol and ethylene oxide in 1,4-dioxane, two hyperbranched poly(ethylene oxide) copolymers were prepared. High molar masses of 374 000 and 438 000 g mol^{-1} were determined by universally calibrated SEC, while the glycidol contents ranged from 0.34 to 0.45, as shown by inverse-gated ^{13}C NMR spectroscopy. Resulting from different molar masses and compositions, total numbers of 1700 and 2600 hydroxy groups (#OH) were calculated. In a second step, esterification of these groups with lauroyl or oleoyl chloride was achieved to different degrees (α = 0.25 or 100). Maximum loadings between 1.58 and 35.33 were evaluated for varying polymer characteristics (molar mass, #OH, α, chain-length and topology) significantly enhancing values reported for nanocapsules based on *hb*PG. Upon encapsulation, the dyes were still affected by changes of the pH value of the surrounding medium. However, release of the cargo was only observed after basic cleavage of the ester bonds.

These materials show similar behavior as reported by Sunder *et al.* offering the potential for application discussed for *hb*PG while significantly improving the maximum loading Y.

Acknowledgment

T. K. is grateful for financial support by a fellowship from the “Fonds der Chemischen Industrie (FCI)”. Furthermore, the authors thank Monika Schmelzer and Ulrike Kemmer-Jonas for technical assistance.

References

(1) Newkome, G. R.; Moorefield, C. N.; Baker, G. R.; Saunders, M. J.; Grossman, S. H. Unimolecular Micelles. *Angew. Chem. Int. Ed.* **1991**, *30*, 1178–1180.

(2) Riess, G. Micellization of block copolymers. *Prog. Polym. Sci.* **2003**, *28*, 1107–1170.

(3) Fréchet, J. M. J.; Tomalia, D. A. *Dendrimers and other dendritic polymers*; Wiley: Chichester, New York, 2010.

(4) Petkov, V.; Parvanov, V.; Tomalia, D.; Swanson, D.; Bergstrom, D.; Vogt, T. 3D structure of dendritic and hyper-branched macromolecules by X-ray diffraction. *Solid State Communications* **2005**, *134*, 671–675.

(5) Voit, B. I.; Lederer, A. Hyperbranched and highly branched polymer architectures--synthetic strategies and major characterization aspects. *Chem. Rev.* **2009**, *109*, 5924–5973.

(6) Yan, D.; Gao, C.; Frey, H. *Hyperbranched polymers: Synthesis, properties, and applications*; Wiley series on polymer engineering and technology; Wiley: Hoboken, N.J, 2011.

(7) Sunder, A.; Hanselmann, R.; Frey, H.; Mülhaupt, R. Controlled Synthesis of Hyperbranched Polyglycerols by Ring-Opening Multibranching Polymerization. *Macromolecules* **1999**, *32*, 4240–4246.

(8) Schömer, M.; Schüll, C.; Frey, H. Hyperbranched aliphatic polyether polyols. *J. Polym. Sci. A Polym. Chem.* **2013**, *51*, 995–1019.

(9) Herzberger, J.; Niederer, K.; Pohlit, H.; Seiwert, J.; Worm, M.; Wurm, F. R.; Frey, H. Polymerization of Ethylene Oxide, Propylene Oxide, and Other Alkylene Oxides: Synthesis, Novel Polymer Architectures, and Bioconjugation. *Chem. Rev.* **2016**, *116*, 2170–2243.

(10) Haag, R.; Stumbé, J.-F.; Sunder, A.; Frey, H.; Hebel, A. An Approach to Core−Shell-Type Architectures in Hyperbranched Polyglycerols by Selective Chemical Differentiation. *Macromolecules* **2000**, *33*, 8158–8166.

(11) Krämer, M.; Stumbé, J.-F.; Türk, H.; Krause, S.; Komp, A.; Delineau, L.; Prokhorova, S.; Kautz, H.; Haag, R. pH-Responsive Molecular Nanocarriers Based on Dendritic Core-Shell Architectures. *Angew. Chem. Int. Ed.* **2002**, *41*, 4252–4256.

(12) Sunder, A.; Krämer, M.; Hanselmann, R.; Mülhaupt, R.; Frey, H. Molecular Nanocapsules Based on Amphiphilic Hyperbranched Polyglycerols. *Angew. Chem. Int. Ed.* **1999**, *38*, 3552–3555.

(13) Kainthan, R. K.; Janzen, J.; Kizhakkedathu, J. N.; Devine, D. V.; Brooks, D. E. Hydrophobically derivatized hyperbranched polyglycerol as a human serum albumin substitute. *Biomaterials* **2008**, *29*, 1693–1704.

(14) Haag, R. Supramolekulare Wirkstoff-Transportsysteme auf der Basis polymerer Kern-Schale-Architekturen. *Angew. Chem.* **2004**, *116*, 280–284.

(15) Kainthan, R. K.; Mugabe, C.; Burt, H. M.; Brooks, D. E. Unimolecular micelles based on hydrophobically derivatized hyperbranched polyglycerols: ligand binding properties. *Biomacromolecules* **2008**, *9*, 886–895.

(16) Kainthan, R. K.; Brooks, D. E. Unimolecular micelles based on hydrophobically derivatized hyperbranched polyglycerols: biodistribution studies. *Bioconjug. Chem.* **2008**, *19*, 2231–2238.

(17) Stefan Mecking; Ralf Thomann; Holger Frey; Alexander Sunder. Preparation of Catalytically Active Palladium Nanoclusters in Compartments of Amphiphilic Hyperbranched Polyglycerols. *Macromolecules* **2000**, *33*, 3958–3960.

(18) Slagt, M. Q.; Stiriba, S.-E.; Klein Gebbink, R. J. M.; Kautz, H.; Frey, H.; van Koten, G. Encapsulation of Hydrophilic Pincer−Platinum(II) Complexes in Amphiphilic Hyperbranched Polyglycerol Nanocapsules. *Macromolecules* **2002**, *35*, 5734–5737.

(19) Slagt, M. Q.; Stiriba, S.-E.; Kautz, H.; Klein Gebbink, R. J. M.; Frey, H.; van Koten, G. Optically Active Hyperbranched Polyglycerol as Scaffold for Covalent and Noncovalent Immobilization of Platinum(II) NCN-Pincer Complexes. Catalytic Application and Recovery. *Organometallics* **2004**, *23*, 1525–1532.

(20) Chen, Y.; Frey, H.; Thomann, R.; Stiriba, S.-E. Optically active amphiphilic hyperbranched polyglycerols as templates for palladium nanoparticles. *Inorganica Chimica Acta* **2006**, *359*, 1837–1844.

(21) Kurniasih, I. N.; Keilitz, J.; Haag, R. Dendritic nanocarriers based on hyperbranched polymers. *Chem. Soc. Rev.* **2015**, *44*, 4145–4164.

(22) Garamus, V. M.; Maksimova, T. V.; Kautz, H.; Barriau, E.; Frey, H.; Schlotterbeck, U.; Mecking, S.; Richtering, W. Hyperbranched Polymers: Structure of Hyperbranched Polyglycerol and Amphiphilic Poly(glycerol ester)s in Dilute Aqueous and Nonaqueous Solution. *Macromolecules* **2004**, *37*, 8394–8399.

(23) Stiriba, S.-E.; Kautz, H.; Frey, H. Hyperbranched molecular nanocapsules: comparison of the hyperbranched architecture with the perfect linear analogue. *J. Am. Chem. Soc.* **2002**, *124*, 9698–9699.

(24) Kainthan Rajesh Kumar; Donald E. Brooks. Comparison of Hyperbranched and Linear Polyglycidol Unimolecular Reverse Micelles as Nanoreactors and Nanocapsules. *Macromol. Rapid Commun.* **2005**, *26*, 155–159.

(25) Zou, J.; Zhao, Y.; Shi, W. Encapsulation mechanism of molecular nanocarriers based on unimolecular micelle forming dendritic core-shell structural polymers. *J. Phys. Chem. B.* **2006**, *110*, 2638–2642.

(26) Kautz, H.; Sunder, A.; Frey, H. Control of the molecular weight of hyperbranched polyglycerols. *Macromol. Symp.* **2001**, *163*, 67–74.

(27) Kainthan, R. K.; Muliawan, E. B.; Hatzikiriakos, S. G.; Brooks, D. E. Synthesis, Characterization, and Viscoelastic Properties of High Molecular Weight Hyperbranched Polyglycerols. *Macromolecules* **2006**, *39*, 7708–7717.

(28) Frey, H.; Hölter, D. Degree of branching in hyperbranched polymers. 3 Copolymerization of ABm-monomers with AB and ABn-monomers. *Acta Polym.* **1999**, *50*, 67–76.

(29) Wilms, D.; Schömer, M.; Wurm, F.; Hermanns, M. I.; Kirkpatrick, C. J.; Frey, H. Hyperbranched PEG by random copolymerization of ethylene oxide and glycidol. *Macromol. Rapid Commun.* **2010**, *31*, 1811–1815.

(30) Schömer, M.; Seiwert, J.; Frey, H. Hyperbranched Poly(propylene oxide): A Multifunctional Backbone-Thermoresponsive Polyether Polyol Copolymer. *ACS Macro Lett.* **2012**, *1*, 888–891.

(31) Seiwert, J.; Leibig, D.; Kemmer-Jonas, U.; Bauer, M.; Perevyazko, I.; Preis, J.; Frey, H. Hyperbranched Polyols via Copolymerization of 1,2-Butylene Oxide and Glycidol: Comparison of Batch Synthesis and Slow Monomer Addition. *Macromolecules* **2016**, *49*, 38–47.

(32) Leibig, D.; Seiwert, J.; Liermann, J. C.; Frey, H. Copolymerization Kinetics of Glycidol and Ethylene Oxide, Propylene Oxide, and 1,2-Butylene Oxide: From Hyperbranched to Multiarm Star Topology. *Macromolecules* **2016**, *49*, 7767–7776.

(33) Perevyazko, I.; Seiwert, J.; Schömer, M.; Frey, H.; Schubert, U. S.; Pavlov, G. M. Hyperbranched Poly(ethylene glycol) Copolymers: Absolute Values of the Molar Mass, Properties in Dilute Solution, and Hydrodynamic Homology. *Macromolecules* **2015**, *48*, 5887–5898.

(34) Wang, Z. Einhorn Acylation. In *Comprehensive Organic Name Reactions and Reagents*; Wang, Z., Ed.; John Wiley & Sons, Inc: Hoboken, NJ, USA, 2010; p 95.

(35) Roumanet, P.-J.; Laflèche, F.; Jarroux, N.; Raoul, Y.; Claude, S.; Guégan, P. Novel aliphatic polyesters from an oleic acid based monomer. Synthesis, epoxidation, cross-linking and biodegradation. *European Polymer Journal* **2013**, *49*, 813–822.

(36) Maier, S.; Sunder, A.; Frey, H.; Mülhaupt, R. Synthesis of poly(glycerol)-block-poly(methyl acrylate) multi-arm star polymers. *Macromol. Rapid Commun.* **2000**, *21*, 226–230.

(37) Hölter, D.; Burgath, A.; Frey, H. Degree of branching in hyperbranched polymers. *Acta Polym.* **1997**, *48*, 30–35.

(38) Hölter, D.; Frey, H. Degree of branching in hyperbranched polymers. 2. Enhancement of the db: Scope and limitations. *Acta Polym.* **1997**, *48*, 298–309.

Supporting Information

Supplemental Analysis Data

SEC Data

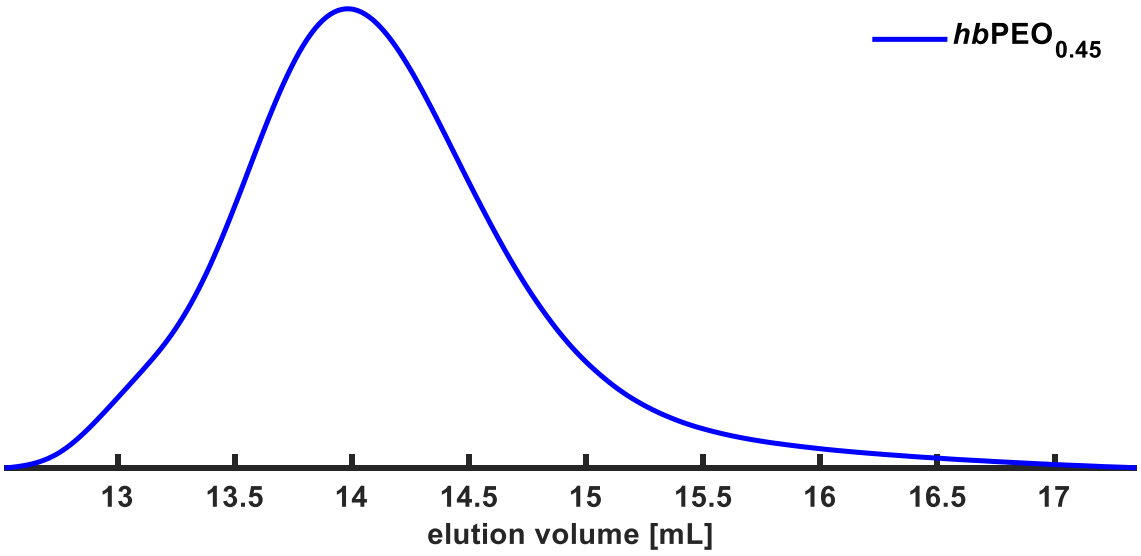

Figure S 1. SEC trace of *hb*PEO$_{0.45}$ (DMF, RI detector).

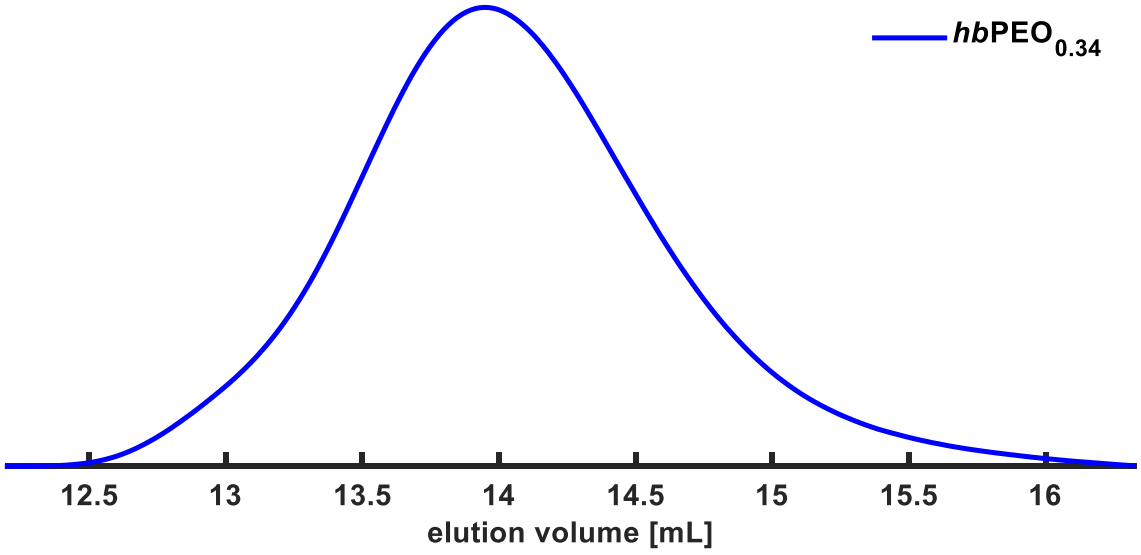

Figure S 2. SEC trace of *hb*PEO$_{0.34}$ (DMF, RI detector).

Supplemental NMR Spectroscopy

Calculation of the degree of branching for AB_2/AB systems (S 1: experimental values, S 2: theoretical values) according to Frey *et al.*:[28,37,38]

$$DB = \frac{2\,D}{2\,D + L_{1,3G} + L_{1,4G} + L_{EO}} \qquad S\,1$$

$$DB_{AB2/AB} = 2\,\frac{r+1}{(r+2)^2};\ r = \frac{[AB]}{[AB_2]} \qquad S\,2$$

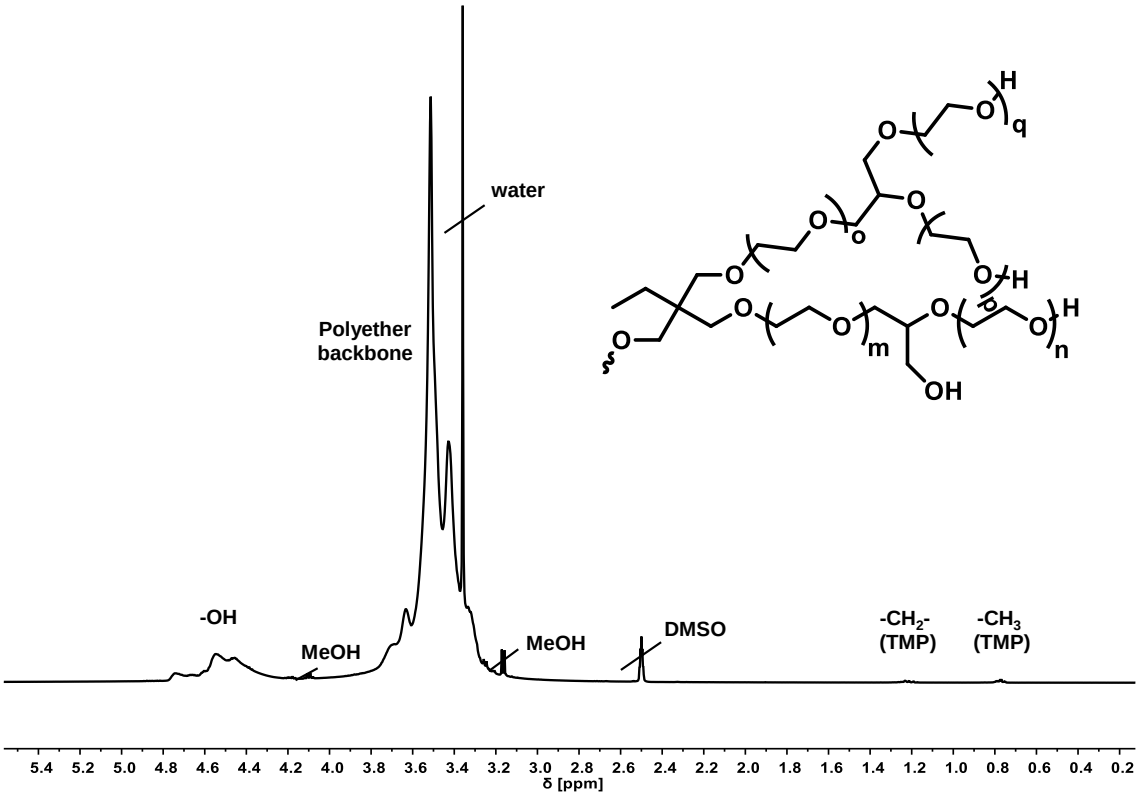

Figure S 3. ^{1}H NMR spectrum of *hb*$PEO_{0.45}$ (400 MHz, DMSO-d_6).

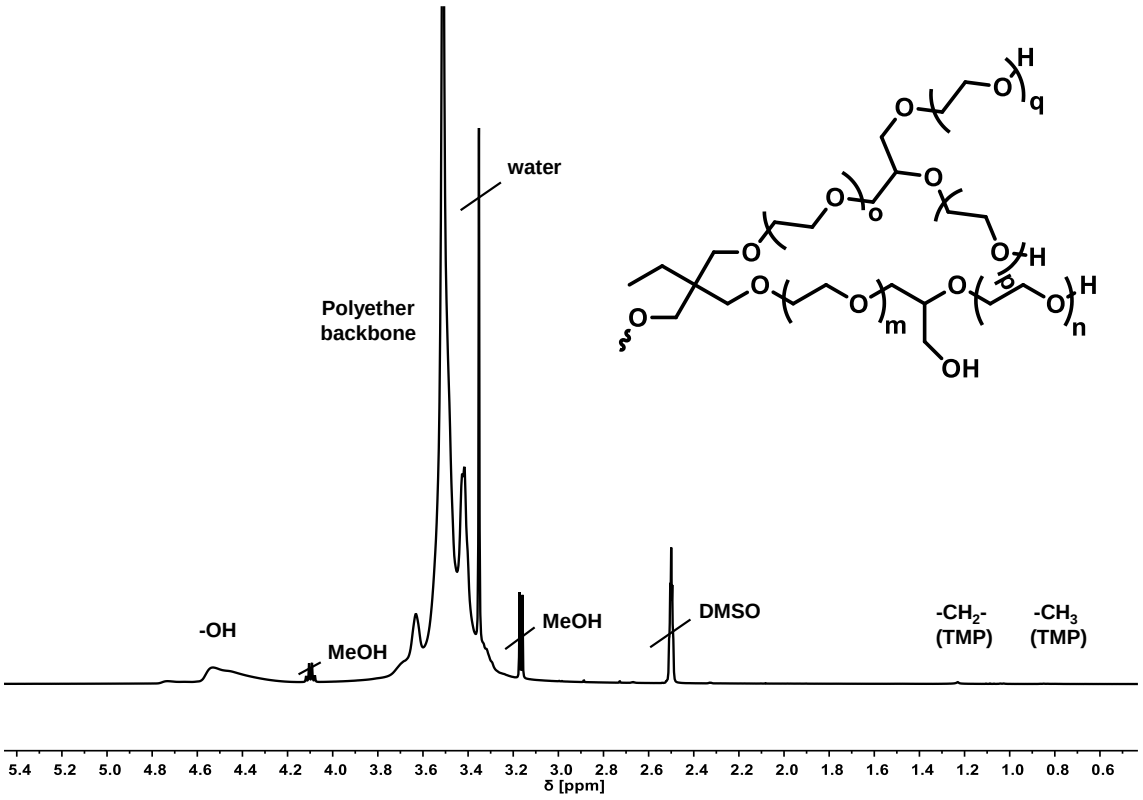

Figure S 4. ^{1}H NMR spectrum of *hb*PEO$_{0.34}$ (400 MHz, DMSO-d_6)

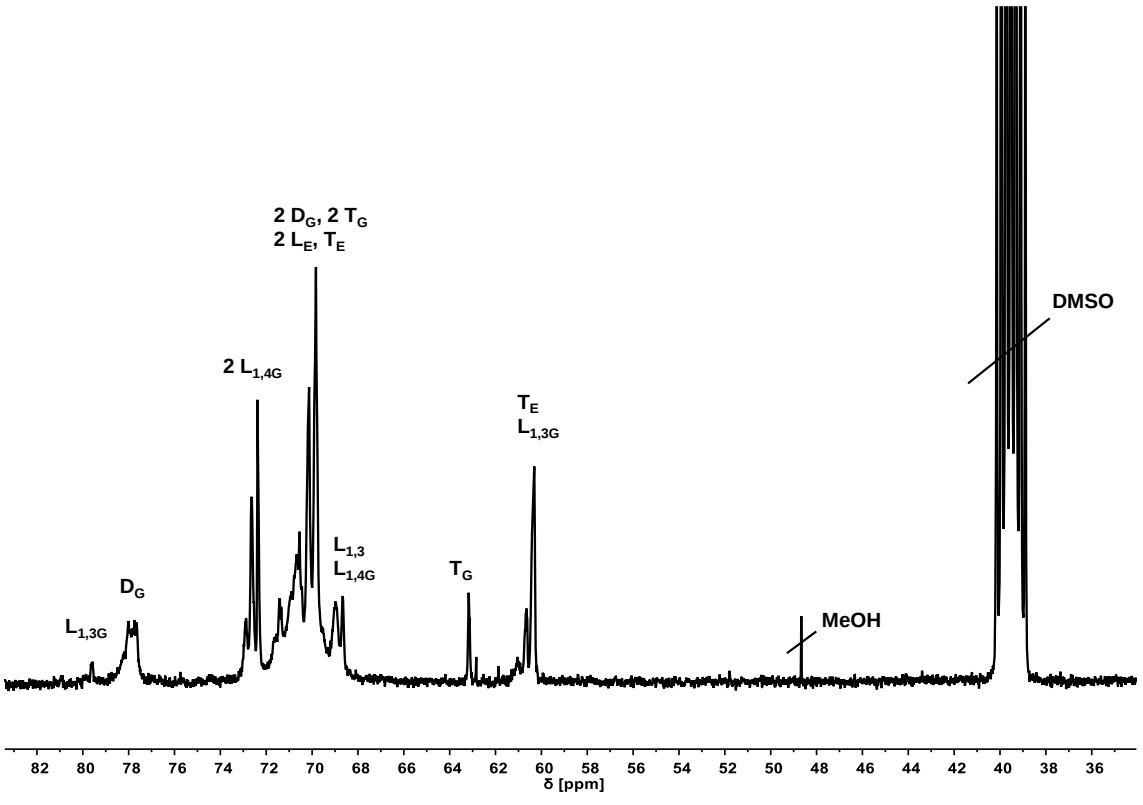

Figure S 5. ^{13}C NMR spectrum of *hb*PEO$_{0.45}$ (100 MHz, DMSO-d_6).

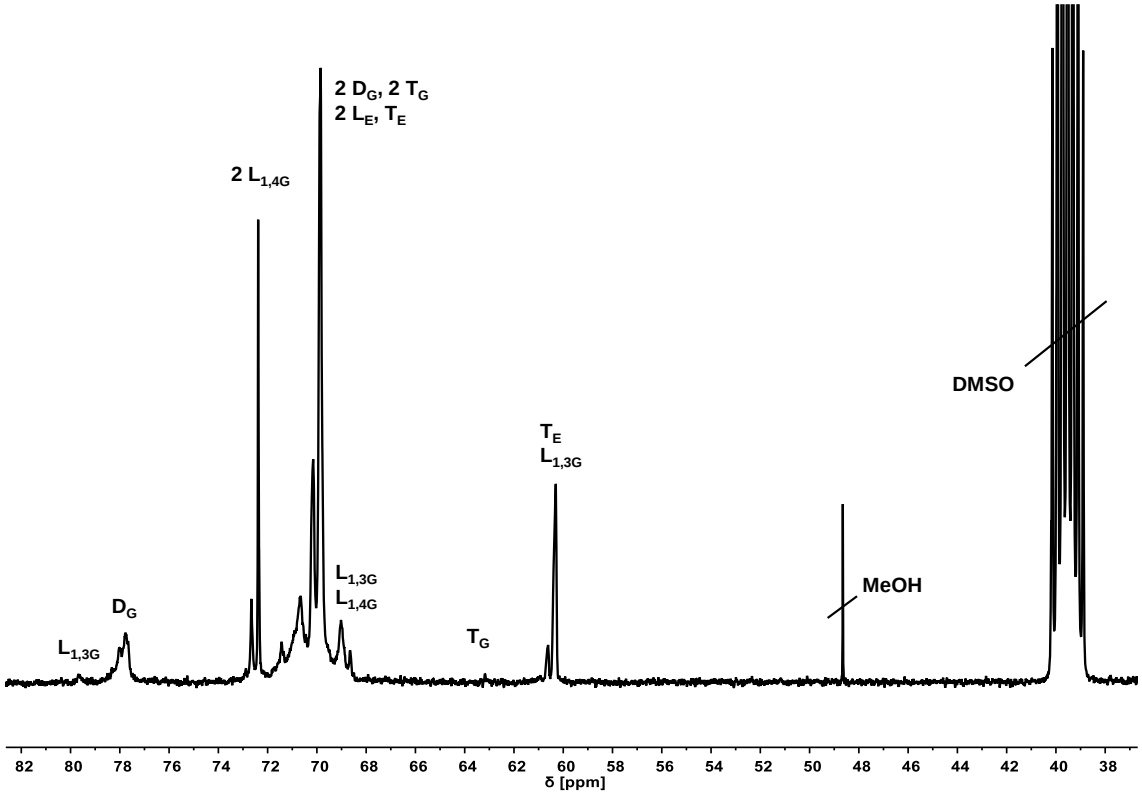

Figure S 6. ^{13}C NMR spectrum of *hb*$PEO_{0.34}$ (100 MHz, DMSO-d_6).

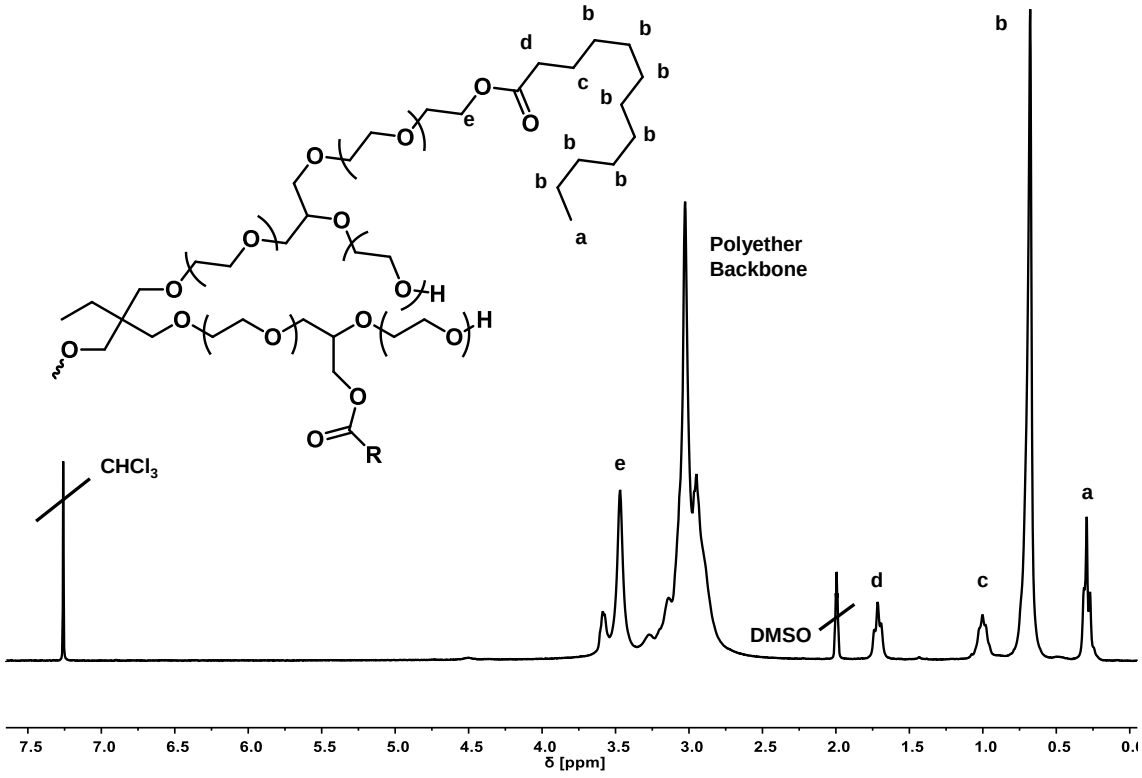

Figure S 7. ^{1}H NMR spectrum of *hb*$PEO_{0.45}$-$C12_{0.25}$ (300 MHz, $CDCl_3$ + DMSO-d_6).

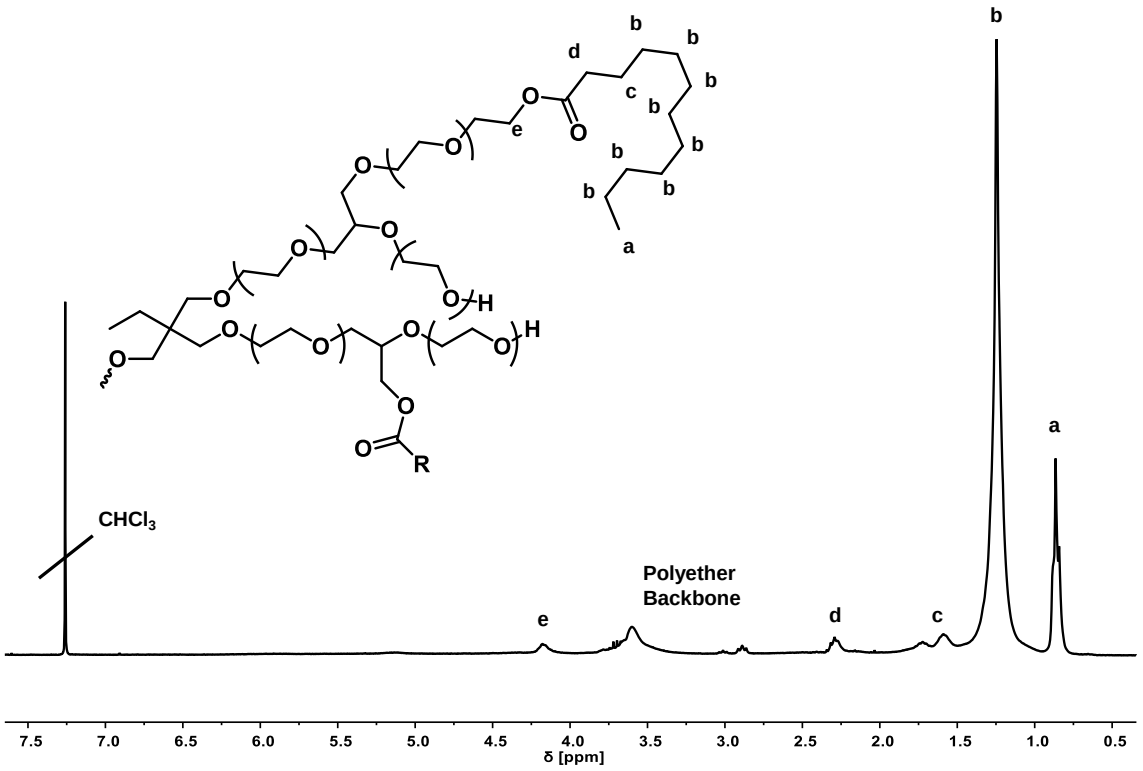

Figure S 8. ^{1}H NMR spectrum of *hb*PEO$_{0.45}$-C12$_{1.00}$ (300 MHz, $CDCl_3$).

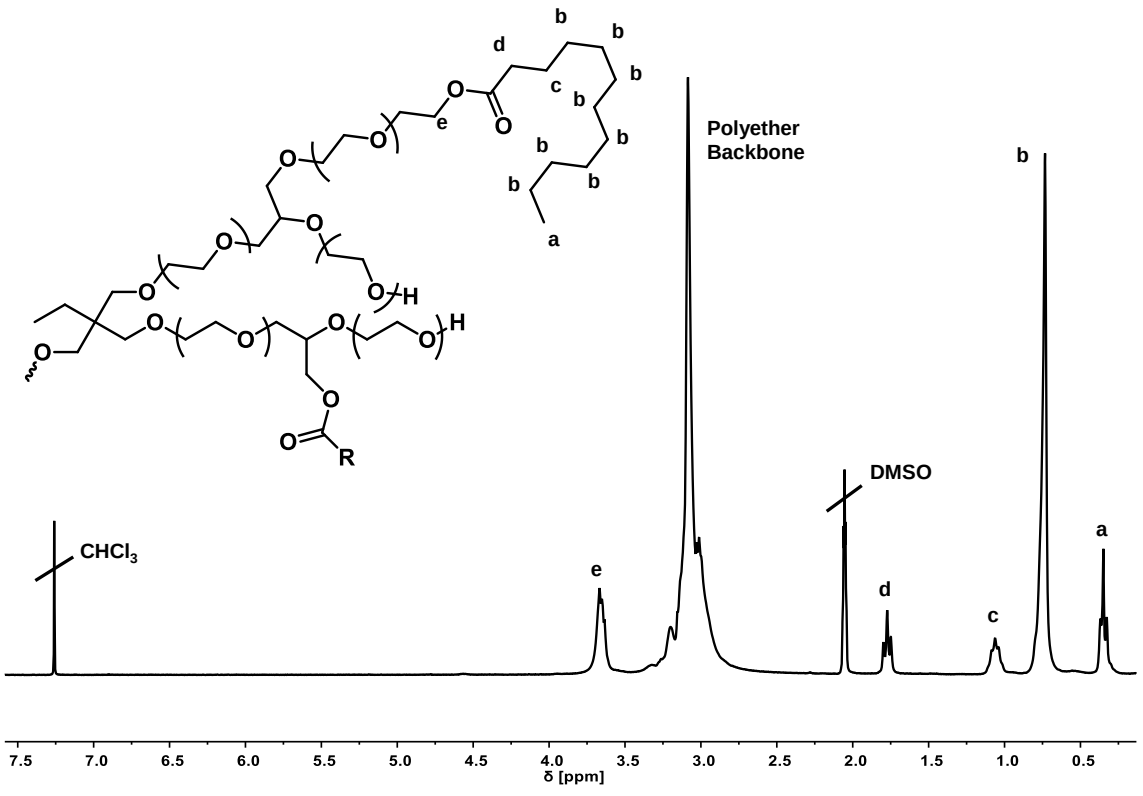

Figure S 9. ^{1}H NMR spectrum of *hb*PEO$_{0.34}$-C12$_{0.23}$ (300 MHz, $CDCl_3$ + DMSO-d_6).

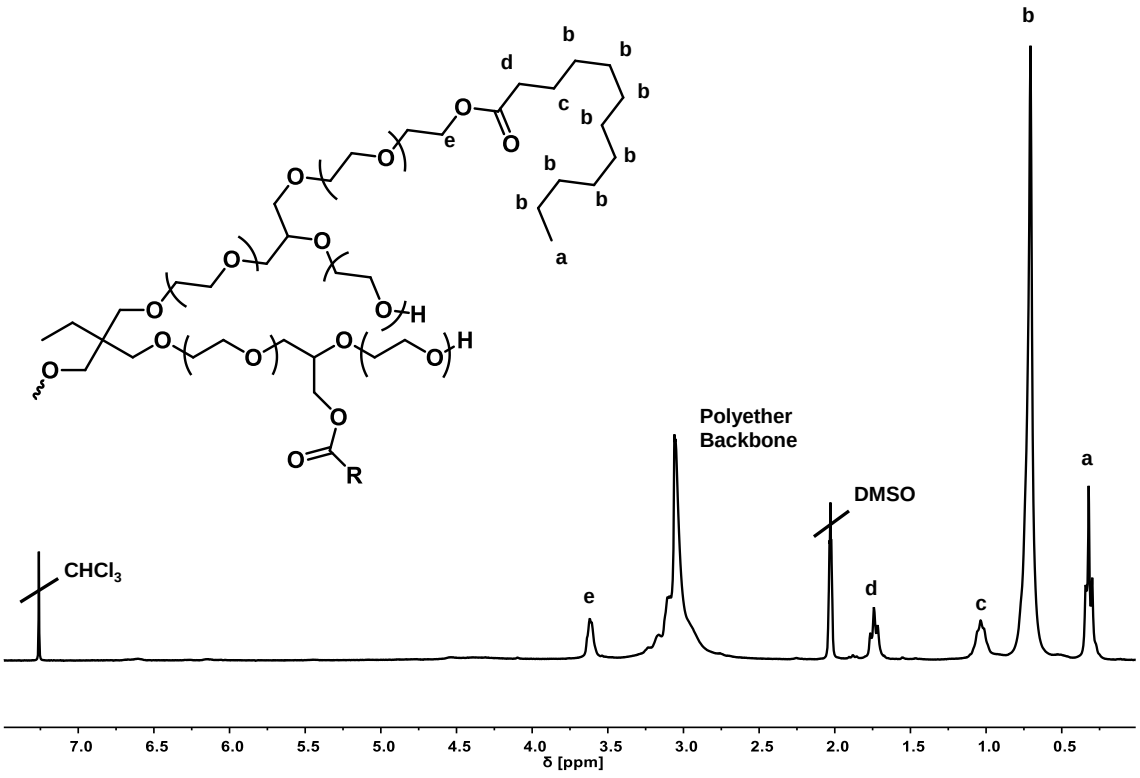

Figure S 10. ^{1}H NMR spectrum of *hb*$PEO_{0.34}$-$C12_{0.95}$ (300 MHz, $CDCl_3$).

Supplemental FTIR Spectroscopy

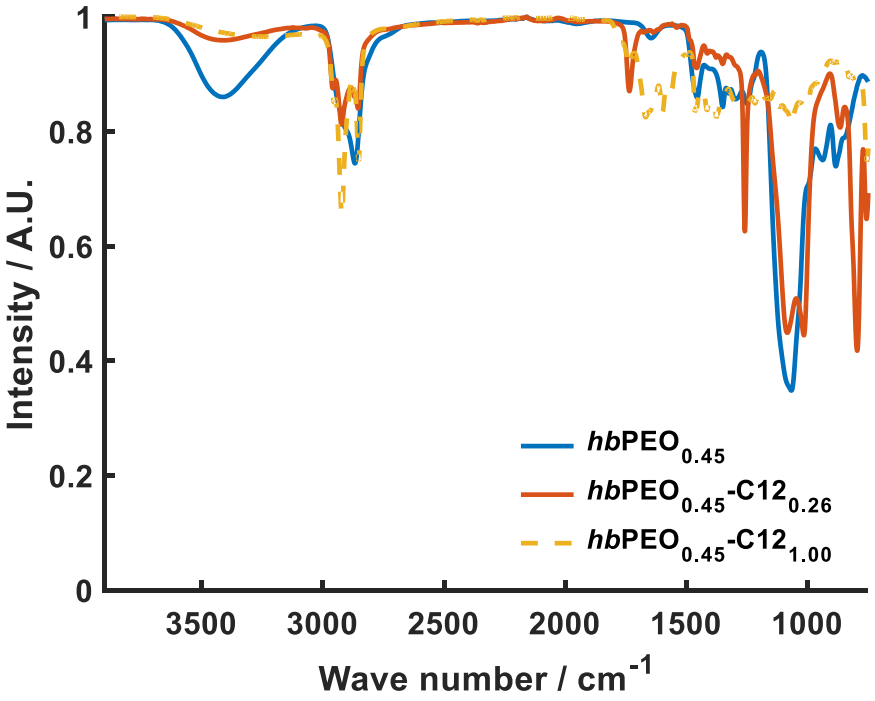

Figure S 11. FTIR spectra of *hb*PEO$_{0.45}$, *hb*PEO$_{0.45}$-C12$_{0.26}$ and *hb*PEO$_{0.45}$-C12$_{1.00}$.

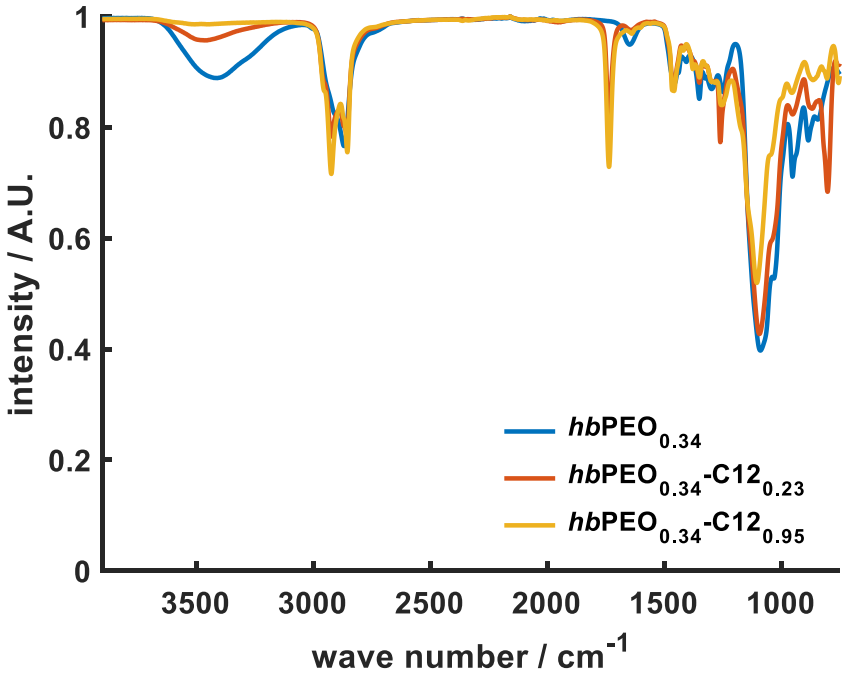

Figure S 12. FTIR spectra of *hb*PEO$_{0.34}$, *hb*PEO$_{0.34}$-C12$_{0.23}$ and *hb*PEO$_{0.34}$-C12$_{0.95}$.

Supplemental UV-Vis Spectroscopy

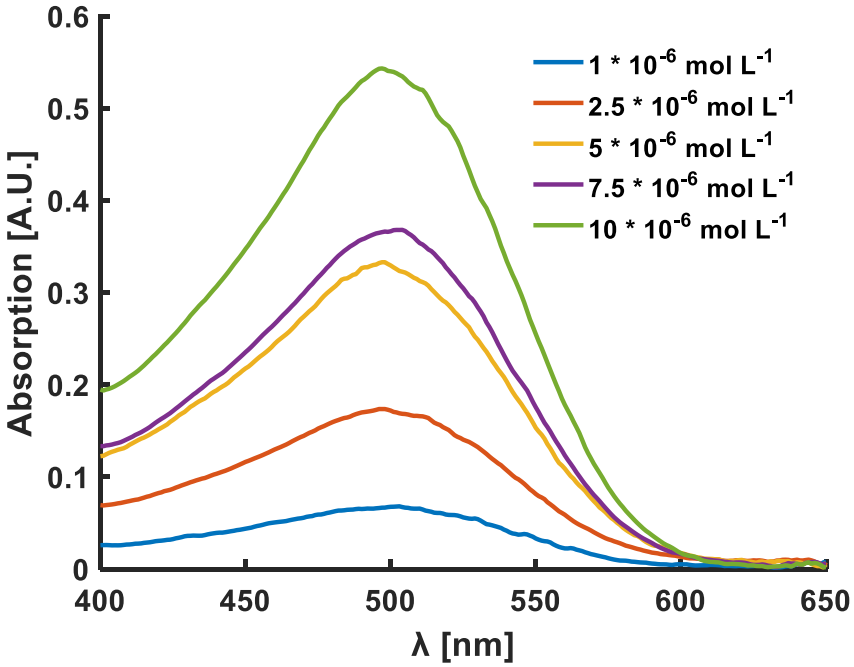

Figure S 13. UV-Vis absorption spectra (λ = 400 – 650 nm) of aqueous congo red solutions with varying concentrations.

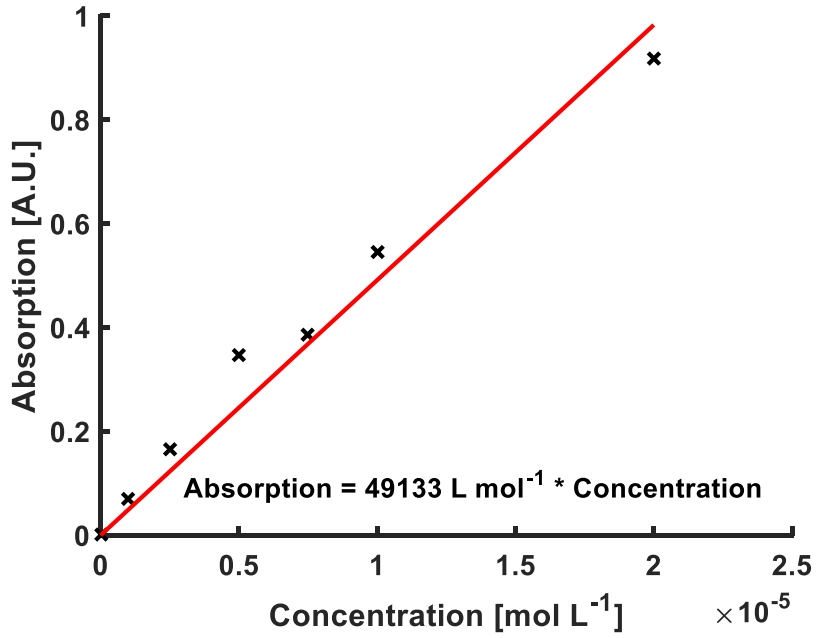

Figure S 14. A_{max} (λ = 495 nm) of aqueous congo red solutions plotted against the respective concentrations.

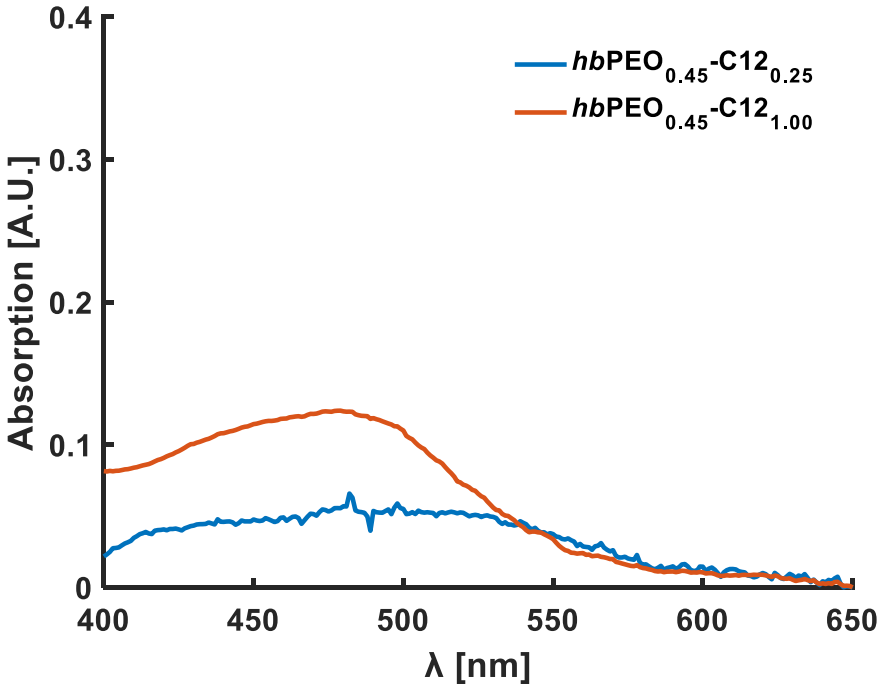

Figure S 15. UV-Vis absorption spectra (λ =400 - 650 nm) of *hb*PEO$_{0.45}$-C12$_{0.25}$ and *hb*PEO$_{0.45}$-C12$_{1.00}$ after saturation with congo red.

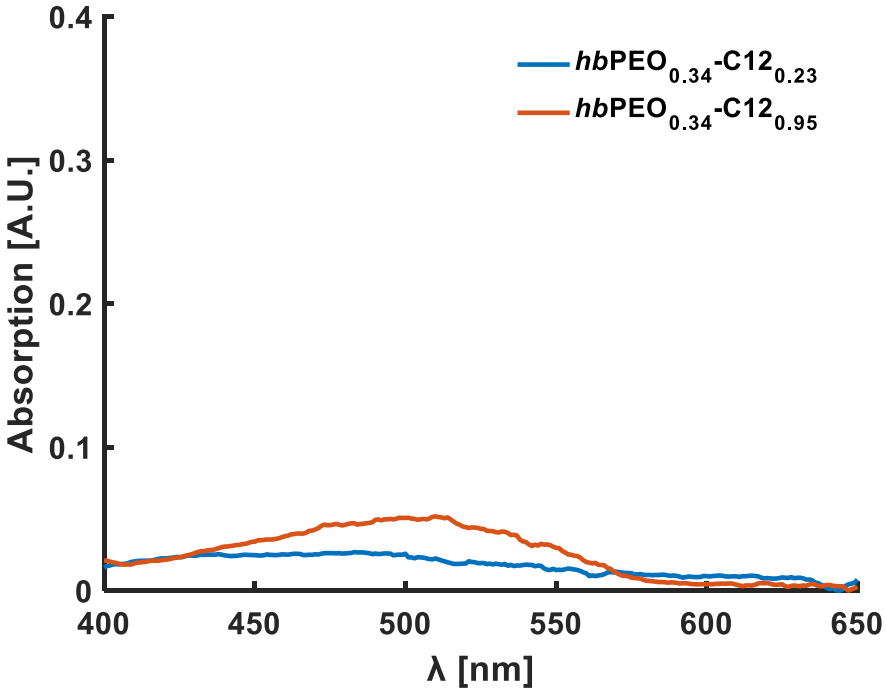

Figure S 16 UV-Vis absorption spectra (λ = 400 – 650 nm) of *hb*PEO$_{0.34}$-C12$_{0.23}$ and *hb*PEO$_{0.34}$-C12$_{0.95}$ after saturation with congo red.

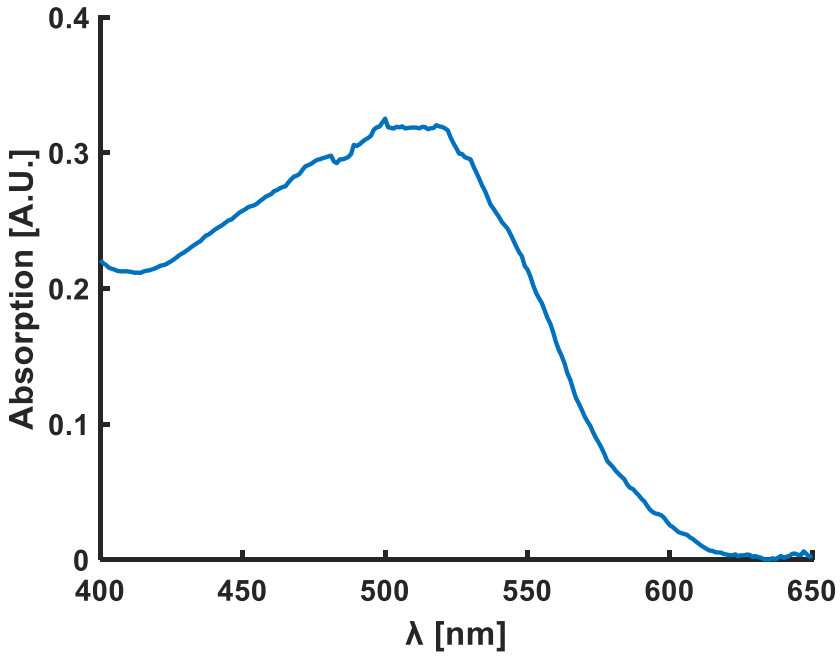

Figure S 17. UV-Vis absorption spectrum (λ = 400 – 650 nm) of *hb*PEO$_{0.34}$-C18$_{1.00}$ after extraction of an aqueous solution of congo red (1000 10^{-6} mol L^{-1}).

Behavior Towards pH Changes

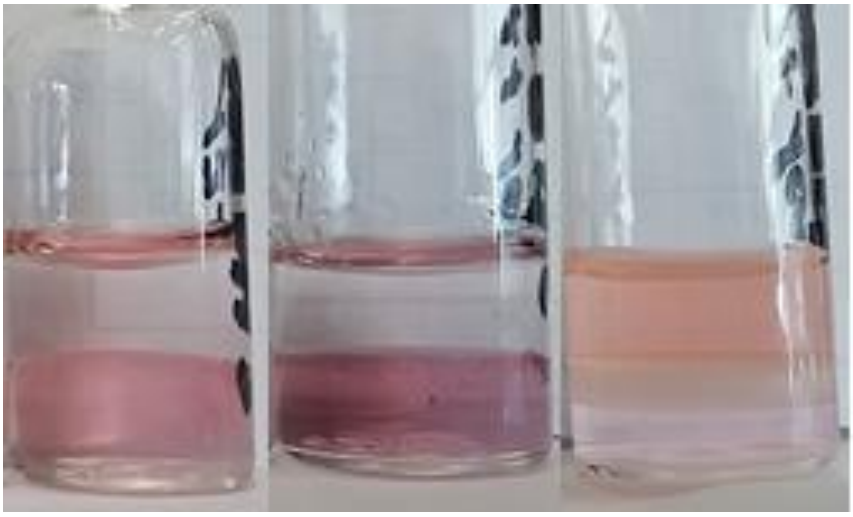

Figure S 18. Solutions of *hb*$PEO_{0.34}$-$C18_{1.00}$ (0.01 wt%) saturated with dye (bottom layer) after agitation with aqueous solutions of sodium hydroxide with increasing concentration (from left to right: pH 11, pH 14 and concentrated aqueous NaOH) (top layer).

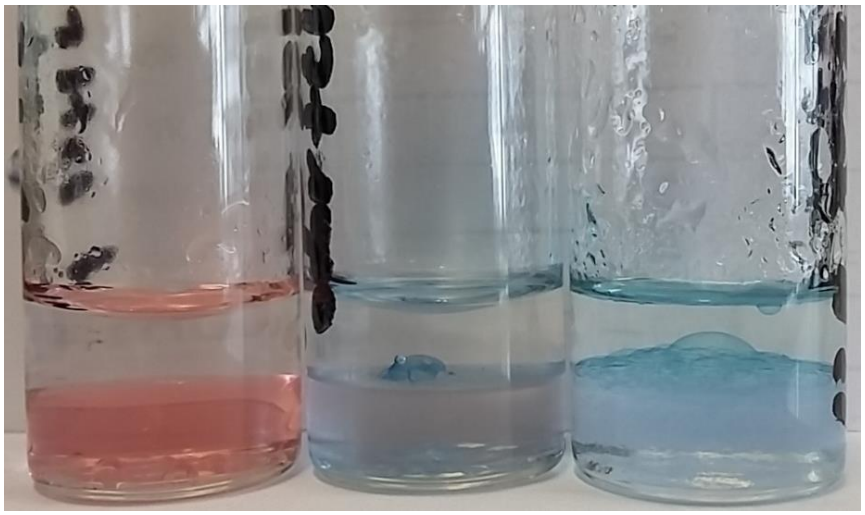

Figure S 19. Solutions of *hb*$PEO_{0.34}$-$C18_{1.00}$ (0.01 wt%) saturated with dye (bottom layer) after agitation with aqueous hydrochloric acid with increasing concentration (from left to right: pH 3, pH 0 and concentrated hydrochloric acid) (top layer).

3.4 Synthesis of *h*bPEO-*b*-PMMA Multi-Arm Star Polymers *via* Atom Transfer Radical Polymerization

Tobias Kaiser[a], Patrick Roth[a], Jasmin Preis[b], Holger Frey[a,]*

[a]Department of Chemistry, Johannes Gutenberg University, 55128 Mainz, Germany

[b]PSS Polymer Standards Service GmbH, In der Dalheimer Wiese 5, 55120 Mainz, Germany

To be submitted.

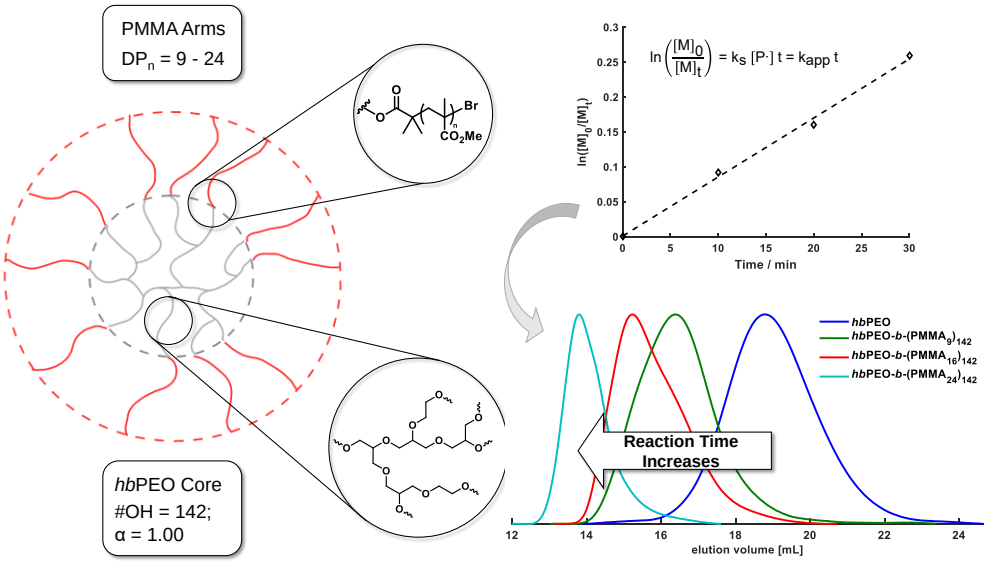

Abstract

The synthesis of the multi-arm star copolymers based on *hb*PEO with a total of 142 arm of different lengths via three steps is reported. A hyperbranched poly(ethylene oxide) copolymer (M_n = 36 700 g mol^{-1}, X_G = 0.28, #OH = 142) was synthesized by simultaneous slow monomer addition of ethylene oxide and glycidol. Quantitative esterification with 2-bromoisobutyryl bromide, as confirmed by FTIR spectroscopy, yielded multifunctional ATRP macroinitiators. The esterified *hb*PEO carrying an average of 142 initiation sites per polymer was subsequently used for the controlled radical polymerization of methyl methacrylate (MMA) using an ATRP catalyst system of CuBr/PMDETA in DMF at 70 °C *in vacuo*. By variation of the reaction times between 10 and 30 min, three different PMMA chain lengths (DP_n = 9, 16, 24) and molar masses of 930 to 2400 g mol^{-1} per arm were obtained. The SEC traces showed mainly monomodal distributions with narrow dispersities, i.e. narrower than the macroinitiator. Interestingly, despite rather low degrees of polymerization, the thermal properties of *hb*PEO-*b*-$(PMMA_{24})_{142}$ approaches the properties of linear PMMA. In the observed time frame, the reaction followed first order kinetics resulting in a linear increase of both the chain-length and the conversion index with time.

Introduction

Multi-arm star polymers possess a range of rather peculiar properties both in bulk and solution.[1,2] An elegant strategy for the synthesis of these sophisticated polymer architectures is summarized as the “core-first” approach.[3] Following this method, a multi-functional core is employed which exhibits functional groups enabling the

initiation of a living polymerization, for example anionic ring-opening or controlled radical polymerizations. Due to a well-defined structure, ease of synthesis and large number of functional end groups, hyperbranched polymers, e.g. hyperbranched polyglycerol (*hb*PG), are commonly employed as macroinitiators.[4] Hyperbranched polyglycerol is typically prepared by the anionic ring-opening polymerization of glycidol by slowly adding the monomer to a partially deprotonated initiator.[5] Following this technique, control of the molar mass, moderate dispersities and elevated degrees of branching are obtained.[6–8] The hydroxy groups of *hb*PGs have been used as initiator moieties for the ring-opening polymerization of cyclic ethers or esters, e.g. EO,[9,10] PO,[11] ε-caprolactone,[12] L-lactide[13] or glycolide.[14] The functionalization of the hydroxy groups by esterification with 2-bromoisobutyryl bromide on the other hand enables the controlled radical polymerization of different vinyl and (meth-)acrylate monomers by ATRP.[15–17] For example, multi-arm star polymers with polystyrene,[18] poly(methyl acrylate),[19] poly(tert-butyl acrylate) and poly(acrylate),[20,21] poly(2-hydroxymethyl acrylate),[22,23] poly(hexafluorobutyl acrylate)[24] and poly(methyl methacrylate)[25] arms have been reported before.

As each glycidol unit introduces exactly one hydroxy group upon polymerization, the overall functionality of hyperbranched homopolyglycerol can be tuned by varying the degree of polymerization.[26–29] To change the number of functional hydroxy groups (#OH) and overall functionality independent from the molar mass, however, the copolymerization of glycidol with suitable AB type monomers, e.g. glycidyl ethers or alkylene oxides, is a commonly employed strategy.[30] By substitution of a fraction of glycidol with the comonomer, #OH is limited while retaining a constant degree of polymerization. Specifically the copolymerization of glycidol with common alkylene oxides, i.e. ethylene oxide, propylene oxide or

butylene oxide, yields interesting hyperbranched analogues of widely used linear alkylene oxides.[31–36] Several multi-arm star polymers based on a *hb*PEO macroinitiator have been reported, for example with polyester[37,38] or polycarbonate arms.[39,40] Due to the inherently high number of growing chains, the main challenge to overcome during the synthesis of multi-arm star polymers is the high probability of radical-radical-coupling, leading to deactivation and gelation by cross-linking, despite following controlled radical polymerization techniques. As reported by Frey and coworkers, during the synthesis of multi-arm stars comprised of a *hb*PG core and 17 to 108 poly(tert-butyl acrylate) arms, cross-linking occurs at conversions higher than 30 %.[20] Lederer and coworkers successfully employed AGET ATRP to grow PMMA arms from a *hb*PG core carrying 45 to 85 arms. The authors emphasize the importance of the number of arms and arm length for the properties and fields of application, i.e. processability.[25]

In this work, we present the synthesis and characterization of multi-arm star polymers based on well-defined *hb*PEO as the core moiety further expanding the number of arms per polymer reported by Lederer and coworkers. After functionalization, the hyperbranched polyether polyol core carries 142 ATRP initiation sites which are used for the controlled polymerization of methyl methacrylate by ATRP to yield individual degrees of polymerization between 9 and 24. The average molar masses per polymer ranged from 190 000 to 400 000 g mol^{-1} resulting in similar thermal behavior as linear homopolymers of MMA.

Experimental Section

Materials

All Materials were purchased from Sigma Aldrich, TCI chemicals, VWR chemicals, Fisher Scientific and Deutero. CuBr (99.9 %) was purified with glacial acetic acid for two weeks, washed with pure ethanol and stored under argon. Prior to use, DMF (stabilized) and MMA (99 %, stabilized) were filtered through a basic alumina column to remove the stabilizer. All other materials were used without further purification.

Measurements

NMR spectroscopy. ^{1}H NMR spectra were either recorded on a Bruker Avance III HD 300 (5 mm BBFO-SmartProbe with z-gradient and ATM) at 300 MHz or on a Bruker Avance II HD 400 (5 mm BBFO-SmartProbe with z-gradient and ATM) at 400 MHz. Inverse gated ^{13}C NMR spectra were recorded on a Bruker Avance II HD 400 (5 mm BBFO-SmartProbe with z-gradient and ATM) at 100 MHz. The residual signals of the deuterated solvent were utilized as an internal reference.

Size-exclusion chromatography (SEC). SEC measurements in DMF (containing 0.25 g L^{-1} of lithium bromide) were performed using an integrated Agilent 1100 series instrument, equipped with a PSS HEMA column combination ($10^6/10^4/10^2$ Å porosity), UV and RI detector. Calibration is based on linear poly (ethylene oxide) standards (Polymer Standards Service).

SEC with integrated viscosity measurements were performed in DMF (containing 5 g L^{-1} lithium bromide) employing a PSS GRAM column combination (10/300/300

Å porosity), an Agilent MDS refractive index detector and an Agilent MDS viscometer. The calibration is based on linear poly (methyl methacrylate) standards (Polymer Standards Service), molar mass averages were calculated via universal calibration.

Fourier-transform infrared spectroscopy (FTIR). FTIR measurements were performed using a Nicolet iS10 FTIR spectrometer (Thermo Fisher Scientific) equipped with diamond ATR sample holder.

Differential Scanning Calorimetry. DSC measurements were performed using a PerkinElmer 8500 thermal analysis system and a Perkin-Elmer CLN2 thermal analysis controller in the temperature range of -90 to +150 °C at a heating rate of 10 K min^{-1}.

Synthesis of *hb*PEO *via* SMA

The synthesis of *hb*PEO (36 700 g mol^{-1}, c_{OH} = 5.33 mmol g^{-1}) *via* SMA was performed as reported elsewhere.[32] To achieve elevated molar masses without elongated addition times, a partially deprotonated *hb*PEO macroinitiator (M_n = 9600 g mol^{-1}, universally calibrated SEC) was employed.

^{1}H NMR (DMSO-d_6, 400 MHz): δ (ppm) = 4.76 – 4.35 (m, br, OH), 3.90 – 3.15 (m, O-CH, O-CH_2), 1.36 – 1.18 (m, 2H, CH_3-CH_2 (TMP)), 0.87 – 0.75 (m, 3H, CH_3 (TMP)).

^{13}C NMR (DMSO-d_6, 100 MHz): δ (ppm) = 80.25 – 79.45 ($L_{1,3G}$), 78.52 – 77.42 (D_G), 73.22 – 72.10 ($L_{1,4G}$), 72.04 – 69.62 (D_G, L_E, T_E, 2 T_G), 69.61 – 68.37 ($L_{1,3G}$, $L_{1,4G}$), 63.39 – 62.96 (T_G), 60.87 – 60.07 (T_E, $L_{1,3G}$).

FTIR: $\tilde{\nu}$ (cm^{-1}) = 3600 – 3000 (-OH), 1100 (C-O-C).

Esterification

200 mg of the *hb*PEO copolymer (1 mmol in relation to functional groups, 1 eq.) was dissolved in 1 mL methanol was transferred to a two-neck flask equipped with a Teflon seal and a magnetic stirrer. The solution was mixed with 3 mL of benzene and the polymer was dried *in vacuo* overnight. Afterwards, the polymer was dissolved in anhydrous pyridine (20 mL) under inert gas atmosphere and the solution was cooled to 0 °C. 2-Bromoisobutyryl bromide (0.13 mL, 1 mmol, 1 eq) was added dropwise and the resulting mixture was stirred over night at room temperature. After the addition of potassium carbonate (1.1 eq) and stirring for 30 minutes, precipitated salts and other solids were removed by filtration and pyridine was removed azeotropically *in vacuo* using toluene. The crude product was dialyzed in chloroform (benzoylated cellulose MWCO = 2000 g mol^{-1}) to yield the product as pale yellow to brown wax.

^{1}H NMR ($CDCl_3$, 400 MHz): δ (ppm) = 5.30 – 5.03 (-CH-OCOR), 4.34 – 4.09 (m, -CH_2-OCOR), 3.90 – 3.28 (m, polyether backbone), 1.97 – 1.83 (s, -C(CH_3)$_2$Br).

^{13}C NMR (CDCl3, 100 MHz): δ (ppm) = 171.93 (C=O) 79.53 – 67.40 (polyether backbone), 65.77 – 64.77 (-CH_2-OCOR), 56.30 (-C-(CH_3)$_2$Br), 30.34 (-C-(CH_3)$_2$Br).

FTIR: $\tilde{\nu}$ (cm^{-1}) = 1730 (C=O), 1377 (-CH_3), 1100 (C-O-C).

ATRP of MMA

The macroinitiator (50 mg, 0.27 mmol in relation to ATRP initiation sites, 1 eq.) was placed in a round-bottom flask equipped with a magnetic stirrer and dissolved in 3 mL DMF. Subsequently, CuBr (15 mg, 0.07 mmol, 0.25 eq.) and *N*,*N*,*N'*,*N''*,*N''*-pentamethyldiethylenetriamine (PMDETA) (0.03 mL, 0.13 mmol, 0.5 eq.) were added and the mixture was degassed by three freeze-pump-thaw cycles. In a separate flask, methyl methacrylate (MMA) was degassed by argon bubbling. 3 mL of degassed MMA (2.82 g, 27 mmol, 106 eq.) were added to the reaction mixture. After evacuation, the reaction mixture was immediately heated to 70 °C and the polymerization was conducted for either 10, 20 or 30 min. To terminate the polymerization, the reaction flask was immersed in liquid nitrogen. Afterwards, the mixture was diluted with THF and filtered through silica gel to remove the copper catalyst. After precipitation in cold n-hexane, the polymers were retrieved as colorless solids. The yields varied depending on the reaction time (76 mg after 10 min, 144 mg after 20 min, 315 mg after 30 min).

^{1}H NMR ($CDCl_3$, 400 MHz): δ (ppm) = 4.34 – 4.09 (m, -C$\underline{H}_2$-OCOR), 3.69 – 3.51 (s, -O-C$\underline{H}_3$ (PMMA)), 2.06 – 1.72 (m, -CH_2- (PMMA)), 1.17 – 0.74 (s, -C$\underline{H}_3$ (PMMA)).

^{13}C NMR (CDCl3, 100 MHz): δ (ppm) = 177.88 ($\underline{C}$=O (PMMA) 171.93 ($\underline{C}$=O) 79.53 – 67.40 (polyether backbone), 65.77 – 64.77 (-$\underline{C}H_2$-OCOR), 56.30 (-$\underline{C}$-$(CH_3)_2$Br), 54.96 – 53.78 (-$\underline{C}H_2$- (PMMA)), 52.21 – 51.40 (-O-$\underline{C}H_3$ (PMMA)), 30.34 (-C-($\underline{C}H_3)_2$Br), 20.31 – 15.23 (-$\underline{C}H_3$ (PMMA)).

Results and Discussion

Multi-arm star copolymers based on well-defined *hb*PEO were prepared in a facile three-step process.

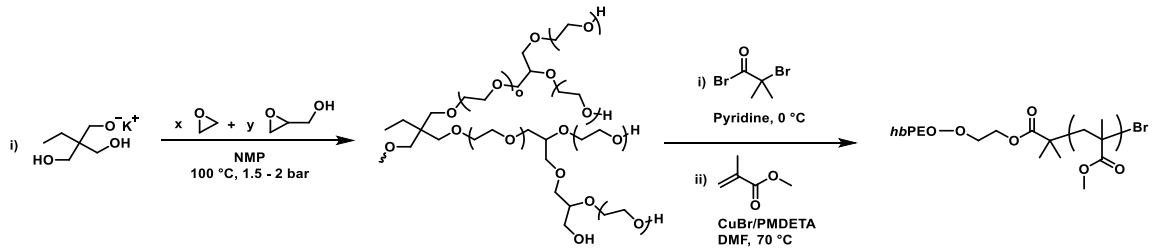

Scheme 1. Schematic synthesis of multi-arm star polymers by controlled radical polymerization of MMA using esterified *hb*PEO macroinitiators.

First, hyperbranched poly(ethylene oxide) was synthesized *via* simultaneous slow monomer addition of glycidol and ethylene using a *hb*PEO macroinitiator (9600 g mol^{-1}) to fully control the molar mass.[6,41,42] The polymer was analyzed by a combination of universally calibrated SEC in DMF as well as ^{1}H and ^{13}C NMR spectroscopy to determine the molar mass and copolymer composition. Table 1 summarizes the analytical data obtained from SEC and NMR spectroscopy (see supporting information for further detail).

Table 1. ^{13}C NMR and SEC characterization data of the hyperbranched poly(ethylene oxide) copolymer.

Sample	M_n[a)] [g mol^{-1}]	Đ[a)]	X_G[b)]	DB[b)]	#OH[c)]
*hb*PEO	36700	1.91	0.28	0.34	142

[a)]Determined by universally calibrated SEC (DMF, 70 °C, online viscosimetry), [b)]determined by Inverse Gated ^{13}C NMR spectroscopy, [c)]calculated using equation 1 and data obtained ^{13}C NMR spectroscopy and universally calibrated SEC.

For further functionalization, precise knowledge of the total number of functional groups is important. As each glycidol unit introduces exactly one hydroxy group in addition to the functional groups of the initiator TMP (f = 3), the total number #OH can be calculated according to equation 1 using the values summarized in Table 1:

$$\#OH = \frac{M_n X_G}{M_G} + 3 \qquad 1$$

With a molar mass (M_n) of 36 700 g mol^{-1} and glycidol content (X_G) of 0.28, a total of 142 hydroxy groups per polymer is calculated using the molar mass of a single repeating unit (M_G). Subsequently, the hydroxy groups were quantitatively functionalized by esterification with an excess of 2-bromoisobutyryl bromide (2-BIBB) in pyridine to introduce multiple ATRP initiation sites (cf. Scheme 1). To remove unreacted acid halide, the crude product *hb*PEO-Br$_{142}$ was dialyzed in chloroform (MWCO = 2000 g mol^{-1}) for two days.

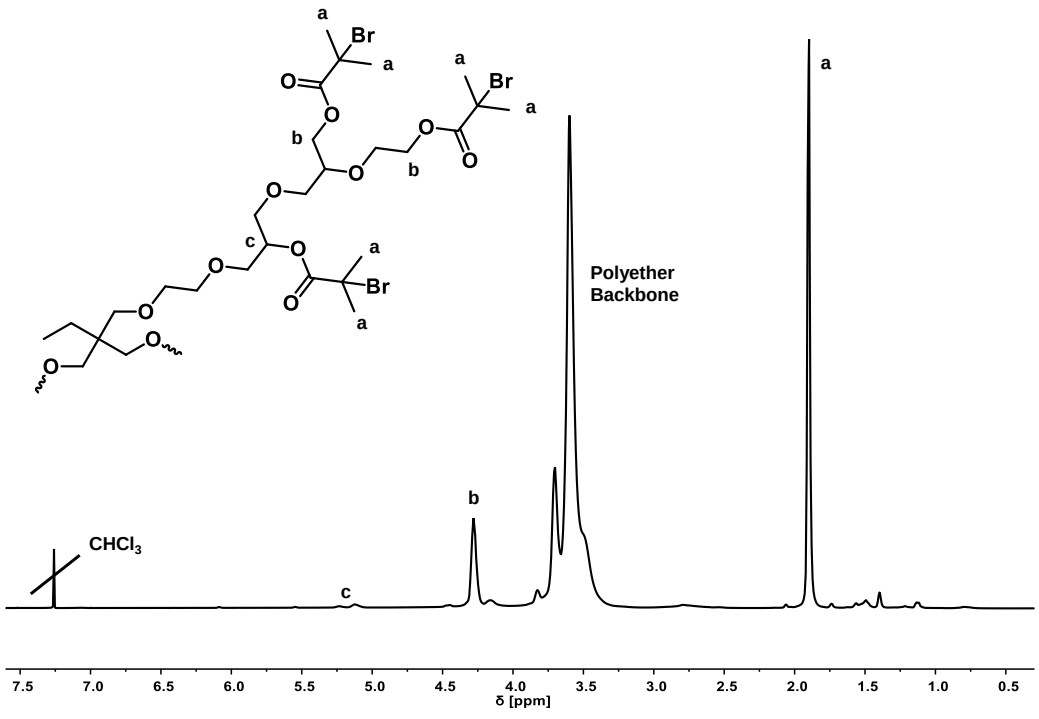

Figure 1. ^{1}H NMR spectrum of *hb*PEO-Br$_{142}$ (400 MHz, $CDCl_3$).

The ^{1}H NMR spectrum of *hb*PEO-Br$_{142}$ (Figure 1) after dialysis shows the signal of the 2-bromoisobutyryl moiety (methyl groups (signal a), 1.67 – 2.09 ppm) alongside the polyether backbone of *hb*PEO (3.18 – 4.38 ppm). Upon functionalization, the signals of the methine groups (esterified primary hydroxy group, signal c, 5.28 – 5.04 ppm) and of the methylene groups carrying the ester (esterified secondary hydroxy group, signal b, 4.05 - 4.38 ppm) are clearly shifted and distinguishable from the polyether backbone. Further analytical data, i.e. 2D spectra, are found in the supporting information (cf. Figure S 5). For the following discussion, only signal b will be considered because of the low intensity of the methine signal (see also Figure S 5). Additionally, the copolymer composition (X_G = 0.28 and X_{EO} = 0.72) results in an abundance of ethylene oxide units, making up the most part of the readily addressable primary hydroxy groups (see Figure S 2). Due to a signal intensity ratio of 6:2 of the signals a and b, no unreacted 2-bromoisobutyryl bromide is present after work-up by dialysis despite using an excess of 2-BIBB. Hence, *hb*PEO-Br$_{142}$ will be utilized as an ATRP initiator without further purification. However, because of the insufficient resolution of the hydroxy signal in $CDCl_3$, quantitative functionalization cannot be confirmed using only ^{1}H NMR spectroscopy. Hence, FTIR spectroscopy is employed to confirm full conversion of the hydroxy groups, as both hydroxy groups and carbonyl groups result in rather intensive bands. Figure 2shows the FTIR spectra of both *hb*PEO (blue) and *hb*PEO-Br$_{142}$ (orange). Upon esterification, the intensive O-H band (3000 – 3600 cm^{-1}) of *hb*PEO disappears completely, whereas the C=O band of the ester moiety is found at 1730 cm^{-1}. Therefore, in combination with the results obtained from NMR spectroscopy, quantitative functionalization of the hydroxy groups is assumed. Consequently, the total number of ATRP initiator moieties

equals the number of hydroxy groups (#OH = #Br = 142) resulting in a molar mass of the macroinitiator of 57800 g mol^{-1}.

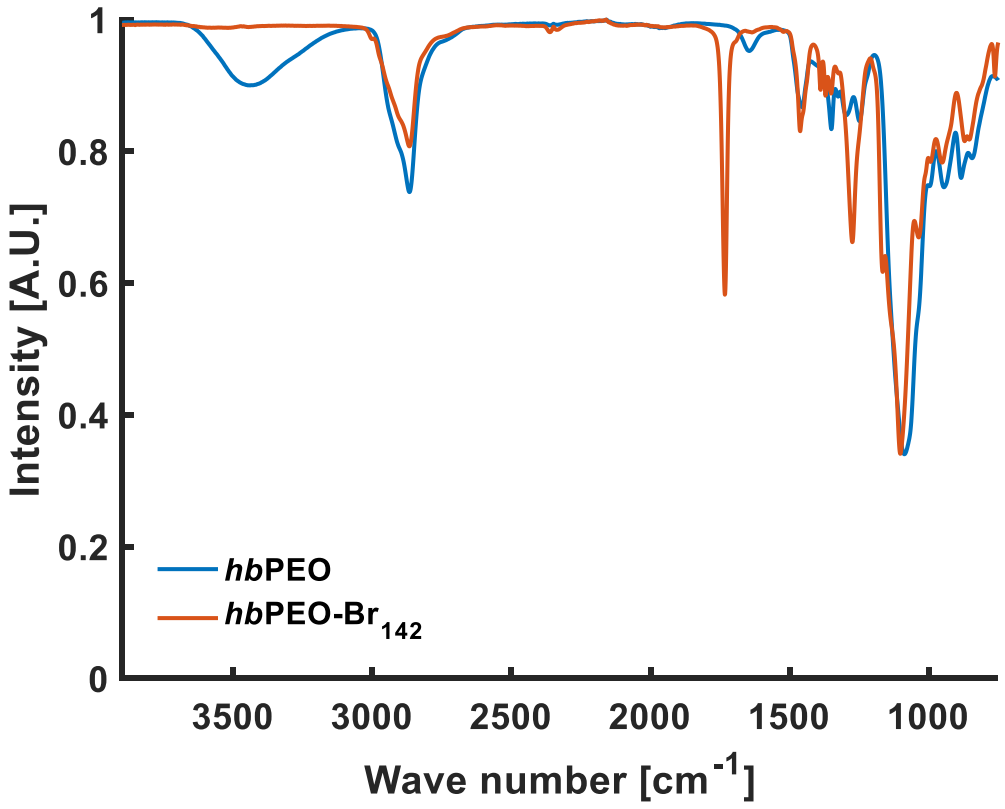

Figure 2. FTIR spectra of *hb*PEO before (blue) and after reaction with 2-bromo-isobutyryl bromide (orange).

The subsequent controlled radical polymerization of methyl methacrylate employing the macroinitiator *hb*PEO-Br$_{142}$ was performed using CuBr/PMDETA as the catalytic system. The polymerizations were conducted in analogy to modified literature reports,[19,25] as initial tests showed the best results for the reaction in DMF at 70 °C *in vacuo*. To prevent side-reactions, such as star-star-coupling, ultimately resulting in gelation, the polymerization was conducted in high dilution with smaller amounts of catalyst and only for short durations up to 30 min.[19] Three multi-arm star polymers characterized by different arm lengths were synthesized by variation

of the reaction time between 10 and 30 min. After the desired reaction time, the polymerization was terminated by immersing the reaction flask in liquid nitrogen. Afterwards, the reaction mixture was diluted with THF and the copper catalyst was removed by filtration using silica gel. The star polymers were then isolated by precipitation in cold n-hexane. Macroscopically no gelation occurred under the reaction conditions discussed above and all samples showed good solubility in various organic solvents, e.g. THF, DMF, chloroform. Figure 3 shows the SEC traces of star copolymers retrieved after individual reaction times of 10, 20 and 30 min and *hb*PEO representing the macroinitiator. The indices describe the individual chain-length of each PMMA arm as calculated using ^{1}H NMR data (*vide infra*).

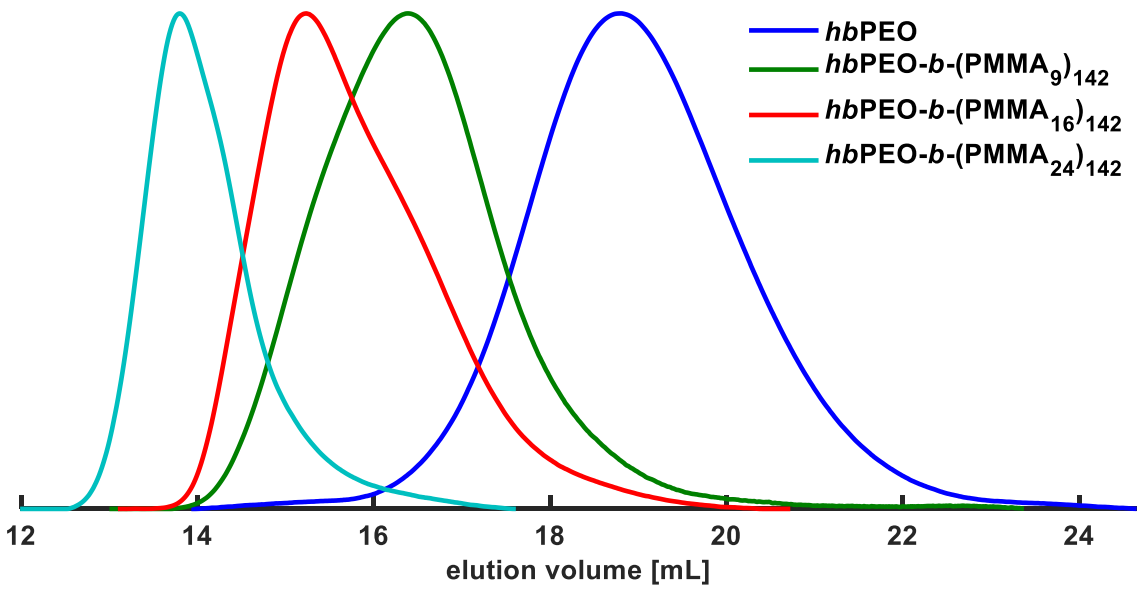

Figure 3. SEC traces of *hb*PEO and the multi-arm star polymers *hb*PEO-*b*-$(PMMA_9)_{142}$, *hb*PEO-*b*-$(PMMA_{16})_{142}$ and *hb*PEO-*b*-$(PMMA_{26})_{142}$ (DMF, RI detector).

Upon longer reaction time, the SEC traces are clearly shifted towards lower elution volumes in comparison to *hb*PEO indicating an increase in hydrodynamic radius. The molar masses determined using linear PMMA standards increase from 40800 to 58100 and 72300 g mol^{-1} with increasing reaction time. The polydispersities

decrease from 1.30 after 10 min to 1.22 after 20 min and 1.14 min after 30 min approaching typical polydispersities obtained for linear polymers prepared by controlled radical polymerization (M_w / M_n ≈ 1.1 – 1.2)[43]. Despite showing a positive trend, linear SEC typically underestimates the molar masses of branched polymers due to their compact structure.[33] Therefore, ^{1}H NMR spectroscopy and different 2D experiments were performed to confirm the star architecture and to determine the individual arm lengths. As a general example, Figure 4 shows the ^{1}H NMR spectrum of *hb*PEO-b-$(PMMA_9)_{142}$.

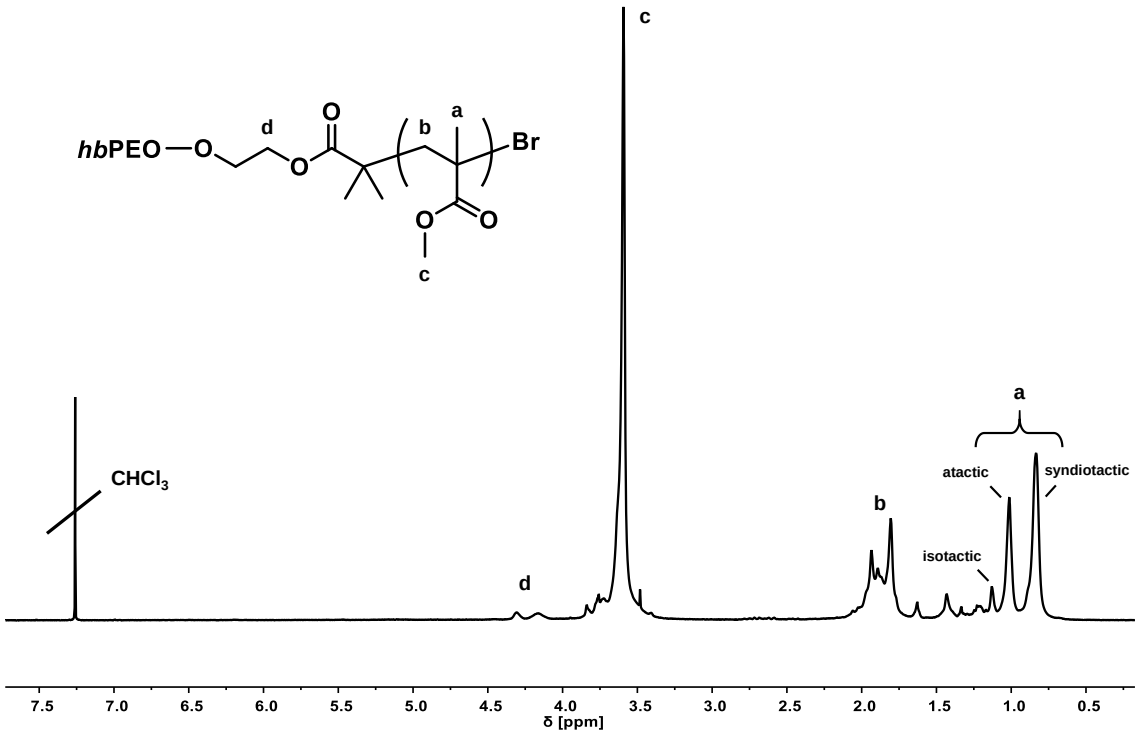

Figure 4. ^{1}H NMR spectrum of *hb*PEO-*b*-$(PMMA_9)_{142}$ (400 MHz, $CDCl_3$).

The spectrum shows each of the signals of the PMMA arms: the methyl group (a) at 0.75 - 1.15 ppm (58 % syndiotactic, 34 % atactic, 8 % isotactic), the backbone methylene group (b) at 1.70 – 2.15 ppm and the methoxy group (c) at 3.55 – 3.70 ppm. As the latter overlaps with the signal of the polyether backbone,

representing the macroinitiator, only the signal of the groups carrying the ATRP initiator site (d, 4.07 – 4.37 ppm) is visible in the spectrum.

A HSQC experiment (heteronuclear single quantum correlation) was performed to differentiate between the signals of the macroinitiator and the PMMA arms. Figure 5 shows the ^{1}H-^{13}C HSQC NMR spectrum of *hb*PEO-*b*-$(PMMA_9)_{142}$, the respective ^{13}C 2D spectra of hb*PEO*-b-$(PMMA_{16})_{142}$ and *hb*PEO-*b*-$(PMMA_{26})_{142}$ are found in the supporting information (cf.). For the correlation, 13C DEPT NMR spectra are used to facilely distinguish between methylene groups and methyl or methine groups *via* phase correlation.

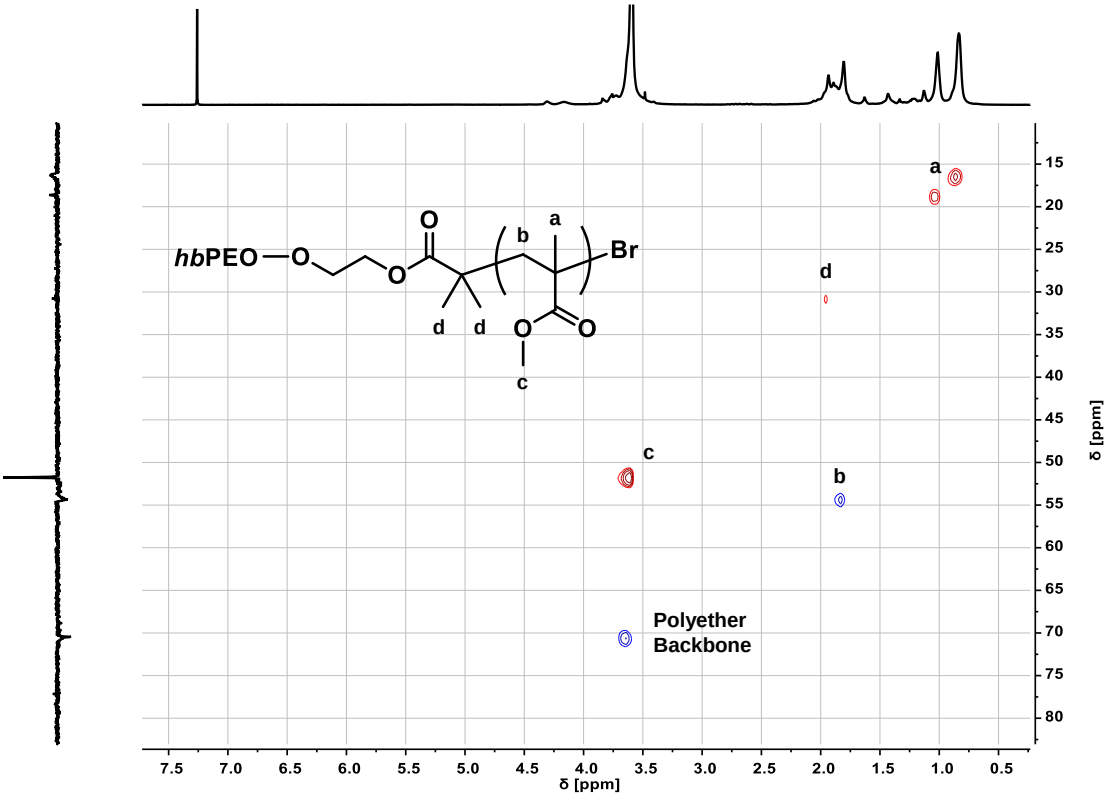

Figure 5. ^{1}H-^{13}C HSQC NMR spectrum of *hb*PEO-*b*-$(PMMA_9)_{142}$ (400/100MHz, $CDCl_3$). ^{1}H and ^{13}C NMR spectra can be found on the horizontal and vertical axis, respectively. Phase correlation is given by correlation of cross peaks (red: methyl, methine, Blue: methylene).

Several signals of the macroinitiator, i.e. the signals of the polyether backbone (^{1}H = 3.78 – 3.57 ppm; ^{13}C = 68.44 – 71.93 ppm), and of the isobutyryl moieties attached to the core (^{1}H = 1.94 – 1.94 ppm; ^{13}C = 29.84 – 32.04 ppm) are clearly distinguishable. However, to unambiguously confirm the attachment of the PMMA arms to the hyperbranched polyether polyol core, a DOSY (diffusion ordered spectroscopy) experiment was conducted. In the case of a successful initiation by the *hb*PEO core, each polymer should possess the same diffusion coefficient since being covalently attached.

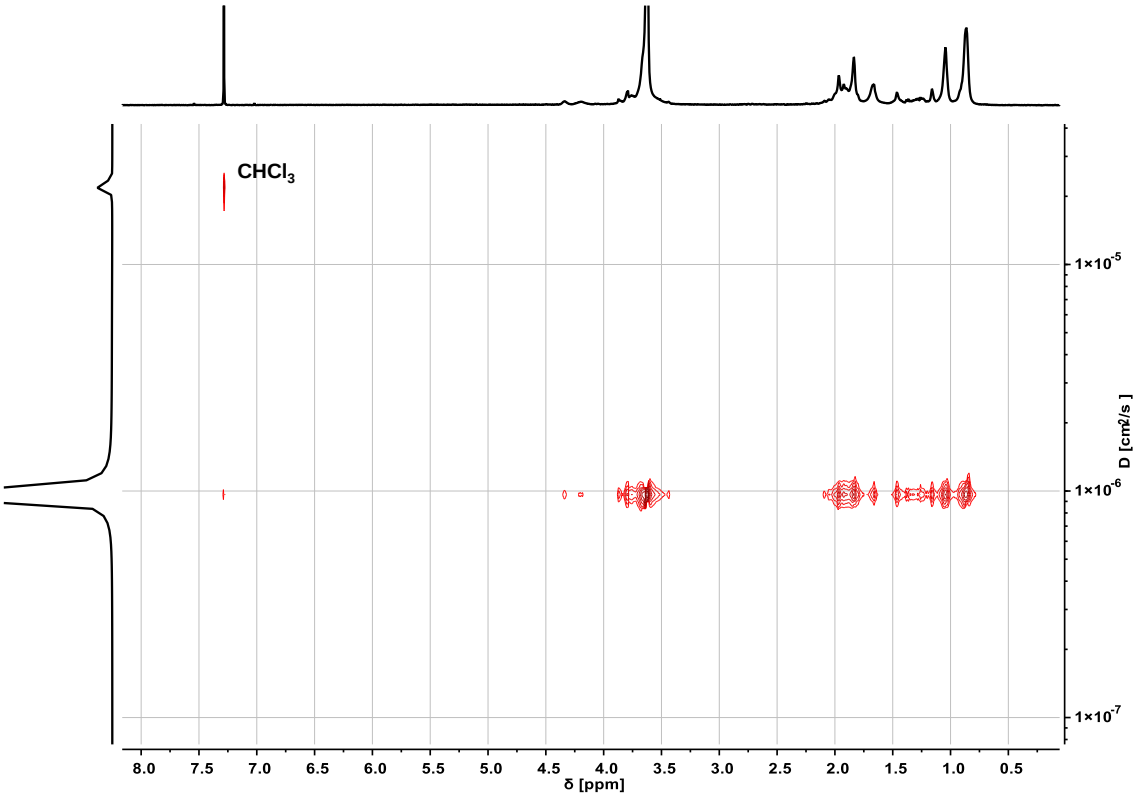

Figure 6. DOSY of *hb*PEO-*b*-$(PMMA_9)_{142}$ (400 MHz, $CDCl_3$). The ^{1}H NMR spectrum and the diffusion coefficient D [cm^2 s^{-1}] can be found on the horizontal and the vertical axis, respectively.

Figure 6 shows the DOSY of *hb*PEO-*b*-$(PMMA_9)_{142}$ measured in $CDCl_3$. The signals of both individual polymers (*hb*PEO and PMMA) are projected to a single

diffusion coefficient D. The same observations are made for *hb*PEO-*b*-$(PMMA_{14})_{142}$ and *hb*PEO-*b*-$(PMMA_{9})_{142}$ (cf. Figure S 13 and Figure S 14) confirming the attachment of the arms to the macroinitiator to form multi-arm star copolymers.

Table 2. ^{1}H NMR data of the multi-arm star copolymers *hb*PEO-*b*-$(PMMA_{9})_{142}$, *hb*PEO-*b*-$(PMMA_{16})_{142}$ and *hb*PEO-*b*-$(PMMA_{24})_{142}$.

Sample[a)]	**Time [min]**	**Conv.**[b)] **[%]**	**$DP_{n,arms}$**[b)]	**$M_{n,arms}$**[b)] **[g mol^{-1}]**	**$M_{n,calc}$**[c)] **[kg mol^{-1}]**
*hb*PEO-*b*-$(PMMA_{9})_{142}$	10	9	9	930	189
*hb*PEO-*b*-$(PMMA_{16})_{142}$	20	15	16	1570	280
*hb*PEO-*b*-$(PMMA_{24})_{142}$	30	23	24	2400	401

[a)]Terminology *hb*PEO-*b*-$(PMMA_x)_y$: x = degree of polymerization as determined by ^{1}H NMR spectroscopy, y = total number of arms per star copolymer, [b)]calculated based on ^{1}H NMR spectroscopy, [c)]$M_{n,calc}=(M_{n,\,hbPEO}+142\,(\,M_{2\text{-}BIBB}-M_{HBr})\,)+(DP_n\,M_{MMA})$.

Following the qualitative verification of the formation of multi-arm star polymers, the copolymers, specifically the PMMA arm will be analyzed quantitatively based on the ^{1}H NMR spectra (see Table 2). Employing signal d (two protons) as normation, the methyl group a (three protons per repeating unit per repeating unit) (cf. Figure 4) can be used to calculate the average chain length of each PMMA arm:

$$DP_{n,PMMA}=\frac{I_a}{3} \qquad 2$$

Depending on the reaction time, the degree of polymerization of PMMA ranges from 9 to 24 per arm. Considering the total number of ATRP initiation sites, the overall molar mass of the multi-arm stars can be calculated accordingly.

Interestingly, due to the high number of arms growing simultaneously, an average molar mass of 400 000 g mol^{-1} is achieved after only 30 min of reaction time.

Considering the high overall molar mass of the PMMA in comparison to the macroinitiator, the appearance of micro-phase separation is highly unlikely. Accordingly, only one T_g was found for all multi-arm star polymers assuming values of 54 °C (10 min), 94 °C (20 min) and 104 °C (30 min). Interestingly, the individual values approach the T_g of PMMA (T_g = 105 °C) at a DP_n of only 24 repeating units, which translates to an average molar mass of 2400 g mol^{-1} – an observation already discussed for other multi-arm star copolymers based on hyperbranched polyether polyols.[19]

For controlled or living radical polymerizations, the overall radical concentration [P·] is constant due to the absence of termination reactions, e.g. radical-radical coupling. In this specific case, the rate constant k_s and [P·] form an apparent rate constant k_{app} and the reaction shows first order kinetics, i.e. the conversion index $\ln\left(\frac{[M]_o}{[M]_t}\right)$ depends linearly on the reaction time t as expressed by equation 3:[43]

$$\ln\left(\frac{[M]_0}{[M]_t}\right) = k_s[P\cdot]t = k_{app}t \qquad 3$$

Figure 7 shows the degrees of polymerization and conversion indices $\ln\left(\frac{[M]_o}{[M]_t}\right)$ plotted against the reaction time. In both cases a linear (first order) dependence is observed. Considering equation 2, the overall radical concentration [P·] is constant in a time frame of up to 30 minutes, i.e. conversions of up to 23 %. Therefore, under the specific reaction conditions employed, the simultaneous growth of 142 chains per polymer can proceed in a controlled manner without termination reactions.

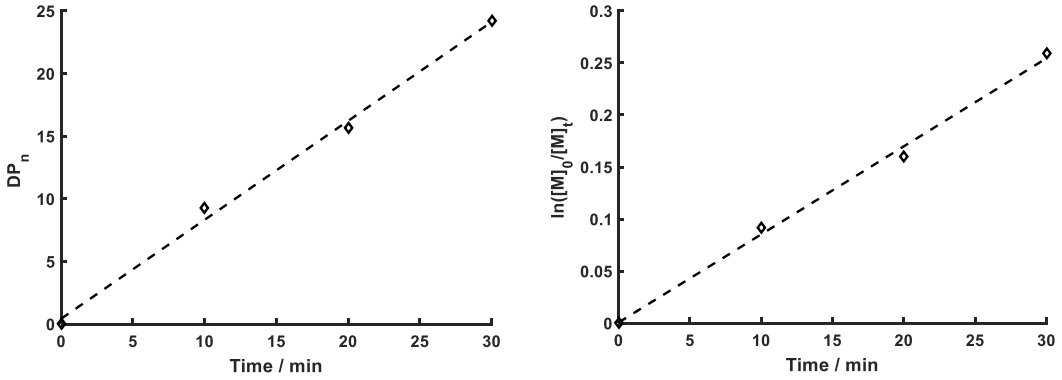

Figure 7. DP_n vs. reaction time (left) and conversion index $\ln\left(\frac{[M]_o}{[M]_t}\right)$ vs. reaction time (right).

The combination of the different NMR experiments and the kinetical evaluation of the reaction proves the proposed multi-arm star architecture of the *hb*PEO-*b*-(PMMA) copolymers prepared under well-controlled reaction conditions. The amphiphilic materials show promising properties, e.g. solubility in various organic solvents and thermal behavior, from which interesting applications might arise, e.g. as micellar structures. The main variables available to tune the properties of multi-arm star polymers are the number and the molar mass of the arms. For example, the thermal properties can be adjusted by variation of the arm length as discussed above. However, by increasing the molar mass fraction of the arms, the processability in melt declines due to entanglements being more probable[25]. On the other hand, processability is improved again by a reduced number of arms. Therefore, a delicate balance is needed to tailor the properties of multi-arm star polymers.

Conclusion

Multi-arm star polymers are a peculiar copolymer class possessing a range of interesting properties. These properties show a strongly dependence on the total number of arms per polymer and the individual arm lengths. Several multi-arm star polymers based on hyperbranched polyglycerol as the multifunctional core moiety for a core-first approach have been reported already, however, only with a limited number of arms, e.g. up to 85 arms in the case of *hb*PG-*b*-PMMA star copolymers.

Here, by employing a high molar mass polyether polyol core, several *hb*PEO-b-PMMA multi-arm star copolymers with an unprecedented average number of arms of 142 were synthesized. By simultaneous slow monomer addition of glycidol and ethylene oxide to a *hb*PEO macroinitiator (Mn = 9600 g mol^{-1}), a well-defined *hb*PEO copolymer with a molar mass of 36700 g mol^{-1} (determined by universally calibrated SEC) was obtained. In combination with a glycidol content of X_G = 0.28, an average number of 142 hydroxy groups per polymer was calculated. In a second step, the functional groups were quantitatively esterified with 2-bromoisobutyryl bromide, as confirmed by a combination of ^{1}H spectroscopy, various 2D NMR experiments (HSQC and DOSY) and FTIR spectroscopy, to yield multifunctional ATRP macroinitiators *hb*PEO-Br$_{142}$. The controlled radical polymerization of MMA using *hb*PEO-Br$_{142}$ and a typical ATRP catalyst system (CuBr/PMDETA, in DMF, 70 °C) followed first-order kinetics up to a conversion of 23 % without gelation. The molar masses determined by SEC strongly depend on the reaction time and range from 40 800 to 72 300 g mol^{-1} with narrow dispersities (M_w / M_n = 1.30 – 1.14). The molar masses and degrees of polymerization of the individual arms were calculated by ^{1}H NMR spectroscopy. With increasing reaction time, DP_n of 9, 16 and 24 were obtained, translating to molar masses between 930 and 2400 g mol^{-1} per arm or

189 000 and 401 000 g mol^{-1} per polymer after a reaction time of only 30 min. These polymers show good solubility in a wide range of organic solvents and thermal properties similar to linear homopolymers of PMMA despite relatively low degrees of polymerization.

Acknowledgment

T. K. is grateful for financial support by a fellowship from the “Fonds der Chemischen Industrie (FCI)”. Furthermore, the authors thank Monika Schmelzer and Ulrike Kemmer-Jonas for technical assistance.

References

(1) Archer, L. A.; Varshney, S. K. Synthesis and Relaxation Dynamics of Multiarm Polybutadiene Melts. *Macromolecules* **1998**, *31*, 6348–6355.

(2) Roovers, J.; Zhou, L. L.; Toporowski, P. M.; van der Zwan, M.; Iatrou, H.; Hadjichristidis, N. Regular star polymers with 64 and 128 arms. Models for polymeric micelles. *Macromolecules* **1993**, *26*, 4324–4331.

(3) Gao, H.; Matyjaszewski, K. Synthesis of Star Polymers by A New “Core-First” Method: Sequential Polymerization of Cross-Linker and Monomer. *Macromolecules* **2008**, *41*, 1118–1125.

(4) Schömer, M.; Schüll, C.; Frey, H. Hyperbranched aliphatic polyether polyols. *J. Polym. Sci. Polym. Chem.* **2013**, *51*, 995–1019.

(5) Sunder, A.; Hanselmann, R.; Frey, H.; Mülhaupt, R. Controlled Synthesis of Hyperbranched Polyglycerols by Ring-Opening Multibranching Polymerization. *Macromolecules* **1999**, *32*, 4240–4246.

(6) Hölter, D.; Frey, H. Degree of branching in hyperbranched polymers. 2. Enhancement of the db: Scope and limitations. *Acta Polym.* **1997**, *48*, 298–309.

(7) Radke, W.; Litvinenko, G.; Müller, A. H. E. Effect of Core-Forming Molecules on Molecular Weight Distribution and Degree of Branching in the Synthesis of Hyperbranched Polymers. *Macromolecules* **1998**, *31*, 239–248.

(8) Hanselmann, R.; Hölter, D.; Frey, H. Hyperbranched Polymers Prepared via the Core-Dilution/Slow Addition Technique: Computer Simulation of Molecular Weight Distribution and Degree of Branching. *Macromolecules* **1998**, *31*, 3790–3801.

(9) Sunder, A.; Mülhaupt, R.; Frey, H. Hyperbranched Polyether−Polyols Based on Polyglycerol: Polarity Design by Block Copolymerization with Propylene Oxide. *Macromolecules* **2000**, *33*, 309–314.

(10) Doycheva, M.; Berger-Nicoletti, E.; Wurm, F.; Frey, H. Rapid Synthesis and MALDI-ToF Characterization of Poly(ethylene oxide) Multiarm Star Polymers. *Macromol. Chem. Phys.* **2010**, *211*, 35–44.

(11) Knischka, R.; Lutz, P. J.; Sunder, A.; Mülhaupt, R.; Frey, H. Functional Poly(ethylene oxide) Multiarm Star Polymers: Core-First Synthesis Using Hyperbranched Polyglycerol Initiators. *Macromolecules* **2000**, *33*, 315–320.

(12) Burgath, A.; Sunder, A.; Neuner, I.; Mülhaupt, R.; Frey, H. Multi-arm star block copolymers based on ε-caprolactone with hyperbranched polyglycerol core. *Macromol. Chem. Phys.* **2000**, *201*, 792–797.

(13) Gottschalk, C.; Wolf, F.; Frey, H. Multi-Arm Star Poly(L-lactide) with Hyperbranched Polyglycerol Core. *Macromol. Chem. Phys.* **2007**, *208*, 1657–1665.

(14) Wolf, F. K.; Fischer, A. M.; Frey, H. Poly(glycolide) multi-arm star polymers: Improved solubility via limited arm length. *Beilstein J. Org. Chem.* **2010**, *6*.

(15) Kato, M.; Kamigaito, M.; Sawamoto, M.; Higashimura, T. Polymerization of Methyl Methacrylate with the Carbon Tetrachloride/Dichlorotris-(triphenylphosphine)ruthenium(II)/Methylaluminum Bis(2,6-di-tert-butylphenoxide) Initiating System: Possibility of Living Radical Polymerization. *Macromolecules* **1995**, *28*, 1721–1723.

(16) Wang, J.-S.; Matyjaszewski, K. Controlled/"living" radical polymerization. atom transfer radical polymerization in the presence of transition-metal complexes. *J. Am. Chem. Soc.* **1995**, *117*, 5614–5615.

(17) Matyjaszewski, K. Atom Transfer Radical Polymerization (ATRP): Current Status and Future Perspectives. *Macromolecules* **2012**, *45*, 4015–4039.

(18) Iocozzia, J.; Lin, Z. Solution-Stable Colloidal Gold Nanoparticles via Surfactant-Free, Hyperbranched Polyglycerol-b-polystyrene Unimolecular Templates. *Langmuir* **2016**, *32*, 7180–7188.

(19) Maier, S.; Sunder, A.; Frey, H.; Mülhaupt, R. Synthesis of poly(glycerol)-block-poly(methyl acrylate) multi-arm star polymers. *Macromol. Rapid Commun.* **2000**, *21*, 226–230.

(20) Shen, Z.; Chen, Y.; Barriau, E.; Frey, H. Multi-Arm Star Polyglycerol-block-poly(tert-butyl acrylate) and the Respective Multi-Arm Poly(acrylic acid) Stars. *Macromol. Chem. Phys.* **2006**, *207*, 57–64.

(21) Shen, Z.; Duan, H.; Frey, H. Water-Soluble Fluorescent Ag Nanoclusters Obtained from Multiarm Star Poly(acrylic acid) as “Molecular Hydrogel” Templates. *Adv. Mater.* **2007**, *19*, 349–352.

(22) Chen, Y.; Shen, Z.; Barriau, E.; Kautz, H.; Frey, H. Synthesis of multiarm star poly(glycerol)-block-poly(2-hydroxyethyl methacrylate). *Biomacromolecules* **2006**, *7*, 919–926.

(23) Liu, H.; Chen, Y.; Shen, Z.; Frey, H. Multiarm star polyglycerol-block-poly(HEMA) as a versatile precursor for the preparation of micellar nanocapsules with different properties. *React. Funct. Polym.* **2007**, *67*, 156–164.

(24) Zhang, Y.; Yan, Y.; Wang, Y.; Li, Y.; Wang, X.; Zhang, H.; Liu, J.; Wang, F. The synthesis and solution properties of hyperbranched polyglycerols modified with hexafluorobutyl acrylate. *Colloids and Surfaces A: Physicochem. Eng. Aspects* **2013**, *436*, 563–569.

(25) Morell, M.; Voit, B.; Ramis, X.; Serra, À.; Lederer, A. Synthesis, characterization, and rheological properties of multiarm stars with poly(glycidol) core and poly(methyl methacrylate) arms by AGET ATRP. *J. Polym. Sci. Polym. Chem.* **2011**, *49*, 3138–3151.

(26) Kautz, H.; Sunder, A.; Frey, H. Control of the molecular weight of hyperbranched polyglycerols. *Macromol. Symp.* **2001**, *163*, 67–74.

(27) Kainthan, R. K.; Muliawan, E. B.; Hatzikiriakos, S. G.; Brooks, D. E. Synthesis, Characterization, and Viscoelastic Properties of High Molecular Weight Hyperbranched Polyglycerols. *Macromolecules* **2006**, *39*, 7708–7717.

(28) ul-haq, M. I.; Shenoi, R. A.; Brooks, D. E.; Kizhakkedathu, J. N. Solvent-assisted anionic ring opening polymerization of glycidol: Toward medium and high molecular weight hyperbranched polyglycerols. *J. Polym. Sci. Polym. Chem.* **2013**, *51*, 2614–2621.

(29) Moore, E.; Zill, A. T.; Anderson, C. A.; Jochem, A. R.; Zimmerman, S. C.; Bonder, C. S.; Kraus, T.; Thissen, H.; Voelcker, N. H. Synthesis and Conjugation of Alkyne-Functional Hyperbranched Polyglycerols. *Macromol. Chem. Phys.* **2016**, *217*, 2252–2261.

(30) Sunder, A.; Türk, H.; Haag, R.; Frey, H. Copolymers of Glycidol and Glycidyl Ethers: Design of Branched Polyether Polyols by Combination of Latent Cyclic AB 2 and ABR Monomers. *Macromolecules* **2000**, *33*, 7682–7692.

(31) Wilms, D.; Schömer, M.; Wurm, F.; Hermanns, M. I.; Kirkpatrick, C. J.; Frey, H. Hyperbranched PEG by random copolymerization of ethylene oxide and glycidol. *Macromol. Rapid Commun.* **2010**, *31*, 1811–1815.

(32) Kaiser, T.; Seiwert, J.; Vitz, J.; Preis, J.; Nischang, I.; Schubert, U. S.; Frey, H. Control of the Molar Mass of Hyperbranched Poly(ethylene oxide) by Slow Monomer Addition. *to be submitted*.

(33) Perevyazko, I.; Seiwert, J.; Schömer, M.; Frey, H.; Schubert, U. S.; Pavlov, G. M. Hyperbranched Poly(ethylene glycol) Copolymers: Absolute Values of the Molar Mass, Properties in Dilute Solution, and Hydrodynamic Homology. *Macromolecules* **2015**, *48*, 5887–5898.

(34) Schömer, M.; Seiwert, J.; Frey, H. Hyperbranched Poly(propylene oxide): A Multifunctional Backbone-Thermoresponsive Polyether Polyol Copolymer. *ACS Macro Lett.* **2012**, *1*, 888–891.

(35) Seiwert, J.; Leibig, D.; Kemmer-Jonas, U.; Bauer, M.; Perevyazko, I.; Preis, J.; Frey, H. Hyperbranched Polyols via Copolymerization of 1,2-Butylene Oxide and Glycidol: Comparison of Batch Synthesis and Slow Monomer Addition. *Macromolecules* **2016**, *49*, 38–47.

(36) Leibig, D.; Seiwert, J.; Liermann, J. C.; Frey, H. Copolymerization Kinetics of Glycidol and Ethylene Oxide, Propylene Oxide, and 1,2-Butylene Oxide: From Hyperbranched to Multiarm Star Topology. *Macromolecules* **2016**, *49*, 7767–7776.

(37) Schömer, M.; Frey, H. Organobase-Catalyzed Synthesis of Multiarm Star Polylactide With Hyperbranched Poly(ethylene glycol) as the Core. *Macromol. Chem. Phys.* **2011**, *212*, 2478–2486.

(38) Geschwind, J.; Rathi, S.; Tonhauser, C.; Schömer, M.; Hsu, S. L.; Coughlin, E. B.; Frey, H. Stereocomplex Formation in Polylactide Multiarm Stars and Comb Copolymers with Linear and Hyperbranched Multifunctional PEG. *Macromol. Chem. Phys.* **2013**, *214*, 1434–1444.

(39) Hilf, J.; Schulze, P.; Seiwert, J.; Frey, H. Controlled synthesis of multi-arm star polyether-polycarbonate polyols based on propylene oxide and CO2. *Macromol. Rapid Commun.* **2014**, *35*, 198–203.

(40) Scharfenberg, M.; Seiwert, J.; Scherger, M.; Preis, J.; Susewind, M.; Frey, H. Multiarm Polycarbonate Star Polymers with a Hyperbranched Polyether Core from CO 2 and Common Epoxides. *Macromolecules* **2017**, *50*, 6577–6585.

(41) Kaiser, T.; Seiwert, J.; Vitz, J.; Preis, J.; Nischang, I.; Schubert, U. S.; Frey, H. Control of the Molar Mass of Hyperbranched Poly(ethylene glycol) Via Slow Monomer Addition. *to be submitted*.

(42) Wilms, D.; Wurm, F.; Nieberle, J.; Böhm, P.; Kemmer-Jonas, U.; Frey, H. Hyperbranched Polyglycerols with Elevated Molecular Weights: A Facile Two-Step Synthesis Protocol Based on Polyglycerol Macroinitiators. *Macromolecules* **2009**, *42*, 3230–3236.

(43) Matyjaszewski, K.; Davis, T. P. *Handbook of Radical Polymerization*; John Wiley & Sons, Inc: Hoboken, NJ, USA, 2002.

(44) Hölter, D.; Burgath, A.; Frey, H. Degree of branching in hyperbranched polymers. *Acta Polym.* **1997**, *48*, 30–35.

(45) Frey, H.; Hölter, D. Degree of branching in hyperbranched polymers. 3 Copolymerization of ABm-monomers with AB and ABn-monomers. *Acta Polym.* **1999**, *50*, 67–76.

Supporting Information

*hb*PEO

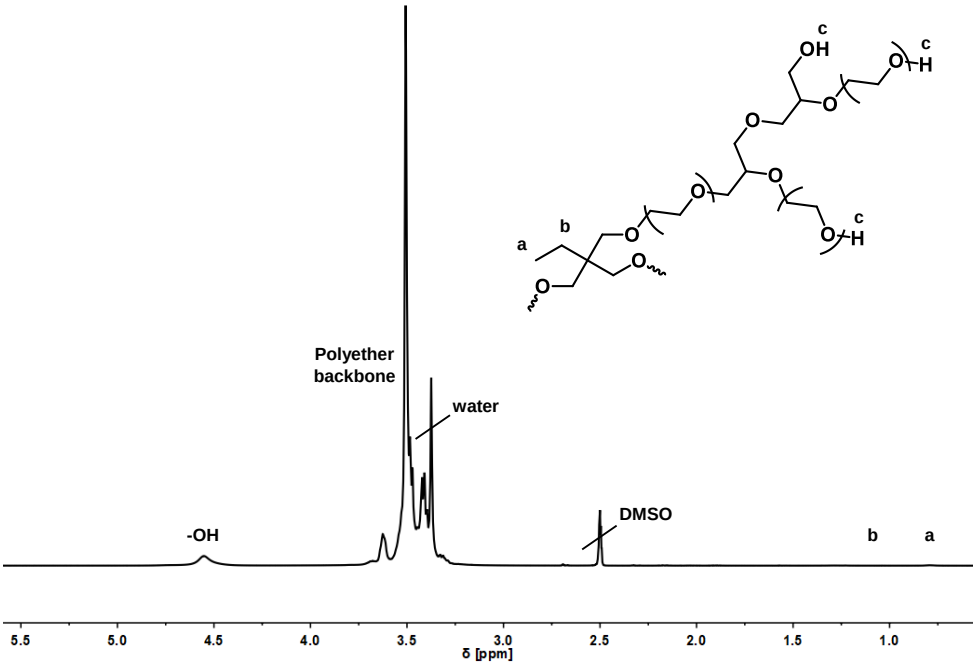

Figure S 1. ^{1}H NMR spectrum of *hb*PEO (400 MHz, DMSO-d_6).

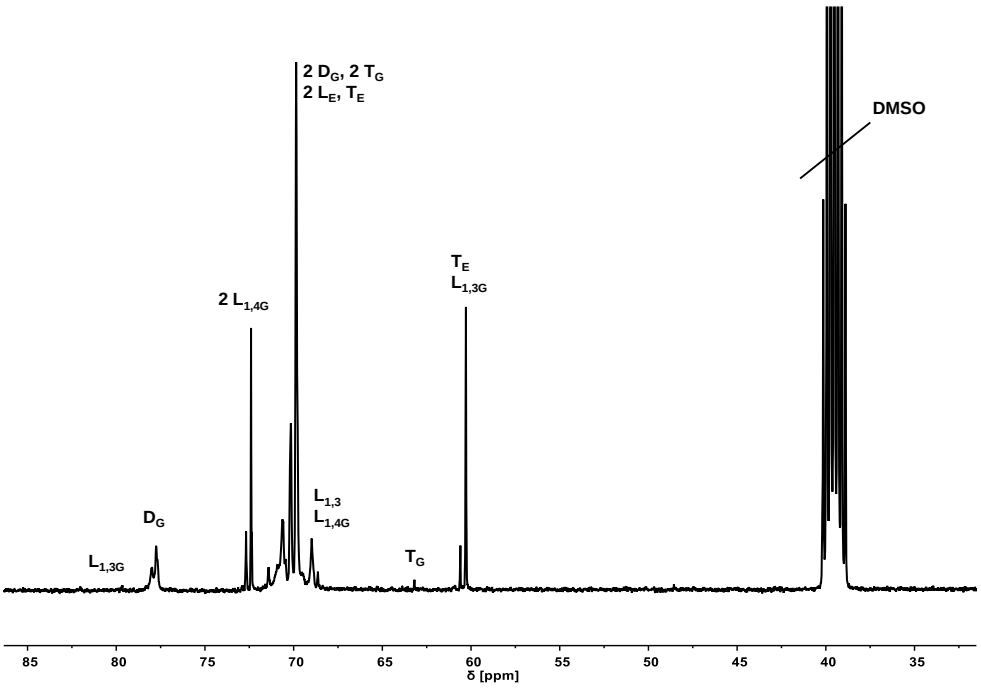

Figure S 2. ^{13}C NMR spectrum of *hb*PEO (100 MHz, DMSO-d_6). The signals were assigned according to literature reports.[31]

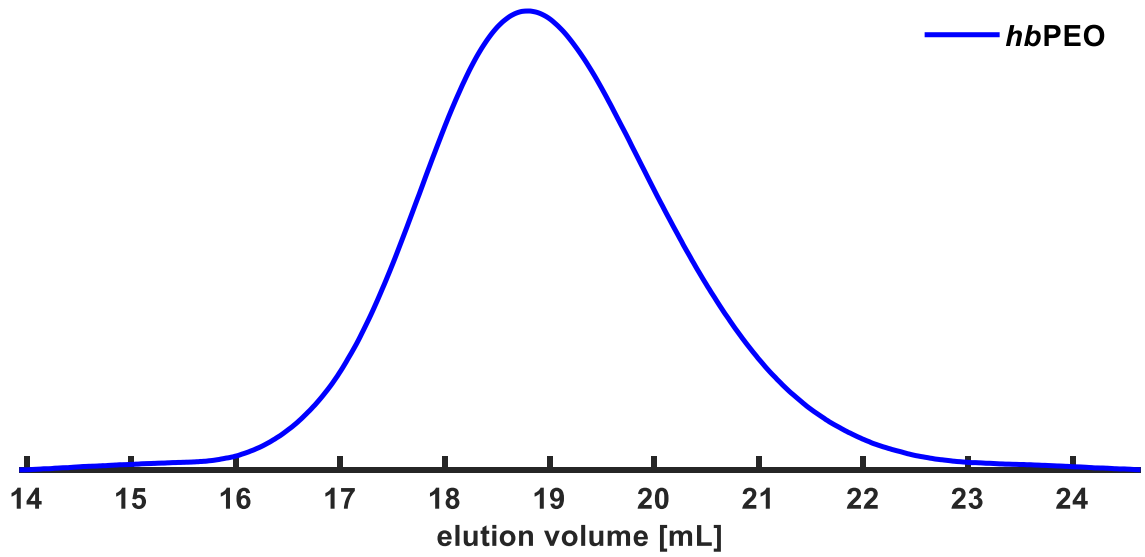

Figure S 3. SEC trace of *hb*PEO (DMF, RI detector).

Degrees of Branching

Degree of branching and copolymer composition according to Frey and coworkers:[44,45]

$$DB = \frac{2\,D}{2\,D + L} \qquad S\ 1$$

$$X_G = \frac{D_G + L_{1,3G} + L_{1,4G} + T_G}{D_G + L_{1,3G} + L_{1,4G} + T_G + L_E + T_E} \qquad S\ 2$$

*hb*PEO-Br$_{142}$

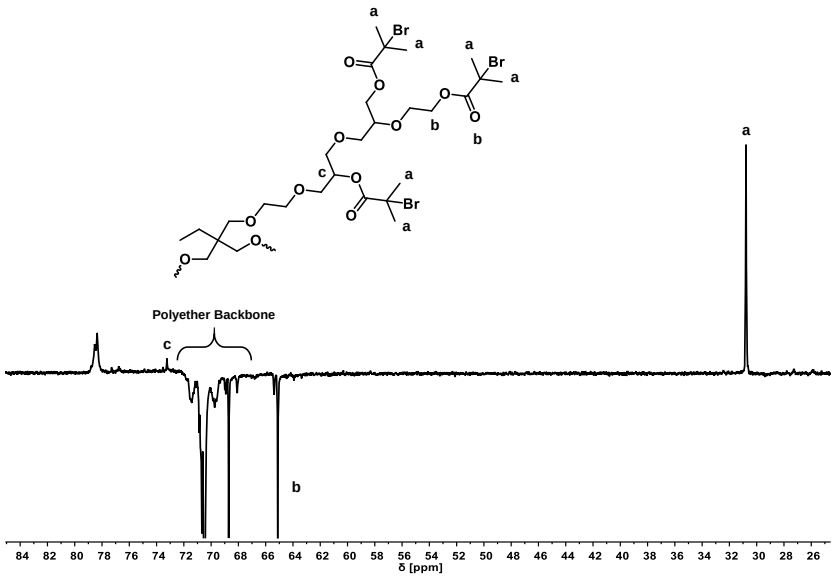

Figure S 4. ^{13}C DEPT NMR spectrum of *hb*PEO-Br$_{142}$ (100 MHz, DMSO-d_6). The different phases found in the spectrum represent different carbon substitution patterns (positive: primary and secondary, negative: methylene; quartary carbon atoms are not depicted).

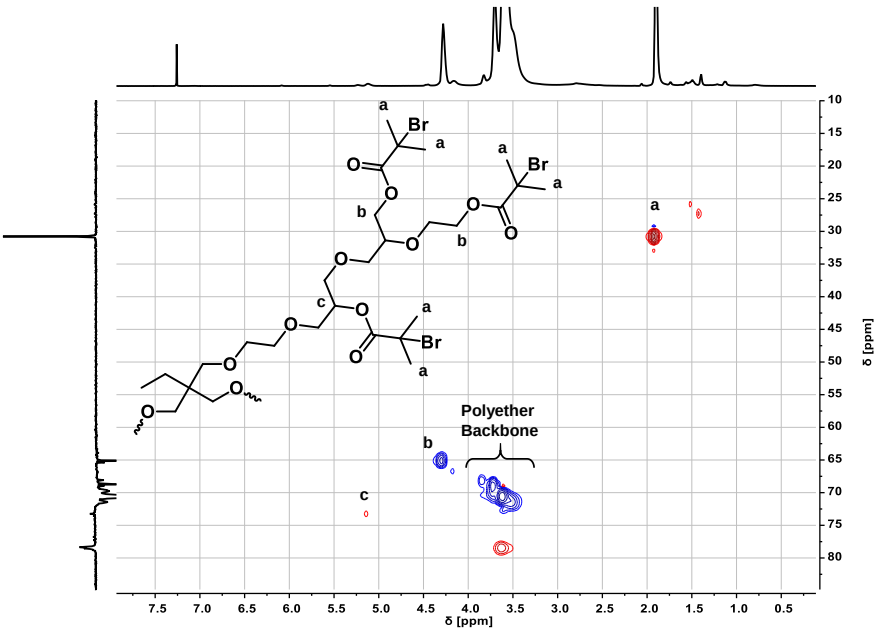

Figure S 5. HSQC spectrum of *hb*PEO-Br$_{142}$ (400/100MHz, $CDCl_3$). ^{1}H and ^{13}C NMR spectra can be found on the horizontal and vertical axis, respectively. Phase correlation is given by correlation of cross peaks (red: methyl, methine, Blue: methylene).

*hb*PEO-*b*-PMMA multi-arm star polymers

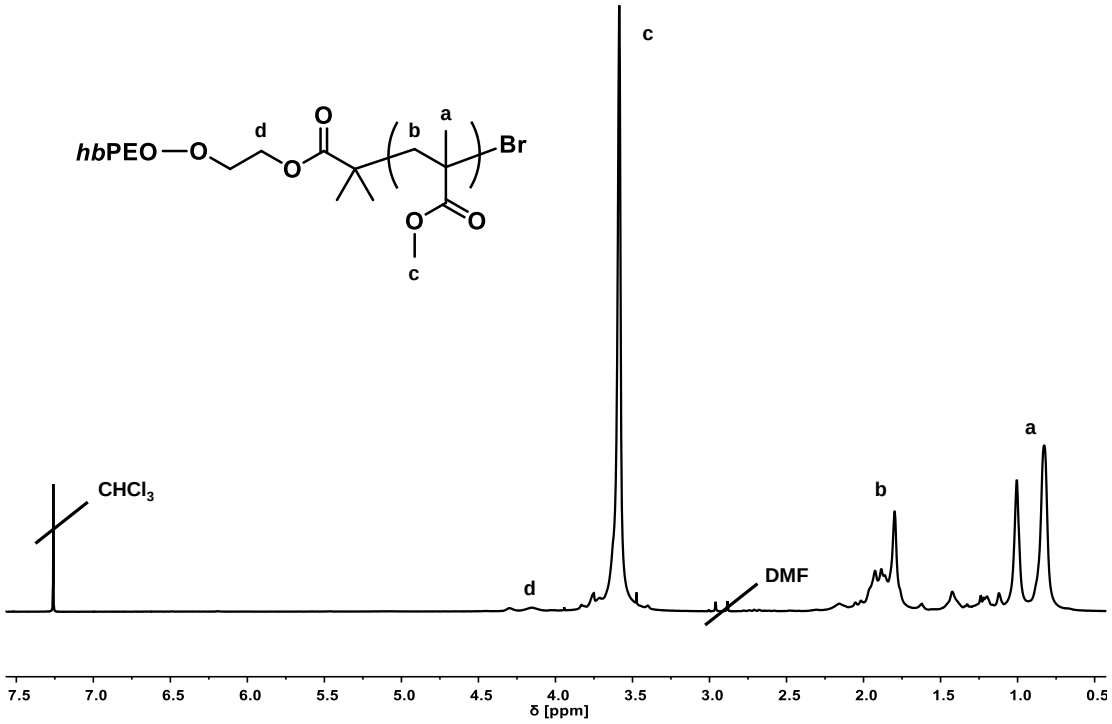

Figure S 6. ^{1}H NMR spectrum of *hb*PEO-*b*-$(PMMA_{16})_{142}$ (400 MHz, $CDCl_3$).

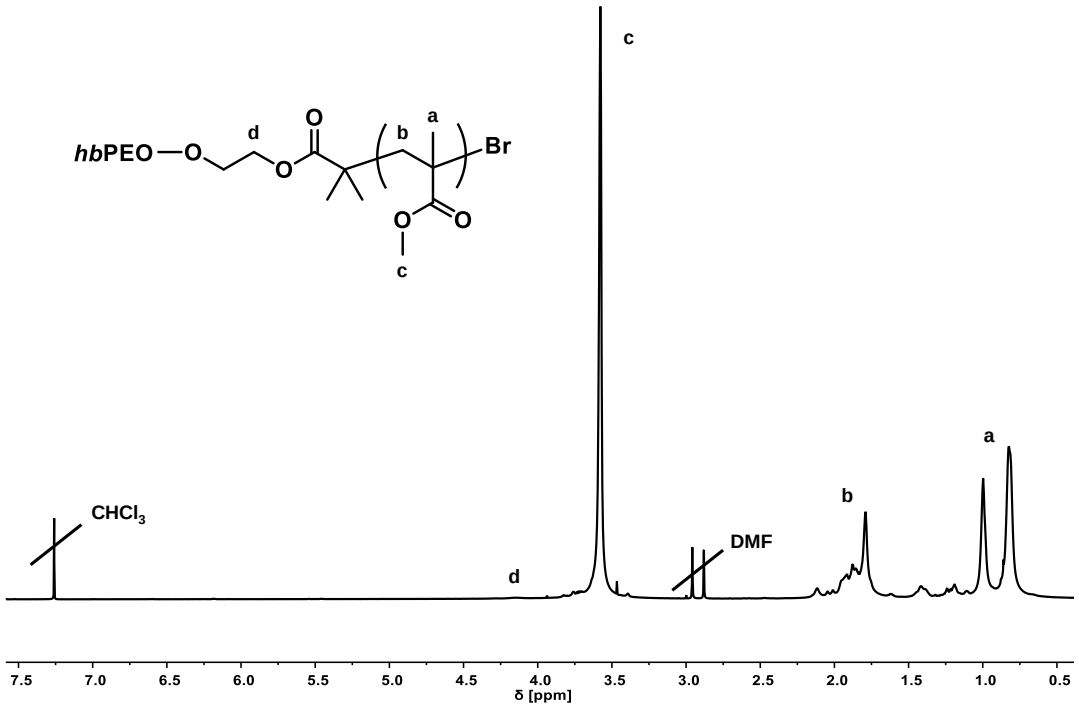

Figure S 7. ^{1}H NMR spectrum of *hb*PEO-*b*-$(PMMA_{24})_{142}$ (400 MHz, $CDCl_3$).

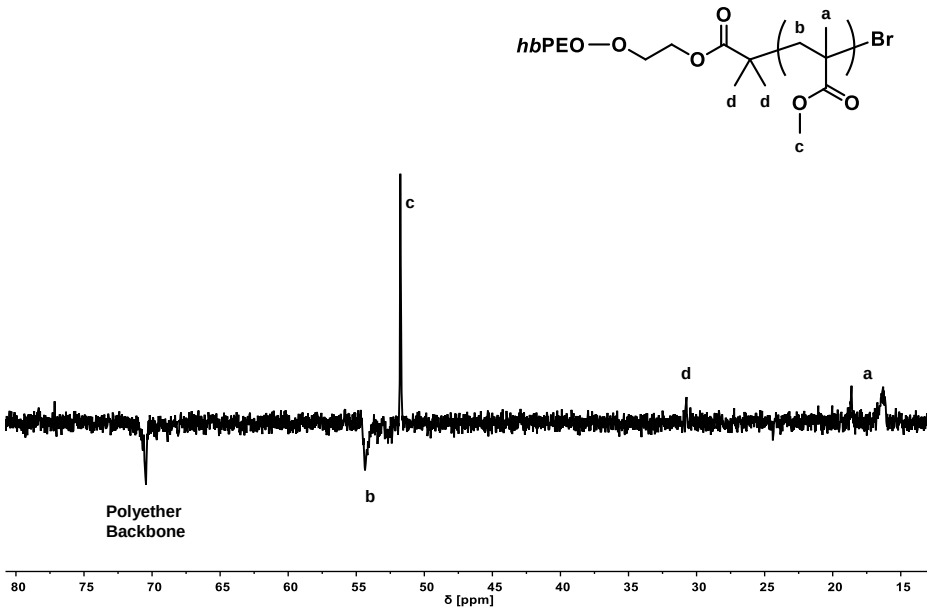

Figure S 8. ^{13}C DEPT NMR spectrum of *hb*PEO-*b*-$(PMMA_9)_{142}$ (100 MHz, DMSO-d_6). The different phases found in the spectrum represent different carbon substitution patterns (positive: primary and secondary, negative: methylene; quartary carbon atoms are not depicted).

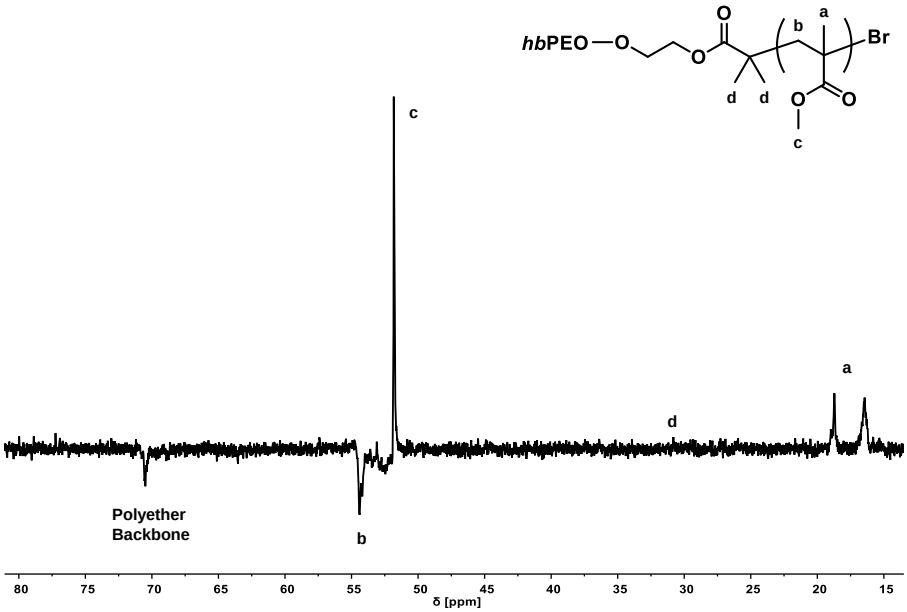

Figure S 9. ^{13}C DEPT NMR spectrum of *hb*PEO-*b*-$(PMMA_{16})_{142}$ (100 MHz, DMSO-d_6). The different phases found in the spectrum represent different carbon substitution patterns (positive: primary and secondary, negative: methylene; quartary carbon atoms are not depicted).

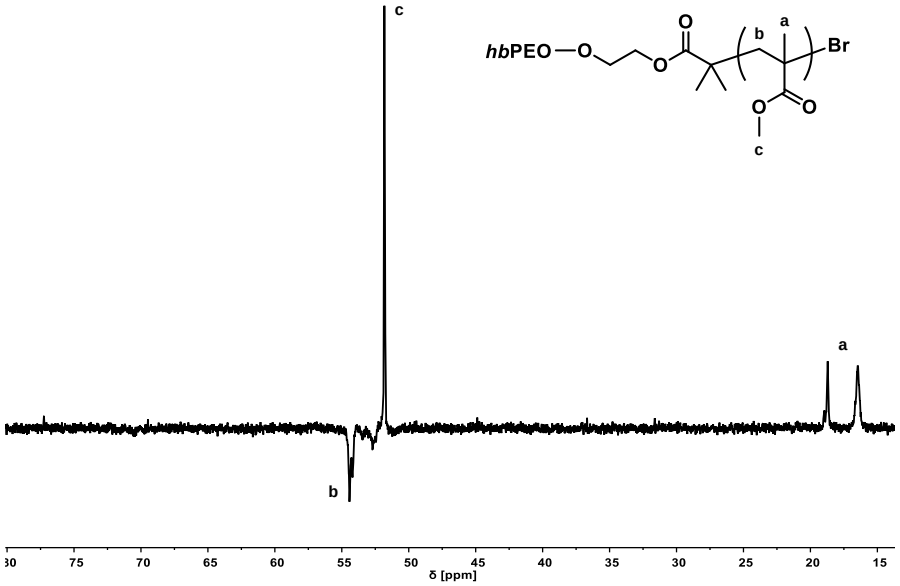

Figure S 10. ^{13}C DEPT NMR spectrum of *hb*PEO-*b*-$(PMMA_{24})_{142}$ (100 MHz, DMSO-d_6). The different phases found in the spectrum represent different carbon substitution patterns (positive: primary and secondary, negative: methylene; quartary carbon atoms are not depicted).

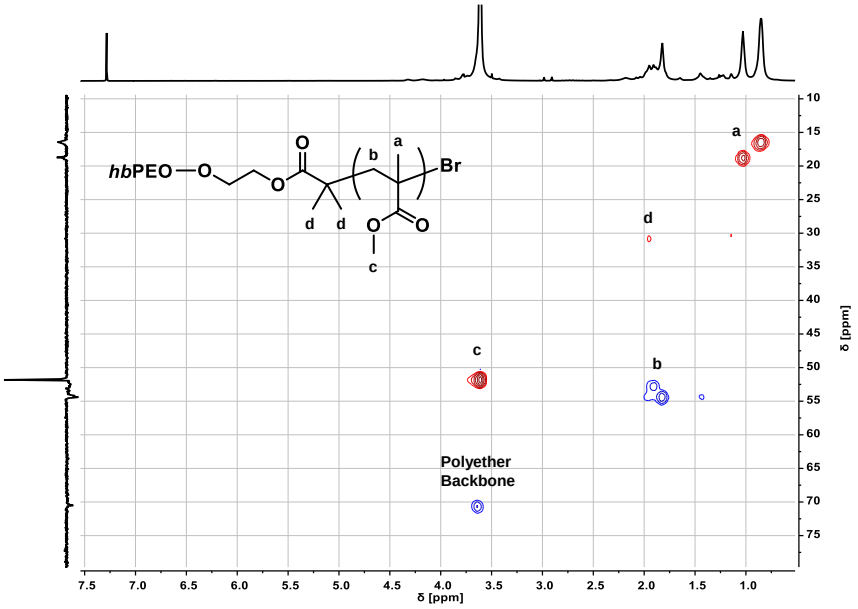

Figure S 11. ^{1}H-^{13}C HSQC NMR spectrum of *hb*PEO-*b*-$(PMMA_{16})_{142}$ (400/100MHz, $CDCl_3$). ^{1}H and ^{13}C NMR spectra can be found on the horizontal and vertical axis, respectively. Phase correlation is given by correlation of cross peaks (red: methyl, methine, Blue: methylene).

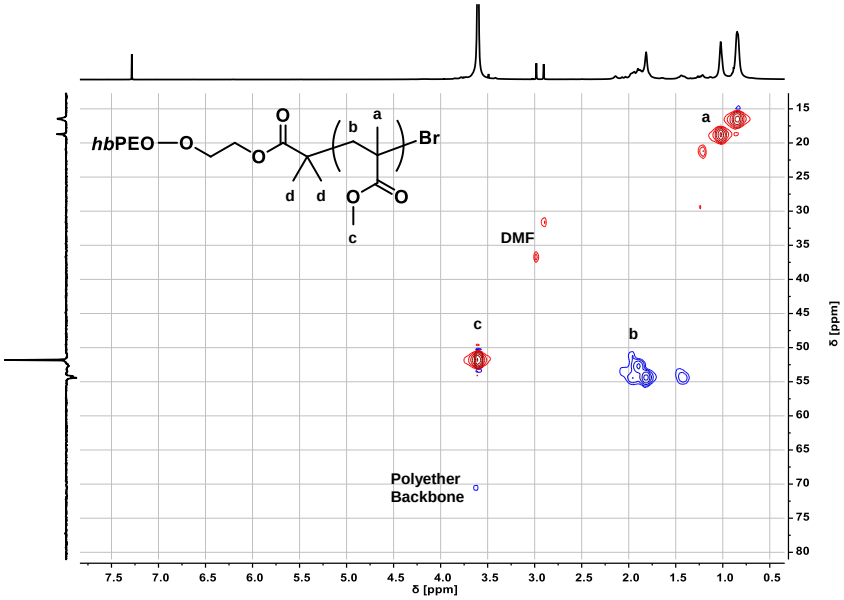

Figure S 12. ^{1}H-^{13}C HSQC NMR spectrum of *hb*PEO-*b*-$(PMMA_{24})_{142}$ (400/100MHz, $CDCl_3$). ^{1}H and ^{13}C NMR spectra can be found on the horizontal and vertical axis, respectively. Phase correlation is given by correlation of cross peaks (red: methyl, methine, Blue: methylene).

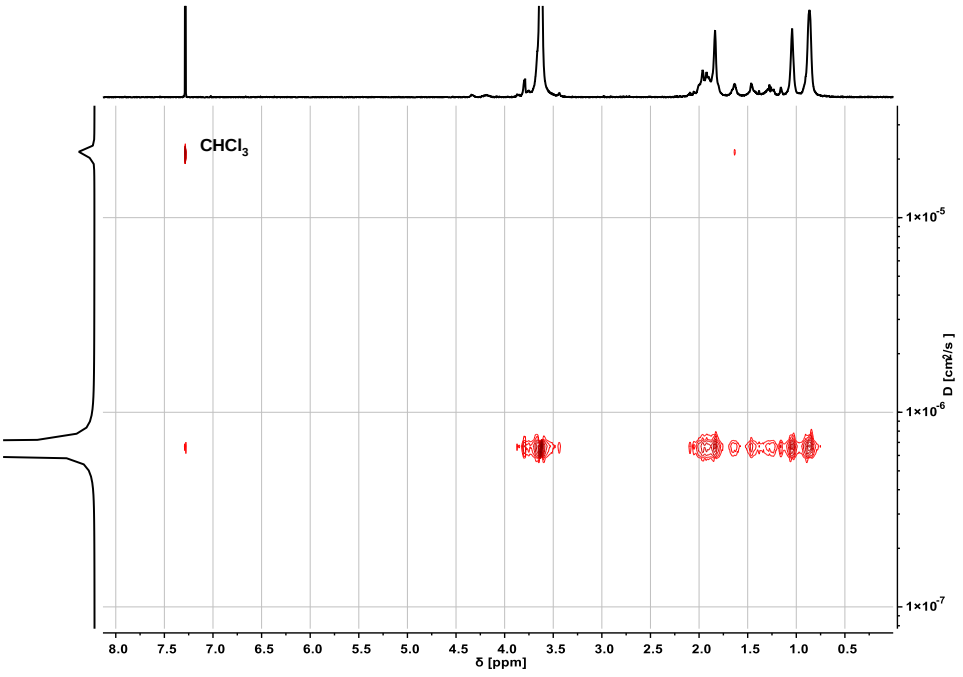

Figure S 13. DOSY of *hb*PEO-*b*-$(PMMA_{16})_{142}$ (400 MHz, $CDCl_3$). The ^{1}H NMR spectrum and the diffusion coefficient D [cm^2 s^{-1}] can be found on the horizontal and the vertical axis, respectively.

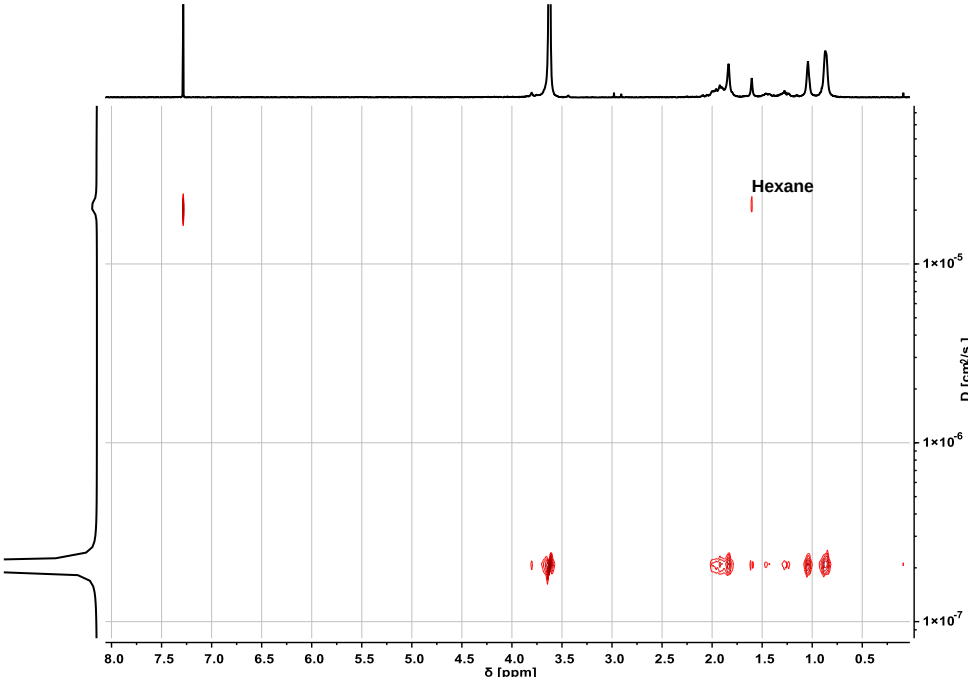

Figure S 14. DOSY of *hb*PEO-*b*-$(PMMA_{24})_{142}$ (400 MHz, $CDCl_3$). The ^1H NMR spectrum and the diffusion coefficient D [$cm^2\ s^{-1}$] can be found on the horizontal and the vertical axis, respectively.

A. Appendix

A.1 Curriculum Vitae

A.2 List of Publications

Peer-Reviewed Publications

Control of the Molar Mass of Hyperbranched Poly(ethylene oxide) *via* Slow Monomer Addition

Tobias Kaiser, Jan Seiwert, Jürgen Vitz, Jasmin Preis, Ivo Nischang, Ulrich S. Schubert, Holger Frey, **2020**, *to be submitted*.

Variation of the Degree of Branching of Hyperbranched Polyether Polyols by Copolymerization of Glycidol with 1-Substituted Analogs

Tobias Kaiser, Tobias Johann, Holger Frey, **2020**, *to be submitted*.

“Hard” Sphere-Behavior of “Soft”, Globular Hyperbranched Polyglycerols - Extensive Molecular Hydrodynamic and Light Scattering Studies

Alexey Lezov, Alexander Gubarev, Tobias Kaiser, Nikolay Tsvetkov, Ivo Nischang, Ulrich S. Schubert, Holger Frey, Igor Perevyazko, **2020**, *to be submitted*.

Synthesis of Stimuli-Responsive Organobases by Copolymerization of Glycidol and a N,N-Dibutylamino-Functional Glycidyl Ether

Tobias Kaiser, Mika Donabauer, Matthias Bros, Holger Frey, **2020**, *in preparation*.

***In-Situ* End-Group Functionalization of Hyperbranched Polyglycerols by Copolymerization of Glycidol with a Bulky Glycidyl Ester**

Tobias Kaiser, Holger Frey, **2020**, *to be submitted*.

Synthesis of Unimolecular Nanocapsules by Partial Esterification of Hyperbranched Poly(ethylene oxide)

Tobias Kaiser, Jessica Emsermann, Jasmin Preis, Holger Frey, **2020**, *to be submitted*.

Synthesis of *hb*PEO-*b*-PMMA Multi-Arm Star Copolymers *via* Atom Transfer Radical Polymerization

Tobias Kaiser, Patrick Roth, Jasmin Preis, Holger Frey, **2020**, *to be submitted*.

Conference Contributions

Control of the Molar Mass of Hyperbranched Poly(ethylene oxide) *via* Slow Monomer Addition (Poster)

Tobias Kaiser, Jan Seiwert, Jürgen Vitz, Jasmin Preis, Ulrich S. Schubert, Holger Frey, *Bordeaux Polymer Conference BPC*, Bordeaux, France, **2018**.

Synthesis of Unimolecular Nanocapsules by Partial Esterification of Hyperbranched Poly(ethylene oxide) (Poster)

Tobias Kaiser, Jessica Emsermann, Jasmin Preis, Holger Frey, *International Symposium on Ionic Polymerization IP*, Beijing, China, **2019**.

Variation of the Degree of Branching of Hyperbranched Polyether Polyols by Copolymerization of Glycidol with 1-Substituted Analogs (Poster)

Tobias Kaiser, Tobias Johann, Holger Frey, *Makromolekulares Kolloquium*, Freiburg, **2020**.